

# *MODFLOW 6 – Example problems*

*MODFLOW 6 Development Team,  
with contributions from Chieh Ying Chen and Mike Toews*

05/23/2024

## Preface

The document presents example problems for MODFLOW 6. The MODFLOW 6 program can be downloaded from the USGS for free. The performance of MODFLOW 6 has been tested with these examples and other tests. Future testing, however, might reveal errors that were not detected in the test simulations. Updates are routinely made to the MODFLOW 6 program and to these examples. Users can check for updates on the MODFLOW Web page (<https://doi.org/10.5066/F76Q1VQV>).

## Acknowledgements

In addition to those listed on the cover page, the following individuals contributed to one or more of the examples presented here: David Krcmar and Yu-Feng Lin.

# Contents

<b>Introduction</b>	<b>0–2</b>
<b>1 TWRI</b>	<b>1–1</b>
1.1 Example Description . . . . .	1–1
1.2 Example Results . . . . .	1–2
<b>2 BCF2SS Model</b>	<b>2–1</b>
2.1 Conceptual Model . . . . .	2–1
2.2 Example Description . . . . .	2–2
2.3 Example Results . . . . .	2–3
<b>3 Tidal Model</b>	<b>3–1</b>
3.1 Example Description . . . . .	3–1
3.2 Example Results . . . . .	3–3
<b>4 Flow and Head Boundary (FHB) Package Replication</b>	<b>4–1</b>
4.1 Example Description . . . . .	4–1
4.2 Example Results . . . . .	4–1
<b>5 Nested Grid Problem</b>	<b>5–1</b>
5.1 Example Description . . . . .	5–1
5.2 Scenario Results . . . . .	5–1
5.2.1 Standard Groundwater Flow Formulation . . . . .	5–1
5.2.2 XT3D . . . . .	5–1
<b>6 Nested Grid Problem, Two Domains</b>	<b>6–1</b>
6.1 Example Description . . . . .	6–2
6.2 Scenario Results . . . . .	6–3
<b>7 MODFLOW-NWT Problem 2</b>	<b>7–1</b>
7.1 Example Description . . . . .	7–1
7.2 Scenario Results . . . . .	7–2
<b>8 MODFLOW-NWT Problem 3</b>	<b>8–1</b>
8.1 Example Description . . . . .	8–1
8.2 Scenario Results . . . . .	8–1
<b>9 Zaidel Problem</b>	<b>9–1</b>
9.1 Example Description . . . . .	9–1
9.2 Example Results . . . . .	9–1
<b>10 Streamflow Routing Package Problem 1</b>	<b>10–1</b>
10.1 Conceptual Model . . . . .	10–1
10.2 Example Description . . . . .	10–2
10.3 Example Results . . . . .	10–3
<b>11 Advanced Packages with MVR</b>	<b>11–1</b>
11.1 Example Results . . . . .	11–1

<b>12 Lake Package Problem 1</b>	<b>12–1</b>
12.1 Example Description . . . . .	.12–1
12.2 Example Results . . . . .	.12–3
<b>13 Lake Package Problem 2</b>	<b>13–1</b>
13.1 Example Description . . . . .	.13–1
13.2 Example Results . . . . .	.13–3
<b>14 Neville-Tonkin Multi-Aquifer Well Problem</b>	<b>14–1</b>
14.1 Example Description . . . . .	.14–1
14.2 Example Results . . . . .	.14–2
<b>15 Multi-Aquifer Well Problem, Flowing Well Option</b>	<b>15–1</b>
15.1 Example Description . . . . .	.15–1
15.2 Example Results . . . . .	.15–2
<b>16 Reilly Multi-Aquifer Well Problem</b>	<b>16–1</b>
16.1 Example Description . . . . .	.16–1
16.1.1 Regional Model . . . . .	.16–1
16.1.2 Local Model . . . . .	.16–2
16.2 Example Results . . . . .	.16–4
<b>17 Flow Diversion</b>	<b>17–1</b>
17.1 Example Description . . . . .	.17–1
17.2 Scenario Results . . . . .	.17–2
17.2.1 Newton-Raphson Formulation . . . . .	.17–2
17.2.2 Standard Conductance Formulation with rewetting . . . . .	.17–2
17.2.3 Newton-Raphson Formulation with a cylindrical obstruction . . . . .	.17–4
<b>18 Circular Island with Triangular Mesh</b>	<b>18–1</b>
18.1 Example Description . . . . .	.18–1
18.2 Example Results . . . . .	.18–1
<b>19 Hani Problem</b>	<b>19–1</b>
19.1 Example Description . . . . .	.19–1
19.2 Scenario Results . . . . .	.19–2
<b>20 Groundwater Whirls</b>	<b>20–1</b>
20.1 Example Description . . . . .	.20–1
20.2 Example Results . . . . .	.20–1
<b>21 LGR with MVR and SFR</b>	<b>21–1</b>
21.1 Example description . . . . .	.21–1
<b>22 Vilhelmsen LGR</b>	<b>22–1</b>
22.1 Example Description . . . . .	.22–1
22.2 Example Results . . . . .	.22–2
<b>23 Laatooe Periodic Boundary Condition</b>	<b>23–1</b>
23.1 Example Description . . . . .	.23–1

23.2 Example Results . . . . .	.23-1
<b>24 Elastic Aquifer Loading</b>	<b>24-1</b>
24.1 Example Description . . . . .	.24-1
24.2 Example Results . . . . .	.24-4
<b>25 Delay Interbed Drainage</b>	<b>25-1</b>
25.1 Theory . . . . .	.25-1
25.2 Example Description . . . . .	.25-2
25.2.1 Head-Based Formulation . . . . .	.25-2
25.2.2 Effective Stress-Based Formulation . . . . .	.25-4
25.2.3 Effect of Interbed Thickness on the Effective Stress-Based Formulation . . . . .	.25-5
<b>26 One-Dimensional Compaction</b>	<b>26-1</b>
26.1 Site Description . . . . .	.26-1
26.2 Example Description . . . . .	.26-2
26.3 Example Results . . . . .	.26-6
<b>27 One-Dimensional Compaction in a Three-Dimensional Flow Field</b>	<b>27-1</b>
27.1 Example Description . . . . .	.27-1
27.2 Example Results . . . . .	.27-4
27.2.1 Simulated Stresses . . . . .	.27-4
27.2.2 Simulated Compaction . . . . .	.27-4
27.2.3 Simulated Storage Changes . . . . .	.27-4
<b>28 Drainage Discharge Scaling</b>	<b>28-1</b>
28.1 Example Description . . . . .	.28-1
28.2 Example Results . . . . .	.28-3
<b>29 Sagehen UZF1 Package Problem 1</b>	<b>29-1</b>
29.1 Example description . . . . .	.29-1
29.2 Example results . . . . .	.29-2
<b>30 Capture Fraction Analysis</b>	<b>30-1</b>
30.1 Example Description . . . . .	.30-1
30.2 Example Results . . . . .	.30-2
<b>31 Keating Problem</b>	<b>31-1</b>
31.1 Example description . . . . .	.31-1
31.2 Example Results . . . . .	.31-2
<b>32 MOC3D Problem 1</b>	<b>32-1</b>
32.1 Example description . . . . .	.32-1
32.2 Example Scenarios . . . . .	.32-1
32.2.1 Scenario Results . . . . .	.32-2
<b>33 MOC3D Problem 2</b>	<b>33-1</b>
33.1 Example description . . . . .	.33-1
33.2 Example Results . . . . .	.33-2

<b>34 MOC3D Problem 2 with Triangular Grid</b>	<b>34–1</b>
34.1 Example description . . . . .	.34–1
34.2 Example Results . . . . .	.34–2
<b>35 MT3DMS Problem 1</b>	<b>35–1</b>
35.1 Example description . . . . .	.35–1
35.2 Example Results . . . . .	.35–2
<b>36 MT3DMS Problem 2</b>	<b>36–1</b>
36.1 Example description . . . . .	.36–2
36.2 Example Results . . . . .	.36–2
<b>37 MT3DMS Problem 3</b>	<b>37–1</b>
37.1 Example description . . . . .	.37–1
<b>38 MT3DMS Problem 4</b>	<b>38–1</b>
<b>39 MT3DMS Problem 5</b>	<b>39–1</b>
<b>40 MT3DMS Problem 6</b>	<b>40–1</b>
<b>41 MT3DMS Problem 7</b>	<b>41–1</b>
<b>42 MT3DMS Problem 8</b>	<b>42–1</b>
42.1 Example description . . . . .	.42–1
42.2 Example results . . . . .	.42–2
<b>43 MT3DMS Problem 9</b>	<b>43–1</b>
43.1 Example description . . . . .	.43–1
43.2 Example results . . . . .	.43–3
<b>44 MT3DMS Problem 10</b>	<b>44–1</b>
44.1 Example description . . . . .	.44–1
44.2 Example results . . . . .	.44–2
<b>45 MT3DMS Problem 10, Two Domains</b>	<b>45–1</b>
45.1 Example description . . . . .	.45–1
45.2 Example Results . . . . .	.45–1
<b>46 MT3DMS Supplemental Guide Problem 6.3.1</b>	<b>46–1</b>
46.1 Example description . . . . .	.46–1
46.2 Example Results . . . . .	.46–1
<b>47 MT3DMS Supplemental Guide Problem 6.3.2</b>	<b>47–1</b>
47.1 Example description . . . . .	.47–1
47.2 Example Scenarios . . . . .	.47–2
47.2.1 Scenario Results . . . . .	.47–2
<b>48 MT3DMS Supplemental Guide Problem 8.2</b>	<b>48–1</b>
48.1 Example description . . . . .	.48–1

48.2 Example Results . . . . .	48-2
<b>49 SFR1 Manual Problem 2</b>	<b>49-1</b>
49.1 Example description . . . . .	49-1
49.2 Example Results . . . . .	49-3
<b>50 Two-Dimensional Test of Unsaturated-Saturated Transport</b>	<b>50-1</b>
50.1 Example description . . . . .	50-2
50.2 Example results . . . . .	50-3
<b>51 Henry Problem</b>	<b>51-1</b>
51.1 Example Description . . . . .	51-1
51.2 Scenario Results . . . . .	51-2
<b>52 Salt Lake Problem</b>	<b>52-1</b>
52.1 Example description . . . . .	52-1
52.2 Example Results . . . . .	52-3
<b>53 Rotating Interface Problem</b>	<b>53-1</b>
53.1 Example description . . . . .	53-1
53.2 Example Results . . . . .	53-2
<b>54 Hecht-Mendez 3D Borehole Heat Exchanger Problem</b>	<b>54-1</b>
54.1 Example description . . . . .	54-1
54.2 Analytical solutions . . . . .	54-3
54.3 Example results . . . . .	54-4
<b>55 Stallman Problem</b>	<b>55-1</b>
55.1 Example Description . . . . .	55-1
55.2 Example Results . . . . .	55-2
<b>56 Synthetic Valley Problem</b>	<b>56-1</b>
56.1 Example description . . . . .	56-1
56.2 Example Results . . . . .	56-3
<b>57 Radial Groundwater Flow Model</b>	<b>57-1</b>
57.1 Example description . . . . .	57-1
57.2 Radial Setup with Unstructured Discretization (DISU) . . . . .	57-2
57.3 Example Results . . . . .	57-3
<b>58 Curvilinear Groundwater Flow Model</b>	<b>58-1</b>
58.1 Example Description . . . . .	58-1
58.2 Example Results . . . . .	58-2
<b>59 Multipart Curvilinear Groundwater Flow Model</b>	<b>59-1</b>
59.1 Example Description . . . . .	59-1
59.2 Example Results . . . . .	59-3
<b>60 Radial Heat Transport</b>	<b>60-1</b>
60.1 Example description . . . . .	60-1

60.2 Example Results . . . . .	.60–5
<b>61 Interacting Borehole Heat Exchangers in a Geothermal Setting</b>	<b>61–1</b>
61.1 Example description . . . . .	.61–1
61.2 Example Results . . . . .	.61–5
<b>62 Infiltrating Heat Front</b>	<b>62–1</b>
62.1 Example description . . . . .	.62–1
62.2 Example Results . . . . .	.62–3
<b>63 Forward Particle Tracking, Structured Grid, Steady-State Flow</b>	<b>63–1</b>
63.1 Example description . . . . .	.63–1
63.2 Example Results . . . . .	.63–2
<b>64 Forward Particle Tracking, Structured Grid, Transient Flow</b>	<b>64–1</b>
64.1 Example description . . . . .	.64–1
64.2 Example Results . . . . .	.64–1
<b>65 Thermal Profile along a Particle Path</b>	<b>65–1</b>
65.1 Example description . . . . .	.65–1
65.2 Example Results . . . . .	.65–2
<b>References Cited</b>	<b>R–1</b>

## List of Figures

1–1	Illustration of the system simulated in the TWRI example problem, from McDonald and Harbaugh (1988). . . . .	1–1
1–2	Simulated water levels and normalized specific discharge vectors in the unconfined, upper, and lower aquifers. <i>A</i> . MODFLOW 6 unconfined aquifer results. <i>B</i> . MODFLOW 6 middle aquifer results. <i>C</i> . MODFLOW 6 lower aquifer results. <i>D</i> . MODFLOW-2005 unconfined aquifer results. <i>E</i> . MODFLOW-2005 middle aquifer results. <i>F</i> . MODFLOW-2005 lower aquifer results. . . . .	1–3
2–1	Diagram showing the model domain. <i>A</i> , plan view, and <i>B</i> , cross-section view. The locations of river cells, and wells are also shown. The steady-state water-table is shown in the cross-section view. . . . .	2–1
2–2	WETDRY parameter values used in the upper aquifer. Cells with negative values can only rewet when the head in an underlying cells exceeds the bottom of the cell. Cells with positive values can rewet if the head in an underlying cells exceeds the bottom of the cell or from adjacent connected cells. . . . .	2–3
2–3	Simulated water levels and normalized specific discharge vectors in the upper and lower aquifers under natural and pumping conditions using the rewetting option in the Node Property Flow (NPF) Package with the Standard Conductance Formulation. <i>A</i> . Upper aquifer results under natural conditions. <i>B</i> . Lower aquifer results under natural conditions <i>C</i> . Upper aquifer results under pumping conditions. <i>D</i> . Lower aquifer results under pumping conditions . . . . .	2–4
2–4	Simulated water levels and normalized specific discharge vectors in the upper and lower aquifers under natural and pumping conditions using the Newton-Raphson Formulation. <i>A</i> . Upper aquifer results under natural conditions. <i>B</i> . Lower aquifer results under natural conditions <i>C</i> . Upper aquifer results under pumping conditions. <i>D</i> . Lower aquifer results under pumping conditions . . . . .	2–5
3–1	Model grid and boundary conditions used for the Tidal example problem: (A) river and well boundaries in layer 1; (B) general-head boundaries in layer 2; (C) general-head and well boundaries in layer 3; and (D) zones used to assign recharge to layer 1. . . . .	3–2
3–2	Simulated groundwater head in model cell (1, 13, 8). . . . .	3–3
3–3	Simulated groundwater flow for model cell (1, 5, 6) and its connection with model cell (1, 6, 6). Positive values indicate flow into model cell (1, 5, 6). . . . .	3–3
3–4	Simulated flow between general-head boundary cells and the groundwater flow model. ESTUARY2 is the combined flow for all general-head cells in layer 2. ESTUARY3 is the combined flow for all general-head cells in layer 3. A positive value represents from from the general-head boundary into the groundwater model. . . . .	3–4
4–1	Model grid and boundary conditions used for the FHB example problem. . . . .	4–2
4–2	Simulated groundwater head in model cells (1, 2, 1) and (1, 2, 10). . . . .	4–2
4–3	Simulated groundwater flow for model cell (1, 2, 2) and its connection with model cell (1, 2, 1). Positive values indicate flow into model cell (1, 2, 2). . . . .	4–3
5–1	Model grid used for the nested grid problem. Constant-head cells are marked in blue. Cell numbers are shown inside each model cell. Vertices are also numbered and are shown in red. . . . .	5–2
5–2	Simulated head (A) and errors in simulated head (B) for the nested grid problem simulated with the standard groundwater flow formulation. . . . .	5–3
5–3	Simulated head (A) and errors in simulated head (B) for the nested grid problem simulated with the XT3D groundwater flow formulation (Provost and others, 2017). . . . .	5–4

6-1	A top view of the grids of the outer and inner model used in this example. The dashed red line indicates the interface between the two. The blue shaded areas are the cells with a constant head boundary condition. . . . .	6-1
6-2	Flow calculation stencils for XT3D for the coupled model system. Details in the text. . . . .	6-2
6-3	Results for scenario 1: simulated head (A) and differences in head with respect to the analytical result (B) for a system of coupled models without XT3D. . . . .	6-4
6-4	Results for scenario 2: simulated head (A) and differences in head with respect to the analytical result (B) for a system of coupled models with XT3D active in both models but not at the exchange between them. . . . .	6-4
6-5	Results for scenario 3: simulated head (A) and differences in head with respect to the analytical result (B) for a system of coupled models with XT3D active in both models and at the exchange between them. . . . .	6-5
6-6	Results for scenario 4: simulated head (A) and differences in head with respect to the analytical result (B) for a system of coupled models without XT3D in the models but with XT3D enabled at the exchange between them. . . . .	6-5
7-1	Hydrogeology, model grid, and model boundary conditions (from McDonald and others, 1992). . . . .	7-1
7-2	Comparison of water-table elevations simulated using the Newton-Raphson Formulation and Standard Conductance Formulation with rewetting. Water-table altitudes in row 1 are shown for <i>A</i> , 190 days, <i>B</i> , 708 days, <i>C</i> , 2,630 days, and <i>D</i> , at steady state. The location of the uppermost constant head boundary cell is also shown. . . . .	7-4
8-1	Distribution of layer-bottom elevations. The location of constant head boundary cells is also shown. . . . .	8-2
8-2	Distribution of groundwater recharge applied in the model scenarios. <i>A</i> , higher recharge rates, and <i>B</i> , lower recharge rates. The location of constant head boundary cells is also shown. . . . .	8-3
8-3	Distribution of heads and saturated thicknesses for the high recharge scenario. <i>A</i> , heads, and <i>B</i> , saturated thicknesses. The location of constant head boundary cells is also shown. . . . .	8-4
8-4	Distribution of heads and saturated thicknesses for the low recharge scenario. <i>A</i> , heads, and <i>B</i> , saturated thicknesses. The white regions indicate cells that have saturated thicknesses less than 1 mm. The location of constant head boundary cells is also shown. . . . .	8-5
9-1	Discontinuous water table configuration over a multistep impervious base. Simulated results for the case where the constant head in column 200 is equal to 1 meter is shown. The impervious model base and the location of constant head boundary cells is also shown. . . . .	9-2
9-2	Discontinuous water table configuration over a multistep impervious base. Simulated results for the case where the constant head in column 200 is equal to 10 meters is shown. The impervious model base and the location of constant head boundary cells is also shown. . . . .	9-2
10-1	Land surface and aquifer bottom elevations. <i>A</i> . Land surface elevation. The location of inactive cells and cells with streamflow routing reaches are also shown. <i>B</i> . Aquifer bottom elevations. The location of cells with general-head and well boundaries are also shown. . . . .	10-1
10-2	Simulated water levels and normalized specific discharge vectors under steady state and pumping conditions. <i>A</i> . steady-state results. <i>B</i> . results after 50 years of pumping. . . . .	10-4

10–3 Simulated reach depth and downstream discharge at select reaches. <i>A.</i> Stage in reach 4. <i>B.</i> Downstream discharge in reach 4. <i>C.</i> Stage in reach 15. <i>D.</i> Downstream discharge in reach 15. <i>E.</i> Stage in reach 27. <i>F.</i> Downstream discharge in reach 27. <i>G.</i> Stage in reach 36. <i>H.</i> Downstream discharge in reach 36. . . . .	.10–6
11–1 Plan view of lakes and stream reaches in the MODFLOW 6 model that demonstrates usage of the MVR package with the advanced packages (i.e., UZF, SFR, LAK) and includes a linkage with the WEL package. . . . .	.11–2
11–2 Simulated infiltration and recharge to and from the unsaturated-zone (left y-axis), respectively, for the cells located at row 5 column 2, including the moisture content of the cell in layer 1 (right y-axis). . . . .	.11–3
11–3 Monthly totals of pumped water from all 10 simulated wells transferred to UZF cells via the MVR package. Total monthly runoff amounts transferred to the surface water network are also shown. . . . .	.11–4
12–1 Lateral and vertical grid discretization. <i>A.</i> Map view. The location of lake and constant head boundary cells are also shown. Simulated heads and lake stage at the end of stress period 1, normalized specific discharge vectors, and the location of two observation locations are also shown. <i>B.</i> Cross-section view. The location of lake and constant head boundaries are also shown. The water table and lake stage at the end of stress period 1 are also shown. . . . .	.12–2
12–2 Selected heads in the aquifer and the lake stage. The location of points A and B are shown in figure 12–1. . . . .	.12–3
13–1 Lateral grid discretization. The location of lake and constant head boundary cells are also shown. Simulated heads and lake stage at the end of stress period 1, normalized specific discharge vectors, and the location of three observation locations are also shown. . . . .	.13–2
13–2 Lake stages and selected heads in the aquifer. <i>A.</i> Lake stages. The location of lake 1 and 2 are shown in figure 13–1. <i>B.</i> Heads in the aquifer. The location of points A, B, and C are shown in figure 13–1. . . . .	.13–4
14–1 Location of inactive cells and the multi-aquifer well. . . . .	.14–1
14–2 Simulated aquifer discharges to the multi-aquifer well. Discharge rates are relative to the multi-aquifer well; positive and negative discharge rates represent inflow to and outflow from the multi-aquifer, respectively. <i>A.</i> Non-pumping case. <i>B.</i> Pumping case. . . . .	.14–3
15–1 Location of inactive cells and the multi-aquifer well. . . . .	.15–1
15–2 Simulated aquifer discharges to the multi-aquifer well and flowing well discharge. Discharge rates are relative to the multi-aquifer well; positive and negative discharge rates represent inflow to and outflow from the multi-aquifer, respectively. <i>A.</i> Aquifer discharge to the multi-aquifer well. <i>B.</i> Flowing well discharge. . . . .	.15–3
16–1 Diagram showing the regional cross-section model with the location of the local three-dimensional model simulating flow through a wellbore. Steady-state water-table elevation and heads along with the location of the downgradient constant head boundary. . . . .	.16–2
16–2 Diagram showing the horizontal discretization used in the local three-dimensional model simulating flow through a wellbore. Steady-state water-table contours are shown along with the location of the multi-aquifer well and constant head boundaries. . . . .	.16–3
16–3 Graph of flow between the aquifer and the borehole with depth for the three-dimensional local model with the well represented as a multi-aquifer well and using high hydraulic conductivity. Positive discharge values indicate flow from the aquifer to the wellbore. Negative discharge values indicate flow from the wellbore to the aquifer. . . . .	.16–5

17–1 Bottom elevation of the flow diversion problem in meters. Bottom elevation are lowest at the edges of the domain and highest in the center of the domain. The location of constant head boundary cells is also shown. . . . .	17–1
17–2 Simulated heads and normalized specific discharge vectors for the scenario using the Newton-Raphson Formulation. Bottom elevation contours are shown in areas with dry cells. The location of constant head boundary cells is also shown. . . . .	17–3
17–3 Simulated heads and normalized specific discharge vectors for the scenario using the Standard Conductance Formulation with rewetting. Bottom elevation contours are shown in areas with dry cells. The location of constant head boundary cells is also shown. . . . .	17–4
17–4 Simulated heads and normalized specific discharge vectors for the scenario using the Newton-Raphson Formulation with a cylindrical obstruction. The location of constant head boundary cells is also shown. . . . .	17–5
18–1 Model grid and boundary conditions used for the circular island problem. General-head boundaries are shown in blue, and represent an off-shore boundary condition. Cell not colored represent the island and are assigned groundwater recharge. . . . .	18–2
18–2 Simulated groundwater head in (A) model layer 1 and (B) model layer 2. . . . .	18–3
19–1 Model grid and boundary conditions used for the horizontal anisotropy problem. Blue cells are constant-head cells and the pumping well is located in the cell shown in red. . . . .	19–2
19–2 Simulated drawdown for anisotropic groundwater flow to a pumping well for scenario 1. The dominant hydraulic conductivity ellipse is aligned with the x-axis. . . . .	19–3
19–3 Simulated drawdown for anisotropic groundwater flow to a pumping well for scenario 2. The dominant hydraulic conductivity ellipse axis is rotated 25 degrees counter clockwise from the x-axis. The XT3D option is required for this scenario because the ellipse axes do not align with the row and column directions. . . . .	19–3
19–4 Simulated drawdown for anisotropic groundwater flow to a pumping well for scenario 3. The dominant hydraulic conductivity ellipse axis is rotated 90 degrees counter clockwise from the x-axis so that the ellipse axes align with the column and row directions. . . . .	19–4
20–1 Diagram showing the model domain for the whirl problem, which consists of a three-dimensional box with two hydrogeologic units (light and dark shading). Groundwater is injected into one end of the box (column 1, pink shading) at a rate of 0.01 cubic meters per day ( $m^3/d$ ) into each cell and is removed from the opposite end of the box (column 51, pink shading) at a rate of 0.01 $m^3/d$ from each cell. From Provost and others (2017). . . . .	20–2
20–2 Cross section showing vectors of specific discharge for column 1 of the groundwater whirl problem. Vectors show the swirling flow pattern caused by the contrast in the hydraulic conductivity ellipsoid which occurs and the interface between model layer 5 and model layer 6. . . . .	20–3
21–1 Plan view of a three-dimensional aquifer system used to test the local grid refinement method in MODFLOW 6. A $15 \times 15$ horizontal grid discretization is shown for the parent grid and the locally refined grid ( $15 \times 18$ ) spacing is equivalent to a $45 \times 45$ discretization over the whole domain. Two between-model MVR connections are invoked for the SFR packages (parent and child) where the river crosses between domains . . . . .	21–1
21–2 Simulated streamflow and groundwater surface-water exchange for each stream reach in figure 21–1. The transfer of water between adjacent stream reaches in the parent versus child models occurs at locations identified by the vertical black lines on the plot. Bar widths are indicative of the relative stream reach lengths within the host grid cell (figure 21–1). . . . .	21–3

22–1 Globally refined model grid showing top elevation and river cells. Area of interest is shown as a dashed line.	22–2
22–2 Cross section for $y = 3000\text{ m}$ showing globally refined model grid. Color flood of hydraulic conductivity shows overburden material, valley fill, and deposits into which the valley is incised.	22–3
22–3 Globally coarsened model grid showing top elevation and river cells. Area of interest is shown as a dashed line.	22–3
22–4 Cross section for $y = 3000\text{ m}$ showing globally coarsened model grid. Color flood of hydraulic conductivity shows overburden material, valley fill, and deposits into which the valley is incised.	22–4
22–5 Local grid refinement model showing the outer coarse grid and the inner refined model grid. Top elevation and river cells are shown for both the outer and inner grids. Refinement area is shown as a dashed line.	22–4
22–6 Simulated head in layer 1 for the GR model.	22–5
22–7 Simulated head in layer 1 for the GC model.	22–6
22–8 Simulated head in layer 1 for the LGR model. Dashed line indicates location of inset model with higher resolution than the outer coarse model.	22–7
23–1 Cross section showing simulated head and vectors of specific discharge for the spatial periodic boundary condition example problem. Vectors of specific discharge are shown for every fifth cell in the layer and column directions.	23–2
24–1 Diagram showing the model domain for the elastic aquifer loading problem. <i>A</i> , plan view, and <i>B</i> , cross-section view	24–1
24–2 Graphs showing the applied loading and water-level fluctuations for the elastic aquifer loading problem. <i>A</i> , shows the loading applied to the top of the first column in layer 1, and <i>B</i> , shows simulated and offset water-level fluctuations at well S-201	24–3
25–1 Model domain and setup for the delay interbed drainage problem. Interbed drainage is the result of step decrease in head in the aquifer	25–3
25–2 Graphs showing comparisons of simulated compaction with the head-based formulation and the analytical solution for the delay interbed drainage problem. <i>A</i> , comparison of the compaction history simulated with the analytical solution to the problem, and <i>B</i> , difference between the analytical solution and simulated compaction	25–4
25–3 Graphs showing comparisons of simulated compaction for head- and effective stress-based formulations for the delay interbed drainage problem. <i>A</i> , comparison of the compaction history simulated with the head- and effective stress-based formulation solution to the problem, and <i>B</i> , difference between the simulated head- and effective stress-based formulation compaction	25–5
25–4 Graphs showing the difference between head- and effective stress-based compaction for different interbed thicknesses for the delay interbed drainage problem. <i>A</i> , difference between the head- and effective stress-based formulation compaction, and <i>B</i> , difference between drainage at the top and bottom of the interbed relative to the head-based formulation interbed drainage	25–6
25–5 Graphs showing differences between head- and effective stress-based formulation interbed heads relative to head-based interbed heads for variable interbed thicknesses at select fractions of the time constant ( $\tau_0$ ) for the delay interbed drainage problem. <i>A</i> , 1 percent of $\tau_0$ , <i>B</i> , 5 percent of $\tau_0$ , <i>C</i> , 10 percent of $\tau_0$ , <i>D</i> , 50 percent of $\tau_0$ , and <i>E</i> , 100 percent of $\tau_0$	25–7

26–1 Maps showing the location of the study area for the one-dimensional compaction problem in southern California. <i>A</i> , location of the study area in southern California and <i>B</i> , location of the Holly site and Edwards Air Force Base in the Antelope Valley. Cross-blended hypsometric tints with relief, water, drains and ocean bottom background image from Natural Earth and is available at <a href="https://www.naturalearthdata.com/downloads/50m-raster-data/50m-cross-blend-hypso/">https://www.naturalearthdata.com/downloads/50m-raster-data/50m-cross-blend-hypso/</a> , accessed on July 9, 2019 . . . . .	26–1
26–2 Diagram showing the model domain and setup for the one-dimensional compaction problem. <i>A</i> , hydrostratigraphy, <i>B</i> , interbed types used in aquifer and confining units, and <i>C</i> , location of constant-head boundary conditions . . . . .	26–3
26–3 Graph showing depth to water values used in the one-dimensional compaction problem for the upper, middle, and lower aquifers at the Holly site, Edwards Air Force Base, Antelope Valley, California. Modified from Sneed (2008) . . . . .	26–5
26–4 Graphs showing simulated compaction in different material types using head- and effective stress based formulations for the one-dimensional compaction problem. <i>A</i> , Total compaction, <i>B</i> , compaction in interbeds in the thick aquitard, <i>C</i> , compaction in delay interbeds contained in aquifers, <i>D</i> , compaction in interbeds in the confining unit, <i>E</i> , compaction in no-delay interbeds contained in aquifers, and <i>F</i> , compaction in coarse-grained materials . . . . .	26–8
26–5 Graphs showing history matches for simulated and measured aquifer-system compaction in the one-dimensional compaction problem. <i>A</i> , compaction in the different material types for the full simulation period (for 1908–2006 ), <i>B</i> , comparison of simulated and observed compaction at the Holly site for the period from 1990 to 2007, and <i>C</i> , simulated and observed stress/displacement for the period from October 1, 1992 to September 4, 2006. Elastic and inelastic specific storage values were calibrated using observed Holly site compaction data for the period from October 1, 1992 to September 4, 2006 and simulated compaction from the model based on Sneed (2008), which used a head-based formulation to simulate compaction . . . . .	26–9
26–6 Graph showing simulated vertical head profiles and approximately decadal head changes in the one-dimensional compaction problem. Vertical head profiles are shown for 1908, 1916, 1926, 1936, 1946, 1956, 1966, 1976, 1986, 1996, and 2006. The colored area between plotted years represents the simulated head change over approximately decadal period of time between simulated vertical head profiles. The vertical location of model layer tops and bottom and layers with constant-head boundaries are also shown. . . . .	26–10
27–1 Diagram showing the model domain for the one-dimensional compaction in a three-dimensional flow field problem. <i>A</i> , plan view, and <i>B</i> , cross-section view. The locations of active and inactive areas of the model domain, steady-state heads in model layer 1, and locations of recharge cells, constant-head cells, and wells are also shown . . . . .	27–3
27–2 Graphs showing computed stresses for row 9, column 10 for the one-dimensional compaction in a three-dimensional flow field problem. <i>A</i> , Effective and preconsolidation stress in layer 1, <i>B</i> , geostatic stress in layer 1, <i>C</i> , effective and preconsolidation stress in layer 2, and <i>D</i> , geostatic stress in layer 2 . . . . .	27–5
27–3 Graphs showing computed downward displacement for the tops of model layers 1–4 for the one-dimensional compaction in a three-dimensional flow field problem. <i>A</i> , interbed compaction at row 9, column 10, <i>B</i> , interbed compaction at row 12, column 7, <i>C</i> , coarse-grained material compaction at row 9, column 10, <i>D</i> , coarse-grained material compaction at row 12, column 7, <i>E</i> , total compaction at row 9, column 10, and <i>F</i> , total compaction at row 12, column 7 . . . . .	27–6

28–1 Simulated infiltration to the unsaturated zone and groundwater seepage to the land surface using the drain and unsaturated zone flow packages. The colored vertical bars delineate different stress periods. <i>A</i> . Infiltration to the unsaturated zone. <i>B</i> . Groundwater seepage to the land surface. . . . .	28–3
29–1 3-Dimensional perspective view of the Sagehen watershed looking westward. Colors depict zones of varying hydraulic conductivity within the active grid domain. . . . .	29–3
29–2 Plot of static infiltration factors used to spatially vary infiltration rates within the watershed. Infiltration factors were multiplied by a time series of infiltration rates shown in figure 29–4 . . . . .	29–4
29–3 Calculated depth to groundwater during the steady-state stress period at the beginning of the simulation. . . . .	29–5
29–4 Volumetric rates of infiltration, recharge, and evapotranspiration from the unsaturated and saturated zones summed over the model domain. . . . .	29–6
29–5 Volumetric flow rates of surface-water generation and runoff. . . . .	29–6
30–1 Diagram showing the model domain and the simulated streamflow capture fraction. The location of river cells, constant head cells, and wells are also shown. . . . .	30–2
31–1 Color shaded plot of heads simulated by MODFLOW 6 for the Keating and Zyvoloski (2009) problem involving groundwater flow and transport through an unsaturated zone. Recharge is applied to the narrow strip shown in red on the top of the model domain. . . . .	31–2
31–2 Color shaded plots of concentrations simulated by MODFLOW 6 for the Keating and Zyvoloski (2009) problem involving groundwater flow and transport through an unsaturated zone. This plot can be compared to figure 11 in Bedekar and others (2016), which shows similar plots for MT3D-USGS results. Plots of concentration versus time are shown in figure 31–3 for the two points shown in yellow. . . . .	31–3
31–3 Concentrations versus time for two observation points as simulated by MODFLOW 6 and by Keating and Zyvoloski (2009) for a problem involving groundwater flow and transport through an unsaturated zone. This plot can be compared to figure 12 in Bedekar and others (2016), which shows a similar plot for MT3D-USGS results. . . . .	31–4
32–1 Concentrations simulated by the MODFLOW 6 GWT Model and calculated by the analytical solution for one-dimensional flow with transport for the low dispersion case. Circles are for the GWT Model results; the lines represent the analytical solution by Wexler (1992). Results are shown for three different distances (0.05, 4.05, and 11.05 cm from the end of the first cell). Every fifth time step is shown for the MODFLOW 6 results. . . . .	32–2
32–2 Concentrations simulated by the MODFLOW 6 GWT Model and calculated by the analytical solution for one-dimensional flow with transport for the low dispersion case. Circles are for the GWT Model results; the lines represent the analytical solution by Wexler (1992). Results are shown for three different times (6, 60, and 120 s). Every fifth cell is shown for the MODFLOW 6 results. . . . .	32–3
32–3 Concentrations simulated by the MODFLOW 6 GWT Model and calculated by the analytical solution for one-dimensional flow with transport for the high dispersion case. Circles are for the GWT Model results; the lines represent the analytical solution by Wexler (1992). Results are shown for three different distances (0.05, 4.05, and 11.05 cm from the end of the first cell). Every fifth time step is shown for the MODFLOW 6 results. . . . .	32–4

32-4 Concentrations simulated by the MODFLOW 6 GWT Model and calculated by the analytical solution for one-dimensional flow with transport for the high dispersion case. Circles are for the GWT Model results; the lines represent the analytical solution by Wexler (1992). Results are shown for three different times (6, 60, and 120 s). Every fifth cell is shown for the MODFLOW 6 results. . . . .	32-4
32-5 Concentrations simulated by the MODFLOW 6 GWT Model and calculated by the analytical solution for one-dimensional flow with transport for the high dispersion case and a retardation factor of 2. Circles are for the GWT Model results; the lines represent the analytical solution by Wexler (1992). Results are shown for three different distances (0.05, 4.05, and 11.05 cm from the end of the first cell). Every fifth time step is shown for the MODFLOW 6 results. . . . .	32-5
32-6 Concentrations simulated by the MODFLOW 6 GWT Model and calculated by the analytical solution for one-dimensional flow with transport for the high dispersion case and a retardation factor of 2. Circles are for the GWT Model results; the lines represent the analytical solution by Wexler (1992). Results are shown for three different times (6, 60, and 120 s). Every fifth cell is shown for the MODFLOW 6 results. . . . .	32-5
32-7 Concentrations simulated by the MODFLOW 6 GWT Model and calculated by the analytical solution for one-dimensional flow with transport for the high dispersion case and a decay rate of $0.01\text{ s}^{-1}$ . Circles are for the GWT Model results; the lines represent the analytical solution by Wexler (1992). Results are shown for three different distances (0.05, 4.05, and 11.05 cm from the end of the first cell). Every fifth time step is shown for the MODFLOW 6 results. . . . .	32-6
32-8 Concentrations simulated by the MODFLOW 6 GWT Model and calculated by the analytical solution for one-dimensional flow with transport for the high dispersion case and a decay rate of $0.01\text{ s}^{-1}$ . Circles are for the GWT Model results; the lines represent the analytical solution by Wexler (1992). Results are shown for three different times (6, 60, and 120 s). Every fifth cell is shown for the MODFLOW 6 results. . . . .	32-6
33-1 Concentrations simulated by the MODFLOW 6 GWT Model and calculated by the analytical solution for three-dimensional flow with transport. Results are for the end of the simulation (time=400 d) and for layer 1. Black lines represent solute concentration contours from the analytical solution (Wexler, 1992); blue lines represent solute concentration contours simulated by MODFLOW 6. An aspect ratio of 4.0 is specified to enhance the comparison. . . . .	33-2
34-1 Triangular model grid used for the MODFLOW 6 simulation. Model grid is shown using an aspect ratio of 4. . . . .	34-1
34-2 Concentrations simulated by the MODFLOW 6 GWT Model and calculated by the analytical solution for three-dimensional flow with transport. Results are for the end of the simulation (time=400 d) and for layer 1. Black lines represent solute concentration contours from the analytical solution (Wexler, 1992); blue lines represent solute concentration contours simulated by MODFLOW 6. An aspect ratio of 4.0 is specified to enhance the comparison. . . . .	34-3
35-1 Comparison of the MT3DMS and MODFLOW 6 numerical solutions for a one-dimensional advection dominated test problem. The analytical solution for this problem was originally given in Van Genuchten and Alves (1982) and is not shown here . . . . .	35-2
35-2 Comparison of the MT3DMS and MODFLOW 6 numerical solutions for a one-dimensional test problem with dispersion ( $\alpha_L = 10\text{ cm}$ ). The analytical solution for this problem was originally given in Van Genuchten and Alves (1982) and is not shown here . . . . .	35-3

35–3 Comparison of the MT3DMS and MODFLOW 6 numerical solutions for a one-dimensional test problem with dispersion ( $\alpha_L = 10 \text{ cm}$ ) and retardation ( $R = 5.0$ ). The analytical solution for this problem was originally given in Van Genuchten and Alves (1982) and is not shown here . . . . .	35–4
35–4 Comparison of the MT3DMS and MODFLOW 6 numerical solutions for a one-dimensional test problem with dispersion ( $\alpha_L = 10 \text{ cm}$ ), retardation ( $R = 5.0$ ) and decay ( $\lambda = 0.002 \text{ d}^{-1}$ ). The analytical solution for this problem was originally given in Van Genuchten and Alves (1982) and is not shown here . . . . .	35–5
36–1 Comparison of the MT3DMS and MODFLOW 6 results for nonlinear sorption represented with the Freundlich isotherm. . . . .	36–3
36–2 Comparison of the MT3DMS and MODFLOW 6 results for nonlinear sorption represented with the Langmuir isotherm. . . . .	36–3
36–3 Comparison of the MT3DMS (solid lines) and MODFLOW 6 (circles) results for four different values of the nonequilibrium exchange coefficient (beta). The results for MODFLOW 6 are shown for every 20th time step. . . . .	36–4
37–1 Comparison of the MT3DMS and MODFLOW 6 numerical solutions for a two-dimensional advection-dispersion test problem. The analytical solution for this problem was originally given in Wilson and Miller (1978) and is not shown here . . . . .	37–2
38–1 Comparison of the MT3DMS and MODFLOW 6 numerical solutions for two-dimensional transport in a diagonal flow field. Both models are using their respective finite difference solutions without the TVD option . . . . .	38–2
38–2 Comparison of the MT3DMS and MODFLOW 6 numerical solutions for two-dimensional transport in a diagonal flow field. Both models are using their respective finite difference solutions with the use of the TVD option, which serves as the main difference with results displayed in figure 38–2 . . . . .	38–3
38–3 Comparison of the MT3DMS and MODFLOW 6 numerical solutions for two-dimensional transport in a diagonal flow field. Here, MT3DMS is using a MOC technique to find a solution while MODFLOW 6 uses finite difference without TVD activated. . . . .	38–4
39–1 Comparison of the MT3DMS and MODFLOW 6 numerical solutions for a point source in a two-dimensional radial flow field simulation. The thick black line in figure 39–2 shows the location of this profile view of concentrations. The analytical solution for this problem was originally given in (Moench and Ogata, 1981) and is not shown here . . . . .	39–2
39–2 Comparison of the MT3DMS and MODFLOW 6 numerical solutions for two-dimensional transport in a radial flow field. The thick black line shows the location of the concentration profile shown in figure 39–1. Both models are using their respective finite difference solutions with the use of the TVD option. . . . .	39–3
40–1 Comparison of the MT3D-USGS and MODFLOW 6 numerical solutions at an injection/extraction well. The analytical solution for this problem was originally given in (Gelhar and Collins, 1971) and is not shown here . . . . .	40–2
41–1 Comparison of the MT3D-USGS and MODFLOW 6 numerical solutions for three-dimensional transport in a uniform flow field. The analytical solution for this problem was originally given in (Hunt, 1978) and is not shown here . . . . .	41–2
42–1 MT3DMS test problem 8 configuration showing flow (upper figure) and transport (lower figure) boundary conditions (from Sudicky (1989)). . . . .	42–1
42–2 Migrating contaminant plume as calculated by (A) MT3D-USGS and (B) MODFLOW 6 after 8 years. The original problem was given in (Sudicky, 1989) . . . . .	42–3
42–3 Migrating contaminant plume as calculated by (A) MT3D-USGS and (B) MODFLOW 6 after 12 years. The original problem was given in (Sudicky, 1989) . . . . .	42–4

42–4 Migrating contaminant plume as calculated by (A) MT3D-USGS and (B) MODFLOW 6 after 20 years. The original problem was given in (Sudicky, 1989) . . . . .	42–5
43–1 MT3DMS test problem 9 configuration showing grid discretization, constant head boundaries, and the locations of injection and pumping wells (from Zheng and Wang (1999)). . . . .	43–2
43–2 Migrating contaminant plume as calculated by (A) MT3D-USGS and (B) MODFLOW 6 after one year of simulation time. The original problem was given in (Zheng and Wang, 1999). Cells shaded in blue show the location of constant head boundary cells. Light brown shaded cells show the location of the aquitard. . . . .	43–3
44–1 MT3DMS test problem 10 showing the numerical model configuration. Image not to scale. (11,600 ft = 3,535.68 m; 20,450 ft = 6,233 m; 25 ft = 7.62 m) . . . . .	44–3
44–2 (A) Initial and simulated contaminant plume concentrations as calculated by MT3DMS and MODFLOW 6 after (B) 500 days, (C) 750 days, and (D) 1,000 days. . . . .	44–4
45–1 The model grid for the studied problem. The red dashed rectangle shows where the GWF and GWT Model Exchange connects the inner to the outer models. . . . .	45–2
45–2 (A) Initial and simulated contaminant plume concentrations in model layer 3 as calculated by MODFLOW 6 with the multi-model setup after (B) 500 days, (C) 750 days, and (D) 1,000 days. . . . .	45–3
45–3 Difference in simulated head in model layer 3 with the multi-model setup with respect to the results from a setup containing a coupling between a single GWF and a single GWT model after (A) 1 day, (B) 500 days, (C) 750 days, and (D) 1,000 days. . . . .	45–4
45–4 Difference in simulated concentrations in model layer 3 with the multi-model setup when compared to the results with a single GWF and single GWT model after (A) 1 day, (B) 500 days, (C) 750 days, and (D) 1,000 days. . . . .	45–5
46–1 Concentrations simulated by the MODFLOW 6 GWT Model and MT3DMS for zero-order growth in a uniform flow field. . . . .	46–2
47–1 Concentrations simulated by the MODFLOW 6 GWT Model and MT3DMS for zero-order growth in a dual-domain system. Circles are for the GWT Model results; the lines represent simulated concentrations for MT3DMS. . . . .	47–2
48–1 Concentrations simulated by MODFLOW 6 and MT3DMS for a problem involving a recirculating well. This figure can be compared to figure 8.2 in Zheng (2010). . . . .	48–2
49–1 Model grid, boundary conditions and locations of lakes and streams used for the stream-lake interaction with solute transport problem. From Pradic and others (2004). . . . .	49–1
49–2 Contours of head simulated by the MODFLOW 6 GWF Model for the stream-lake interaction example. Contours are for (A) layer 1, and (B) layer 2. This figure can be compared with figure 14 in Pradic and others (2004), which shows head contours as simulated by MODFLOW-2000. . . . .	49–4
49–3 Concentration versus time simulated by MODFLOW 6 for the stream-lake interaction example. Solid lines represent the MODFLOW 6 simulated change in boron concentration in lake 1 and at the end of stream segments 2, 3, and 4. Dashed lines are results from the MODFLOW-GWT simulation (Pradic and others, 2004). . . . .	49–6
49–4 Contours of concentration simulated by the MODFLOW 6 GWT Model for the stream-lake interaction example. Contours are shown for (A) layer 1, (B) layer 3, (C) layer 5, and (D) layer 8. This figure can be compared with figure 17 in Pradic and others (2004), which shows an equivalent plot using model results simulated by MODFLOW-GWT. . . . .	49–7
50–1 A two-dimensional problem first published in Morway and others (2013). MT3D-USGS results closely match a benchmark solution calculated by VS2DT (Lappala and others, 1987). The light blue shaded region shows the location of the saturated zone. . . . .	50–3

50–2 A two-dimensional transport problem with no dispersive fluxes in either MODFLOW 6 or MT3D-USGS within the unsaturated-zone. The light blue shaded region shows the location of the saturated zone. . . . .	50–4
51–1 Simulation results for the classic Henry problem. . . . .	51–3
51–2 Simulation results for the low-inflow version of the Henry problem. . . . .	51–4
52–1 Model grid and boundary conditions used for the salt lake problem. Evaporation occurs from the cells highlighted in red. Inflow into the model grid occurs through the constant-head cells shown in blue. . . . .	52–2
52–2 Color-shaded plots of concentration simulated by MODFLOW 6 for the Simmons and others (1999) problem involving density-driven groundwater flow and solute transport. Panels can be compared with the panels shown for the Hele-Shaw experient (Wooding and others, 1997b) and for the SEAWAT-2000 numerical simulation (Langevin and others, 2003). . . . .	52–4
53–1 Configuration and variable definition for the rotating interface problem. From Bakker and others (2004) and Langevin and others (2003). Note that the constant-head boundary is not needed for the MODFLOW 6 simulation. . . . .	53–1
53–2 Model grid and initial conditions used for the rotating interface problem. Colors represent three different water types. . . . .	53–3
53–3 Initial horizontal velocity versus vertical position of the left interface, exact (solid), and MODFLOW 6 (blue circles). . . . .	53–4
53–4 Color-shaded plots of concentration simulated by MODFLOW 6 for the Bakker and others (2004) problem involving rotating interfaces. . . . .	53–5
54–1 Example of a closed ground source heat pump extracting heat beneath a private residence, from Hecht-Mendez (2008). . . . .	54–1
54–2 Model setup, from Hecht-Mendez and others (2010). . . . .	54–3
54–3 (A) Depiction of a heat plume spreading down gradient of a planar source (or sink) for which (Domenico and Robbins, 1985) gives an analytical solution for (B) two spreading directions in both y and z and finally (C) two spreading directions in y and one spreading direction in z, from Hecht-Mendez (2008). . . . .	54–4
54–4 MODFLOW 6 simulated temperatures are compared to analytical solutions in a steady flow model with a Peclet number equal to 1.0. For this scenario, thermal transport is roughly split between convective and conductive processes. Temperature profiles are calculated along the centerline down gradient of a planar heat sink as shown in figure 54–3 . . . . .	54–5
54–5 MODFLOW 6 simulated temperatures are compared to analytical solutions in a steady flow model with a Peclet number equal to 10.0. For this scenario, thermal transport is dominated by convective transport. Temperature profiles are calculated along the centerline down gradient of a planar heat sink as shown in figure 54–3 . . . . .	54–5
55–1 Comparison of the temperature profile simulated with MODFLOW 6 (blue circles) and calculated with the Stallman (1965) analytical solution (dashed line). . . . .	55–2
56–1 Map showing the Voronoi grid used to discretize the model domain and the location of Blue Lake, Straight River, and the areal extent of the confining unit separating the upper and lower aquifer units for the Synthetic Valley example in Hughes and others (2023). . . . .	56–1
56–2 Color shaded plot of (A) topography and (B) simulated steady-state heads and specific discharge rates in model layer 1. . . . .	56–4

56–3 Contours of concentrations at the end of 30 years in model layer (A) 1, (B) 2, (C) 3, (D) 4, (E) 5, and (F) 6. The extent of the confining unit in model layer 3 is also shown on (C). . . . .	.56–5
57–1 Plan view of the two-dimensional, radial model grid. <i>A</i> , plan view of entire model grid containing 22 radial bands, and <i>B</i> , plan view of the 5 innermost radial bands and the well location is marked in red. . . . .	.57–1
57–2 Radial model analytical solution (Neuman, 1974) and simulated groundwater (MF6) head 40 <i>ft</i> from the well (radial band 12) at the model's Top (1 <i>ft</i> depth; layer 1), Middle (25 <i>ft</i> depth; layer 13), and Bottom (49 <i>ft</i> depth; layer 25). . . . .	.57–4
57–3 Radial model analytical dimensionless solution (Neuman, 1974) and simulated groundwater (MF6) dimensionless drawdown 40 <i>ft</i> from the well (radial band 12) at the model's Top (1 <i>ft</i> depth; layer 1), Middle (25 <i>ft</i> depth; layer 13), and Bottom (49 <i>ft</i> depth; layer 25). . . . .	.57–4
58–1 Model grid used for the 90° curvilinear vertex model. Constant-head cells are marked in blue. The inner constant head is 10 <i>ft</i> and the outer constant head is 3.33 <i>ft</i> . Cell numbers are shown inside each model cell. Vertices are also numbered and are shown in red. . . . .	.58–3
58–2 Steady state head solution and specific discharge vectors from the MODFLOW 6 curvilinear vertex model. . . . .	.58–4
58–3 Steady state head solution from the MODFLOW 6 curvilinear vertex model (MF6) compared with the analytical solution (Crank, 1975). The MF6 head values are taken from each radial band along column 10. The radial distance of each MF6 solution is the distance from the vertex axis origin to the cell center. . . . .	.58–5
59–1 Three regions that combine to construct the hypothetical, curvilinear grid. <i>A</i> , Left curvilinear grid from 180° to 270°, <i>B</i> , Center 16 by 18 rectangular grid , and <i>C</i> , Right curvilinear grid from 90° to 0°. Grid vertices are marked in yellow. Note, the x, y coordinate positions are included for relative comparisons and not for the specific spatial location. . . . .	.59–1
59–2 Plan view of the hypothetical, curvilinear grid with a meandering, curved flow path. Constant-head cells are marked in blue. The cell numbers 1, 19, . . . , 253, 271 constant head is 10 <i>ft</i> . The cell numbers 577, 595, . . . , 829, 847 constant head is 3.33 <i>ft</i> . Grid cell numbers are shown inside each model cell. Grid vertices are yellow with vertex numbers in red. . . . .	.59–2
59–3 Steady state head solution and specific discharge vectors from the MODFLOW 6 curvilinear grid with a meandering, curved flow path. . . . .	.59–3
60–1 Configuration of the DISV model grid used in the radial transport problem. Model grid originally published in Al-Khoury and others (2020). Please refer to figure 60–2 for a zoomed-in view of the model grid in the vicinity of the BHE. . . . .	.60–2
60–2 A zoomed-in view showing the refined discretization in close proximity to the BHE. Cell dimensions are sub-centimeter scale around the perimeter of the BHE. The radius of the BHE is 7.5 <i>cm</i> . . . . .	.60–3
60–3 A head gradient is established in the outer-most ring of grid cells to drive groundwater flow from left to right. The combination of the groundwater head gradient with the hydraulic conductivity (table 60–1) results in a groundwater velocity of $1 \times 10^{-5} \frac{m}{s}$ . . . . .	.60–4
60–4 Simulation results for the GWE model run compared with an analytical solution. . . . .	.60–5

61–1 Configuration of the DISV model grid used to demonstrate the use of GWE in a geothermal transport problem. The original numerical model grid was published in Al-Khoury and others (2021). The red box shows the location of figure 61–2 which provides zoomed-in detail of the model grid in the vicinity of the BHEs. . . . .	61–2
61–2 A zoomed-in view showing the refined discretization in close proximity to the BHEs. Cell dimensions are on the scale of centimeters around the perimeter of the BHEs. The diameter of each BHE is 10.0 cm. . . . .	61–3
61–3 The established head gradient drives groundwater flow from left to right with a velocity of $1 \times 10^{-5} \frac{m}{s}$ . . . . .	61–4
61–4 Simulated and analytical isotherm contours for the geothermal example problem. The solid lines correspond to the GWE solution while the dashed line represents the analytical solution published by Al-Khoury and others (2021). . . . .	61–5
62–1 View of 1-dimensional model setup. Total thickness of the unsaturated zone is 10 m and is discretized with 100 cells that are each 10 cm thick. . . . .	62–2
62–2 Comparison of simulated migration of infiltrating heat front to an analytical solution .	62–4
62–3 The same infiltrating heat fronts as shown in figure 62–2, but highlights the advective and conductive heat fluxes separately . . . . .	62–5
63–1 Conceptual model. Image reproduced from the MODPATH 7 examples document (Pollock, 2017). . . . .	63–1
63–2 Heads simulated by the MODFLOW 6 groundwater flow (GWF) model. . . . .	63–3
63–3 Particle pathlines and 1000-day points for subproblem 1A. Points are colored by layer. .	63–4
63–4 Particle pathlines, colored by destination: particles with red pathlines are captured by the well, particles with blue pathlines are captured by the river. . . . .	63–5
63–5 Particle release points, colored by destination. . . . .	63–6
63–6 Particle release points, colored by travel time. . . . .	63–7
64–1 Head simulated by the MODFLOW 6 groundwater flow (GWF) model. . . . .	64–2
64–2 2000-day particle path points. Points are colored by travel time. . . . .	64–3
64–3 Three-dimensional perspective of pathlines and 2000-day points. Points are colored by destination. . . . .	64–4
64–4 Particle release and termination points, colored by destination. . . . .	64–5
65–1 (Top) Model grid color-filled with the steady-state temperature field and specific discharge arrows. Dashed blue lines show the paths of particles 1 and 2 and they traverse the simulation domain. (Middle) The x-position of each particle is plotted against its temperature as it traverses the simulation domain. (Bottom) The travel time of each particle is plotted against its temperature as it traverses the simulation domain. . . . .	65–3

## List of Tables

1	List of example problems and simulation characteristics.	0–2
1–1	Model parameters for example ex-gwf-twri.	1–1
1–1	Model parameters for example ex-gwf-twri.	1–2
2–1	Model parameters for example ex-gwf-bcf2ss.	2–2
3–1	Model parameters for example ex-gwf-advtidal.	3–1
4–1	Model parameters for example ex-gwf-fhb.	4–1
5–1	Model parameters for example ex-gwf-u1disv.	5–1
5–2	Scenario parameters for example ex-gwf-u1disv.	5–1
6–1	Model parameters for example ex-gwf-u1gwfgrwf.	6–2
6–1	Model parameters for example ex-gwf-u1gwfgrwf.	6–3
6–2	Scenario parameters for example ex-gwf-u1gwfgrwf.	6–3
7–1	Model parameters for example ex-gwf-nwt-p02.	7–2
7–2	Scenario parameters for example ex-gwf-nwt-p02.	7–3
8–1	Model parameters for example ex-gwf-nwt-p03.	8–1
9–1	Model parameters for example ex-gwf-zaidel.	9–1
10–1	Model parameters for example ex-gwf-sfr-p01.	10–2
11–1	Model parameters for example ex-gwf-sfr-p01b.	11–1
12–1	Model parameters for example ex-gwf-lak-p01.	12–1
13–1	Model parameters for example ex-gwf-lak-p02.	13–1
14–1	Model parameters for example ex-gwf-maw-p01.	14–2
15–1	Model parameters for example ex-gwf-maw-p02.	15–2
16–1	Model parameters for example ex-gwf-maw-p03.	16–1
17–1	Model parameters for example ex-gwf-bump.	17–2
17–2	Scenario parameters for example ex-gwf-bump.	17–2
18–1	Model parameters for example ex-gwf-disvmesh.	18–1
19–1	Model parameters for example ex-gwf-hani.	19–1
19–2	Scenario parameters for example ex-gwf-hani.	19–1
20–1	Model parameters for example ex-gwf-whirl.	20–1
21–1	Model parameters for example ex-gwf-lgr.	21–2
22–1	Model parameters for example ex-gwf-lgrv.	22–1
22–1	Model parameters for example ex-gwf-lgrv.	22–2
22–2	Scenario parameters for example ex-gwf-lgrv.	22–2
23–1	Model parameters for example ex-gwf-spbc.	23–1
24–1	Assumed train properties for example ex-gwf-csub-p01.	24–2
24–2	Model parameters for example ex-gwf-csub-p01.	24–2
25–1	Model parameters for example ex-gwf-csub-p02.	25–2
25–2	Scenario parameters for example ex-gwf-csub-p02.	25–3
26–1	Aquifer properties for example ex-gwf-csub-p03.	26–2
26–2	Interbed properties for example ex-gwf-csub-p03.	26–4
26–3	Aquifer storage properties for example ex-gwf-csub-p03.	26–6
26–4	Interbed storage properties for example ex-gwf-csub-p03.	26–6
26–4	Interbed storage properties for example ex-gwf-csub-p03.	26–7
27–1	Model parameters for example ex-gwf-csub-p04.	27–1
27–1	Model parameters for example ex-gwf-csub-p04.	27–2
28–1	Model parameters for example ex-gwf-drn-p01.	28–1
28–2	Infiltration and pumping rates for example ex-gwf-drn-p01.	28–2

29–1 Model parameters for example ex-gwf-sagehen.	29–1
29–1 Model parameters for example ex-gwf-sagehen.	29–2
30–1 Model parameters for example ex-gwf-capture.	30–1
31–1 Model parameters for example ex-gwt-keating.	31–1
31–1 Model parameters for example ex-gwt-keating.	31–2
32–1 Model parameters for example ex-gwt-moc3d-p01.	32–1
32–2 Scenario parameters for example ex-gwt-moc3d-p01.	32–2
33–1 Model parameters for example ex-gwt-moc3d-p02.	33–1
33–1 Model parameters for example ex-gwt-moc3d-p02.	33–2
34–1 Model parameters for example ex-gwt-moc3d-p02tg.	34–2
35–1 Scenario parameters for example ex-gwt-mt3dms-p01.	35–1
35–2 Model parameters for example ex-gwt-mt3dms-p01.	35–1
35–2 Model parameters for example ex-gwt-mt3dms-p01.	35–2
36–1 Scenario parameters for example ex-gwt-mt3dms-p02.	36–1
36–1 Scenario parameters for example ex-gwt-mt3dms-p02.	36–2
36–2 Model parameters for example ex-gwt-mt3dms-p02.	36–2
37–1 Model parameters for example ex-gwt-mt3dms-p03.	37–1
38–1 Scenario parameters for example ex-gwt-mt3dms-p04.	38–1
38–2 Model parameters for example ex-gwt-mt3dms-p04.	38–1
39–1 Model parameters for example ex-gwt-mt3dms-p05.	39–1
40–1 Model parameters for example ex-gwt-mt3dms-p06.	40–1
41–1 Model parameters for example ex-gwt-mt3dms-p07.	41–1
42–1 Model parameters for example ex-gwt-mt3dms-p08.	42–2
43–1 Model parameters for example ex-gwt-mt3dms-p09.	43–1
44–1 Model parameters for example ex-gwt-mt3dms-p10.	44–1
44–1 Model parameters for example ex-gwt-mt3dms-p10.	44–2
46–1 Model parameters for example ex-gwt-mt3dsupp631.	46–1
47–1 Model parameters for example ex-gwt-mt3dsupp632.	47–1
47–2 Scenario parameters for example ex-gwt-mt3dsupp632.	47–2
48–1 Model parameters for example ex-gwt-mt3dsupp82.	48–1
49–1 Model parameters for example ex-gwt-prudic2004t2.	49–2
50–1 Scenario parameters for example ex-gwt-uzt-2d.	50–1
50–1 Scenario parameters for example ex-gwt-uzt-2d.	50–2
50–2 Model parameters for example ex-gwt-uzt-2d.	50–2
51–1 Model parameters for example ex-gwt-henry.	51–1
51–1 Model parameters for example ex-gwt-henry.	51–2
51–2 Scenario parameters for example ex-gwt-henry.	51–2
52–1 Model parameters for example ex-gwt-saltlake.	52–1
53–1 Model parameters for example ex-gwt-rotate.	53–2
54–1 Scenario parameters for example ex-gwt-hecht-mendez.	54–2
54–2 Model parameters for example ex-gwt-hecht-mendez.	54–2
55–1 Model parameters for example ex-gwt-stallman.	55–1
55–1 Model parameters for example ex-gwt-stallman.	55–2
56–1 Model parameters for example ex-gwt-synthetic-valley.	56–2
57–1 Model parameters for example ex-gwf-radial.	57–2
58–1 Model parameters for example ex-gwf-curvilinear-90.	58–1
58–1 Model parameters for example ex-gwf-curvilinear-90.	58–2
59–1 Model parameters for example ex-gwf-curvilinear.	59–2

59–1 Model parameters for example ex-gwf-curvilinear.	.59–3
60–1 Model parameters for example ex-gwe-radial.	.60–1
61–1 Model parameters for example ex-gwe-geotherm.	.61–1
62–1 Model parameters for example ex-gwe-danckwerts.	.62–2
62–1 Model parameters for example ex-gwe-danckwerts.	.62–3
63–1 Model parameters for example ex-prt-mp7-p01.	.63–1
63–1 Model parameters for example ex-prt-mp7-p01.	.63–2
64–1 Model parameters for example ex-prt-mp7-p03.	.64–1
65–1 Model parameters for example ex-gwe-prt.	.65–1

# Introduction

This document describes MODFLOW 6 example scenarios. The examples demonstrate the capabilities of select components of MODFLOW 6. Examples have been included for the MODFLOW 6 components summarized in table 1.

Table 1: List of example problems and simulation characteristics.

Example	Simulation	Namefile(s)	Grid Dimensions	Packages
1	ex-gwf-twri01	ex-gwf-twri01.nam	(5, 15, 15)	CHD DIS DRN IC IMS NPF OC RCHA TDIS WEL
2	ex-gwf-bcf2ss-p01a	ex-gwf-bcf2ss.nam	(2, 10, 15)	DIS IC IMS NPF OC RCHA RIV TDIS WEL
	ex-gwf-bcf2ss-p02a	ex-gwf-bcf2ss.nam	(2, 10, 15)	DIS IC IMS NPF OC RCHA RIV TDIS WEL
3	ex-gwf-advtidal	ex-gwf-advtidal.nam	(3, 15, 10)	DIS EVT GHB IC IMS NPF OBS OC RCH RIV STO TDIS TS WEL
4	ex-gwf-fhb	ex-gwf-fhb.nam	(1, 3, 10)	CHD DIS IC IMS NPF OBS OC STO TDIS TS WEL
5	ex-gwf-u1disv	ex-gwf-u1disv.nam	(1, 121)	CHD DISV IC IMS NPF OC TDIS
	ex-gwf-u1disv-x	ex-gwf-u1disv-x.nam	(1, 121)	CHD DISV IC IMS NPF OC TDIS XT3D
6	ex-gwf-u1gwgwf-s1	outer.nam	(1, 7, 7)	CHD DIS GWFGWF IC IMS NPF OC TDIS
		inner.nam	(1, 9, 9)	CHD DIS GWFGWF IC IMS NPF OC TDIS
	ex-gwf-u1gwgwf-s2	outer.nam	(1, 7, 7)	CHD DIS GWFGWF IC IMS NPF OC TDIS XT3D
		inner.nam	(1, 9, 9)	CHD DIS GWFGWF IC IMS NPF OC TDIS XT3D
	ex-gwf-u1gwgwf-s3	outer.nam	(1, 7, 7)	CHD DIS GWFGWF IC IMS NPF OC TDIS XT3D
		inner.nam	(1, 9, 9)	CHD DIS GWFGWF IC IMS NPF OC TDIS XT3D
	ex-gwf-u1gwgwf-s4	outer.nam	(1, 7, 7)	CHD DIS GWFGWF IC IMS NPF OC TDIS
		inner.nam	(1, 9, 9)	CHD DIS GWFGWF IC IMS NPF OC TDIS
	ex-gwf-nwt-p02a	ex-gwf-nwt-p02.nam	(14, 40, 40)	CHD DIS IC IMS NPF OC RCH STO TDIS
		ex-gwf-nwt-p02b	(14, 40, 40)	CHD DIS ICIMS NPF OC RCH STO TDIS
8	ex-gwf-nwt-p03a	ex-gwf-nwt-p03.nam	(1, 80, 80)	CHD DIS ICIMS NPF OC RCHA TDIS
	ex-gwf-nwt-p03b	ex-gwf-nwt-p03.nam	(1, 80, 80)	CHD DIS ICIMS NPF OC RCHA TDIS
9	ex-gwf-zaidel	ex-gwf-zaidel.nam	(1, 1, 200)	CHD DIS ICIMS NPF OC TDIS

<b>Example</b>	<b>Simulation</b>	<b>Namefile(s)</b>	<b>Grid Dimensions</b>	<b>Packages</b>
10	ex-gwf-sfr-p01	ex-gwf-sfr-p01.nam	(1, 15, 10)	DIS EVTA GHB IC IMS NPF OBS OC RCHA SFR STO TDIS WEL
11	ex-gwf-sfr-p01b	ex-gwf-sfr-p01b.nam	(2, 15, 10)	DIS GHB IC IMS LAK MVR NPF OBS OC SFR STO TDIS UZF WEL
12	ex-gwf-lak-p01	ex-gwf-lak-p01.nam	(5, 17, 17)	CHD DIS EVTA IC IMS LAK NPF OBS OC RCHA STO TDIS
13	ex-gwf-lak-p02	ex-gwf-lak-p02.nam	(5, 27, 17)	CHD DIS EVTA IC IMS LAK MVR NPF OBS OC RCHA SFR STO TDIS
14	ex-gwf-maw-p01a	ex-gwf-maw-p01.nam	(2, 101, 101)	DIS IC IMS MAW NPF OBS OC STO TDIS
	ex-gwf-maw-p01b	ex-gwf-maw-p01.nam	(2, 101, 101)	DIS IC IMS MAW NPF OBS OC STO TDIS
15	ex-gwf-maw-p02	ex-gwf-maw-p02.nam	(2, 101, 101)	DIS IC IMS MAW NPF OBS OC STO TDIS
16	ex-gwf-maw-p03a	ex-gwf-maw-p03.nam	(21, 1, 200)	CHD DIS IC IMS NPF OC RCHA TDIS
	ex-gwf-maw-p03b	ex-gwf-maw-p03.nam	(41, 16, 27)	CHD DIS ICIMS MAW NPF OBS OC RCHA TDIS
	ex-gwf-maw-p03c	ex-gwf-maw-p03.nam	(41, 16, 27)	CHD DIS ICIMS NPF OBS OC RCHA TDIS
17	ex-gwf-bump-p01a	ex-gwf-bump.nam	(1, 51, 51)	CHD DIS ICIMS NPF OC TDIS
	ex-gwf-bump-p01b	ex-gwf-bump.nam	(1, 51, 51)	CHD DIS ICIMS NPF OC TDIS
	ex-gwf-bump-p01c	ex-gwf-bump.nam	(1, 51, 51)	CHD DIS ICIMS NPF OC TDIS
18	ex-gwf-disvmesh	ex-gwf-disvmesh.nam	(2, 5240)	DISV GHB ICIMS NPF OC RCH TDIS XT3D
19	ex-gwf-hanic	ex-gwf-hanic.nam	(1, 51, 51)	CHD DIS ICIMS NPF OC TDIS WEL
	ex-gwf-hanir	ex-gwf-hanir.nam	(1, 51, 51)	CHD DIS ICIMS NPF OC TDIS WEL
	ex-gwf-hanix	ex-gwf-hanix.nam	(1, 51, 51)	CHD DIS ICIMS NPF OC TDIS WEL XT3D
20	ex-gwf-whirl	ex-gwf-whirl.nam	(10, 10, 51)	DIS ICIMS NPF OC TDIS WEL XT3D
21	ex-gwf-lgr	gwf-lgr-parent.nam	(3, 15, 15)	CHD DIS GWFGWF IC IMS MVR NPF OC SFR TDIS
		gwf-lgr-child.nam	(6, 15, 18)	CHD DIS GWFGWF IC IMS MVR NPF OC SFR TDIS
22	ex-gwf-lgrv-gc	parent.nam	(9, 61, 49)	DIS ICIMS NPF OC RCHA RIV TDIS
	ex-gwf-lgrv-gr	parent.nam	(25, 183, 147)	DIS ICIMS NPF OC RCHA RIV TDIS
	ex-gwf-lgrv-lgr	parent.nam	(9, 61, 49)	DIS GWFGWF ICIMS NPF OC RCHA RIV TDIS

Example	Simulation	Namefile(s)	Grid Dimensions	Packages
		child.nam	(25, 90, 78)	DIS GWFGWF IC IMS NPF OC RCHA RIV TDIS
23	ex-gwf-spbc	ex-gwf-spbc.nam	(190, 1, 100)	CHD DIS GWFGWF IC IMS NPF OC TDIS
24	ex-gwf-csub-p01	ex-gwf-csub-p01.nam	(3, 1, 35)	CSUB DIS IC IMS NPF OBS OC STO TDIS TS
25	ex-gwf-csub-p02a	ex-gwf-csub-p02a.nam	(1, 1, 3)	CHD CSUB DIS IC IMS NPF OBS OC STO TDIS
	ex-gwf-csub-p02b	ex-gwf-csub-p02b.nam	(1, 1, 3)	CHD CSUB DIS IC IMS NPF OBS OC STO TDIS
26	ex-gwf-csub-p03a	ex-gwf-csub-p03a.nam	(14, 1, 1)	CHD CSUB DIS IC IMS NPF OBS OC STO TDIS TS
	ex-gwf-csub-p03b	ex-gwf-csub-p03b.nam	(14, 1, 1)	CHD CSUB DIS ICIMS NPF OBS OC STO TDIS TS
27	ex-gwf-csub-p04	ex-gwf-csub-p04.nam	(4, 20, 15)	CHD CSUB DIS ICIMS NPF OBS OC RCH STO TDIS WEL
28	ex-gwf-drn-p01a	ex-gwf-drn-p01.nam	(1, 15, 10)	DIS DRN GHB ICIMS MVR NPF OBS OC SFR STO TDIS UZF WEL
	ex-gwf-drn-p01b	ex-gwf-drn-p01.nam	(1, 15, 10)	DIS GHB ICIMS MVR NPF OBS OC SFR STO TDIS UZF WEL
29	ex-gwf-sagehen	ex-gwf-sagehen.nam	(1, 73, 81)	CHD DIS DRN ICIMS MVR NPF OC SFR STO TDIS UZF
30	ex-gwf-capture	ex-gwf-capture.nam	(1, 40, 20)	CHD DIS ICIMS NPF OC RCHA RIV TDIS WEL
31	ex-gwt-keating	trans.nam	(80, 1, 400)	ADV DIS DSP FMI ICIMS MST OBS OC SSM TDIS
		flow.nam	(80, 1, 400)	CHD DIS ICIMS NPF OC RCH TDIS
32	ex-gwt-moc3d-p01a	trans.nam	(1, 1, 122)	ADV DIS DSP FMI ICIMS MST OBS OC SSM TDIS
		flow.nam	(1, 1, 122)	CHD DIS ICIMS NPF OC TDIS WEL
	ex-gwt-moc3d-p01b	trans.nam	(1, 1, 122)	ADV DIS DSP FMI ICIMS MST OBS OC SSM TDIS
		flow.nam	(1, 1, 122)	CHD DIS ICIMS NPF OC TDIS WEL
	ex-gwt-moc3d-p01c	trans.nam	(1, 1, 122)	ADV DIS DSP FMI ICIMS MST OBS OC SSM TDIS
		flow.nam	(1, 1, 122)	CHD DIS ICIMS NPF OC TDIS WEL
	ex-gwt-moc3d-p01d	trans.nam	(1, 1, 122)	ADV DIS DSP FMI ICIMS MST OBS OC SSM TDIS
		flow.nam	(1, 1, 122)	CHD DIS ICIMS NPF OC TDIS WEL
33	ex-gwt-moc3d-p02	trans.nam	(40, 12, 30)	ADV DIS DSP FMI ICIMS MST OBS OC SRC SSM TDIS

Example	Simulation	Namefile(s)	Grid Dimensions	Packages
34	ex-gwt-moc3d-p02tg	flow.nam	(40, 12, 30)	CHD DIS IC IMS NPF OC TDIS WEL
		trans.nam	(40, 695)	ADV DISV DSP FMI IC IMS MST OBS OC SRC SSM TDIS
35	ex-gwt-mt3dms-p01a	flow.nam	(40, 695)	CHD DISV IC IMS NPF OC TDIS WEL XT3D
		gwf-p01-mf6.nam	(1, 1, 101)	CHD DIS GWFGWT IC IMS NPF OC TDIS
35	ex-gwt-mt3dms-p01b	gwt-p01-mf6.nam	(1, 1, 101)	ADV CHD CNC DIS GWFGWT IC IMS MST NPF OC SSM TDIS
		gwf-p01-mf6.nam	(1, 1, 101)	CHD DIS GWFGWT IC IMS NPF OC TDIS
35	ex-gwt-mt3dms-p01c	gwt-p01-mf6.nam	(1, 1, 101)	ADV CHD CNC DIS DSP GWFGWT IC IMS MST NPF OC SSM TDIS
		gwf-p01-mf6.nam	(1, 1, 101)	CHD DIS GWFGWT IC IMS NPF OC TDIS
35	ex-gwt-mt3dms-p01d	gwt-p01-mf6.nam	(1, 1, 101)	ADV CHD CNC DIS DSP GWFGWT IC IMS MST NPF OC SSM TDIS
		gwf-p01-mf6.nam	(1, 1, 101)	CHD DIS GWFGWT IC IMS NPF OC TDIS
36	ex-gwt-mt3dms-p02a	trans.nam	(1, 1, 101)	ADV DIS DSP FMI IC IMS MST OBS OC SSM TDIS
		flow.nam	(1, 1, 101)	CHD DIS IC IMS NPF OC TDIS WEL
36	ex-gwt-mt3dms-p02b	trans.nam	(1, 1, 101)	ADV DIS DSP FMI IC IMS MST OBS OC SSM TDIS
		flow.nam	(1, 1, 101)	CHD DIS IC IMS NPF OC TDIS WEL
36	ex-gwt-mt3dms-p02c	trans.nam	(1, 1, 101)	ADV DIS DSP FMI IC IMS MST OBS OC SSM TDIS
		flow.nam	(1, 1, 101)	CHD DIS IC IMS NPF OC TDIS WEL
36	ex-gwt-mt3dms-p02d	trans.nam	(1, 1, 101)	ADV DIS DSP FMI IC IMS IST MST OBS OC SSM TDIS
		flow.nam	(1, 1, 101)	CHD DIS IC IMS NPF OC TDIS WEL
36	ex-gwt-mt3dms-p02e	trans.nam	(1, 1, 101)	ADV DIS DSP FMI IC IMS IST MST OBS OC SSM TDIS
		flow.nam	(1, 1, 101)	CHD DIS IC IMS NPF OC TDIS WEL
36	ex-gwt-mt3dms-p02f	trans.nam	(1, 1, 101)	ADV DIS DSP FMI IC IMS IST MST OBS OC SSM TDIS

<b>Example</b>	<b>Simulation</b>	<b>Namefile(s)</b>	<b>Grid Dimensions</b>	<b>Packages</b>
37	ex-gwt-mt3dms-p03	flow.nam	(1, 1, 101)	CHD DIS IC IMS NPF OC TDIS WEL
		gwf-p03-mf6.nam	(1, 31, 46)	CHD DIS GWFGWT IC IMS NPF OC STO TDIS WEL
38	ex-gwt-mt3dms-p04a	gwf-p04-mf6.nam	(1, 100, 100)	ADV CHD CNC DIS DSP GWFGWT IC IMS MST NPF OC SSM STO TDIS WEL
		gwt_p04-mf6.nam	(1, 100, 100)	CHD DIS GWFGWT IC IMS NPF OC STO TDIS WEL
	ex-gwt-mt3dms-p04b	gwf-p04-mf6.nam	(1, 100, 100)	ADV CHD DIS DSP GWFGWT IC IMS MST NPF OC SSM STO TDIS WEL
		gwt_p04-mf6.nam	(1, 100, 100)	CHD DIS GWFGWT IC IMS NPF OC STO TDIS WEL
	ex-gwt-mt3dms-p04c	gwf-p04-mf6.nam	(1, 100, 100)	ADV CHD DIS DSP GWFGWT IC IMS MST NPF OC SSM STO TDIS WEL
		gwt_p04-mf6.nam	(1, 100, 100)	CHD DIS GWFGWT IC IMS NPF OC STO TDIS WEL
39	ex-gwt-mt3dms-p05	gwf-p05-mf6.nam	(1, 31, 31)	ADV CHD CNC DIS DSP GWFGWT IC IMS MST NPF OC SSM STO TDIS WEL
		gwt_p05-mf6.nam	(1, 31, 31)	CHD DIS GWFGWT IC IMS NPF OC STO TDIS WEL
40	ex-gwt-mt3dms-p06	gwf-p06-mf6.nam	(1, 31, 31)	ADV CHD DIS DSP GWFGWT IC IMS MST NPF OBS OC SSM STO TDIS WEL
		gwt_p06-mf6.nam	(1, 31, 31)	CHD DIS GWFGWT IC IMS NPF OC STO TDIS WEL
41	ex-gwt-mt3dms-p07	gwf-p07-mf6.nam	(8, 15, 21)	ADV CHD DIS DSP GWFGWT IC IMS MST NPF OC SSM TDIS WEL
		gwt_p07-mf6.nam	(8, 15, 21)	CHD DIS GWFGWT IC IMS NPF OC TDIS WEL
42	ex-gwt-mt3dms-p08	gwf_p08_mf6.nam	(27, 1, 50)	CHD DIS GWFGWT IC IMS NPF OC RCHA STO TDIS

Example	Simulation	Namefile(s)	Grid Dimensions	Packages
		gwt_p08_mf6.nam	(27, 1, 50)	ADV CHD CNC DIS DSP GWFGWT IC IMS MST NPF OC RCHA SSM STO TDIS
43	ex-gwt-mt3dms-p09	gwf-p09-mf6.nam	(1, 18, 14)	CHD DIS GWFGWT IC IMS NPF OC STO TDIS WEL
		gwt-p09-mf6.nam	(1, 18, 14)	ADV CHD DIS DSP GWFGWT IC IMS MST NPF OC SSM STO TDIS WEL
44	ex-gwt-mt3dms-p10	gwf-p10-mf6.nam	(4, 61, 40)	CHD DIS GWFGWT IC IMS NPF OC RCHA STO TDIS WEL
		gwt-p10-mf6.nam	(4, 61, 40)	ADV CHD DIS DSP GWFGWT IC IMS MST NPF OC RCHA SSM STO TDIS WEL
45	ex-gwt-gwtgwt-p10	gwf-outer.nam	(4, 61, 40)	CHD DIS GWFGWF GWFGWT GWTGWT IC IMS NPF OC RCHA STO TDIS
		gwf-inner.nam	(4, 45, 28)	CHD DIS GWFGWF GWFGWT GWTGWT IC IMS NPF OC RCHA STO TDIS WEL
		gwt-outer.nam	(4, 61, 40)	ADV CHD DIS DSP GWFGWF GWFGWT GWTGWT IC IMS MST NPF OC RCHA SSM STO TDIS WEL
		gwt-inner.nam	(4, 45, 28)	ADV CHD DIS DSP GWFGWF GWFGWT GWTGWT IC IMS MST NPF OC RCHA SSM STO TDIS WEL
46	ex-gwt-mt3dsupp631	trans.nam	(1, 1, 101)	ADV DIS DSP FMI IC IMS MST OBS SSM TDIS
		flow.nam	(1, 1, 101)	CHD DIS IC IMS NPF OC TDIS WEL
47	ex-gwt-mt3dsupp632a	trans.nam	(1, 1, 401)	ADV CNC DIS DSP FMI IC IMS IST MST OBS SSM TDIS
		flow.nam	(1, 1, 401)	CHD DIS IC IMS NPF OC TDIS WEL
	ex-gwt-mt3dsupp632b	trans.nam	(1, 1, 401)	ADV CNC DIS DSP FMI IC IMS IST MST OBS SSM TDIS
		flow.nam	(1, 1, 401)	CHD DIS IC IMS NPF OC TDIS WEL

Example	Simulation	Namefile(s)	Grid Dimensions	Packages
48	ex-gwt-mt3dsupp632c	trans.nam	(1, 1, 401)	ADV CNC DIS DSP FMI IC IMS IST MST OBS SSM TDIS
		flow.nam	(1, 1, 401)	CHD DIS IC IMS NPF OC TDIS WEL
49	ex-gwt-mt3dsupp82	trans.nam	(1, 31, 46)	ADV DIS DSP FMI IC IMS MST MVT MWT OC SSM TDIS
		flow.nam	(1, 31, 46)	CHD DIS IC IMS MAW MVR NPF OC TDIS
50	ex-gwt-prudic2004t2	trans.nam	(8, 36, 23)	ADV CNC DIS DSP FMI IC IMS LKT MST MVT OBS OC SFT SSM TDIS
		flow.nam	(8, 36, 23)	CHD DIS IC IMS LAK MVR NPF OBS OC RCHA SFR TDIS
51	ex-gwt-uzt-2d-a	gwf-uzt-2d-mf6.nam	(20, 1, 40)	CHD DIS GWFGWT IC IMS NPF OC STO TDIS UZF
		gwt-uzt-2d-mf6.nam	(20, 1, 40)	ADV CHD DIS DSP GWFGWT IC IMS MST NPF OC SSM STO TDIS UZF UZT
	ex-gwt-uzt-2d-b	gwf-uzt-2d-mf6.nam	(20, 1, 40)	CHD DIS GWFGWT IC IMS NPF OC STO TDIS UZF
		gwt-uzt-2d-mf6.nam	(20, 1, 40)	ADV CHD DIS DSP GWFGWT IC IMS MST NPF OC SSM STO TDIS UZF UZT
52	ex-gwt-henry-a	flow.nam	(40, 1, 80)	BUY DIS GHB GWFGWT IC IMS NPF OC TDIS WEL
		trans.nam	(40, 1, 80)	ADV BUY DIS DSP GHB GWFGWT IC IMS MST NPF OC SSM TDIS WEL
	ex-gwt-henry-b	flow.nam	(40, 1, 80)	BUY DIS GHB GWFGWT IC IMS NPF OC TDIS WEL
		trans.nam	(40, 1, 80)	ADV BUY DIS DSP GHB GWFGWT IC IMS MST NPF OC SSM TDIS WEL
53	ex-gwt-saltlake	flow.nam	(57, 1, 135)	BUY CHD DIS GWFGWT IC IMS NPF OC RCH STO TDIS
		trans.nam	(57, 1, 135)	ADV BUY CHD CNC DIS DSP GWFGWT IC IMS MST NPF OC RCH SSM STO TDIS
54	ex-gwt-rotate	flow.nam	(80, 1, 300)	BUY DIS GWFGWT IC IMS NPF OC TDIS
		trans.nam	(80, 1, 300)	ADV BUY DIS GWFGWT IC IMS MST NPF OC TDIS

Example	Simulation	Namefile(s)	Grid Dimensions	Packages
54	ex-gwt-hecht-mendez-b	gwt-hecht-mendez.nam	(13, 83, 247)	ADV DIS DSP FMI IC IMS MST OC SRC SSM TDIS
		gwf-hecht-mendez.nam	(13, 83, 247)	CHD DIS IC IMS NPF OC STO TDIS
	ex-gwt-hecht-mendez-c	gwt-hecht-mendez.nam	(13, 83, 247)	ADV DIS DSP FMI IC IMS MST OC SRC SSM TDIS
		gwf-hecht-mendez.nam	(13, 83, 247)	CHD DIS ICIMS NPF OC STO TDIS
55	ex-gwt-stallman	flow.nam	(120, 1, 1)	CHD DIS GWFGWT IC IMS NPF OC TDIS
		trans.nam	(120, 1, 1)	ADV CHD CNC DIS DSP GWFGWT IC IMS MST NPF OC SSM TDIS
56	ex-gwt-synthetic-valley	trans.nam	(6, 6343)	ADV DISV DSP FMI IC IMS MST OC SSM TDIS
		flow.nam	(6, 6343)	DISV DRN EVTA IC IMS LAK NPF OC RCHA SFR TDIS WEL XT3D
60	ex-gwe-radial-slow	gwf-radial.nam	(1, 19981)	CHD DISV IC IMS NPF OC STO TDIS XT3D
		gwe-radial.nam	(1, 19981)	ADV CND DISV ESL EST FMI IC IMS OC SSM TDIS
61	ex-gwe-geotherm	gwf-geotherm.nam	(1, 18815)	CHD DISV IC IMS NPF OC STO TDIS XT3D
		gwe-geotherm.nam	(1, 18815)	ADV CND DISV ESL EST FMI IC IMS OC SSM TDIS
62	ex-gwe-danckwerts	gwf-danckwerts.nam	(101, 1, 1)	CHD DIS GWFGWE IC IMS NPF OC STO TDIS UZF
		gwe-danckwerts.nam	(101, 1, 1)	ADV CHD CND DIS EST GWFGWE IC IMS NPF OC SSM STO TDIS UZE UZF
63	ex-prt-mp7-p01	mp7-p01-prt.nam	(3, 21, 20)	DIS EMS FMI MIP OC PRP TDIS
		mp7-p01-gwf.nam	(3, 21, 20)	DIS ICIMS NPF OC RCHA RIV TDIS WEL
64	ex-prt-mp7-p03	mp7-p03-prt.nam	(3, 21, 20)	DIS EMS FMI MIP OC PRP TDIS
		mp7-p03-gwf.nam	(3, 21, 20)	DIS DRN ICIMS NPF OC RCHA RIV STO TDIS WEL
65	ex-gwe-prt	ex-gwe-prt-prt.nam	(1, 1692)	DISV EMS FMI MIP OC PRP TDIS
		ex-gwe-prt-gwe.nam	(1, 1692)	ADV CND DISV EST FMI ICIMS OC SSM TDIS
		ex-gwe-prt-gwf.nam	(1, 1692)	CHD DISV ICIMS NPF OC STO TDIS WEL XT3D

# 1 TWRI

This example is a modified version of the original MODFLOW example (TWRI) described in [McDonald and Harbaugh \(1988\)](#) and duplicated in [Harbaugh and McDonald \(1996\)](#). This problem is also is distributed with MODFLOW-2005 ([Harbaugh, 2005](#)). The problem has been modified from a quasi-3D problem, where confining beds are not explicitly simulated, to an equivalent three-dimensional problem.

## 1.1 Example Description

There are three simulated aquifers, which are separated from each other by confining layers (fig. 1–1). The confining beds are 50 ft thick and are explicitly simulated as model layers 2 and 4, respectively. Each layer is a square 75,000 ft on a side and is divided into a grid with 15 rows and 15 columns, which forms squares 5,000 ft on a side. A single steady-stress period with a total length of 86,400 seconds (1 day) is simulated.

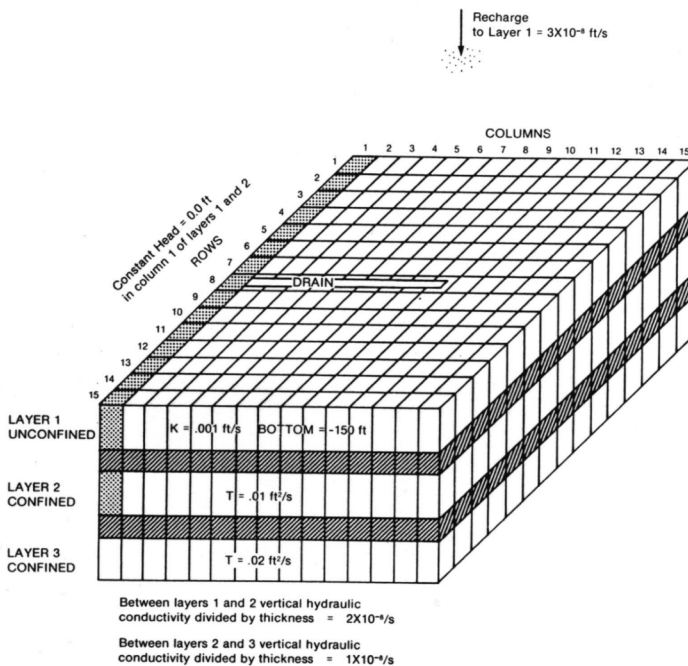


Figure 1–1: Illustration of the system simulated in the TWRI example problem, from [McDonald and Harbaugh \(1988\)](#).

The transmissivity of the middle and lower aquifers (fig. 1–1) was converted to a horizontal hydraulic conductivity using the layer thickness (table 1–1). The vertical hydraulic conductivity in the aquifers was set equal to the horizontal hydraulic conductivity. The vertical hydraulic conductivity of the confining units was calculated from the vertical conductance of the confining beds defined in the original problem and the confining unit thickness (table 1–1); the horizontal hydraulic conductivity of the confining bed was set to the vertical hydraulic conductivity and results in vertical flow in the confining unit.

Table 1–1: Model parameters for example ex-gwf-twri.

Parameter	Value
Number of periods	1
Number of layers	5
Number of columns	15
Number of rows	15
Column width (ft)	5000.0
Row width (ft)	5000.0
Top of the model (ft)	200.0
Layer bottom elevations (ft)	-150.0, -200.0, -300.0, -350.0, -450.0
Starting head (ft)	0.0
Cell conversion type	1, 0, 0, 0, 0
Horizontal hydraulic conductivity (ft/s)	1.0e-3, 1.0e-8, 1.0e-4, 5.0e-7, 2.0e-4
Vertical hydraulic conductivity (ft/s)	1.0e-3, 1.0e-8, 1.0e-4, 5.0e-7, 2.0e-4
Recharge rate (ft/s)	3e-8

An initial head of zero *ft* was specified in all model layers. Any initial head exceeding the bottom of model layer 1 (-150 *ft*) could be specified since the model is steady-state.

Flow into the system is from infiltration from precipitation and was represented using the recharge (RCH) package. A constant recharge rate of  $3 \times 10^{-7}$  *ft/s* was specified for every cell in model layer 1. Flow out of the model is from buried drain tubes represented by drain (DRN) package cells in model layer 1, discharging wells represented by well (WEL) package cells in all three aquifers, and a lake represented by constant head (CHD) packages cells in the unconfined and middle aquifers (fig. 1–1).

## 1.2 Example Results

Simulated results in the unconfined, middle, and lower aquifers are shown in figure 1–2. Simulated results for a quasi-3D MODFLOW-2005 simulation are also shown in figure 1–2. MODFLOW 6 and MODFLOW-2005 results differ by less than 0.05 *ft* in any aquifer unit.

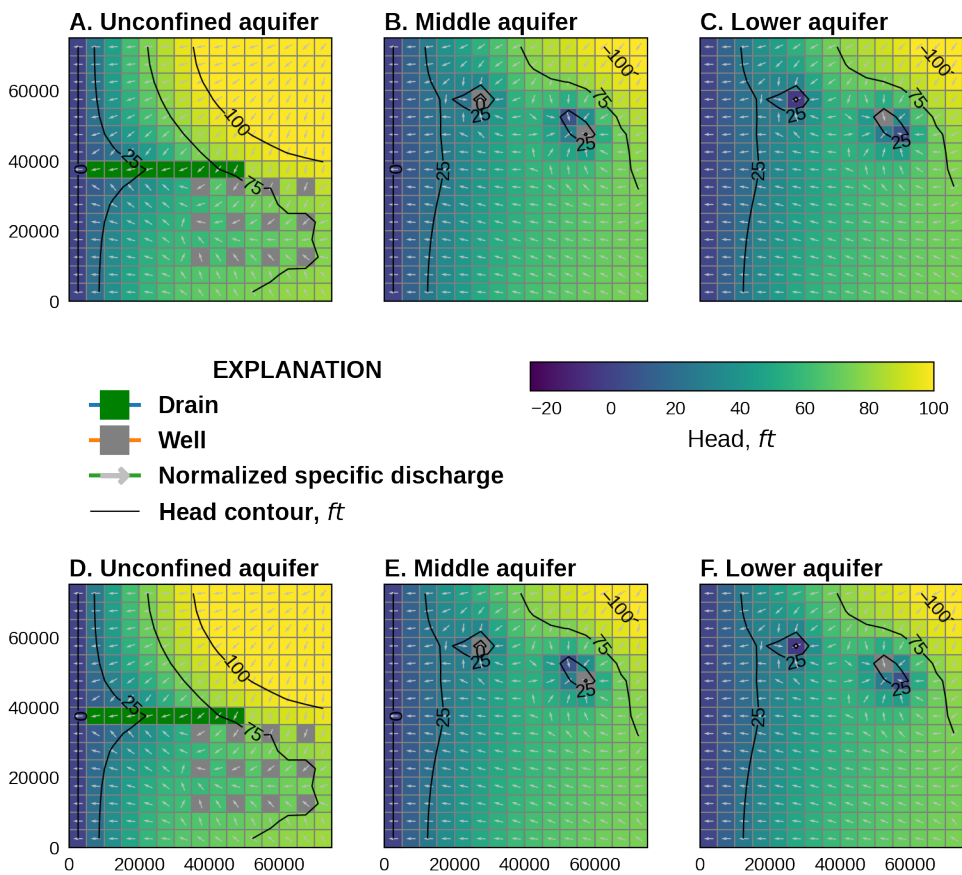


Figure 1–2: Simulated water levels and normalized specific discharge vectors in the unconfined, upper, and lower aquifers. *A.* MODFLOW 6 unconfined aquifer results. *B.* MODFLOW 6 middle aquifer results. *C.* MODFLOW 6 lower aquifer results. *D.* MODFLOW-2005 unconfined aquifer results. *E.* MODFLOW-2005 middle aquifer results. *F.* MODFLOW-2005 lower aquifer results.

## 2 BCF2SS Model

In an aquifer system where two aquifers are separated by a confining bed, large pumpage withdrawals from the bottom aquifer can desaturate parts of the upper aquifer. If pumpage is discontinued, resaturation of the upper aquifer can occur. This problem demonstrates the capability of the Node Property Flow (NPF) Package to successfully simulate this common hydrologic situation which is difficult or impossible to simulate without use of the rewetting option and the Standard Formulation or the Newton-Raphson Formulation.

This example is a version of the original MODFLOW rewetting example (BCF2SS) described in [McDonald and others \(1992\)](#). This problem is also distributed with MODFLOW-2005 ([Harbaugh, 2005](#)). The problem has been modified to use a vertical hydraulic conductivity that is equivalent to the original quasi-3D vertical conductance (VCONT) value used in the original problem.

### 2.1 Conceptual Model

The hypothetical aquifer system consists of an upper aquifer and a lower aquifer separated by a confining unit. No-flow boundaries surround the system on all sides, except that the lower aquifer discharges to a stream along the right side of the area (fig. 2–1). Recharge from precipitation is applied evenly over the entire area. The stream penetrates the lower aquifer; in the region above the stream, the upper aquifer and confining unit are missing (see [McDonald and others, 1992](#), figure 1). Under natural conditions, recharge flows through the system to the stream. Under stressed conditions, two wells withdraw water from the lower aquifer. If enough water is pumped, cells in the upper aquifer will desaturate. Removal of the stresses will then cause the desaturated areas to resaturate.

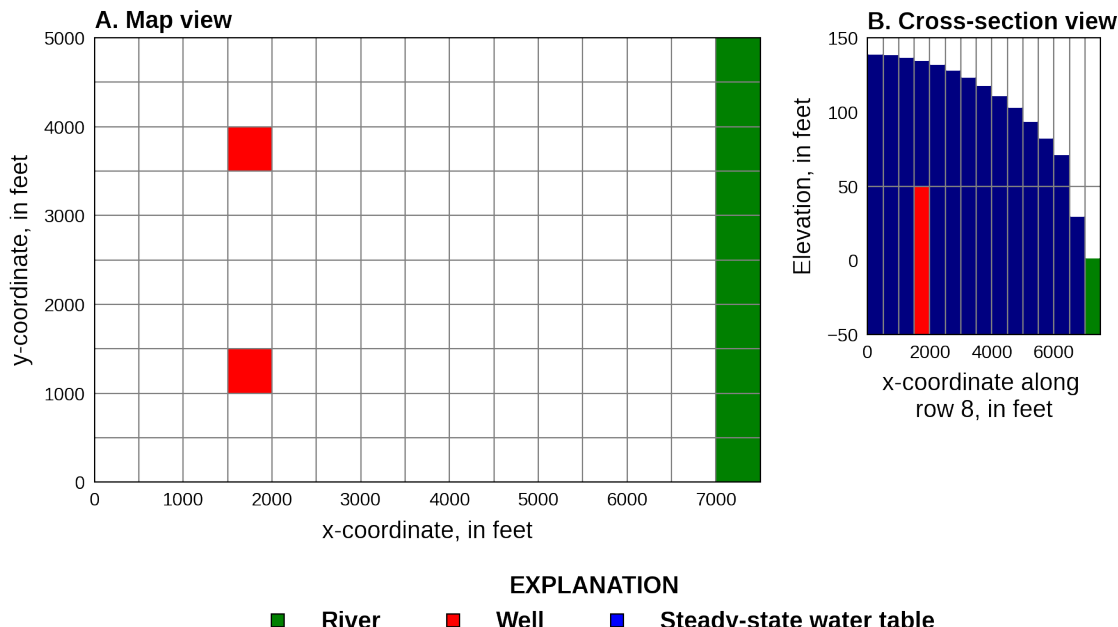


Figure 2–1: Diagram showing the model domain. A, plan view, and B, cross-section view. The locations of river cells, and wells are also shown. The steady-state water-table is shown in the cross-section view.

## 2.2 Example Description

The model consists of two layers—one for each aquifer. A uniform horizontal grid of 10 rows and 15 columns is used (fig. 2–1). Two steady-state solutions were obtained to simulate natural conditions and pumping conditions.

Because horizontal flow in the confining bed is small compared to horizontal flow in the aquifers and storage is not a factor in steady-state simulations, the confining bed is not treated as a separate layer. A horizontal hydraulic conductivity of 10 and 5  $ft/day$  is specified for the upper and lower aquifers, respectively (table 1–1); the horizontal conductivity of the lower aquifer is calculated based on the transmissivity ( $500 ft^2/day$ ) and 100  $ft$  layer thickness used in the original problem (McDonald and others, 1992). The vertical hydraulic conductivity of the confining units is calculated from the vertical conductance of the confining beds defined in the original problem ( $0.999999 \times 10^{-3}$  per day) (table 1–1).

Table 2–1: Model parameters for example ex-gwf-bcf2ss.

Parameter	Value
Number of periods	2
Number of layers	2
Number of rows	10
Number of columns	15
Column width (ft)	500.0
Row width (ft)	500.0
Top of the model (ft)	150.0
Layer bottom elevations (ft)	50.0, -50.
Cell conversion type	1, 0
Horizontal hydraulic conductivity (ft/d)	10.0, 5.0
Vertical hydraulic conductivity (ft/d)	0.1
Starting head (ft)	0.0
Recharge rate (ft/d)	0.004

An initial head of zero  $ft$  is specified in all model layers. Flow into the system is from infiltration from precipitation and was represented using the recharge (RCH) package. A constant recharge rate of  $4 \times 10^{-3} ft/day$  was specified for every cell in the upper aquifer. Flow out of the model is from a stream represented by river (RIV) package cells in the lower aquifer, discharging wells represented by well (WEL) package cells in the lower aquifer. River cells are located in column 15 of every row in the lower aquifer and have a river stage, conductance, and bottom elevation of 0  $ft$ ,  $10,000 ft^2/day$ , and -5  $ft$ , respectively (fig. 2–1). Two wells are included in the second stress period, each pumping  $35,000 ft^3/day$ , at (row 3, column 4) and (row 8, column 4) in the lower aquifer.

The WETDRY parameter used in upper aquifer is shown in figure 2–2. On the right side of the model, the WETDRY parameter is negative in order to cause a cell to become wet only when head in the layer below exceeds the wetting threshold. This was done to avoid incorrectly converting dry cells to wet because of the large head differences between adjacent horizontal cells (McDonald and others, 1992). On the left side of the model, horizontal head changes between adjacent cells generally are small, so head in the neighboring horizontal cells is a good indicator of whether or not a dry cell should become wet. Therefore, positive WETDRY parameters are used in most of this area to allow wetting to occur either from the cell below or from horizontally adjacent cells. Near the well, the horizontal head gradients under pumping conditions also are relatively large; consequently, a negative WETDRY parameter was used at the cells above the well. This prevents these cells from incorrectly becoming wet (McDonald and others, 1992). Rewetting is not enabled in the lower aquifer.

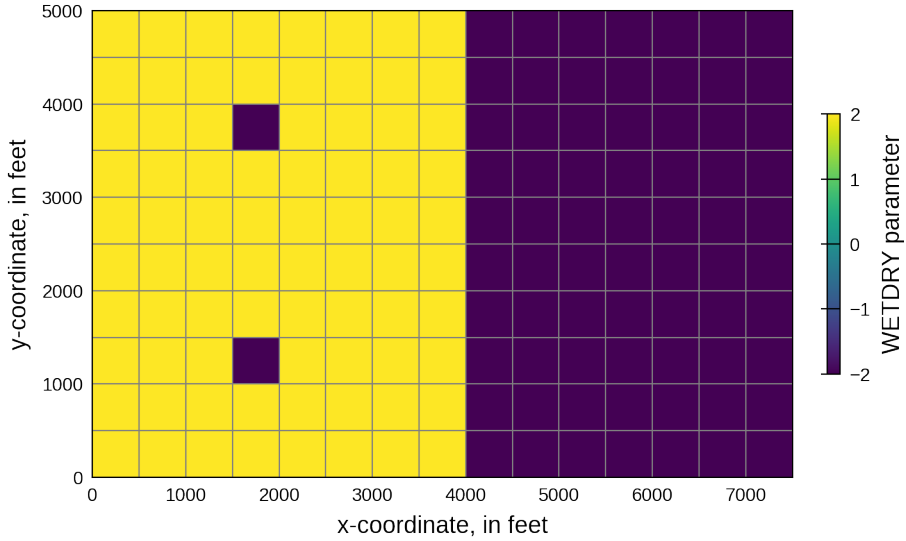


Figure 2–2: WETDRY parameter values used in the upper aquifer. Cells with negative values can only rewet when the head in an underlying cells exceeds the bottom of the cell. Cells with positive values can rewet if the head in an underlying cells exceeds the bottom of the cell or from adjacent connected cells.

### 2.3 Example Results

Two steady-state solutions were obtained to simulate natural conditions and pumping conditions. The two solutions are designed to demonstrate the ability of the rewetting option of the NPF Package to handle a broad range of possibilities for cells converting between wet and dry in the top aquifer. When solving for natural conditions, the top aquifer initially is specified as being entirely dry and many cells must convert to wet. When solving for pumping conditions, the top aquifer is initially specified to be under natural conditions and many cells must convert to dry. The first stress period simulates natural conditions (fig. 2–3A and B) and the second period simulates the addition of pumping wells (fig. 2–3C and D).

Simulated results for the example problem using the Newton-Raphson Formulation instead of the rewetting option and the Standard Formulation is shown in figure 2–4. In general, the simulated results are comparable for the Standard Formulation with the NPF Package rewetting option and the Newton-Raphson formulation. The largest differences between the two approaches occur in the upper aquifer under pumping conditions and is the result of differences in horizontal conductance weighting. Upstream weighting, which is used with the Newton-Raphson Formulation, increases the volumetric horizontal flow and decreases water-levels. Also note how saturated conditions propagate further into the domain in the upper aquifer under pumping conditions using the Newton-Raphson Formulation than when the Standard Formulation with the NPF Package rewetting option is used.

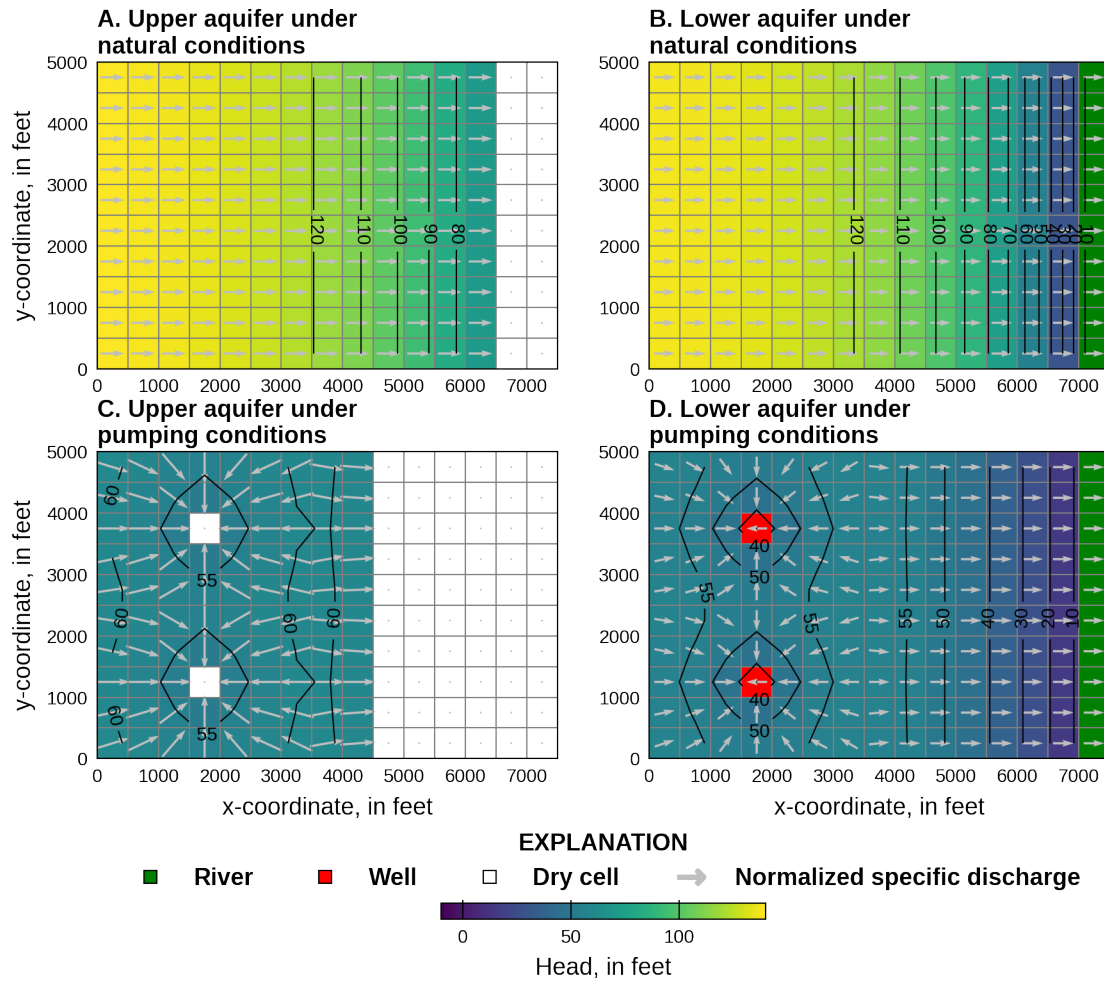


Figure 2–3: Simulated water levels and normalized specific discharge vectors in the upper and lower aquifers under natural and pumping conditions using the rewetting option in the Node Property Flow (NPF) Package with the Standard Conductance Formulation. *A.* Upper aquifer results under natural conditions. *B.* Lower aquifer results under natural conditions *C.* Upper aquifer results under pumping conditions. *D.* Lower aquifer results under pumping conditions

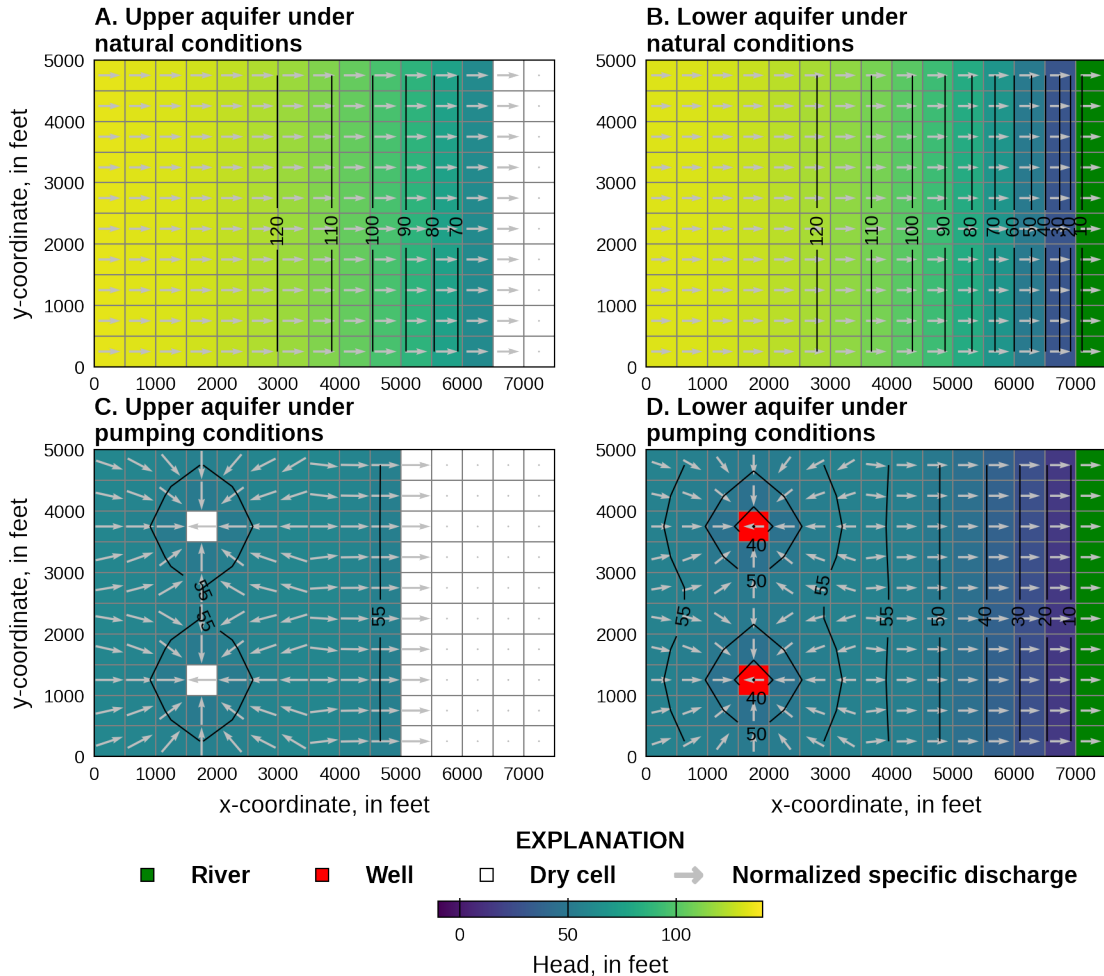


Figure 2–4: Simulated water levels and normalized specific discharge vectors in the upper and lower aquifers under natural and pumping conditions using the Newton-Raphson Formulation. *A*. Upper aquifer results under natural conditions. *B*. Lower aquifer results under natural conditions. *C*. Upper aquifer results under pumping conditions. *D*. Lower aquifer results under pumping conditions

## 3 Tidal Model

This example demonstrates use of MODFLOW 6 observations and time series and the capability to use multiple stress packages of the same type in a single groundwater flow model. This is a synthetic example problem that has not been documented elsewhere.

### 3.1 Example Description

The problem consists of two aquifers, which are separated from each other by a confining layer. The upper aquifer is unconfined and the lower aquifer is confined. The confining layer is 15 m thick and is explicitly simulated as model layer 2. The grid consists of 15 rows and 10 columns. Each cell is 500 m on a side. A single steady-stress period of 1 day is followed by three 10-day transient stress periods, each with 120 time steps. Model parameters are listed in table 3–1.

Table 3–1: Model parameters for example ex-gwf-advtidal.

Parameter	Value
Number of periods	4
Number of layers	3
Number of columns	10
Number of rows	15
Column width (m)	500.0
Row width (m)	500.0
Top of the model (m)	50.0
Layer bottom elevations (m)	5.0, -10.0, -100.0
Starting head (m)	50.0
Cell conversion type	1, 0, 0
Horizontal hydraulic conductivity (m/d)	5.0, 0.1, 4.0
Vertical hydraulic conductivity (m/d)	0.5, 5.0e-3, 0.1
Specific storage (/m)	1.0e-6
Specific yield (unitless)	0.2

An initial head of 50 m was specified in all model layers. Any initial head exceeding the bottom of model layer 1 (5 m) could be specified since the model is steady-state.

The model demonstrates use of the GHB, WEL, RIV RCH, and EVT stress packages. Locations for these boundaries are shown in figure 3–1. The GHB is used to apply a tidally varying boundary condition to the right side of the model in layers 2 and 3. The GHB Package uses the time series capability to represent tidally varying stage for these stress boundaries. Stage values are linearly interpolated to each time step from a time series of tidal fluctuations. The WEL Package also uses time series to change pumping rates by well according to a time series of pumping records. The pumping rates are interpolated using the stepwise option, which indicates that rates are held constant at the specified value until a new value is specified. This is an alternative to the linear interpolation method. The WEL Package contains pumping rates specified with time series and pumping rates specified with a constant value for the stress period. A simple RIV Package is also used with time series to change the river stage by time step.

The RCH and EVT Packages are used to assign and calculate recharge and evapotranspiration, respectively. Three separate RCH Packages are used in this example to assign a different recharge rate to each of the three zones shown in figure 3–1D.

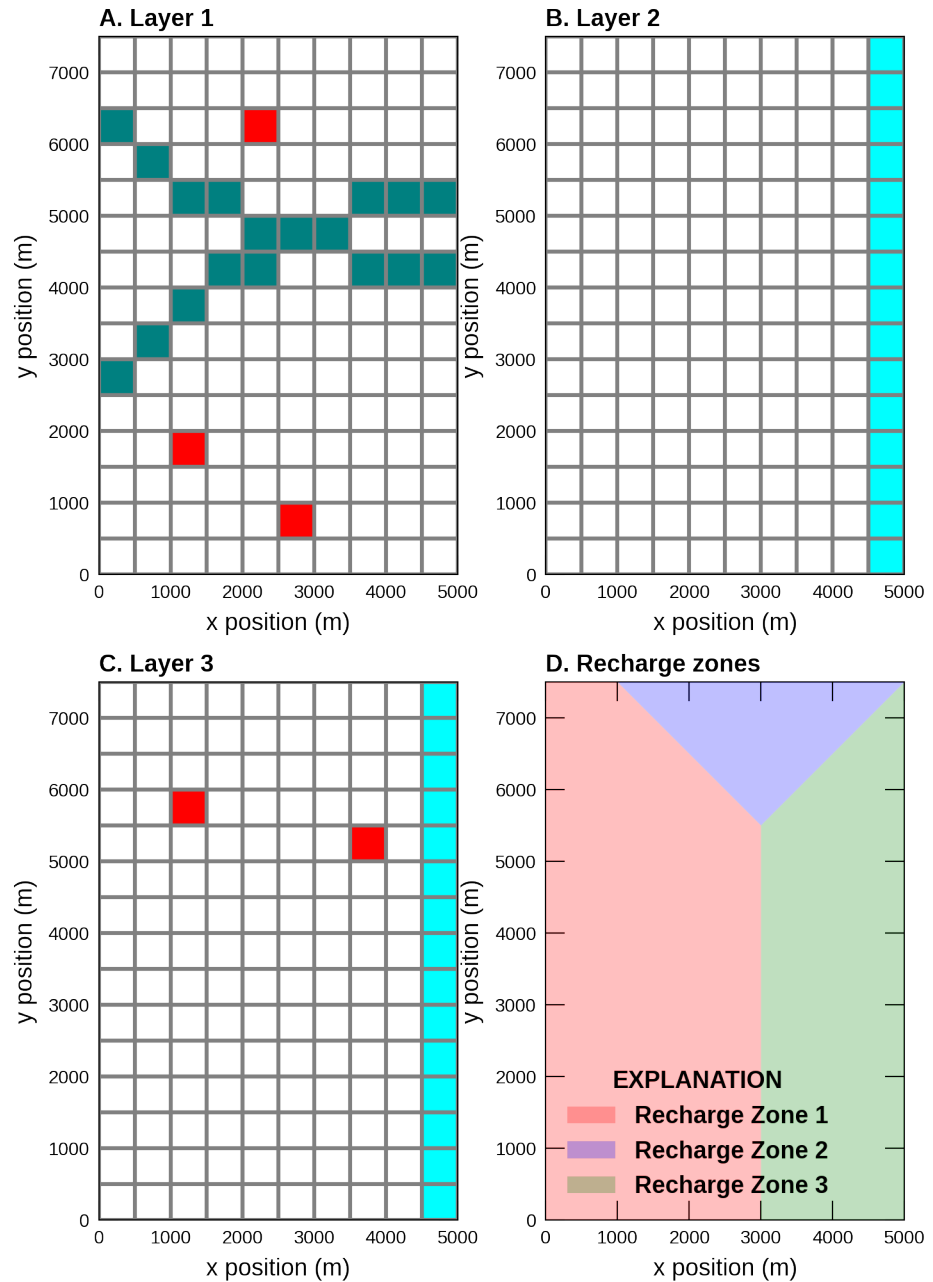


Figure 3–1: Model grid and boundary conditions used for the Tidal example problem: (A) river and well boundaries in layer 1; (B) general-head boundaries in layer 2; (C) general-head and well boundaries in layer 3; and (D) zones used to assign recharge to layer 1.

### 3.2 Example Results

The observation capability in MODFLOW 6 was used to extract time series of simulated heads and flows. Time series of model results are shown in figures 3–2, 3–3, and 3–4.

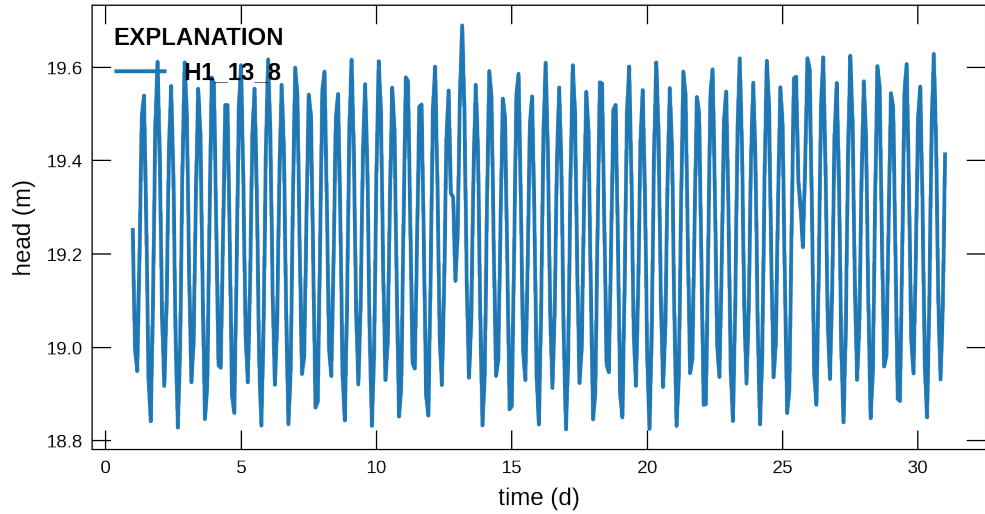


Figure 3–2: Simulated groundwater head in model cell (1, 13, 8).

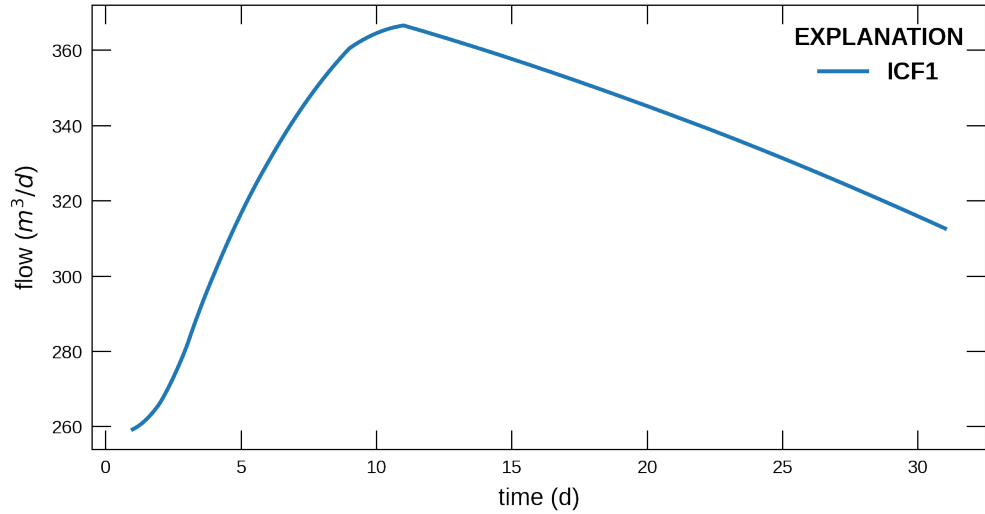


Figure 3–3: Simulated groundwater flow for model cell (1, 5, 6) and its connection with model cell (1, 6, 6). Positive values indicate flow into model cell (1, 5, 6).

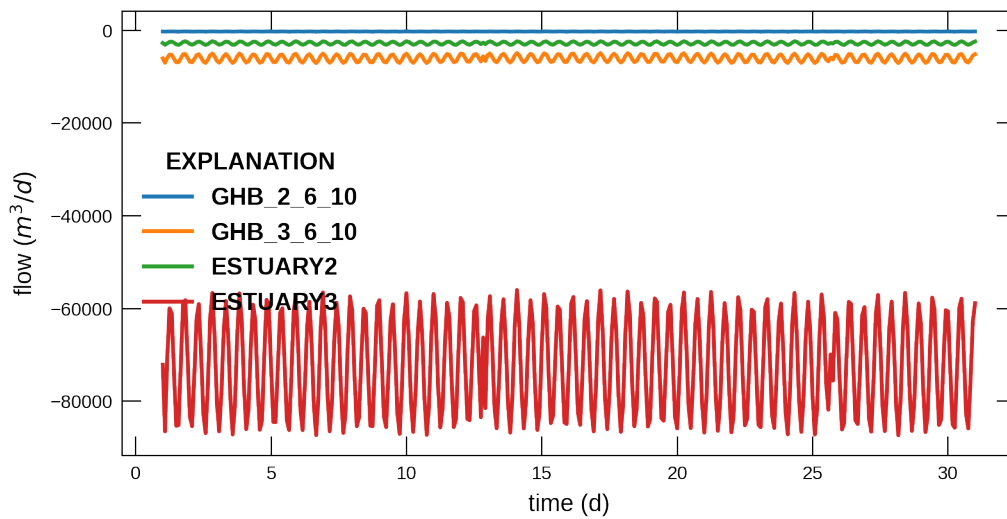


Figure 3–4: Simulated flow between general-head boundary cells and the groundwater flow model. ESTUARY2 is the combined flow for all general-head cells in layer 2. ESTUARY3 is the combined flow for all general-head cells in layer 3. A positive value represents from the general-head boundary into the groundwater model.

## 4 Flow and Head Boundary (FHB) Package Replication

This example shows how the time series capability in MODFLOW 6 can be combined with the constant-head (CHD) and Well (WEL) Packages to replicate the capabilities of the Flow and Head Boundary (FHB) Package in previous versions of MODFLOW. This synthetic example problem has been released with previous MODFLOW versions, such as MODFLOW-2005 ([Harbaugh, 2005](#)) and was first described by [Leake and Lilly \(1997\)](#).

### 4.1 Example Description

The problem consists of a very simple single-layer model representing a confined aquifer. The grid consists of 3 rows and 10 columns. Each cell is 1000 m on a side. There are three transient stress periods with lengths of 400, 200, and 400 days. There are 10, 4, and 6 time steps per stress period. Model parameters are listed in table 4–1.

Table 4–1: Model parameters for example ex-gwf-fhb.

Parameter	Value
Number of periods	3
Number of layers	1
Number of columns	10
Number of rows	3
Column width (m)	1000.0
Row width (m)	1000.0
Top of the model (m)	50.0
Layer bottom elevations (m)	-200.0
Starting head (m)	0.0
Cell conversion type	0
Horizontal hydraulic conductivity (m/d)	20.0
Specific storage (/m)	0.01

An initial head of 0 m was specified for the model. The value is important as the model begins with a transient stress period.

The model demonstrates use of the CHD and WEL packages. Locations for these boundaries are shown in figure 4–1. Both of these packages use time varying values for the constant head and the well flow rate.

### 4.2 Example Results

The observation capability in MODFLOW 6 was used to extract time series of simulated heads and flows. Time series of model results are shown in figures 4–2 and 4–3.

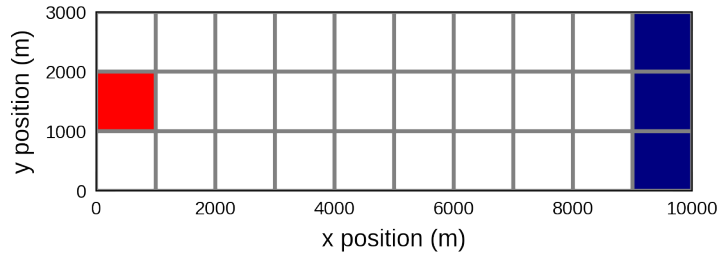


Figure 4-1: Model grid and boundary conditions used for the FHB example problem.

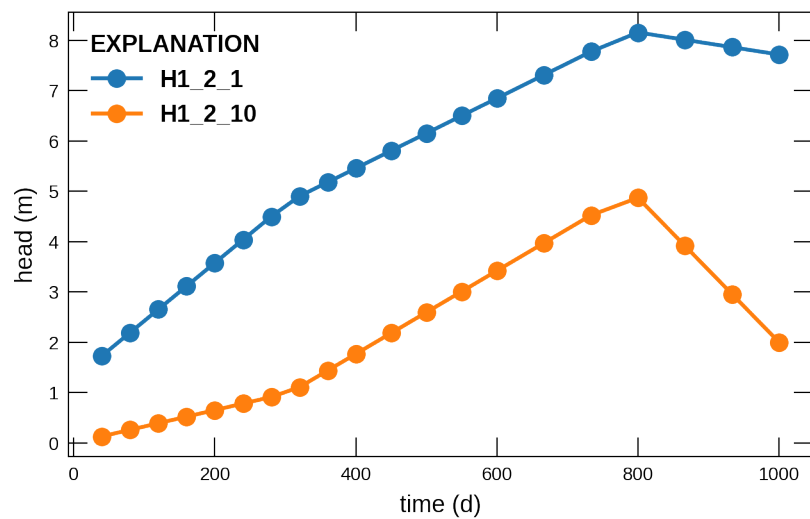


Figure 4-2: Simulated groundwater head in model cells (1, 2, 1) and (1, 2, 10).

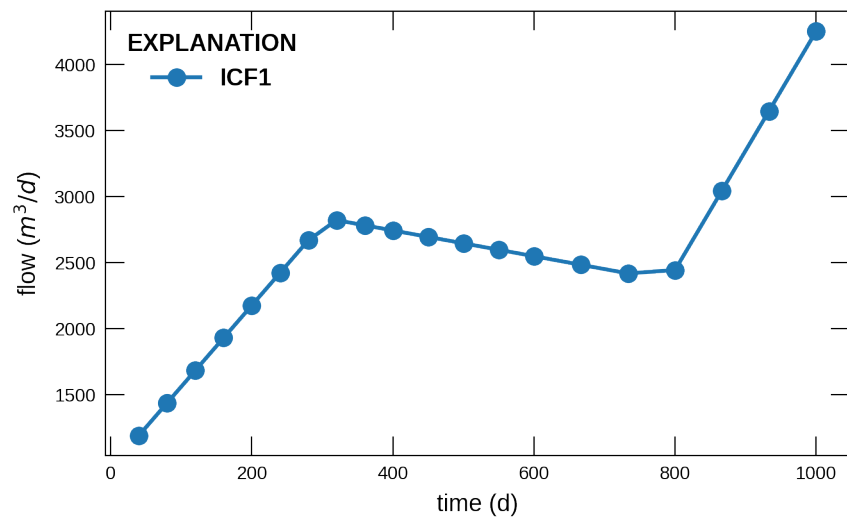


Figure 4-3: Simulated groundwater flow for model cell (1, 2, 2) and its connection with model cell (1, 2, 1). Positive values indicate flow into model cell (1, 2, 2).

## 5 Nested Grid Problem

This example reproduces the nested grid problem described in the MODFLOW-USG documentation ([Panday and others, 2013](#)). The problem is recreated here using the Discretization by Vertices (DISV) input and is run with the standard groundwater flow formulation and the XT3D formulation ([Provost and others, 2017](#)), which provides more accurate results for nested grids.

### 5.1 Example Description

The problem consists of a nested grid as shown in figure 5–1. The outer grid has cells that are 100 m on a side; the nested grid has cells with sides that are 1/3 this length. Cells and vertices are numbered in figure 5–1 and can be compared to the vertices and cell information listed in the input file for the DISV Package. The top of the model is uniform and set to zero (table 5–1). The bottom of the model is also uniform, and is set to -100 m. The simulation consists of a single steady-state stress period with a length of one day. The simulation starts with an initial head of zero.

Constant-heads are assigned a value of 1.0 m on the left side of the model and 0.0 m on the right side of the model.

Table 5–1: Model parameters for example ex-gwf-u1disv.

Parameter	Value
Number of periods	1
Number of layers	1
Top of the model (m)	0.0
Layer bottom elevations (m)	-100.0
Starting head (m)	0.0
Cell conversion type	0
Horizontal hydraulic conductivity (m/d)	1.0

### 5.2 Scenario Results

The nested grid problem was run with the standard groundwater flow formulation and the XT3D formulation ([Provost and others, 2017](#)) (table 5–2).

Table 5–2: Scenario parameters for example ex-gwf-u1disv.

Scenario	Scenario Name	Parameter	Value
1	ex-gwf-u1disv	xt3d	False
2	ex-gwf-u1disv-x	xt3d	True

#### 5.2.1 Standard Groundwater Flow Formulation

Model results for the simulation with the standard groundwater flow formulation are shown in figure 5–2. Flow is from left to right and should be perfectly one dimensional. The head surface should represent a flat plane with a value of 1.0 on the left and zero on the right. Because the configuration of a nested grid violates the control-volume finite-difference assumptions, there are errors in the simulated heads as shown in figure 5–2B. Head errors are larger than solution tolerances.

#### 5.2.2 XT3D

Model results for the simulation with the XT3D groundwater flow formulation ([Provost and others, 2017](#)) are shown in figure 5–3. In this simulation, the XT3D formulation gives a much better solution

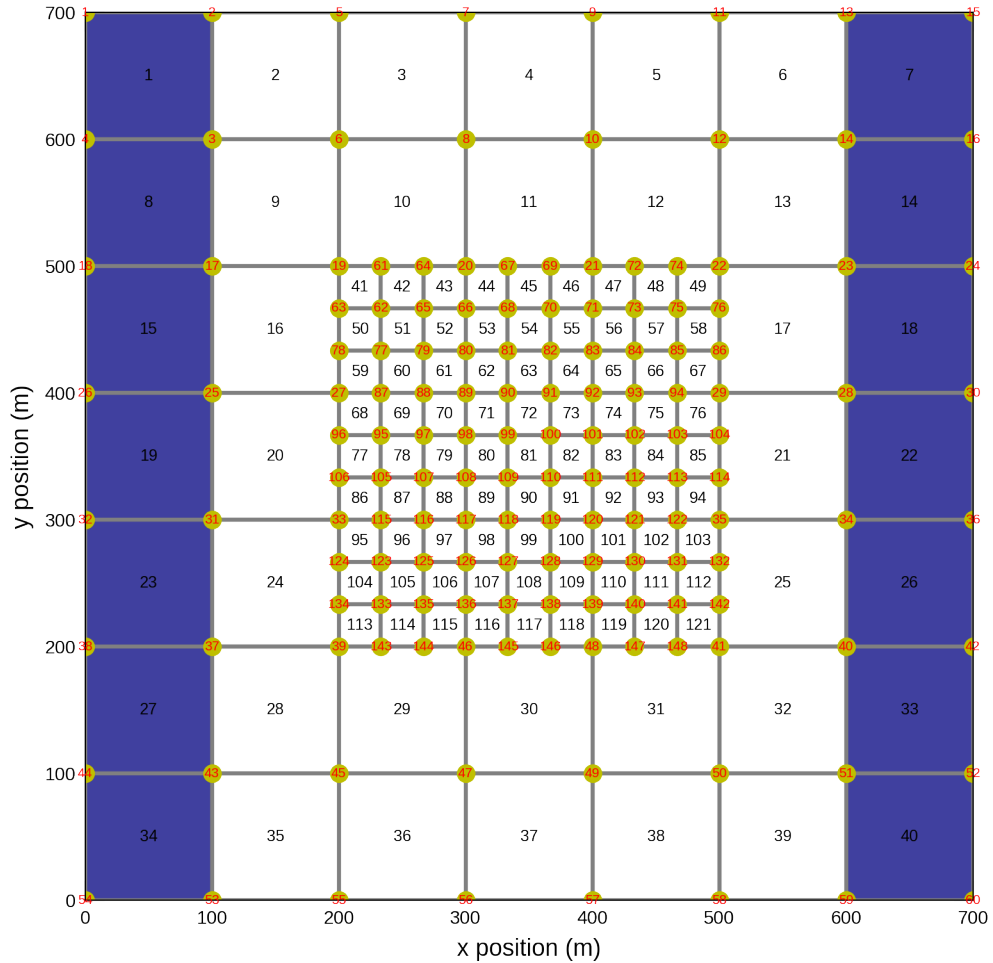


Figure 5–1: Model grid used for the nested grid problem. Constant-head cells are marked in blue. Cell numbers are shown inside each model cell. Vertices are also numbered and are shown in red.

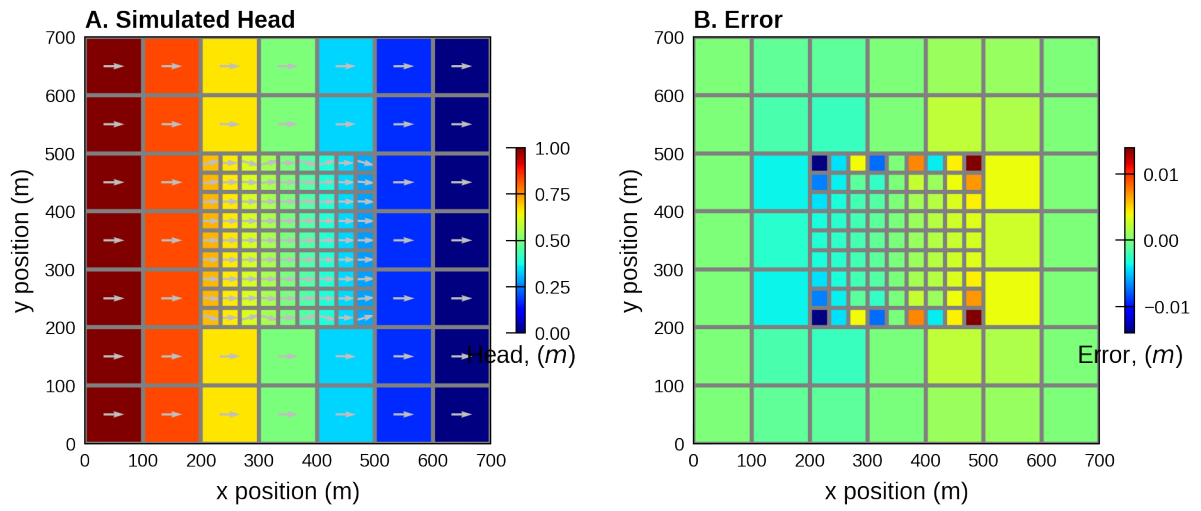


Figure 5–2: Simulated head (A) and errors in simulated head (B) for the nested grid problem simulated with the standard groundwater flow formulation.

than the standard groundwater flow formulation. Errors in simulated head (figure 5–3B) are smaller than the tolerances used for the problem.

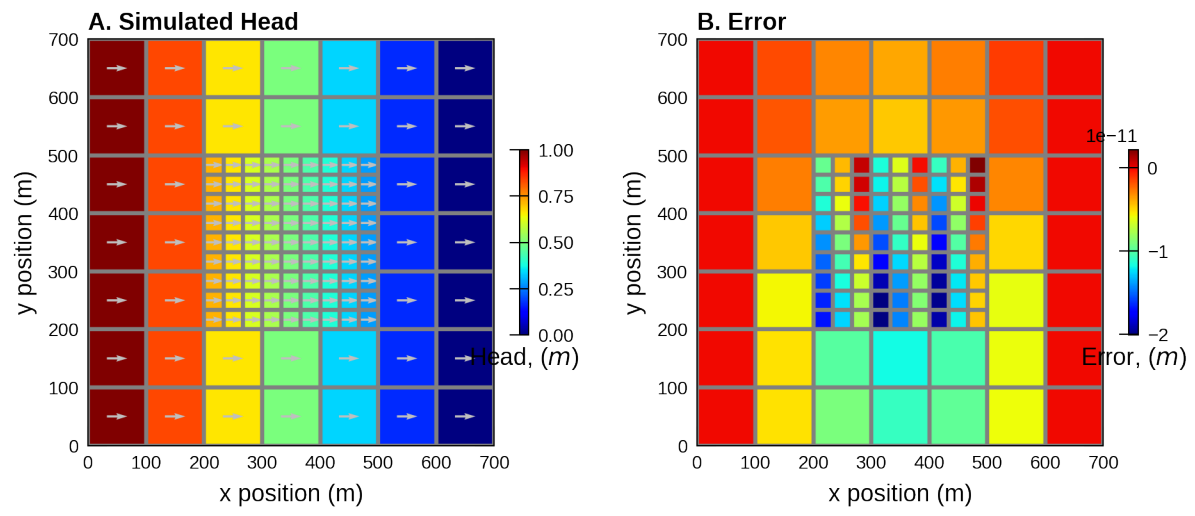


Figure 5–3: Simulated head (A) and errors in simulated head (B) for the nested grid problem simulated with the XT3D groundwater flow formulation ([Provost and others, 2017](#)).

## 6 Nested Grid Problem, Two Domains

This example reproduces the nested grid problem described in the MODFLOW-USG documentation ([Panday and others, 2013](#)). A single model setup with a grid based on the Discretization by Vertices (DISV) input is presented elsewhere in these examples. This problem is set up using two individual GWF models with a regular grid (DIS) that are coupled through a GWF Exchange. A plan view of the combined grid for the two models is shown in figure 6–1. The XT3D option in the NPF package can be applied to avoid inaccuracies at the cell refinement interface ([Provost and others, 2017](#)), which is the model boundary in this example. However, for this coupled system it is not sufficient to enable XT3D for the models independently: the correct flow calculation around the model interface relies on information from both models.

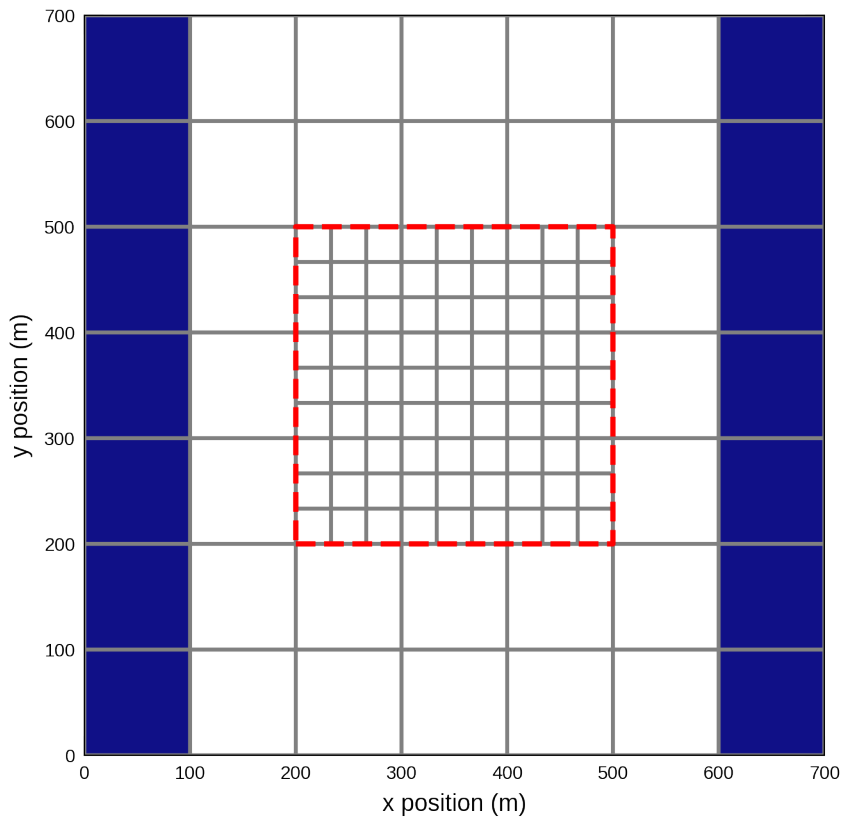


Figure 6–1: A top view of the grids of the outer and inner model used in this example. The dashed red line indicates the interface between the two. The blue shaded areas are the cells with a constant head boundary condition.

This is illustrated in more detail in figure 6–2. The red dots show (examples of) cell connections where the flow relies on data from both models. The cells which are involved in the flow calculation are colored blue. In the left panel this is the case for flows that cross the model boundary. On the right it is shown how interior connections can still be dependent on cell data from the neighboring

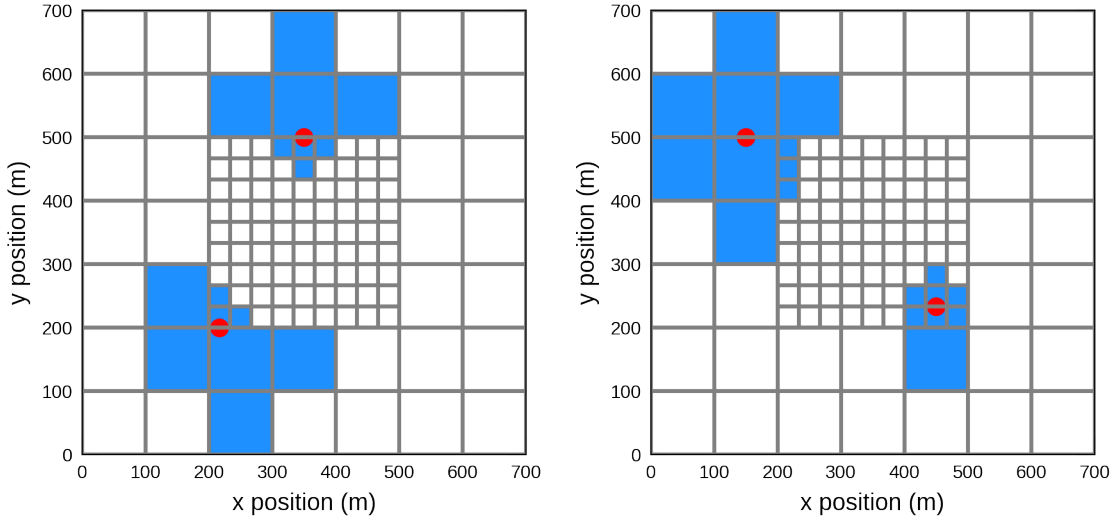


Figure 6–2: Flow calculation stencils for XT3D for the coupled model system. Details in the text.

model. With the release of the generalized coupling framework in MODFLOW 6 (as of version 6.3.0) it is now possible to activate XT3D not just for the internal model connections, but also for connections between models. Additionally, it will correctly calculate the XT3D fluxes near the model boundary using data from both models (c.f. the right panel in figure 6–2). In this example problem we study how these options affect the accuracy of the simulation results.

## 6.1 Example Description

This is a typical Local Grid Refinement (LGR) example with the coarse outer cells ( $100m \times 100m$ ) being part of one model and the refined inner cells part of the other. Some essential and uniform parameters are given in table 6–1. The two models are connected by a GWF Exchange which enables groundwater flow through the grid faces marked by the dashed red square. The blue cells indicate where a constant head boundary condition is imposed. The condition is set to  $1m$  for the cells on the left and to  $0m$  for the right. As a result, the analytical solution of the problem is trivial and given by the expression

$$h = 1.0 - \frac{x - 50.0}{600.0} m \quad (6-1)$$

for the head  $h$  and  $x \in (50.0, 650.0)$ . This formula will be used to test the accuracy of the simulated results presented below.

Table 6–1: Model parameters for example ex-gwf-u1gwgwf.

Parameter	Value
Number of periods	1
Number of layers	1
Top of the model (m)	0.0
Layer bottom elevations (m)	-100.0
Starting head (m)	0.0
Constant head boundary LEFT (m)	1.0

Table 6–1: Model parameters for example ex-gwf-u1gwgwf.

Parameter	Value
Constant head boundary RIGHT (m)	0.0
Cell conversion type	0
Horizontal hydraulic conductivity (m/d)	1.0

## 6.2 Scenario Results

The nested grid problem was run for 4 different scenarios using the parameter configuration listed in table 6–2.

Table 6–2: Scenario parameters for example ex-gwf-u1gwgwf.

Scenario	Scenario Name	Parameter	Value
1	ex-gwf-u1gwgwf-s1	XT3D in models	False
		XT3D at exchange	False
2	ex-gwf-u1gwgwf-s2	XT3D in models	True
		XT3D at exchange	False
3	ex-gwf-u1gwgwf-s3	XT3D in models	True
		XT3D at exchange	True
4	ex-gwf-u1gwgwf-s4	XT3D in models	False
		XT3D at exchange	True

Model results for the simulation of these scenarios are shown in figures 6–3, 6–4, 6–5, 6–6. Flow is from left to right and should be perfectly one-dimensional. The head surface should represent a flat plane with a value of 1.0 on the left and zero on the right, following the analytical expression given in equation 6–1.

Because the configuration of a nested grid with a refinement violates the control-volume finite-difference assumptions, there are errors in the simulated heads for scenario 1 with the standard NPF flow formulation, as shown in figure 6–3B. Enabling the XT3D method in both models as done in scenario 2, is insufficient to get rid of these inaccuracies as can be seen from figure 6–4B. Scenario 3 applies the advanced XT3D calculation globally on both models *and* at the interface. This setup is now equivalent to what was presented in the “Nested Grid Problem” elsewhere in these examples for the case of a single DISV-based model with XT3D enabled. And as expected, figure 6–5B illustrates how in this case the deviation from the analytical result is well within the solver tolerance ( $h_{close} = 1 \times 10^{-9}$ ). Scenario 4 is a new capability of the generalized coupling and allows to apply XT3D where it is needed: in the exchange region between the models (c.f. figure 6–2B). Because the XT3D calculation is quite costly, this is an efficient alternative to the setup in scenario 3 which leads to the same level of accuracy. The latter is clearly demonstrated by the error plot in figure 6–6B.

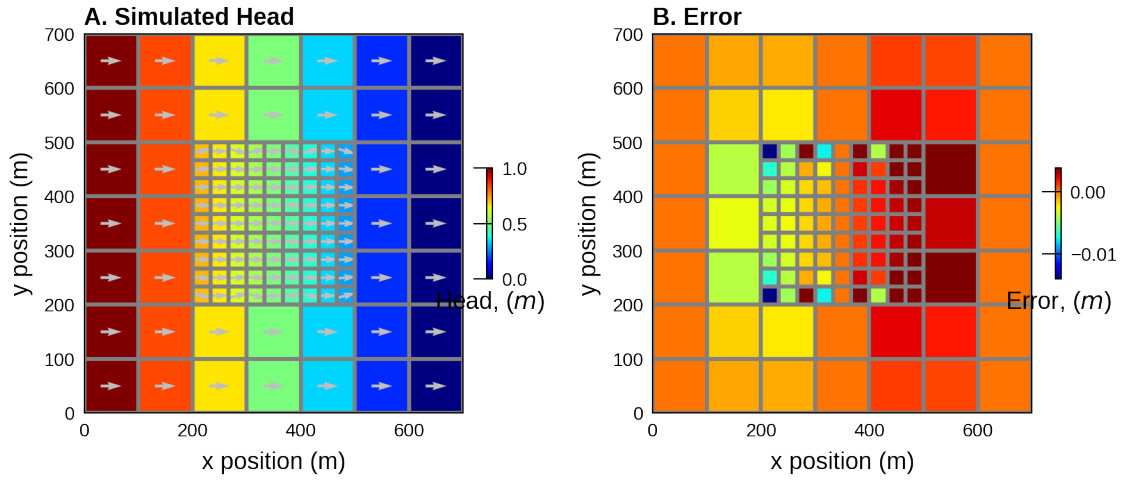


Figure 6–3: Results for scenario 1: simulated head (A) and differences in head with respect to the analytical result (B) for a system of coupled models without XT3D.

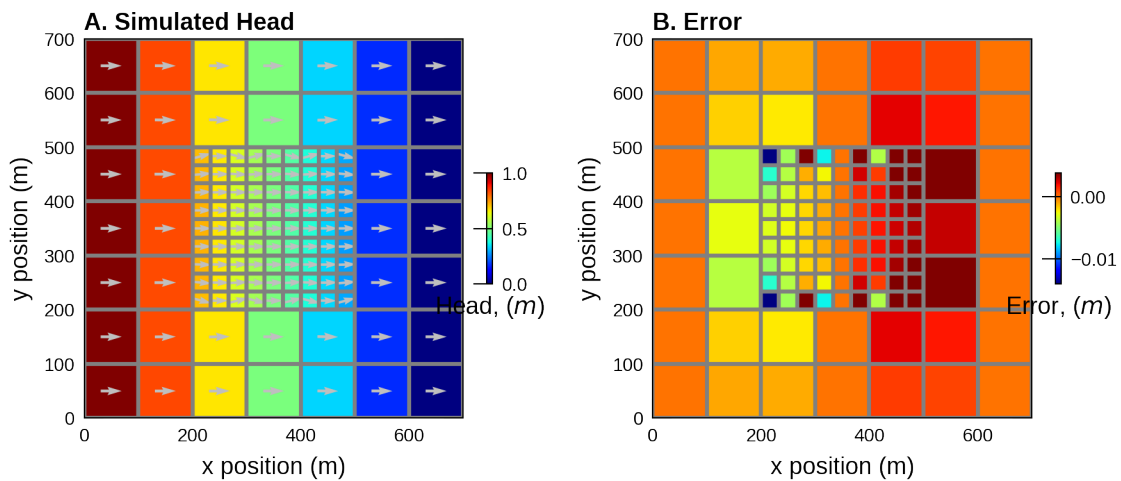


Figure 6–4: Results for scenario 2: simulated head (A) and differences in head with respect to the analytical result (B) for a system of coupled models with XT3D active in both models but not at the exchange between them.

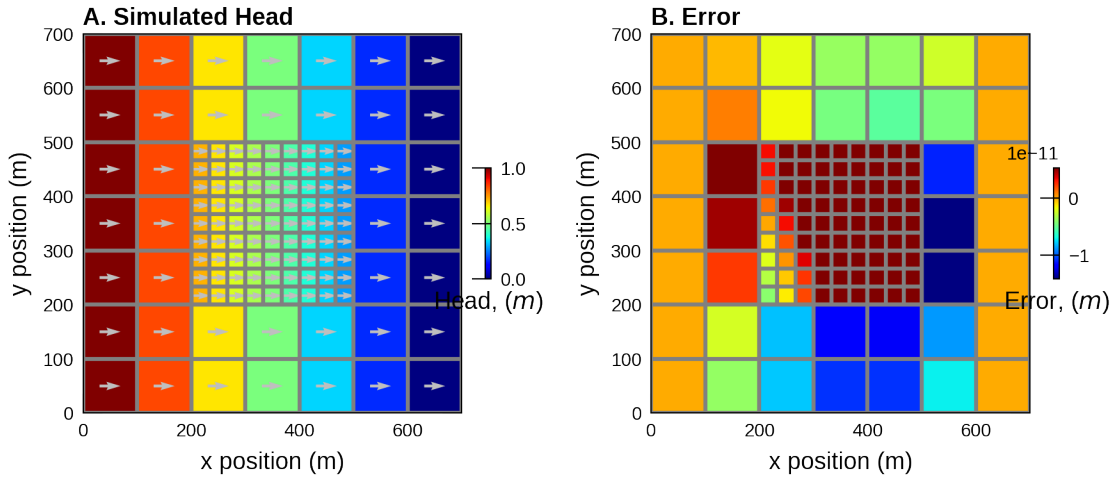


Figure 6–5: Results for scenario 3: simulated head (A) and differences in head with respect to the analytical result (B) for a system of coupled models with XT3D active in both models and at the exchange between them.

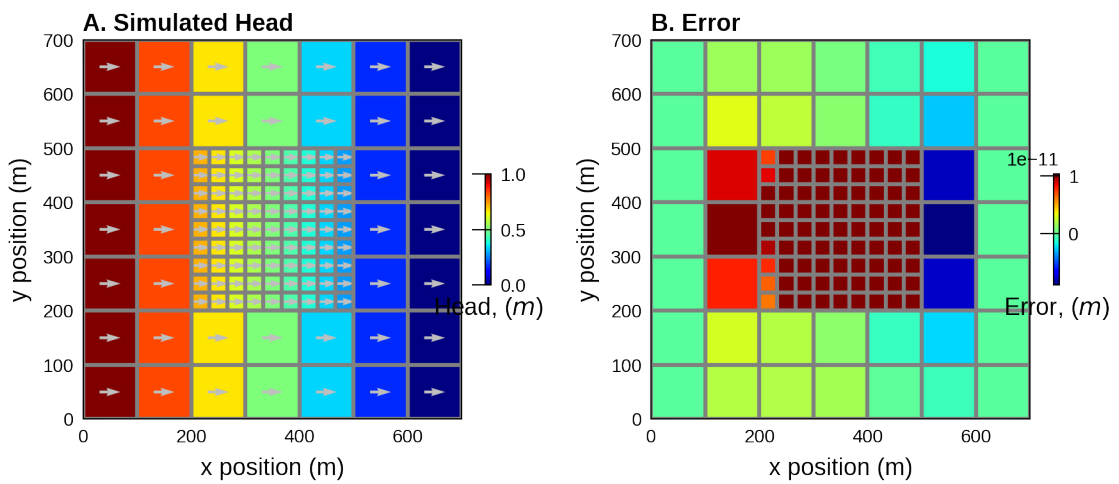


Figure 6–6: Results for scenario 4: simulated head (A) and differences in head with respect to the analytical result (B) for a system of coupled models without XT3D in the models but with XT3D enabled at the exchange between them.

## 7 MODFLOW-NWT Problem 2

This example is based on problem 2 in [Niswonger and others \(2011\)](#) which used the Newton-Raphson formulation to simulate dry cells under a recharge pond. This problem is also described in [McDonald and others \(1992\)](#) and used the MODFLOW rewetting option to rewet dry cells.

### 7.1 Example Description

The simulation represents a rectangular, unconfined aquifer with a deep water table. The model uses symmetry to simplify the problem by simulating one-quarter of the pond and the downgradient model domain (fig. 7-1). Model parameters for the example are summarized in table 7-1

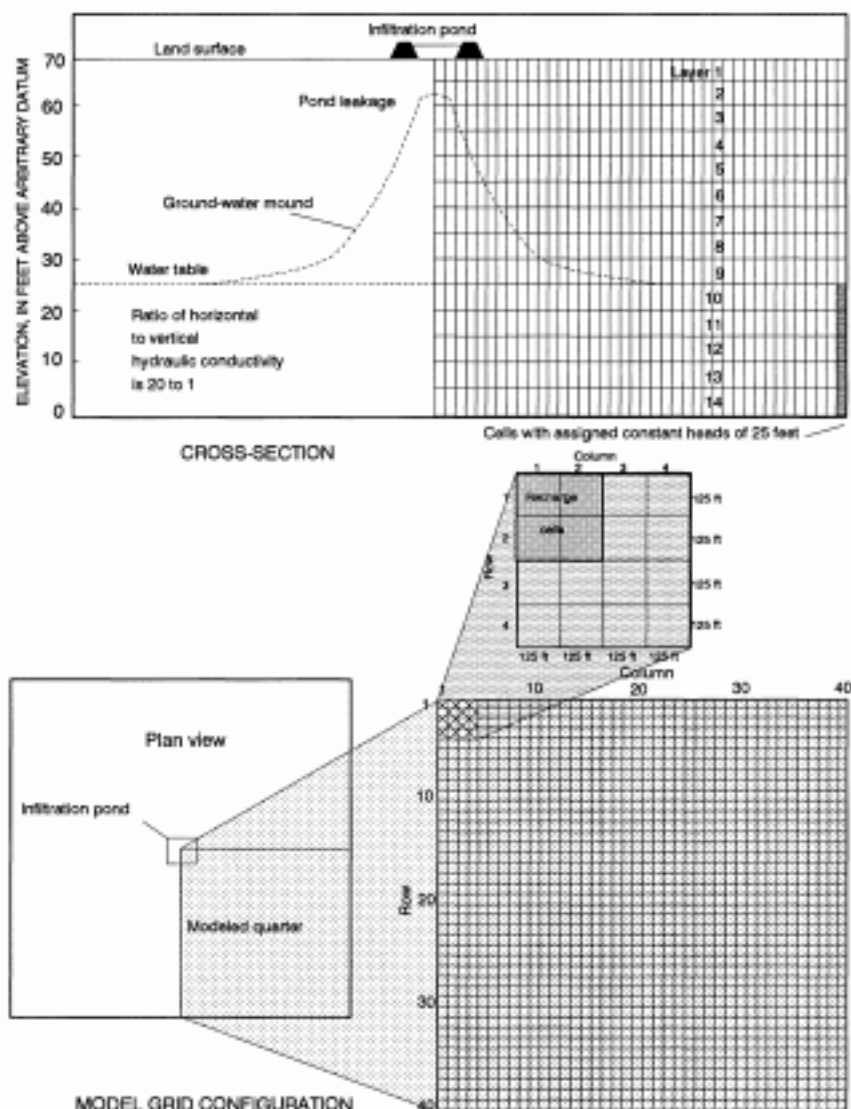


Figure 7-1: Hydrogeology, model grid, and model boundary conditions (from [McDonald and others, 1992](#)).

The model consists of a grid of 40 columns, 40 rows, and 14 layers. The model domain is 5,000 *ft* in the x- and y-directions. The discretization is 125 *ft* in the row and column direction for all cells. The upper model layer is 15 *ft* thick and the remaining model layers (layers 2 through 14) are 5 *ft* thick. Four stress periods are simulated. The first three stress periods are transient and the last stress period is steady state. The stress periods are 190, 518, 1921, and 1 days in length and are broken up into 10, 2, 17, and 1 time steps of equal length. The total simulation time at the end of the four stress periods are 190, 708, 2,630, and 2,631 days, respectively.

Table 7–1: Model parameters for example ex-gwf-nwt-p02.

Parameter	Value
Number of periods	4
Number of layers	14
Number of rows	40
Number of columns	40
Column width ( <i>ft</i> )	125.0
Row width ( <i>ft</i> )	125.0
Top of the model ( <i>ft</i> )	80.0
Horizontal hydraulic conductivity ( <i>ft/day</i> )	5.0
Horizontal hydraulic conductivity ( <i>ft/day</i> )	0.25
Specific storage (1/ <i>day</i> )	0.0002
Specific yield (unitless)	0.2
Constant head along left and lower edges and starting head ( <i>ft</i> )	25.0
Recharge rate ( <i>ft/day</i> )	0.05

The horizontal hydraulic conductivity is 5 *ft/day* and vertical hydraulic conductivity is 0.25 *ft/day*. The upper ten model layers are convertible and the lower four model layers are confined. The specific yield is 0.2 (unitless) and the specific storage is 0.0002 1/*day*. Unconfined and confined storage change is simulated in the upper ten model layers; confined storage change is simulated in the lower four model layers.

A initial head of 25 *ft* was specified in all model cells, which results in the upper 9 model layers being dry at the start of the simulation. Constant heads boundary condition cells with a specified value of 25 *ft* were specified on the right and lower edges of the model in model layer 10 through 14. The pond area above the aquifer is approximately 6 acres and recharge is added to four cells in the upper left corner of the model (fig. 7–1). A constant recharge rate of 0.05 *ft/day* is applied to the pond area and results in a total pond leakage rate equal to 12,500 *ft<sup>3</sup>/day* for the full model domain.

## 7.2 Scenario Results

Example model results are evaluated using the Newton-Raphson Formulation and the Standard Conductance Formulation with rewetting (table 7–2). Complex and simple complexity Iterative Model Solver options were used for the simulation using the Newton-Raphson formulation and the Standard Conductance Formulation with rewetting scenarios, respectively. Rewetting was only activated in the upper 9 layers. The pseudo-transient continuation option ([Hughes and others, 2017](#)) was disabled in the Newton-Raphson Formulation scenario.

Water-table elevations were compared for four simulation times: 190 days; 708 days; 2,630 days; and at steady state (2,631 days). Water-table elevation in row 1 were very similar for the two solutions (fig. 7–2), with a maximum difference in head of 2.5 *ft* directly under the pond (row 2, column 2). The mean absolute water-table error for the model domain ranged from 0.061 to 0.012 *ft*.

(fig. 7–2). A portion of the difference between the two scenarios is likely a result of the upstream horizontal conductance weighting used with the Newton-Raphson formulation.

Table 7–2: Scenario parameters for example ex-gwf-nwt-p02.

Scenario	Scenario Name	Parameter	Value
1	ex-gwf-nwt-p02a	newton	newton
2	ex-gwf-nwt-p02b	rewet	True
		wetfct	0.5
		iwetit	1
		ihdwet	1
		wetdry	-0.5

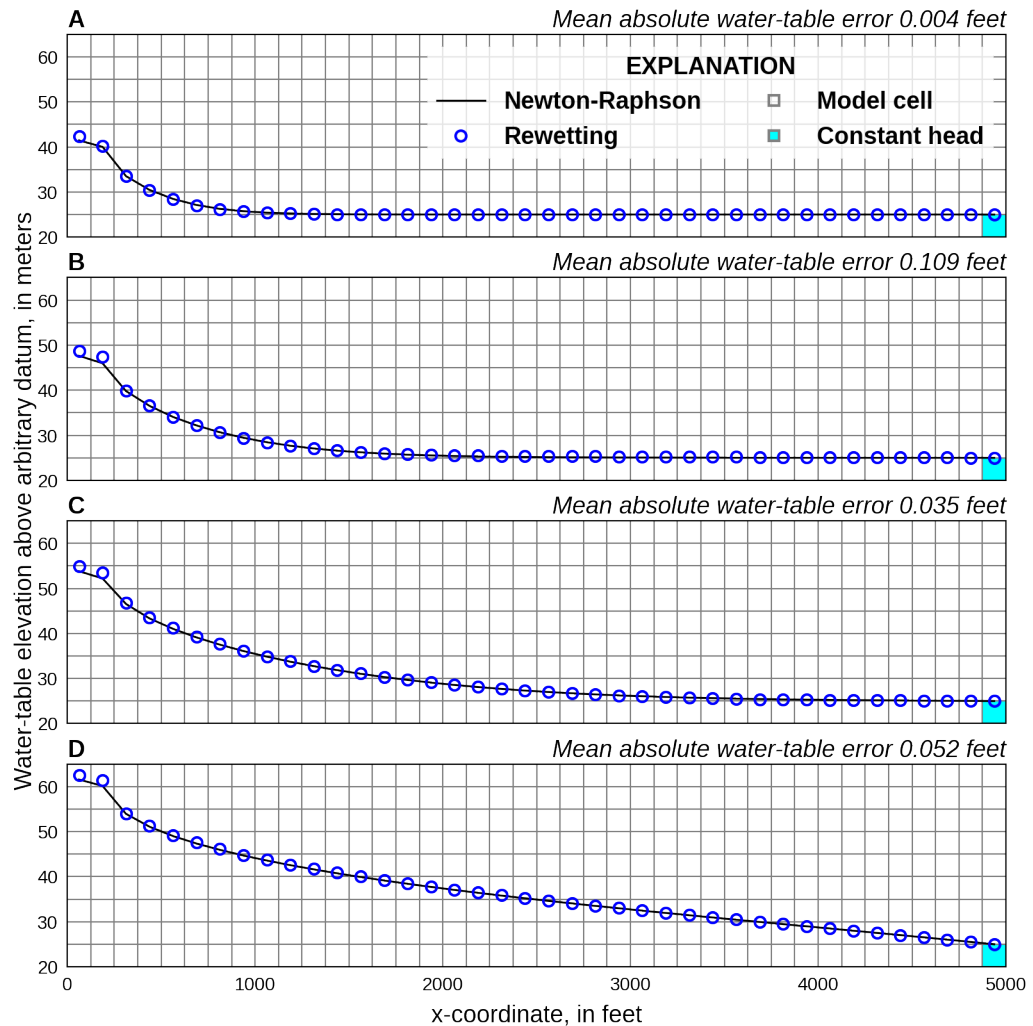


Figure 7-2: Comparison of water-table elevations simulated using the Newton-Raphson Formulation and Standard Conductance Formulation with rewetting. Water-table altitudes in row 1 are shown for A, 190 days, B, 708 days, C, 2,630 days, and D, at steady state. The location of the uppermost constant head boundary cell is also shown.

## 8 MODFLOW-NWT Problem 3

This example is based on problem 3 in [Niswonger and others \(2011\)](#) which used the Newton-Raphson formulation to simulate water levels in a rectangular, unconfined aquifer with a complex bottom elevation and receiving areally distributed recharge. This problem provides a good example of the utility of Newton-Raphson Formulation for solving problems with wetting and drying of cells.

### 8.1 Example Description

Model parameters for the example are summarized in table 8–1.

Table 8–1: Model parameters for example ex-gwf-nwt-p03.

Parameter	Value
Number of periods	1
Number of layers	1
Number of rows	80
Number of columns	80
Cell size in the x-direction (m)	100.0
Cell size in y-direction (m)	100.0
Top of the model (m)	200.0
Horizontal hydraulic conductivity (m/day)	1.0
Constant head water level (m)	24.0

The model consists of a grid of 40 columns, 40 rows, and 1 layer. The model domain is 8,000 m in the x- and y-directions. The discretization is 100 m in the row and column direction for all cells. The top of the model is specified to be 200 m and the bottom of the model ranges from about 4 to 80 m (fig. 8–1). A single steady-state stress period, 365 days in length, with a single time step is simulated.

The horizontal hydraulic conductivity is 1 m/day and each cell is convertible. A initial head 20 m above the cell bottom was specified in all model cells.

Constant heads boundary condition cells with a specified value of 24 m are specified in column 80 for rows 46 through 48 (fig. 8–1). Recharge that is a function of the bottom elevation is specified for each active cells; two different recharge distributions are specified and are discussed further below.

Newton under-relaxation to maintain water-levels above the aquifer bottom ([Hughes and others, 2017](#)). The simple complexity Iterative Model Solver option and preconditioned bi-conjugate gradient stabilized linear accelerator was used for both scenarios.

### 8.2 Scenario Results

The model was evaluated using high and low recharge rates (fig. 8–2). Low recharge rates are 3 orders of magnitude less than the high recharge rates and simulate more arid conditions. Simulation results with large recharge rates are shown in figure 8–3. The entire model domain is saturated and simulated saturated thickness ranges between zero and 25 m (fig. 8–3B). Simulation results with low recharge rates are shown in figure 8–4. Only a small portion of the model domain has heads that are significantly above the cell bottom. However, all cells in the simulation have a non-zero saturated thickness (greater than 2 mm), which allows the applied recharge to flow horizontally toward the constant-head boundaries at the outlet of the aquifer.

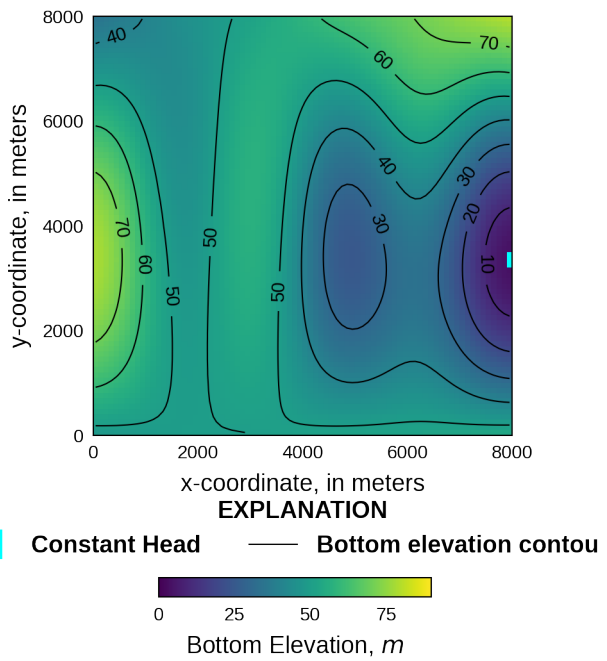


Figure 8–1: Distribution of layer-bottom elevations. The location of constant head boundary cells is also shown.

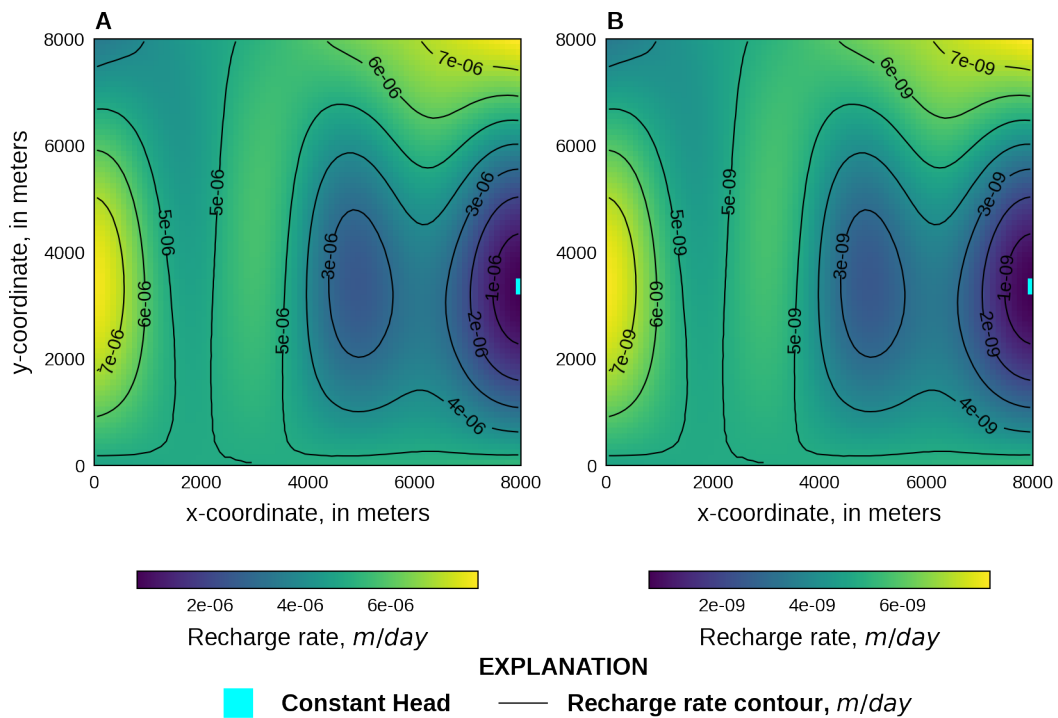


Figure 8–2: Distribution of groundwater recharge applied in the model scenarios. *A*, higher recharge rates, and *B*, lower recharge rates. The location of constant head boundary cells is also shown.

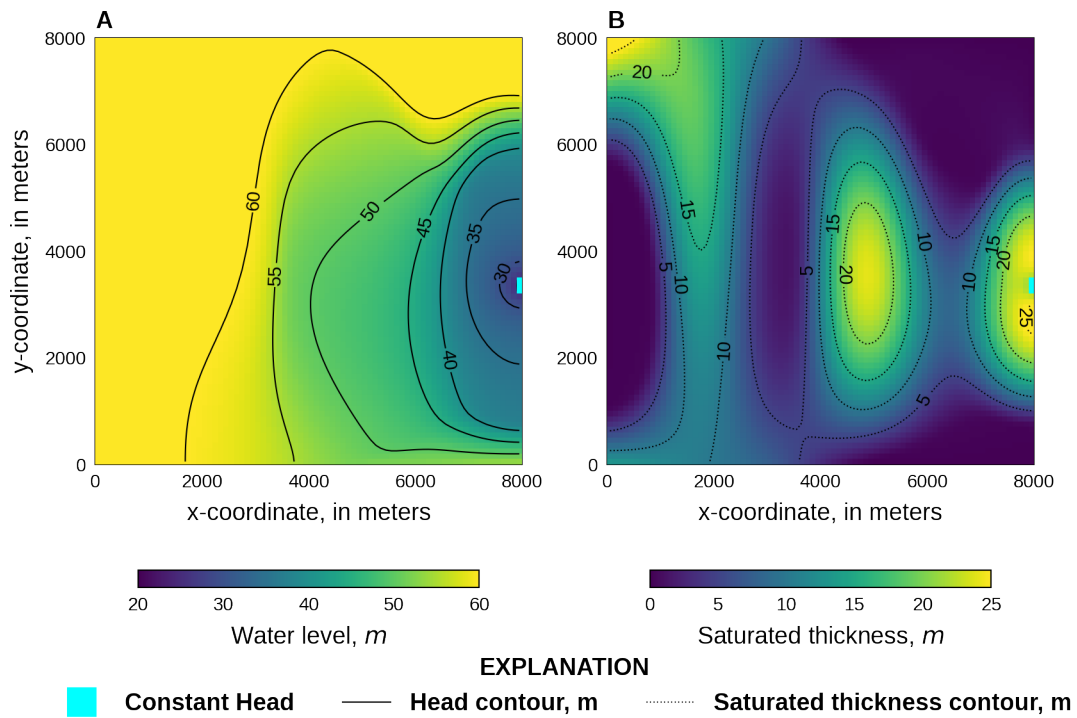


Figure 8–3: Distribution of heads and saturated thicknesses for the high recharge scenario. *A*, heads, and *B*, saturated thicknesses. The location of constant head boundary cells is also shown.

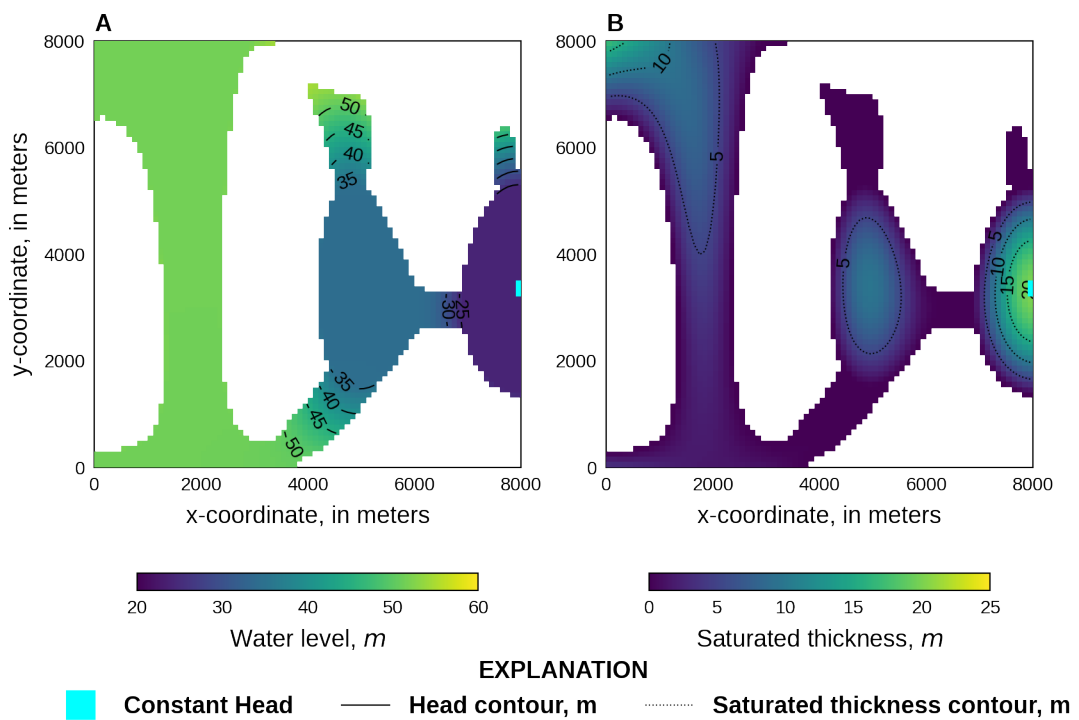


Figure 8–4: Distribution of heads and saturated thicknesses for the low recharge scenario. *A*, heads, and *B*, saturated thicknesses. The white regions indicate cells that have saturated thicknesses less than 1 mm. The location of constant head boundary cells is also shown.

## 9 Zaidel Problem

One of the most challenging numerical cases for MODFLOW arises from drying-rewetting problems often associated with abrupt changes in the elevations of impervious base of a thin unconfined aquifer. This problem simulates a discontinuous water table configuration over a stairway impervious base and flow between constant-head boundaries at the left and right sides of the model domain. This problem is based on the problems that compared the analytical solution of [Zaidel \(2013\)](#) to MODFLOW-NWT (see [Zaidel, 2013](#), figure 6).

### 9.1 Example Description

Model parameters for the example are summarized in table 9–1. The model consists of a grid of 200 columns, 1 row, and 1 layer and a bottom altitude of ranging from 20 to 0 m (fig. 9–1). The discretization is 5 m in the row direction and 1 m in the column direction for all cells. A single steady-stress period with a total length of 1 day is simulated.

Table 9–1: Model parameters for example ex-gwf-zaidel.

Parameter	Value
Number of periods	1
Number of layers	1
Number of rows	1
Number of columns	200
Column width ( <i>m</i> )	5.0
Row width ( <i>m</i> )	1.0
Top of the model ( <i>m</i> )	25.0
Starting head ( <i>m</i> )	23.0
Cell conversion type	1
Horizontal hydraulic conductivity ( <i>m/day</i> )	0.0001
Constant head in column 1 ( <i>m</i> )	23.0

A constant horizontal hydraulic conductivity of 0.0001 *m/d* was specified in all cells. An initial head of 23 *m* was specified in all model cells. Constant head boundary cells were specified in column 1 and 200. The constant head value in column 1 is 23 *m* and was used in all simulations. A constant head value of 1 and 10 *m* was specified in column 200 based on the values evaluated by [Zaidel \(2013\)](#).

### 9.2 Example Results

Simulated results for the case with the constant head in column 200 equal to 1 *m* and 10 *m* are shown in figures 9–1 and 9–2, respectively. Simulated results compare well with the results in [Zaidel \(2013\)](#).

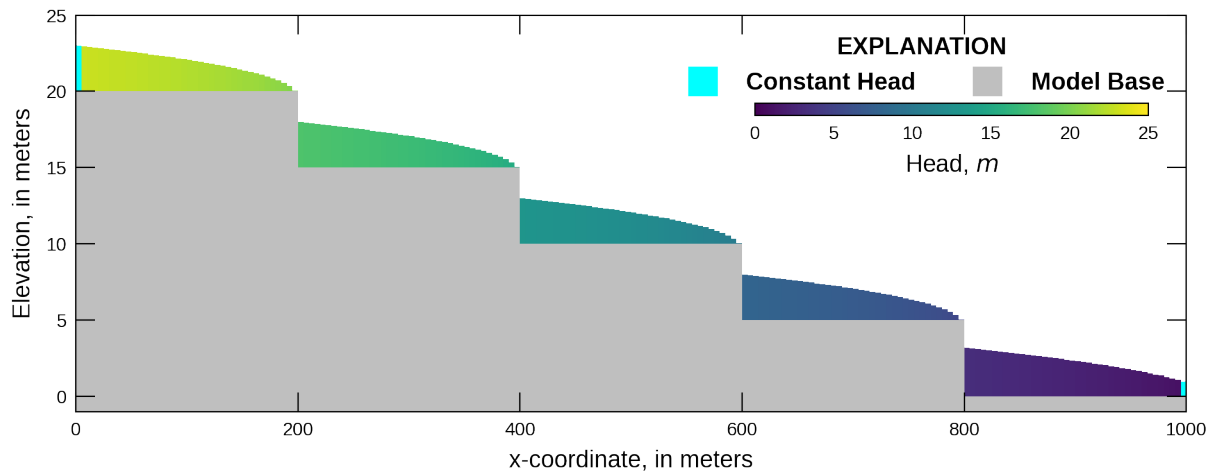


Figure 9–1: Discontinuous water table configuration over a multistep impervious base. Simulated results for the case where the constant head in column 200 is equal to 1 meter is shown. The impervious model base and the location of constant head boundary cells is also shown.

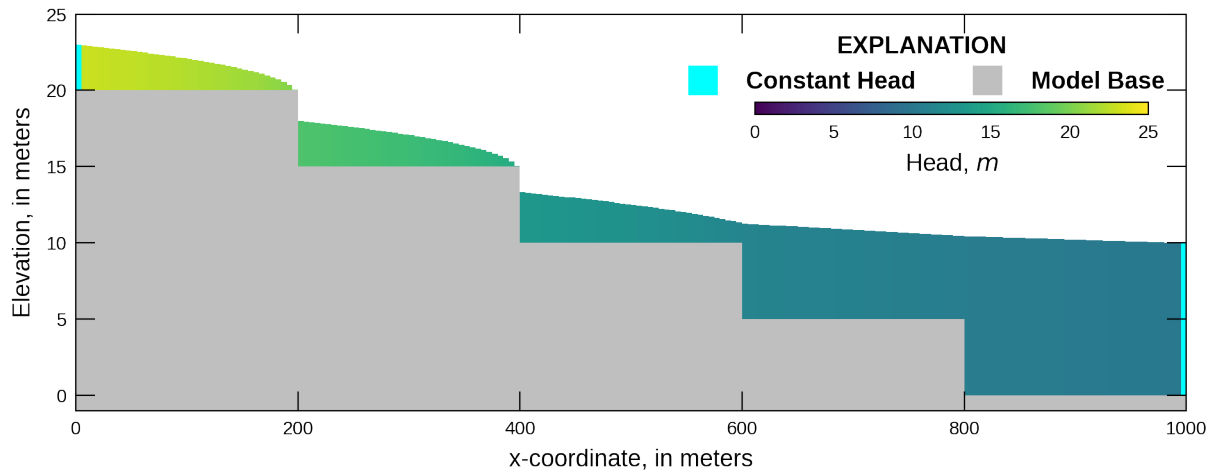


Figure 9–2: Discontinuous water table configuration over a multistep impervious base. Simulated results for the case where the constant head in column 200 is equal to 10 meters is shown. The impervious model base and the location of constant head boundary cells is also shown.

## 10 Streamflow Routing Package Problem 1

This example is a modified version of the Streamflow Routing (SFR) Package described in Prudic and others (2004). The problem has been modified by converting all of the SFR reaches to use rectangular channels.

### 10.1 Conceptual Model

The example represents a hypothetical problem of stream-aquifer interaction for an alluvial basin in a semiarid region in which recharge to the aquifer is primarily leakage from streams that enter the basin from mountains on the northwest, northeast, and southeast (fig. 10–1).

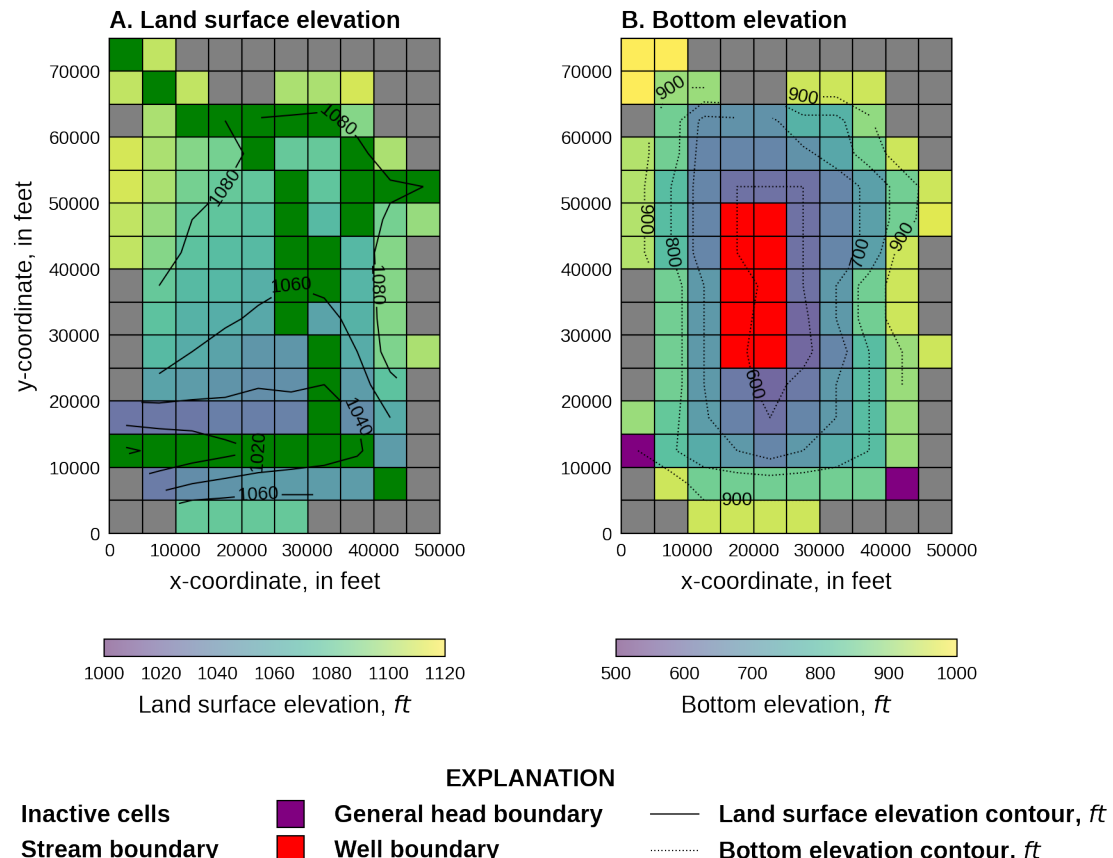


Figure 10–1: Land surface and aquifer bottom elevations. *A.* Land surface elevation. The location of inactive cells and cells with streamflow routing reaches are also shown. *B.* Aquifer bottom elevations. The location of cells with general-head and well boundaries are also shown.

The principal aquifer is unconsolidated deposits of mostly sand and gravel. The mountains consist of bedrock that is many times less permeable than the unconsolidated deposits. Upland areas adjacent to the basin contribute some recharge to the aquifer either as underflow through the perimeter bedrock or from intermittent channels that have small drainage areas. The southern stream is perennial across the valley. Groundwater flow trends in the same direction as the streams.

## 10.2 Example Description

Model parameters for the example are summarized in table 10–1. The model consists of a grid of 10 columns, 15 rows, and 1 layer. The model domain is 50,000 *ft* and 80,000 *ft* in the x- and y-directions, respectively. The discretization is 5,000 *ft* in the row and column direction for all cells. The top of the model ranges from about 1,000 to 1,100 *ft* (fig. 10–1A) and the bottom of the model ranges from about 500 to 1,000 *ft* (fig. 10–1B).

Three stress periods are simulated. The first stress period is steady state and the remaining stress periods are transient. The stress periods are 0, 50, and 50 years in length and are broken up into 1, 50, and 50 time steps. A time step multiplier of 1, 1.1, and 1.1 are used in stress periods 1 through 3, respectively.

Table 10–1: Model parameters for example ex-gwf-sfr-p01.

Parameter	Value
Number of periods	3
Number of layers	1
Number of rows	15
Number of columns	10
Column width ( <i>ft</i> )	5000.0
Row width ( <i>ft</i> )	5000.0
Starting head ( <i>ft</i> )	1050.0
Hydraulic conductivity near the stream ( <i>ft/s</i> )	0.002
Hydraulic conductivity in the basin ( <i>ft/s</i> )	0.0004
Specific storage ( <i>1/s</i> )	1e-6
Specific yield near the stream (unitless)	0.2
Specific yield in the basin (unitless)	0.1
Evapotranspiration rate ( <i>ft/s</i> )	9.5e-8
Evapotranspiration extinction depth ( <i>ft</i> )	15.0

The basin fill thickens toward the center of the valley and hydraulic conductivity of the basin fill is highest in the region of the stream channels. Hydraulic conductivity is  $173 \text{ ft/day}$  ( $2 \times 10^{-4} \text{ ft/s}$ ) in the vicinity of the stream channels and  $35 \text{ ft/day}$  ( $4 \times 10^{-4} \text{ ft/s}$ ) elsewhere in the alluvial basin. A constant specific storage value of  $1 \times 10^{-6}$  ( $1/\text{day}$ ) was specified throughout the alluvial basin. Specific yield is 0.2 (unitless) in the vicinity of the stream channels and 0.1 (unitless) elsewhere in the alluvial basin.

An initial head of 1,050 *ft* is specified in all model layers. Any initial head exceeding the bottom of each cell could be specified since the model is steady-state.

Flow into the system is from infiltration from precipitation and was represented using the recharge (RCH) package. Recharge rates applied to each cell ranged  $2.5 \times 10^{-10}$  to  $2 \times 10^{-9} \text{ ft/s}$ , with lower rates in the vicinity of the stream channels and higher rates elsewhere in the alluvial basin. Flow out of the model is from groundwater evapotranspiration represented by evapotranspiration (EVT) package cells and discharging wells represented by well (WEL) package cells. Groundwater evapotranspiration occurs where depth to water is within 15 *ft* of land surface,

has a maximum rate of 3  $ft/yr$  at land surface, and is coincident with the valley lowland through which several streams flow. Wells are only active in the second stress period and were located in ten cells (rows 6 through 10 and columns 4 and 5) along the west side of the valley (fig. 10–1B). Each well extracted 10  $ft^3/s$  of groundwater for a total withdrawal rate of 100  $ft^3/s$  (about twice the steady-state ground-water inflow). Two general-head boundary cells were added in (row 13, column 1) and (row 14, column 8) with a specified head equal to 988 and 1,045  $ft$ , respectively, and a constant conductance of 0.038  $ft^2/s$ .

The streams in the model domain were represented using a total of 36 reaches. External inflows of 25, 10, and 100  $ft^3/s$  were specified for reach 1, 16, and 28, respectively. Reach 1 is located in (row 1, column 1), reach 16 is in (row 5, column 10), and reach 28 is in (row 14, column 9).

Streamflow discharges from the model at the downstream end of reach 36 in (row 13, column 1). Reach widths were specified to be 12, 0, 5, 12, 55, and 40  $ft$  for reaches 1–9, 10–18, 19–22, 23–27, 28–30, and 31–36, respectively. The remaining streambed properties and stream dimensions used for each stream reach are the same as those used in Pradic and others (2004) (see Pradic and others, 2004, Table 1). Constant stage reaches were used to define the ditch represented by reaches 10–15 and ranged from approximately 1,075.5–1061.6  $ft$ . A diversion from reach 4 to 10 was specified to represent managed inflows to the ditch. Ditch inflows were specified to be 10  $ft^3/s$  except if the downstream flow in reach 4 is less than the specified diversion rate; in cases where the downstream flow in reach 4 is less than the specified diversion rate all of the downstream flow in reach 4 is diverted to the ditch and the inflow to reach

The model uses the Newton-Raphson Formulation. The simple complexity Iterative Model Solver option and preconditioned bi-conjugate gradient stabilized linear accelerator is also used.

### 10.3 Example Results

Simulated results for the initial steady-state stress period and at the end of the stress period with groundwater pumping (stress period 2) are shown in figure 10–2. Reach stage and downstream discharge were also evaluated for reach 4, 14, 27, and 36.

Simulated stage and flow for reach 4 in (row 3, column 4) is shown in figure 10–3A and B. Flow out decreased rapidly when pumping began, but the decrease slowed after only 3 years. The marked change in flow and stream depth was caused by a decline in ground-water levels relative to the head in the stream for all cells corresponding to all the upstream reaches. After 3 years, cells upstream of the reach 4 began to decline below the streambed causing the slope of the decline in flow to decrease. Flow in the stream no longer changed after about 9 years of pumping because the ground-water level in cells corresponding to the reaches upstream of reach 4 had declined below the streambed and the leakage rates had become constant. Once withdrawals ceased, flow began to increase in the last reach of segment 5 after about 21 yrs after pumping had ceased and after about 19 yrs in reach 4. The increase of flow in reach 4 during the recovery period was slower than the decrease in flow during the pumping period and largely was controlled by the gradual recovery of ground-water levels in areas distant from the pumping wells.

The last reach (reach 15) along the ditch (reaches 10–15) was used to illustrate how the option of specifying stream stage works when flow in a channel ceases and when flow commences again (fig. 10–3C and D). The stream stage and related depth is constant in reaches 10–15 as long as there is flow in the reach. Once flow in the reach ceases, the streambed elevation (depth = 0) is used for comparing head differences between the stream and groundwater. The slight lag between when flow out of the reach went to zero and when stream depth went to zero during the rapid decline was the result of all inflow into the reach leaking through the streambed. Inflow into the reach ceases during the following time step and consequently the entire reach became dry and stream depth became zero.

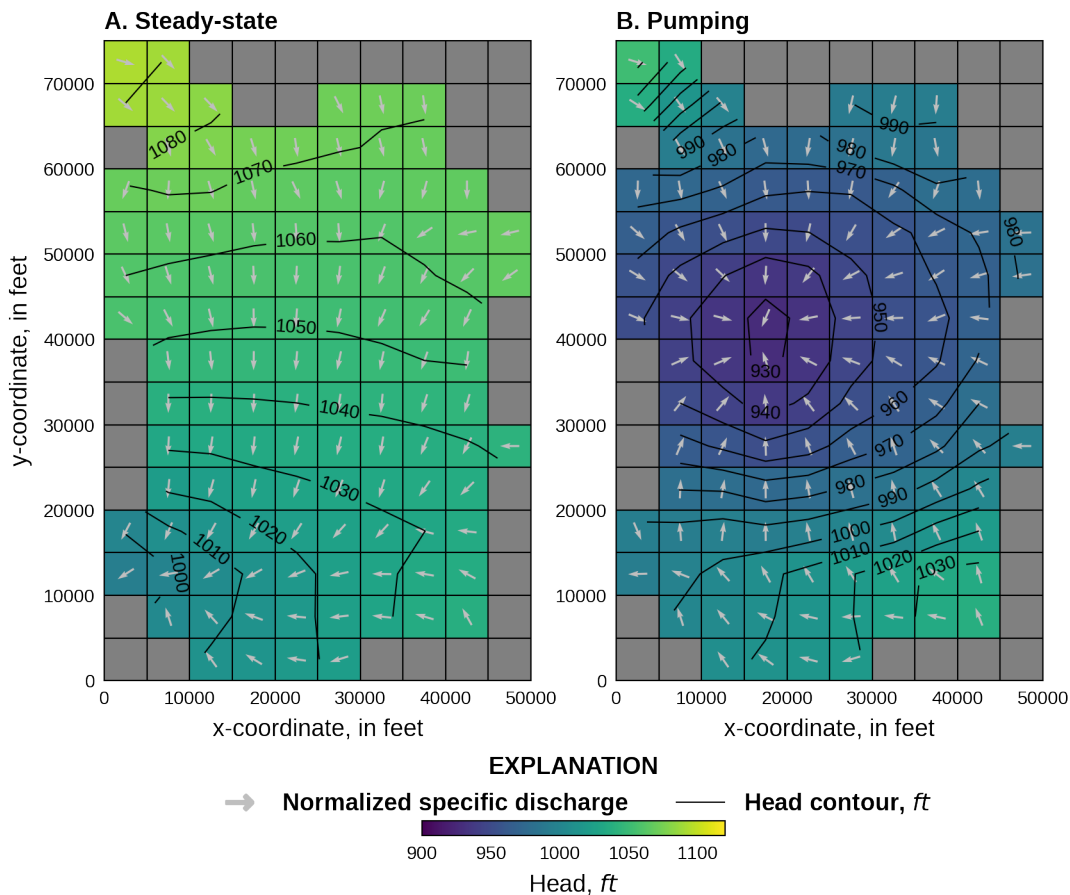


Figure 10–2: Simulated water levels and normalized specific discharge vectors under steady state and pumping conditions. *A.* steady-state results. *B.* results after 50 years of pumping.

The same lag occurred during the recovery period and was again caused by all inflow into the reach leaking through the streambed. Outflow from the last reach did not occur until inflow into the reach exceeded that which could leak through the streambed.

Flow in reach 27 (fig. 10-3E and F) is used to illustrate what happens when there is no inflow from upstream reaches, but the groundwater level in the corresponding model cell is higher than the elevation of the streambed. Flow and stream depth decreased rapidly in the pumping (second stress) period and depth became zero after only 2 years, even though there was still a small quantity of outflow from the reach. The reason for stream depth being zero with minor outflow is that the only source of water to the reach is from ground-water leakage. When this occurs, stream depth at the midpoint of the reach is set to zero and the stream head at the midpoint is equal to the streambed elevation.

In the steady-state stress period (stress period 1), reach 36 is generally gaining, but became losing during the pumping period (stress period 2). Streamflow out of the reach and the depth decreased during the pumping period (fig. 10-3G and H) because inflow from upstream reaches declined and because leakage in the reach switched from flow out of the aquifer into the stream to flow from the stream into the aquifer. Although the water table declined in all cells corresponding to reaches 28–36, the water table did not decline below the streambed and consequently, streambed leakage did not become constant. Once pumping ceases, flow in the reach increases in a manner similar to how it decreased. The slight increase in flow after 70 years was due to an increase in flow from reaches upstream of reach 27. The response in reach 36 after pumping ceases in stress period 3 was much different than that for reach 4 and 27 (compare fig. 10-3H with fig. 10-3B) because groundwater levels did not decline below the bottom of the streambed beneath reaches 31–36 whereas they did beneath reaches 1–4.

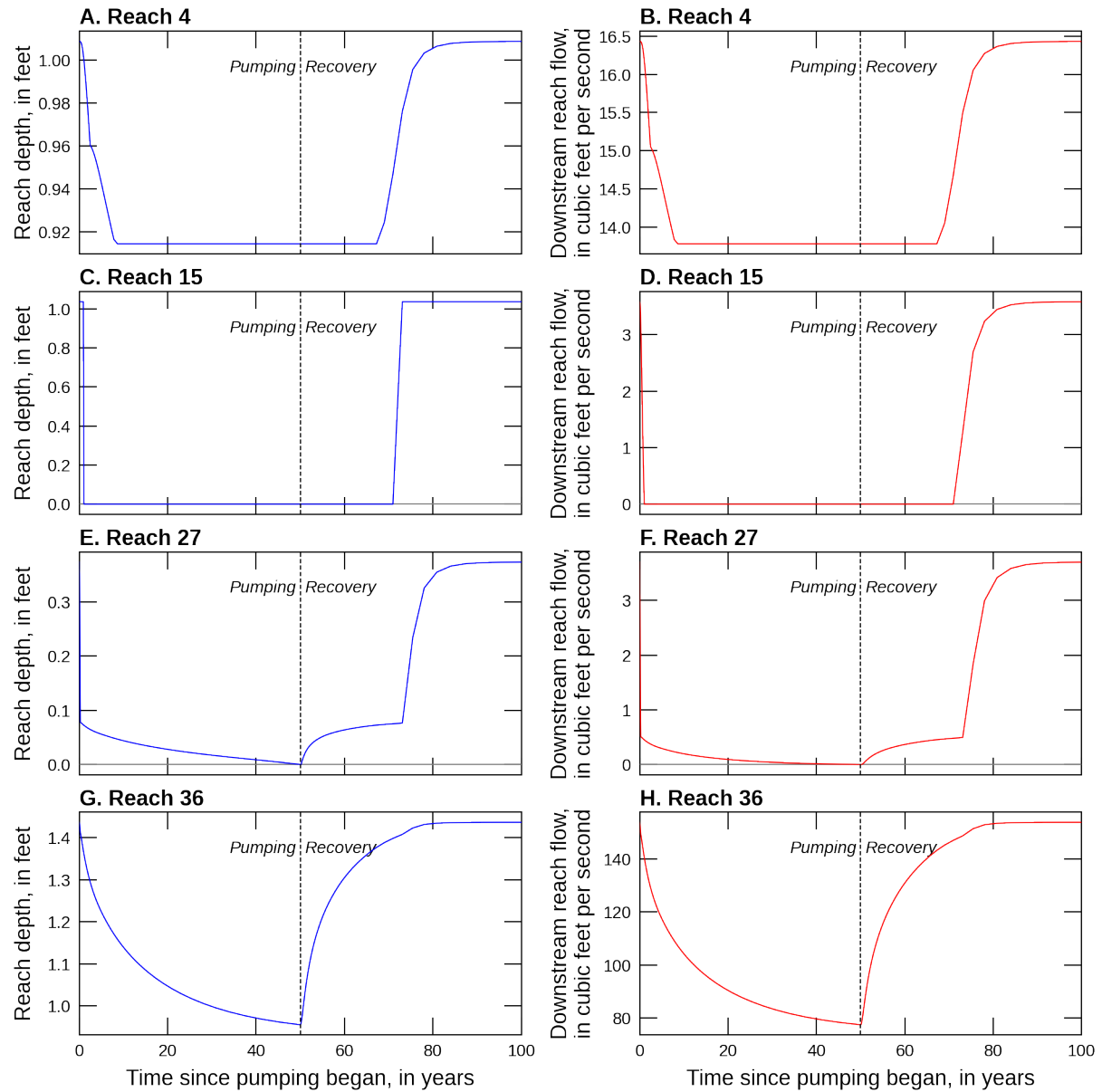


Figure 10-3: Simulated reach depth and downstream discharge at select reaches. *A.* Stage in reach 4. *B.* Downstream discharge in reach 4. *C.* Stage in reach 15. *D.* Downstream discharge in reach 15. *E.* Stage in reach 27. *F.* Downstream discharge in reach 27. *G.* Stage in reach 36. *H.* Downstream discharge in reach 36.

## 11 Advanced Packages with MVR

The Advanced MODFLOW 6 Packages example problem is designed to demonstrate the combined use of the UZF, SFR and LAK Packages in MODFLOW 6. It originally appeared in the “Getting Started” pdf document in the MODFLOW 6-docs.git repository, and is included here for completeness of the examples.

Flows exchanged between the advanced packages (i.e., UZF, SFR, and LAK) and the WEL package are made with the MVR Package. The problem was adapted from a previously developed test problem documented in [Pradic and others \(2004\)](#) and [Niswonger and Pradic \(2005\)](#) and represents a developed basinfill aquifer in the northern Great Basin. Streamflow enters the valley from three perennial streams. Because the valley is much lower in altitude than the surrounding uplands, recharge in the valley floor is relatively low as compared to recharge from streams and lakes that receive flow from precipitation falling in the mountains. In the lowland areas, native plants use the ground water. Two lakes were added to the original test problem to illustrate the capabilities of the Lake Package (figure 11-1).

The topography, and the locations of streams and lakes within the basin are shown in figure 11-1. Note that unlike the streamflow routing package for MODFLOW-2005, the SFR Package for MODFLOW 6 does not support designation of stream segments. Stream networks now consist solely of reaches that are numbered consecutively from 1 to the total number of reaches, and all stream property information is input on a reach basis. The simulation also includes and general head boundary conditions (GHB Package) and 10 agricultural wells. Aquifer properties are provided in table 11-1.

Table 11-1: Model parameters for example ex-gwf-sfr-p01b.

Parameter	Value
Number of periods	24
Number of layers	2
Number of rows	15
Number of columns	10
Column width (ft)	5000.0
Row width (ft)	5000.0
Starting head (ft)	varies
Hydraulic conductivity near the stream (ft/s)	0.002
Hydraulic conductivity in the basin (ft/s)	varies
Lakebed leakance (1/s)	2e-9
Specific storage (1/s)	0.1e-5
Specific yield near the stream (unitless)	0.2
Specific yield in the basin (unitless)	0.1
Evapotranspiration rate (ft/s)	9.5e-8
Evapotranspiration extinction depth (ft)	15.0

### 11.1 Example Results

Unlike the original UZF1 Package ([Niswonger and others, 2006](#)) for MODFLOW-2005, the UZF Package for MODFLOW 6 can simulate unsaturated flow separately for each layer. Thus, rather than simulating homogenous unsaturated flow between the water table and land surface, the unsaturated zone in cells in different MODFLOW layers can be specified with different unsaturated hydraulic properties to represent vertical heterogeneity. Results from the UZF Package are shown below for the cell at row 5, column 2, layers 1 and 2 (the infiltration is shown for the cell in layer 1 while the

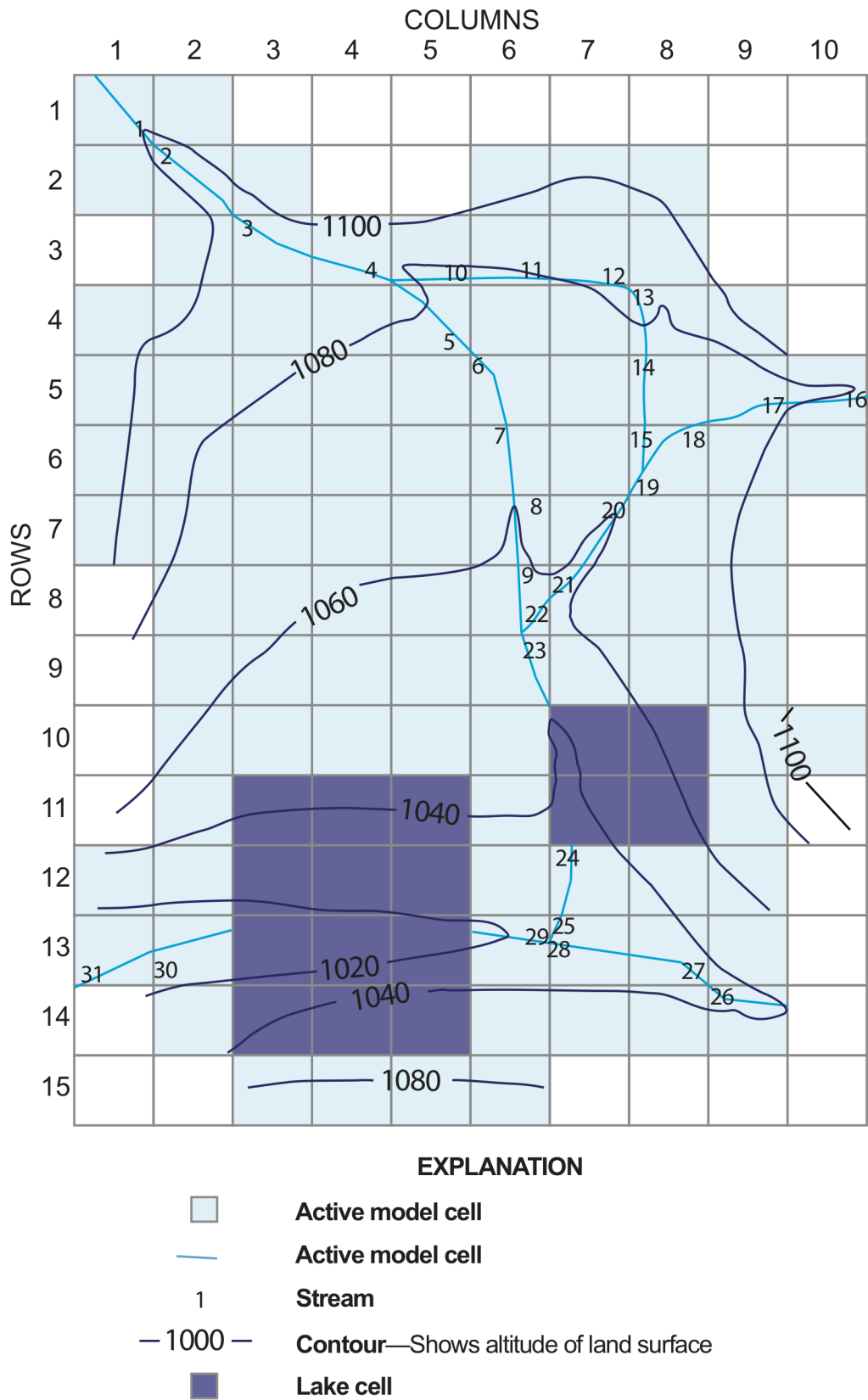


Figure 11–1: Plan view of lakes and stream reaches in the MODFLOW 6 model that demonstrates usage of the MVR package with the advanced packages (i.e., UZF, SFR, LAK) and includes a linkage with the WEL package.

recharge occurs in layer 2. The moisture content is for the cell located in layer 1). The unsaturated-zone package is ideal for simulating the delay between when water infiltrates at land-surface and recharges the saturated zone.

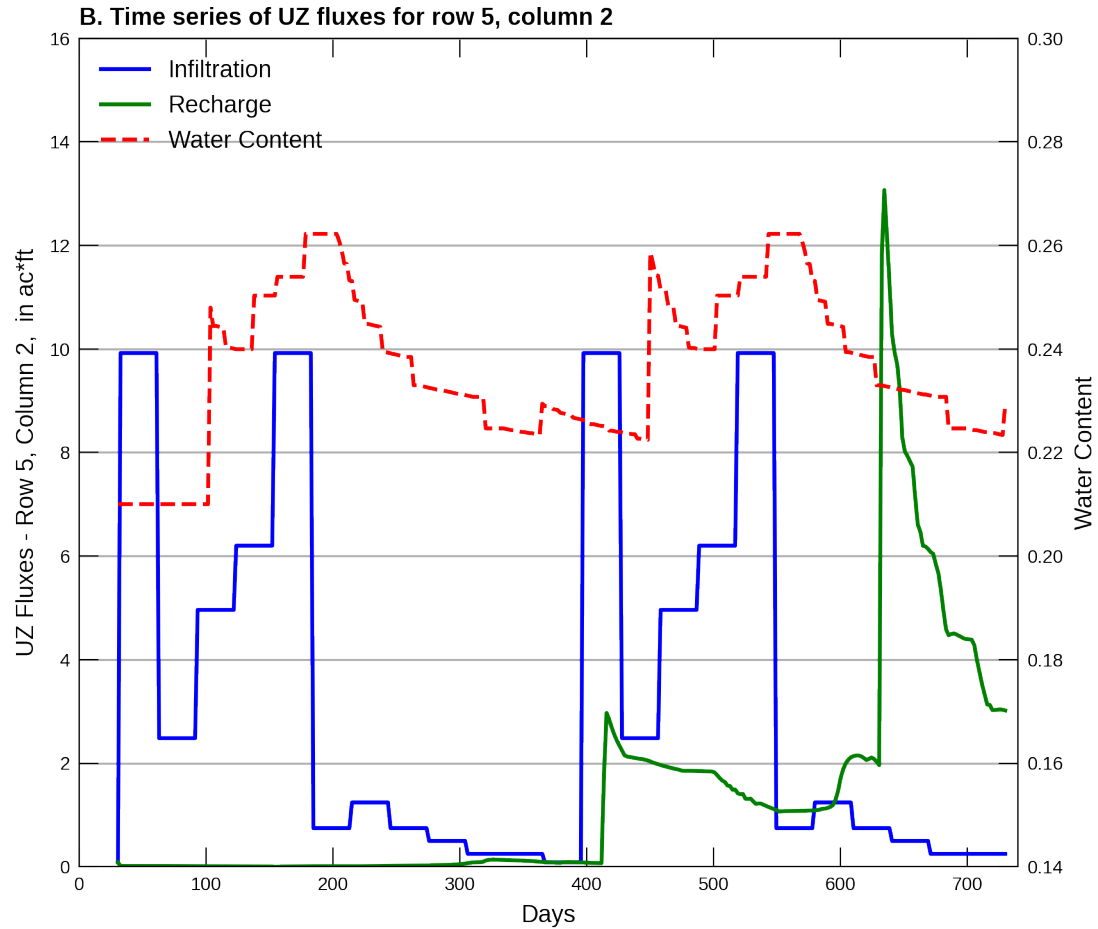


Figure 11–2: Simulated infiltration and recharge to and from the unsaturated-zone (left y-axis), respectively, for the cells located at row 5 column 2, including the moisture content of the cell in layer 1 (right y-axis).

Additionally, after calculating any rejected infiltration based on the user-specified infiltration rate, the unsaturated-zone package will partition the net infiltration into evapotranspiration (ET), changes in soil moisture storage, and recharge as mentioned above. For this problem, the MVR package is used to transfer pumped groundwater (WEL package) to land surface for simulating irrigation with groundwater. Figure 11–3 shows the monthly totals of pumped water used for irrigation for each month of the simulation. Figure 11–3 also shows the total runoff, primarily groundwater discharge to land surface (spring flow) that is transferred to the stream network (or lakes) using the MVR package.

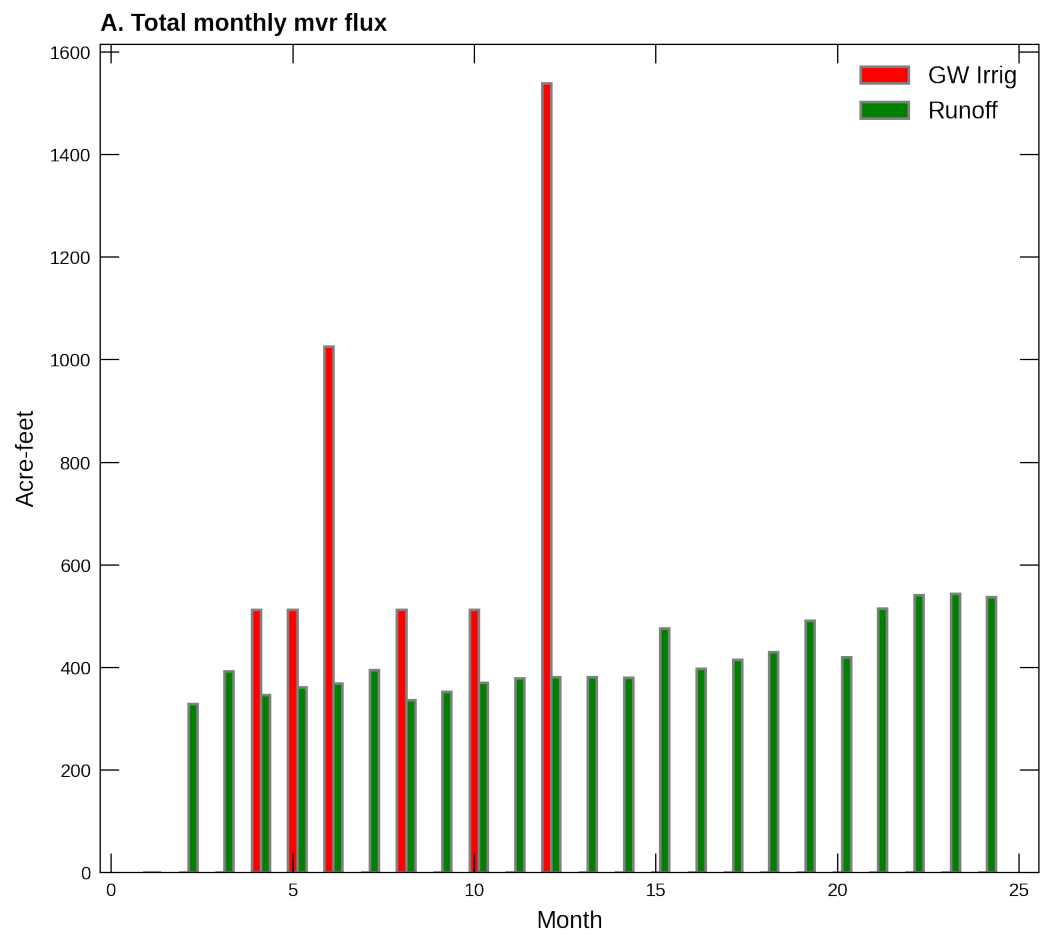


Figure 11–3: Monthly totals of pumped water from all 10 simulated wells transferred to UZF cells via the MVR package. Total monthly runoff amounts transferred to the surface water network are also shown.

## 12 Lake Package Problem 1

This example is based on problem 1 in the Lake (LAK) Package for MODFLOW-2000 described in [Merritt and Konikow \(2000\)](#). The example represents a lake surrounded by a surficial aquifer (fig. 12–1).

### 12.1 Example Description

Model parameters for the example are summarized in table 12–1. The model consists of a grid of 17 columns, 17 rows, and 5 layers. The model domain is 13,000 *ft* in the x- and y-directions. The discretization is in the row and column directions ranges from 250 to 1,000 *ft* and is 500 *ft* in the center of the model domain where the lake is located (fig. 12–1). The top of the model is specified to be 500 *ft* and the bottom of each layer is specified to be 107, 97, 87, 77, and 67 *ft*. Groundwater flow was inactivated in the location of the lake in model layers 1 and 2 by specifying an IDOMAIN value of zero in these cells.

One transient stress period 5,000 days in length is simulated. The stress period has 100 time steps and uses a time step multiplier equal to 1.02, which results in time step lengths that range 16.01 to 113.74 days.

Table 12–1: Model parameters for example ex-gwf-lak-p01.

Parameter	Value
Number of periods	1
Number of layers	5
Number of rows	17
Number of columns	17
Top of the model ( <i>ft</i> )	500.0
Bottom elevations ( <i>ft</i> )	107., 97., 87., 77., 67.
Starting head ( <i>ft</i> )	115.0
Horizontal hydraulic conductivity ( <i>ft/d</i> )	30.0
Vertical hydraulic conductivity ( <i>ft/d</i> )	1179., 30., 30., 30., 30.
Specific storage ( <i>1/d</i> )	3e-4
Specific yield (unitless)	0.2
Constant head on left side of model ( <i>ft</i> )	160.0
Constant head on right side of model ( <i>ft</i> )	140.0
Aereal recharge rate ( <i>ft/d</i> )	0.0116
Maximum evapotranspiration rate ( <i>ft/d</i> )	0.0141
Evapotranspiration extinction depth ( <i>ft</i> )	15.0
Starting lake stage ( <i>ft</i> )	110.0
Lake evaporation rate ( <i>ft/d</i> )	0.0103
Lakebed leakance ( <i>1/d</i> )	0.1

The horizontal and vertical hydraulic conductivity is 30 *ft/day* except for the vertical hydraulic conductivity of layer 1 which was specified to be 1,179 *ft/d*. A constant specific storage value of  $3 \times 10^{-4}$  (*1/day*) and specific yield of 0.2 (unitless) were specified. All model layers were specified to convert between confined and unconfined conditions. An initial head of 115 *ft* was specified in all model layers.

Flow into the system is from infiltration from precipitation and was represented using the recharge (RCH) package and a constant recharge rate of 0.0116 *ft/d*. Flow out of the model is from groundwater evapotranspiration represented by evapotranspiration (EVT) package cells. Groundwater evapotranspiration occurs where depth to water is within 15 *ft* of land surface, has a

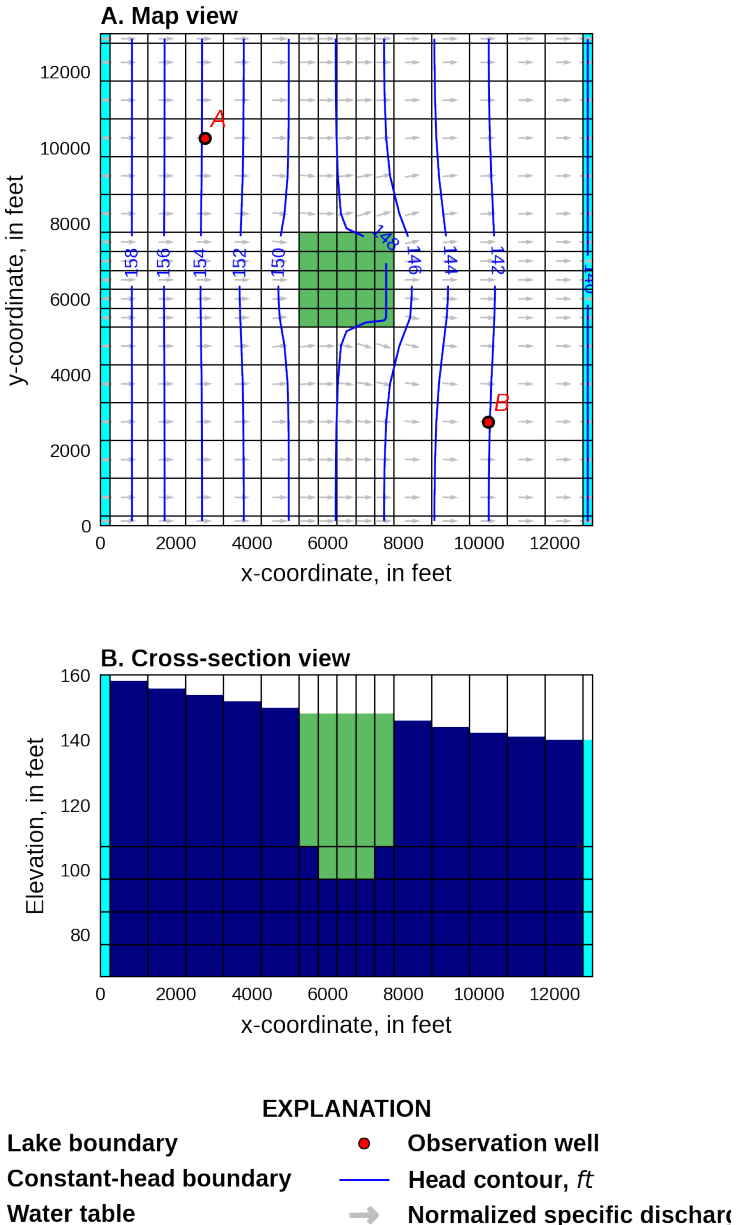


Figure 12–1: Lateral and vertical grid discretization. *A.* Map view. The location of lake and constant head boundary cells are also shown. Simulated heads and lake stage at the end of stress period 1, normalized specific discharge vectors, and the location of two observation locations are also shown. *B.* Cross-section view. The location of lake and constant head boundaries are also shown. The water table and lake stage at the end of stress period 1 are also shown.

maximum rate of  $0.0141 \text{ ft/d}$  at land surface. The evapotranspiration surface, the elevation in the aquifer below which evapotranspiration is assumed to decline linearly, is represented as linearly sloping from  $160 \text{ ft}$  on the left side of the model to  $140 \text{ ft}$  on the right side of the model, except in the lake area, where the elevation is specified as  $3 \text{ ft}$  below the lakebed, which is equal to  $2 \text{ ft}$  below the layer bottom elevation. This means that in the possible case of lake drying, land-surface evapotranspiration from the water table under the dry lakebed is at the maximum rate if the water table is not deeper than  $3 \text{ ft}$  below the lakebed. Away from the lake, the evapotranspiration surface is an implicit representation of land surface, since the latter is normally equal to or slightly above the evapotranspiration surface. Constant head boundary cells were added in column 1 and column 17 in all rows and layers; constant heads are specified to be  $160$  and  $140 \text{ ft}$  on the left and right sides of the model, respectively.

The lake is located in the center of the model domain in model layers 1 and 2 and has an initial stage of  $110 \text{ ft}$ . The lake is connected horizontally to the aquifer in model layers 1 and 2 and vertically to cells in model layer 2 and 3 that directly underly the lake. A lakebed leakance value of  $0.1 \text{ 1/d}$  was specified for all lake connections to the aquifer. The connection length for horizontal lake connections were calculated from grid dimensions and are  $500 \text{ ft}$  in layer 1 and  $250 \text{ ft}$  in layer 2; the connection width for horizontal connections was  $500 \text{ ft}$ . Rainfall and evaporation rates equal to  $0.0116$  and  $0.0103 \text{ ft/d}$  are specified for the lake, respectively.

The model uses the Newton-Raphson Formulation. The simple complexity Iterative Model Solver option and preconditioned bi-conjugate gradient stabilized linear accelerator is also used.

## 12.2 Example Results

Simulated results at the end of the stress period are shown in figure 12–1. Transient results for the lake stage and groundwater heads at two aquifer locations are shown in figure 12–2. Both water-table elevations and the lake stage converge asymptotically to equilibrium values. The water-table elevations approximately converge in about 1,000 days and the lake stage in about 2,000 days of simulation time.

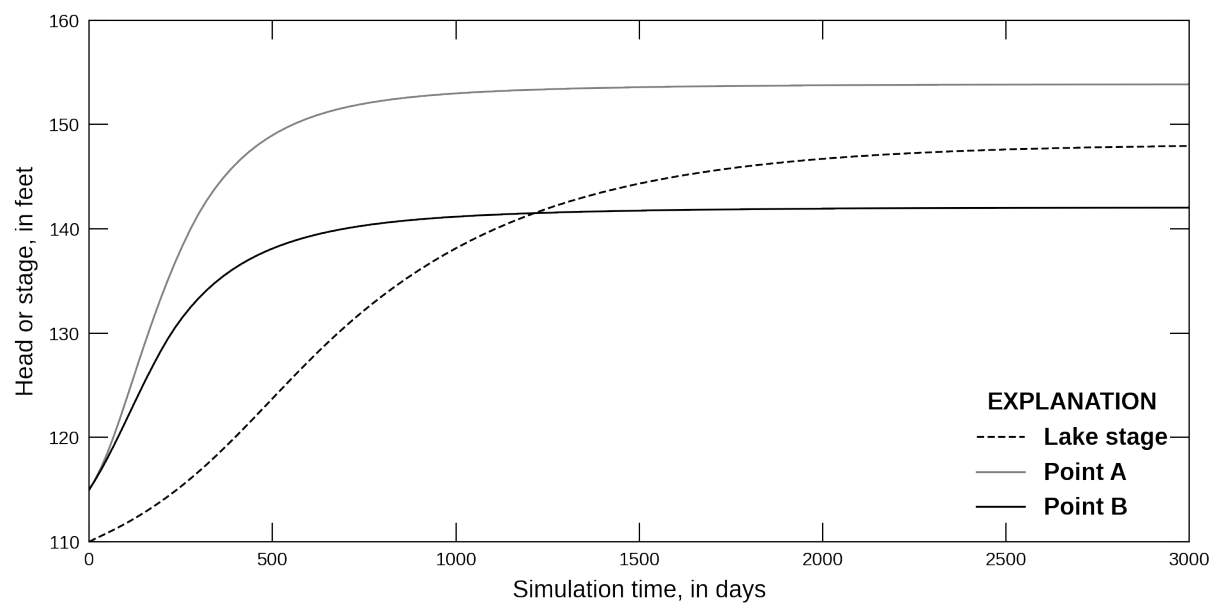


Figure 12–2: Selected heads in the aquifer and the lake stage. The location of points A and B are shown in figure 12–1.

## 13 Lake Package Problem 2

This example is based on problem 2 in the Lake (LAK) Package for MODFLOW-2000 described in [Merritt and Konikow \(2000\)](#). The example represents a two lakes connected by a stream surrounded by a surficial aquifer (fig. 13-1). The problem has been modified to use the Newton-Raphson Formulation instead of the Standard Conductance Formulation with Node Property Flow (NPF) Package rewetting option.

### 13.1 Example Description

Model parameters for the example are summarized in table 13-1. The model consists of a grid of 17 columns, 27 rows, and 5 layers. The model domain is 13,000 and 20,500 *ft* in the x- and y-directions, respectively. The discretization is in the row and column directions ranges from 250 to 1,000 *ft* and is 500 *ft* where the lakes are located (fig. 13-1). The top of the model is specified to be 200 *ft* and the bottom of each layer is specified to be 102, 97, 87, 77, and 67 *ft*. Groundwater flow was inactivated in the location of the lakes in model layers 1 and 2 by specifying an IDOMAIN value of zero in these cells.

One transient stress period 1,500 days in length is simulated. The stress period has 200 time steps and uses a time step multiplier equal to 1.005, which results in time step lengths that range 4.40 to 11.82 days.

Table 13-1: Model parameters for example ex-gwf-lak-p02.

Parameter	Value
Number of periods	1
Number of layers	5
Number of rows	27
Number of columns	17
Top of the model ( <i>ft</i> )	200.0
Bottom elevations ( <i>ft</i> )	102., 97., 87., 77., 67.
Starting head ( <i>ft</i> )	115.0
Horizontal hydraulic conductivity ( <i>ft/d</i> )	30.0
Vertical hydraulic conductivity ( <i>ft/d</i> )	30.0
Specific storage ( <i>1/d</i> )	3e-4
Specific yield (unitless)	0.2
Constant head on left side of model ( <i>ft</i> )	160.0
Constant head on right side of model ( <i>ft</i> )	140.0
Areal recharge rate ( <i>ft/d</i> )	0.0116
Maximum evapotranspiration rate ( <i>ft/d</i> )	0.0141
Evapotranspiration extinction depth ( <i>ft</i> )	15.0
Starting lake stage ( <i>ft</i> )	130.0
Lake evaporation rate ( <i>ft/d</i> )	0.0103
Lakebed leakance ( <i>1/d</i> )	0.1

The horizontal and vertical hydraulic conductivity is 30 *ft/d*. A constant specific storage value of  $3 \times 10^{-4}$  (*1/day*) and specific yield of 0.2 (unitless) were specified. All model layers were specified to convert between confined and unconfined conditions. An initial head of 115 *ft* was specified in all model layers.

Flow into the system is from infiltration from precipitation and was represented using the recharge (RCH) package and a constant recharge rate of 0.0116 *ft/d*. Flow out of the model is from groundwater evapotranspiration represented by evapotranspiration (EVT) package cells. Groundwater evapotranspiration occurs where depth to water is within 15 *ft* of land surface, has a

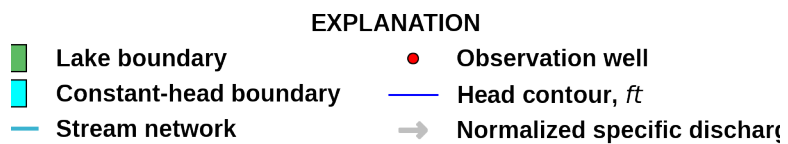
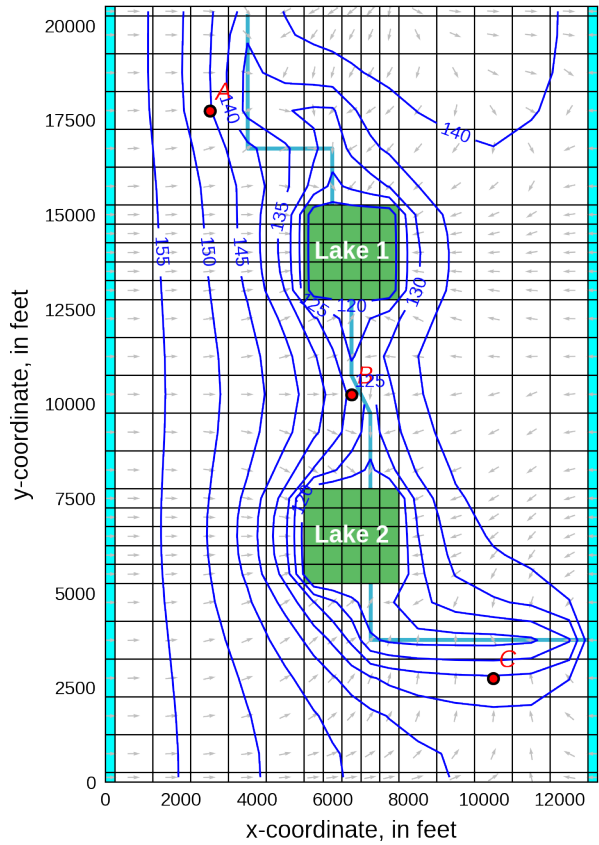


Figure 13–1: Lateral grid discretization. The location of lake and constant head boundary cells are also shown. Simulated heads and lake stage at the end of stress period 1, normalized specific discharge vectors, and the location of three observation locations are also shown.

maximum rate of  $0.0141 \text{ ft/d}$  at land surface. The evapotranspiration surface, the elevation in the aquifer below which evapotranspiration is assumed to decline linearly, is represented as linearly sloping from  $160 \text{ ft}$  on the left side of the model to  $140 \text{ ft}$  on the right side of the model, except in the lake area, where the elevation is specified as  $3 \text{ ft}$  below the lakebed, which is equal to  $2 \text{ ft}$  below the layer bottom elevation. This means that in the possible case of lake drying, land-surface evapotranspiration from the water table under the dry lakebed is at the maximum rate if the water table is not deeper than  $3 \text{ ft}$  below the lakebed. Away from the lake, the evapotranspiration surface is an implicit representation of land surface, since the latter is normally equal to or slightly above the evapotranspiration surface. Constant head boundary cells were added in column 1 and column 17 in all rows and layers; constant heads are specified to be  $160$  and  $140 \text{ ft}$  on the left and right sides of the model, respectively.

The lakes are located in the center of the finest resolution model cells ( $500 \text{ ft}$ ) in model layers 1 and 2 and have an initial stage of  $130 \text{ ft}$ . The lakes are connected horizontally to the aquifer in model layers 1 and 2 and vertically to cells in model layer 2 and 3 that directly underly the lake. A lakebed leakage value of  $0.1 \text{ l/d}$  was specified for all lake connections to the aquifer. The connection length for horizontal lake connections were calculated from grid dimensions and are  $500 \text{ ft}$  in layer 1 and  $250 \text{ ft}$  in layer 2; the connection width for horizontal connections was  $500 \text{ ft}$ . Rainfall and evaporation rates equal to  $0.0116$  and  $0.0103 \text{ ft/d}$  are specified for the lake, respectively. Outlets were defined for both lakes in order to connect the lakes with the stream network. Outlet discharge for lake 1 and 2 were calculated by Manning's formula, an outlet width of  $5 \text{ ft}$ , and a roughness coefficient of  $0.05$ . The outlet elevation and slope for lake 1 is  $114.85 \text{ ft}$  and  $8.21 \times 10^{-4} \text{ ft/ft}$ . The outlet elevation and slope for lake 2 is  $109.43 \text{ ft}$  and  $9.46 \times 10^{-4} \text{ ft/ft}$ .

The stream network was represented using the Streamflow Routing (SFR) Package. The stream network was discretized using 22 reaches. The length of each reach is obtained from the dimensions of the model grid ( [13-1](#) ). Most reaches are specified to be  $1,000 \text{ ft}$  in length and all are at least  $500 \text{ ft}$  in length. The stream network flowing into lake 1 has 8 reaches. The elevation of the top of the streambed drops from  $124$  to  $117 \text{ ft}$  between the centers of the upper and lower reaches. The stream network connecting lake 1 and 2 has 6 reaches and flows out of lake 1 and into lake 2. The elevation of the top of the streambed at the reach centers drops from  $114.5$  to  $111 \text{ ft}$  in the segment. The stream network flowing out of lake 2 and discharging from the model domain has 8 reaches. The top of the streambed at the reach centers drops from  $109$  to  $103 \text{ ft}$  in the segment. The streambed is assumed to be  $0.5 \text{ ft}$  thick everywhere, and arbitrary uniform values are assigned for streambed hydraulic conductivity ( $0.5 \text{ ft/d}$ ), stream width ( $5 \text{ ft}$ ), and roughness coefficient ( $0.05$ ). Stream stage is calculated by Manning's formula. The streambed hydraulic conductivity value is sufficiently high to allow small exchanges of water with the surficial aquifer. In this example, it is assumed that there is no precipitation on the stream surface, evaporation from the stream surface, or overland runoff to the stream. An arbitrary inflow amount of  $6.9 \times 10^5 \text{ ft}^3/\text{d}$  is assigned to the uppermost reach in the system.

The Mover (MVR) Package is used to move water from the stream (reach 8) flowing into lake 1, lake 1 into the stream (reach 9) connecting lake 1 and 2, the reach connecting lake 1 and 2 (reach 14) into lake 2, and flowing from lake 2 in to the stream (reach 15) discharging from the model in reach 22.

The model uses the Newton-Raphson Formulation. The simple complexity Iterative Model Solver option and preconditioned bi-conjugate gradient stabilized linear accelerator is also used.

## 13.2 Example Results

Simulated results at the end of the stress period are shown in figure 13–1. Transient results for lake stages and groundwater heads at three aquifer locations are shown in figure 13–2.

Because of the stream connections, lake stages decrease from the initial stage of 130 ft (fig. 13–2A) and remain well below the stage computed for the isolated lake in Lake Package Problem 1. Lake stages decrease during the first 60 days of the simulation and increase slightly during the remainder of the simulation as aquifer heads increase. By time step 200, at the end of the 1,500 day simulation, aquifer heads in the interior part of the grid have greatly increased from the initial head of 115 ft except in the immediate vicinity of the lakes (figs 13–1 and 13–2B). With an outflow elevation to a stream segment of 114.85 ft, the stage of lake 1 converges to 116.98 ft, and with a stream outflow elevation of 109.4 ft, the stage of lake 2 converges to 111.93 ft. These stages are 30–35 ft below the equilibrium stage of the isolated lake of Lake Package Problem 1 (148.14 ft).

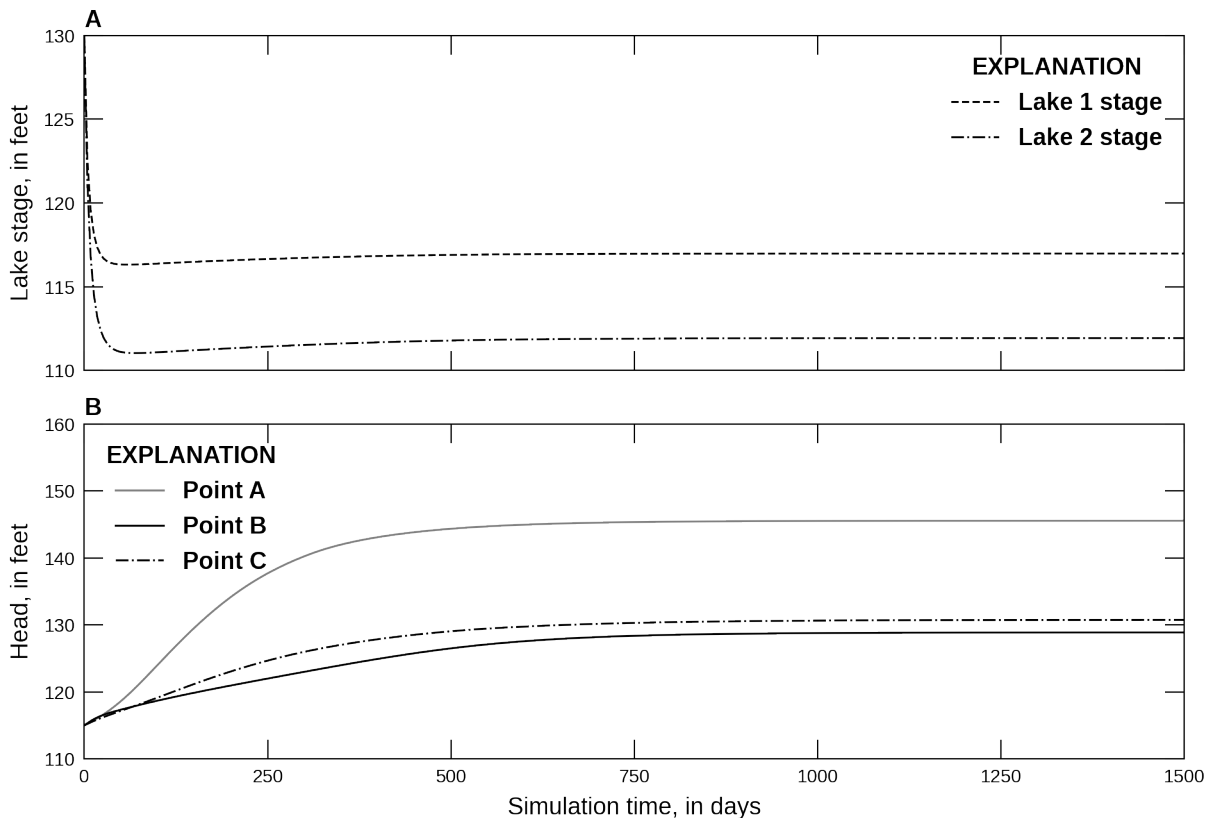


Figure 13–2: Lake stages and selected heads in the aquifer. A. Lake stages. The location of lake 1 and 2 are shown in figure 13–1. B. Heads in the aquifer. The location of points A, B, and C are shown in figure 13–1.

The stream system acts as a highly effective drain for the lake/aquifer system. The depth of flow in stream connecting lake 1 and 2 is about 2.1–2.3 ft and the depth of flow in stream discharging from lake 2 is generally is about 1.6–2 ft. The volume of water leaking from the aquifer to the stream generally is about 2 to 7 percent of the downstream flow in each reach.

## 14 Neville-Tonkin Multi-Aquifer Well Problem

This is the multi-aquifer well simulation described in [Neville and Tonkin \(2004\)](#). The example simulates an upper and lower aquifer separated by an impermeable confining unit but connected by a well that is open across both aquifers.

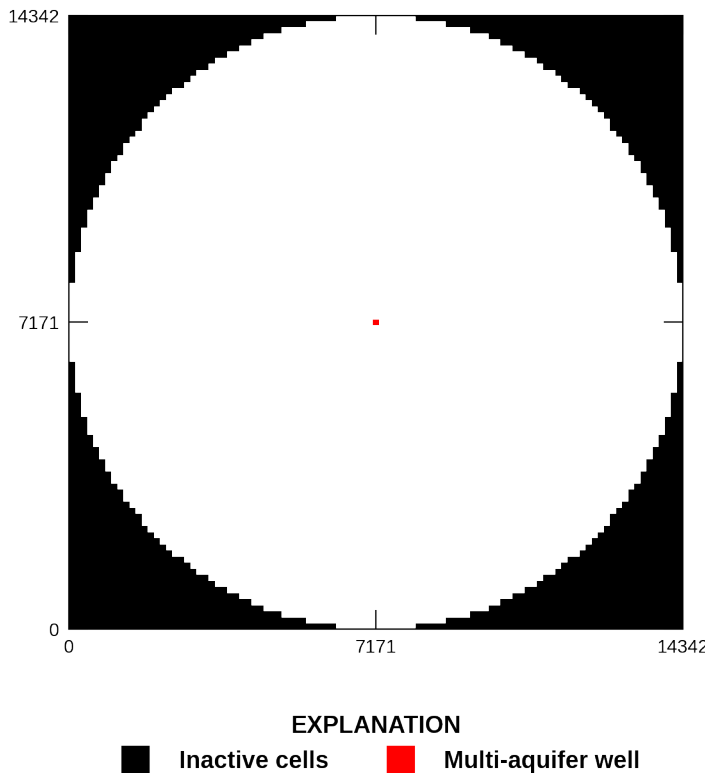


Figure 14–1: Location of inactive cells and the multi-aquifer well.

### 14.1 Example Description

Model parameters for the example are summarized in table 14–1. The model consists of a grid of 101 columns, 101 rows, and 2 layers. The model domain is 14,342 m in the x- and y-directions (fig. 14–1). The discretization is in the row and column directions is 142 m. The top of the model is specified to be -50 m and the bottom of each layer is specified to be 142.9 and -514.5 m. Groundwater flow was inactivated beyond a distance of 7,163 m from the center cell (row 51, column 51) in model layers 1 and 2 by specifying an IDOMAIN value of zero in these cells (fig. 14–1).

One transient stress period 2.1314815 days in length is simulated. The stress period has 50 time steps and uses a time step multiplier equal to 1.2, which results in time step lengths that range  $0.51 \times 10^{-4}$  to 0.39 days. A short simulation time is specified to prevent the effect of the well propagating to the model boundary.

Table 14–1: Model parameters for example ex-gwf-maw-p01.

Parameter	Value
Number of periods	1
Number of layers	2
Number of rows	101
Number of columns	101
Column width ( $m$ )	142.0
Row width ( $m$ )	142.0
Top of the model ( $m$ )	-50.0
Bottom elevations ( $m$ )	-142.9, -514.5
Starting head ( $m$ )	3.05, 9.14
Horizontal hydraulic conductivity ( $m/d$ )	1.0
Vertical hydraulic conductivity ( $m/d$ )	1.0e-16
Specific storage ( $1/d$ )	1e-4
Well radius ( $m$ )	0.15

The horizontal and vertical hydraulic conductivity is 1 and  $1 \times 10^{-16} m/d$ . The transmissivity of the upper and lower aquifer is 92.9 and  $371.6 m^2/d$ . A constant specific storage value of  $1 \times 10^{-4} (1/d)$  is specified. All model layers are specified to be confined. An initial head of 3.05 and 9.14 m are specified in the upper and lower aquifer, respectively.

The multi-aquifer well was the only boundary condition specified in the model. The well is located in the center of the model domain (fig. 14–1), fully penetrates both aquifers, and has a well radius of 0.15 m. The Thiem conductance equation was used to calculate the well conductance in each aquifer. The initial head in the well was set equal to the initial head in the lower aquifer (9.14 m) and well storage was not simulated.

## 14.2 Example Results

The model was run for the case where the well was not pumping and a case where the well is pumping  $1,767 m^3/d$ . Transient results for non-pumping and pumping case are shown in figure 14–2. For the non-pumping case, the flow from the lower aquifer is balanced by flow to the upper aquifer (fig. 14–2A). The water level in the multi-aquifer well under non-pumping can be calculated using the Sokol solution (Sokol, 1963). The Sokol solution is

$$h_w = \frac{\sum_{m=1}^N T_m h_m}{\sum_{m=1}^N T_m} \quad (14-1)$$

where  $h_w$  is the water-level in the well (L),  $T_m$  is the aquifer transmissivity ( $L^2/T$ ), and  $h_m$  is the aquifer head at the outer-constant head boundary (L). For the non-pumping case, the water-level in the well calculated using equation 14–1 is 7.922 m, which is identical the water-level in the multi-aquifer well.

For the pumping case, the flow from the upper aquifer is actually initially negative, indicating that at early time water flows up the wellbore and into the upper aquifer, rather than discharging from it (fig. 14–2B).

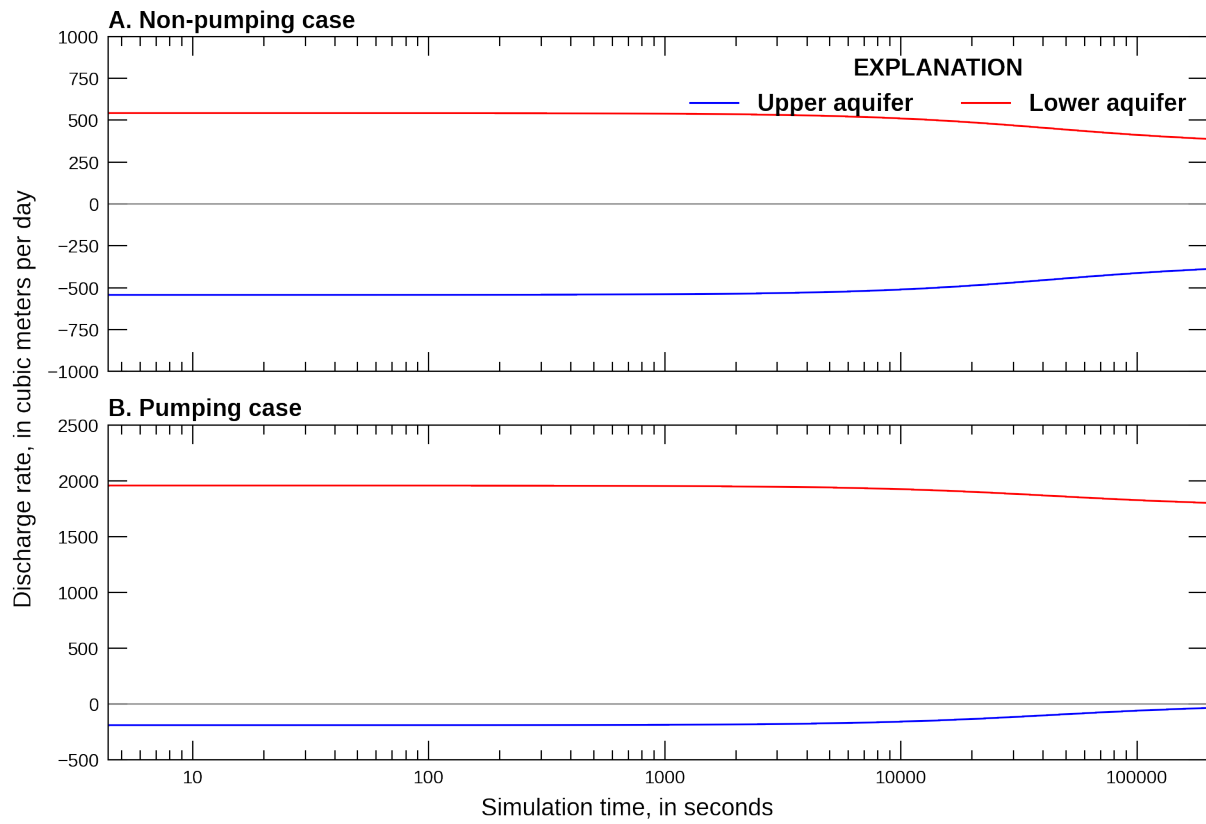


Figure 14–2: Simulated aquifer discharges to the multi-aquifer well. Discharge rates are relative to the multi-aquifer well; positive and negative discharge rates represent inflow to and outflow from the multi-aquifer, respectively. *A.* Non-pumping case. *B.* Pumping case.

## 15 Multi-Aquifer Well Problem, Flowing Well Option

This is a modified version of the multi-aquifer well simulation described in [Neville and Tonkin \(2004\)](#). The example simulates an upper and lower aquifer separated by an impermeable confining unit but connected by a well that is open across both aquifers. The multi-aquifer well uses the flowing well Multi-Aquifer Well (MAW) Package option to simulate discharge of water from the well at land surface.

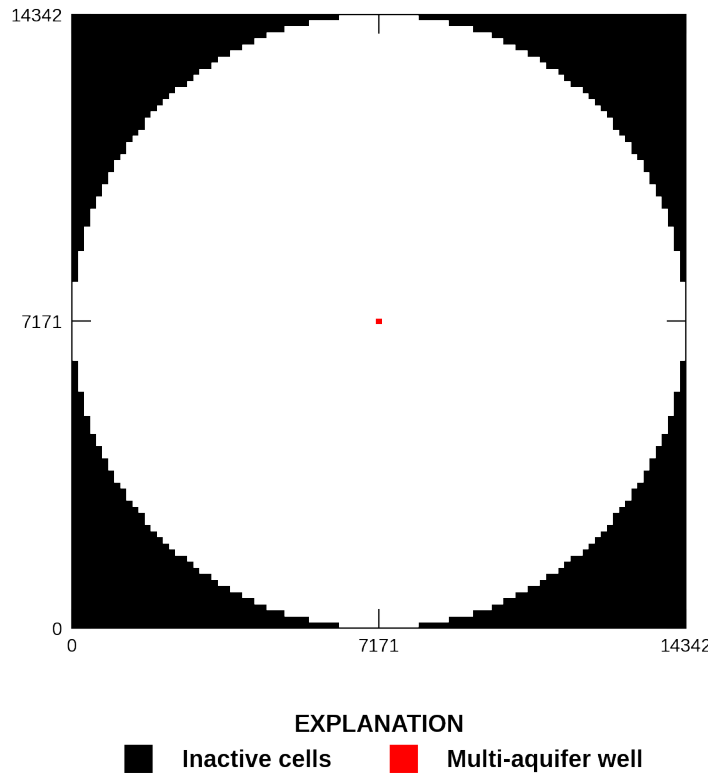


Figure 15–1: Location of inactive cells and the multi-aquifer well.

### 15.1 Example Description

Model parameters for the example are summarized in table 15–1. The model consists of a grid of 101 columns, 101 rows, and 2 layers. The model domain is 14,342 m in the x- and y-directions (fig. 15–1). The discretization is in the row and column directions is 142 m. The top of the model is specified to be -50 m and the bottom of each layer is specified to be 142.9 and -514.5 m. Groundwater flow was inactivated beyond a distance of 7,163 m from the center cell (row 51, column 51) in model layers 1 and 2 by specifying an IDOMAIN value of zero in these cells (fig. 15–1).

One transient stress period 2.1314815 days in length is simulated. The stress period has 50 time steps and uses a time step multiplier equal to 1.2, which results in time step lengths that range  $0.51 \times 10^{-4}$  to 0.39 days. A short simulation time is specified to prevent the effect of the well propagating to the model boundary.

Table 15–1: Model parameters for example ex-gwf-maw-p02.

Parameter	Value
Number of periods	1
Number of layers	2
Number of rows	101
Number of columns	101
Column width ( $m$ )	142.0
Row width ( $m$ )	142.0
Top of the model ( $m$ )	-50.0
Bottom elevations ( $m$ )	-142.9, -514.5
Starting head ( $m$ )	3.05, 9.14
Horizontal hydraulic conductivity ( $m/d$ )	1.0
Vertical hydraulic conductivity ( $m/d$ )	1.0e-16
Specific storage ( $1/d$ )	1e-4
Well radius ( $m$ )	0.15
Well pumping rate ( $m^3/d$ )	0.0

The horizontal and vertical hydraulic conductivity is 1 and  $1 \times 10^{-16} m/d$ . The transmissivity of the upper and lower aquifer is 92.9 and  $371.6 m^2/d$ . A constant specific storage value of  $1 \times 10^{-4} (1/d)$  is specified. All model layers are specified to be confined. An initial head of 3.05 and 9.14 m are specified in the upper and lower aquifer, respectively.

The multi-aquifer well was the only boundary condition specified in the model. The well is located in the center of the model domain (fig. 15–1), fully penetrates both aquifers, has a well radius of 0.15 m, and is not pumping. The well conductance is specified to be 111.3763 and  $445.9849 m^2/d$  in the upper and lower aquifer, respectively. The initial head in the well was set equal to the initial head in the lower aquifer (9.14 m) and well storage is simulated. The flowing well discharge elevation and conductance are specified to be 0.0 m and  $m^2/d$ .

## 15.2 Example Results

Transient results for non-pumping and pumping case are shown in figure 15–2. Inflow to the well from the upper and lower aquifers is equal to the flowing well discharge. Initially the water level in the well and aquifers is above the flowing well discharge elevation. As a result, flowing well discharge begins immediately and continues throughout the simulation. Flowing well discharge decreases during the simulation as water-levels in the well and in the aquifer adjacent to the well decrease during the simulation.

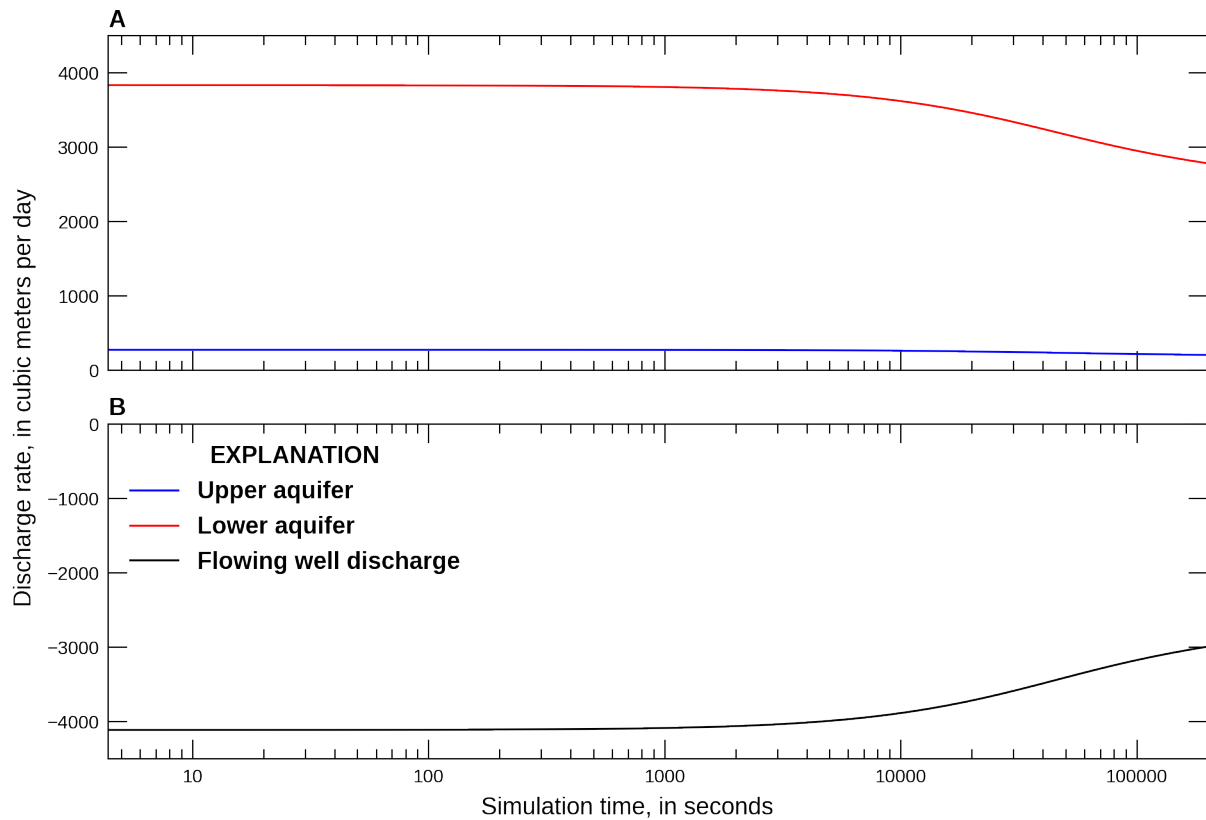


Figure 15–2: Simulated aquifer discharges to the multi-aquifer well and flowing well discharge. Discharge rates are relative to the multi-aquifer well; positive and negative discharge rates represent inflow to and outflow from the multi-aquifer, respectively. *A.* Aquifer discharge to the multi-aquifer well. *B.* Flowing well discharge.

## 16 Reilly Multi-Aquifer Well Problem

This is the unstressed multi-aquifer well simulation described in [Reilly and others \(1989\)](#). The example simulates a unconfined groundwater system that exhibits two-dimensional flow in vertical section and quantify the movement of water through a well under nonpumping conditions.

### 16.1 Example Description

A two-dimensional cross-section model was developed to provide lateral boundary conditions for a local scale model that included the effects of a nonpumping well screened across multiple model layers. The multi-aquifer well was represented using a multi-aquifer well and a vertical string of high hydraulic conductivity cells in order to compare multi-aquifer well results to the results of [Reilly and others \(1989\)](#). Model parameters for the regional and local model examples are summarized in table 16–1.

Table 16–1: Model parameters for example ex-gwf-maw-p03.

Parameter	Value
Number of periods	1
Number of layers (regional)	21
Number of rows (regional)	1
Number of columns (regional)	200
Number of layers (local)	41
Number of rows (local)	16
Number of columns (local)	27
Regional column width (ft)	50.0
Regional row width (ft)	1.0
Top of the model (ft)	10.0
Model bottom elevation (ft)	-205.0
Starting head (ft)	10.0
Horizontal hydraulic conductivity (ft/d)	250.0
Vertical hydraulic conductivity (ft/d)	50.0
Areal recharge (ft/d)	0.004566
Regional downgradient constant head (ft)	0.0
Row, column location of well	(15, 13)
Layers with well screen	(1, 12)
Well radius (ft)	0.1333
Bottom of the well (ft)	-65.0
Hydraulic conductivity for well (ft/d)	1e9

#### 16.1.1 Regional Model

The regional model consists of a grid of 200 columns, 1 row, and 21 layers. The model domain is 10,000 and 1 *ft* in the x- and y-directions (fig. 16–1). The discretization is in the column directions is 50 *ft*. The top of the model is specified to be 10 *ft* and the bottom of the aquifer is specified to be -205 *ft*. The bottom of the first model layer is -5 *ft* and layers 2 through 21 are 10 *ft* thick. A single steady-state stress period 1 day in length is simulated. The stress period has 1 time step.

The horizontal and vertical hydraulic conductivity is 250 and 50 *ft/d*. The upper model layer was specified to be convertible (unconfined) and all other model layers are specified to be confined. An initial head of 10 *ft* is specified, but any value above the bottom of each layer could have been specified since the simulation is steady state.

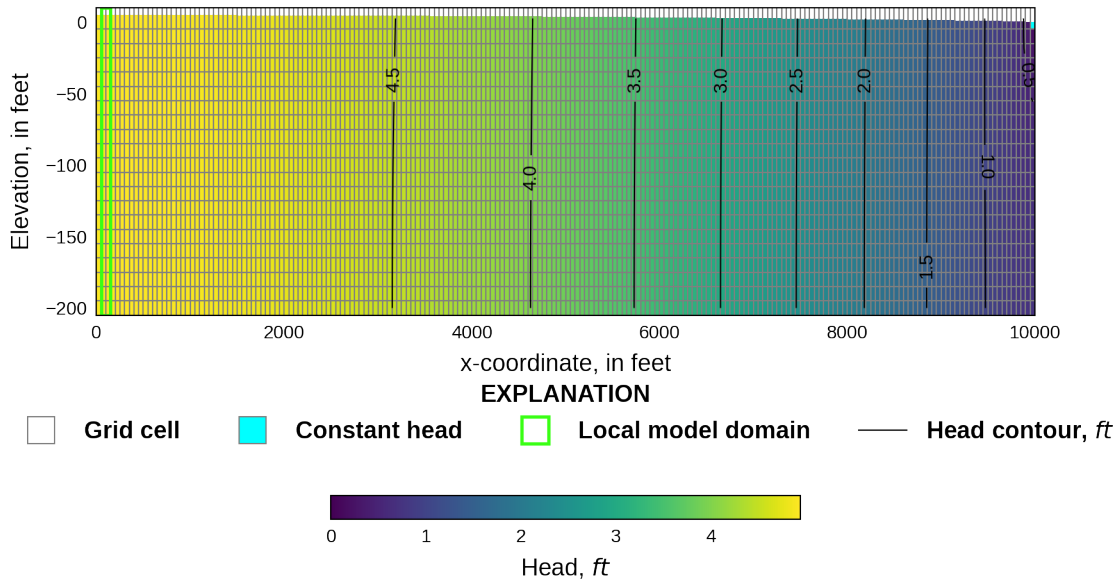


Figure 16–1: Diagram showing the regional cross-section model with the location of the local three-dimensional model simulating flow through a wellbore. Steady-state water-table elevation and heads along with the location of the downgradient constant head boundary.

Flow into the system is from infiltration from precipitation and was represented using the recharge (RCH) package. A constant recharge rate of  $4.566 \times 10^{-3} \text{ ft/d}$  (20 in/yr) was specified for every cell in model layer 1. Flow out of the model is from a specified downgradient outflow boundary represented by a constant head (CHD) package cells in model layer 1.

### 16.1.2 Local Model

Since the flow system is symmetric around the well, only half of the local domain was simulated. The local model consists of a grid of 27 columns, 16 rows, and 41 layers. The model domain is 100 and 50 ft in the x- and y-directions (fig. 16–2). The discretization is in the column and row directions, ranging from 10 to 0.1665 ft. In the cell containing the well (row 16, column 14) the discretization is 0.333 and 0.1665 ft (4 and 2 in) in the x- and y-directions, respectively. The top of the model is specified to be 10 ft and the bottom of the aquifer is specified to be -205 ft. The bottom of the first model layer is -5 ft and layers 2 through 41 are 5 ft thick. A single steady-state stress period 1 day in length is simulated. The stress period has 1 time step.

The horizontal and vertical hydraulic conductivity is 250 and 50 ft/d. The upper model layer was specified to be convertible (unconfined) and all other model layers are specified to be confined. An initial head of 10 ft is specified, but any value above the bottom of each layer could have been specified since the simulation is steady state.

Flow into the system is from infiltration from precipitation and was represented using the recharge (RCH) package. A constant recharge rate of  $4.566 \times 10^{-3} \text{ ft/d}$  (20 in/yr) was specified for every cell in model layer 1. Simulated regional results were used to define constant head values specified in columns 1 and 27. The heads in column 1 and 2 of the regional model were linearly

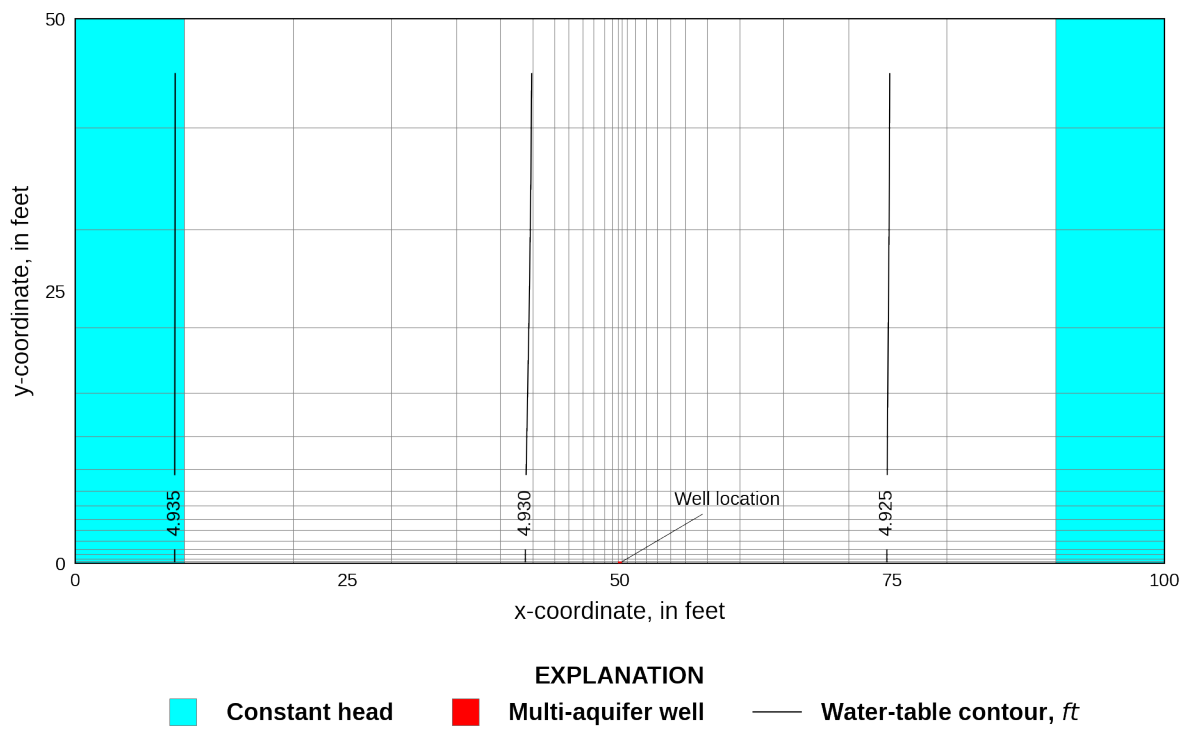


Figure 16–2: Diagram showing the horizontal discretization used in the local three-dimensional model simulating flow through a wellbore. Steady-state water-table contours are shown along with the location of the multi-aquifer well and constant head boundaries.

interpolated to the node position in column 1 to define constant heads in the first column of the local model. The heads in column 3 and 4 of the regional model were linearly interpolated to the node position in column 27 to define constant heads in the last column of the local model. Vertically, linearly interpolated heads from layer 2 through 21 in the regional model were applied to the two equivalent layers in the local model.

The well is located in the lower center of the model domain (fig. 16–2), has a 60 *ft* screened interval that fully penetrates model layers 2 through 13, has a well radius of 0.1333 *ft*, the well bottom is at -65 *ft*, and is not pumping. In order to compare results to a version of the local model that simulated the well using high hydraulic conductivity the well is located in (row 16, column 14) but physically connected to the three cells horizontally connected to the cell. Furthermore, the top and bottom of the well are connected to the overlying and underlying cells in layer 1 and layer 14.

The conductance for each connection was calculated using the same harmonic average used by MODFLOW 6 to calculate intercell conductance (see [Langevin and others, 2017a](#), eq.4-24). The equivalent hydraulic conductivity of the cell containing the well is based on the Hagen-Poiseuille equation for laminar pipe flow by an equivalent form of Darcy's law and is used in MODFLOW 6. For laminar flow, the Hagen-Poiseuille equation is

$$Q_{\text{pipe}} = VA = \frac{gd^2A}{32\nu L} \Delta h, \quad (16-1)$$

where  $Q_{\text{pipe}}$  is the flow through the pipe (in this case wellbore) ( $\text{L}^3/\text{T}$ ),  $V$  is the velocity ( $\text{L}/\text{T}$ ),  $A$  is the cross-sectional area of the pipe ( $\text{L}^2$ ),  $d$  is the diameter of the pipe ( $\text{L}$ ),  $g$  is the acceleration due to gravity ( $\text{L}/\text{T}^2$ ),  $\nu$  is the kinematic viscosity of the flowing fluid ( $\text{L}^2/\text{T}$ ), and  $\Delta h$  is the head loss ( $\text{L}$ ). Darcy's law is

$$Q = \frac{KA}{L} \Delta h, \quad (16-2)$$

where  $Q$  is the flow through a block of porous medium,  $K$  is the hydraulic conductivity of the medium ( $\text{L}/\text{T}$ ), and  $L$  is the length of flow section ( $\text{L}$ ). The equivalent hydraulic conductivity ( $K_{\text{eq}}$ ) representing the wellbore can be calculated by equating equations 16–1 and 16–2 and rearranging to solve for  $K_{\text{eq}}$ . The equivalent hydraulic conductivity is

$$K_{\text{eq}} = \frac{gd^2}{32\nu} = 1 \times 10^9 \text{ ft}/\text{d}. \quad (16-3)$$

A total of 38 multi-aquifer well connections to the connected aquifer were defined and had conductances values equal to 1.11 (connections to layer 1 and 14), 832.50 (connections to column 13 and 15 in layers 2 through 13), and 3330.000  $\text{ft}^2/\text{d}$  (connection to row 15 in all layers). The initial head in the well was set equal to the initial head in the aquifer (10.0 *ft*). For the case where the well represented as a multi-aquifer well, the cell in row 16, column 14, and layers 2 through 13 was inactivated by specifying an IDOMAIN value of 0 in these cells. For the case where the well was represented using high hydraulic conductivity, the horizontal and vertical hydraulic conductivity in row 16, column 14, and layers 2 through 13 was set to  $1 \times 10^9 \text{ ft}/\text{d}$  (see eq. 16–3).

## 16.2 Example Results

Steady-state results for the regional model are shown in figure 16–1. Steady-state water-table elevations for the local three-dimensional model with the well simulated using a multi-aquifer well are shown in figure 16–2. The flow with depth into or from the wellbore is shown in figure 16–3. The flow to or from the wellbore for the case where the multi-aquifer well and high hydraulic conductivity

were used is in close agreement and the mean error for all of the cells connected to the wellbore is  $-2.14 \times 10^{-6} \text{ ft}^3/\text{d}$ . The total flow into and out of the wellbore is 9.53 and  $9.52 \text{ ft}^3/\text{d}$  for the case with the multi-aquifer well and high hydraulic conductivity, respectively. The steady-state head in the wellbore and the average head for all cells representing the well in the high hydraulic conductivity case are both 4.93 ft.

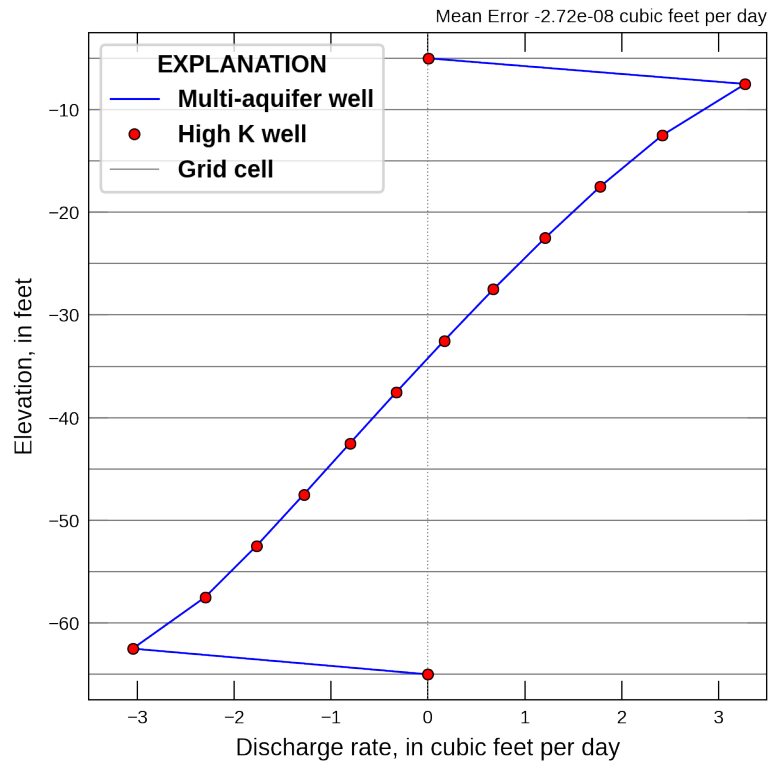


Figure 16–3: Graph of flow between the aquifer and the borehole with depth for the three-dimensional local model with the well represented as a multi-aquifer well and using high hydraulic conductivity. Positive discharge values indicate flow from the aquifer to the wellbore. Negative discharge values indicate flow from the wellbore to the aquifer.

## 17 Flow Diversion

This problem simulates unconfined groundwater flow in an aquifer with a high bottom elevation in the center of the aquifer and groundwater flow around a high bottom elevation.

### 17.1 Example Description

Model parameters for the example are summarized in table 17–1. The model consists of a grid of 51 columns, 51 rows, and 1 layer. The discretization is 1.96 m in the row and column direction for all cells. The top of the aquifer is 25 m and the bottom elevation of the aquifer ranges from 0 m at the edges of the domain to 10 m in the center of the domain (fig. 17–1). A single steady-stress period with a total length of 1 day is simulated.

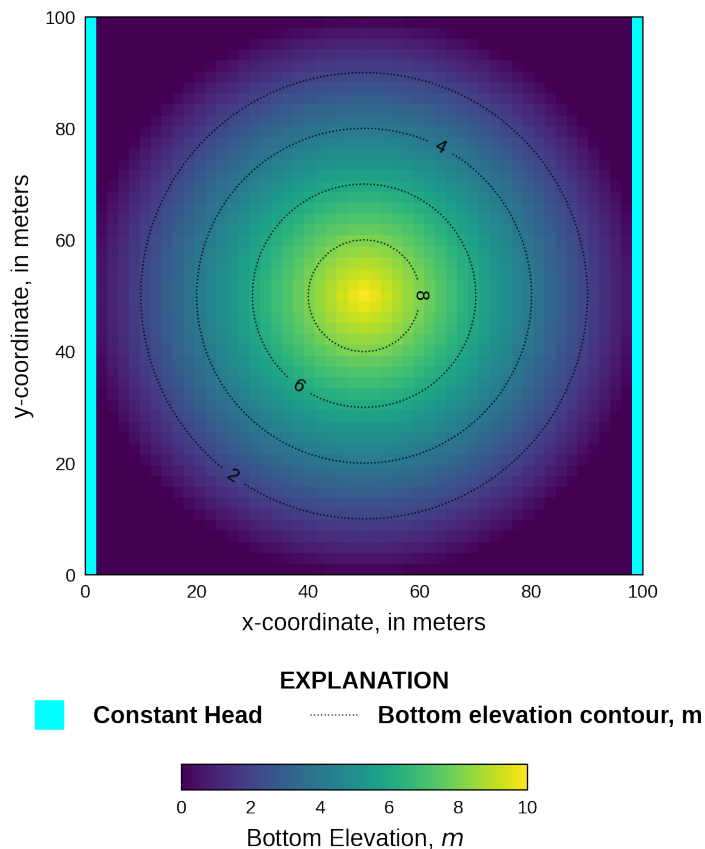


Figure 17–1: Bottom elevation of the flow diversion problem in meters. Bottom elevation are lowest at the edges of the domain and highest in the center of the domain. The location of constant head boundary cells is also shown.

Table 17–1: Model parameters for example ex-gwf-bump.

Parameter	Value
Number of periods	1
Number of layers	1
Number of rows	51
Number of columns	51
Model length in x-direction (m)	100.0
Model length in y-direction (m)	100.0
Top of the model (m)	25.0
Horizontal hydraulic conductivity (m/day)	1.0
Constant head in column 1 and starting head (m)	7.5
Constant head in column 51 (m)	2.5

A constant horizontal hydraulic conductivity of 1  $m/day$  was specified in all cells. An initial head of 7.5  $m$  was specified in all model cells. Constant head boundary cells were specified for all rows in column 1 and 51. A constant head value of 7.5 and 2.5  $m$  is specified in column 1 and 51, respectively.

## 17.2 Scenario Results

The flow diversion model was evaluated using the Newton-Raphson Formulation and the Standard Conductance Formulation with rewetting (table 17–2). A scenario that used a cylindrical obstruction and the Newton-Raphson Formulation was also evaluated.

Table 17–2: Scenario parameters for example ex-gwf-bump.

Scenario	Scenario Name	Parameter	Value
1	ex-gwf-bump-p01a	newton	newton
2	ex-gwf-bump-p01b	rewet	True
		wetfct	1.0
		iwetit	1
		ihdwet	0
		wetdry	2.0
		newton	newton
3	ex-gwf-bump-p01c	cylindrical	True

### 17.2.1 Newton-Raphson Formulation

Simulated results using the Newton-Raphson Formulation is shown in figure 17–2. Newton under-relaxation is used with the Newton-Raphson Formulation to maintain water-levels above the aquifer bottom (Hughes and others, 2017). Cells with bottom elevation ranging from approximately 7.5 to 10  $m$  are dry and normalized specific discharge vectors show that groundwater is flowing around the dry cells. Note the relatively constant heads of approximately 7.5  $m$  adjacent to the dry cells. A total of 10.94  $m^3/day$  is discharged to the constant head cells in column 51.

### 17.2.2 Standard Conductance Formulation with rewetting

Rewetting parameters specified in the Node Property Flow Package for this scenario are summarized in table 17–2. A positive WETDRY parameter value of 2 is used to allow wetting to occur from horizontally adjacent cells. Simulated results using the Standard Conductance Formulation with rewetting is shown in figure 17–3. Although the rewetting allows the model to converge the area of

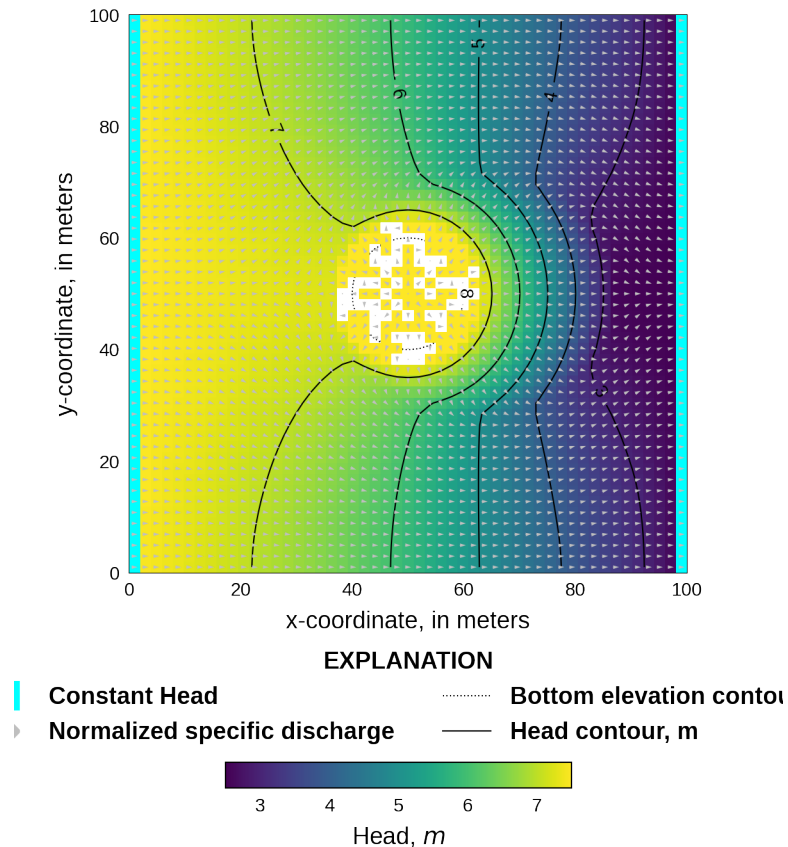


Figure 17–2: Simulated heads and normalized specific discharge vectors for the scenario using the Newton-Raphson Formulation. Bottom elevation contours are shown in areas with dry cells. The location of constant head boundary cells is also shown.

dry cells is significantly larger than the area of dry cells in the Newton-Raphson Formulation scenario. Furthermore, the increase in the area of dry cells is not symmetric and extends further in areas where there is a significant component of downstream flow. Simulated heads for both scenarios are comparable in areas that are not dry in both scenarios. A total of  $10.50 \text{ m}^3/\text{day}$  is discharged to the constant head cells in column 51. The slight flow reduction for this scenario is a result of upstream horizontal conductance weighting used with the Newton-Raphson formulation and the slightly reduced total simulated horizontal conductance for the rewetting scenario.

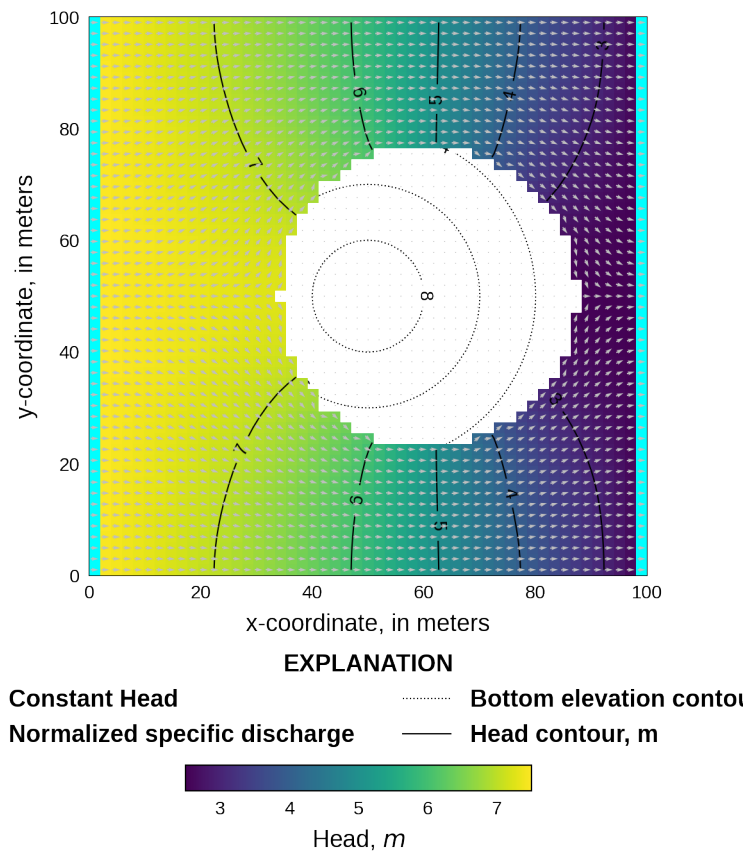


Figure 17–3: Simulated heads and normalized specific discharge vectors for the scenario using the Standard Conductance Formulation with rewetting. Bottom elevation contours are shown in areas with dry cells. The location of constant head boundary cells is also shown.

### 17.2.3 Newton-Raphson Formulation with a cylindrical obstruction

The model setup for this scenario is identical to the Newton-Raphson Formulation scenario except for the aquifer bottom elevations, which are used to represent the cylindrical obstruction. Aquifer bottom elevations are derived from aquifer bottom elevations shown in figure 17–1 and are equal to 0 and 20

$m$  where elevations are less than  $7.5\text{ m}$  and greater than or equal to  $7.5\text{ m}$ , respectively. Simulated results using the Newton-Raphson Formulation and a cylindrical obstruction is shown in figure 17–4. Dry cells are limited to the location of the cylindrical obstruction. Simulated heads for this scenario show the typical characteristics of flow around a cylinder including increased heads on the upstream side of the cylinder and decreased heads on the downstream side of the cylinder. A total of  $23.10\text{ m}^3/\text{day}$  is discharged to the constant head cells in column 51, which is more than double to discharge rate in the other scenarios as a result of an increase in total simulated horizontal conductance resulting from bottom elevations equal to  $0\text{ m}$  except in the location of the cylindrical obstruction.

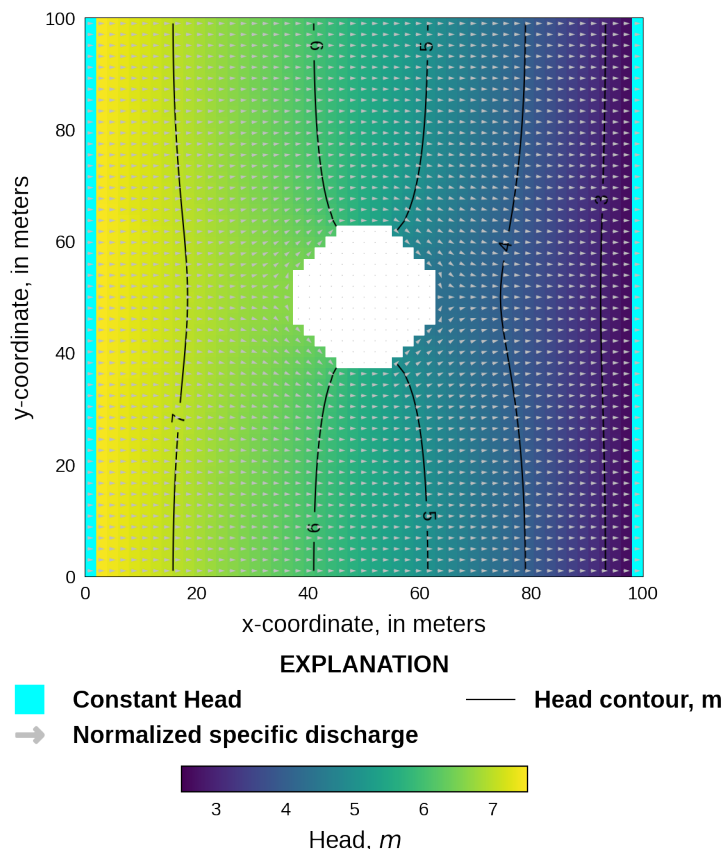


Figure 17–4: Simulated heads and normalized specific discharge vectors for the scenario using the Newton-Raphson Formulation with a cylindrical obstruction. The location of constant head boundary cells is also shown.

## 18 Circular Island with Triangular Mesh

This example shows how a triangular mesh can be used to simulate a circular island. This is a synthetic example problem that has not been documented elsewhere.

### 18.1 Example Description

The problem consists of a simple two-layer model representing groundwater flow in a circular island. The island has a radius of 1025 m. The extent of the grid extends out to 1500 m from the island center. The grid consists of 5240 triangular cells and 2778 vertices per layer. The grid was created using an external mesh generator. Vertices and cell definitions are provided to MODFLOW 6 using the Discretization by Vertices (DISV) Package. There is a single steady-state stress period with a length of 1 day. Model parameters are listed in table 18–1.

Table 18–1: Model parameters for example ex-gwf-disvmesh.

Parameter	Value
Number of periods	1
Number of layers	2
Top of the model (m)	0.0
Layer bottom elevations (m)	-20.0, -40.0
Starting head (m)	0.0
Cell conversion type	0
Horizontal hydraulic conductivity (m/d)	10.0
Vertical hydraulic conductivity (m/d)	0.2
Recharge rate (m/d)	4.0e-3

An initial head of 0 m was specified for the model. The value is not important as the model is steady state.

Recharge is assigned to cells in layer one that are within the 1025 m radius of the island. Outside the island, general-head boundaries (GHB) are assigned with a stage of zero. GHB locations are shown in cyan in figure 18–1. Cells not colored in figure 18–1 are assigned recharge.

### 18.2 Example Results

Simulated heads for model layers 1 and 2 are shown in figure 18–2.

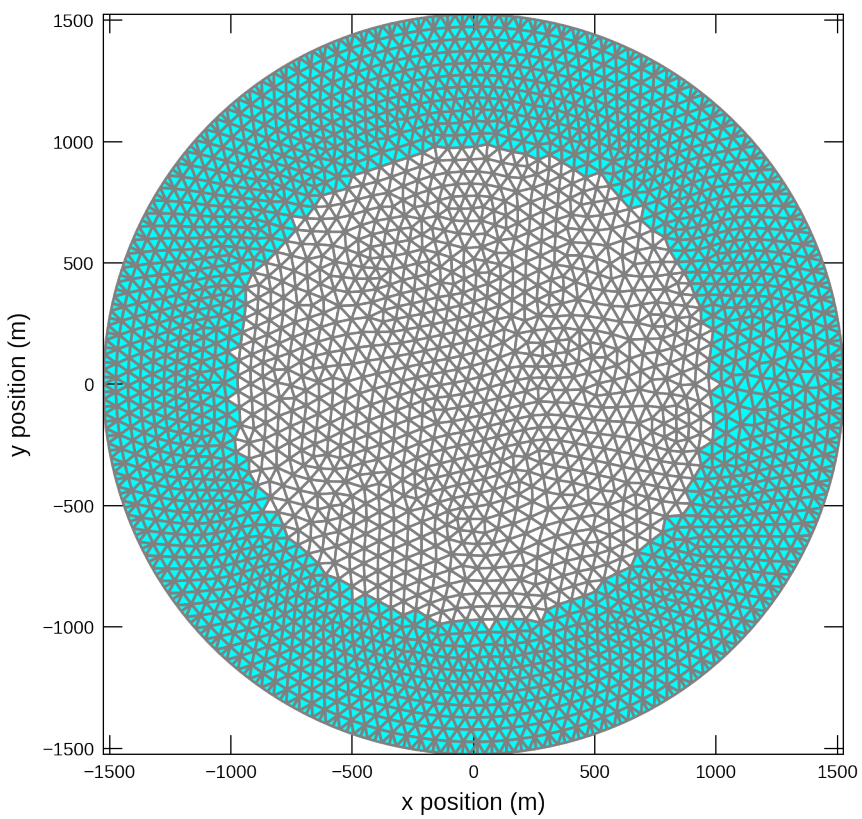


Figure 18–1: Model grid and boundary conditions used for the circular island problem. General-head boundaries are shown in blue, and represent an off-shore boundary condition. Cell not colored represent the island and are assigned groundwater recharge.

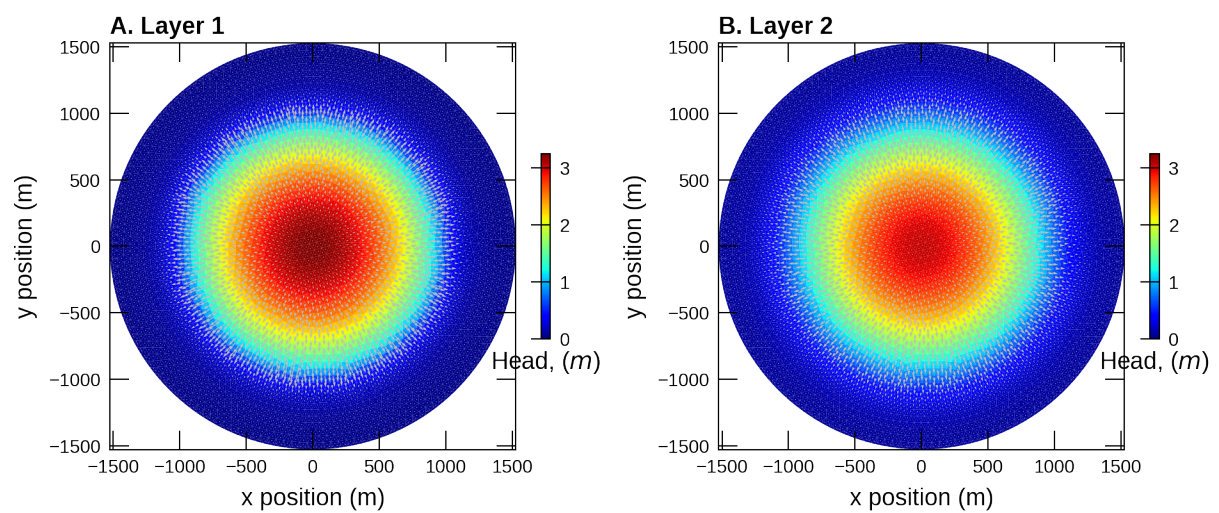


Figure 18–2: Simulated groundwater head in (A) model layer 1 and (B) model layer 2.

## 19 Hani Problem

This problem simulates groundwater flow to a pumping well under horizontally anisotropic groundwater flow conditions. This is a synthetic example problem that has not been documented elsewhere.

### 19.1 Example Description

Model parameters for the example are summarized in table 19–1. The model consists of a grid of 51 columns, 51 rows, and 1 layer. The discretization is 10  $m$  in the row and column direction for all cells (fig. 19–1). The top of the aquifer is zero and the bottom elevation of the aquifer is -10  $m$ . A single steady-stress period with a total length of 1 day is simulated.

Table 19–1: Model parameters for example ex-gwf-hani.

Parameter	Value
Number of periods	1
Number of layers	1
Number of rows	51
Number of columns	51
Spacing along rows ( $m$ )	10.0
Spacing along columns ( $m$ )	10.0
Top of the model ( $m$ )	0.0
Layer bottom elevations ( $m$ )	-10.0
Starting head ( $m$ )	0.0
Cell conversion type	0
Horizontal hydraulic conductivity in the 11 direction ( $m/d$ )	1.0
Horizontal hydraulic conductivity in the 22 direction ( $m/d$ )	0.01
Pumping rate ( $m^3/d$ )	-1.0

For this problem, hydraulic conductivity is anisotropic with K11 specified as 100 times larger than K22. For the first scenario the hydraulic conductivity ellipse is not rotated. For the second scenario, the ellipse is rotated 25 degrees counter clockwise in the horizontal plane. Because the ellipse axes do not align with the model grid, the XT3D option (Provost and others, 2017) is required to simulate this scenario. For the third scenario, the ellipse is rotated 90 degrees, so that groundwater flows more easily in the column direction.

Table 19–2: Scenario parameters for example ex-gwf-hani.

Scenario	Scenario Name	Parameter	Value
1	ex-gwf-hanir	angle1	0
		xt3d	False
2	ex-gwf-hanix	angle1	25
		xt3d	True
3	ex-gwf-hanic	angle1	90
		xt3d	False

An initial head of zero was specified in all model cells. Constant head boundary cells with a value of zero were specified for all perimeter model cells. A pumping well with a rate of -1.0  $m^3/d$  is located in the center of the model domain.

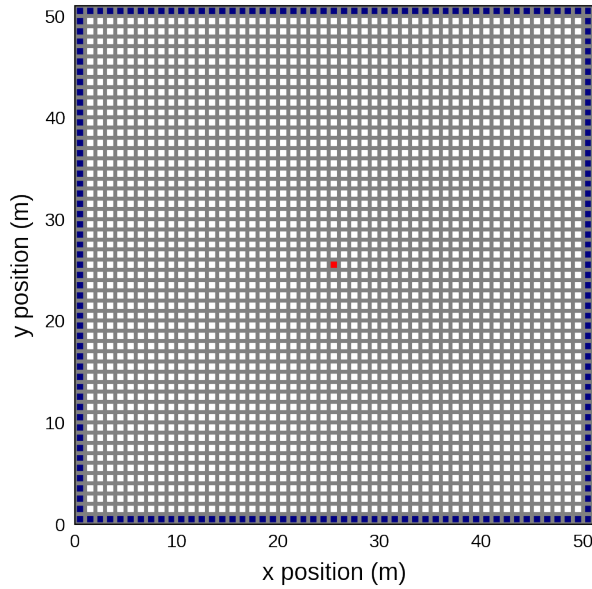


Figure 19–1: Model grid and boundary conditions used for the horizontal anisotropy problem. Blue cells are constant-head cells and the pumping well is located in the cell shown in red.

## 19.2 Scenario Results

Simulated drawdown for the three scenarios are shown in figures 19–2, 19–3, and 19–4.

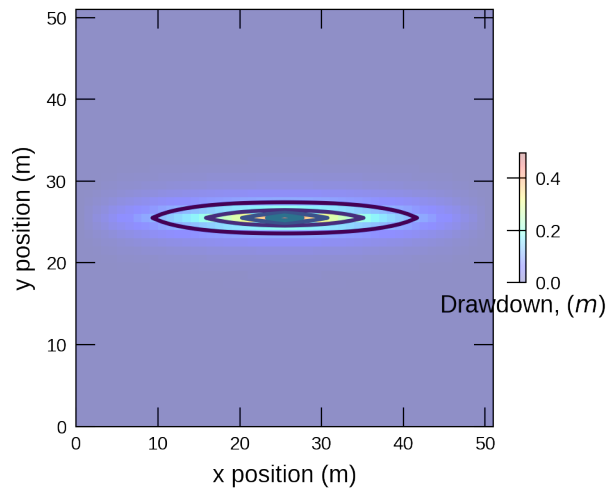


Figure 19–2: Simulated drawdown for anisotropic groundwater flow to a pumping well for scenario 1. The dominant hydraulic conductivity ellipse is aligned with the x-axis.

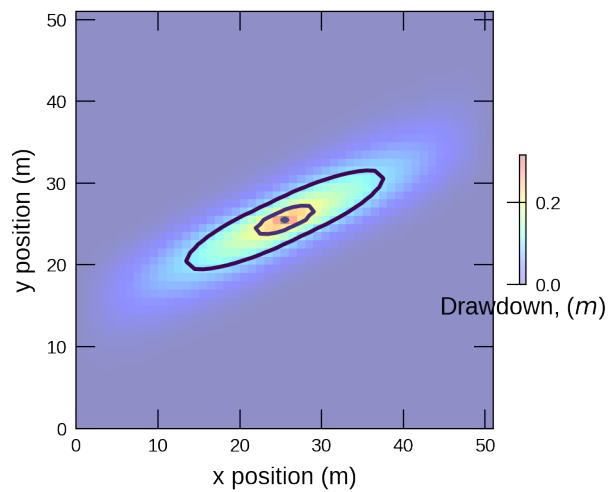


Figure 19–3: Simulated drawdown for anisotropic groundwater flow to a pumping well for scenario 2. The dominant hydraulic conductivity ellipse axis is rotated 25 degrees counter clockwise from the x-axis. The XT3D option is required for this scenario because the ellipse axes do not align with the row and column directions.

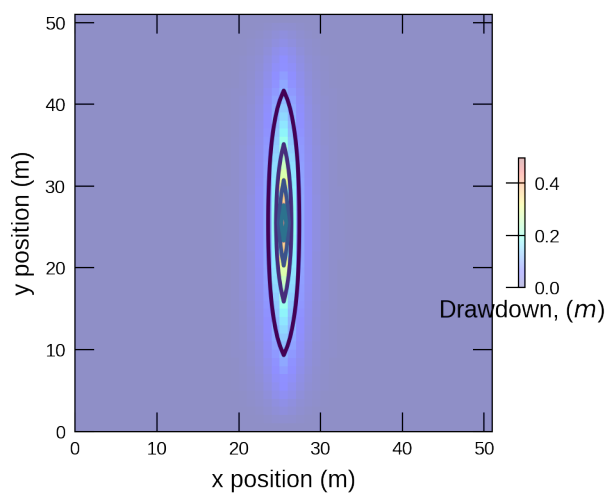


Figure 19–4: Simulated drawdown for anisotropic groundwater flow to a pumping well for scenario 3. The dominant hydraulic conductivity ellipse axis is rotated 90 degrees counter clockwise from the x-axis so that the ellipse axes align with the column and row directions.

## 20 Groundwater Whirls

This problem is based on the first whirl problem described by [Provost and others \(2017\)](#). Using steady-state groundwater flow simulations, [Hemker and others \(2004\)](#) have shown that “spiraling flow lines occur in layered aquifers that have different anisotropic horizontal hydraulic conductivities in adjacent layers.” They refer to such spiraling flow lines as “groundwater whirls.” This example demonstrates the use of the XT3D option to implement anisotropy that induces groundwater whirls in a highly idealized two-aquifer system.

### 20.1 Example Description

The model domain (fig. 20–1) is a box that is 5,100 m by 1,000 m horizontally and 1,000 m thick, discretized into a regular grid of 10 rows, 51 columns, and 10 layers. The top five model layers form the top aquifer, and the bottom five model layers form the bottom aquifer. All cells are confined. Aquifer properties are homogeneous within each aquifer but differ between the aquifers. Groundwater recharges one end of the box at a total rate of 1 m<sup>3</sup>/d, distributed equally among 100 cells, and is removed from the opposite end of the box at the same rate, also distributed equally among 100 cells. There is a single steady-state stress period with a length of 1 day. Model parameters are listed in table 20–1. An initial head of 0 m was specified for the model. The value is not important as the model is steady state.

The simulation reported, which corresponds to the first whirl problem presented by [Provost and others \(2017\)](#) here uses 10:1 horizontal anisotropy ( $K_{11} = K_{33} = 1 \text{ m/d}$ ,  $K_{22} = 0.1 \text{ m/d}$ ) rotated 45 degrees counterclockwise from the  $x$  axis in the top aquifer and 45 degrees clockwise from the  $x$  axis in the bottom aquifer.

Table 20–1: Model parameters for example ex-gwf-whirl.

Parameter	Value
Number of periods	1
Number of layers	10
Number of rows	10
Number of columns	51
Spacing along rows (m)	100.0
Spacing along columns (m)	100.0
Top of the model (m)	0.0
Layer bottom elevations (m)	-100, -200, -300, -400, -500, -600, -700, -800, -900, -1000
Starting head (m)	0.0
Cell conversion type	0
Hydraulic conductivity in the 11 direction (m/d)	1.0
Hydraulic conductivity in the 22 direction (m/d)	0.1
Hydraulic conductivity in the 33 direction (m/d)	1.0
Rotation of the hydraulic conductivity ellipsoid in the x-y plane	45, 45, 45, 45, 45, -45, -45, -45, -45
Inflow rate (m <sup>3</sup> /d)	0.01

### 20.2 Example Results

The whirl flow pattern is shown by plotting specific discharge vectors in cross section for column 1 (fig. 20–2).

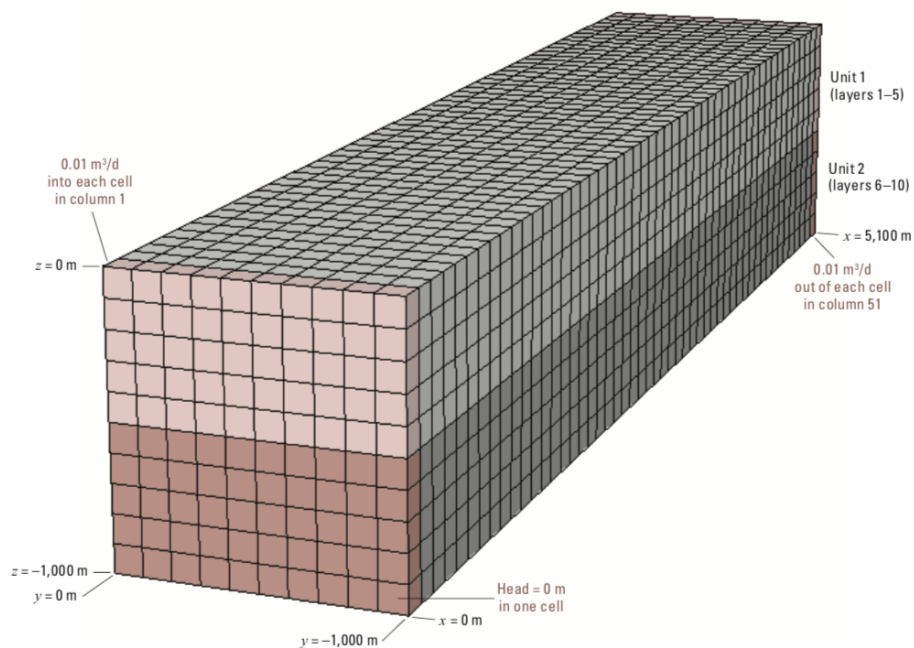


Figure 20–1: Diagram showing the model domain for the whirl problem, which consists of a three-dimensional box with two hydrogeologic units (light and dark shading). Groundwater is injected into one end of the box (column 1, pink shading) at a rate of 0.01 cubic meters per day ( $\text{m}^3/\text{d}$ ) into each cell and is removed from the opposite end of the box (column 51, pink shading) at a rate of  $0.01 \text{ m}^3/\text{d}$  from each cell. From [Provost and others \(2017\)](#).

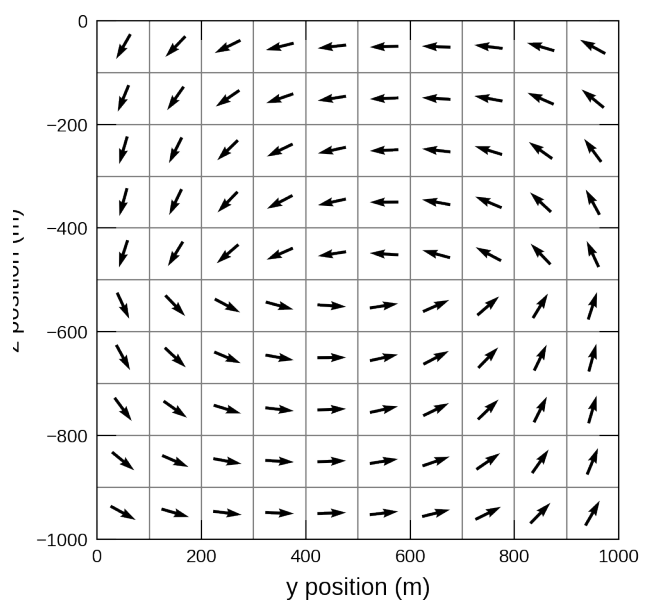


Figure 20–2: Cross section showing vectors of specific discharge for column 1 of the groundwater whirl problem. Vectors show the swirling flow pattern caused by the contrast in the hydraulic conductivity ellipsoid which occurs and the interface between model layer 5 and model layer 6.

## 21 LGR with MVR and SFR

This example is based on LGR2 Problem 3 in [Mehl and Hill \(2013\)](#), which includes two models arranged in a nested parent-child grid setup, where the parent model uses a coarse grid that surrounds the finely-gridded child model (Figure 21–1). Parent-child model setups limit grid refinement to localized regions of interest within large model domains to keep model runtimes to a minimum. Owing to the relative ease of setup for this type of model arrangement in MODFLOW 6, particularly when developing a model (i.e., simulation) with a support utility like flop (Bakker and others, 2016), the use of multi-model arrangements necessitates a generalized supporting package like MVR to transfer water among features within a simulation. To demonstrate, this example uses MVR to cascade streamflow from an upstream SFR reach in the parent model to a downstream SFR reach in the child model. Further downstream MVR again cascades streamflow from the last child model SFR reach to the appropriate SFR reach in the parent model.

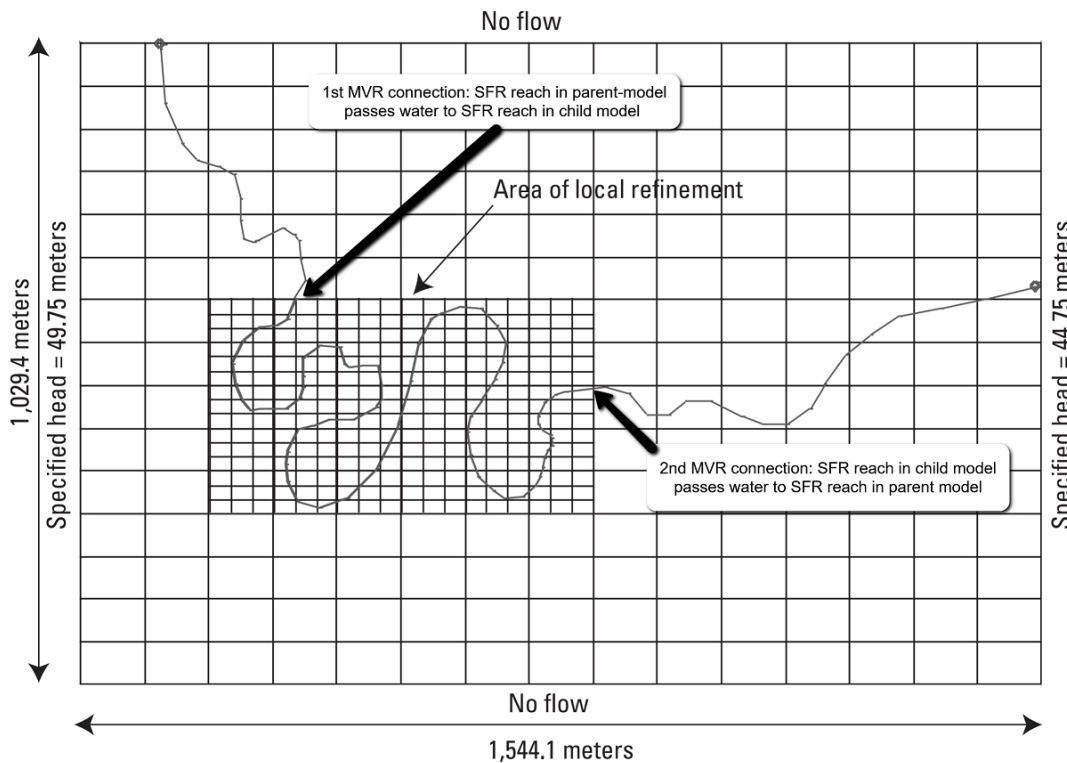


Figure 21–1: Plan view of a three-dimensional aquifer system used to test the local grid refinement method in MODFLOW 6. A  $15 \times 15$  horizontal grid discretization is shown for the parent grid and the locally refined grid ( $15 \times 18$ ) spacing is equivalent to a  $45 \times 45$  discretization over the whole domain. Two between-model MVR connections are invoked for the SFR packages (parent and child) where the river crosses between domains

### 21.1 Example description

The parent model is 15 rows by 15 columns by 3 layers with the child model occupying a 5 row by 6 column by 2 layer portion of the parent grid as shown in figure 21–1. The child model applies a 3:1

refinement to each parent grid cell, including in the vertical direction, resulting in a 15 row by 18 column by 6 layer child model. In this way, each parent grid cell is replaced by 27 ( $3^3$ ) child model grid cells. Aquifer properties are uniform and equal throughout both model domains. Interested readers are referred to [Mehl and Hill \(2013\)](#) for additional model details.

Table 21–1: Model parameters for example ex-gwf-lgr.

Parameter	Value
Number of layers in parent model	3
Number of rows in parent model	15
Number of columns in parent model	15
Parent model column width (m)	102.94
Parent model row width (m)	68.63
Number of child model columns per parent model columns	5
Number of child model rows per parent model rows	5
Child model column width (m)	20.588
Child model row width (m)	13.725
Horizontal hydraulic conductivity (m/d)	1.0
Vertical hydraulic conductivity (m/d)	1.0

Figure 21–2 demonstrates that both MVR connections transfer streamflow to the appropriate stream reach in the receiving downstream model. This is evidenced by the continuous and smooth downward trend in streamflow at the first MVR connection as well as by the uninterrupted upward trend in streamflow at the second MVR connection.

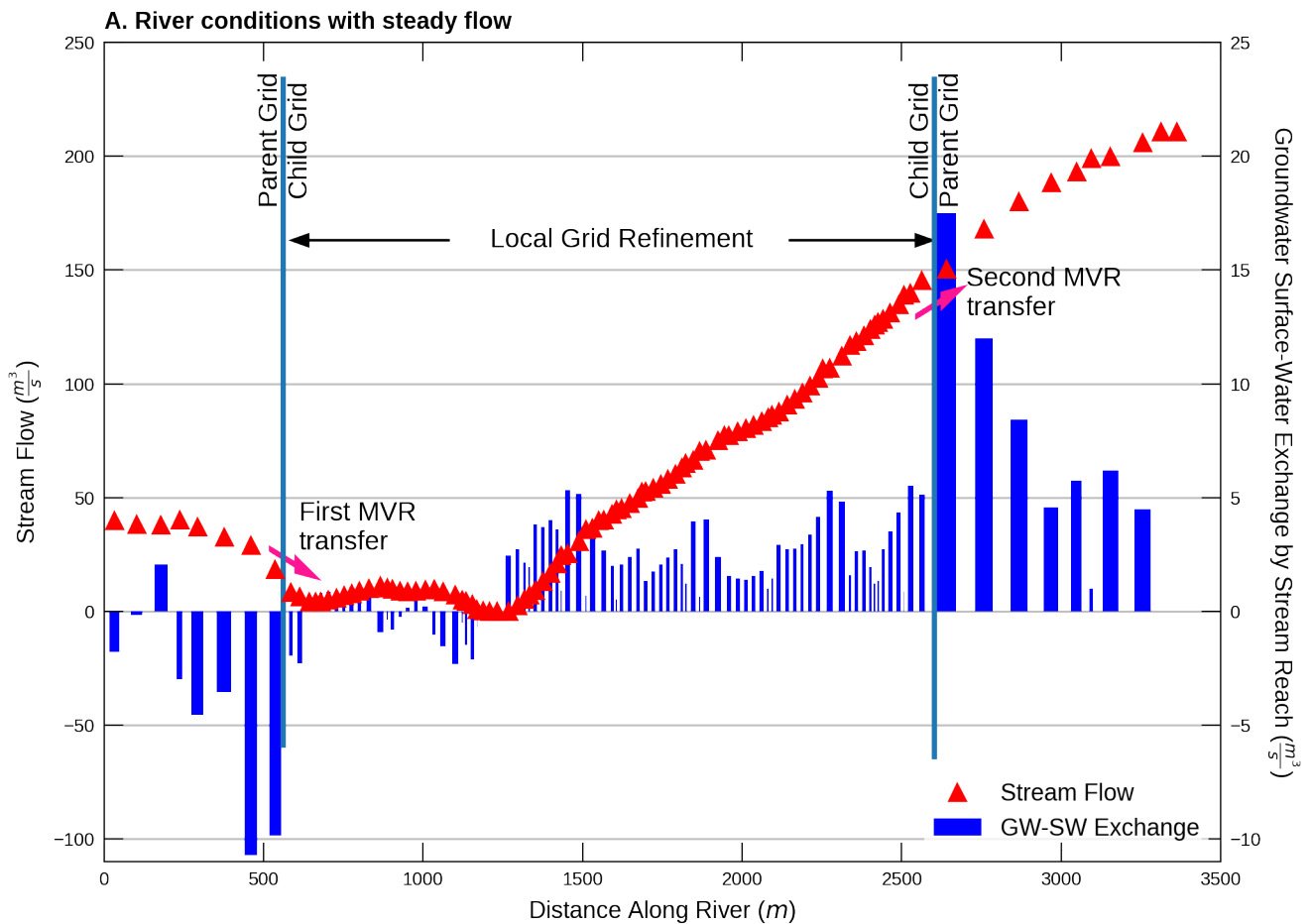


Figure 21–2: Simulated streamflow and groundwater surface-water exchange for each stream reach in figure 21–1. The transfer of water between adjacent stream reaches in the parent versus child models occurs at locations identified by the vertical black lines on the plot. Bar widths are indicative of the relative stream reach lengths within the host grid cell (figure 21–1).

## 22 Vilhelmsen LGR

This example reproduces several models described by [Vilhelmsen and others \(2012\)](#), which simulate groundwater flow in a buried valley aquifer at different grid resolution. The domain is simulated using a globally refined (GR) grid, a globally coarsened (GC) grid, and a coarse outer grid with a locally refined inset grid (LGR).

### 22.1 Example Description

Groundwater flow is simulated using three different simulations corresponding to three different grid configurations: GR, GC, and LGR (tab. 22–2). The GR grid consists of 25 layers, 183 rows and 147 columns. The grid spacing along rows is 35 m and the grid spacing along columns is 25 m. The top of the model is variable, based on topography in the area (fig. 22–1). Layer bottoms are flat. The bottom for layer 1 is set to 30 m. Bottom elevations for layers 2 through 25 are calculated using a uniform layer thickness of 5 m. A cross section for the GR grid is shown in figure 22–2.

The GC grid fits evenly into the GF grid, and has 1/3 the number of cells in the row and column directions. Instead of 25 layers, the GC grid has only 9 layers. Layer 1 corresponds to layer 1 in the GF model; however, each underlying layer in the GC grid corresponds to three layers in the GF model. The GC grid is shown in map view in figure 22–3 and as a cross section in figure 22–4.

The LGR grid is a combination of the GF and GC grids (fig. 22–5). The coarse outer parent grid is comprised of the GC grid, whereas the inset child grid consists of the GF grid. The LGR simulation consists of two separate model input files, one for the parent model and one for the child model. The two models are connected in MODFLOW 6 using the GWF-GWF Exchange, which is used to connect cells from the parent model to cells in the child model.

There are three different hydrogeologic units. The upper layer represents overburden material. The buried valley is filled with valley sediments, and the bottom material consists of the deposits into which the valley is incised. These three units are assigned a single value for hydraulic conductivity.

Recharge is uniformly applied to the water table at a rate of 1.1098e-9 m/s. A river is represented in model layer 1 using the River (RIV) Package. The models are run as steady state using a single time step with a duration of 1 second.

Table 22–1: Model parameters for example ex-gwf-lgrv.

Parameter	Value
Number of periods	1
Number of layers in refined model	25
Number of rows in refined model	183
Number of columns in refined model	147
Number of layers in coarsened model	9
Number of rows in coarsened model	61
Number of columns in coarsened model	49
Column width (m) in refined model	35.0
Row width (m) in refined model	25.0
Layer thickness (m) in refined model	5.0
Column width (m) in coarsened model	105.0
Row width (m) in coarsened model	75.0
Layer thickness (m) in coarsened model	15.0
Top of the model (m)	variable
Layer bottom elevations (m)	30 to -90
Cell conversion type	0
Recharge rate (m/s)	1.1098e-09

Table 22–1: Model parameters for example ex-gwf-lgrv.

Parameter	Value
Horizontal hydraulic conductivity ( $m/s$ )	5.e-07, 1.e-06, 5.e-05

Table 22–2: Scenario parameters for example ex-gwf-lgrv.

Scenario	Scenario Name	Parameter	Value
1	ex-gwf-lgrv-gr	configuration	Refined
2	ex-gwf-lgrv-gc	configuration	Coarse
3	ex-gwf-lgrv-lgr	configuration	LGR

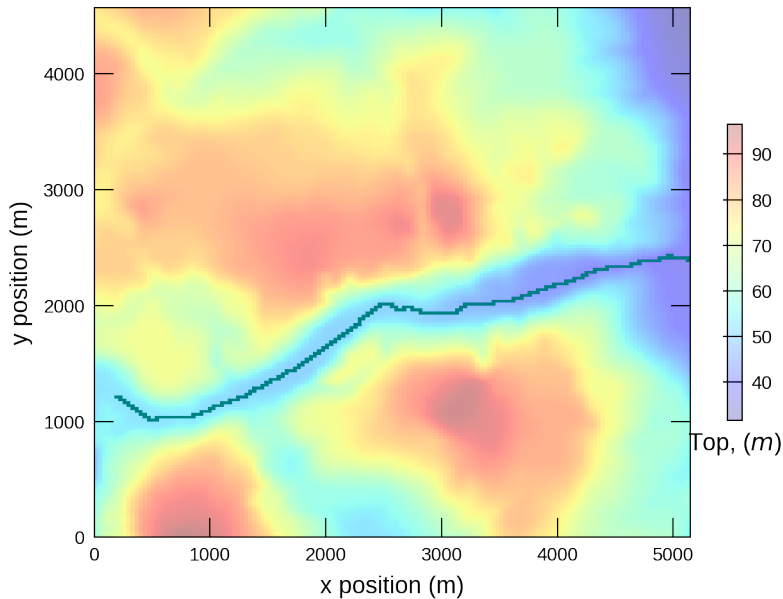


Figure 22–1: Globally refined model grid showing top elevation and river cells. Area of interest is shown as a dashed line.

## 22.2 Example Results

Model results for the three different simulations are shown in figures 22–6, 22–7, and 22–8. Simulated results from the three simulations are in good agreement and demonstrate the different levels of detail that can be achieved with the three grids. Testing of the three simulations indicates that the LGR model is about 25 times slower than the GC model; however the GF model is about 100 times slower than the GC. These numbers indicate that LGR can be used effectively in MODFLOW 6 to include refined inset models within coarser regional models.

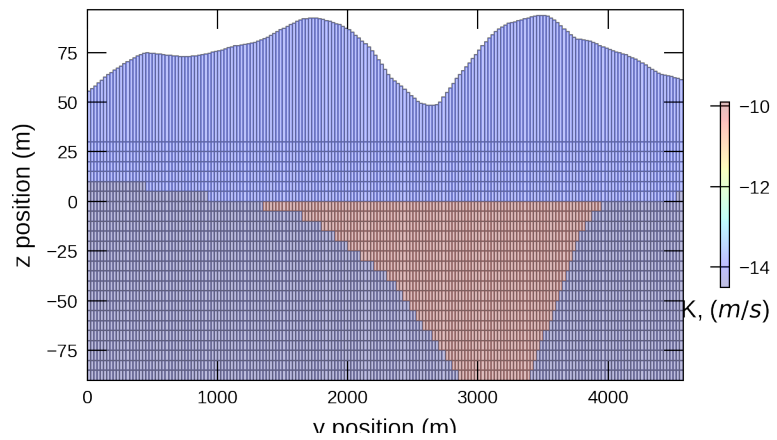


Figure 22–2: Cross section for  $y = 3000\text{ m}$  showing globally refined model grid. Color flood of hydraulic conductivity shows overburden material, valley fill, and deposits into which the valley is incised.

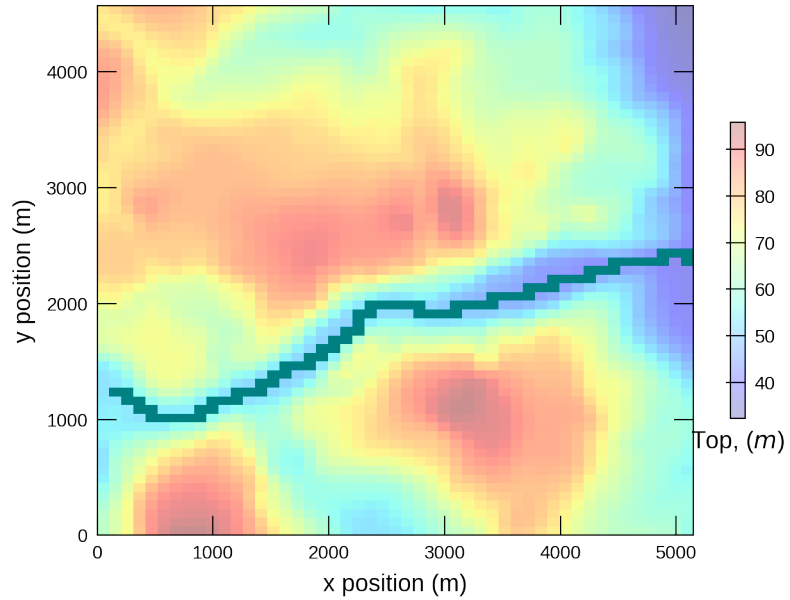


Figure 22–3: Globally coarsened model grid showing top elevation and river cells. Area of interest is shown as a dashed line.

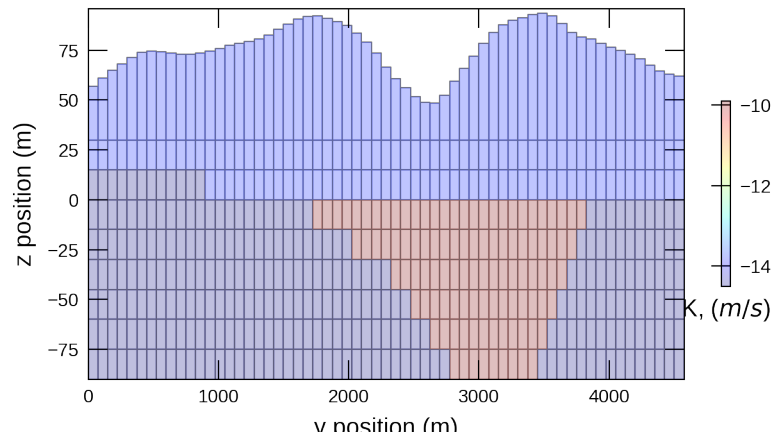


Figure 22–4: Cross section for  $y = 3000\text{ m}$  showing globally coarsened model grid. Color flood of hydraulic conductivity shows overburden material, valley fill, and deposits into which the valley is incised.

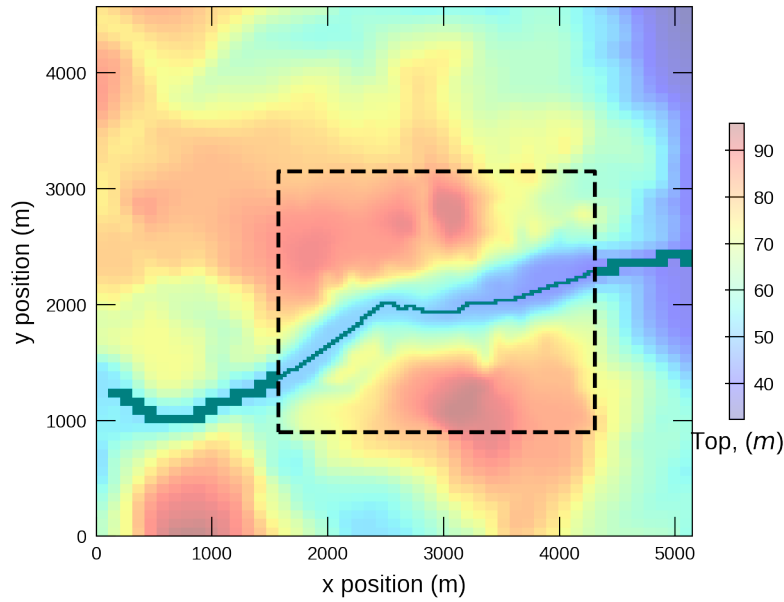


Figure 22–5: Local grid refinement model showing the outer coarse grid and the inner refined model grid. Top elevation and river cells are shown for both the outer and inner grids. Refinement area is shown as a dashed line.

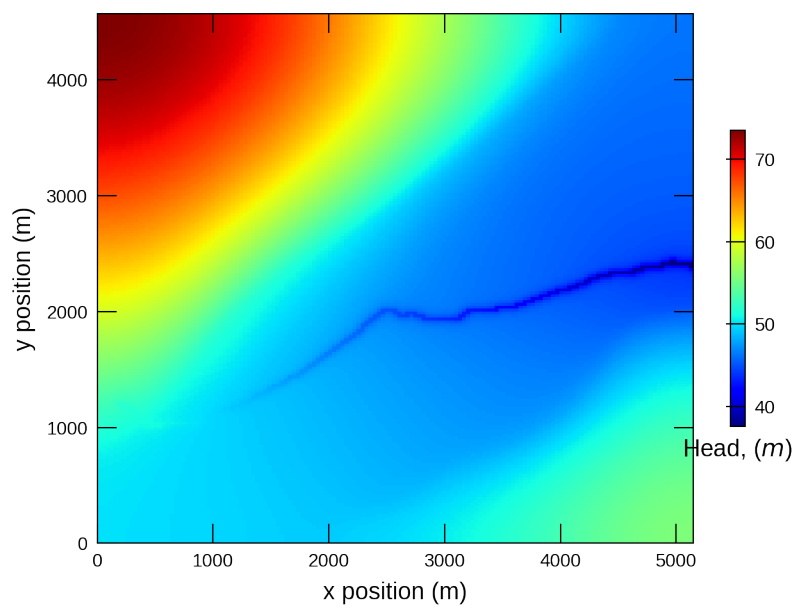


Figure 22–6: Simulated head in layer 1 for the GR model.

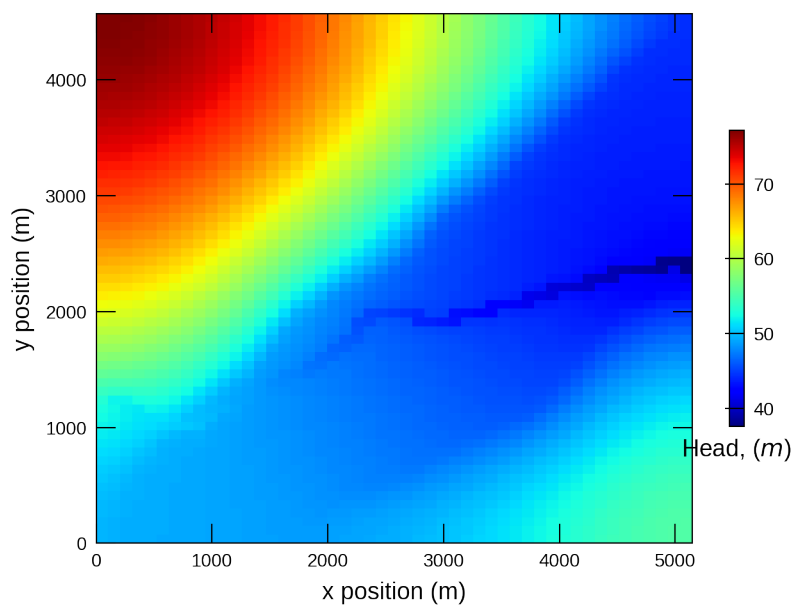


Figure 22–7: Simulated head in layer 1 for the GC model.

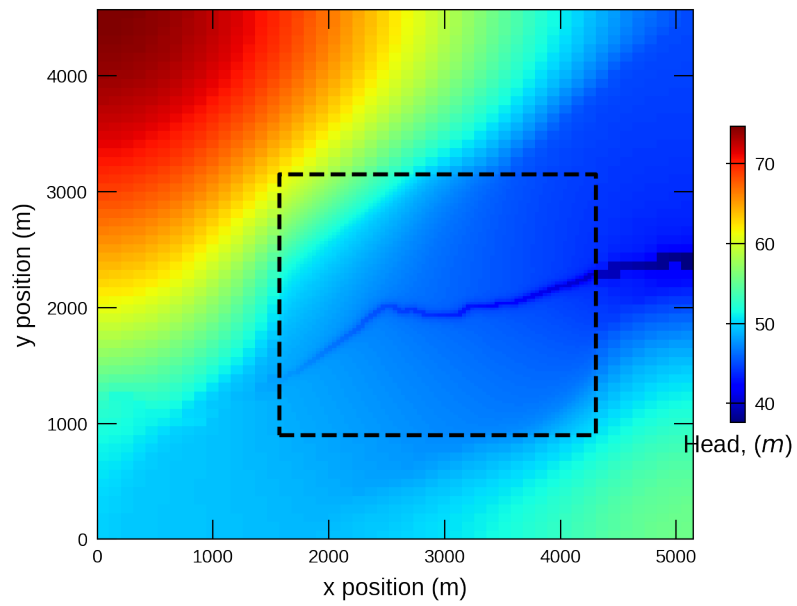


Figure 22–8: Simulated head in layer 1 for the LGR model. Dashed line indicates location of inset model with higher resolution than the outer coarse model.

## 23 Laat toe Periodic Boundary Condition

This example shows how the exchange capability in MODFLOW 6 can be used to simulate spatial periodic boundary conditions (SPBC), such as the one described by [Laat toe and others \(2014\)](#). A SPBC can be used to represent spatially repeating groundwater flow conditions, such as those that might form beneath repeating bedforms on the sea floor. The example simulated here is equivalent to the first MODFLOW simulation reported by [Laat toe and others \(2014\)](#).

### 23.1 Example Description

The problem consists of a two-dimensional cross-section model consisting of 190 layers and 100 columns. Each cell is 0.06 m wide and each layer has a width of 0.03 m. Model parameters are listed in table 23–1.

Table 23–1: Model parameters for example ex-gwf-spbc.

Parameter	Value
Number of periods	1
Number of layers	190
Number of columns	100
Number of rows	1
Column width (m)	0.06
Row width (m)	1.0
Layer thickness (m)	0.03
Top of the model (m)	0.0
Starting head (m)	0.0
Cell conversion type	0
Horizontal hydraulic conductivity (m/d)	1.0

An initial head of 0 m was specified for the model; however this model is not important as the model represents steady-state conditions.

The top of model has a constant-head condition assigned to layer 1. A different constant-head value is assigned to each cell based on a sine wave with an amplitude of 1.0 m and a wavelength of 6 m, which is the length of the model in the x direction. The GWF-GWF Exchange is used to connect the cells on the left side of the model with the cells on the right side of the model. The first cell in each model cell is hydraulically connected to the last cell in each model layer. For example, the cell in (1, 1, 1) is hydraulically connected to the cell in (1, 1, 100). In MODFLOW 6, these cells are connected at the matrix solution level, rather than through outer iterations as was done by [Laat toe and others \(2014\)](#).

### 23.2 Example Results

Model results are shown in figure 23–1. Groundwater flowing into cells on the left side of the model is instantaneously applied to cells on the right side of the model. Because the first column of cells is hydraulically connected to the last column of cell through the GWF-GWF Exchange, flow exiting the model through the left face automatically flows back into the model through the right face.

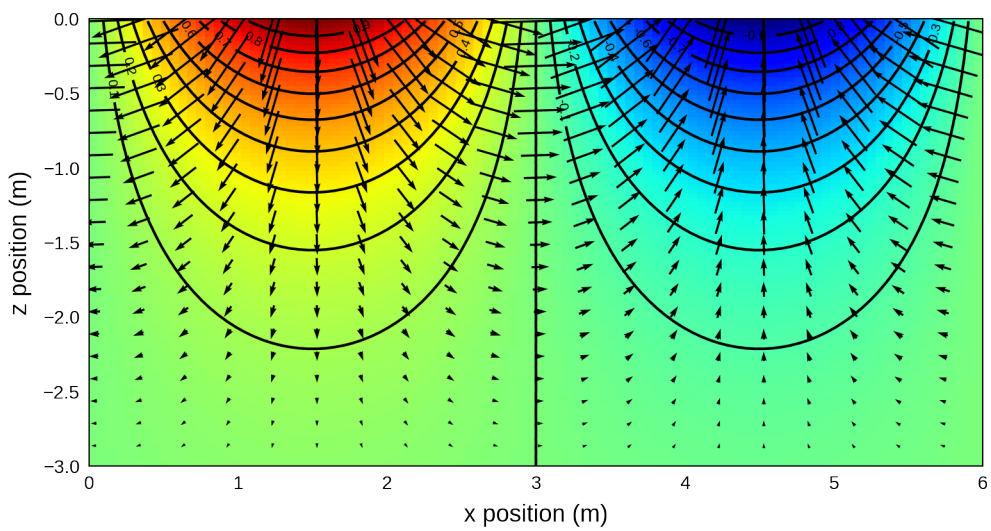


Figure 23–1: Cross section showing simulated head and vectors of specific discharge for the spatial periodic boundary condition example problem. Vectors of specific discharge are shown for every fifth cell in the layer and column directions.

## 24 Elastic Aquifer Loading

This problem simulates elastic compaction of aquifer materials in response to the loading of an aquifer by a passing train. Water-level responses were simulated for an eastbound train leaving the Smithtown Station in Long Island, New York at 13:04 on April 23, 1937 ([Jacob, 1939](#)).

### 24.1 Example Description

The problem is simulated as a two-dimensional half-cell cross-section model. The model grid for this problem consists of three layers, 1 row, and 35 columns (fig. 24–1). The model layers were defined based on hydrostratigraphic information in [Jacob \(1939\)](#). The upper and lower layer represent an unconfined upper aquifer and confined lower aquifer separated by a confining unit (fig. 24–1B). The upper and lower aquifers are composed of sand and gravel, respectively, and the confining unit is composed of clay.

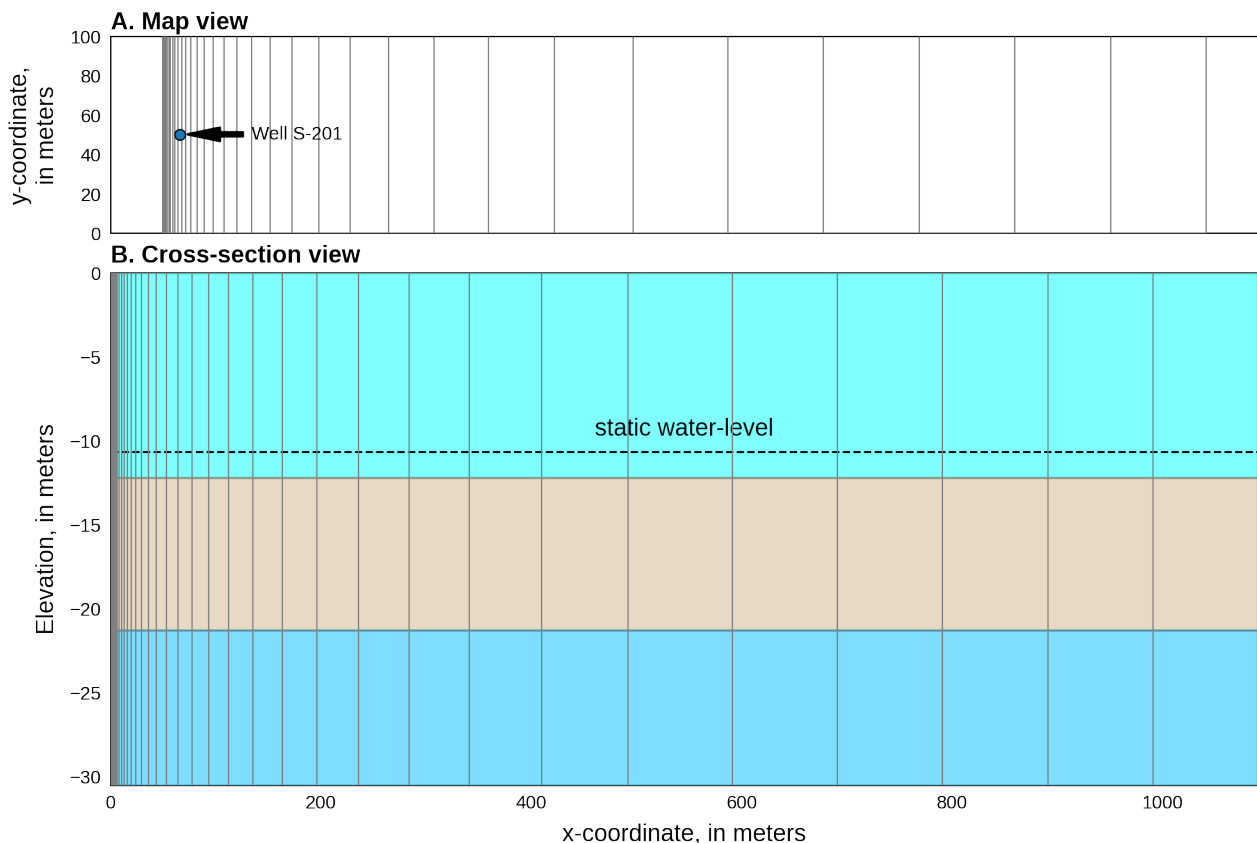


Figure 24–1: Diagram showing the model domain for the elastic aquifer loading problem. *A*, plan view, and *B*, cross-section view

The model has a top elevation of 0 meters and layer bottom elevations of -12.2, -21.3, and -30.5 meters, for layers 1, 2, and 3 respectively. DELR increases from 0.5 to 98.9 meters in columns 1 to 30, using a multiplier of 1.2; a DELR value of 100 meters is specified in columns 31 to 35. DELC is specified with a constant value of 100.6 meters and is based on the an estimate of the total length of the train (table 24–1). The simulation consists of two stress periods. The first stress period is

steady-state with a single time step and is 0.5 seconds in length. The second stress period is transient, 58.5 seconds in length, and is divided into 117 equally sized time steps.

Table 24–1: Assumed train properties for example ex-gwf-csub-p01.

Type	Number	Length, in meters	Weight, in kilograms
Engine	2	21.3	108,862.08
Car	4	79.3	199,580.48
Total	–	100.6	308,442.56

Initial hydraulic properties were based on aquifer material data in [Freeze and Cherry \(1979\)](#) and are summarized in table 24–2. Hydraulic conductivity was assumed to be isotropic in the horizontal and vertical directions in each layer. Hydraulic conductivity and specific storage values were modified from initial values during model calibration, which is described below. The specific storage was defined to be 0 for all layers in the storage (STO) package. All model layers were defined to be convertible for hydraulic conductivity and storage properties. Default flow property (NPF) and storage (STO) package settings were used. An initial head of -10.7 meters was defined for each layer.

Table 24–2: Model parameters for example ex-gwf-csub-p01.

Parameter	Value
Number of periods	2
Number of layers	3
Number of columns	35
Number of rows	1
Initial column width (m)	0.5
Maximum column width	100.0
Row width (m)	100.6
Top of the model (ft)	0.0
Layer bottom elevations (m)	-12.2, -21.3, -30.5
Starting head (m)	-10.7
Cell conversion type	1, 0, 0
Horizontal hydraulic conductivity (m/s)	1.8e-5, 3.5e-10, 3.1e-5
Specific yield (unitless)	0.1, 0.05, 0.25
Specific gravity of moist soils (unitless)	1.7
Specific gravity of saturated soils (unitless)	2.0
Coarse grained elastic storativity (1/m)	3.3e-5, 6.6e-4, 4.5e-7
Coarse-grained porosity (unitless)	0.25, 0.50, 0.30

The effective stress formulation of the CSUB package was used to simulate one-dimensional compaction of aquifer materials. A specific gravity of 1.7 and 2.0 was defined for moist and saturated sediments, respectively. Water compressibility was simulated using a specific gravity of water of 9,806.65 Newtons per cubic meters and water compressibility of  $4.6512 \times 10^{-10}$  per Pascal. The thickness of compressible materials and total porosity were updated during the simulation in response compaction.

[Jacob \(1939\)](#) measured water-level fluctuations in well S-201 (fig. 24–1A). S-201 is located 16.5 meters north of the tracks (column 12) and has a total depth of 27.1 meters (model layer 3). A limited amount of data on the position of the train relative to well S-201 was provided by [Jacob \(1939\)](#). As a result, it was assumed that the original water-level fluctuation data is a proxy for train loading. The maximum water-level fluctuation value was assumed to correspond to loading by the full weight of the train (table 24–1) and a zero water-level fluctuation corresponded to complete

unloading. The estimated loading of the aquifer (fig. 24–2A) was converted to an equivalent height of water over the first cell of the model using the cell area, one-half the total train weight (because the problem is simulated as a half-cell problem), and the density of water (1,000 kilograms per cubic meters). Because well S-201 is located 16.5 meters north of the tracks, the estimated loading was translated in time by -1.5 seconds to account for the time for loading to cause water-level fluctuations at the well; the -1.5 second adjustment was determined through trial and error. Train loading was applied in column 1 using a time series file. Flow was not allowed to leave the model domain and no sources/sinks were applied to the model. The left and right side of the model domain are represented as a free-slip (roller) boundaries.

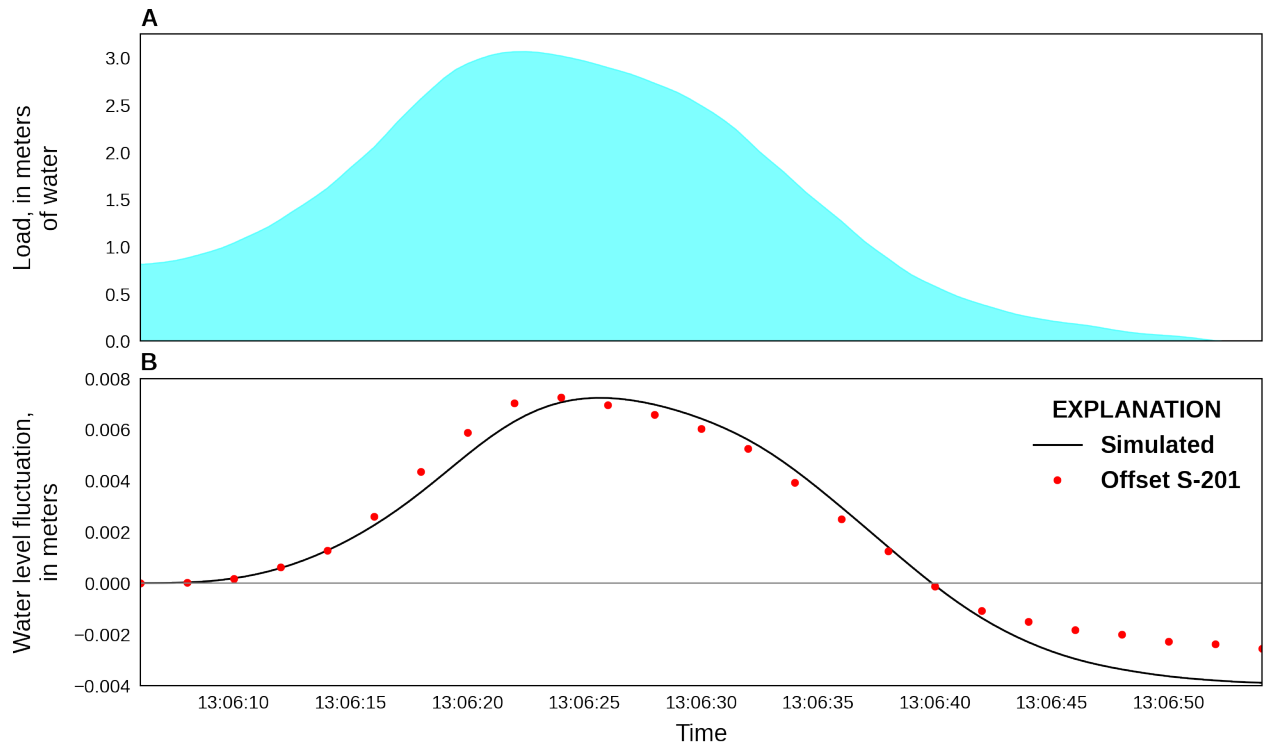


Figure 24–2: Graphs showing the applied loading and water-level fluctuations for the elastic aquifer loading problem. A, shows the loading applied to the top of the first column in layer 1, and B, shows simulated and offset water-level fluctuations at well S-201

The water-level fluctuation data used to calibrate the hydraulic parameters was offset so that the initial water-level fluctuation reported (after rewinding the pen-carriage cable) corresponded to a zero value. The adjusted water-level at the end of the simulation period is less than zero since loading of the aquifer by the train was already occurring at the beginning of the data presented in Jacob (1939) (fig 24–2B). The water-level fluctuation data was offset rather than extended because of uncertainties about the train velocity and acceleration prior to the simulation period.

PEST++ (Welter and others, 2015) was used to calibrate the horizontal hydraulic conductivity in layers 1 and 3, the vertical hydraulic conductivity in layer 2, and specific storage values in all model layers. The water-level fluctuation observations were weighted by  $\max(0.01, h_i/\max(h))$  to force PEST++ to favor the peak water-level fluctuations. The water-level fluctuations were only sensitive to the hydraulic conductivity and specific storage of model layer 3; as a result, PEST++ only

modified the hydraulic properties of layer 3. Final hydraulic properties used in the model are shown in table 24–2.

## 24.2 Example Results

A comparison of simulated and observed water-level fluctuations is shown in figure 24–2B. For this problem, the MODFLOW 6 solution does not show perfect agreement with the offset water-level fluctuations. The primary source of model error is likely due primarily to inaccuracies in the loading being applied in the model. Use of a two-dimensional cross-section model instead of a three-dimensional model may also be responsible for a portion of the model error shown in figure 24–2B. Horizontal strain has also been found to be significant in close proximity pumping wells (the source of strain) and may also contribute to the model error (Burbey, 2001).

## 25 Delay Interbed Drainage

This problem simulates the drainage of a thick interbed caused by a step decrease in hydraulic head in the aquifer and is based on sample problem 1 in [Hoffmann and others \(2003\)](#).

### 25.1 Theory

The equilibration of hydraulic heads in thick interbeds imbedded in an aquifer system typically lags head changes in the surrounding aquifer as a result of the characteristically low vertical hydraulic conductivity of fine-grained silts and clays that constitute the interbeds. Similarly, the hydraulic gradient within the interbeds can be treated as vertical if the horizontal extents of the interbeds are much greater than their thicknesses, the delayed dissipation of unequilibrated heads within the interbeds can be described by the one-dimensional diffusion equation,

$$\frac{\partial^2 h}{\partial z^2} = \frac{S'_S}{K'_v} \frac{\partial h}{\partial t}, \quad (25-1)$$

where  $z$  is the vertical spatial coordinate (L),  $S'_S$  is the specific storage of the interbed (unitless),  $K'_v$  is the vertical hydraulic conductivity of the interbed (L/T), and  $t$  is time (T). The solution of this diffusion problem is identical to heat diffusion. [Carslaw and Jaeger \(1959\)](#) developed an analytical solution for heat diffusion from a slab with the ends at a constant temperature that can be recast to solve equation 25-1 for delayed flow from a thick interbed. If the initial head at  $t = 0$  is  $h_0$  throughout the thickness of the interbed ( $b_0$ ), and the head in the surrounding aquifer is  $\Delta h$  above  $h_0$  for  $t > 0$ , the head distribution [ $h(z, t)$ ] for the interbed can be written as the infinite series

$$h(z, t) - h_0 = \Delta h - \frac{4\Delta h}{\pi} \sum_{k=0}^{\infty} \frac{-1^k}{2k+1} e^{-\frac{\pi^2}{4}\frac{t}{\tau_k}} \cos\left(\frac{(2k+1)\pi z}{b_0}\right), \quad (25-2)$$

where the time constant,  $\tau_k$ , is defined as

$$\tau_k = \frac{\left(\frac{b_0}{2}\right)^2 S'_S}{(2k+1)^2 K'_v}. \quad (25-3)$$

In equation 25-2,  $z = 0$  is assumed to be at the midplane of the interbed, with the boundaries at  $\pm \frac{b_0}{2}$ . Note that both the coefficients in the sum and the  $\tau_k$  decrease as  $k$  increases. Thus, the true head distribution can be adequately described by a finite number of addends ( $k$ ), particularly for later times. In the context of interbed compaction and land subsidence, the time delay caused by slow dissipation of transient overpressures is often given in terms of the time constant

$$\tau_0 = \frac{\left(\frac{b_0}{2}\right)^2 S'_S}{K'_v}, \quad (25-4)$$

which is the time during which about 93 percent of the ultimate compaction for a given decrease in head occurs ([Riley, 1969](#)). Because  $\tau_0$  is proportional to  $S'_S$ , which generally is much larger for inelastically deforming interbeds than for elastically deforming interbeds, deformation in elastically deforming interbeds is often assumed to occur instantaneously. The same is true for very thin inelastically deforming interbeds. Thus, equation 25-4 can be used to determine in which interbeds the time constant exceeds the model time step, necessitating consideration of use of delay-interbeds, which account for delayed drainage processes, instead of no-delay interbeds.

Under constant geostatic stress conditions, compaction in the interbed can be directly related head changes using

$$\Delta b = S'_S \Delta h, \quad (25-5)$$

where  $\Delta b$  is the change in thickness of the interbed (L).

## 25.2 Example Description

Static model parameters are summarized in table 25–1. The model grid for this problem consists of 1 layer, 1 row, and 3 columns (fig. 25–1). The model has a top elevation of 0 meters and bottom elevation of -1,000 meters. DELR and DELC are equal to 1 meter. The simulation consists of one transient stress period 1,000 days in length, and is divided into 100 variable length time steps calculated using a time step multiplier equal to 1.05.

Table 25–1: Model parameters for example ex-gwf-csub-p02.

Parameter	Value
Number of periods	1
Number of layers	1
Number of columns	3
Number of rows	1
Column width (m)	1.0
Row width (m)	1.0
Top of the model (ft)	0.0
Layer bottom elevations (m)	-1000.0
Starting head (m)	0.0
Cell conversion type	0
Horizontal hydraulic conductivity (m/d)	1.0e6
Specific gravity of moist soils (unitless)	1.7
Specific gravity of saturated soils (unitless)	2.0
Interbed drainage time constant (unitless)	1000.0
Coarse-grained material porosity (unitless)	0.2
Elastic specific storage (1/m)	1.0e-5
Inelastic specific storage (1/m)	1.0e-2
Interbed porosity (unitless)	0.45
Initial interbed head (m)	1.0
Initial preconsolidation head (m)	1.0

The hydraulic conductivity in the aquifer was set to a very large value ( $1 \times 10^6$  meters per day), so that the head in the aquifer in the center cell remains constant. The specific yield and specific storage in the STO package were set to 0. Default flow property (NPF) and storage (STO) package settings were used. Initial heads were specified to be 0 meters.

### 25.2.1 Head-Based Formulation

Initially, the head-based formulation of the CSUB package was used to simulate compaction of the delay interbed and compare to analytical results calculated using equations 25–2 and 25–5 (table 25–2). Ten finite-difference nodes represent the half-thickness of the interbed. The time constant,  $\tau_0$  (eq. 25–4), was chosen to be 1,000 with vertical hydraulic conductivity set to  $2.5 \times 10^{-6}$  meters per day, interbed thickness set to 1 meters, and elastic skeletal specific storage set to  $1 \times 10^{-5}$  per meter and inelastic skeletal specific storage set to 0.01 per meter. Meters and days units have

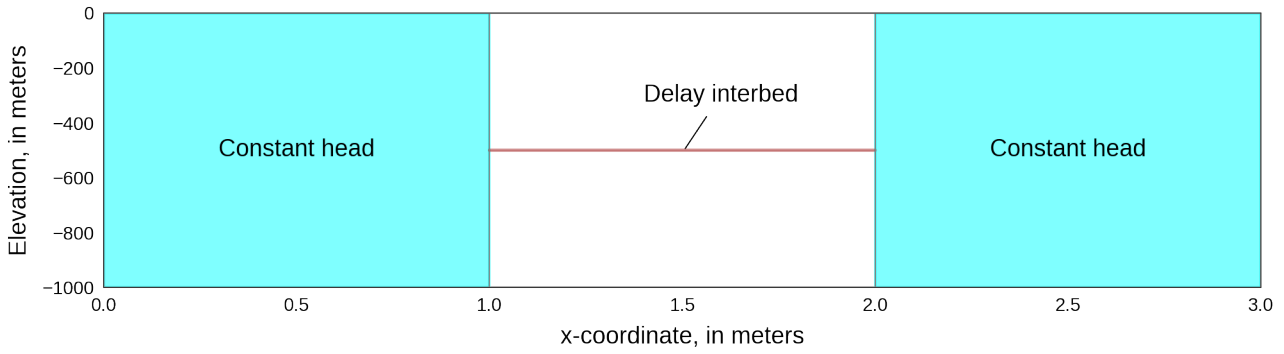


Figure 25–1: Model domain and setup for the delay interbed drainage problem. Interbed drainage is the result of step decrease in head in the aquifer

been used in this problem but any consistent set of length and time units results in the same solution. The specific storage of coarse-grained aquifer material were specified to be  $0 \times 10^{-6}$  per meter. Water compressibility was not simulated in this problem and the thickness of compressible materials and total porosity were not updated during the simulation.

Table 25–2: Scenario parameters for example ex-gwf-csub-p02.

Scenario	Scenario Name	Parameter	Value
1	ex-gwf-csub-p02a	head based	True
		bed thickness	(1.0,)
		kv	(2.5e-06,)
		ndelaycells	19
2	ex-gwf-csub-p02b	head based	False
		bed thickness	(1.0,)
		kv	(2.5e-06,)
		ndelaycells	19
3	ex-gwf-csub-p02c	head based	True
		bed thickness	(1.0, 2.0, 5.0, 10.0, 20.0, 50.0, 100.0)
		kv	(2.5e-06, 1e-05, 6.25e-05, 0.00025, 0.001, 0.00625, 0.025)
		ndelaycells	1001

Constant-head cells, with a value of 0 meters, bound the delay interbed in column 2. The water released from the interbed during the simulation can leave the system through these constant-head cells. The starting head and the preconsolidation head in the delay interbed were specified to be 1 meter higher than the initial head in the surrounding aquifer.

The resulting compaction of the interbed is compared to the analytical solution (derived using equations 25–2, 25–4, and 25–5) in figure 25–1. The CSUB-computed values closely match the analytical values. The small differences, particularly at early times, may be at least partly due to the

fact that the aquifer head in the simulation does not remain exactly constant as a result of water entering the aquifer from the interbed. Because of the finite transmissivity of the aquifer, the head in the aquifer briefly rises to about 2 percent of the starting head in the interbed during the first time step.

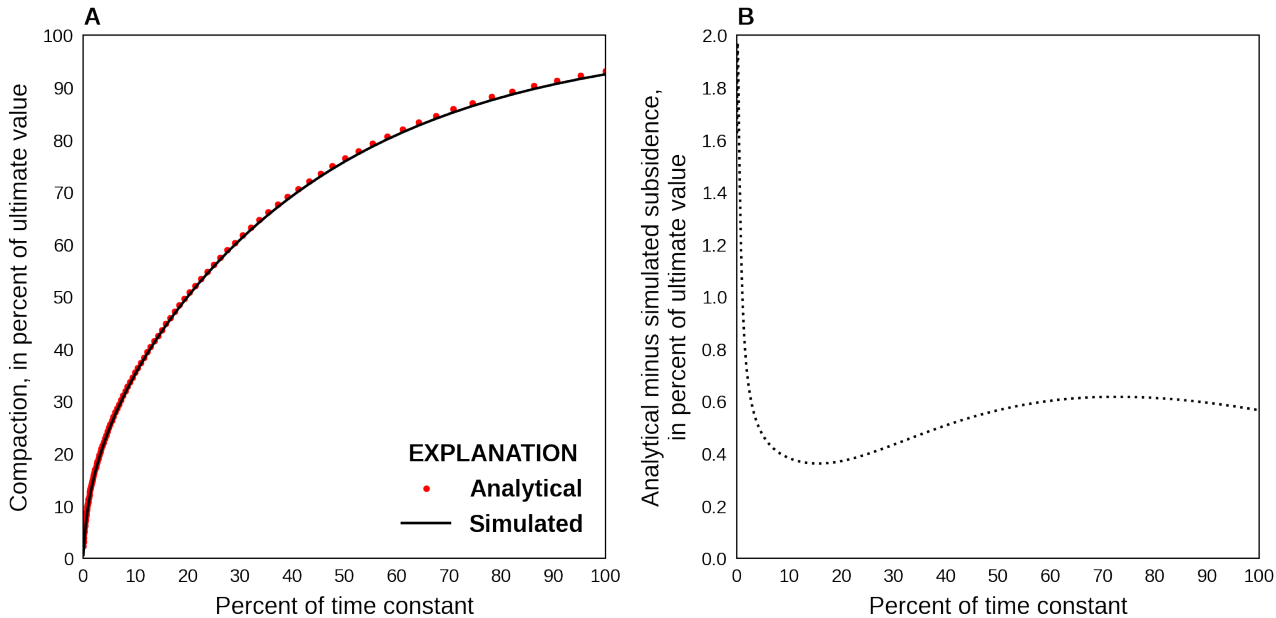


Figure 25–2: Graphs showing comparisons of simulated compaction with the head-based formulation and the analytical solution for the delay interbed drainage problem. *A*, comparison of the compaction history simulated with the analytical solution to the problem, and *B*, difference between the analytical solution and simulated compaction

### 25.2.2 Effective Stress-Based Formulation

To evaluate differences between the head- and effective stress-based formulations, the problem shown in figure 25–1 was modified to use the effective stress-formulation (table 25–2). A total of 19 finite-difference nodes were used in the effective stress-based formulation so that results could be directly compared to the head-based formulation that used 10 finite-difference cells to represent the half-thickness of the interbed. A specific gravity of 1.7 and 2.0 was defined for moist and saturated sediments, respectively. The initial preconsolidation stress was set to be 1 meter less than the initial effective stress of 1,000 meters and is based on the initial preconsolidation head, which was defined to be 1 meter above the initial head in the head-based formulation.

The resulting effective stress-based compaction of the interbed is compared to the head-based solution in figure 25–3. The effective stress-based values closely match the head-based values. The small differences (< 0.1%) are partly due to the fact that calculated specific storage values are not constant in the effective stress-formulation. Furthermore, the inelastic and elastic compression indices (41.8 and  $4.18 \times 10^{-2}$  (unitless)), respectively, which are internally calculated from the initial effective stress and the user-provided inelastic and elastic specific storage values, results in a slightly smaller initial inelastic storativity value ( $9.5 \times 10^{-3}$  versus  $1.0 \times 10^{-2}$ ) that increase to values slightly larger than the user-provided inelastic storativity in subsequent time steps.

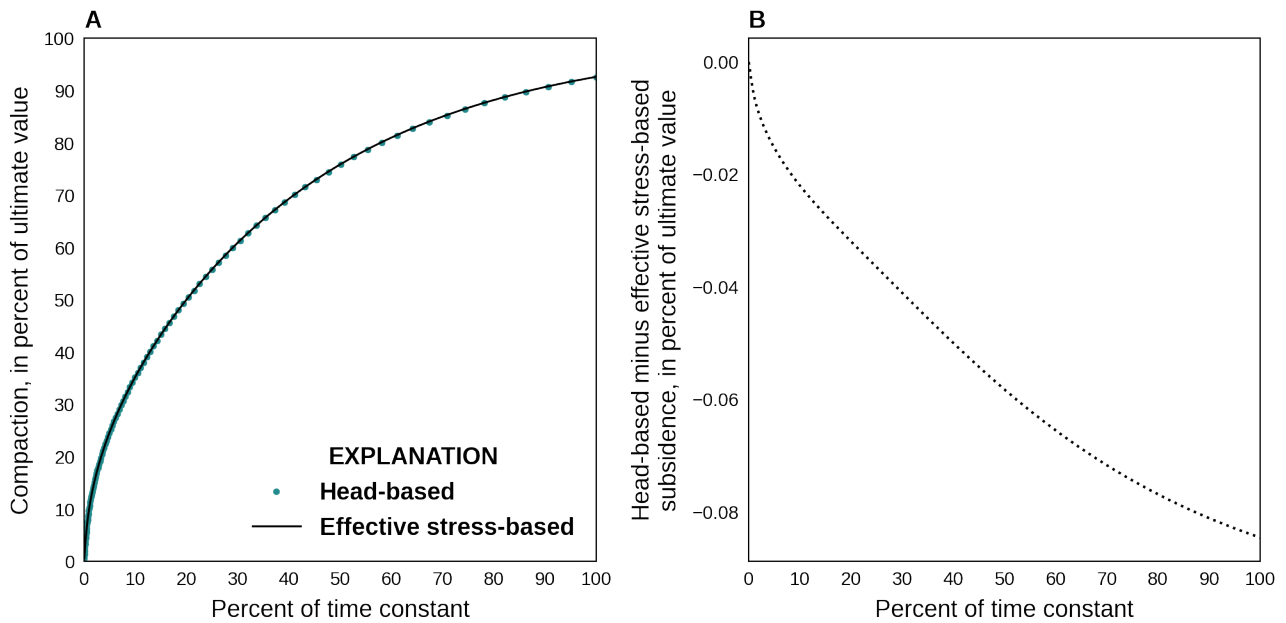


Figure 25–3: Graphs showing comparisons of simulated compaction for head- and effective stress-based formulations for the delay interbed drainage problem. *A*, comparison of the compaction history simulated with the head- and effective stress-based formulation solution to the problem, and *B*, difference between the simulated head- and effective stress-based formulation compaction

Another reason the difference between the head- and effective stress-based compaction shown in figure 25–3 is small is the interbed thickness is small (1 meter) and as a result the difference between the effective stress at the top and bottom of the interbed is also small.

### 25.2.3 Effect of Interbed Thickness on the Effective Stress-Based Formulation

To evaluate the effect of the interbed thickness affects compaction, head- and effective stress-based models were run with interbed thicknesses ranging from 1 to 100 m (table 25–2). A time constant ( $\tau_0$ ) of 1,000 was used with elastic and inelastic skeletal specific storage values of  $1 \times 10^{-5}$  and 0.01 per meter, respectively, were used for each interbed thickness evaluated. The vertical hydraulic conductivity for each interbed thickness evaluated was calculated using equation 25–3 and the specified  $\tau_0$  and specific storage values. The calculated vertical hydraulic conductivity ranged from  $2.5 \times 10^{-6}$  to 0.025 meters per day for interbed thickness ranging from 1 to 100 meters, respectively. A total of 1,001 finite-difference nodes were used to simulate the interbed for the head- and effective stress-based formulation simulations to provide additional spatial resolution for simulated interbed heads; the head-based simulations were simulated using a full-cell formulation. All other model parameters for the simulations that evaluated different interbed thicknesses were unchanged from the original values.

The difference between the analytical and simulated compaction and drainage rates at the top and bottom of the interbed relative to analytical drainage rates are shown in figure 25–4. The difference between head- and effective stress-based compaction for a 1 meter interbed thickness shown in figure 25–4A are identical to the results shown in figure 25–3B. In general, the differences between the simulated results and the analytical solution are comparable for interbed thickness less

than 20 meters. Coincident with compaction differences, the average difference in drainage from the top and bottom of the interbed to the aquifer is greater than 0.7% (fig. 25–4B) for interbed thicknesses greater than 10 meters as a result of larger differences in the effective stress at the top and bottom of the interbed. The average difference between the effective stress at the bottom and top of the interbed is 2.02%, 5.13%, and 10.5% of the average interbed effective stress for the simulations with 20, 50, and 100 meters interbed thicknesses, respectively.

Figure 25–5 shows the vertical distribution of the difference in head- and effective stress-based formulation interbed heads relative to head-based interbed heads for each of the interbed thicknesses evaluated. Head-based interbed heads are symmetric about the center line of the interbed, with lower heads at the top and bottom of the interbed and the highest heads at the center of the interbed. As a result, negative and positive differences shown in figure 25–5 represent higher and lower interbed heads in the effective stress-based formulation than the head-based formulation, respectively. Generally, effective stress-based interbed heads are higher and lower in the top and bottom halves of the interbed, respectively, and differences are greatest for interbed thicknesses greater than 10 meters. The spatial distribution of interbed head differences is controlled by the decrease in the inelastic specific storage value resulting from the increase in effective stress with depth and the reduction in the water released from storage with depth in the interbed, which results in increased head changes with depth with the effective stress-formulation. As the simulation progresses, differences propagate from the top and bottom of interbed into the interbed as the maximum difference decreases.

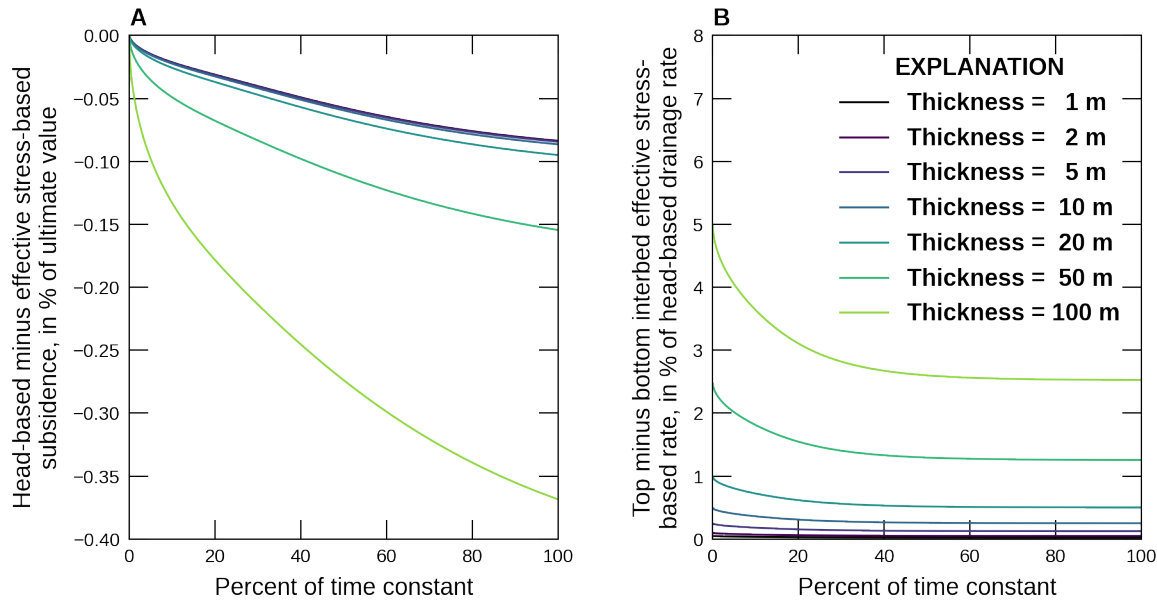


Figure 25–4: Graphs showing the difference between head- and effective stress-based compaction for different interbed thicknesses for the delay interbed drainage problem. A, difference between the head- and effective stress-based formulation compaction, and B, difference between drainage at the top and bottom of the interbed relative to the head-based formulation interbed drainage

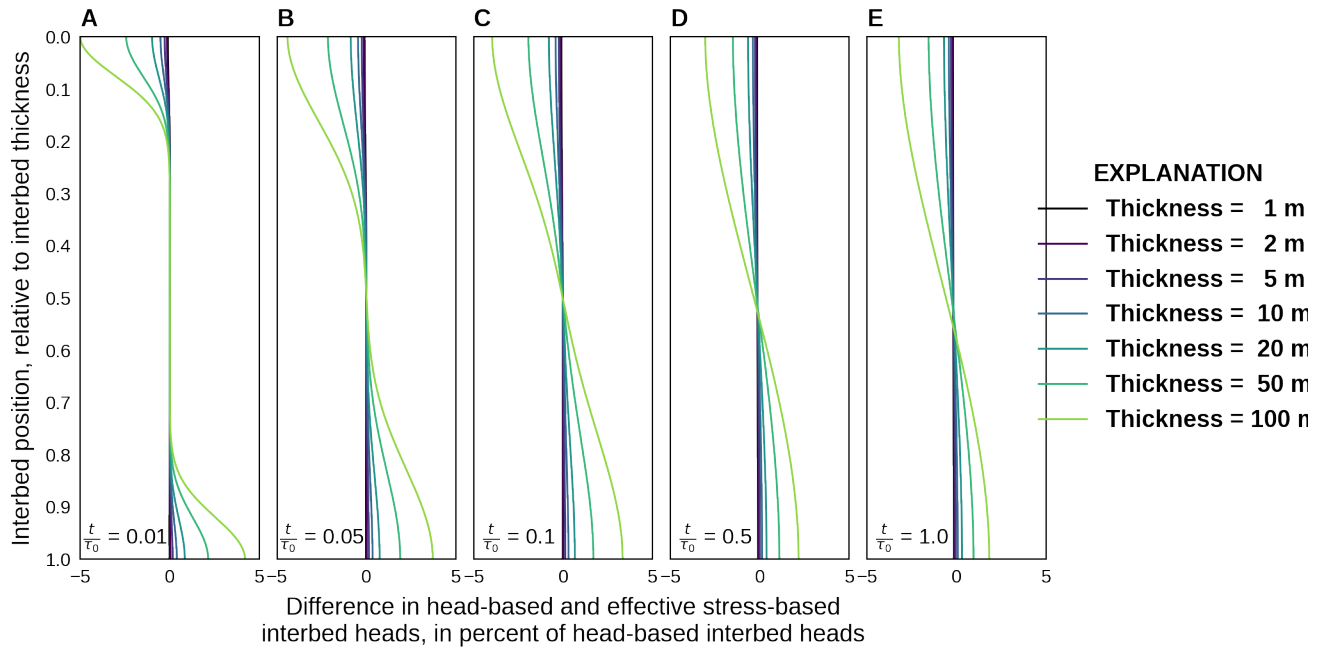


Figure 25-5: Graphs showing differences between head- and effective stress-based formulation interbed heads relative to head-based interbed heads for variable interbed thicknesses at select fractions of the time constant ( $\tau_0$ ) for the delay interbed drainage problem. A, 1 percent of  $\tau_0$ , B, 5 percent of  $\tau_0$ , C, 10 percent of  $\tau_0$ , D, 50 percent of  $\tau_0$ , and E, 100 percent of  $\tau_0$

## 26 One-Dimensional Compaction

A one-dimensional MODFLOW 6 model was developed by [Sneed \(2008\)](#) to simulate aquitard drainage, compaction and, land subsidence at the Holly site, located at the Edwards Air Force base, in response to effective stress changes caused by groundwater pumpage in the Antelope Valley in southern California (fig. 26–1). Land subsidence resulting from groundwater level declines, has long been recognized as a problem in Antelope Valley, California. The original one-dimension compaction model was calibrated to extensometer data from the USGS Holly site (station name [008N010W01Q005S](#)) for the period from 1990 to 2006, and used a head based-formulation to represent compaction. The model of [Sneed \(2008\)](#) has been modified to use the effective stress formulation available in the CSUB package for MODFLOW 6.

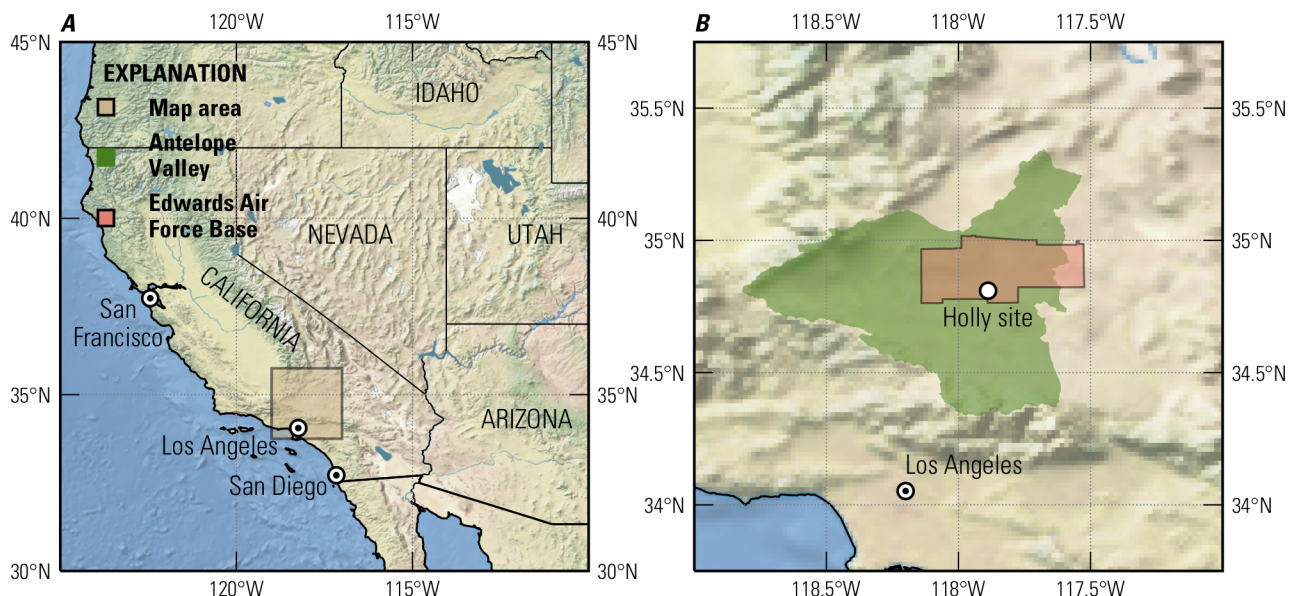


Figure 26–1: Maps showing the location of the study area for the one-dimensional compaction problem in southern California. *A*, location of the study area in southern California and *B*, location of the Holly site and Edwards Air Force Base in the Antelope Valley. Cross-blended hypsometric tints with relief, water, drains and ocean bottom background image from Natural Earth and is available at <https://www.naturalearthdata.com/downloads/50m-raster-data/50m-cross-blend-hypso/>, accessed on July 9, 2019

### 26.1 Site Description

The subsurface geology at the Holly site comprises Quaternary alluvial and lacustrine deposits from land surface to about 260 meters below land surface, consolidated late Tertiary and early Quaternary sedimentary continental deposits from about 260 to 330 meters below land surface, and decomposed basement complex. Lithologic and geophysical logs of the Holly site indicate the presence of relatively thin interbedded aquitards, ranging from 0.3 to 5 meters thick, and two thicker aquitards 20 meters (37–57 meters below land surface) and 19 meters (92–111 meters below land surface) thick. The

upper aquitard is interpreted as a regionally extensive, confining unit. The groundwater system at the Holly site is comprises two aquifer systems—an unconfined system and a confined system, which are separated by lacustrine blue-clay deposits that constitute the confining unit. The upper aquifer is unconfined, about 37 meters thick and the water table is about 20 meters below land surface. The confined-aquifer system at the site extends about 275 meters below the confining unit, where it is underlain by weathered bedrock. The middle aquifer is the source of most of the groundwater pumped from the well field closest to the Holly site. Additional information on the hydrogeology of the Holly site and the Antelope Valley can be found in [Sneed and Galloway \(2000\)](#) and [Sneed \(2008\)](#).

Compaction at the Holly site for the period from 1990 through 2006 was measured using a counterweighted pipe extensometer designed to measure compaction in the interval from 4.6 to about 260 meters below land surface. The principal mode of compaction at the Holly site is a seasonally dependent step response. Larger rates of compaction are associated with summer water-level drawdowns and despite groundwater level recoveries of more than 3 meters during the winter, compaction continues, at a reduced rate. The absence of aquifer-system expansion during seasonal water-level recovery is consistent with the delayed drainage and resultant delayed, or residual, compaction of thick aquitards.

## 26.2 Example Description

The model grid for this problem consists of 14 layers, 1 row, and 1 column (fig. 26–2). The model layers are based on the model of [Sneed \(2008\)](#), with the exception of the top of model layer 1 which was modified from the original value of -27.74 meters to 0 meters to allow the model to account for unsaturated conditions above the water table when calculating geostatic and effective-stresses. Model layer thicknesses are summarized in table 26–1. DELR and DELC are equal to 1 meter. The model consists of 353 stress periods covering the period from May 8, 1908 to September 4, 2006. The duration of model stress periods and time steps for the period from May 8, 1908 to May 9, 1990 (“early time”) were annual and monthly—365.25 and 30.4375 days, respectively, and were 22 and 1 days, respectively, for the period from May 9, 1990 to September 4, 2006 (“late time”). The nearly century duration of the simulations allows for comparisons of aquifer-system compaction owing to sustained groundwater pumpage and water-level declines through the period of groundwater development and seasonal groundwater level cycling since 1990.

Table 26–1: Aquifer properties for example ex-gwf-csub-p03.

<b>Layer</b>	<b>Thickness</b>	<b>Hydraulic conductivity</b>	<b>Initial head</b>
1	36.88	9.14e-3	0.00
2	5.49	3.66e-6	1.57
3	8.23	3.66e-6	3.38
4	6.40	3.66e-6	5.56
5	12.80	9.14e-3	6.77
6	0.30	9.14e-3	6.77
7	21.95	9.14e-3	6.77
8	5.18	4.57e-6	6.77
9	8.53	4.57e-6	6.77
10	5.49	4.57e-6	6.77
11	0.30	9.14e-3	6.77
12	167.34	9.14e-3	6.77
13	0.30	9.14e-3	5.55
14	53.34	9.14e-3	5.55

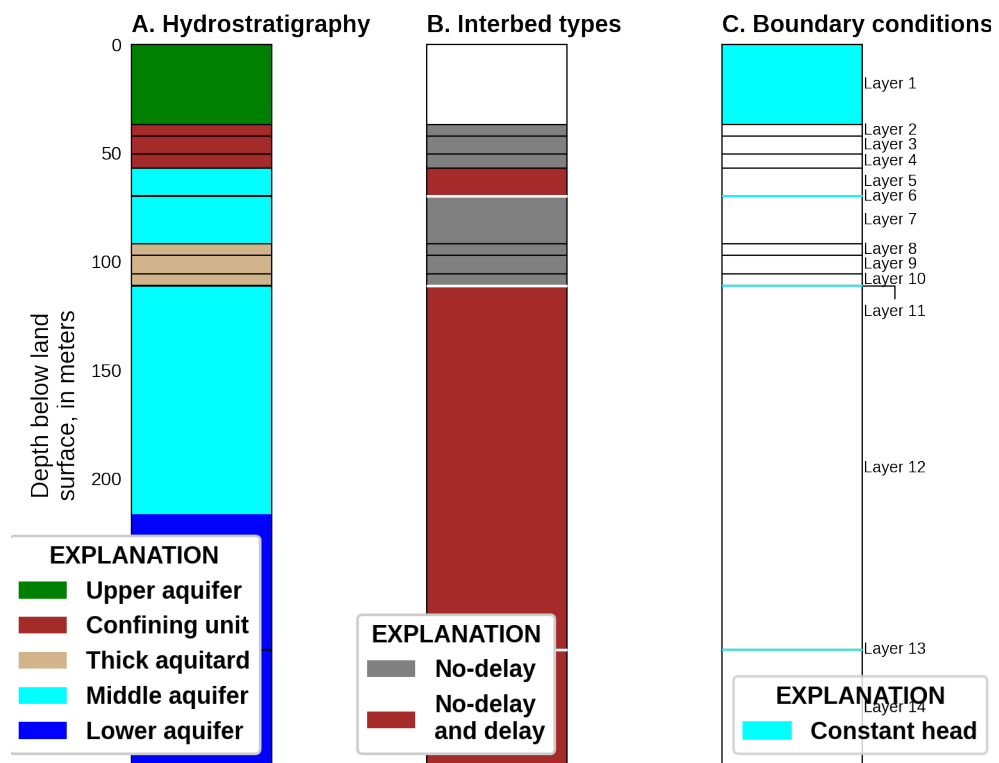


Figure 26–2: Diagram showing the model domain and setup for the one-dimensional compaction problem. *A*, hydrostratigraphy, *B*, interbed types used in aquifer and confining units, and *C*, location of constant-head boundary conditions

---

Hydraulic properties used in the model are shown in table 26–1. Sneed (2008) specified different horizontal and vertical hydraulic conductivity values for each layer; however, vertical hydraulic conductivity values from Sneed (2008) were assigned as the horizontal hydraulic conductivity values in each layer since there is no horizontal flow in this one-dimensional problem. The specific yield and specific storage in the STO package were defined to be 0 for all layers. All model layers are defined to be non-convertible for hydraulic conductivity and storage properties. Default NPF and STO package settings were used. Initial heads in the model range from 0. to 6.77 meters (table 26–1).

The effective stress formulation of the CSUB package was used to simulate compaction of aquifer materials. Fine-grained materials defined as delay interbeds were discretized using 39 cells and assigned a uniform vertical hydraulic conductivity of  $4.57 \times 10^{-6}$  meters per day. A specific gravity of 1.7 and 2.0 was defined for moist and saturated sediments, respectively. Water compressibility was simulated using a specific gravity of water of 9,806.65 Newtons per cubic meters and water compressibility of  $4.6512 \times 10^{-10}$  per Pascal. The thickness of compressible materials and total porosity were updated during the simulation in response compaction.

Interbedded aquitards ranged from 0.3 to 5.5 meters in thickness. The Holly model simulates interbedded aquitards less than 1.5 meters thick using no-delay interbeds (ultimate compaction occurs within a model time step), and simulates interbedded aquitards 1.5 meters thick or greater using delay-interbeds (ultimate compaction does not occur within a model time step). A total of 18 interbedded aquitards ranging from approximately 0.3 to 1.2 meters thick, with a total aggregate thickness of approximately 12 meters, were modeled as no-delay interbeds and 10 interbedded aquitards ranging from approximately 1.5 to 5.5 meters thick, with a total aggregate thickness of approximately 27 meters, were modeled as delay interbeds (table 26–2). The confining unit (approximately 20 meters thick) and the thick aquitard (approximately 19 meters thick), were modeled as no-delay interbeds (table 26–2). Simulation of delayed drainage and residual compaction in each of these units was simulated implicitly using 3 model layers as recommended in Hoffmann and others (2003). Compaction was not simulated for the upper aquifer because the upper aquifer is relatively coarse grained and heads are changing very slowly and are hydraulically isolated from seasonal groundwater fluctuations in the production zones of the aquifer system. A constant porosity of 0.30 was used for the coarse- and fine-grained materials in the model.

Table 26–2: Interbed properties for example ex-gwf-csub-p03.

Interbed	Layer	Thickness	Initial stress
1	2	5.49	47.27
2	3	8.23	55.93
3	4	6.40	62.76
4	5	2.74	75.90
5	7	0.61	98.15
6	8	5.18	103.33
7	9	8.53	111.86
8	10	5.49	117.35
9	12	7.62	285.60
10	14	0.91	339.25
11	5	5.27	75.90
12	12	5.06	285.60
13	14	7.82	339.25

Initial preconsolidation stresses were calculated from initial preconsolidation heads developed by [Sneed \(2008\)](#) and effective stresses calculated using initial heads (table 26–1). Initial preconsolidation stresses for no-delay and delay interbeds are summarized in table 26–2, respectively. [Sneed \(2008\)](#) estimated initial preconsolidation heads from the time series for paired bench marks near the Holly site and middle aquifer water levels (fig. 26–3). Delay beds in the middle aquifer (model layers 5 and 12) and the lower aquifer (model layer 12) were specified to be 6.77 and 5.55 meters above land surface, respectively, which are the same as initial heads in these layers.

Boundary conditions in the one-dimensional compaction model of the Holly site consist of constant (time-variant) heads for those parts of the coarse-grained aquifer that represent measured (or estimated) hydraulic head (fig. 26–2C). The upper, middle, and lower aquifers at the Holly site are represented in the model by specifying heads in each aquifer using data from [Sneed \(2008\)](#) and are shown in figure 26–3. The upper model boundary is a time-variant, constant-head boundary that represents measured or estimated heads in the upper aquifer (model layer 1) at the Holly site and is about 28 meters below land surface (fig. 26–2C). Three boundaries within the model domain consist of time-variant, specified heads that represent measured or estimated heads in the middle (model layers 6 and 11) and lower aquifers (model layer 13) at the Holly site (fig. 26–2C). Time-varying heads for constant-head cells were defined using a time series file. Although compaction is not thought to be important in the upper aquifer it should be noted that compaction and related release/storage of water are not simulated in cells with constant-head boundaries.

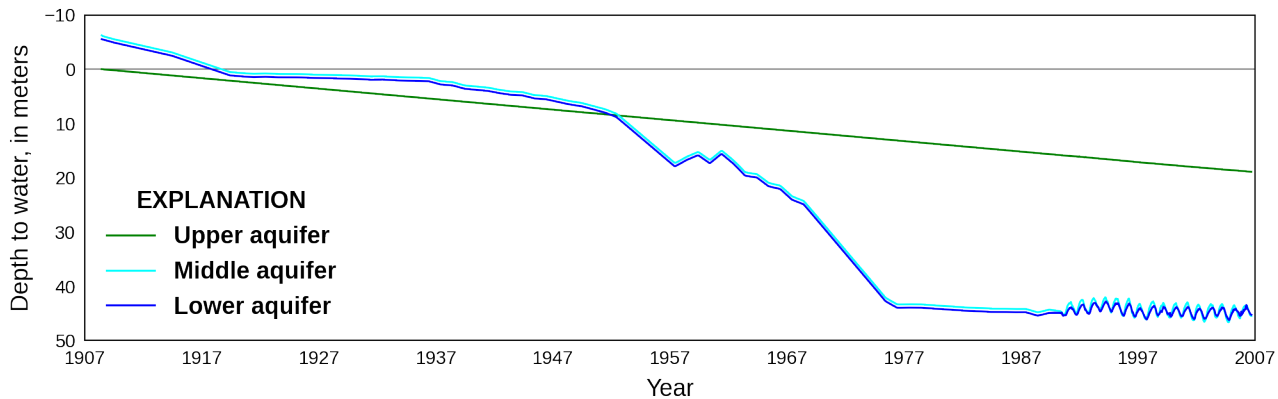


Figure 26–3: Graph showing depth to water values used in the one-dimensional compaction problem for the upper, middle, and lower aquifers at the Holly site, Edwards Air Force Base, Antelope Valley, California. Modified from [Sneed \(2008\)](#)

The compaction at the end of the simulation for the confining unit (0.28 meters), the thick aquitard (0.66 meters), no-delay interbeds contained in aquifer units (0.06 meters), delay interbeds contained in aquifer units (0.35 meters), and coarse grained materials (0.06 meters) from a modified MODFLOW 6 version of the model of [Sneed \(2008\)](#) were used to calibrate initial specific storage values used in the model. The specific storage values used by [Sneed \(2008\)](#) were uniformly scaled by a factor of  $9.9408 \times 10^{-1}$  to better match the observed compaction at the Holly site for the period from October 1, 1992 to May 9, 2006. The total compaction at the end of the simulation period (1.42 meters) and the total compaction from October 1, 1992 to May 9, 2006 (0.19 meters) were also used to calibrate initial specific storage values used in the model.

PEST++ ([Welter and others, 2015](#)) was used to calibrate 1) the elastic specific storage value for coarse grained materials in model layers 5, 7, 12, and 14; 2) inelastic and elastic specific storage values for the confining unit (model layers 2–4); 3) inelastic and elastic specific storage values for the thick aquitard (model layers 8–10); and 4) inelastic and elastic specific storage value were calibrated for no-delay and delay interbeds contained in aquifer units (model layers 5, 6, 12, and 14).

Compaction values simulated using the head-based formulation for the confining unit, the thick aquitard, no-delay interbeds contained in aquifer units, delay interbeds contained in aquifer units, and coarse grained materials were given a weight of 1; total compaction and the total compaction from October 1, 1992 to May 9, 2006 were given an increased weight of 5 to favor fitting the total compaction and observed change in total compaction over material based compaction values.

### 26.3 Example Results

Comparison of head- and effective stress-based compaction results are shown in figure [26–4](#). The compaction at the end of the simulation in the model using head- and effective stress-based formulation were essentially identical and mean errors calculated for the entire simulation ranged from -0.0045 meters (confining unit compaction) to 0.0042 meters (compaction in delay interbeds contained in aquifer units), with the largest differences occurring between approximately 1947 and 1977.

The thickness of compressible materials and calibrated specific storage values for coarse-grained materials, fine-grained materials represented as no-delay interbeds, and fine-grained materials represented as delay interbeds are summarized in tables [26–3](#) and [26–4](#), respectively. Calibrated specific storage values are larger than values used with the head-based formulation. Percent differences relative to values used by [Sneed \(2008\)](#) were 27.0% for the elastic specific storage values of coarse-grained materials, averaged 79.2 and 210.2% for the inelastic and elastic specific storage values of no-delay interbeds, and averaged 20.6 and 52.2% for the inelastic and elastic specific storage values of delay interbeds. Larger specific storage values are expected for the effective stress-based formulation since effective-stress values increase during the simulation, as a result of groundwater pumpage induced water-level declines, and result in reduced specific storage values and compaction with time relative to the head-based formulation model using the uniformly scaled specific storage values from [Sneed \(2008\)](#).

Table 26–3: Aquifer storage properties for example ex-gwf-csub-p03.

<b>Layer</b>	<b>Specific Storage</b>
5	6.88e-6
7	6.88e-6
12	6.88e-6
14	6.88e-6

Table 26–4: Interbed storage properties for example ex-gwf-csub-p03.

<b>Interbed</b>	<b>Layer</b>	<b>Inelastic Specific Storage</b>	<b>Elastic Specific Storage</b>
1	2	1.35e-3	8.57e-6
2	3	1.35e-3	8.57e-6
3	4	1.35e-3	8.57e-6
4	5	2.69e-4	1.26e-5

Table 26–4: Interbed storage properties for example ex-gwf-csub-p03.

Interbed	Layer	Inelastic Specific Storage	Elastic Specific Storage
5	7	2.71e-4	1.15e-5
6	8	1.92e-3	3.42e-5
7	9	1.92e-3	3.42e-5
8	10	1.92e-3	3.42e-5
9	12	1.46e-4	6.40e-6
10	14	2.17e-4	9.24e-6
11	5	2.27e-4	1.03e-5
12	12	4.87e-4	7.59e-6
13	14	1.02e-3	6.86e-6

The simulations for the period 1908–2006 provide information about how the aquifer-system components, aquifers and aquitards, contributed to overall compaction because of the continual lowering of water levels throughout the 1900s and because of seasonal water-level cycling since 1990. Simulated compaction totaled 1.42 meters for the period 1908–2006. Of the total simulated compaction, the confining unit (thickness = 20.12 meters) accounted for 20.0% of the total; the thick aquitard (thickness = 19.20 meters) accounted for 46.7% of the total; delay interbeds in aquifers (aggregate thickness = 18.14 meters) accounted for 24.6%; coarse-grained materials (aggregate thickness = 225.39 meters) accounted for 4.5% of the total; and no-delay interbeds in aquifers (aggregate thickness = 11.89 meters) accounted for 4.4% of the total (fig. 26–5A). During 1990–2006, a total of 0.23 meters of compaction was simulated; the confining unit accounted for 31.2% of the total; the thick aquitard accounted for 66.3% of the total; delay interbeds in aquifers accounted for 1.7%; coarse-grained materials accounted for -0.1% (representing expansion of coarse grained materials); and no-delay interbeds in aquifers accounted for 0.9% of the total. For these relatively quickly equilibrating thin aquitards, the fairly stable stresses since the mid-1970s and cyclic stresses during the late time were often in the elastic range of stress. In fact, beginning in about 1976, the delay and no-delay interbeds in aquifers had significantly reduced compaction rates, contributing only 0.01 meters (2.4%) and 0.004 meters (0.1%) of compaction, respectively, during the last 30 years of the simulation. These thin aquitards deformed mostly elastically during the late time (fig. 26–5).

The simulated stress/displacement trajectory also compares well in magnitude and timing with the measured stress/displacement trajectory between October 1, 1992 and September 4, 2006 (fig. 26–5C). The effective stress at the base of the lower aquifer was estimated using water-level data for the upper and lower aquifers (fig. 26–3). The estimated stress/displacement trajectory fit is poorest from 1993 to 1996 when seasonal compaction changes lag behind observed changes. After April 1997, simulated compaction is generally consistent with observed compaction.

Vertical distributions of hydraulic head in the aquitards can be used as a direct measure of residual compaction (Riley, 1969, 1998). A linear profile showing deviations in the simulated 1908 to 2006 head distributions for the two thick clay sequences—the confining unit and the thick aquitard—indicate large residual excess pore pressures exist at the end of the simulation (fig. 26–6). Residual excess pore pressures in these thick aquitards began accumulating in about 1950, when water levels in the aquifers began declining at rate faster (fig. 26–3) than these aquitards could dissipate excess pore pressures. The simulations indicate that about 98% of the compaction during late time is residual compaction occurring in these two thick clay sequences (fig. 26–5A).

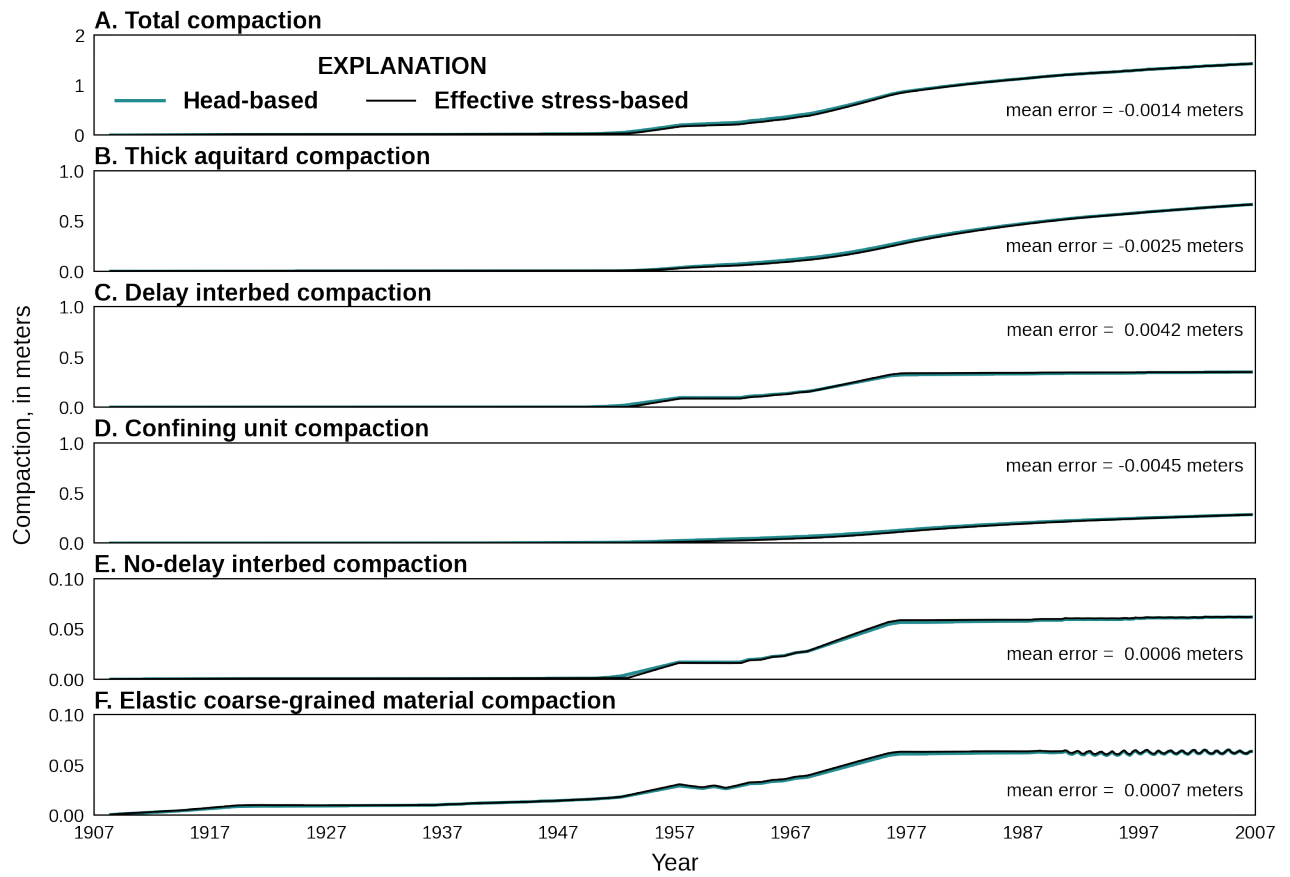


Figure 26–4: Graphs showing simulated compaction in different material types using head- and effective stress based formulations for the one-dimensional compaction problem. *A*, Total compaction, *B*, compaction in interbeds in the thick aquitard, *C*, compaction in delay interbeds contained in aquifers, *D*, compaction in interbeds in the confining unit, *E*, compaction in no-delay interbeds contained in aquifers, and *F*, compaction in coarse-grained materials

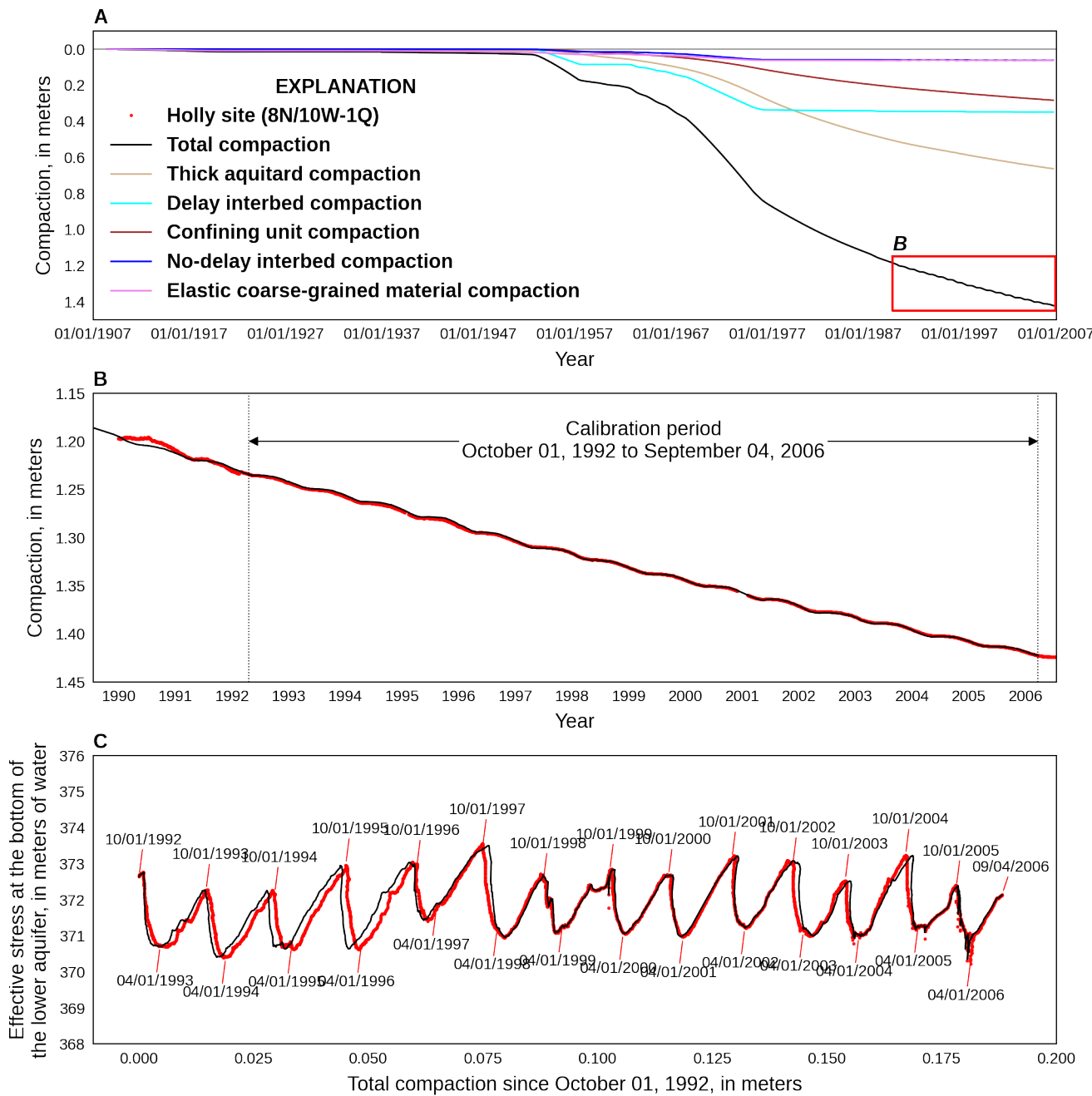


Figure 26–5: Graphs showing history matches for simulated and measured aquifer-system compaction in the one-dimensional compaction problem. A, compaction in the different material types for the full simulation period (for 1908–2006), B, comparison of simulated and observed compaction at the Holly site for the period from 1990 to 2007, and C, simulated and observed stress/displacement for the period from October 1, 1992 to September 4, 2006. Elastic and inelastic specific storage values were calibrated using observed Holly site compaction data for the period from October 1, 1992 to September 4, 2006 and simulated compaction from the model based on Sneed (2008), which used a head-based formulation to simulate compaction

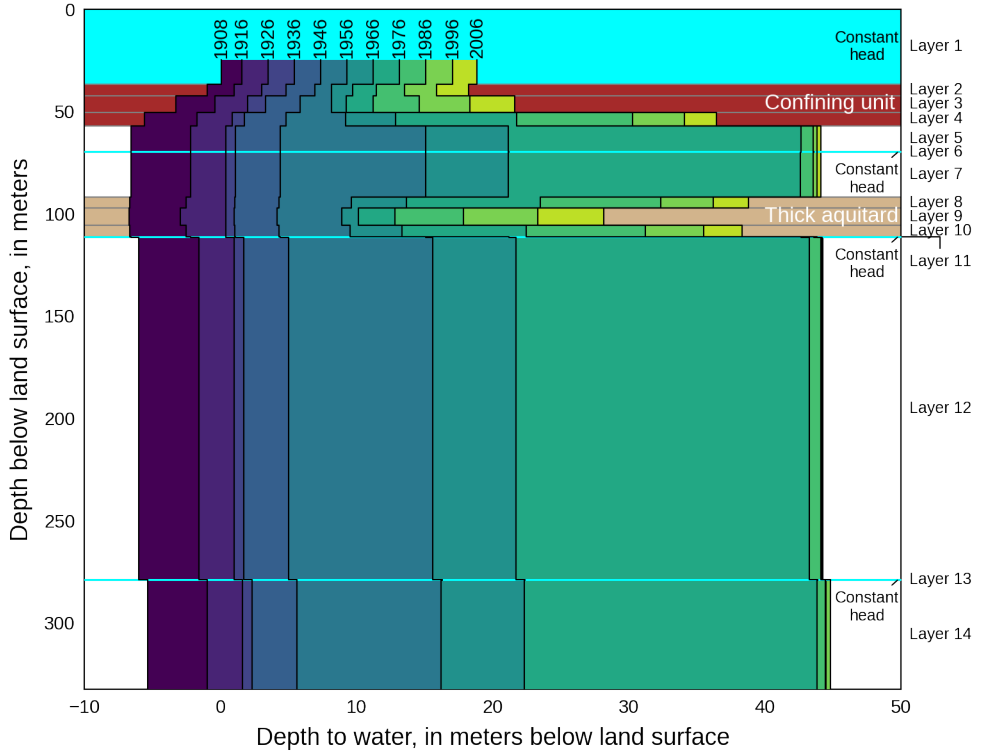


Figure 26–6: Graph showing simulated vertical head profiles and approximately decadal head changes in the one-dimensional compaction problem. Vertical head profiles are shown for 1908, 1916, 1926, 1936, 1946, 1956, 1966, 1976, 1986, 1996, and 2006. The colored area between plotted years represents the simulated head change over approximately decadal period of time between simulated vertical head profiles. The vertical location of model layer tops and bottom and layers with constant-head boundaries are also shown.

## 27 One-Dimensional Compaction in a Three-Dimensional Flow Field

This problem is based on the problem presented in the SUB-WT report ([Leake and Galloway, 2007](#)) and represent groundwater development in a hypothetical aquifer that includes some features typical of basin-fill aquifers in an arid or semi-arid environment. The problem of [Leake and Galloway \(2007\)](#) was modified to include compaction of coarse-grained aquifer materials and water compressibility. Specific stress packages were also modified but net inflows to the model domain are identical.

### 27.1 Example Description

The model grid for this problem consists of four layers, 20 rows, and 15 columns (fig. [27-1](#)). The model has a top elevation of 150 meters and layer bottom elevations of 50, -100, -150, and -350 meters for layers 1, 2, 3, and 4, respectively. DELR and DELC are specified with a constant value of 2,000 meters. The simulation consists of three stress periods. The first is an initial steady-state period for the purpose of computing the head distribution, which is used with other quantities to compute the initial hydrostatic, effective, geostatic, and preconsolidation stresses. The second stress period is used to simulate 60 years of pumping by the two wells at locations shown in figure [27-1](#). The third stress period is used to simulate 60 years of recovery following cessation of pumping. The second and third stress periods are divided into 60, 1-year time steps.

The aquifer system consists of an unconfined upper aquifer, an extensive confining unit, and a confined lower aquifer (fig. [27-1B](#)). The model uses two layers to represent the water-table aquifer and one layer each to represent the confining unit and the lower aquifer. Hydraulic conductivity was assumed to be isotropic in the horizontal and vertical directions in each layer. Hydraulic properties for coarse-grained materials are listed in table [27-1](#). The specific storage was defined to be 0 for all layers in the STO package. Model layer 1 and layers 2–4 were defined to be convertible and non-convertible, respectively, for hydraulic conductivity and storage properties. Default NPF and STO package settings were used. An initial head of 100 meters was defined for each layer.

Table 27-1: Model parameters for example ex-gwf-csub-p04.

Parameter	Value
Number of periods	3
Number of layers	4
Number of rows	20
Number of columns	15
Column width (m)	2000.0
Row width (m)	2000.0
Top of the model (ft)	150.0
Layer bottom elevations (m)	50., -100., -150., -350.
Starting head (m)	100.0
Cell conversion type	1, 0, 0, 0
Horizontal hydraulic conductivity (m/d)	4., 4., 0.01, 4.
Vertical hydraulic conductivity (m/d)	0.4, 0.4, 0.01, 0.4
Specific yield (unitless)	0.3, 0.3, 0.4, 0.3
Compressibility of water (Newtons/(m <sup>3</sup> ))	9806.65
Specific gravity of water (1/Pa)	4.6612e-10
Specific gravity of moist soils (unitless)	1.77, 1.77, 1.60, 1.77
Specific gravity of saturated soils (unitless)	2.06, 2.05, 1.94, 2.06
Coarse-grained material porosity (unitless)	0.32, 0.32, 0.45, 0.32
Elastic specific storage (1/m)	0.005, 0.005, 0.01, 0.005

Table 27–1: Model parameters for example ex-gwf-csub-p04.

Parameter	Value
Interbed thickness (m)	45., 70., 50., 90.
Interbed initial porosity (unitless)	0.45
Interbed recompression index (unitless)	0.01
Interbed compression index (unitless)	0.25
Initial preconsolidation stress offset (m)	15.0

The effective stress formulation of the CSUB package was used to simulate compaction of aquifer materials. Storage properties for coarse- and fine-grained materials were specified using compression indices. No-delay interbeds were specified in each active model cell. Hydraulic properties for fine-grained materials represented as no-delay interbeds are listed in table 27–1; no-delay interbeds in model 3 comprise the full thickness of the confining unit.

The specific gravity of fully- and partially-saturated materials for each layer was calculated using

$$G = (1 - \bar{\theta})G_{\text{solid}} + k_r \bar{\theta} G_{\text{water}}, \quad (27-1)$$

where  $G$  is the specific gravity of a control volume that includes solids and water (unitless),  $\bar{\theta}$  is the thickness weighted porosity of coarse- and fine-grained materials in a control volume (unitless),  $G_{\text{solid}}$  is the specific gravity of the solids in a control volume (unitless),  $k_r$  is a scaling factor used to scale the specific gravity of water if a control volume is not fully saturated (unitless), and  $G_{\text{water}}$  is the specific gravity of water (unitless).  $k_r$  is 1 for saturated materials or the ratio of the volume of water to the total volume for materials that are not fully saturated.

The specific gravity of saturated materials for each layer was calculated using the thickness weighted porosity listed in table 27–1, a  $G_{\text{solid}}$  value of 2.7, and a  $G_{\text{water}}$  value of 1.0. The specific gravity of moist materials was calculated using a  $k_r$  value of 0.25 and the other values used to calculate the specific gravity of saturated materials. The specific gravity of saturated and moist materials used for the one-dimensional compaction in a three-dimensional flow field problem are listed in table 27–1

Water compressibility was simulated and default specific gravity of water ( $\gamma_{\text{water}} = 4.6512 \times 10^{-10}$  per Pascal) and the compressibility of water ( $\beta = 9806.65$  Newtons per cubic meter) values were used. Initial specific storage values related to the compressibility of water ( $S_{s,\text{water}} = \theta \beta \gamma_{\text{water}}$ ) were  $1.46 \times 10^{-6}$  and  $2.05 \times 10^{-6}$  per meter for coarse- and fine-grained materials, respectively. The porosity and thickness of coarse- and fine-grained materials were adjusted during the simulation in response to compaction. The initial preconsolidation stress for the no-delay interbeds was specified to be 15 meters greater than the steady-state effective stress calculated in each cell at the end of stress period 1.

Inflow to the flow system is simulated using the recharge package at 18 recharge locations in layer 1 shown on figure 27–1A. Recharge at each of these locations is specified at a rate of  $5.5 \times 10^{-4}$  meters per day throughout the entire simulation, resulting in a total recharge rate of 39,600 cubic meters per day. Under steady-state conditions, all of the flow leaves the system through eight constant-head cells, two of which are in each layer at the horizontal locations shown on figure 27–1A. Head at the eight constant-head cells is specified to be 100 meters. During stress period 2, each of the two wells shown on figure 27–1A withdraw water from the upper and lower aquifer at a rate of 72,000 cubic meters per day.

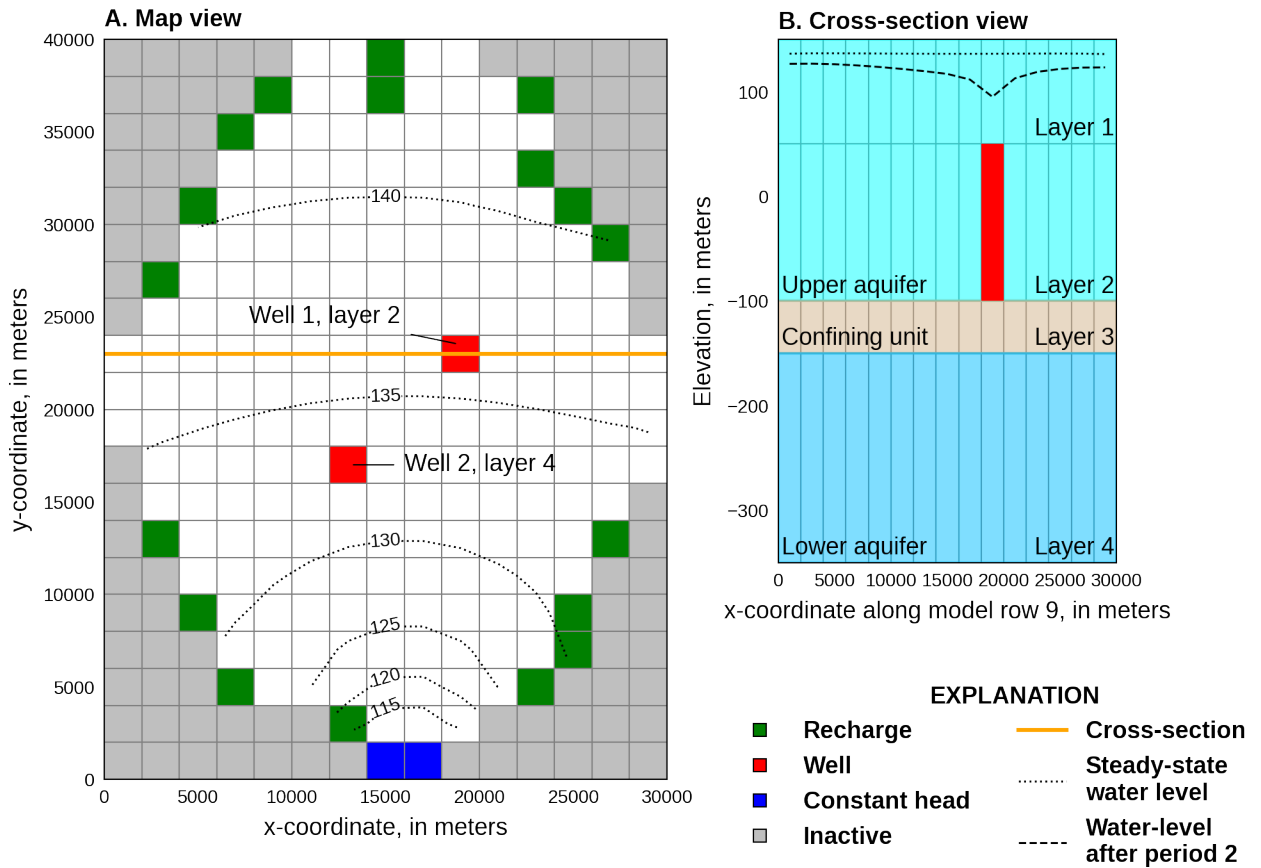


Figure 27-1: Diagram showing the model domain for the one-dimensional compaction in a three-dimensional flow field problem. *A*, plan view, and *B*, cross-section view. The locations of active and inactive areas of the model domain, steady-state heads in model layer 1, and locations of recharge cells, constant-head cells, and wells are also shown

## 27.2 Example Results

The initial steady-state stress period results in a maximum head of 143.0 meters in row 1, column 8. Steady-state hydraulic gradients slope down valley and toward the center of the valley to the constant-head cells in row 20, layers 1–4 (fig. 27–1). The steady-state head distribution is used to compute initial effective stress, preconsolidation stress, and geostatic stress for the transient part of the simulation. For the location of the well in row 9, column 10, layer 2, these stress values are 273.3, 288.3, and 509.5 meters, respectively.

Equivalent skeletal specific storage values were calculated from recompression and compression indices and the initial effective stress distribution. Computed values of elastic skeletal specific storage at row 9, column 10, were  $2.03 \times 10^{-5}$ ,  $8.58 \times 10^{-6}$ ,  $7.33 \times 10^{-6}$ , and  $4.41 \times 10^{-6}$  per meter for layers 1–4, respectively. Values of inelastic (virgin) skeletal specific storage for the same location were  $2.03 \times 10^{-4}$ ,  $8.58 \times 10^{-5}$ ,  $7.33 \times 10^{-5}$ , and  $4.41 \times 10^{-5}$  per meter for layers 1–4, respectively. These values are not used explicitly in further calculations by the CSUB package, but are provided to illustrate how effective stress influences the spatial distribution of specific storage.

### 27.2.1 Simulated Stresses

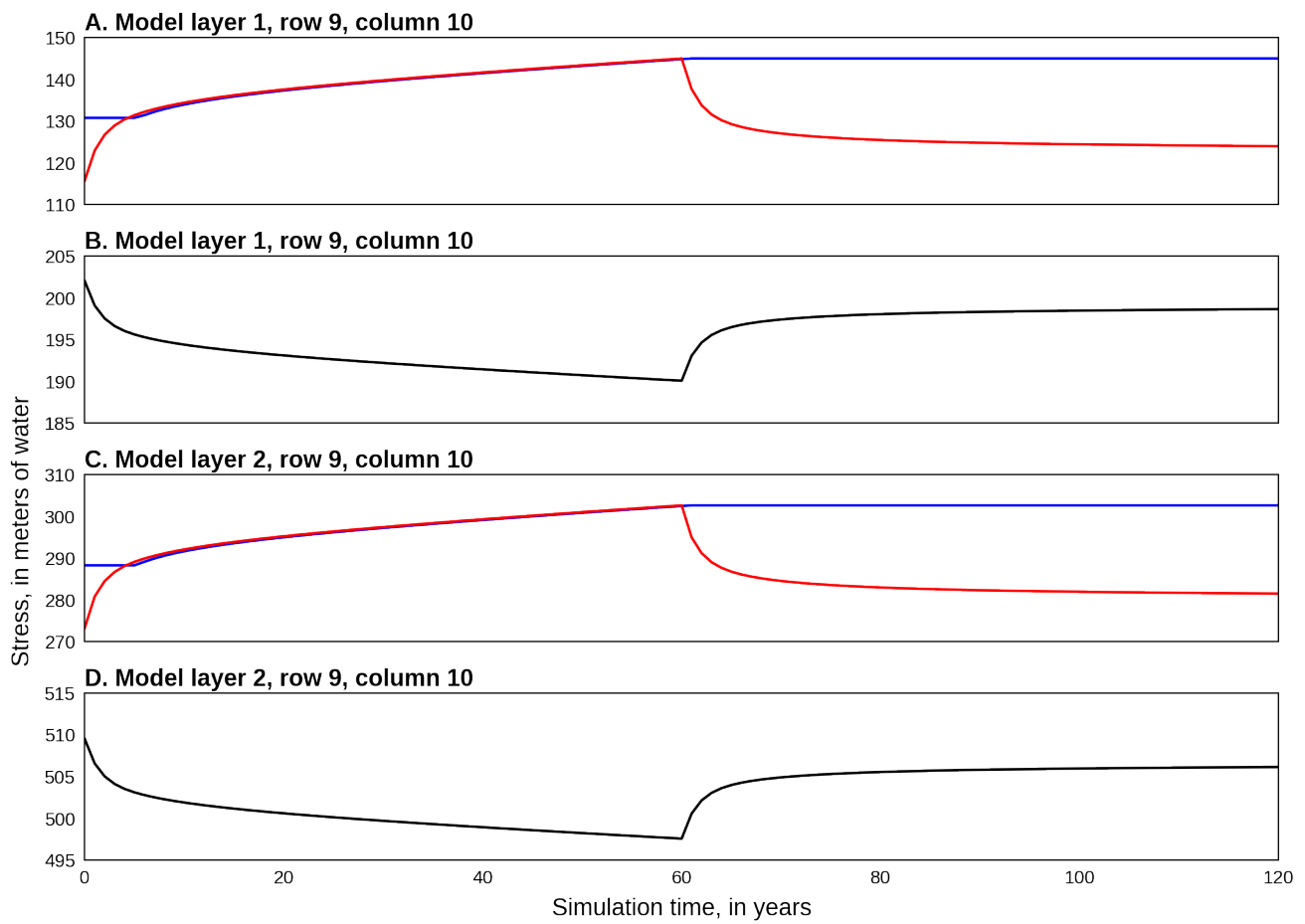
Values of effective stress, preconsolidation stress, and geostatic stress at the bottom of the cell for the 60-year pumping and 60-year recovery periods are shown in figure 27–2 for row 9, column 10, layers 1 and 2. In both layers, preconsolidation stress is exceeded early in the simulation and tracks with increases in effective stress until recovery of water levels after the start of stress period 3 (year 60). Head change at this location is similar in layers 1 and 2, and the shapes and magnitudes of change-of-effective- and preconsolidation-stress curves are nearly the same (figs. 27–2A, C). The curves, however, are at different head elevations because of the increase in magnitude of stress with depth. The shapes of curves representing geostatic stress in layers 1 and 2 (figs. 27–2B, D) are identical because all of the change results from movement of the water table in layer 1 (fig. 27–1B). Note how simulated effective stress and geostatic stress does not return to initial values 60 years after cessation of pumpage; approximately 2,000 years without pumping is required for simulated effective stress and geostatic stress at row 9, column 10, layers 1 and 2 to return initial values.

### 27.2.2 Simulated Compaction

The computed vertical displacements for the tops of layers 1–4 resulting from fine- (interbed) and coarse-grained material compaction at the locations of the two pumping wells are shown in figure 27–3. The total compaction at the top of layer 1 represent the time series of land subsidence for the two locations (fig. 27–3E, F). Similarly, differences between displacement curves for adjacent layers are the time distributions of compaction in the each layer. At both locations, compaction is greatest in the layer in which pumping takes place. Coarse-grained compaction is small relative to inelastic compaction of fine-grained interbeds. Similar to stress results (fig. 27–2), elastic compaction of coarse-grained materials does not fully recover 60 years after cessation of pumpage.

### 27.2.3 Simulated Storage Changes

At the end of the second stress period a total of 3,155,760,128 cubic meters of water was pumped from the water-table and confined aquifers. Water released from specific yield, elastic coarse-grained materials, elastic fine-grained materials, inelastic fine-grained materials, and water compressibility accounted for 96.31% (3,039,304,920 cubic meters) of groundwater pumpage; the remainder of groundwater pumpage came from reduction in the discharge to the eight constant-head cells.



#### EXPLANATION

— Preconsolidation stress    — Effective stress    — Geostatic stress

Figure 27–2: Graphs showing computed stresses for row 9, column 10 for the one-dimensional compaction in a three-dimensional flow field problem. *A*, Effective and preconsolidation stress in layer 1, *B*, geostatic stress in layer 1, *C*, effective and preconsolidation stress in layer 2, and *D*, geostatic stress in layer 2

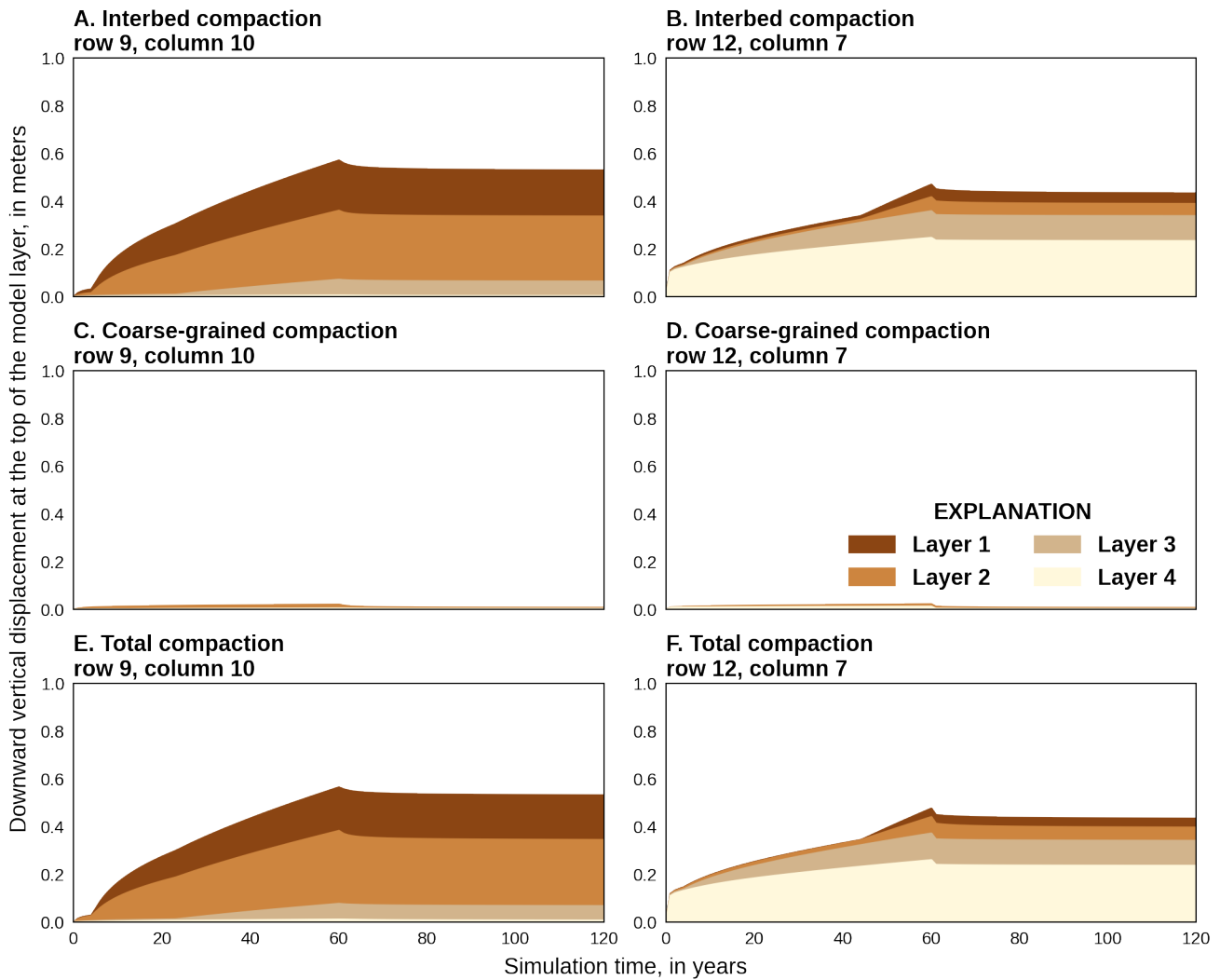


Figure 27–3: Graphs showing computed downward displacement for the tops of model layers 1–4 for the one-dimensional compaction in a three-dimensional flow field problem. *A*, interbed compaction at row 9, column 10, *B*, interbed compaction at row 12, column 7, *C*, coarse-grained material compaction at row 9, column 10, *D*, coarse-grained material compaction at row 12, column 7, *E*, total compaction at row 9, column 10, and *F*, total compaction at row 12, column 7

Individually specific yield, elastic coarse-grained materials, elastic fine-grained materials, inelastic fine-grained materials, and water compressibility accounted for 94.80%, 0.40%, 0.63%, 0.21%, and 0.27%, respectively, of total groundwater pumpage. For the cell containing well 1 (layer 2, row 9, column 10) elastic coarse-grained materials, elastic fine-grained materials, inelastic fine-grained materials, and water compressibility accounted for 5.18%, 3.81%, 87.68%, and 3.33%, respectively, of the total water released from storage (3,628.59 cubic meters) in response to groundwater pumpage. For the cell containing well 2 (layer 4, row 12, column 7) elastic coarse-grained materials, elastic fine-grained materials, inelastic fine-grained materials, and water compressibility accounted for 4.63%, 2.62%, 87.57%, and 5.18%, respectively, of the total water released from storage (3,147.01 cubic meters) in response to groundwater pumpage.

## 28 Drainage Discharge Scaling

This example is a modified version of the Unsaturated Zone Flow (UZF) Package problem 2 described in [Niswonger and others \(2006\)](#). UZF Package problem 2 is based on the Green Valley problem (Streamflow Routing (SFR) Package problem 1) described in [Prudic and others \(2004\)](#). The problem has been modified by converting all of the SFR reaches to use rectangular channels and to use the drain package drainage option to simulate groundwater discharge to the land surface.

### 28.1 Example Description

Model parameters for the example are summarized in table 28–1. The model consists of a grid of 10 columns, 15 rows, and 1 layer. The model domain is 50,000 *ft* and 80,000 *ft* in the x- and y-directions, respectively. The discretization is 5,000 *ft* in the row and column direction for all cells. The top of the model ranges from about 1,000 to 1,100 *ft* and the bottom of the model ranges from about 500 to 1,000 *ft*.

Twelve stress periods are simulated. The first stress period is steady state and the remaining stress periods are transient. The stress periods are  $2.628 \times 10^6$  seconds (30.42 days) in length. The first stress period is broken into one time step. Stress periods 2 through 12 are each broken up into 15 time steps and use a time step multiplier of 1.1.

Table 28–1: Model parameters for example ex-gwf-drn-p01.

Parameter	Value
Number of periods	12
Number of layers	1
Number of rows	15
Number of columns	10
Column width ( <i>ft</i> )	5000.0
Row width ( <i>ft</i> )	5000.0
Starting head ( <i>ft</i> )	1050.0
Hydraulic conductivity near the stream ( <i>ft/s</i> )	0.002
Hydraulic conductivity in the basin ( <i>ft/s</i> )	0.0004
Specific storage (1/ <i>s</i> )	1e-6
Specific yield near the stream (unitless)	0.2
Specific yield in the basin (unitless)	0.1
Vertical saturated hydraulic conductivity ( <i>ft/s</i> )	1e-6
Saturated water content (unitless)	0.3
Initial water content (unitless)	0.1
Base residual water content (unitless)	0.1
Epsilon exponent (unitless)	3.5
Evapotranspiration rate ( <i>ft/s</i> )	5.0e-8
Evapotranspiration extinction wilting content (unitless)	0.10005
Evapotranspiration extinction depth ( <i>ft</i> )	15.0
Surface depression depth ( <i>ft</i> )	1.0

The basin fill thickens toward the center of the valley and hydraulic conductivity of the basin fill is highest in the region of the stream channels. Hydraulic conductivity is  $173 \text{ ft/day}$  ( $2 \times 10^{-4} \text{ ft/s}$ ) in the vicinity of the stream channels and  $35 \text{ ft/day}$  ( $4 \times 10^{-4} \text{ ft/s}$ ) elsewhere in the alluvial basin. A constant specific storage value of  $1 \times 10^{-6}$  ( $1/\text{day}$ ) was specified throughout the alluvial basin. Specific yield is 0.2 (unitless) in the vicinity of the stream channels and 0.1 (unitless) elsewhere in the alluvial basin.

An initial head of 1,050 *ft* is specified in all model layers. Any initial head exceeding the bottom of each cell could be specified since the first stress period is steady-state.

The UZF Package was used to simulate delayed groundwater recharge through the unsaturated zone. A UZF boundary cell is simulated in every active model cell. Constant vertical hydraulic conductivity, saturated water content, initial water content, and Brooks-Corey epsilon exponent ([Brooks and Corey, 1966](#)) are specified for each UZF boundary cell (table 28–2). The specified evapotranspiration extinction water content (table 28–2) is multiplied by a factor of 1 in the valley lowland and 2 elsewhere.

Table 28–2: Infiltration and pumping rates for example ex-gwf-drn-p01.

Stress period	Infiltration rate	Pumping rate
1	1.00e-9	-2.00
2	8.00e-9	-2.00
3	1.00e-8	-1.00
4	2.00e-8	-1.00
5	5.00e-9	-3.00
6	1.00e-8	0.00
7	3.00e-9	-2.00
8	5.00e-9	0.00
9	3.00e-9	-1.00
10	2.00e-9	0.00
11	1.00e-9	-3.00
12	1.00e-9	0.00

Infiltration from precipitation and evapotranspiration are represented using the UZF Package. Specified infiltration rates (table 28–2) are multiplied by a factor ranging from 1 to 8; specified infiltration rates range from  $1.0 \times 10^{-9}$  to  $1.6 \times 10^{-7}$  *ft/s*, with lower rates in the vicinity of the stream channels and higher rates elsewhere in the alluvial basin. Evapotranspiration is represented using the UZF package and occurs where depth to water is within 15 *ft* of land surface, has a maximum rate of  $5.0 \times 10^{-8}$  *ft/s* (1.6 *ft/yr*) at land surface, and is coincident with the valley lowland through which several streams flow.

Wells are located in ten cells (rows 6 through 10 and columns 4 and 5) along the west side of the valley. Withdrawal rates for each well ranged from 0 to -2 *ft<sup>3</sup>/s* during the simulation (table 28–2). Two general-head boundary cells were added in (row 13, column 1) and (row 14, column 8) with a specified head equal to 988 and 1,045 *ft*, respectively, and a constant conductance of 0.038 *ft<sup>2</sup>/s*.

The streams in the model domain were represented using a total of 36 reaches. External inflows of 25, 10, and 100 *ft<sup>3</sup>/s* were specified for reach 1, 16, and 28, respectively. Reach 1 is located in (row 1, column 1), reach 16 is in (row 5, column 10), and reach 28 is in (row 14, column 9).

Streamflow discharges from the model at the downstream end of reach 36 in (row 13, column 1). Reach widths were specified to be 12, 0, 5, 12, 55, and 40 *ft* for reaches 1–9, 10–18, 19–22, 23–27, 28–30, and 31–36, respectively. The remaining streambed properties and stream dimensions used for each stream reach are the same as those used in [Prudic and others \(2004\)](#) (see [Prudic and others, 2004](#), Table 1). Constant stage reaches were used to define the ditch represented by reaches 10–15 and ranged from approximately 1,075.5–1061.6 *ft*. A diversion from reach 4 to 10 was specified to represent managed inflows to the ditch. Ditch inflows were specified to be 10 *ft<sup>3</sup>/s* except if the downstream flow in reach 4 is less than the specified diversion rate; in cases where the downstream flow in reach 4 is less than the specified diversion rate all of the downstream flow in reach 4 is diverted to the ditch and the inflow to reach.

Groundwater discharge to land surface was simulated with the drain (DRN) Package and the UZF Package groundwater seepage option. A surface depression depth of 1 ft was specified. When using the DRN Package to simulate groundwater discharge to land surface, the drain elevation is 0.5 ft below land surface, the drain conductance is  $25 \text{ ft}^2/d$ , and the drainage depth is equal to the surface depression depth.

The mover (MVR) Package was used to route rejected infiltration and groundwater discharge to the land surface calculated by the UZF Package to the stream network. In the case where the DRN Package is used the MVR package routes the drainage discharge representing groundwater discharge to the land surface to the stream network. All of the rejected infiltration and groundwater discharge to the land surface are routed to the stream network using the FACTOR mover type with a value equal to 1.

The model uses the Newton-Raphson Formulation. The simple complexity Iterative Model Solver option and preconditioned bi-conjugate gradient stabilized linear accelerator is also used. Since the Newton-Raphson Formulation is used the simulation using the DRN Package to simulated groundwater discharge to the land surface cubic scaling is used to scale the drain conductance, consisting with groundwater seepage option in the UZF Package.

## 28.2 Example Results

Simulated infiltration to the unsaturated zone and groundwater seepage to the land surface results simulated using the DRN and UZF Packages are shown in figure 28-1. Results using the DRN and UZF Packages are essentially identical (mean error =  $2.72 \times 10^{-8} \text{ ft}^3/\text{s}$ ) indicating the DRN package is capable of duplicating the groundwater seepage results for the UZF Package. Periods of high infiltration to the unsaturated zone correspond to increased in groundwater seepage to the land surface.

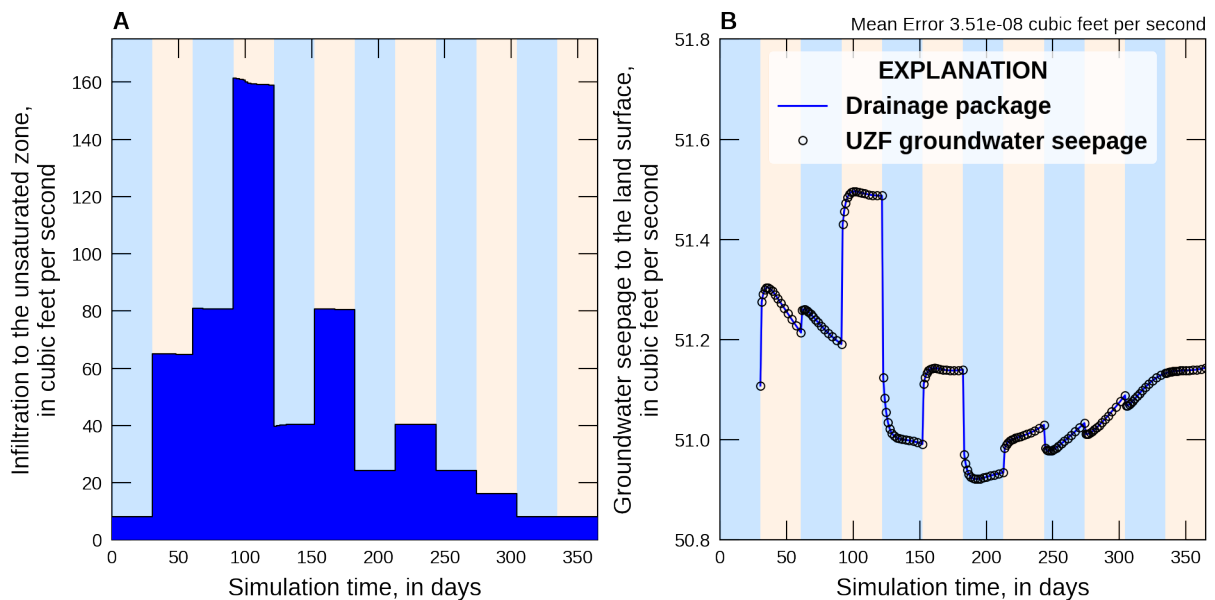


Figure 28-1: Simulated infiltration to the unsaturated zone and groundwater seepage to the land surface using the drain and unsaturated zone flow packages. The colored vertical bars delineate different stress periods. *A.* Infiltration to the unsaturated zone. *B.* Groundwater seepage to the land surface.

## 29 Sagehen UZF1 Package Problem 1

The first test problem in [Niswonger and others \(2006\)](#) presents a conceptual model of the Sagehen watershed that showcased the first version of the unsaturated-zone flow (UZF1) package. The Sagehen watershed is located on the eastern side of the northern Sierra Nevada, north of Lake Tahoe and the city of Truckee (see inset in figure 29–1). The simulation spans the upper 27  $mi^2$  of the watershed. The lowest land surface altitude of 1,928  $m$  above mean sea level occurs where Sagehen Creek exits the model. The highest altitude of 2,649  $m$  above mean sea level occurs on the western-most crest of the watershed, resulting in roughly 720  $m$  of topographic relief across the watershed. Figure 29–1 depicts the setting and topographic relief of the watershed. The geologic setting is primarily comprised of volcanic rocks overlain with a veneer of alluvium. Annual precipitation averages approximately 970  $mm$  which falls primarily in the form of snow.

### 29.1 Example description

For this MODFLOW 6 demonstration of the Sagehen model, a single model layer ranging between 53  $m$  and 899  $m$  thick is used to represent both the saturated and unsaturated zones. Spatially, 73 rows and 81 columns with uniform 90 × 90  $m$  grid cells are used to represent the watershed. The simulated period uses daily stress periods with one time-step per stress period, starting on December 1st and ending on November 30th. The first stress period is steady state, while all others are transient. Because the perimeter of the active model domain follows a topographic watershed divide, a no-flow boundary is used around the perimeter and bottom of the groundwater flow model. However, the cell hosting Sagehen Creek at its exit point as well as the two adjacent cells were specified constant head cells. The specified vertical hydraulic conductivity of the unsaturated zone was set equal to the vertical hydraulic conductivity used in the node-property flow (NPF) package. The stream network is represented with 213 inter-connected stream reaches, all with a constant width of 3  $m$  and range from 30 to 114  $m$  in length.

A set of infiltration factors shown in figure 29–2 tie precipitation rates to land-surface altitude to account for the orographically-driven variations in precipitation. Infiltration factors are three times greater along the western crest of the watershed compared to the lower valley elevations near the outlet. The infiltration factors were multiplied by infiltration rates that varied daily as shown by the “infiltration” time series shown in figure 29–4.

The water content in the unsaturated zone is calculated based on the flux through, and properties of, the unsaturated-zone during the initial steady-state stress period when the recharge rate equals the specified infiltration rate at land surface. A uniform extinction depth of 2.5  $m$  is applied across the entire model. Below 2.5  $m$ , Evapotranspiration (ET) ceases. Using the same approach implemented in UZF1 ([Niswonger and others, 2006](#)), water is first removed from the unsaturated zone in fulfillment of the ET demand. Any remaining residual ET demand is then satisfied using water in the saturated zone when the water table is within 2.5  $m$  of land surface. An extinction water content of 0.10 was specified for the entire model.

A summary of model parameter values are listed in table 29–1. Interested readers are referred to [Niswonger and others \(2006\)](#) for a discussion of additional details, including how the distribution of hydraulic conductivity was derived and aspects of the model calibration, among others.

Table 29–1: Model parameters for example ex-gwf-sagehen.

Parameter	Value
Number of layers in parent model	1
Number of rows in parent model	73

Table 29–1: Model parameters for example ex-gwf-sagehen.

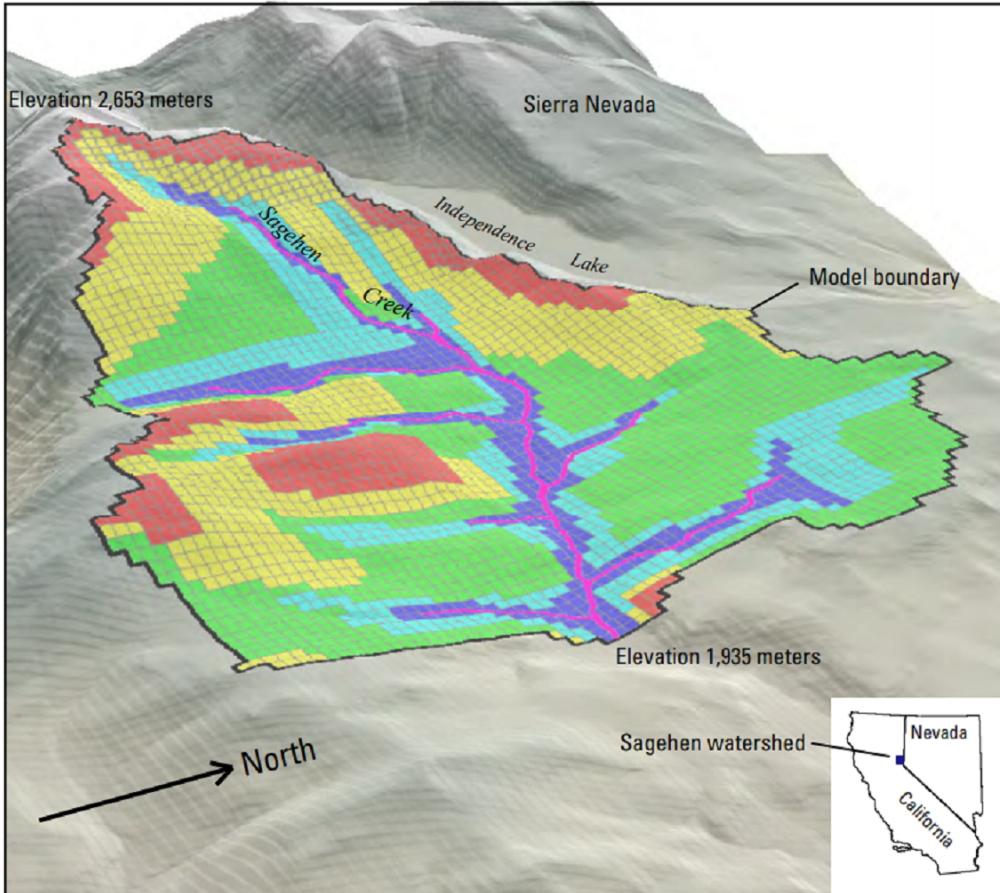
Parameter	Value
Number of columns in parent model	81
Parent model column width ( $m$ )	90.0
Parent model row width ( $m$ )	90.0
Horizontal hydraulic conductivity ( $m/d$ )	0.005 – 0.3
Vertical hydraulic conductivity ( $m/d$ )	0.01 – 0.3
Specific Yield	0.1 – 0.2
Saturated water content	0.15 – 0.25
Extinction water content	0.10
Saturated hydraulic conductivity of unsaturated zone	0.005 – 0.3
Brooks-Corey Epsilon	4.0
Number of SFR stream reaches	213
Hydraulic conductivity of streambed ( $m/d$ )	0.3
Width of stream reaches ( $m$ )	3
Streambed thickness ( $m$ )	1

## 29.2 Example results

Figure 29–3 shows the calculated depth to groundwater during the steady-state stress period. Depths to groundwater varied significantly over the model domain, ranging from more than 25 m below land surface to at, or slightly above, land surface near streams.

The UZF2 package partitions infiltration into runoff, resulting from saturation excess and/or rejected infiltration; recharge; ET; and changes in unsaturated zone storage [Langevin and others \(2017b\)](#). Although changes in unsaturated zone storage are not shown, figure 29–4 shows how the infiltration was partitioned among recharge and ET through time. Runoff processes are depicted in figure 29–5, and together with groundwater discharge directly to streams equal the total streamflow generated by the watershed.

A noteworthy enhancement between this version of the model and that first documented in [\(Niswonger and others, 2006\)](#) is that the drain (DRN) package has been added to the model to capture groundwater discharge to land-surface. In this way, groundwater discharge is kept separate from rejected infiltration, enabling easier viewing of the relative contribution of each of these processes since they are now separated in the calculated model budget. The UZF2 package could be used to simulate both processes; however, if this approach is used the relative contribution of groundwater discharge to land surface and rejected infiltration to stream flow are lumped. In flow-only simulations, this approach may suffice. In a groundwater transport simulation, where these two contributing sources to stream flow may have very different concentrations, the approach taken here will enable improved tracking of solute contributions to surface water. In addition to the DRN package, the mover (MVR) package has been invoked to deliver groundwater discharge and rejected infiltration to the nearest downgradient (i.e., downhill) stream reach. Previously, the IRUNBND array in UZF1 was used to route groundwater discharge and rejected infiltration to the stream network.



Shaded relief base from USGS 10-meter National Elevation Data,  
illumination from the northwest at 45°.  
Albers Equal-Area Conic projection  
Standard parallels 29°30'N and 45°30'N, central meridian 120°00'W  
North American Datum of 1983

### EXPLANATION

Hydraulic Conductivity—  
meter per day

	0.005
	0.01
	0.03
	0.1
	0.3

Figure 29–1: 3-Dimensional perspective view of the Sagehen watershed looking westward. Colors depict zones of varying hydraulic conductivity within the active grid domain.

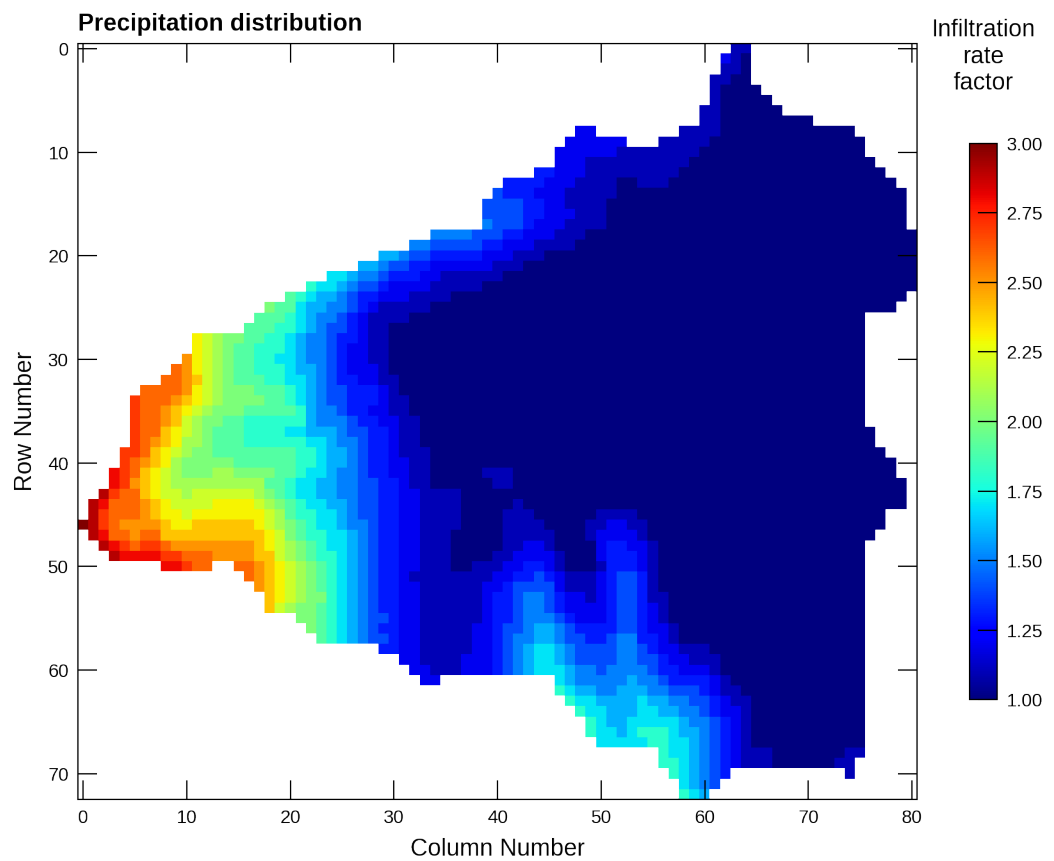


Figure 29–2: Plot of static infiltration factors used to spatially vary infiltration rates within the watershed. Infiltration factors were multiplied by a time series of infiltration rates shown in figure 29–4

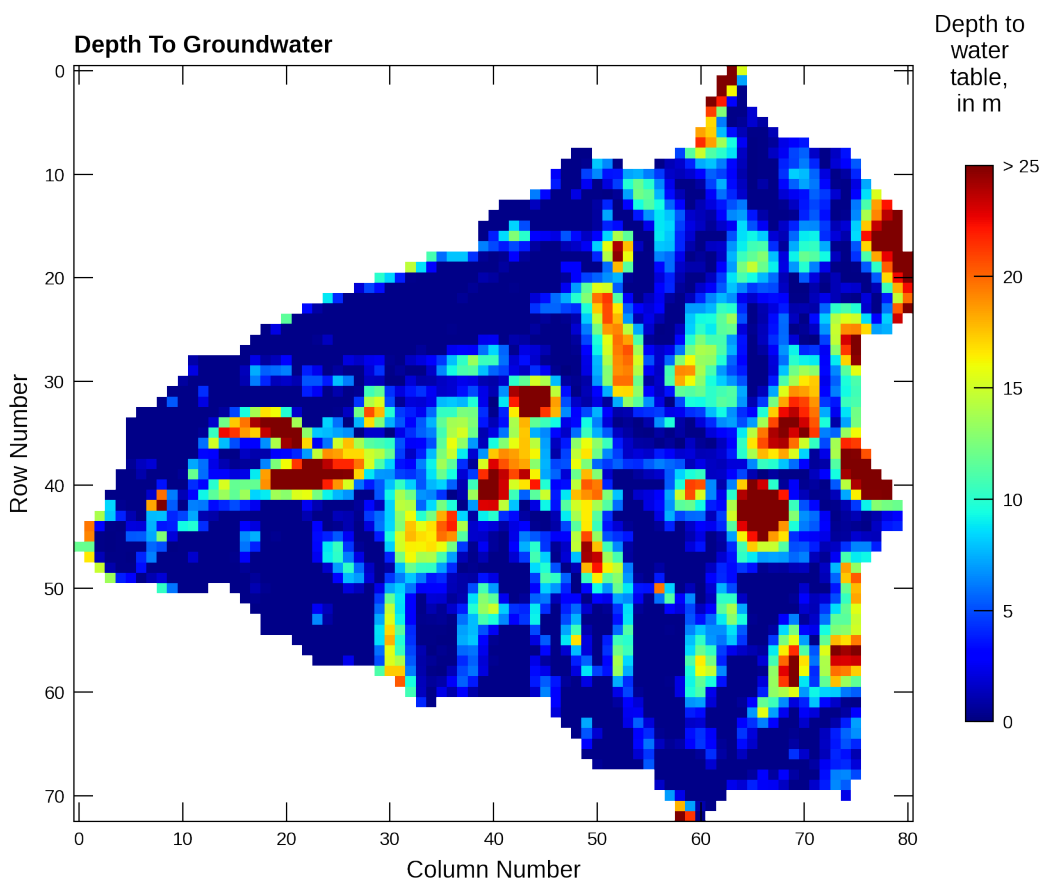


Figure 29–3: Calculated depth to groundwater during the steady-state stress period at the beginning of the simulation.

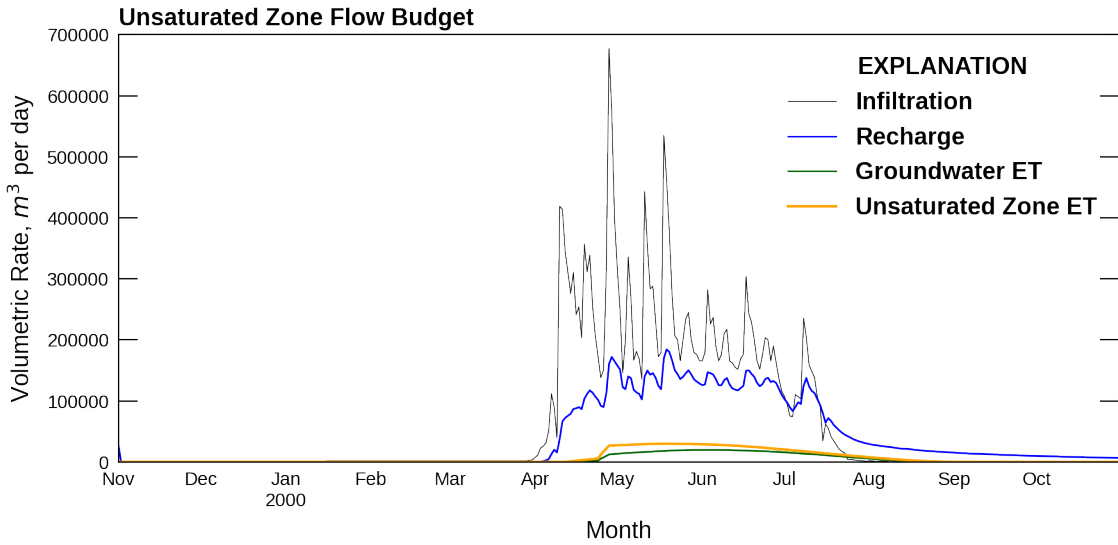


Figure 29–4: Volumetric rates of infiltration, recharge, and evapotranspiration from the unsaturated and saturated zones summed over the model domain.

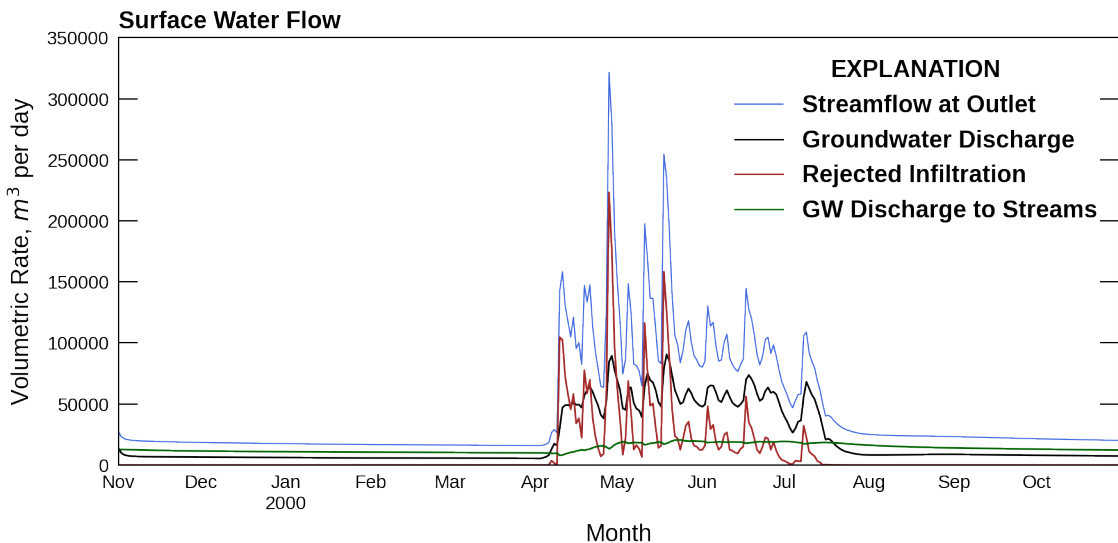


Figure 29–5: Volumetric flow rates of surface-water generation and runoff.

## 30 Capture Fraction Analysis

All groundwater pumped is balanced by removal of water somewhere, initially from storage in the aquifer and later from capture in the form of increase in recharge and decrease in discharge ([Leake and others, 2010](#)). Capture that results in a loss of water in streams, rivers, and wetlands now is a concern in many parts of the United States. Hydrologists commonly use analytical and numerical approaches to study temporal variations in sources of water to wells for select points of interest. Much can be learned about coupled surface/groundwater systems, however, by looking at the spatial distribution of theoretical capture for select times of interest. Development of maps of capture requires (1) a reasonably well-constructed transient or steady state model of an aquifer with head-dependent flow boundaries representing surface water features or evapotranspiration and (2) an automated procedure to run the model repeatedly and extract results, each time with a well in a different cell to evaluate the effect of a flux in a cell on an external boundary condition.

This example presents a streamflow capture analysis of the hypothetical aquifer system of [Freyberg \(1988\)](#) and based on the model datasets presented in [Hunt and others \(2020\)](#). The original problem of [Freyberg \(1988\)](#) documented an exercise where graduate students calibrated a groundwater model and then used it to make forecasts.

### 30.1 Example Description

A single-layer was used to simulate a shallow, water-table aquifer. The aquifer is surrounded by no-flow boundaries on the bottom and north-east-west sides (fig. 30–1). There is an outcrop area within the grid, where the water-table aquifer is missing. The aquifer is discretized using 40 rows and 20 columns (250 m on a side). A single steady-state stress period, with a single time step, was simulated. An arbitrary simulation period of 1 day was simulated. Model parameters for the example are summarized in table 30–1.

The top of the model was set at an arbitrary elevation of 200 m (table 30–1). The bottom elevations were not uniform; the aquifer was relatively flat on the east side and sloped gently to the south and west sides (see [Hunt and others, 2020](#), fig. 1b). In the western area, and southeastern and southwestern corners of the aquifer, the impermeable bottom elevation was higher making for no-flow outcrop areas within the grid.

Table 30–1: Model parameters for example ex-gwf-capture.

Parameter	Value
Number of periods	1
Number of layers	1
Number of rows	40
Number of columns	20
Column width (m)	250.0
Row width (m)	250.0
Top of the model (m)	35.0
Cell conversion type	1
Starting head (m)	45.0
Recharge rate (m/s)	1.6000000e-09
Perturbation flux (m/s)	-1e-3

Hydraulic conductivity (K) consisted of six zones (see [Hunt and others, 2020](#), fig. 1c) with relatively small changes among them; areas of higher values of K were along the north, east and west boundaries, and adjacent to the western outcrop; K was lower in the south.

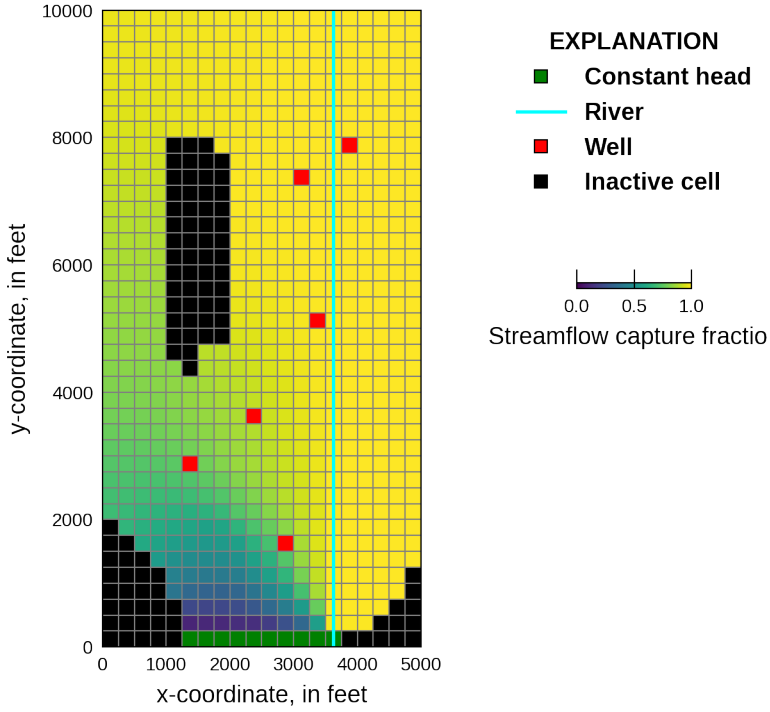


Figure 30–1: Diagram showing the model domain and the simulated streamflow capture fraction. The location of river cells, constant head cells, and wells are also shown.

An initial head of 45 m is specified in each model cell. Flow into the system is from infiltration from precipitation and was represented using the recharge (RCH) package. A constant recharge rate of  $1 \times 10^{-9} \text{ m/s}$  was specified for every active cell in the aquifer. A stream represented by river (RIV) package cells in column 15 in every row in the model and have river stages ranging from 20.1 m in row 1 to 11.25 m in row 40, a conductance of  $0.05 \text{ m}^2/\text{s}$ , and bottom elevations ranging from 20 m in row 1 to 10.25 m in row 40 (fig. 30–1). River cells discharge groundwater from the model in every cells except river cells in row 9 and 10, which are a source of water for the model. Additional discharge of groundwater out of the model is from discharging wells represented by well (WEL) package cells and specified head cells. There are six pumping wells (fig. 30–1) with a total withdrawal rate of  $22.05 \text{ m}^3/\text{s}$ . Heads are specified to be constant on the southern boundary in all active cells in row 40 and range from 16.9 m in column 6 to 11.4 m in column 15.

The Newton-Raphson formulation and Newton-Raphson under-relaxation were used to improve model convergence.

## 30.2 Example Results

The capture fraction analysis was performed using the MODFLOW Application Program Interface (API). An advantage of using the MODFLOW API is that model input files do not need to be regenerated. In this example, the streamflow capture fraction for a cell is calculated as

$$c_{k,i,j} = \frac{Q_{RIV}^+ - Q_{RIV_{\text{base}}}}{|Q^+|}, \quad (30-1)$$

30-2

where  $c_{k,i,j}$  is the streamflow capture fraction for an active cell (unitless),  $Q_{RIV}^+$  is the streamflow in the simulation with the perturbed flow in cell  $(i, j, k)$  ( $L^3/T$ ),  $Q_{RIV_{base}}$  is the streamflow in the base simulation ( $L^3/T$ ), and  $Q^+$  is the flow that is added to an active cell ( $L^3/T$ ).

Use of the MODFLOW API function requires replacement of the time-step loop in MODFLOW with an equivalent time-step loop in the programming language used to access in API. In this example, python is used to control MODFLOW. In addition to defining a replacement time-step loop, use of the MODFLOW API requires accessing program data in memory to control other programs being executed or to change MODFLOW data from the values defined in the MODFLOW input files.

When calculating the streamflow capture fraction, the specified flux in the second WEL package is set to the specified perturbation flux rate (table 30–1) and the node number is modified to reduced node number for the cell being evaluated. The main loop that iterates over all of the active cells and adds the streamflow capture fraction to the appropriate location in the array used to store the values is listed below.

```
ireduced_node = -1
for irow in range(nrow):
    for jcol in range(ncol):

        # skip inactive cells
        if idomain[irow, jcol] < 1:
            continue

        # increment reduced node number
        ireduced_node += 1

        # calculate the perturbed river flow
        qriv = capture_fraction_iteration(mf6, cf_q, inode=ireduced_node)

        # add the value to the capture array
        capture[irow, jcol] = (qriv - qbase) / abs(cf_q)
```

The `idomain` array is a mapping array that identifies cells that have been removed from the simulation. The `capture_fraction_iteration()` function is listed below and returns the net streamflow ( $Q_{RIV}^+$ ) after initializing the simulation (`mobj.initialize()`), adding the perturbation flux rate to the cell being evaluated (`update_wel_pak()`), running each time step in the simulation (`mobj.update()`), getting the net streamflow (`get_streamflow()`), and finalizing the simulation (`mobj.finalize()`).

```
def capture_fraction_iteration(mobj, q, inode=None):
    mobj.initialize()
    # time loop
    current_time = mobj.get_current_time()
    end_time = mobj.get_end_time()
    if inode is not None:
        update_wel_pak(mobj, inode, q)
    while current_time < end_time:
        mobj.update()
        current_time = mobj.get_current_time()
    qriv = get_streamflow(mobj)
    mobj.finalize()
    return qriv
```

The `update_wel_pak()` function is listed below and sets the number of boundaries (`nbound`) in the second WEL package to one, sets the perturbation location (`nodelist`) to the one-based reduced node number, and sets the specified flux rate (`bound`) to the perturbation flux value.

```
def update_wel_pak(mobj, inode, q):
    # set nbound to 1
    tag = mobj.get_var_address("NBOUND", sim_name, "CF-1")
    nbound = mobj.get_value(tag)
    nbound[0] = 1
    mobj.set_value(tag, nbound)
    # set nodelist to inode
    tag = mobj.get_var_address("NODELIST", sim_name, "CF-1")
    nodelist = mobj.get_value(tag)
    nodelist[0] = inode + 1 # convert from zero-based to one-based node number
    mobj.set_value(tag, nodelist)
    # set bound to q
    tag = mobj.get_var_address("BOUND", sim_name, "CF-1")
    bound = mobj.get_value(tag)
    bound[:, 0] = q
    mobj.set_value(tag, bound)
```

The `get_streamflow()` function gets the simulated flow between MODFLOW and the RIV Package and uses `numpy` to sum the flow for all of the RIV package cells into a net stream flow value ( $Q_{RIV}^+$ ).

```
def get_streamflow(mobj):
    tag = mobj.get_var_address("SIMVALS", sim_name, "RIV-1")
    return mobj.get_value(tag).sum()
```

Simulated streamflow capture fraction results are shown in figure 30–1. The stream captures all of the inflow to the model except west of the river in cells close to the constant head boundaries. Cells close to the western-most constant head boundary cells do not contribute any groundwater to the stream.

# 31 Keating Problem

This example is based on an unsaturated flow and transport problem described in [Keating and Zyvoloski \(2009\)](#) under the section “Extension to Mixed Vadose/ Saturated Zone Simulations.” The problem consists of a two-dimensional cross-section model with a perched aquifer overlying a water table aquifer. This problem offers a difficult test for the Newton flow formulation in MODFLOW 6 as well as for the transport model, which must transmit solute through dry cells. This problem was also used by [Bedeckar and others \(2016\)](#) as a test for their solute routing approach implemented in MT3D-USGS for flow models solved with MODFLOW-NWT ([Niswonger and others, 2011](#)).

## 31.1 Example description

The parameters used for this problem are listed in table 31–1. The model grid consists of 1 row, 400 columns, and 80 layers. The flow problem consists of a perched aquifer overlying an unconfined water table aquifer. A perched aquifer forms due the presence of a thin, discontinuous low permeability lens located near the center of the model domain. Flow conditions are simulated as steady state. The solute transport simulation represents transient conditions, which begin with an initial concentration specified as zero everywhere within the model domain. For the first 730 days, recharge enters at a concentration of one. For the remainder of the simulation, recharge has a solute concentration of zero.

Constant-head conditions are prescribed on the left and right sides of the model with head values of 800 m and 100 m, respectively. These constant-head conditions are only assigned if the cell bottom elevation is below the prescribed head value. Water entering the model from the constant head cells is assigned a concentration of zero. Water leaving the constant head cells on the right side of the model leaves at the simulated concentration in the cell.

The Newton formulation is used to simulate flow through the domain. Recharge is assigned to the top of the model, and although upper model cells are dry, this recharge water is instantaneously transmitted down to the perched aquifer. The perched aquifer flows to the left and right and spills over the edges of the confining unit. Water flowing over the edges instantaneously recharges the underlying water table aquifer. A negligible amount of water flows through the low permeability lens and then down into the water table aquifer. The flow problem is challenging to solve and converges best with backtracking, under relaxation, and solver parameters designed for complex problems.

For the transport model, the simulation period is divided into 3000, 10-day time steps. Advection and dispersion are simulated. Because the longitudinal and transverse dispersivities are equal, the computationally demanding XT3D approach is not needed to represent dispersion. The simpler method for calculating dispersion is used instead, and gives comparable results to those obtained with XT3D.

Table 31–1: Model parameters for example ex-gwt-keating.

Parameter	Value
Number of layers	80
Number of rows	1
Number of columns	400
Column width (m)	25.0
Row width (m)	1.0
Layer thickness (m)	25.0
Top of model domain (m)	2000.0
Bottom of model domain (m)	0.0
Permeability of aquifer ( $m^2$ )	1.0e-12
Permeability of aquitard ( $m^2$ )	1.0e-18

Table 31–1: Model parameters for example ex-gwt-keating.

Parameter	Value
Head on left side (m)	800.0
Head on right side (m)	100.0
Recharge (kg/s)	0.5
Normalized recharge concentration (unitless)	1.0
Longitudinal dispersivity (m)	1.0
Transverse horizontal dispersivity (m)	1.0
Transverse vertical dispersivity (m)	1.0
Length of first simulation period (d)	730
Length of second simulation period (d)	29270.0
Porosity of mobile domain (unitless)	0.1
Layer, row, and column for observation 1	(49, 1, 119)
Layer, row, and column for observation 2	(77, 1, 359)

## 31.2 Example Results

Simulated heads from MODFLOW 6 are shown in figure 31–1. Cells with a calculated head beneath the cell bottom are considered “dry” and are not shown with a color. The zone of recharge is shown in red on the top of the plot.

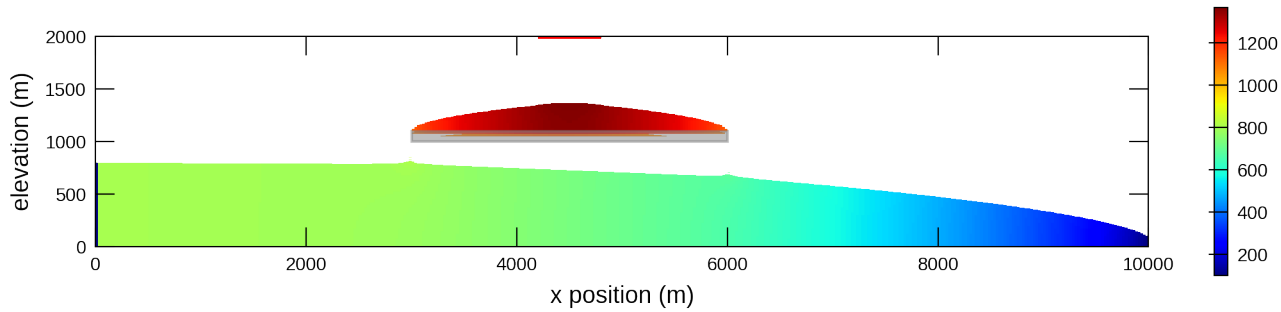


Figure 31–1: Color shaded plot of heads simulated by MODFLOW 6 for the Keating and Zyvoloski (2009) problem involving groundwater flow and transport through an unsaturated zone. Recharge is applied to the narrow strip shown in red on the top of the model domain.

Simulated concentrations from MODFLOW 6 are shown in figure 31–2 for three different times. These plots show the development of the solute plume in the perched aquifer, and then shows flushing of the perched aquifer when the recharge concentration becomes zero. In the underlying water table aquifer, two solute plumes are formed as groundwater flows over the edges of the low permeability lens. These plumes then flow toward the right, and eventually exit through the constant head cells. Plots of concentration versus time for the two yellow points shown in figure 31–2 are

shown in figure 31–3. Results from MODFLOW 6 are shown with the results presented by Keating and Zyvoloski (2009) and are in good agreement considering the complexity of the problem. Similar plots for this problem are also presented by Bedekar and others (2016).

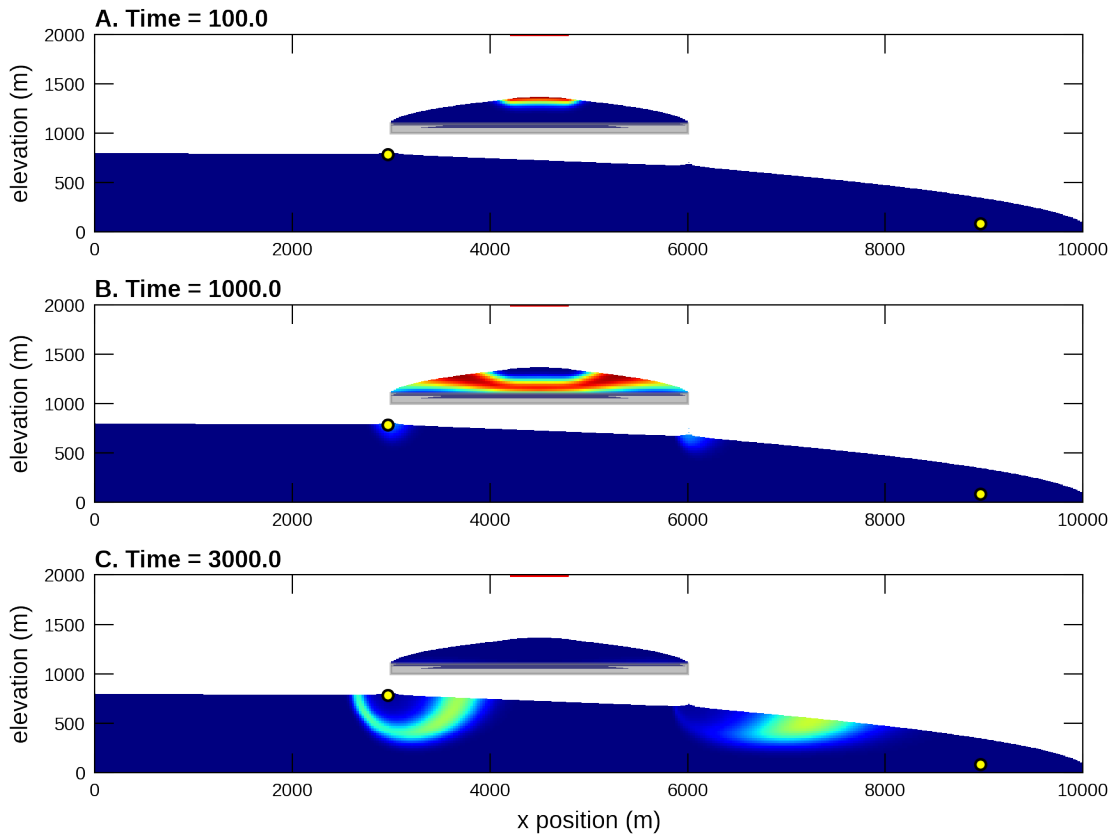


Figure 31–2: Color shaded plots of concentrations simulated by MODFLOW 6 for the Keating and Zyvoloski (2009) problem involving groundwater flow and transport through an unsaturated zone. This plot can be compared to figure 11 in Bedekar and others (2016), which shows similar plots for MT3D-USGS results. Plots of concentration versus time are shown in figure 31–3 for the two points shown in yellow.

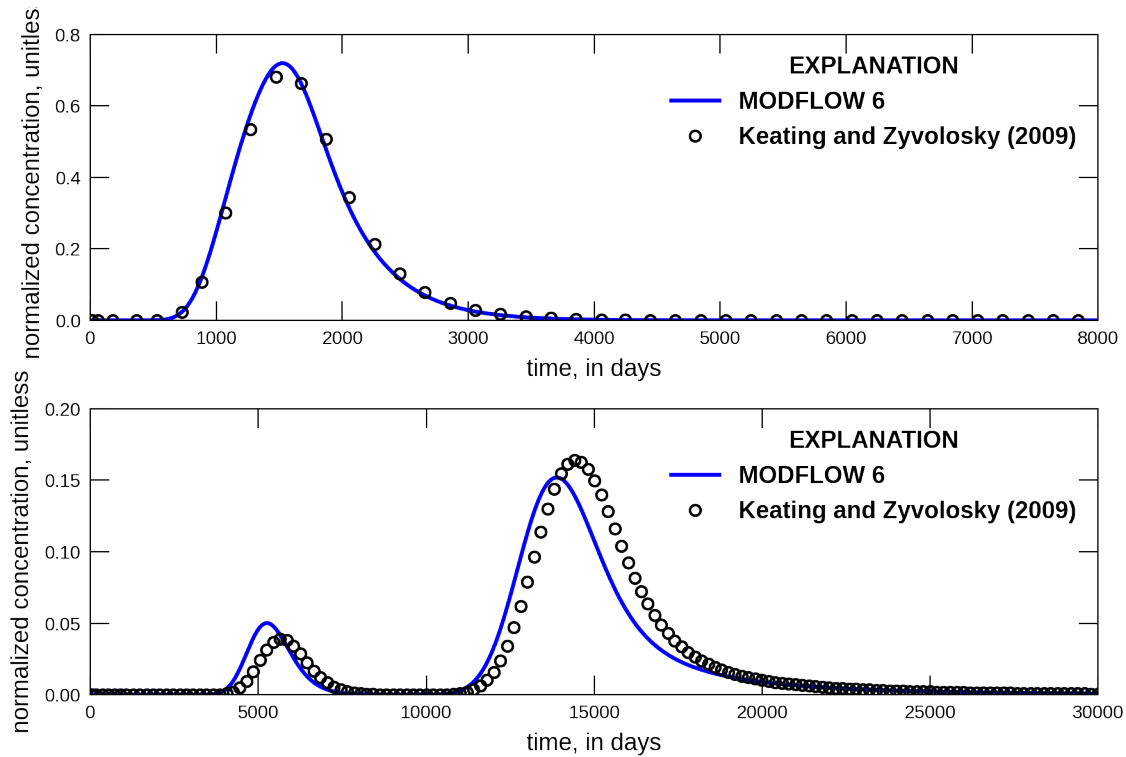


Figure 31–3: Concentrations versus time for two observation points as simulated by MODFLOW 6 and by [Keating and Zyvolosky \(2009\)](#) for a problem involving groundwater flow and transport through an unsaturated zone. This plot can be compared to figure 12 in [Bedekar and others \(2016\)](#), which shows a similar plot for MT3D-USGS results.

## 32 MOC3D Problem 1

This problem corresponds to the first problem presented in the MOC3D report [Konikow and others \(1996\)](#), which involves the transport of a dissolved constituent in a steady, one-dimensional flow field. An analytical solution for this problem is given by [Wexler \(1992\)](#). This example is simulated with the GWT Model in MODFLOW 6, which receives flow information from a separate simulation with the GWF Model in MODFLOW 6. Results from the GWT Model are compared with the results from the [Wexler \(1992\)](#) analytical solution.

### 32.1 Example description

The parameters used for this problem are listed in table 32–1. The model grid for this problem consists of one layer, 120 rows, and 1 columns. The top for each cell is assigned a value of 1.0 cm and the bottom is assigned a value of zero. DELR is set to 1.0 cm and DELC is specified with a constant value of 0.1 cm. The simulation consists of one stress period that is 120 s in length, and the stress period is divided into 240 equally sized time steps. By using a uniform porosity value of 0.1, a velocity value of 0.1 cm/s results from the injection of water at a rate of 0.001 cm<sup>3</sup>/s into the first cell. The last cell is assigned a constant head with a value of zero, though this value is not important as the cells are marked as being confined. The concentration of the injected water is assigned a value of 1.0, and any water that leaves through the constant-head cell leaves with the simulated concentration of the water in that last cell. Advection is solved using the TVD scheme to reduce numerical dispersion.

Table 32–1: Model parameters for example ex-gwt-moc3d-p01.

Parameter	Value
Number of periods	1
Number of layers	1
Number of rows	1
Number of columns	122
Length of system (cm)	12.0
Column width (cm)	0.1
Row width (cm)	0.1
Top of the model (cm)	1.0
Layer bottom elevation (cm)	0
Specific discharge (cms <sup>-1</sup> )	0.1
Hydraulic conductivity (cms <sup>-1</sup> )	0.01
Porosity of mobile domain (unitless)	0.1
Simulation time (s)	120.0
Source concentration (unitless)	1.0
Initial concentration (unitless)	0.0

### 32.2 Example Scenarios

This example problem consists of several different scenarios, as listed in table 32–2. Two different levels of dispersion were simulated, and these simulations are referred to as the low dispersion case and the high dispersion case. The low dispersion case has a dispersion coefficient of 0.01 cm<sup>2</sup>/s, which, for the specified velocity, corresponds to a dispersivity value of 0.1 cm. The high-dispersion case has a dispersion coefficient of 0.1 cm<sup>2</sup>/s, which corresponds to a dispersivity value of 1.0 cm.

Table 32–2: Scenario parameters for example ex-gwt-moc3d-p01.

Scenario	Scenario Name	Parameter	Value
1	ex-gwt-moc3d-p01a	longitudinal dispersivity (cm)	0.1
		retardation factor (unitless)	1.0
		decay rate ( $s^{-1}$ )	0.0
2	ex-gwt-moc3d-p01b	longitudinal dispersivity (cm)	1.0
		retardation factor (unitless)	1.0
		decay rate ( $s^{-1}$ )	0.0
3	ex-gwt-moc3d-p01c	longitudinal dispersivity (cm)	1.0
		retardation factor (unitless)	2.0
		decay rate ( $s^{-1}$ )	0.0
4	ex-gwt-moc3d-p01d	longitudinal dispersivity (cm)	1.0
		retardation factor (unitless)	1.0
		decay rate ( $s^{-1}$ )	0.01

### 32.2.1 Scenario Results

For the first scenario with a relatively small dispersivity value (0.1 cm), plots of concentration versus time and concentration versus distance are shown in figures 32–1 and 32–2, respectively. Figure 32–1 can be compared to figure 18 in [Konikow and others \(1996\)](#). The three separate concentration versus time curves represent the three different distances (0.05, 4.05, and 11.05 cm). For this low-dispersion case, the MODFLOW 6 solution is in relatively good agreement with the analytical solution, but some slight differences are observed. These differences are due primarily to limitations with the second-order TVD scheme implemented in MODFLOW 6, which can suffer from numerical dispersion.

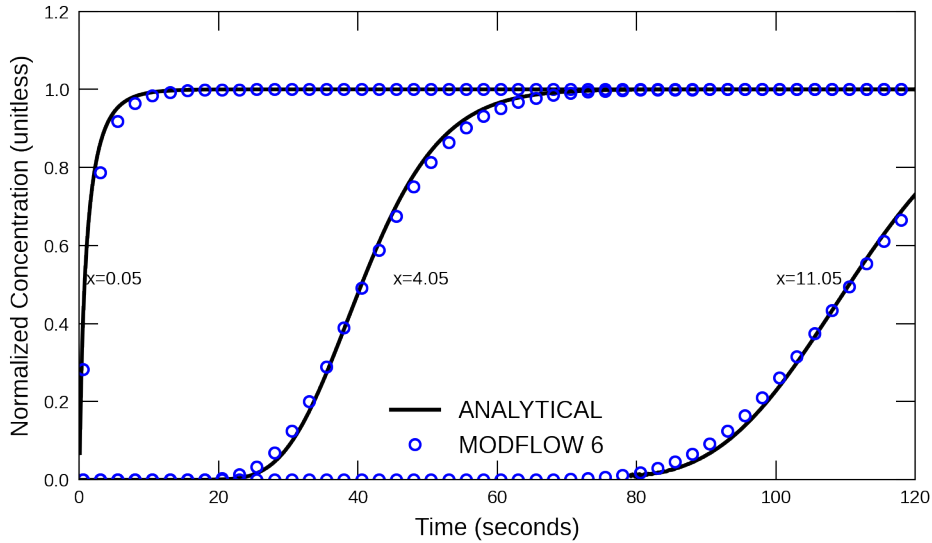


Figure 32–1: Concentrations simulated by the MODFLOW 6 GWT Model and calculated by the analytical solution for one-dimensional flow with transport for the low dispersion case. Circles are for the GWT Model results; the lines represent the analytical solution by [Wexler \(1992\)](#). Results are shown for three different distances (0.05, 4.05, and 11.05 cm from the end of the first cell). Every fifth time step is shown for the MODFLOW 6 results.

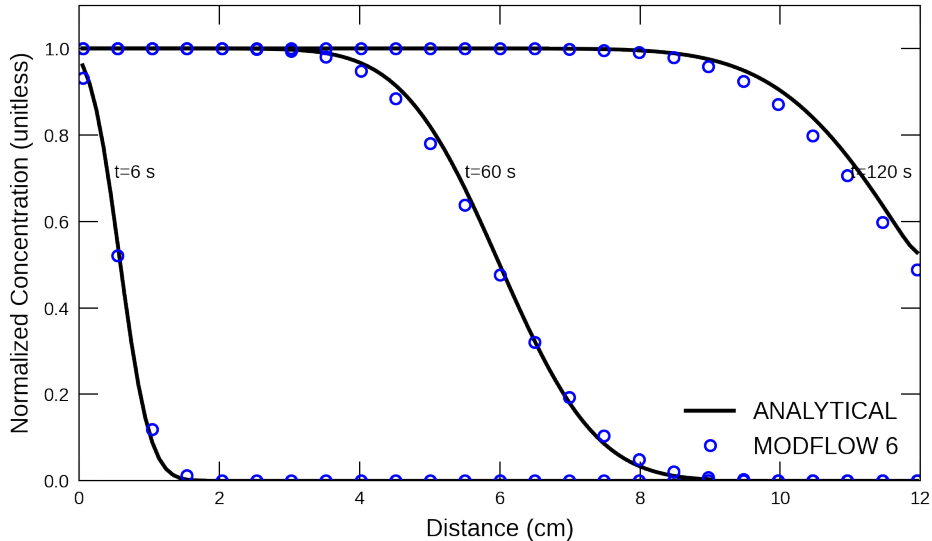


Figure 32–2: Concentrations simulated by the MODFLOW 6 GWT Model and calculated by the analytical solution for one-dimensional flow with transport for the low dispersion case. Circles are for the GWT Model results; the lines represent the analytical solution by Wexler (1992). Results are shown for three different times (6, 60, and 120 s). Every fifth cell is shown for the MODFLOW 6 results.

For the second scenario, which has a relatively large dispersivity value ( $1.0\text{ cm}$ ), plots of concentration versus time and concentration versus distance are shown in figures 32–3 and 32–4, respectively. For the high-dispersion case, the results from the MODFLOW 6 simulation are in better agreement with the analytical solution than for the low dispersion case.

For the remaining scenarios, the results from MODFLOW 6 are compared with the Wexler (1992) analytical solution for two variations of the high-dispersion case. The effects sorption are included in scenario 3 and the effects of decay are included in scenario 4. Plots of concentration versus time and concentration versus distance for a simulation with a retardation factor of 2.0 are shown in figures 32–5 and 32–6, respectively. Plots of concentration versus time and concentration versus distance for a simulation with a decay rate of  $0.01\text{ s}^{-1}$  are shown in figures 32–7 and 32–8, respectively.

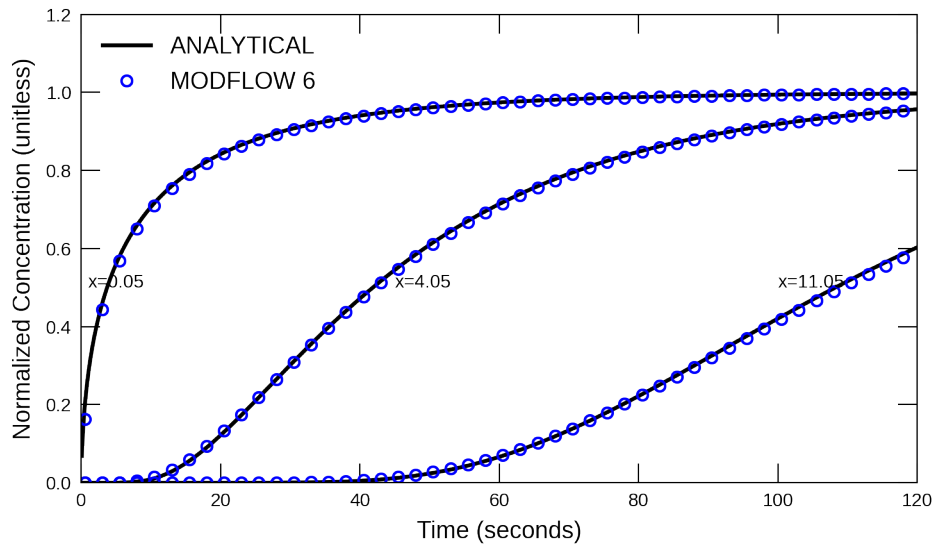


Figure 32–3: Concentrations simulated by the MODFLOW 6 GWT Model and calculated by the analytical solution for one-dimensional flow with transport for the high dispersion case. Circles are for the GWT Model results; the lines represent the analytical solution by Wexler (1992). Results are shown for three different distances ( $0.05, 4.05$ , and  $11.05\text{ cm}$  from the end of the first cell). Every fifth time step is shown for the MODFLOW 6 results.

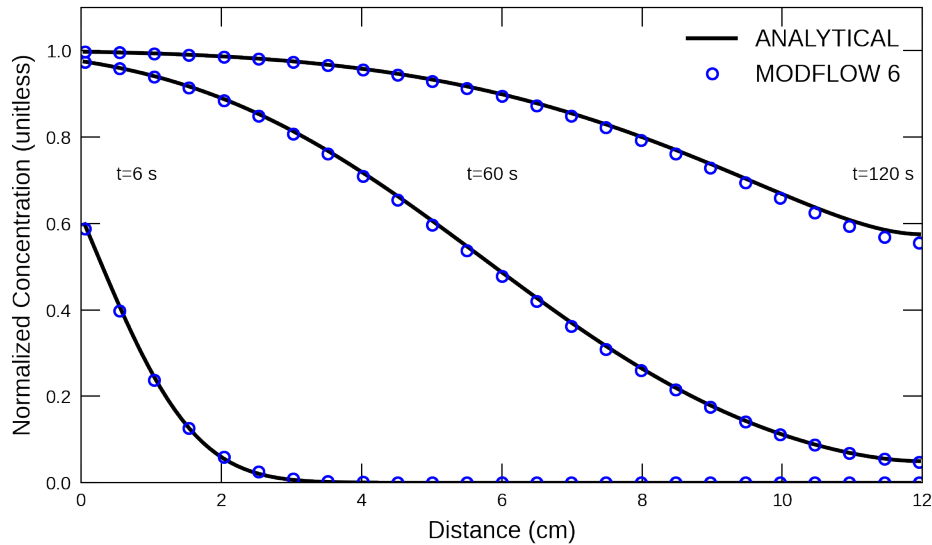


Figure 32–4: Concentrations simulated by the MODFLOW 6 GWT Model and calculated by the analytical solution for one-dimensional flow with transport for the high dispersion case. Circles are for the GWT Model results; the lines represent the analytical solution by Wexler (1992). Results are shown for three different times ( $6, 60$ , and  $120\text{ s}$ ). Every fifth cell is shown for the MODFLOW 6 results.

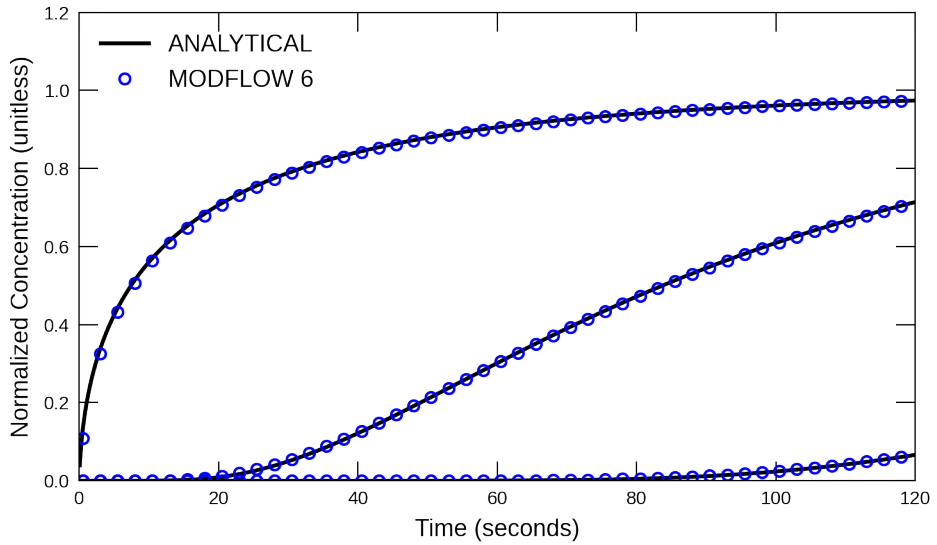


Figure 32–5: Concentrations simulated by the MODFLOW 6 GWT Model and calculated by the analytical solution for one-dimensional flow with transport for the high dispersion case and a retardation factor of 2. Circles are for the GWT Model results; the lines represent the analytical solution by Wexler (1992). Results are shown for three different distances (0.05, 4.05, and 11.05 cm from the end of the first cell). Every fifth time step is shown for the MODFLOW 6 results.

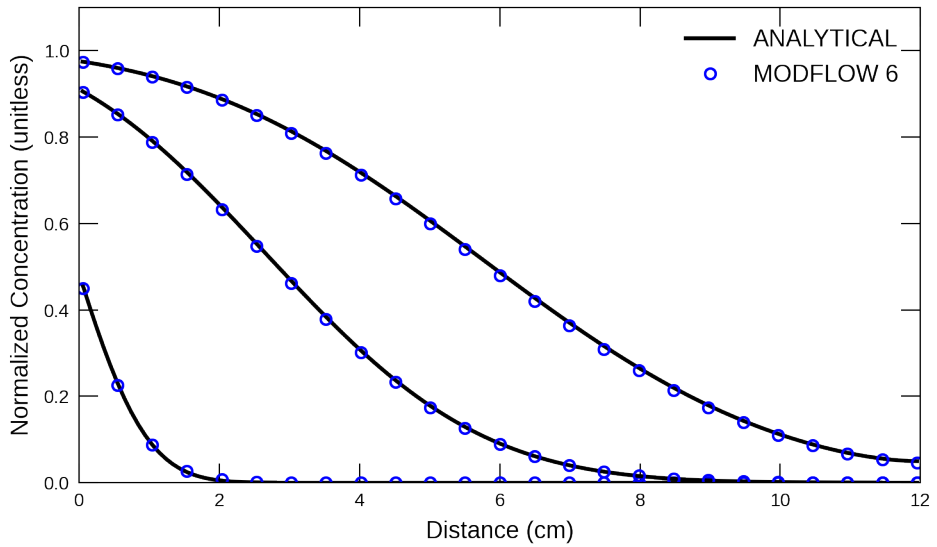


Figure 32–6: Concentrations simulated by the MODFLOW 6 GWT Model and calculated by the analytical solution for one-dimensional flow with transport for the high dispersion case and a retardation factor of 2. Circles are for the GWT Model results; the lines represent the analytical solution by Wexler (1992). Results are shown for three different times (6, 60, and 120 s). Every fifth cell is shown for the MODFLOW 6 results.

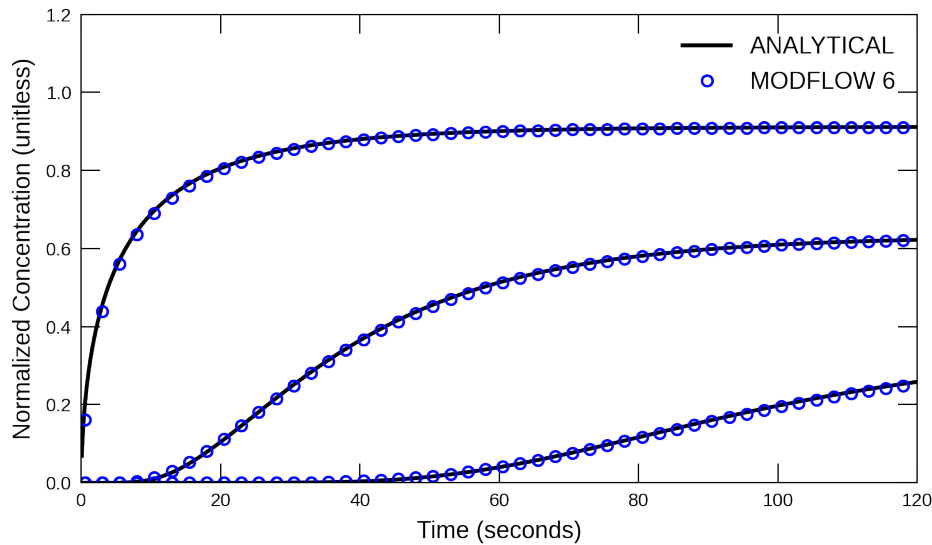


Figure 32–7: Concentrations simulated by the MODFLOW 6 GWT Model and calculated by the analytical solution for one-dimensional flow with transport for the high dispersion case and a decay rate of  $0.01 \text{ s}^{-1}$ . Circles are for the GWT Model results; the lines represent the analytical solution by Wexler (1992). Results are shown for three different distances (0.05, 4.05, and 11.05 cm from the end of the first cell). Every fifth time step is shown for the MODFLOW 6 results.

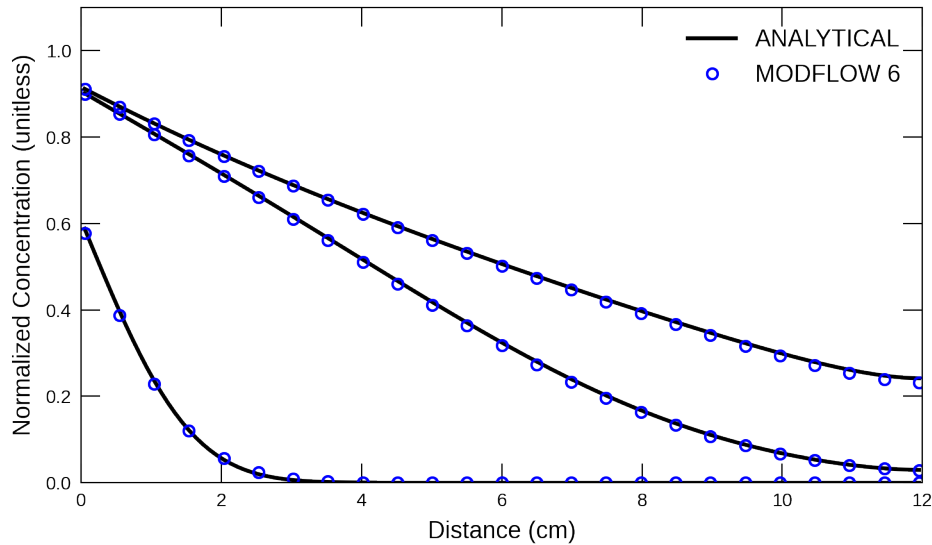


Figure 32–8: Concentrations simulated by the MODFLOW 6 GWT Model and calculated by the analytical solution for one-dimensional flow with transport for the high dispersion case and a decay rate of  $0.01 \text{ s}^{-1}$ . Circles are for the GWT Model results; the lines represent the analytical solution by Wexler (1992). Results are shown for three different times (6, 60, and 120 s). Every fifth cell is shown for the MODFLOW 6 results.

## 33 MOC3D Problem 2

This problem corresponds to the second problem presented in the MOC3D report [Konikow and others \(1996\)](#), which involves the transport of a dissolved constituent in a steady, three-dimensional flow field. An analytical solution for this problem is given by [Wexler \(1992\)](#). This example is simulated with the GWT Model in MODFLOW 6, which receives flow information from a separate simulation with the GWF Model in MODFLOW 6. Results from the GWT Model are compared with the results from the [Wexler \(1992\)](#) analytical solution.

### 33.1 Example description

[Wexler \(1992\)](#) presents an analytical solution for three dimensional solute transport from a point source in a one-dimensional flow field. As described by [Konikow and others \(1996\)](#), only one quadrant of the three-dimensional domain is represented by the numerical model. Thus, the solute mass flux specified for the model is one quarter of the solute mass flux used in the analytical solution.

The parameters used for this problem are listed in table 33–1. The model grid for this problem consists of 40 layers, 12 rows, and 30 columns. The top for layer 1 is set to zero, and flat bottoms are assigned to all layers based on a uniform layer thickness of 0.05 m. DELR is set to 3.0 m and DELC is specified with a constant value of 0.5 m. The simulation consists of one stress period that is 400 d in length, and the stress period is divided into 400 equally sized time steps. Velocity is specified to be 0.1 m/d in the x direction and zero in the y and z directions. The uniform flow field is represented by specifying a constant inflow rate into all of the cells in column 1 and by specifying a constant head condition to all of the cells in column 30. A specified solute flux of 10 grams per day is specified to the cell in layer 1, row 12, and column 8. Any water that leaves through the constant-head cell leaves with the simulated concentration of the water in that last cell. Advection is solved using the TVD scheme to reduce numerical dispersion. In addition to the longitudinal dispersion, transverse dispersion is represented with a different value in the horizontal direction than in the vertical direction. Because the velocity field is perfectly aligned with the model grid, there are no cross-dispersion terms and the problem can be simulated accurately without the need for XT3D.

Table 33–1: Model parameters for example ex-gwt-moc3d-p02.

Parameter	Value
Number of periods	1
Number of layers	40
Number of rows	12
Number of columns	30
Column width (m)	3
Row width (m)	0.5
Layer thickness (m)	0.05
Top of the model (m)	0.0
Model bottom elevation (m)	-2.0
Velocity in x-direction ( $md^{-1}$ )	0.1
Hydraulic conductivity ( $md^{-1}$ )	0.0125
Porosity of mobile domain (unitless)	0.25
Longitudinal dispersivity (m)	0.6
Transverse horizontal dispersivity (m)	0.03
Transverse vertical dispersivity (m)	0.006
Simulation time (d)	400.0
Solute mass flux ( $gd^{-1}$ )	2.5

Table 33–1: Model parameters for example ex-gwt-moc3d-p02.

Parameter	Value
Source location (layer, row, column)	(1, 12, 8)

### 33.2 Example Results

A comparison of the MODFLOW 6 results with the analytical solution of Wexler (1992) is shown for layer 1 in figure 33–1.

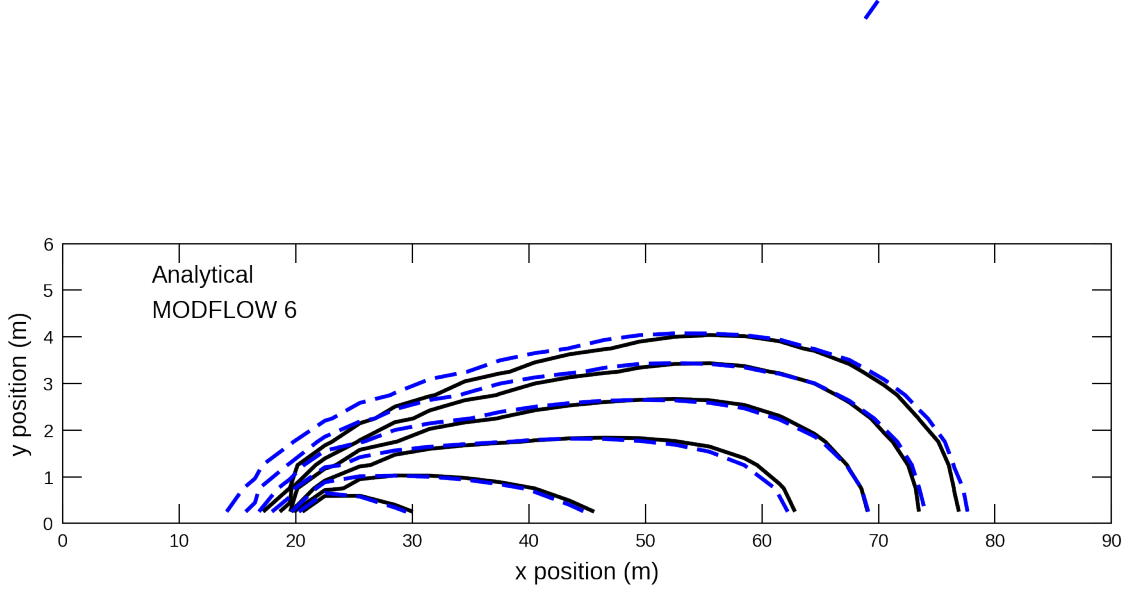


Figure 33–1: Concentrations simulated by the MODFLOW 6 GWT Model and calculated by the analytical solution for three-dimensional flow with transport. Results are for the end of the simulation (time=400 d) and for layer 1. Black lines represent solute concentration contours from the analytical solution (Wexler, 1992); blue lines represent solute concentration contours simulated by MODFLOW 6. An aspect ratio of 4.0 is specified to enhance the comparison.

## 34 MOC3D Problem 2 with Triangular Grid

This problem corresponds to the second problem presented in the MOC3D report [Konikow and others \(1996\)](#), which involves the transport of a dissolved constituent in a steady, three-dimensional flow field. An analytical solution for this problem is given by [Wexler \(1992\)](#). As for the previous example, this example is simulated with the GWT Model in MODFLOW 6, which receives flow information from a separate simulation with the GWF Model in MODFLOW 6. In this example, however, a triangular grid is used for the flow and transport simulation. Results from the GWT Model are compared with the results from the [Wexler \(1992\)](#) analytical solution.

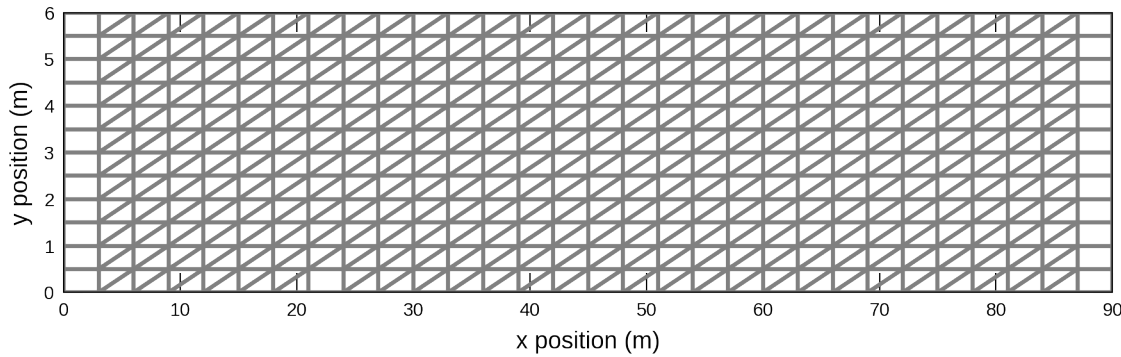


Figure 34–1: Triangular model grid used for the MODFLOW 6 simulation. Model grid is shown using an aspect ratio of 4.

### 34.1 Example description

[Wexler \(1992\)](#) presents an analytical solution for three dimensional solute transport from a point source in a one-dimensional flow field. As described by [Konikow and others \(1996\)](#), only one quadrant of the three-dimensional domain is represented by the numerical model. Thus, the solute mass flux specified for the model is one quarter of the solute mass flux used in the analytical solution.

The parameters used for this problem are listed in table 34–1. The model grid for this problem consists of 40 layers, 695 cells per layer, and 403 vertices in a layer. The top for layer 1 is set to zero, and flat bottoms are assigned to all layers based on a uniform layer thickness of 0.05 m. The remaining parameters are set similarly to the previous simulation with a regular grid, except for in this simulation, the XT3D method is used for flow and dispersive transport.

Table 34–1: Model parameters for example ex-gwt-moc3d-p02tg.

Parameter	Value
Number of periods	1
Number of layers	40
Number of rows	12
Number of columns	30
Column width ( $m$ )	3
Row width ( $m$ )	0.5
Layer thickness ( $m$ )	0.05
Top of the model ( $m$ )	0.0
Model bottom elevation ( $m$ )	-2.0
Velocity in x-direction ( $md^{-1}$ )	0.1
Hydraulic conductivity ( $md^{-1}$ )	0.0125
Porosity of mobile domain (unitless)	0.25
Longitudinal dispersivity ( $m$ )	0.6
Transverse horizontal dispersivity ( $m$ )	0.03
Transverse vertical dispersivity ( $m$ )	0.006
Simulation time ( $d$ )	400.0
Solute mass flux ( $gd^{-1}$ )	2.5
Source location (layer, row, column)	(1, 12, 8)

## 34.2 Example Results

A comparison of the MODFLOW 6 results with the analytical solution of Wexler (1992) is shown for layer 1 in figure 34–2.

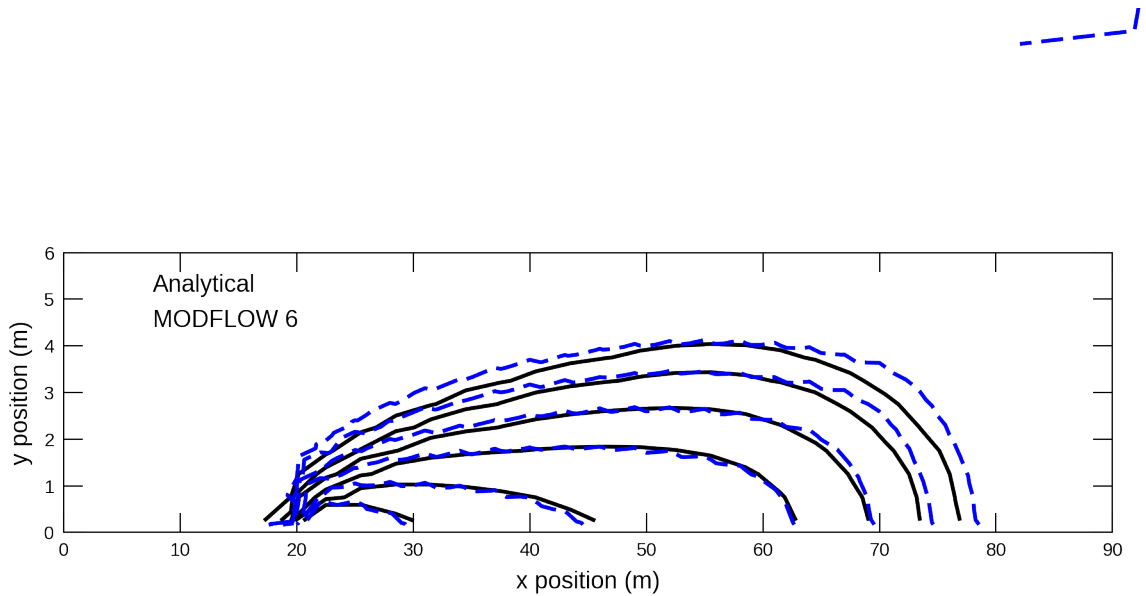


Figure 34–2: Concentrations simulated by the MODFLOW 6 GWT Model and calculated by the analytical solution for three-dimensional flow with transport. Results are for the end of the simulation (time=400 d) and for layer 1. Black lines represent solute concentration contours from the analytical solution (Wexler, 1992); blue lines represent solute concentration contours simulated by MODFLOW 6. An aspect ratio of 4.0 is specified to enhance the comparison.

## 35 MT3DMS Problem 1

Section 7 of [Zheng and Wang \(1999\)](#) details a number of test problems that verify the accuracy of MT3DMS. The first problem presented, titled "one-dimensional transport in a uniform flow field," compared MT3DMS solutions to analytical solutions given by [Van Genuchten and Alves \(1982\)](#). For verifying the accuracy of transport calculations within MODFLOW6, the transport solutions calculated by MT3DMS serve as the benchmark to which the MODFLOW 6 solution is compared. The first 1-dimensional simulation solves for advection only. The second model permutation uses both advection and dispersion to verify MODFLOW 6 results. Next, the accuracy of MODFLOW 6 is verified when advection, dispersion, and some simple chemical reactions represented with sorption processes are used. The fourth and final model permutation adds solute decay to the previous model setup. As of the first release of MODFLOW 6 with transport capabilities, a linear isotherm is the only option available for simulating sorption. Arbitrary values of bulk density and distribution coefficient are uniformly applied to the entire model domain to achieve the indicated retardation factor. The following table summarizes how the four simulations incrementally increase model complexity.

Table 35–1: Scenario parameters for example ex-gwt-mt3dms-p01.

Scenario	Scenario Name	Parameter	Value
1	ex-gwt-mt3dms-p01a	dispersivity (m)	0.0
		retardation (unitless)	1.0
		decay ( $d^{-1}$ )	0.0
2	ex-gwt-mt3dms-p01b	dispersivity (m)	10.0
		retardation (unitless)	1.0
		decay ( $d^{-1}$ )	0.0
3	ex-gwt-mt3dms-p01c	dispersivity (m)	10.0
		retardation (unitless)	5.0
		decay ( $d^{-1}$ )	0.0
4	ex-gwt-mt3dms-p01d	dispersivity (m)	10.0
		retardation (unitless)	5.0
		decay ( $d^{-1}$ )	0.002

### 35.1 Example description

All four model scenarios have 101 columns, 1 row, and 1 layer. The first and last columns use constant-head boundaries to simulate steady flow in confined conditions. Because the analytical solution assumes an infinite 1-dimensional flow field, the last column is set far enough from the source to avoid interfering with the final solution after 2,000 days. Initially, the model domain is devoid of solute; however, the first column uses a constant concentration boundary condition to ensure that water entering the simulation has a unit concentration of 1. Additional model parameters are shown in table 35–2.

Table 35–2: Model parameters for example ex-gwt-mt3dms-p01.

Parameter	Value
Number of periods	1
Number of layers	1
Number of columns	101
Number of rows	1
Column width (m)	10.0
Row width (m)	1.0

Table 35–2: Model parameters for example ex-gwt-mt3dms-p01.

Parameter	Value
Top of the model (m)	0.0
Layer bottom elevations (m)	-1.0
Porosity	0.25
Simulation time (days)	2000
Horizontal hydraulic conductivity (m/d)	1.0

## 35.2 Example Results

Currently no options are available with MODFLOW 6 for simulating solute transport using particle tracking methods [referred to as Method of Characteristics (MOC) in the MT3DMS manual [Zheng and Wang \(1999\)](#)]. Thus, the MODFLOW 6 solution is compared to an MT3DMS solution that uses the third-order total variation diminishing (TVD) option for solving the advection-only problem rather than invoking one of the MOC options available within MT3DMS. Owing to different approaches between the two codes, namely TVD scheme of MT3DMS and the second-order approach of MODFLOW 6, differences between the two solutions and reflected in figure 35–1 are expected. However, the differences are within acceptable tolerances.

The comparison of the MT3DMS and MODFLOW 6 solutions for problem 1a, an advection dominated problem, represents an end-member test as the migrating concentration front is sharp (i.e., discontinuous). In technical terms, the grid Peclet number is infinity for this problem ( $P_e = v\Delta x/D_{xx} = \Delta x/\alpha_L = \infty$ ).

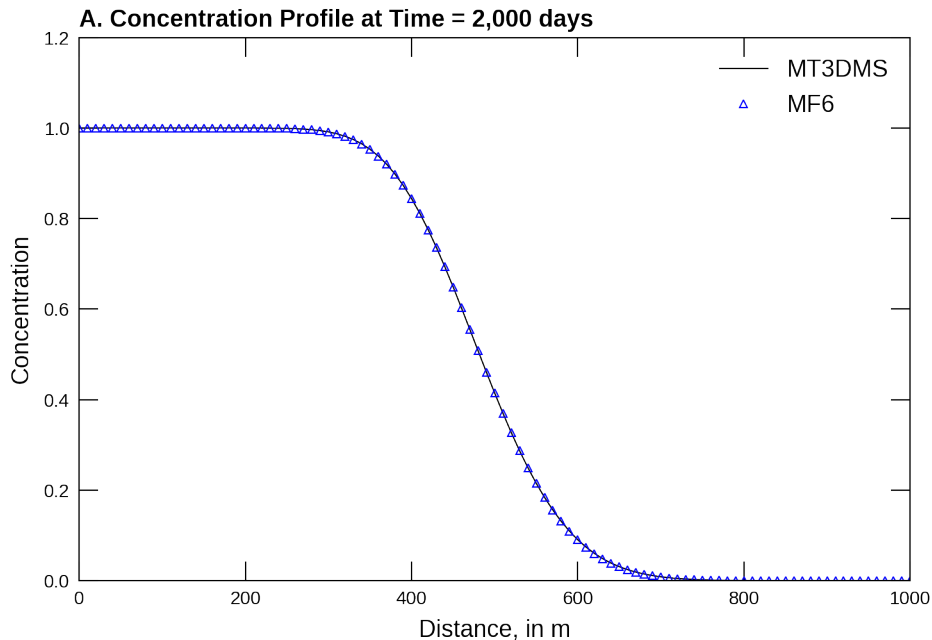


Figure 35–1: Comparison of the MT3DMS and MODFLOW 6 numerical solutions for a one-dimensional advection dominated test problem. The analytical solution for this problem was originally given in [Van Genuchten and Alves \(1982\)](#) and is not shown here

A comparison of MT3DMS and MODFLOW 6 for scenario 2 in the MT3DMS manual represents a more common situation whereby dispersion acts to spread or smooth the advancing concentration front. For this problem, the dispersion term  $\alpha_L$  is set equal to the length of the grid cell in the direction of flow, 10 cm, resulting in a Peclet number equal to one ( $P_e = v\Delta x/D_{xx} = 10/10 = 1$ ). Owing to the presence of dispersion, the finite-difference solutions employed by both MT3DMS and MODFLOW 6 for this problem are more accurate, and as a result are in closer agreement (figure 35–2).

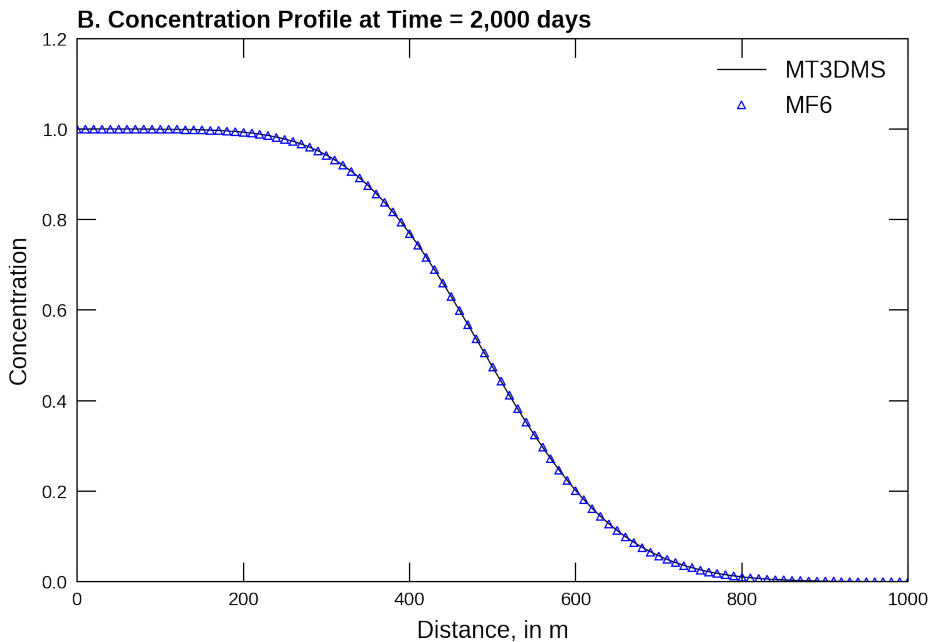


Figure 35–2: Comparison of the MT3DMS and MODFLOW 6 numerical solutions for a one-dimensional test problem with dispersion ( $\alpha_L = 10 \text{ cm}$ ). The analytical solution for this problem was originally given in [Van Genuchten and Alves \(1982\)](#) and is not shown here

The third comparison for the one-dimensional transport in a steady flow field includes uses the same dispersion specified for the second scenario, but adds retardation. For this problem, retardation slows the advance of the migrating concentration front by simulating sorption of the dissolved solute onto the matrix material through which the fluid is moving. In this way, dissolved mass is transferred from the aqueous phase to the solid phase. Appropriate reaction package parameter values are determined for obtaining the specified retardation (5.0) within the code. Figure 35–3 shows a close match between MT3DMS and MODFLOW 6. In addition, figure 35–3 also shows that after 2,000 days, the concentration front did not advance as far as shown in figure 35–2.

The final comparison for the fourth scenario of problem 1 adds decay to the dispersion and retardation simulated in the third scenario. For this case, decay represents the irreversible loss of mass from both the aqueous and sorbed phases, further stunting the advance of the migrating concentration front 35–4.

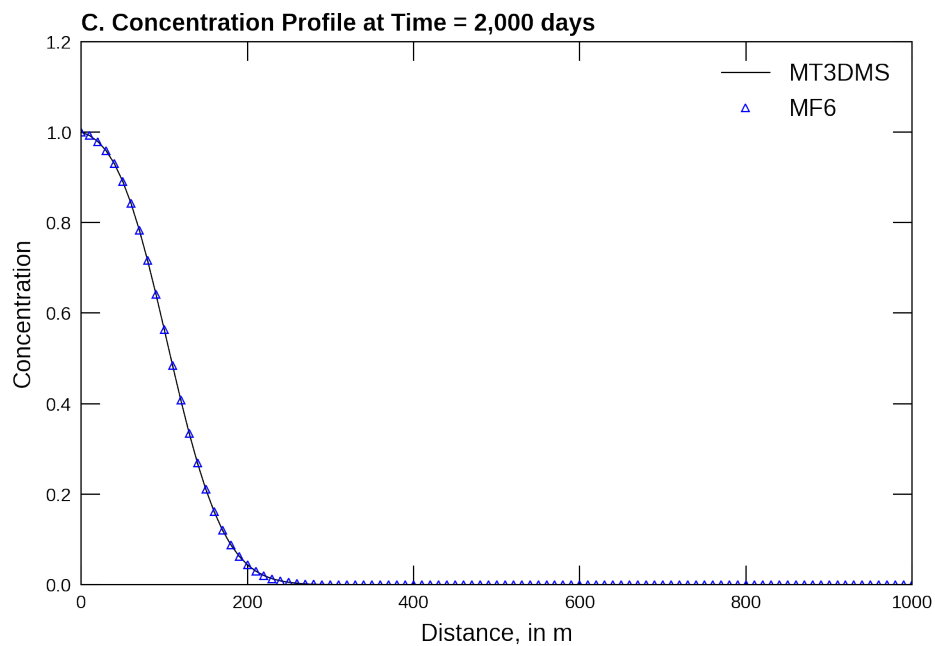


Figure 35-3: Comparison of the MT3DMS and MODFLOW 6 numerical solutions for a one-dimensional test problem with dispersion ( $\alpha_L = 10 \text{ cm}$ ) and retardation ( $R = 5.0$ ). The analytical solution for this problem was originally given in [Van Genuchten and Alves \(1982\)](#) and is not shown here.

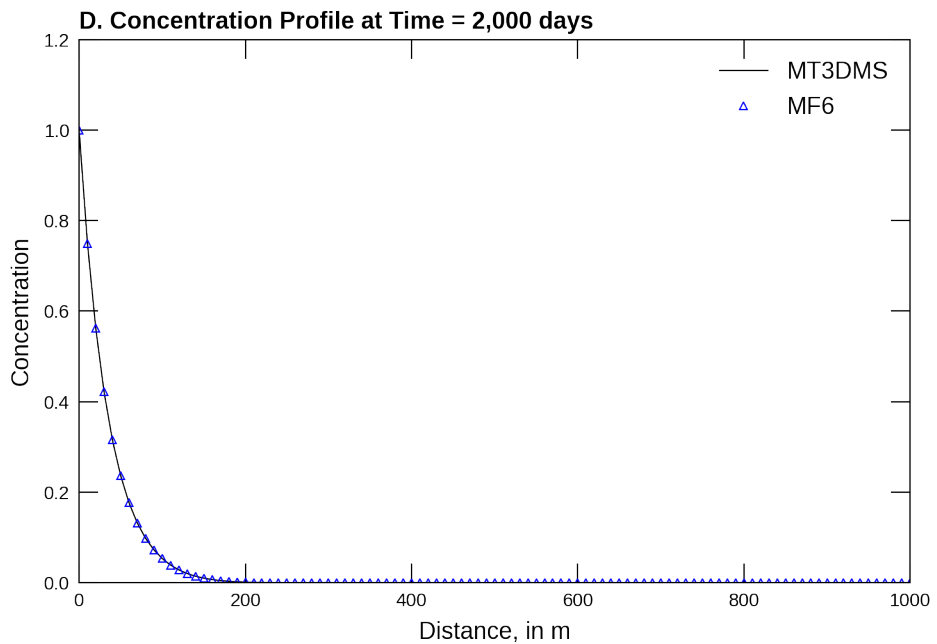


Figure 35–4: Comparison of the MT3DMS and MODFLOW 6 numerical solutions for a one-dimensional test problem with dispersion ( $\alpha_L = 10 \text{ cm}$ ), retardation ( $R = 5.0$ ) and decay ( $\lambda = 0.002 \text{ d}^{-1}$ ). The analytical solution for this problem was originally given in [Van Genuchten and Alves \(1982\)](#) and is not shown here

## 36 MT3DMS Problem 2

This is the second example problem presented in [Zheng and Wang \(1999\)](#), titled “one-dimensional transport with nonlinear or nonequilibrium sorption”. The purpose of this example is to demonstrate simulation of nonlinear and nonequilibrium sorption. For the nonlinear sorption simulations, which use the Freundlich and Langmuir isotherms, [Zheng and Wang \(1999\)](#) compared MT3DMS results to the results from an independent transport simulator called CXTFIT. For the nonequilibrium sorption example, [Zheng and Wang \(1999\)](#) compared the results from MT3DMS to an analytical solution. In this section the results from the MODFLOW 6 GWT Model are compared with the results from MT3DMS.

In MT3DMS, nonequilibrium sorption is represented using the following expression for the dissolved and sorbed solute mass,

$$\rho_b \frac{\partial \bar{C}}{\partial t} = \beta \left( C - \frac{\bar{C}}{K_d} \right), \quad (36-1)$$

where  $\rho_b$  is the bulk density,  $\bar{C}$  is the sorbed concentration,  $C$  is the dissolved aqueous concentration,  $\beta$  is the first-order mass transfer rate between the dissolved aqueous and sorbed phases,  $t$  is time, and  $K_d$  is the linear distribution coefficient.

The current version of the MODFLOW 6 GWT Model does not have the capability to directly represent this type of nonequilibrium sorption. For the example presented by [Zheng and Wang \(1999\)](#), the distribution coefficient has a value close to one (0.933). Because this value is so close to one, we can take advantage of immobile domain capability in MODFLOW 6 to approximate nonequilibrium sorption. For this example there is no separate sorption process within the immobile domain, and there is no decay or production within the immobile domain (as has been defined for this example). Thus, for this problem the transfer of dissolved solute mass between the mobile and immobile domain can be expressed as

$$\theta_{im} \frac{\partial C_{im}}{\partial t} = \zeta (C - C_{im}), \quad (36-2)$$

where  $\theta_{im}$  is the porosity of the immobile domain,  $\zeta$  is the first-order mass transfer rate between the mobile and immobile domains, and  $C_{im}$  is the concentration of the immobile domain. From the similar form of these two equations, it is possible to approximate the nonequilibrium sorption capability in MT3DMS by assigning the immobile domain porosity as bulk density and the first-order mass transfer rate for the mobile and immobile domain as the first-order mass transfer rate for the dissolved and sorbed phases.

There are six scenarios described here (table 36-1). The first two represent nonlinear sorption with the Freundlich and Langmuir isotherms, respectively. The remaining four scenarios represent nonequilibrium sorption with different values for the first-order mass transfer coefficient. These six scenarios and corresponding figures correspond to the ones reported by [Zheng and Wang \(1999\)](#).

Table 36-1: Scenario parameters for example ex-gwt-mt3dms-p02.

Scenario	Scenario Name	Parameter	Value
1	ex-gwt-mt3dms-p02a	sorption (text string)	freundlich
		Kf ( $\mu g L g m g^{-1}$ )	0.3
		a (unitless)	0.7
2	ex-gwt-mt3dms-p02b	sorption (text string)	langmuir
		Kl ( $L m g^{-1}$ )	100.0
		S ( $\mu g g^{-1}$ )	0.003

Table 36–1: Scenario parameters for example ex-gwt-mt3dms-p02.

Scenario	Scenario Name	Parameter	Value
3	ex-gwt-mt3dms-p02c	beta ( $s^{-1}$ )	0.0
4	ex-gwt-mt3dms-p02d	beta ( $s^{-1}$ )	0.002
5	ex-gwt-mt3dms-p02e	beta ( $s^{-1}$ )	0.01
6	ex-gwt-mt3dms-p02f	beta ( $s^{-1}$ )	20.0

### 36.1 Example description

All model scenarios have 101 columns, 1 row, and 1 layer. The first column has a specified inflow rate that results in a velocity of 0.1  $cm/s$ . The last column is assigned as a constant-head boundary to allow water to exit. For the first 160  $s$ , a pulse of solute is introduced to the inflowing water. For the remaining 1340  $s$ , the concentration of inflowing water is zero. Additional model parameters are shown in table 36–2.

Table 36–2: Model parameters for example ex-gwt-mt3dms-p02.

Parameter	Value
Number of periods	2
Number of layers	1
Number of rows	1
Number of columns	101
Length of period 1 ( $s$ )	160
Length of period 2 ( $s$ )	1340
Length of time steps ( $s$ )	1.0
Column width ( $cm$ )	0.16
Row width ( $cm$ )	0.16
Top of the model ( $cm$ )	1.0
Layer bottom elevation ( $cm$ )	0
Velocity ( $cms^{-1}$ )	0.1
Hydraulic conductivity ( $cms^{-1}$ )	0.01
Porosity of mobile domain (unitless)	0.37
Bulk density ( $gcm^{-3}$ )	1.587
Distribution coefficient ( $cm^3g^{-1}$ )	0.933
Longitudinal dispersivity ( $cm$ )	1.0
Source concentration (unitless)	0.05
Initial concentration (unitless)	0.0

### 36.2 Example Results

Simulated results for nonlinear sorption are shown for the Freundlich isotherm in figure 36–1 and for the Langmuir isotherm in figure 36–2. The results from MODFLOW 6 compare well with the results from MT3DMS. Results for the four simulations with different values for beta are shown in figure 36–3. For small beta values, the MODFLOW 6 results compare well with the results from MT3DMS. But for larger beta values, there are small discrepancies between the two models. This is because of the distribution coefficient value (0.933) used for the MT3DMS simulations and the approximation approach for the MODFLOW 6 simulation, which assumes the distribution coefficient is one. If a value of one is used for the distribution coefficient in the MT3DMS simulations, then results are virtually indistinguishable.

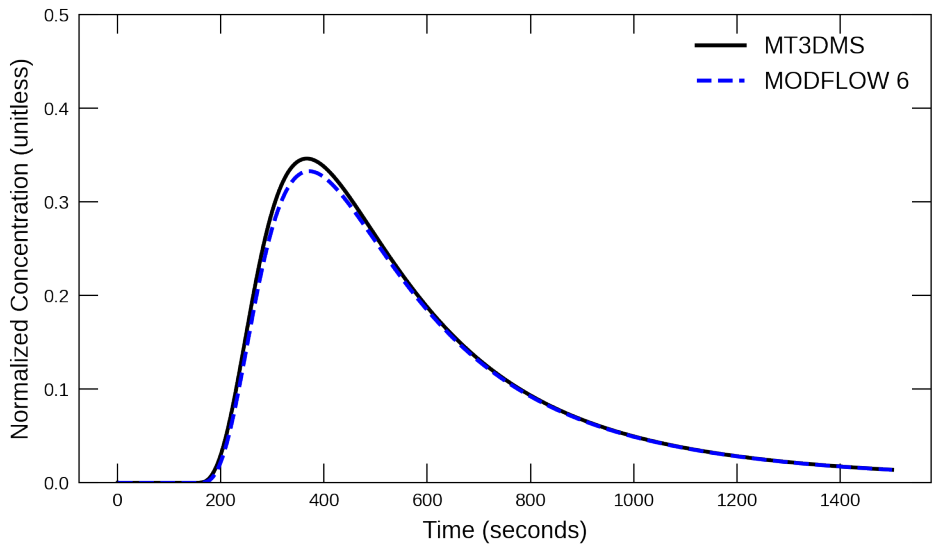


Figure 36–1: Comparison of the MT3DMS and MODFLOW 6 results for nonlinear sorption represented with the Freundlich isotherm.

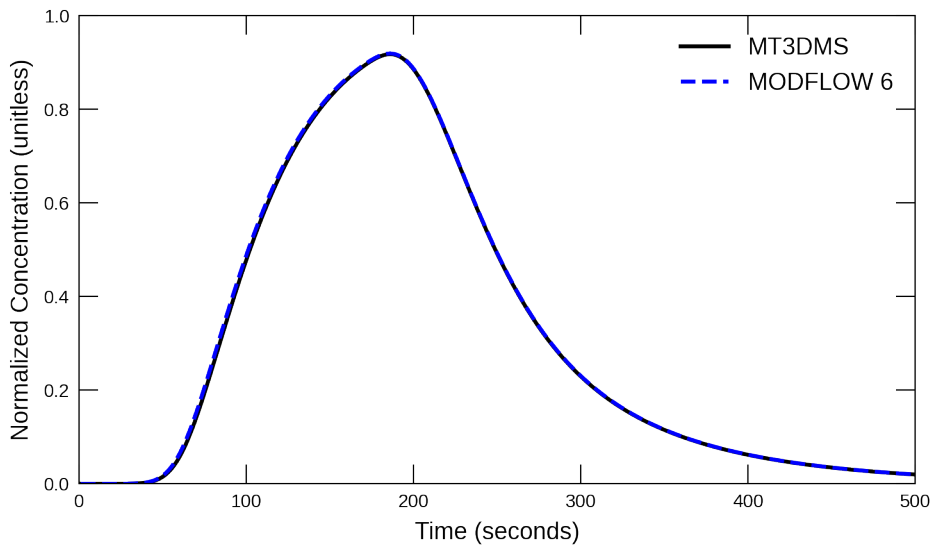


Figure 36–2: Comparison of the MT3DMS and MODFLOW 6 results for nonlinear sorption represented with the Langmuir isotherm.

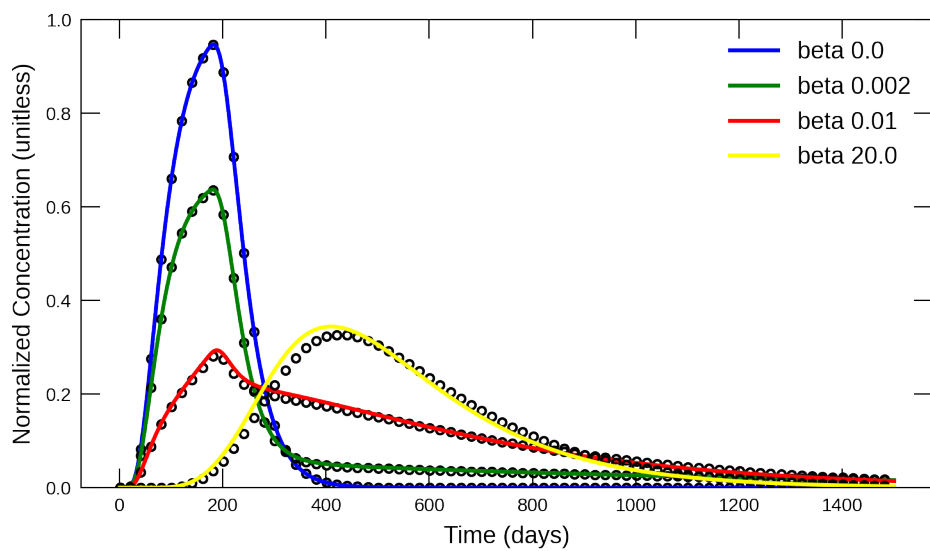


Figure 36–3: Comparison of the MT3DMS (solid lines) and MODFLOW 6 (circles) results for four different values of the nonequilibrium exchange coefficient (beta). The results for MODFLOW 6 are shown for every 20th time step.

## 37 MT3DMS Problem 3

This is the third problem appearing in [Zheng and Wang \(1999\)](#), titled, "two-dimensional transport in a uniform flow field." In contrast to the first demonstrated examples, transport is simulated in two dimensions with dispersion but no reactions. An analytical solution for this problem was originally published in [Wilson and Miller \(1978\)](#). Two assumptions that make the analytical solution possible are that (1) the aquifer is areally infinite and relatively thin to support the assumption that instantaneous mixing occurs in the vertical direction, and (2) that compared to the ambient flow field, the injection rate is insignificant.

### 37.1 Example description

Steady uniform flow enters the left edge of a numerical grid with 31 rows, 46 columns, and 1 layer through a constant head boundary and exits along the right edge. Constant heads are selected to ensure the hydraulic gradient matches with the analytical solution. The other boundaries are all no flow. Boundaries are sufficiently far away from the injection well where the contaminant is released so as not to interfere with the final solution after 365 days. Table 37–1 summarizes model setup:

Table 37–1: Model parameters for example ex-gwt-mt3dms-p03.

Parameter	Value
Number of layers	1
Number of rows	31
Number of columns	46
Column width (m)	10.0
Row width (m)	10.0
Layer thickness (m)	10.0
Top of the model (m)	0.0
Porosity	0.3
Simulation time (days)	365
Horizontal hydraulic conductivity (m/d)	1.0
Volumetric injection rate (m <sup>3</sup> /d)	1.0
Concentration of injected water (mg/L)	1000.0
Longitudinal dispersivity (m)	10.0
Ratio of transverse to longitudinal dispersivity	0.3

After 365 days, the MODFLOW 6 solution aligns well with the MT3DMS solution (fig. 37–1). In addition to the good agreement that was seen in the first MT3DMS test problem, the current comparison confirms that the lateral dispersion is accurately simulated within MODFLOW 6.

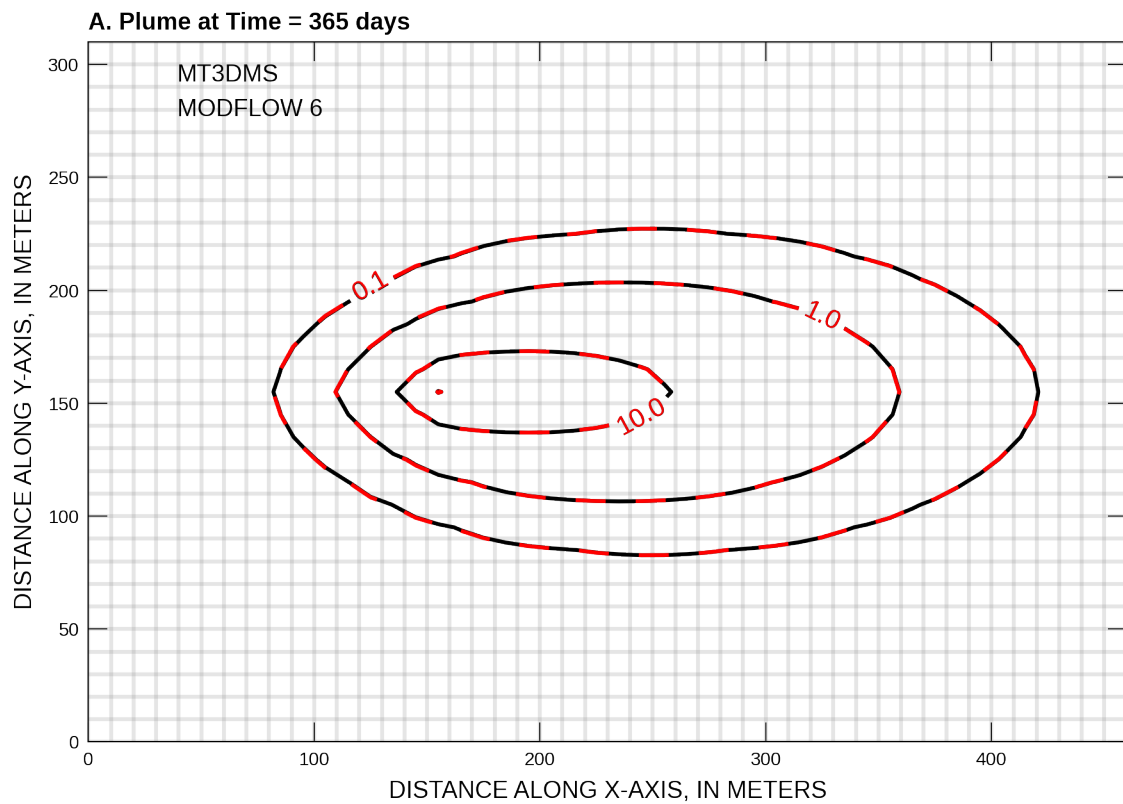


Figure 37–1: Comparison of the MT3DMS and MODFLOW 6 numerical solutions for a two-dimensional advection-dispersion test problem. The analytical solution for this problem was originally given in [Wilson and Miller \(1978\)](#) and is not shown here

## 38 MT3DMS Problem 4

The third demonstrated MT3DMS-MODFLOW 6 transport comparison is for a two-dimensional transport in a diagonal flow field. This problem is similar to the preceding problem with two important changes. First, the flow direction is now oriented at a 45-degree angle relative to rows and columns of the numerical grid. Owing the use of MT3DMS for comparison, the MODFLOW 6 solution uses the traditional DIS package (not DISU or DISV). The second notable change is that the number of rows and columns has been expanded in order to accommodate a longer simulation period of 1,000 days. Because of the orientation of the flow field relative to the model grid, and the sharpness of the migrating concentration front, this test problem presents a challenging set of conditions to simulate. Three scenarios test alternative advection formulations, as summarized in table 38–1

Table 38–1: Scenario parameters for example ex-gwt-mt3dms-p04.

Scenario	Scenario Name	Parameter	Value
1	ex-gwt-mt3dms-p04a	mixelm (unitless)	0
2	ex-gwt-mt3dms-p04b	mixelm (unitless)	-1
3	ex-gwt-mt3dms-p04c	mixelm (unitless)	1

Model parameter values for this problem are provided in table 38–2.

Table 38–2: Model parameters for example ex-gwt-mt3dms-p04.

Parameter	Value
Number of layers	1
Number of rows	100
Number of columns	100
Column width (m)	10.0
Row width (m)	10.0
Layer thickness (m)	1.0
Top of the model (m)	0.0
Porosity	0.14
Simulation time (days)	365
Horizontal hydraulic conductivity (m/d)	1.0
Volumetric injection rate (m <sup>3</sup> /d)	0.01
Concentration of injected water (mg/L)	1000.0
Longitudinal dispersivity (m)	2.0
Ratio of transverse to longitudinal dispersivity	0.1
Molecular diffusion coefficient (m <sup>2</sup> /d)	1.0e-9

The same analytical solution used in the previous problem can be used for this problem after applying the necessary updates to select parameters - most notably the dispersion and porosity terms and that an inter-model comparison is drawn after 1,000 days instead of 365 days. Figure 36 in [Zheng and Wang \(1999\)](#) shows four different solutions for this problem: (1) analytical, (2) Method of Characteristics (MOC), (3) upstream finite difference (FD), and (4) Total Variation Dimishing (TVD) or “ULTIMATE” scheme. Both the MOC and TVD solutions demonstrate a reasonable agreement with the analytical solution. However, the upstream finite difference solution reflects considerably more spread from simulation of too much dispersion - in this case numerical dispersion instead of hydrodynamic dispersion.

The MODFLOW 6 transport solution is compared to all three numerical solutions (FD, TVD, and MOC) presented in [Zheng and Wang \(1999\)](#). The first comparison shows complete agreement

between MT3DMS and the MODFLOW 6 transport solution when the finite difference approach is applied (figure 38–1).

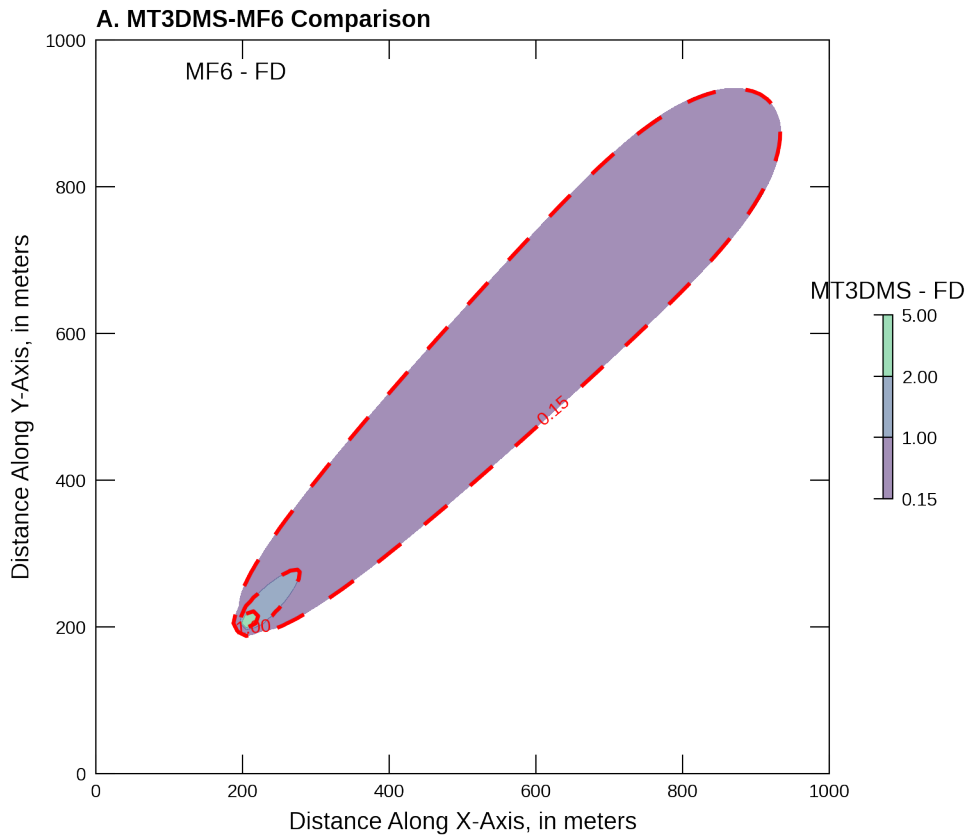


Figure 38–1: Comparison of the MT3DMS and MODFLOW 6 numerical solutions for two-dimensional transport in a diagonal flow field. Both models are using their respective finite difference solutions without the TVD option

Figure 38–2 shows a comparison between the MT3DMS and MODFLOW 6 solution with the respective TVD options for each model activated. Owing to the fact that MT3DMS uses a third-order TVD scheme while MODFLOW 6 uses a second-order scheme, differences between the two solutions are expected.

The third model comparison shows the largest difference between the two solutions (figure 38–3). Because the MOC solution is the closest facsimile of the analytical solution, comparison of MODFLOW 6 with the MT3DMS MOC solution is as close to a comparison with the analytical solution as will be shown for the current set of model runs.

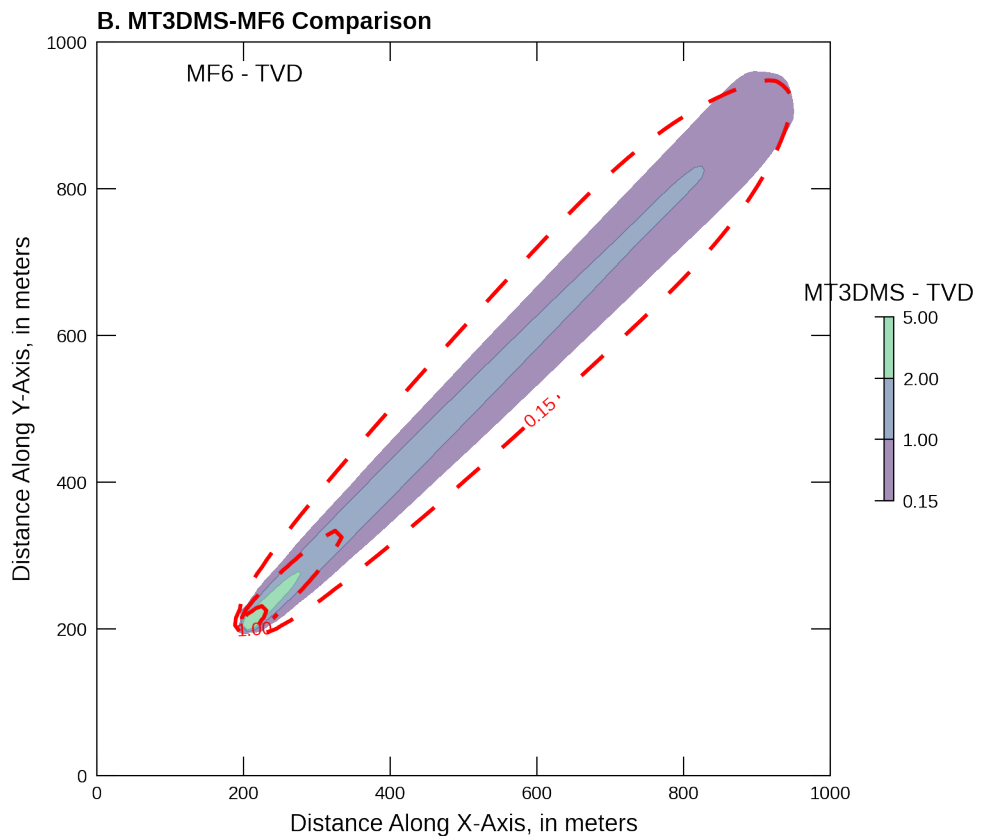


Figure 38–2: Comparison of the MT3DMS and MODFLOW 6 numerical solutions for two-dimensional transport in a diagonal flow field. Both models are using their respective finite difference solutions with the use of the TVD option, which serves as the main difference with results displayed in figure 38–2

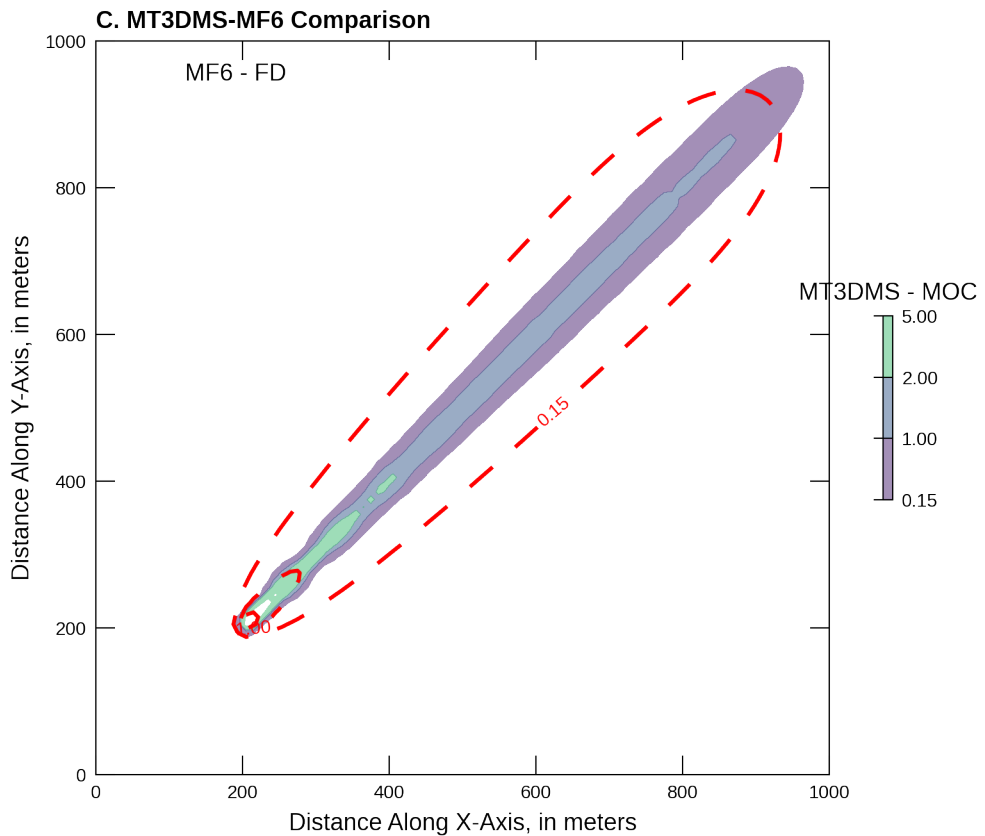


Figure 38–3: Comparison of the MT3DMS and MODFLOW 6 numerical solutions for two-dimensional transport in a diagonal flow field. Here, MT3DMS is using a MOC technique to find a solution while MODFLOW 6 uses finite difference without TVD activated.

## 39 MT3DMS Problem 5

The next example problem tests two-dimensional transport in a radial flow field. The radial flow field is established by injecting water in the center of the model domain (row 16, column 16) and allowing it to flow outward toward the model perimeter. No regional groundwater flow gradient exists as in some of the previous comparisons with MT3DMS. Constant head cells located around the perimeter of the model drain water and solute from the simulation domain. Solute enters the model domain through the injection well with a unit concentration. The starting concentration is zero across the entire domain. Flow remains steady and confined throughout the 27 day simulation period. The aquifer is homogenous, isotropic, and boundaries are sufficiently far from the injection well to avoid solute reaching the boundary during the simulation interval. Table 39–1 summarizes many of the model inputs:

Table 39–1: Model parameters for example ex-gwt-mt3dms-p05.

Parameter	Value
Number of layers	1
Number of rows	31
Number of columns	31
Column width (m)	10.0
Row width (m)	10.0
Layer thickness (m)	1.0
Top of the model (m)	0.0
Porosity	0.3
Simulation time (days)	27
Horizontal hydraulic conductivity (m/d)	1.0
Volumetric injection rate (m <sup>3</sup> /d)	100.0
Concentration of injected water (mg/L)	1.0
Longitudinal dispersivity (m)	10.0
Ratio of transverse to longitudinal dispersivity	1.0
Molecular diffusion coefficient (m <sup>2</sup> /d)	1.0e-9

An analytical solution for this problem was originally given in [Moench and Ogata \(1981\)](#). The MT3DMS solution with the TVD option activated most closely matched the analytical solution. Therefore the TVD option is activated in both MT3DMS and MODFLOW 6 for verifying the transport solution. Figure 39–1 shows a slight under simulation of the outward spread of solute in the MODFLOW 6 solution compared to MT3DMS. Figure 39–2 shows close agreement among the MT3DMS and MODFLOW 6 isoconcentration contours with the TVD advection scheme activated.

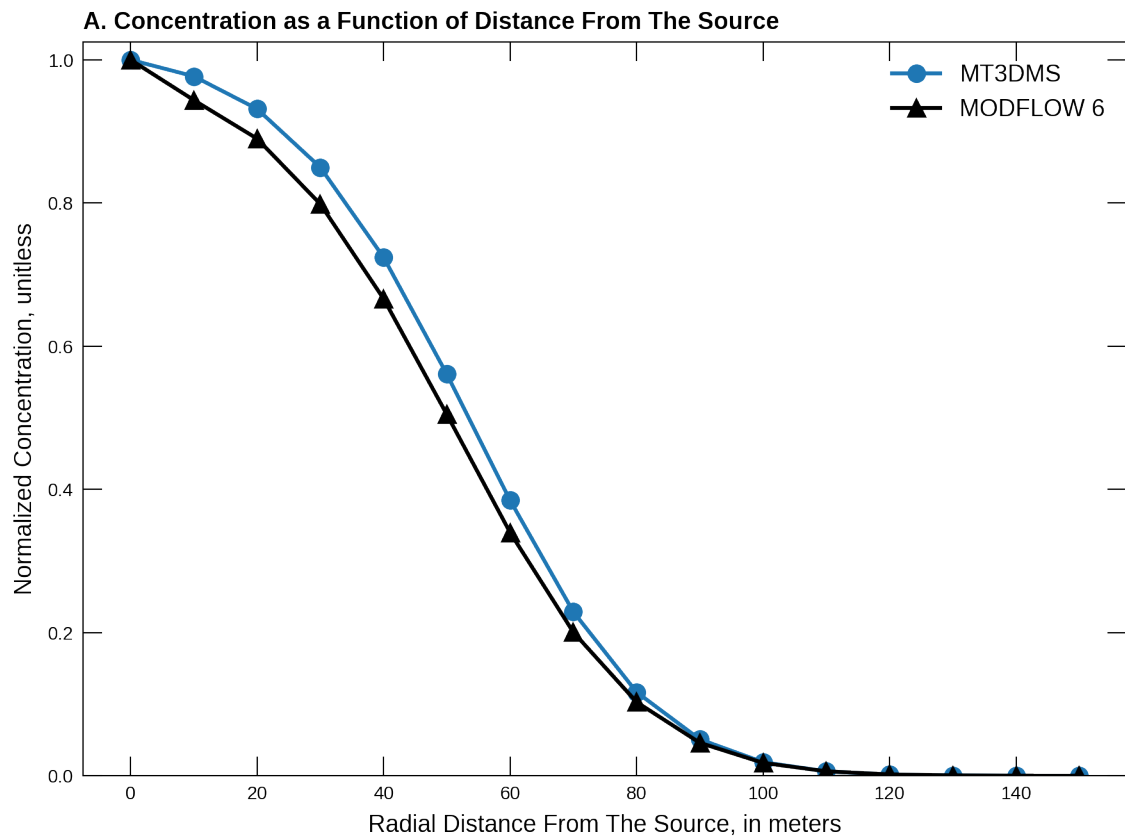


Figure 39–1: Comparison of the MT3DMS and MODFLOW 6 numerical solutions for a point source in a two-dimensional radial flow field simulation. The thick black line in figure 39–2 shows the location of this profile view of concentrations. The analytical solution for this problem was originally given in ([Moench and Ogata, 1981](#)) and is not shown here

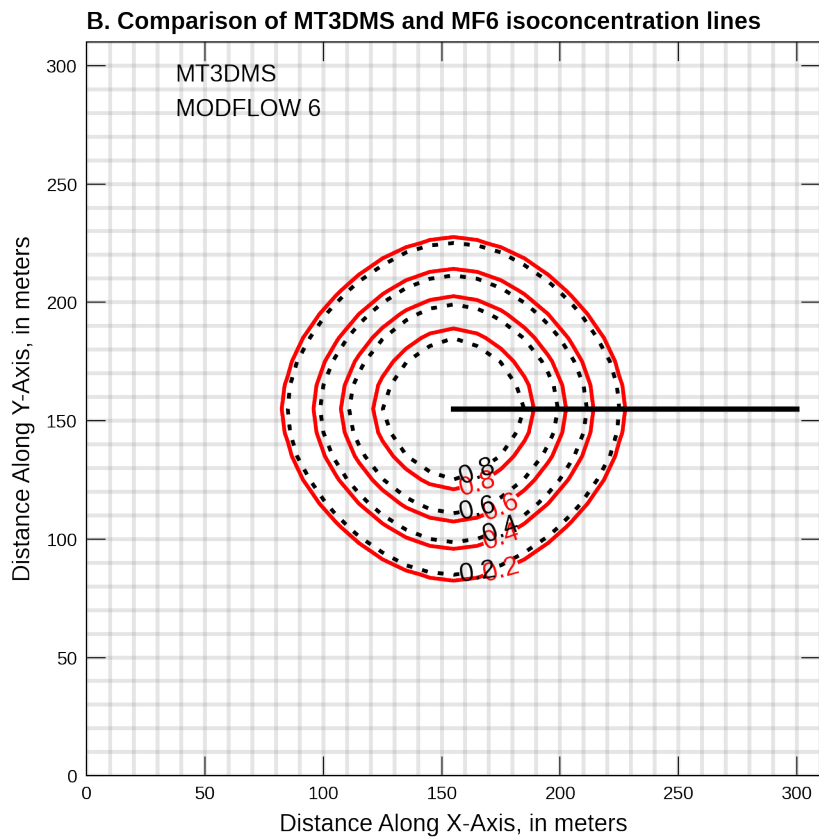


Figure 39–2: Comparison of the MT3DMS and MODFLOW 6 numerical solutions for two-dimensional transport in a radial flow field. The thick black line shows the location of the concentration profile shown in figure 39–1. Both models are using their respective finite difference solutions with the use of the TVD option.

## 40 MT3DMS Problem 6

In this example problem, concentrations are compared between MODFLOW 6 and MT3D-USGS at an injection/extraction well. The well is fully penetrating in a confined aquifer and injects contaminated water for a period of 2.5 years at a rate of  $1 \text{ ft}^3/\text{sec}$ . At the end of 2.5 years, the injection well is reversed and begins pumping (extracting) contaminated groundwater for a period of 7.5 years, also at the rate of  $1 \text{ ft}^3/\text{sec}$ . [El-Kadi \(1988\)](#) was the first to develop the test problem which was later used by [Zheng \(1993\)](#) to test ongoing method-of-characteristics (MOC) developments. The model boundary is placed far enough away from the injection/extraction well to ensure no solute exits the model domain during the injection period. Moreover, steady flow conditions are reached immediately during the injection and extraction stress periods. Problem specifics are provided in table 40–1.

Table 40–1: Model parameters for example ex-gwt-mt3dms-p06.

Parameter	Value
Number of layers	1
Number of rows	31
Number of columns	31
Column width ( $\text{ft}$ )	900.0
Row width ( $\text{ft}$ )	900.0
Layer thickness ( $\text{ft}$ )	20.0
Top of the model ( $\text{ft}$ )	0.0
Porosity	0.35
Length of the injection period ( $\text{years}$ )	2.5
Length of the extraction period ( $\text{years}$ )	7.5
Horizontal hydraulic conductivity ( $\text{ft}/\text{d}$ )	432.0
Volumetric injection rate ( $\text{ft}^3/\text{d}$ )	1.0
Relative concentration of injected water (%)	100.0
Longitudinal dispersivity ( $\text{ft}$ )	100.0
Ratio of transverse to longitudinal dispersivity	1.0

An analytical solution for this problem was originally given in [Gelhar and Collins \(1971\)](#). Because this is an advection dominated problem, both numerical solutions invoke their TVD schemes. The MODFLOW 6 solution shows a quicker rise in concentration at the well site than does the MT3D-USGS solution (figure 40–1).

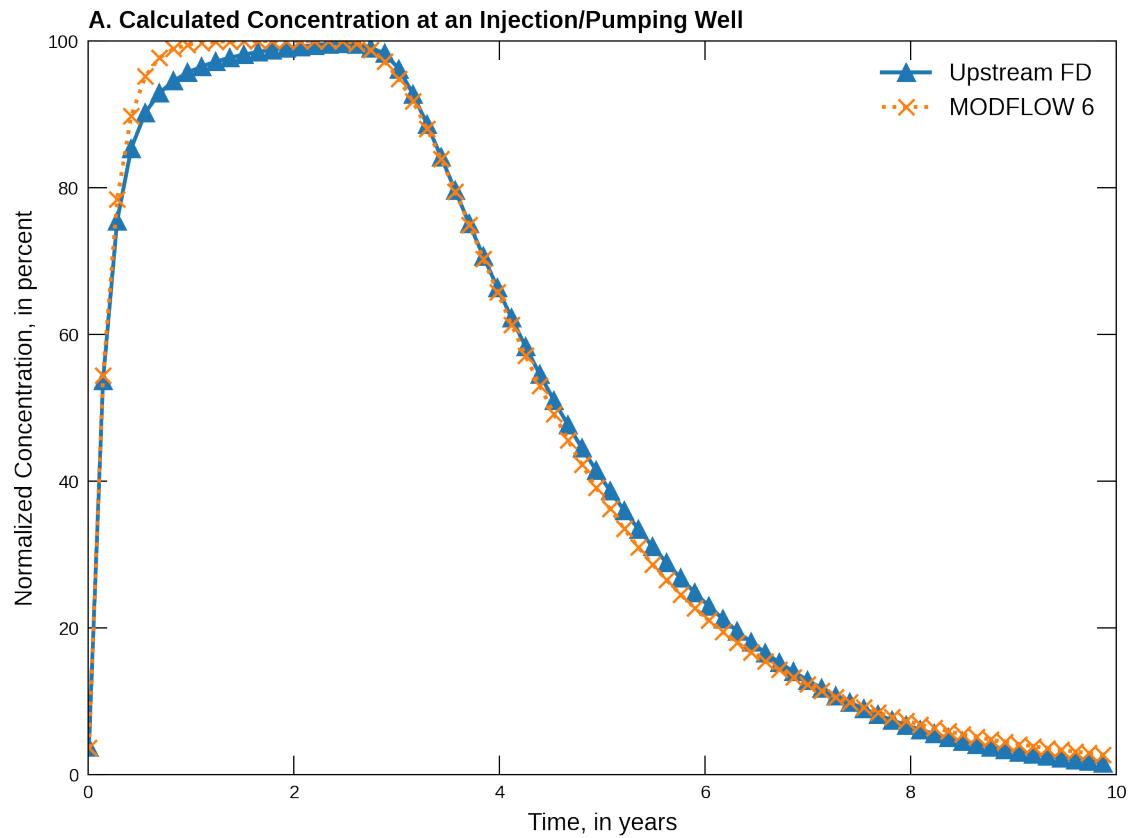


Figure 40–1: Comparison of the MT3D-USGS and MODFLOW 6 numerical solutions at an injection/extraction well. The analytical solution for this problem was originally given in ([Gelhar and Collins, 1971](#)) and is not shown here

## 41 MT3DMS Problem 7

In a previous problem titled “two-dimensional transport in a uniform flow field” concentrations were compared between MODFLOW 6 and MT3D-USGS for a relatively thin aquifer (10 m) wherein instantaneous vertical mixing was assumed. In order to test transport simulation in a thicker aquifer, where all three spatial dimensions are required to adequately simulate the movement of solute, the current problem was devised. Hunt (1978) provides an analytical solution, which is used to verify MT3DMS in Zheng and Wang (1999), but not shown here. Instead, only the MODFLOW 6 and MT3DMS solutions are compared here.

Problem dimensions and aquifer properties are given in table 41–1. The point source is located in layer 7, row 8, and column 3

Table 41–1: Model parameters for example ex-gwt-mt3dms-p07.

Parameter	Value
Number of layers	8
Number of rows	15
Number of columns	21
Column width (m)	10.0
Row width (m)	10.0
Layer thickness (m)	10.0
Top of the model (m)	0.0
Porosity	0.2
Horizontal hydraulic conductivity (m/d)	0.5
Volumetric injection rate (m <sup>3</sup> /d)	0.5
Longitudinal dispersivity (m)	10.0
Ratio of transverse to longitudinal dispersivity	0.3
Ratio of vertical to longitudinal dispersivity	0.3
Simulation time (days)	100.0

An analytical solution for this problem was originally given in Hunt (1978). Both numerical solutions invoke their respective TVD schemes. Moreover, MODFLOW 6 is using the XT3D package for simulating dispersion. The MODFLOW 6 solution shows great agreement with the MT3DMS calculated concentrations for the three layers displayed in figure 40–1.

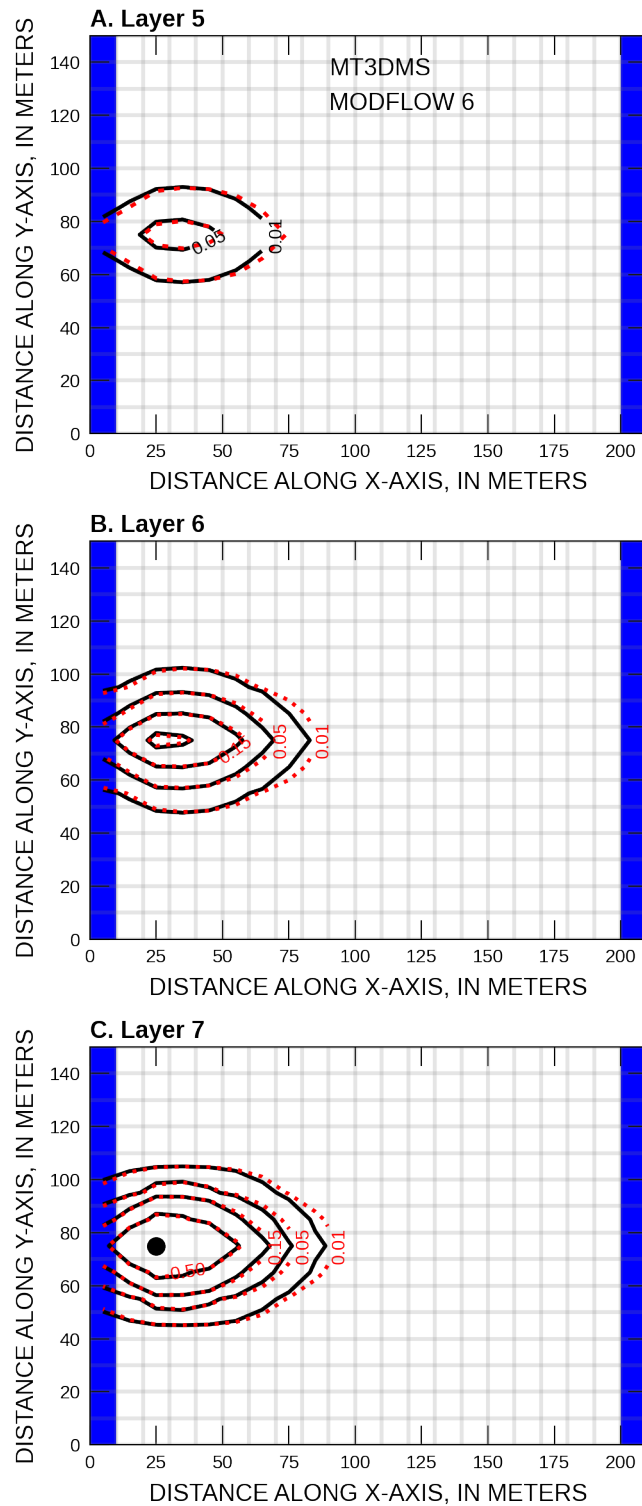


Figure 41–1: Comparison of the MT3D-USGS and MODFLOW 6 numerical solutions for three-dimensional transport in a uniform flow field. The analytical solution for this problem was originally given in ([Hunt, 1978](#)) and is not shown here

## 42 MT3DMS Problem 8

This example problem originally appeared [Sudicky \(1989\)](#) for finding the solution in a hypothetical field-scale example. Among the MT3DMS suite of examples, this is the first one with a heterogeneous hydraulic conductivity field. Defining characteristics that set this problem apart from earlier MT3DMS example problems include a highly irregular flow field and large contrast between longitudinal and transverse dispersivities. [Van der Heijde \(1995\)](#) points out that this particular model test potentially troublesome parameter combinations while at the same time testing the ability of a flow and transport code to simulate real-world problems.

### 42.1 Example description

Using a “deformed quadrilateral” ([Zheng and Wang, 1999](#)), the model domain is 250 m wide by 6.75 m at the left boundary and 5.375 m at the right boundary. The conceptual model is divided into 27 layers and 50 columns all contained within a single row. For the duration of the simulation, steady flow is maintained by a constant recharge rate of 10 cm/yr, no-flow on the left and bottom boundaries and a constant head of 5.375 m on the right boundary (figure 42–1). The simulation uses unconfined conditions to model the water table. Heterogeneity within the aquifer is represented by a fine grained silty sand with a hydraulic conductivity of  $5 \times 10^{-4}$  cm/sec that hosts two lenses of medium-grained sand with a hydraulic conductivity of  $1 \times 10^{-2}$  cm/sec (table 42–1). The vertical hydraulic conductivity is assumed to equal the horizontal conductivity in both materials.

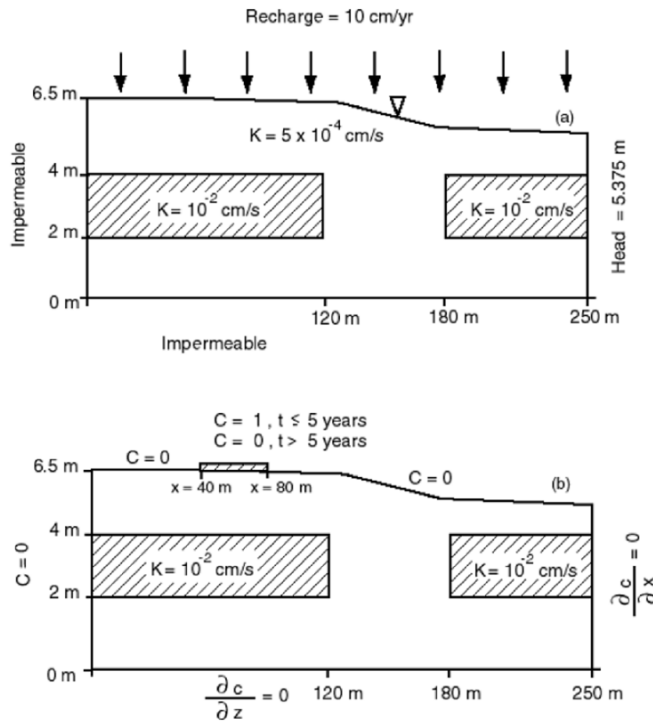


Figure 42–1: MT3DMS test problem 8 configuration showing flow (upper figure) and transport (lower figure) boundary conditions (from [Sudicky \(1989\)](#)).

Table 42–1: Model parameters for example ex-gwt-mt3dms-p08.

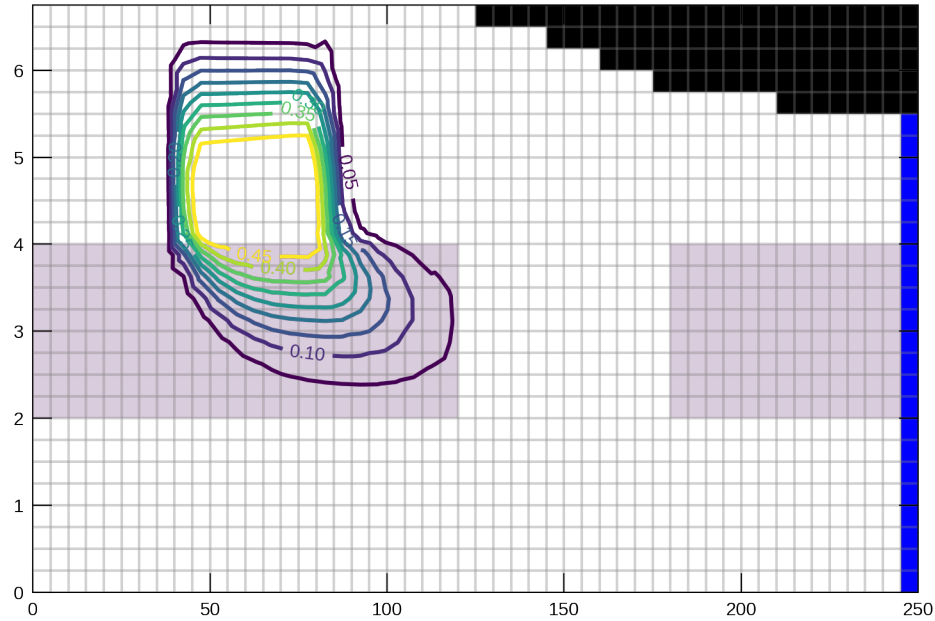
Parameter	Value
Number of layers	27
Number of rows	1
Number of columns	50
Column width ( $m$ )	5.0
Row width ( $m$ )	1.0
Layer thickness ( $m$ )	0.25
Top of the model ( $m$ )	6.75
Porosity	0.35
Horiz. hyd. conductivity of fine grain material ( $cm/sec$ )	5.0e-4
Horiz. hyd. conductivity of medium grain material ( $cm/sec$ )	1.0e-2
Applied recharge rate ( $cm/yr$ )	10.0
Longitudinal dispersivity ( $m$ )	0.5
Transverse vertical dispersivity ( $m$ )	0.005
Effective diffusion coefficient ( $cm^2/sec$ )	1.34e-5
Simulation time ( $years$ )	20.0

Boundary conditions within the transport model also are shown in figure 42–1. A relative concentration of 1.0 is assigned to the recahrge entering the model domain between 40 and 80  $m$  from the left boundary and 0.0 elsewhere. Mass continues to enter the simulation at the given location for the first five years of the simulation, after which time the source is removed and the model continues to run for an additional 15 years. An initial concentration of 0.0 is specified throughout the model domain. A uniform porosity of 0.35 is assigned to the entire model domain. Additional transport-related parameters are listed in table 42–1.

## 42.2 Example results

In order to achieve a close match between MODFLOW 6 and MT3D-USGS, the XT3D solver was activated within MODFLOW 6. Moreover, both solutions use their respective TVD advection schemes. Results are shown after 8, 12, and 20 years (figures 42–2 - 42–4). In each of the selected years for which results are plotted, model results are similar with a couple of small differences. For example, all plots show the leading edge (as defined by the 0.05 isoconcentration contour) of the MT3DMS-calculated plume ahead of the leading the edge of the MODFLOW 6 plume. Also, the MODFLOW 6 plume is less dispersed compared to the MT3DMS plumes as demonstrated by the presence of higher concentrations (i.e., isoconcentration contours) located at the center of the plume, particularly in years 12 and 20.

A. Migrating plume after 8 years, MT3D-USGS



B. Migrating plume after 8 years, MODFLOW 6

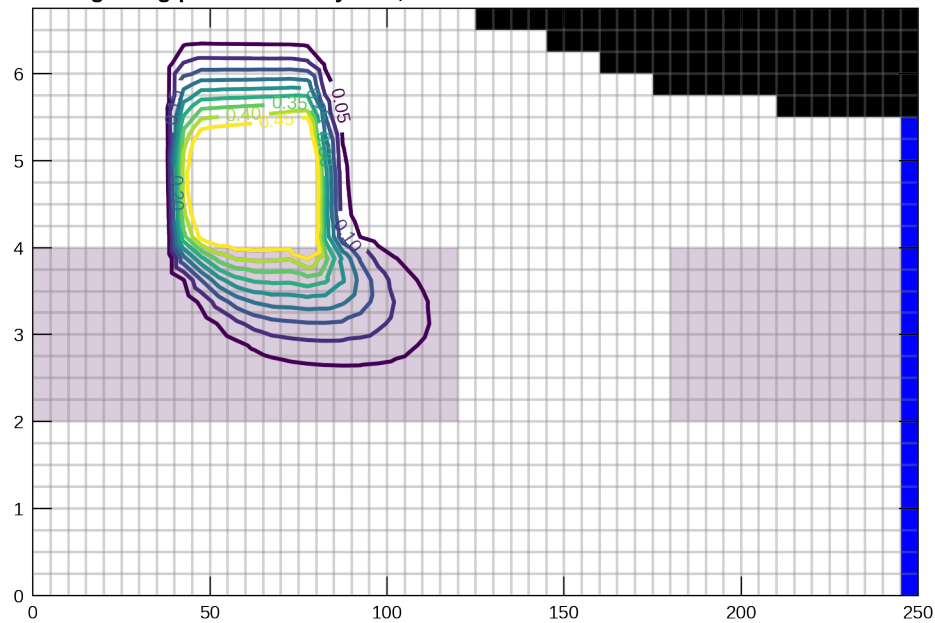
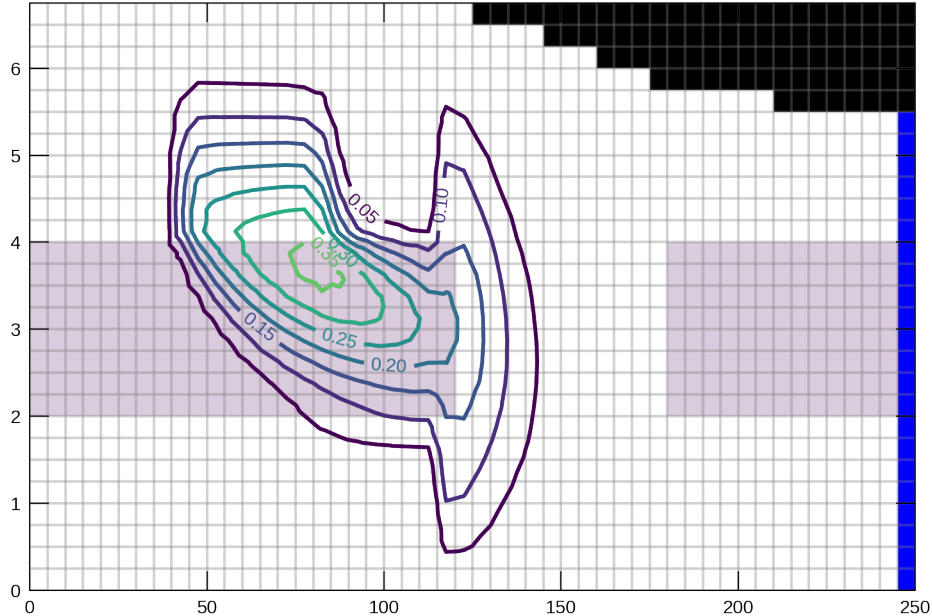


Figure 42–2: Migrating contaminant plume as calculated by (A) MT3D-USGS and (B) MODFLOW 6 after 8 years. The original problem was given in ([Sudicky, 1989](#))

C. Migrating plume after 12 years, MT3D-USGS



D. Migrating plume after 12 years, MODFLOW 6

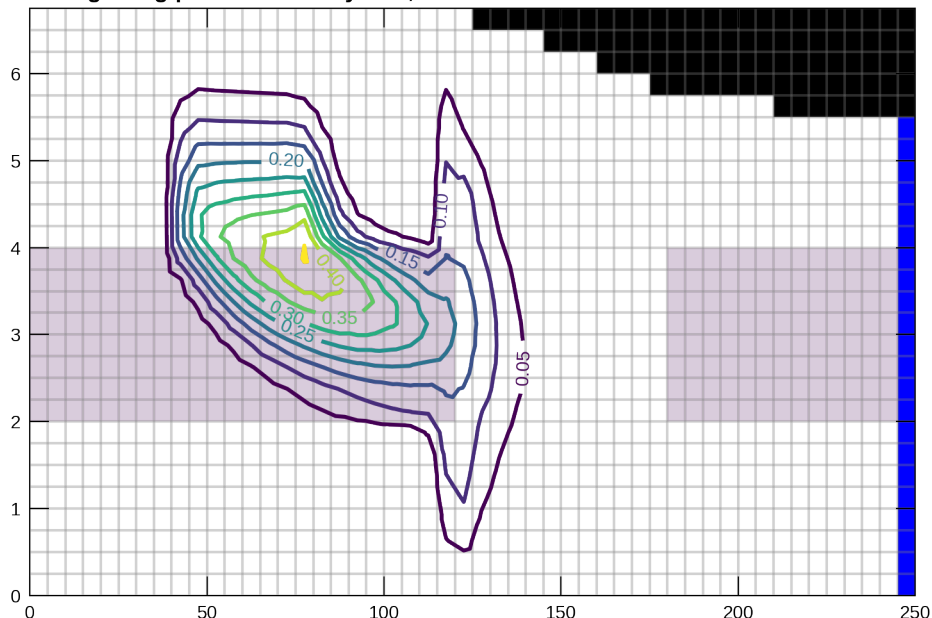
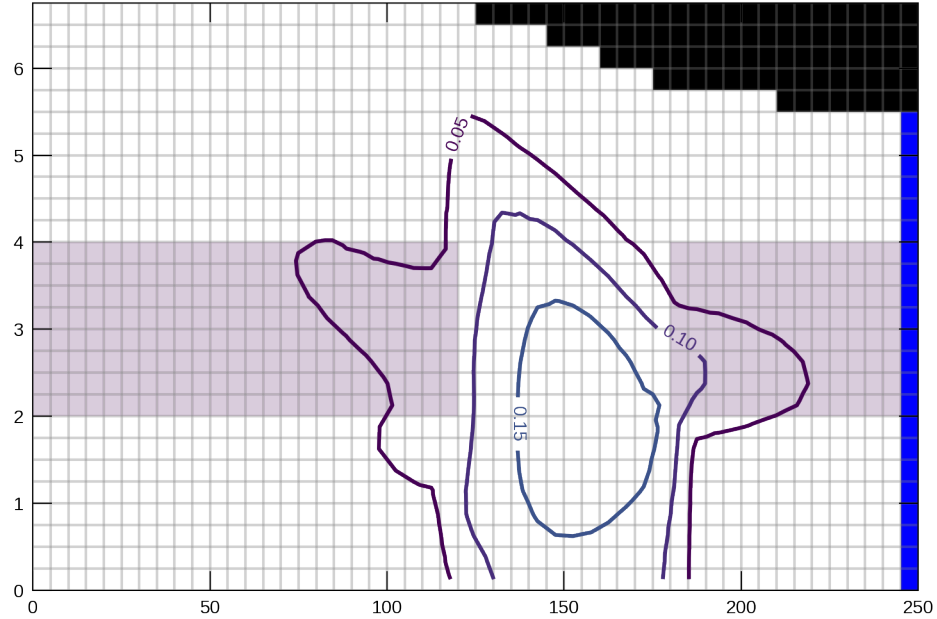


Figure 42-3: Migrating contaminant plume as calculated by (A) MT3D-USGS and (B) MODFLOW 6 after 12 years. The original problem was given in ([Sudicky, 1989](#))

E. Migrating plume after 20 years, MT3D-USGS



F. Migrating plume after 20 years, MODFLOW 6

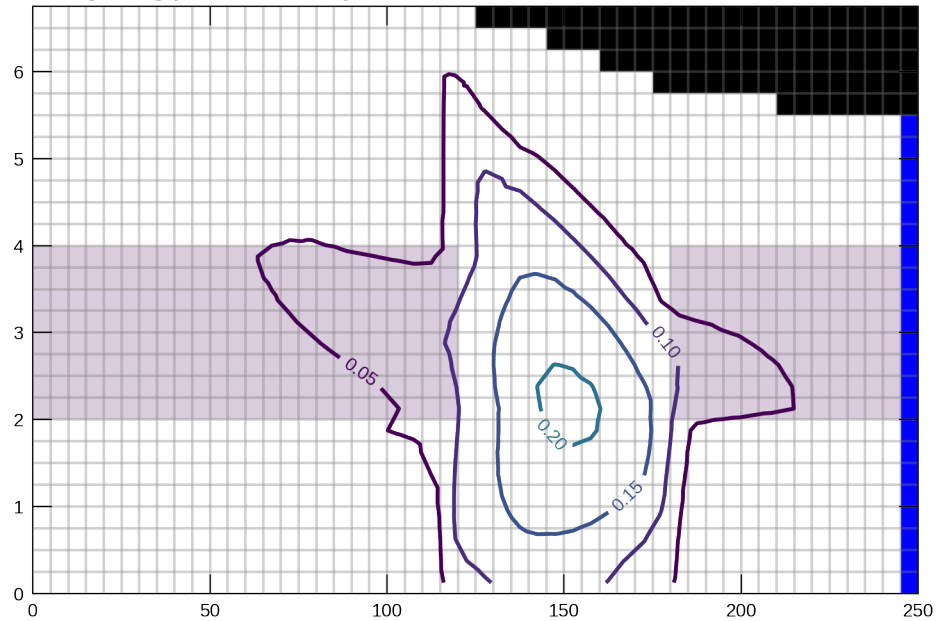


Figure 42–4: Migrating contaminant plume as calculated by (A) MT3D-USGS and (B) MODFLOW 6 after 20 years. The original problem was given in ([Sudicky, 1989](#))

## 43 MT3DMS Problem 9

This example compares MODFLOW 6 and MT3DMS transport solutions in a two-dimensional plan-view setting with heterogeneity in the hydraulic conductivity field. The problem is purely hypothetical and was originally used for comparing different MT3DMS solutions (i.e., finite-difference, method-of-characteristics, and TVD advection schemes) to each other. No analytical solution exists for this problem ([Zheng and Wang, 1999](#)).

### 43.1 Example description

A contaminant plume originates in an injection well located near the upper portion of the model (figure 43–1). After its injection, contaminant migrates toward a pumping well located several rows below a low hydraulic conductivity zone, itself located a couple rows below where contaminant enters the aquifer.

The model domain is discretized by 18 rows, 14 columns, and a single confined layer. Grid cell dimensions are uniformly set to  $100 \times 100\text{ m}$ . The left, right and bottom model boundaries are no-flow. The upper (north) boundary applies a specified head of  $250\text{ m}$  that is held constant throughout the simulation period. Similarly, a specified head is applied to the lower (south) boundary that varies from  $20\text{ m}$  on the left to  $52.5\text{ m}$  on the right, a gradient of  $2.5/100\text{ m/m}$ . Water injected into the aquifer enters at a concentration of  $57.87\text{ ppm}$ . Mass is removed from the aquifer by both the pumping well and with the flow that exits the domain at the lower (south) boundary of the model. Mass that exits the lower boundary does so at the simulated concentration of the water that is removed by the constant head boundary condition. Mass is not allowed to leave through the upper, bottom, left, or right boundaries in the respective transport simulations. All flow boundary conditions are held constant for the duration of the simulation period, resulting in steady-flow conditions. However, the concentration of the injected water is reduced to  $0.0\text{ ppm}$  during the second of two stress periods. Both the injection and pumping wells are assumed to be fully penetrating. Aquifer heterogeneity is depicted in figure 43–1. Model parameters are summarized in table 43–1.

Table 43–1: Model parameters for example ex-gwt-mt3dms-p09.

Parameter	Value
Number of layers	1
Number of rows	18
Number of columns	14
Column width (m)	100.0
Row width (m)	100.0
Layer thickness (m)	10.0
Top of the model (m)	0.0
Porosity	0.3
Horiz. hyd. conductivity of fine grain material (m/sec)	1.474e-4
Horiz. hyd. conductivity of medium grain material (m/sec)	1.474e-7
Injection well rate (m <sup>3</sup> /sec)	0.001
Extraction well pumping rate (m <sup>3</sup> /sec)	-0.0189
Longitudinal dispersivity (m)	20.0
Ratio of horiz. transverse to longitudinal dispersivity (m)	0.2
Simulation time (years)	2.0

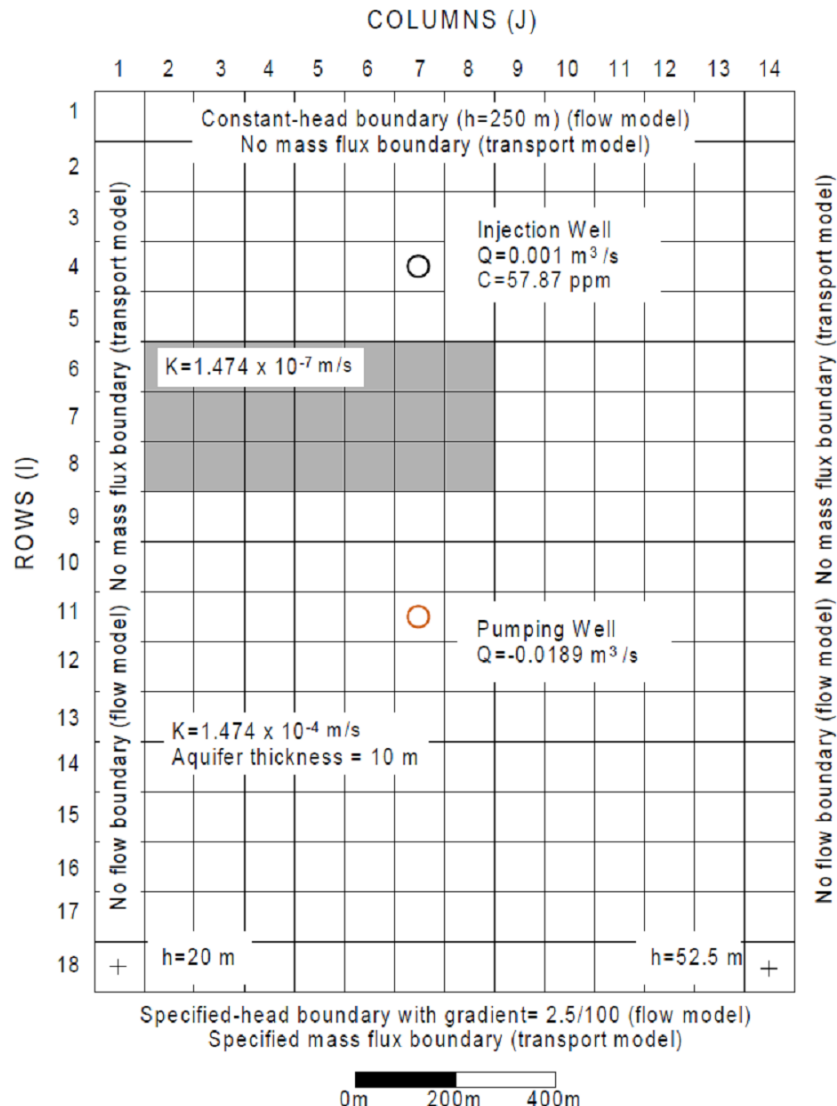


Figure 43–1: MT3DMS test problem 9 configuration showing grid discretization, constant head boundaries, and the locations of injection and pumping wells (from [Zheng and Wang \(1999\)](#)).

In MODFLOW 6, the XT3D solver is not activated; however, both MODFLOW 6 and MT3DMS use their respective TVD advection schemes.

## 43.2 Example results

Contrasting model results after one year, the leading edge of the plume advanced further within the MODFLOW 6 solution (figures 43–2). Confirmation that the same amount of mass entered both simulations (MODFLOW 6 and MT3DMS) was achieved by checking the mass budget information in the respective mode output listing files. In both simulations, the effect of the aquitard aquitard is clearly seen, though the isoconcentration lines appear to have infiltrated the aquitard more with MT3DMS compared to the MODFLOW 6 solution.

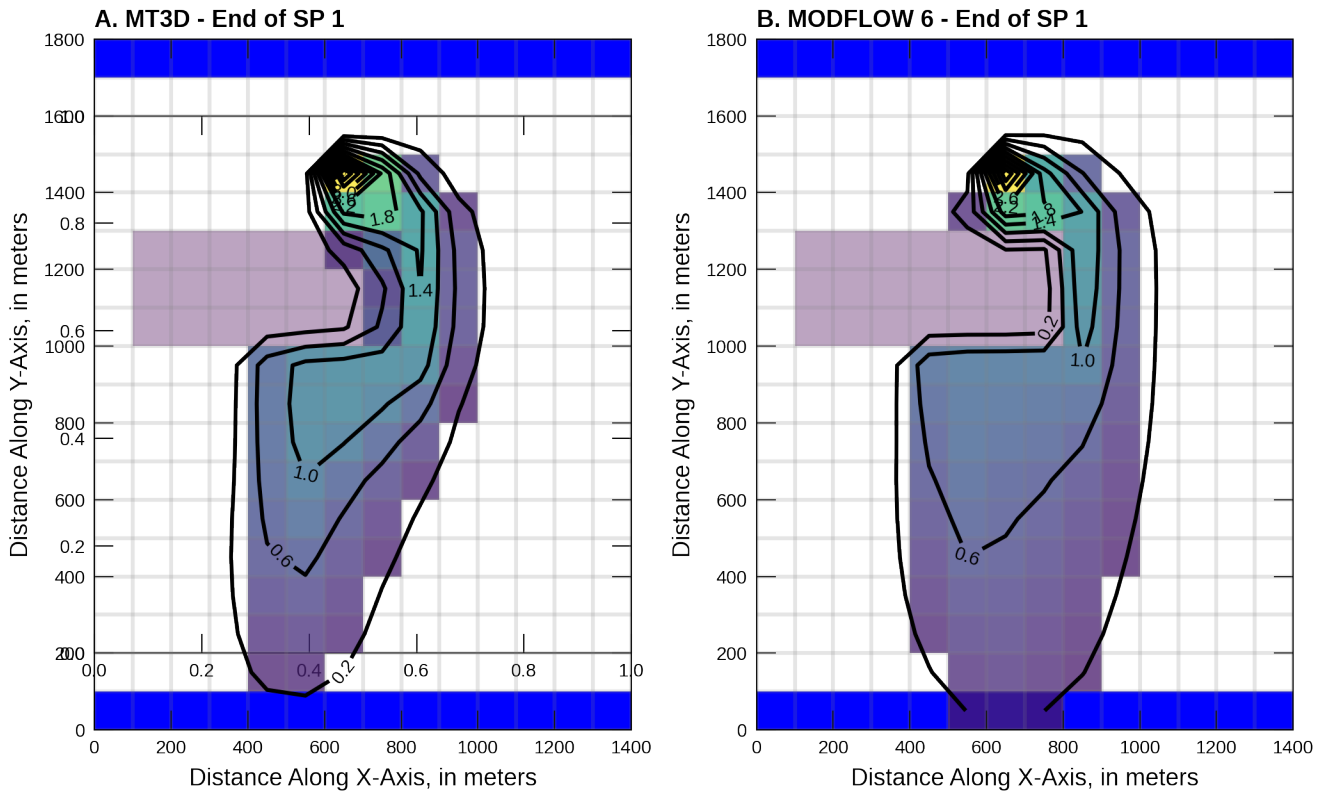


Figure 43–2: Migrating contaminant plume as calculated by (A) MT3D-USGS and (B) MODFLOW 6 after one year of simulation time. The original problem was given in ([Zheng and Wang, 1999](#)). Cells shaded in blue show the location of constant head boundary cells. Light brown shaded cells show the location of the aquitard.

## 44 MT3DMS Problem 10

This example problem describes an actual field problem ([Zheng and Wang, 1999](#)). While the original discussion of this problem compared various MT3MDS solution schemes and evaluated the effectiveness of MT3DMS for solving real-world problems, the current goal is much more modest: to compare the MODFLOW 6 transport solution against the MT3DMS solution.

### 44.1 Example description

The geological setting for this final problem from [Zheng and Wang \(1999\)](#) is roughly shown in figure 44–1. An unconfined aquifer beneath a spill site is approximately divided into an upper and lower zone with hydraulic conductivities of 60 and 520  $ft/day$ , respectively. Each zone is represented by two 25  $ft$  uniformly thick layers, for a total of 4 layers. Each layer is comprised of 61 rows and 40 columns with variable row and column widths. The highest level of grid refinement exists near the detailed study site containing the bulk of the contaminant plume. In this area, row and column widths are  $50 \times 50 ft$  (area denoted by ABCD in figure 44–1). Outside this area, cell lengths and widths progressively increase toward the model boundary. A no-flow no-flux boundary conditions is applied to the bottom boundary while specified head boundaries are used on all four sides. Heads along the sides of the model domain establish a regional flow gradient of  $5 \times 10^{-4}$  from east to west and  $1 \times 10^{-3}$  from north to south. Mass may leave the model domain with the regional flow gradient, but does so at the computed concentration of the groundwater. Water that enters the model domain via the regional flow gradient does so with a concentration of 0.0. However, model boundaries are intentionally set far enough away from the area of concern so that their effect on the flow and transport simulation is minimized. A constant recharge rate of 5  $in/yr$  is applied to the surface of the model. A uniform porosity of 0.30 is applied to the entire model. Owing to the presence of organic contaminants within the groundwater, including 1,2-dichloroethane (1,2-DCA), chemical reactions are simulated using an equilibrium-controlled linear sorption isotherm. Reactive parameters are specified such that the retardation term equals 2. The initial concentration of 1,2-DCA for layer 1 is shown in figure 44–2A. The initial concentration of 1,2-DCA in layer 2 is 20 percent of the layer 1 initial concentration. Layers 3 and 4 start out with no contaminant. The location of extraction wells are given by the black squares in figure 44–2. The extraction wells are used to pump-and-treat contaminated groundwater. The total specified extraction rate among all wells is  $4.25 \times 10^3 m^3/day$  which occurs from layer 3. The Additional model parameter values are listed in table 44–1.

Table 44–1: Model parameters for example ex-gwt-mt3dms-p10.

Parameter	Value
Number of layers	4
Number of rows	61
Number of columns	40
Column width ( $ft$ )	varies
Row width ( $ft$ )	varies
Layer thickness ( $ft$ )	25.0
Top of the model ( $ft$ )	780.0
Saturated thickness ( $ft$ )	100.0
Horiz. hyd. conductivity of layers 1 and 2 ( $ft/day$ )	60.0
Horiz. hyd. conductivity of layers 3 and 4 ( $ft/day$ )	520.0
Ratio of vertical to horizontal hydraulic conductivity	0.1
Recharge rate ( $in/yr$ )	5.0
Concentration of recharge ( $ppm$ )	0.0

Table 44–1: Model parameters for example ex-gwt-mt3dms-p10.

Parameter	Value
Porosity	0.3
Longitudinal dispersivity ( $ft$ )	10.0
Ratio of horizontal transverse dispersivity to longitudinal dispersivity	0.2
Ratio of vertical transverse dispersivity to longitudinal dispersivity	0.2
Aquifer bulk density ( $g/cm^3$ )	1.7
Distribution coefficient ( $cm^3/g$ )	0.176
Simulation time ( $days$ )	1000.0

## 44.2 Example results

The calculated concentration fields are shown for layer 3 at 500, 750, and 1,000 days in figures 44–1B-D, respectively. Both models use their finite-difference solutions and therefore do not invoke their respective TVD scheme. Relatively good agreement between the two simulations is achieved in the lower (southerly) portion of the model for all 3 simulation times displayed. In the upper (northerly) portion of the model, however, several cells separate the isoconcentration contours.

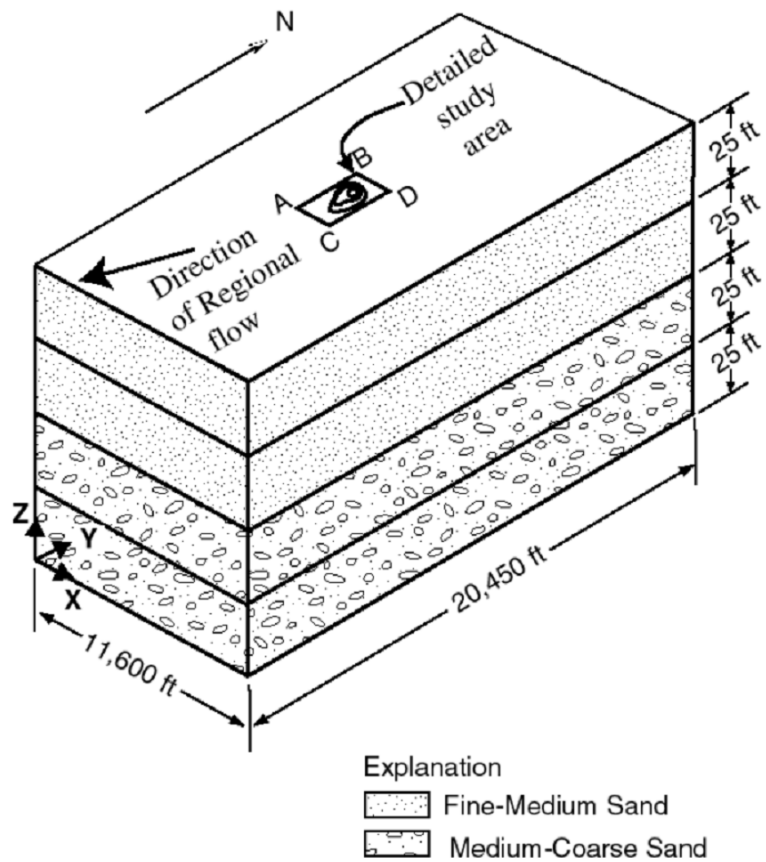


Figure 44–1: MT3DMS test problem 10 showing the numerical model configuration. Image not to scale. (11,600 ft = 3,535.68 m; 20,450 ft = 6,233 m; 25 ft = 7.62 m)

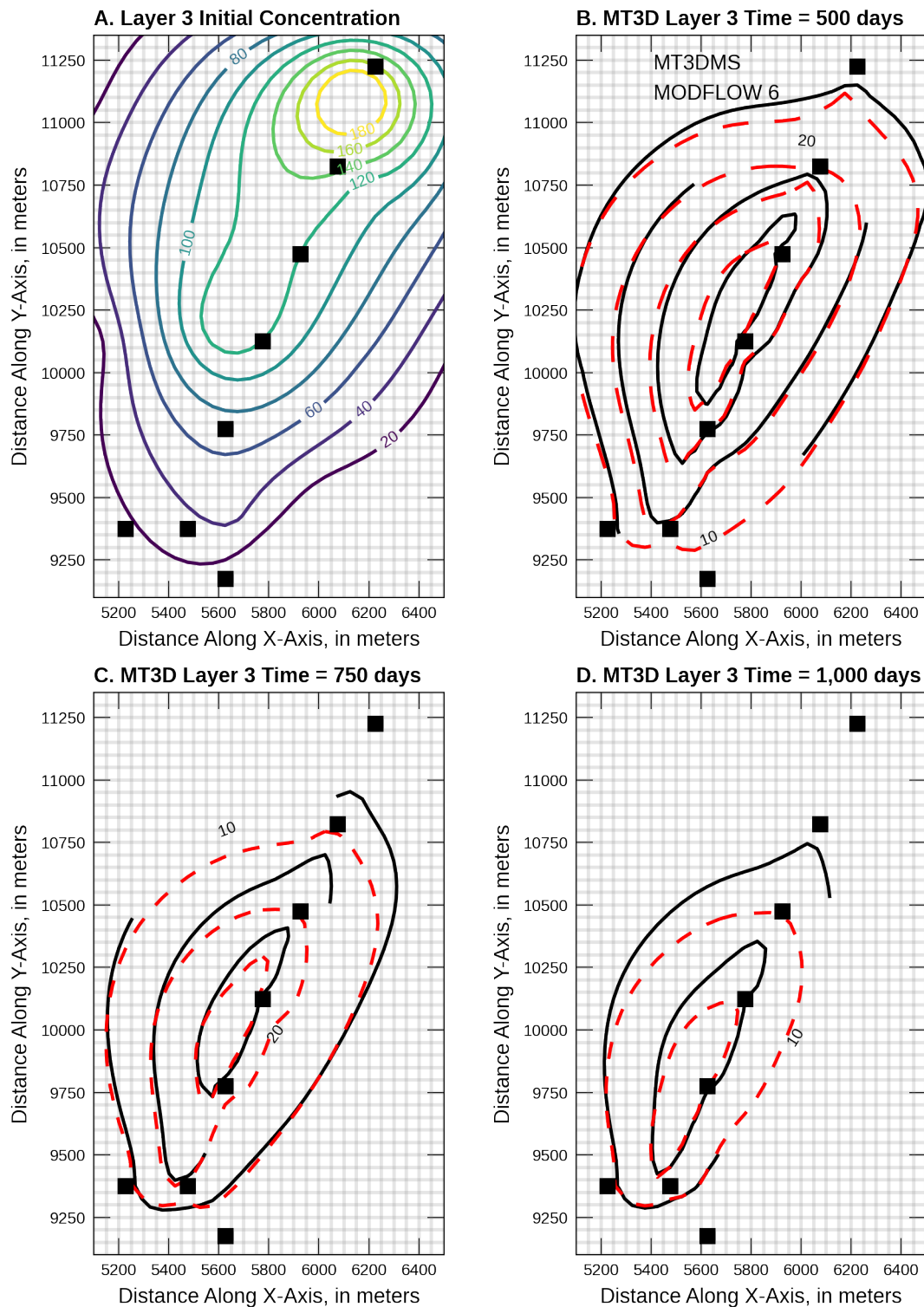


Figure 44–2: (A) Initial and simulated contaminant plume concentrations as calculated by MT3DMS and MODFLOW 6 after (B) 500 days, (C) 750 days, and (D) 1,000 days.

## 45 MT3DMS Problem 10, Two Domains

This example is based on problem 10 from the MT3DMS manual ([Zheng and Wang, 1999](#)). The goal in this example is not to compare the final results to the MT3DMS data presented there, but to show how to create an equivalent setup of that problem using a multi-model approach with the GWF-GWF and GWT-GWT Model Exchanges. To validate its outcome, we can compare the simulated concentration in the study area to the MODFLOW 6 results from the original example.

### 45.1 Example description

The simulated processes and configuration data for this example are identical to those in MODFLOW 6 MT3DMS problem 10 elsewhere in these examples. However, for this example the study site has been modeled as a separate GWF model and a coupled GWT model, embedded in a coarser, surrounding system. Figure 45-4 shows the decomposition of the original grid for the current multi-model approach. By design, this alternative model setup should yield equivalent results.

### 45.2 Example Results

(Explain how the figures prove that the results are identical within the solver's tolerance)

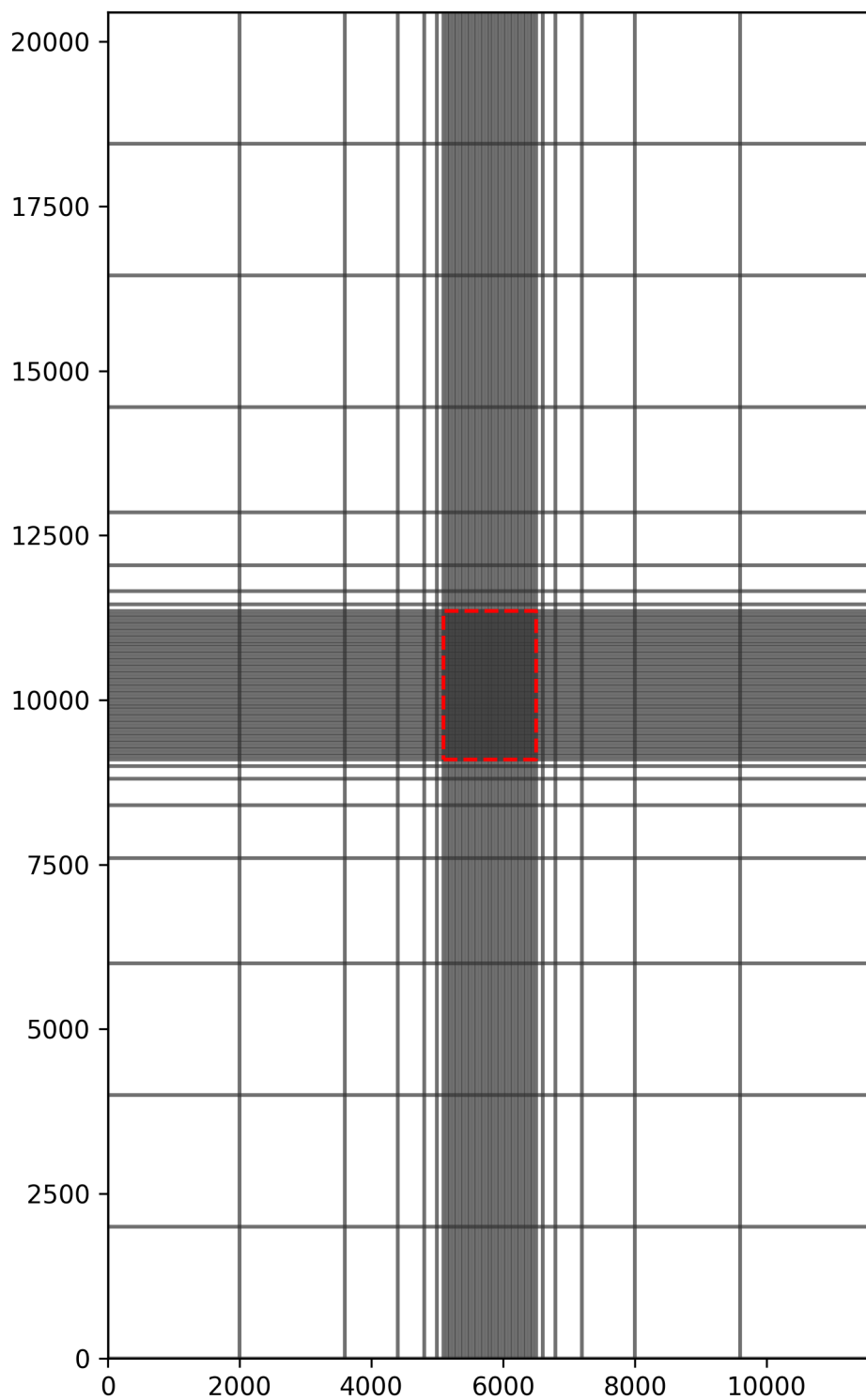


Figure 45–1: The model grid for the studied problem. The red dashed rectangle shows where the GWF and GWT Model Exchange connects the inner to the outer models.

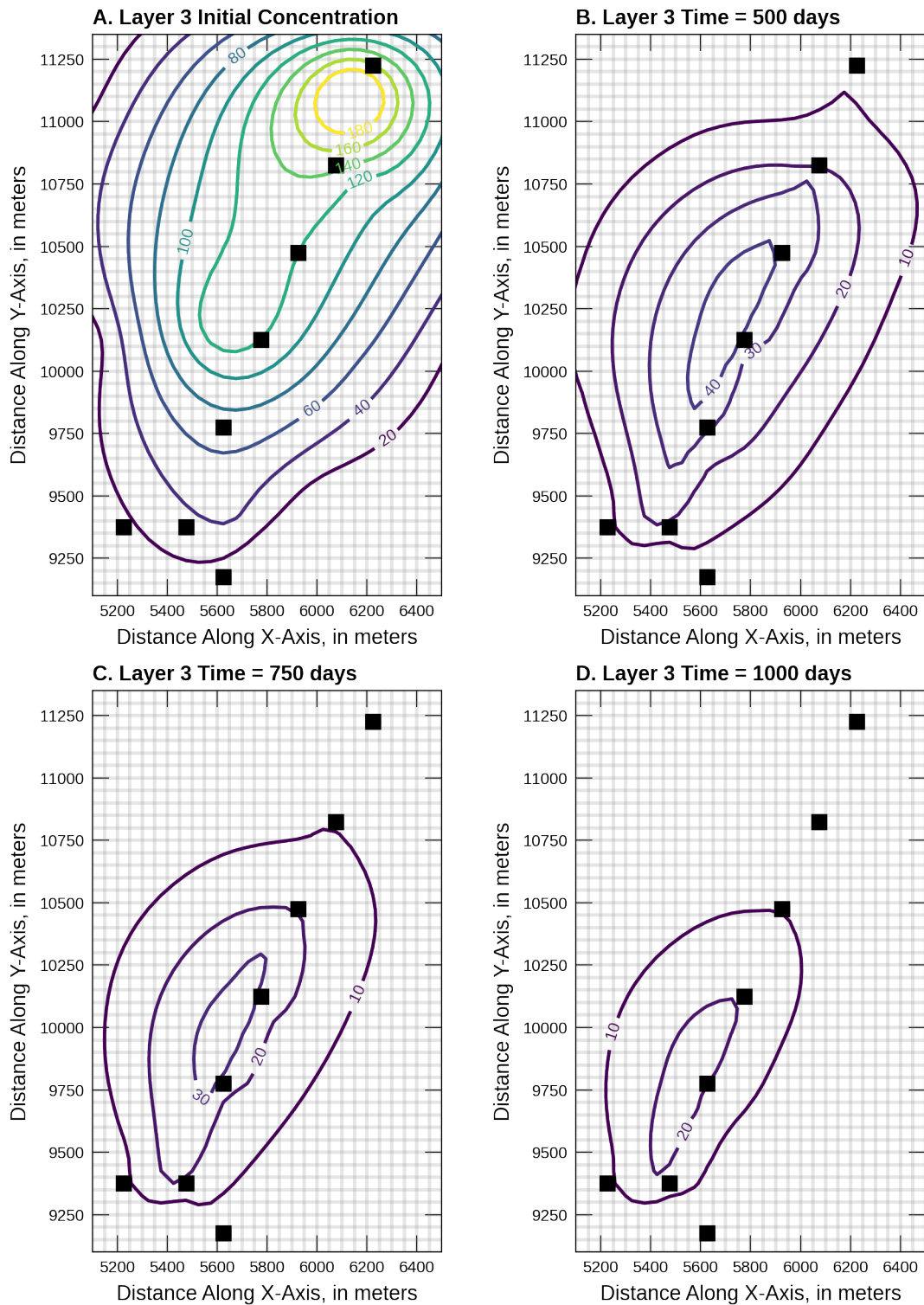


Figure 45–2: (A) Initial and simulated contaminant plume concentrations in model layer 3 as calculated by MODFLOW 6 with the multi-model setup after (B) 500 days, (C) 750 days, and (D) 1,000 days.

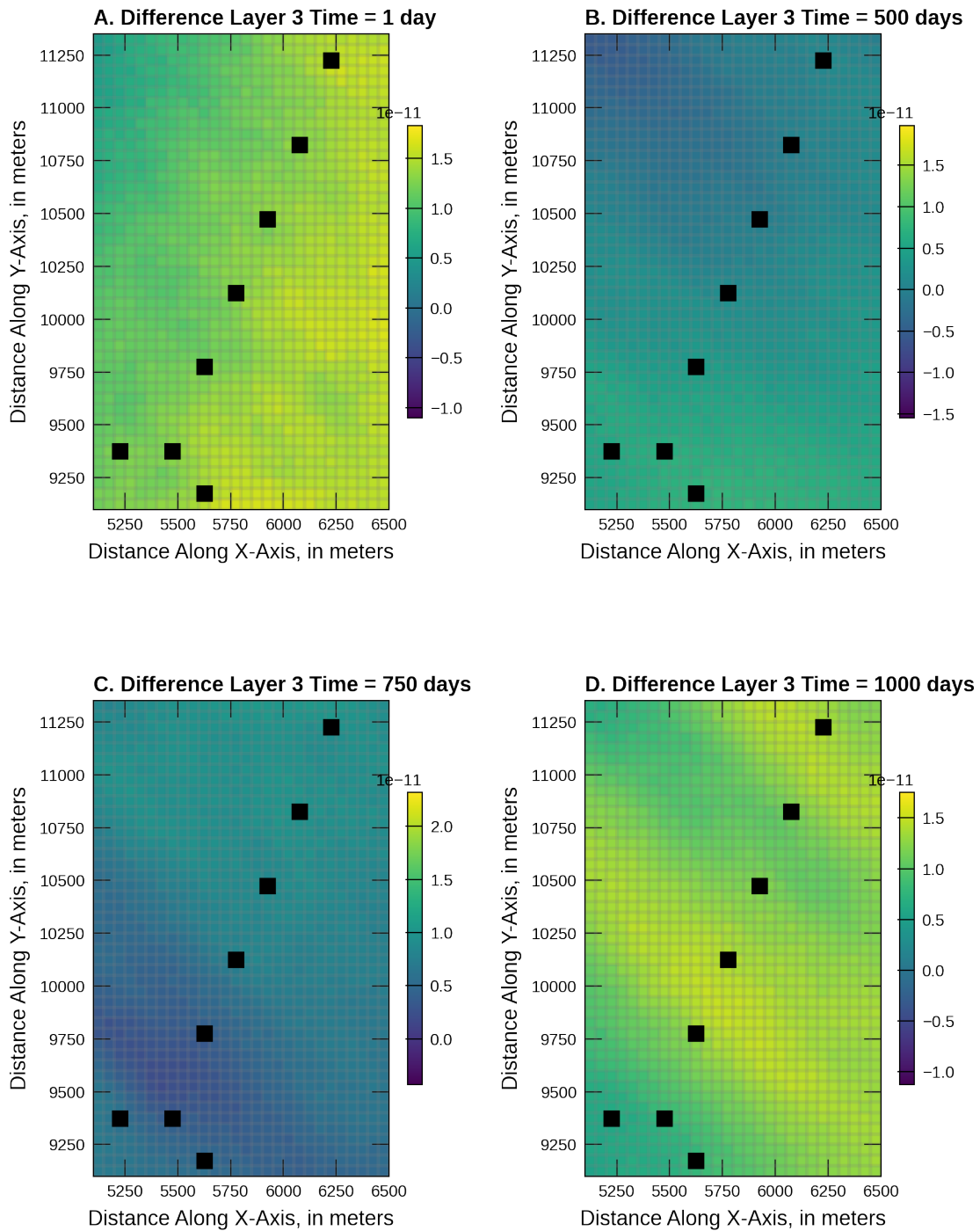


Figure 45–3: Difference in simulated head in model layer 3 with the multi-model setup with respect to the results from a setup containing a coupling between a single GWF and a single GWT model after (A) 1 day, (B) 500 days, (C) 750 days, and (D) 1,000 days.

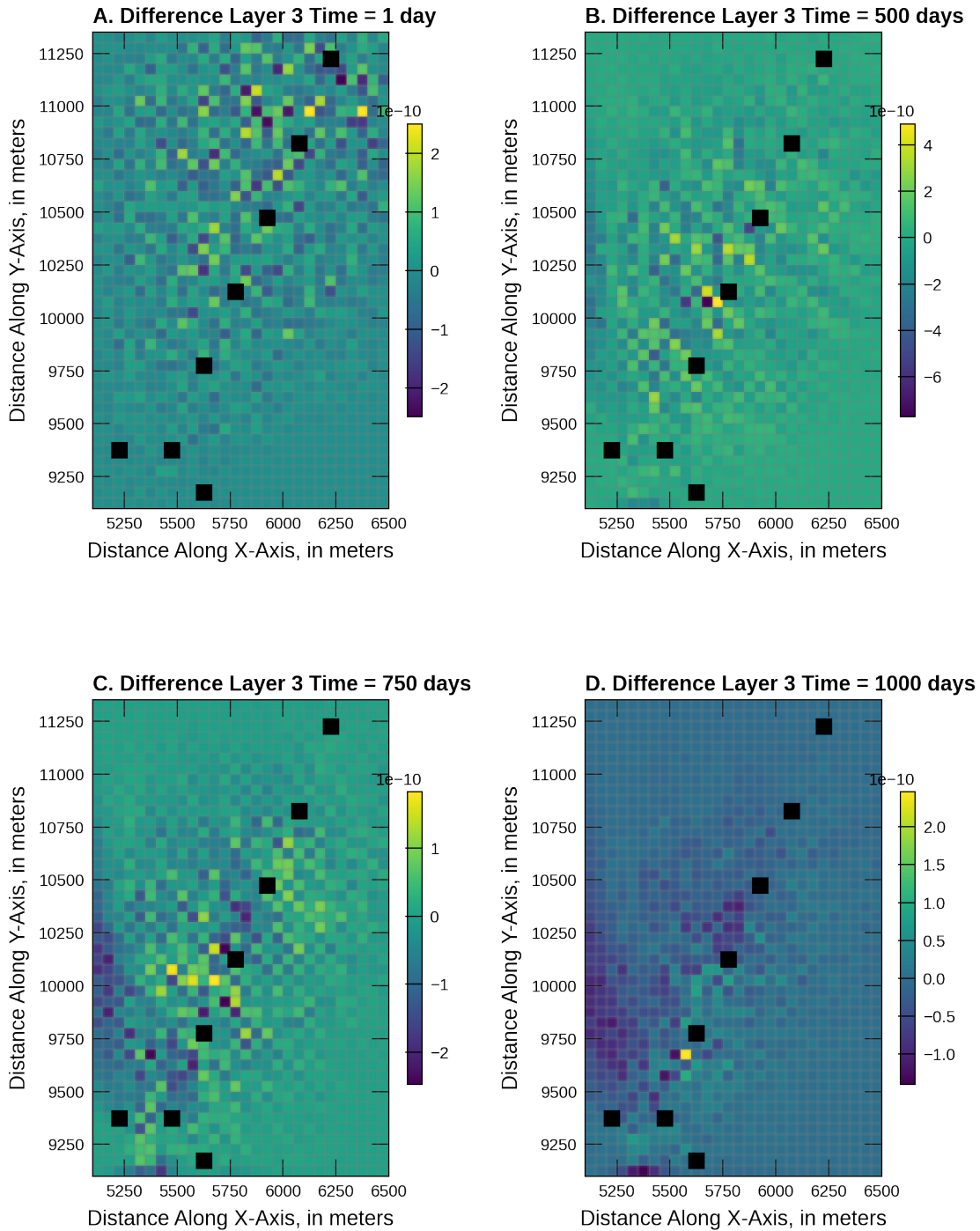


Figure 45–4: Difference in simulated concentrations in model layer 3 with the multi-model setup when compared to the results with a single GWF and single GWT model after (A) 1 day, (B) 500 days, (C) 750 days, and (D) 1,000 days.

## 46 MT3DMS Supplemental Guide Problem 6.3.1

This example is for zero-order production in a uniform flow field. It is based on example problem 6.3.1 described in [Zheng \(2010\)](#). The problem consists of a one-dimensional model grid with inflow into the first cell and outflow through the last cell. This example is simulated with the GWT Model in MODFLOW 6, which receives flow information from a separate simulation with the GWF Model in MODFLOW 6. Results from the GWT Model are compared with the results from a MT3DMS simulation ([Zheng, 1990](#)) that uses flows from a separate MODFLOW-2005 simulation ([Harbaugh, 2005](#)).

### 46.1 Example description

The parameters used for this problem are listed in table 46–1. The model grid consists of 101 columns, 1 row, and 1 layer. The flow problem is confined and steady state with an initial head set to the model top. The solute transport simulation represents transient conditions, which begin with an initial concentration specified as zero everywhere within the model domain. A specified flow condition is assigned to the first model cell. For the source pulse duration, the inflow concentration is specified as one. Following the source pulse duration the inflowing water is assigned a concentration of zero. A specified head condition is assigned to the last model cell. Water exiting the model through the specified head cell leaves with the simulated concentration of that cell.

Table 46–1: Model parameters for example ex-gwt-mt3dsupp631.

Parameter	Value
Number of periods	2
Number of layers	1
Number of rows	1
Number of columns	101
Column width (m)	0.16
Row width (m)	1.0
Top of the model (m)	1.0
Layer bottom elevation (m)	0
Specific discharge ( $md^{-1}$ )	0.1
Longitudinal dispersivity (m)	1.0
Porosity of mobile domain (unitless)	0.37
Zero-order production rate ( $mg/Ld^{-1}$ )	-2.0e-3
Source duration (d)	160.0
Simulation time (t)	840.0
Observation x location (m)	8.0

### 46.2 Example Results

Simulated concentrations from the MODFLOW 6 GWT Model and MT3DMS are shown in figure 46–1. The close agreement between the simulated concentrations demonstrate the zero-order-production capabilities implemented in the GWT Model.

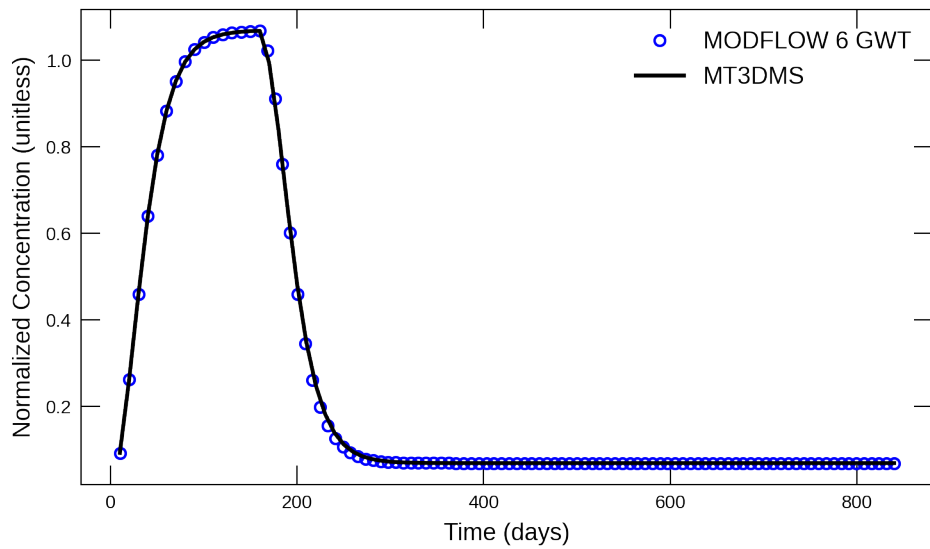


Figure 46–1: Concentrations simulated by the MODFLOW 6 GWT Model and MT3DMS for zero-order growth in a uniform flow field.

## 47 MT3DMS Supplemental Guide Problem 6.3.2

This example is for zero-order production in a dual-domain system. It is based on example problem 6.3.2 described in [Zheng \(2010\)](#). The problem consists of a one-dimensional model grid with inflow into the first cell and outflow through the last cell. This example is simulated with the GWT Model in MODFLOW 6, which receives flow information from a separate simulation with the GWF Model in MODFLOW 6. This example is designed to test the capabilities of the GWT Model to simulate zero-order production in a dual-domain system with and without sorption. Results from the GWT Model are compared with the results from a MT3DMS simulation ([Zheng, 1990](#)) that uses flows from a separate MODFLOW-2005 simulation ([Harbaugh, 2005](#)). This example was described by [Zheng \(2010\)](#) who showed that the results from MT3DMS were in good agreement with an analytical solution.

### 47.1 Example description

The parameters used for this problem are listed in table 47–1. The model grid consists of 401 columns, 1 row, and 1 layer. The flow problem is confined and steady state with an initial head set to the model top. The solute transport simulation represents transient conditions, which begin with an initial concentration specified as zero everywhere within the model domain. A specified flow condition is assigned to the first model cell. For the source pulse duration, a specified concentration with a value of one is assigned to the first model cell. Following the source pulse duration the specified concentration in the first cell is zero. A specified head condition is assigned to the last model cell. Water exiting the model through the specified head cell leaves with the simulated concentration of that cell.

Table 47–1: Model parameters for example ex-gwt-mt3dsupp632.

Parameter	Value
Number of periods	2
Number of layers	1
Number of rows	1
Number of columns	401
Column width (m)	2.5
Row width (m)	1.0
Top of the model (m)	1.0
Layer bottom elevation (m)	0
Specific discharge ( $m d^{-1}$ )	0.06
Longitudinal dispersivity (m)	10
volume fraction that is immobile domain (unitless)	0.2
Porosity of mobile domain (unitless)	0.2
Porosity of immobile domain (unitless)	0.05
Bulk density ( $gL^{-1}$ )	4.0
First-order mass transfer rate between the mobile and immobile domains ( $d^{-1}$ )	1.0e-3
Fraction of sorption sites in contact with mobile water (unitless)	0.8
Source duration (d)	1000
Simulation time (t)	10000
Observation x location (m)	200.0

## 47.2 Example Scenarios

This example problem consists of several different scenarios, as listed in table 47–2. The first two scenarios represent zero-order growth when sorbtion is active. Sorbtion is not active in the last scenario. For all three scenarios, there is mass transfer between the mobile domain and the immobile domain.

Table 47–2: Scenario parameters for example ex-gwt-mt3dsupp632.

Scenario	Scenario Name	Parameter	Value
1	ex-gwt-mt3dsupp632a	distribution ( $mLg^{-1}$ )	coefficient 0.25
		decay ( $g/mLd^{-1}$ )	0.0
		decay sorbed ( $g/mLd^{-1}$ )	-0.001
2	ex-gwt-mt3dsupp632b	distribution ( $mLg^{-1}$ )	coefficient 0.25
		decay ( $g/mLd^{-1}$ )	-0.0005
		decay sorbed ( $g/mLd^{-1}$ )	-0.0005
3	ex-gwt-mt3dsupp632c	distribution ( $mLg^{-1}$ )	coefficient 0.0
		decay ( $g/mLd^{-1}$ )	-0.001
		decay sorbed ( $g/mLd^{-1}$ )	0.0

### 47.2.1 Scenario Results

Results from the three scenarios are shown in figure 47–1. The close agreement between the simulated concentrations for the MODFLOW 6 GWT Model and MT3DMS demonstrate the zero-order growth and immobile-domain transfer capabilities for MODFLOW 6.

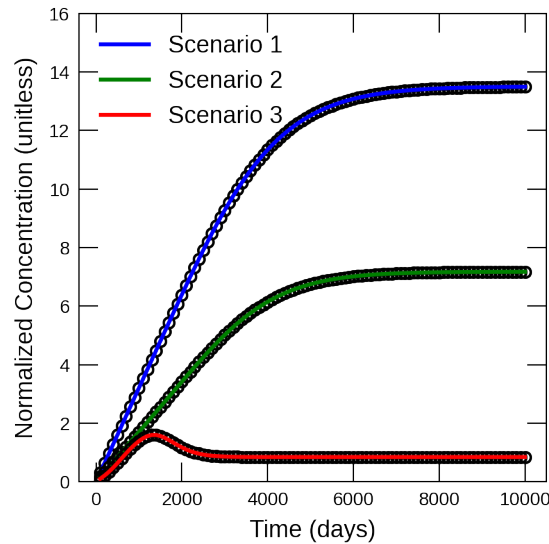


Figure 47–1: Concentrations simulated by the MODFLOW 6 GWT Model and MT3DMS for zero-order growth in a dual-domain system. Circles are for the GWT Model results; the lines represent simulated concentrations for MT3DMS.

## 48 MT3DMS Supplemental Guide Problem 8.2

This example is for a recirculating well. It is based on example problem 8.2 described in [Zheng \(2010\)](#). The problem consists of a two-dimensional, one-layer model with flow from left to right. A solute is introduced into the flow field by an injection well. Downgradient, an extraction well pumps at the same rate as the injection well. This extracted water is then injected into two other injection wells. This example is simulated with the GWT Model in MODFLOW 6, which receives flow information from a separate simulation with the GWF Model in MODFLOW 6. Results from the GWT Model are compared with the results from a MT3DMS simulation ([Zheng, 1990](#)) that uses flows from a separate MODFLOW-2005 simulation ([Harbaugh, 2005](#)).

### 48.1 Example description

The parameters used for this problem are listed in table 48–1. The model grid consists of 31 rows, 46 columns, and 1 layer. The flow problem is confined and steady state. The solute transport simulation represents transient conditions, which begin with an initial concentration specified as zero everywhere within the model domain.

For the MT3DMS representation of this problem, the Well Package is used to inject water at a rate of  $1 \text{ m}^3/\text{d}$  into model cell (1, 16, 16). Water is extracted at a rate of  $-1 \text{ m}^3/\text{d}$  from model cell (1, 16, 21). Two additional wells, located in cells (1, 5, 16) and (1, 27, 16), reinject water at the concentration of the extracted water from cell (1, 16, 21). The injection rate for each of these reinjection wells is  $0.5 \text{ m}^3/\text{d}$ .

For the MODFLOW 6 representation of this problem, the Multi-Aquifer Well (MAW) Package is used for these injection and extraction wells, although because the model is only a single layer, the MAW Package behaves just like the Well Package. The Water Mover (MVR) Package is used to send half of the extracted water into each of the reinjection wells. For the MODFLOW 6 transport simulation, the Multi-Aquifer Transport (MWT) Package is used to calculate the concentration in each of the well bores. The Mover Transport (MVT) Package is used to move the solute from the extraction well to the two reinjection wells based on the simulated flows. Note that this approach used in MODFLOW 6 is slightly different than the approach used in MT3DMS, because MODFLOW 6 is calculating the concentrations in the well boreholes rather than using concentrations directly from the model cells. By specifying a small well radius for the MAW Package, the approaches are similar.

Table 48–1: Model parameters for example ex-gwt-mt3dsupp82.

Parameter	Value
Number of periods	1
Number of layers	1
Number of rows	31
Number of columns	46
Column width (m)	10.0
Row width (m)	10.0
Top of the model (m)	10.0
Layer bottom elevation (m)	0.0
Hydraulic conductivity ( $\text{md}^{-1}$ )	10.0
Longitudinal dispersivity (m)	10.0
Transverse horizontal dispersivity (m)	3.0
Transverse vertical dispersivity (m)	0.3
Simulation time (d)	365.0
Porosity of mobile domain (unitless)	0.3

## 48.2 Example Results

Simulated concentrations from MODFLOW 6 and MT3DMS are shown in figure 48–1. The close agreement between the simulated concentrations demonstrate the ability of MODFLOW 6 to simulate the transfer of water and solute using the mover package capability.

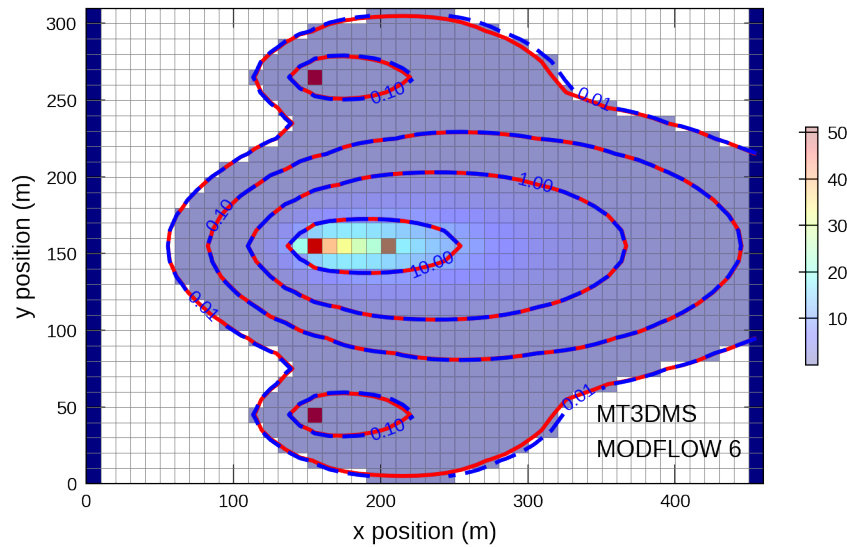


Figure 48–1: Concentrations simulated by MODFLOW 6 and MT3DMS for a problem involving a recirculating well. This figure can be compared to figure 8.2 in [Zheng \(2010\)](#).

## 49 SFR1 Manual Problem 2

This problem is based on the stream-aquifer interaction problem described as test 2 by Prudic and others (2004). Prudic and others (2004) designed their test 2 problem by modifying a variant originally described by Merritt and Konikow (2000). The description in the text and the figures presented here are largely based on the text and figures presented by Prudic and others (2004). The purpose for including this problem here is to demonstrate the use of MODFLOW 6 to simulate solute transport through a coupled system consisting of an aquifer, streams, and lakes. The example requires accurate simulation of transport within the streams and lakes and also between the surface water features and the underlying aquifer.

### 49.1 Example description

The example problem consists of two lakes and a stream network. Figure 49–1 shows the configuration of the hypothetical (but realistic) problem that was used by Prudic and others (2004) to demonstrate integration of the SFR1 Package with the LAK3 Package and the MODFLOW-2000 GWT Process.

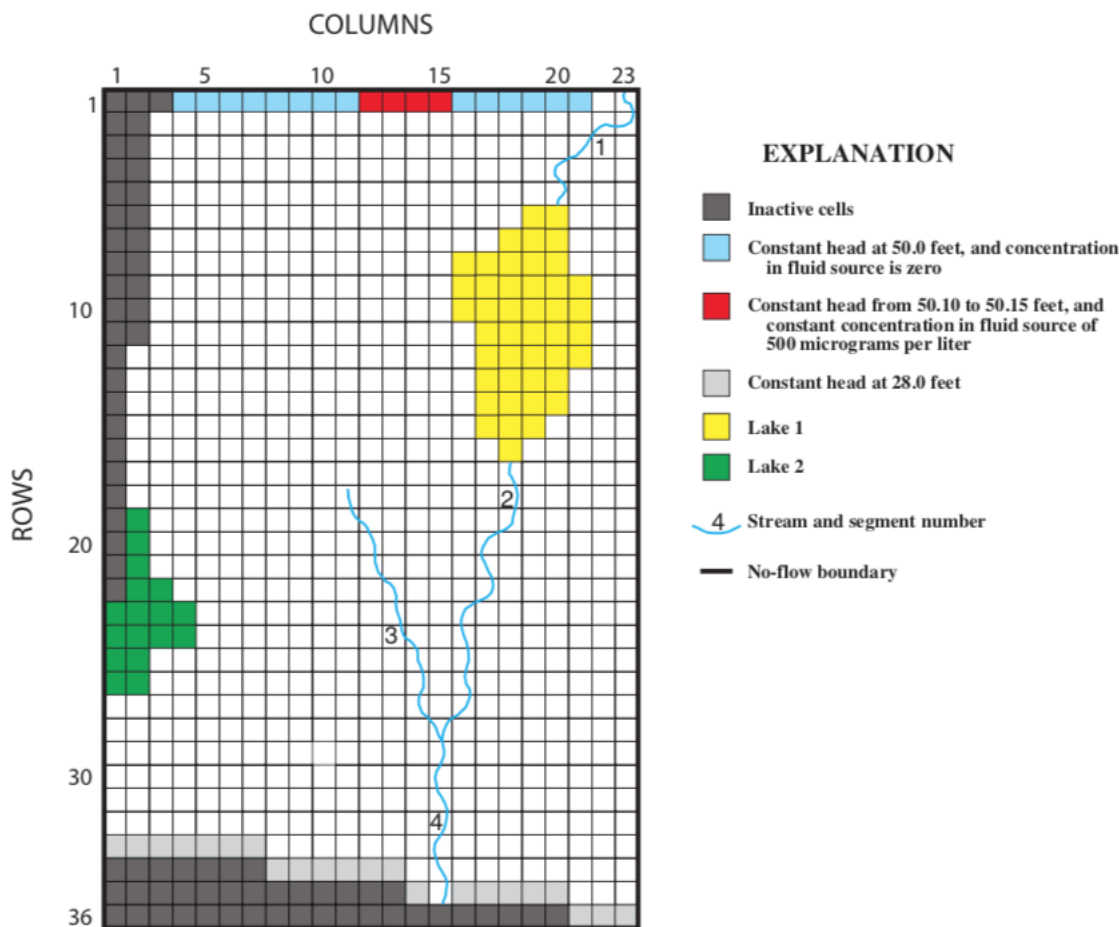


Figure 49–1: Model grid, boundary conditions and locations of lakes and streams used for the stream-lake interaction with solute transport problem. From Prudic and others (2004).

As described in [Prudic and others \(2004\)](#), the aquifer is moderately permeable and has homogeneous properties and uniform thickness (table 49–1). The aquifer was discretized into 8 layers (each 15 ft thick), 36 rows (at equal spacing of 405.7 ft), and 23 columns (at equal spacing of 403.7 ft). The flow field is represented as steady state. Uniform recharge was applied at a rate of 21 in/yr to layer 1 of the model. Two lakes are located within the model domain. Lake 1 has inflow from stream segment 1 and has outflow to stream segment 2. Lake 2 has no stream inflows or outflows. Both streams are in contact with the aquifer. Lakes are in horizontal contact with the aquifer in layer 1 around their edges and in vertical contact with the aquifer in layer 2.

Table 49–1: Model parameters for example ex-gwt-prudic2004t2.

Parameter	Value
Horizontal hydraulic conductivity ( $ft d^{-1}$ )	250.0
Vertical hydraulic conductivity ( $ft d^{-1}$ )	125.0
Storage coefficient (unitless)	0.0
Aquifer thickness (ft)	120.0
Porosity of mobile domain (unitless)	0.30
Recharge rate ( $ft d^{-1}$ )	4.79e-3
Lakebed leakance ( $ft^{-1}$ )	1.0
Streambed hydraulic conductivity ( $ft d^{-1}$ )	100.0
Streambed thickness (ft)	1.0
Stream width (ft)	5.0
Manning's roughness coefficient (unitless)	0.03
Longitudinal dispersivity (ft)	20.0
Transverse horizontal dispersivity (ft)	2.0
Transverse vertical dispersivity (ft)	0.2
Diffusion coefficient ( $ft^2 d^{-1}$ )	0.0
Initial concentration (micrograms per liter)	0.0
Source concentration (micrograms per liter)	500.0
Number of layers	8
Number of rows	36
Number of columns	23
Column width (ft)	405.665
Row width (ft)	403.717
Layer thickness (ft)	15.0
Top of the model (ft)	100.0
Total simulation time (d)	9131.0

The boundary conditions are illustrated in figure 49–1 and were designed to produce flow that is generally from north to south. For the numerical model, constant-head conditions were specified along the northern and southern edges of the model domain, and no-flow boundaries were set along the east and west edges of the grid. In MODFLOW 6 lakes can either sit on top of the model grid, or they can be incised into the model grid as is done with previous MODFLOW versions. For this example, aquifer cells in layer 1 (fig. 49–1) that share the same space as the lake are made inactive in the model grid by setting their IDOMAIN values to zero. The constant-head boundaries were placed in all 8 layers at the map locations shown in figure 49–1, with two exceptions. The first exception is related to the last downstream reach of stream segment 4. The grid cell in which the reach is located and the cell underlying it in layer 2 are both specified as active aquifer cells rather than as constant-head cells because a constant head in that cell with the stream reach would have set the gradient across the streambed. The second exception is related to the contaminant source (from treated sewage effluent), which is only introduced into the upper two model layers (that is, to a total

of 8 cells). The four cells in layer 3 that underlie the contaminant source are specified as active aquifer cells rather than as constant-head cells to simulate transport beneath the source.

Constant-head elevations were specified as 50.0 ft along the north boundary, except at the 4 cells in each of the upper two model layers that represent inflow from the contaminant source, where the fixed heads were 50.15 ft in the two middle cells and 50.10 ft in the two outer cells. The constant-head elevations were set to 28.0 ft along the south boundary.

The stream network consists of four segments and 38 reaches. (In MODFLOW 6 there is no concept of a segment, however the reaches are assigned names based on the segment number so that their combined flows can be compared with the results from MODFLOW-GWT.) The stream depths are calculated using Manning's equation assuming a wide rectangular channel. For all stream reaches, the channel width was assumed constant at 5.0 ft and the roughness coefficient for the channel was 0.03. Inflows to segments 1 and 3 were specified (86,400 and 8,640 ft<sup>3</sup>/d, respectively). The inflow to stream segment 2 was equal to the outflow from lake 1, and it was calculated using Manning's equation assuming a wide rectangular channel with a depth based on the difference between the calculated lake stage and the elevation of the top of the streambed (see [Merritt and Konikow \(2000\)](#), p. 11). The inflow to segment 4 is calculated as the sum of outflows from tributary segments 2 and 3. In MODFLOW 6 the Water Mover Package was used to route the water from the end of segment 1 into lake 1, and from the southern outlet of lake 1 into stream segment 2.

As reported by [Pradic and others \(2004\)](#) the test problem focuses on simulation of a boron plume, which results from sewage effluent. Variables related to the transport simulation are listed in table [49-1](#). For the purposes of this test, boron was assumed nonreactive. Molecular diffusion in the aquifer was assumed a negligible contributor to solute spreading at the scale of the field problem, so that hydrodynamic dispersion was related solely to mechanical dispersion, which was computed in MODFLOW 6 as a function of the specified dispersivity of the medium and the velocity of the flow field. The initial boron concentrations in the aquifer and in the lakes were assumed to be zero, and the sewage effluent concentration was assumed to be 500 micrograms/L. The source concentration in recharge was assumed to be zero and the concentration in specified inflow to stream segments 1 and 3 was also zero. The solute-transport model was run for a period of 25 years.

## 49.2 Example Results

The calculated steady-state head distributions in layers 1 and 2 are shown in figure [49-2](#) for MODFLOW 6. This figure can be compared to figure 14 in [Pradic and others \(2004\)](#). The heads in layers 3 through 8 are almost identical to the heads shown for layer 2 (fig. [49-2](#)). Flow is generally from north to south and predominantly horizontal. Because of recharge at the water table, however, there is a slight vertically downward flow in most areas. The lakes and streams exert a strong influence on the location and magnitude of vertical flow. In layer 2, the good hydraulic connection with the lakebed results in an almost flat horizontal hydraulic gradient in head beneath the lakes (fig. [49-2](#)). In general the simulated water table and aquifer heads simulated by MODFLOW 6 are in good agreement with those simulated by MODFLOW-2000.

The MODFLOW 6 model calculated steady-state stage in lake 1 was 45.07 ft (compared to 44.97 ft in MODFLOW-GWT) and in lake 2 was 37.15 ft (compared to 37.14 ft in MODFLOW-2000). Stream segment 1 was mostly a gaining stream (leakage across streambed was from ground water), and stream segment 2 was losing such that outflow from the last reach in segment 2 was only half of the inflow from lake 1. Stream segment 3 was mostly gaining and outflow from this segment was only from groundwater leakage. Lastly, stream segment 4 was a losing stream and leakage was from the stream to the aquifer in every reach. Simulated flows between MODFLOW 6 and MODFLOW-2000 are in good qualitative agreement, however there are differences in individual flows, which can be

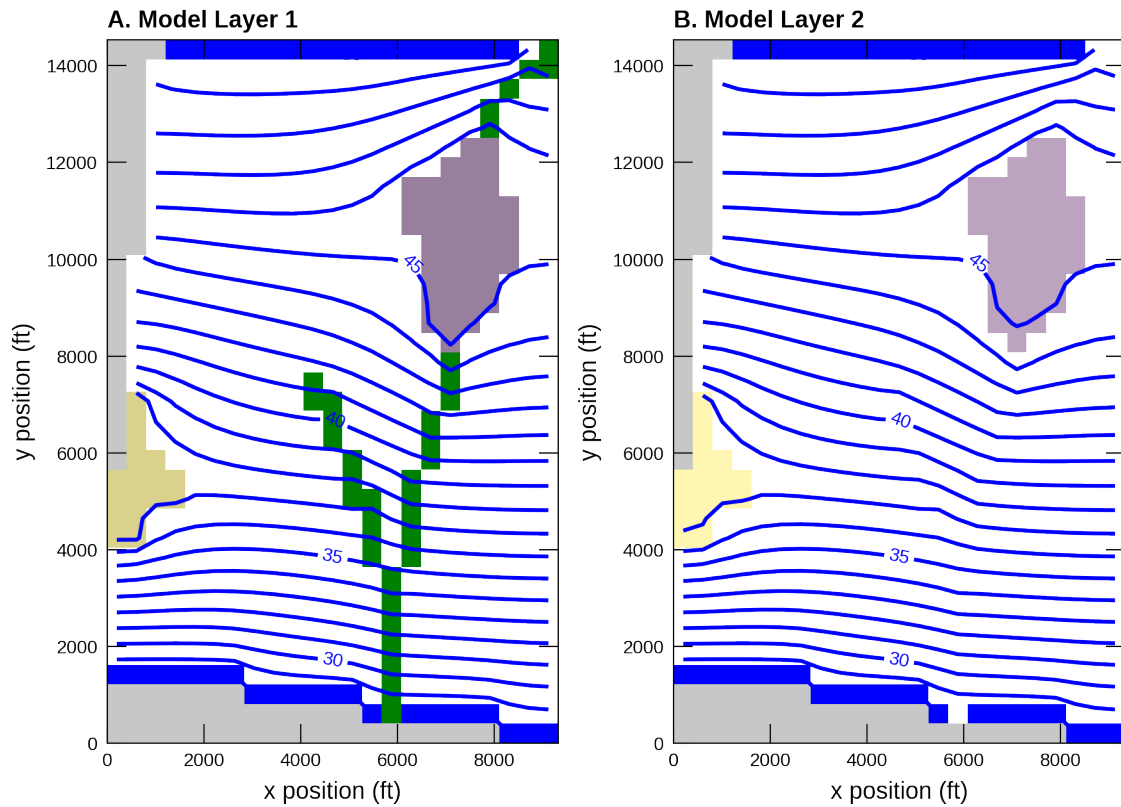


Figure 49–2: Contours of head simulated by the MODFLOW 6 GWF Model for the stream-lake interaction example. Contours are for (A) layer 1, and (B) layer 2. This figure can be compared with figure 14 in [Prudic and others \(2004\)](#), which shows head contours as simulated by MODFLOW-2000.

attributed to slight differences in the way MODFLOW 6 and MODFLOW-2000 simulate lakes, streams, and groundwater flow.

For the MODFLOW 6 simulation, the 25-year period was divided into 300 time steps (compared with 1229 time steps used for the MODFLOW-GWT simulation). Advective groundwater flow was solved using the second-order implicit Total Variation Diminishing (TVD) scheme. Dispersion was solved using the XT3D approach, which was originally designed to represent full three-dimensional anisotropic groundwater flow ([Provost and others, 2017](#)). Transport through the surface water system was solved using the Lake Transport (LKT) Package, the Streamflow Transport (SFT) Package, and the Mover Transport (MVT) Package, which transfers solute between the lake and stream according to simulated flows. Additional detail on the transport parameters for the MODFLOW-GWT simulation are described in [Prudic and others \(2004\)](#) and in [Merritt and Konikow \(2000\)](#). The calculated concentration in lake 1 and in the outflow from the last reach in stream segments 2, 3, and 4 during the 25-year simulation period are shown in figure 49-3 for both the MODFLOW 6 simulation and the MODFLOW-GWT simulation. Note that because stream segment 2 lost flow to ground water in all reaches and its only source was inflow from lake 1, solute concentration in the outflow from the last reach in stream segment 2 was equal to the concentration in the discharge from lake 1 (fig. 49-3). The leading edge of the plume reaches the upstream edge of lake 1 after about 4 years, at which time the concentration in the lake begins to increase rapidly. After about 22 years, the part of the plume close to the source and near the lake has stabilized and the concentration in lake 1 reaches an equilibrium concentration of 37.2 micrograms/L as simulated by MODFLOW 6 and 37.4 micrograms/L as simulated by MODFLOW-GWT. Although there are differences in the surface water concentrations simulated by MODFLOW 6 and MODFLOW-GWT, the general pattern and behavior is quite similar. Differences between the two models are generally attributed to slight differences in simulated flows as well as slight differences in how solute transport is represented. For example, MODFLOW-GWT uses the method-of-characteristics to simulate advective flow, whereas MODFLOW 6 uses an implicit TVD approach. The methods-of-characteristics approach implemented in MODFLOW-GWT is exceptional for reducing numerical dispersion, whereas the second-order TVD approach implemented in MODFLOW 6 is relatively fast and efficient, but it has more numerical dispersion than MODFLOW-GWT.

As the lake concentration increases, it in turn acts as a source of contamination to the aquifer in the areas where the lake is a source of water to the aquifer. Although the lake significantly dilutes the contaminants that enter it from the aquifer, the lake and the stream segments downstream from it in effect provide a short circuit for the relatively fast transmission of low levels of the contaminant. This is evident in figure 49-4, which shows the computed solute distributions in layers 1, 3, 5, and 8 after 25 years. The low-concentration part of the plume emanating from the downgradient side of lake 1 has advanced farther, and is wider, than the main plume that emanated directly from the source at the north edge of the model. The influence of groundwater discharge to stream segment 3 is most apparent in the concentration pattern shown in layer 1 of figure 49-4 (that is, the 25 microgram/L contour). Comparison of concentration levels at different depths in the system indicates that in the southern part of the area, concentrations generally increase with depth. In contrast, in the northern part downgradient from the source, the highest concentrations occur in layer 3. These various patterns result from the dilution effect of recharge of uncontaminated water at the water table coupled with the consequent downward component of flow, which causes the solute to move slowly downward as it migrates to the south. Solute concentrations simulated by MODFLOW 6 and shown in figure 49-4 are generally in good agreement with those simulated by MODFLOW-GWT (figure 17 in [Prudic and others \(2004\)](#)). There are some differences, which can be attributed to the slightly different flow field and the differences in solute transport solution schemes.

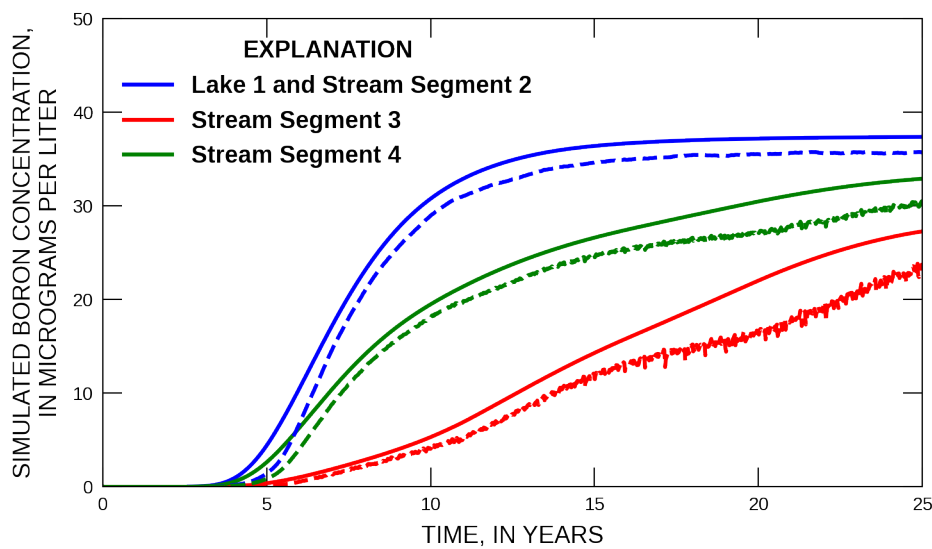


Figure 49–3: Concentration versus time simulated by MODFLOW 6 for the stream-lake interaction example. Solid lines represent the MODFLOW 6 simulated change in boron concentration in lake 1 and at the end of stream segments 2, 3, and 4. Dashed lines are results from the MODFLOW-GWT simulation (Prudic and others, 2004).

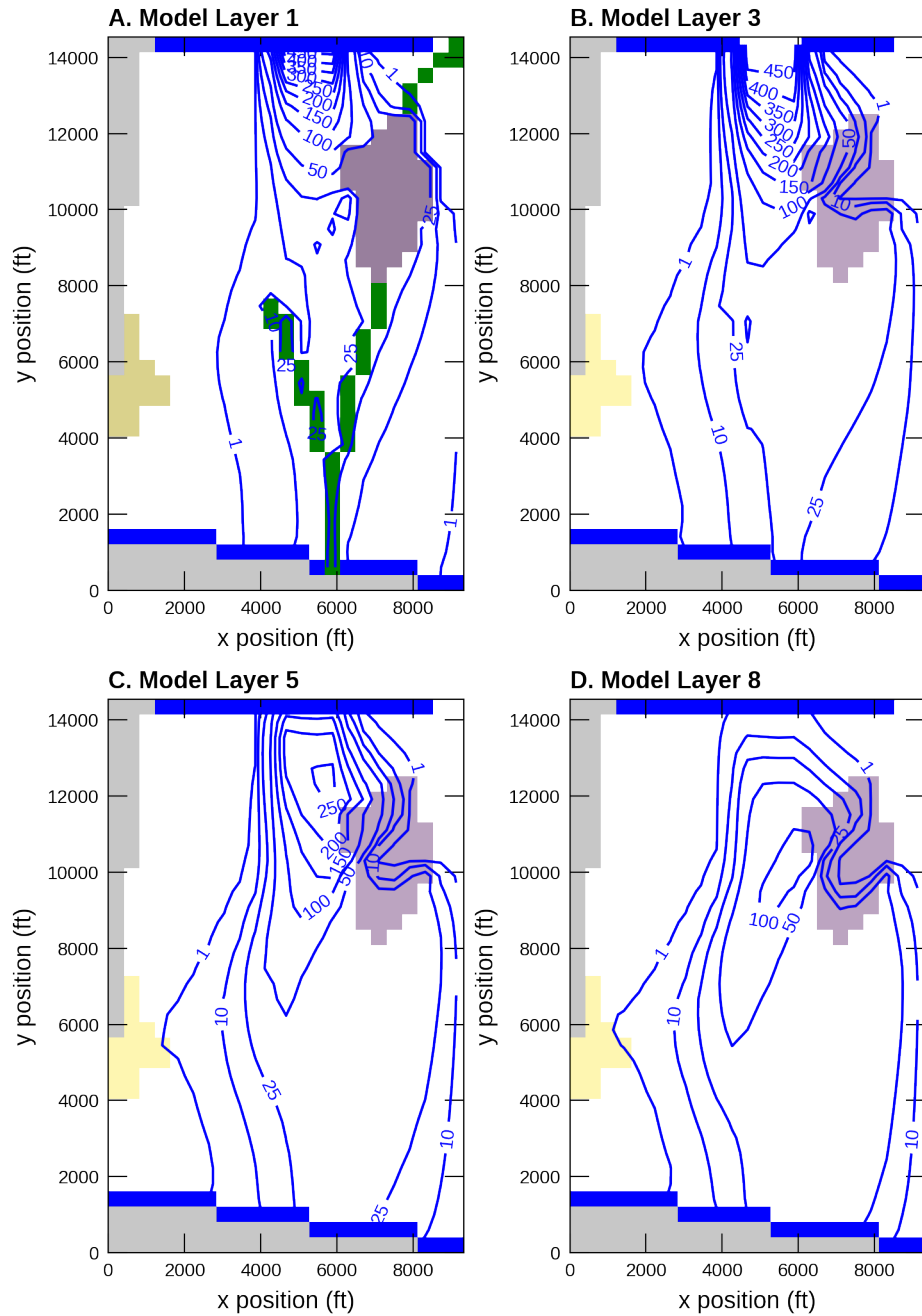


Figure 49–4: Contours of concentration simulated by the MODFLOW 6 GWT Model for the stream-lake interaction example. Contours are shown for (A) layer 1, (B) layer 3, (C) layer 5, and (D) layer 8. This figure can be compared with figure 17 in Prudic and others (2004), which shows an equivalent plot using model results simulated by MODFLOW-GWT.

## 50 Two-Dimensional Test of Unsaturated-Saturated Transport

This example first appeared as scenario 6 in [Morway and others \(2013\)](#). At that time, new capabilities programmed into MT3DMS ([Zheng and Wang, 1999](#)) allowed for simulation of solute transport in the unsaturated-zone using flux terms calculated by the unsaturated-zone flow (UZF1; [Niswonger and others \(2006\)](#)) package. [Morway and others \(2013\)](#) referred to the published MT3DMS variant as UZF-MT3DMS. Eventually, however, these capabilities were better documented and released with MT3D-USGS ([Bedekar and others, 2016](#)). For the purpose of testing unsaturated-zone transport using the UZF/UZT packages inside MODFLOW 6, the MODFLOW 6 solution is compared against the MT3D-USGS solution. Moreover, we note that the results of the MT3D-USGS simulation were compared to results calculated by VS2DT ([Lappala and others, 1987](#)) for establishing the accuracy of the MT3D solution. VS2DT solves Richards' equation and as such can simulate flow and solute fluxes across the unsaturated-saturated interface. Therefore, this example problem tests the ability of MODFLOW 6 to accurately simulate the infiltration, unsaturated-zone transport, recharge, and subsequent saturated transport of dissolved solute.

Currently, the UZT package inside MODFLOW 6 does not simulate dispersion in the unsaturated zone. As a result, two scenarios were setup in both MT3D-USGS and MODFLOW 6. The first maintains fidelity with [Morway and others \(2013\)](#) and simulates dispersion in the unsaturated zone. In the second scenario, no dispersion is simulated in the unsaturated zone by setting the longitudinal, transverse, and vertical dispersion equal to zero in the upper 11 layers as summarized in the following table. Brackets ("[ ]") in the table indicate a list of values, one per layer, is used to define the value for the entire layer. Where only one value appears inside the brackets, a constant value is used throughout the model domain.

Table 50–1: Scenario parameters for example ex-gwt-uzt-2d.

Scenario	Scenario Name	Parameter	Value
1	ex-gwt-uzt-2d-a	longitudinal dispersivity (m)	[0.5]
		ratio horizontal to longitudinal dispersivity (unitless)	[0.4]
		ratio vertical to longitudinal dispersivity (unknown)	[0.4]
2	ex-gwt-uzt-2d-b	longitudinal dispersivity (m)	[0.0, 0.0, 0.0, 0.0, 0.0, 0.0, 0.0, 0.0, 0.0, 0.0, 0.0, 0.0, 0.5, 0.5, 0.5, 0.5, 0.5, 0.5, 0.5, 0.5]
		ratio horizontal to longitudinal dispersivity (unitless)	[0.0, 0.0, 0.0, 0.0, 0.0, 0.0, 0.0, 0.0, 0.0, 0.0, 0.4, 0.4, 0.4, 0.4, 0.4, 0.4, 0.4, 0.4]

Table 50–1: Scenario parameters for example ex-gwt-uzt-2d.

Scenario	Scenario Name	Parameter	Value
		ratio vertical to longitudinal dispersivity (unknown)	[0.0, 0.0, 0.0, 0.0, 0.0, 0.0, 0.0, 0.0, 0.0, 0.0, 0.0, 0.0, 0.0, 0.4, 0.4, 0.4, 0.4, 0.4, 0.4, 0.4, 0.4]

## 50.1 Example description

For this problem, a relatively small, two-dimensional profile that is 10  $m$  wide by 5  $m$  deep is used. Layer thickness, as well as the column widths, are 0.25  $m$ . A constant head boundary of 1.625  $m$  is set on the left and right sides of the active model domain. An infiltration rate of 0.1  $m/day$  is specified all along the top boundary except for the left- and right-most columns where the constant head boundary condition exists. A no-flow boundary is used along the bottom of the simulation domain. The simulation domain starts out clean; however, solute enters with the infiltrating water in the middle 10 columns only. Additional model parameter values are listed in table 50–2.

Table 50–2: Model parameters for example ex-gwt-uzt-2d.

Parameter	Value
Number of layers	20
Number of rows	1
Number of columns	40
Column width ( $m$ )	0.25
Row width ( $m$ )	0.25
Layer thickness ( $m$ )	0.25
Top of the model ( $m$ )	5.0
Horizontal hydraulic conductivity ( $m/day$ )	2.5
Vertical hydraulic conductivity ( $m/day$ )	0.5
Aquifer storativity	1e-5
Specific yield	0.35
Residual water content	0.1
Saturated water content	0.45
Initial water content	0.105
Brooks-Corey Epsilon	4.0
Infiltration rate ( $m/d$ )	0.1
Concentration of recharge in select cells( $ppm$ )	1.0
Porosity	0.45
Longitudinal dispersivity ( $ft$ )	0.5
Ratio of horizontal transverse dispersivity to longitudinal dispersivity	0.4
Ratio of vertical transverse dispersivity to longitudinal dispersivity	0.4
Simulation time ( $days$ )	60.0

Given the relatively dry initial condition within the unsaturated zone, the infiltrating front reaches the water table on day 8 of the 60 day simulation period. Once the infiltrating wave reaches the saturated zone, the water table rises into the unsaturated zone and further tests the accuracy of the transport solution.

## 50.2 Example results

Because MODFLOW 6 does not (yet) simulate dispersion in the unsaturated-zone, there are some significant differences between the two solutions (figure 50–1). Whereas longitudinal and transverse dispersive fluxes spread solute ahead and to the side of the downward migrating plume within the MT3D-USGS unsaturated zone solution, the UZF/UZT formulation within MODFLOW 6 simulates purely advective transport in the unsaturated zone. However, once solute reaches the saturated zone, dispersion is simulated using the XT3D package (the default setting).

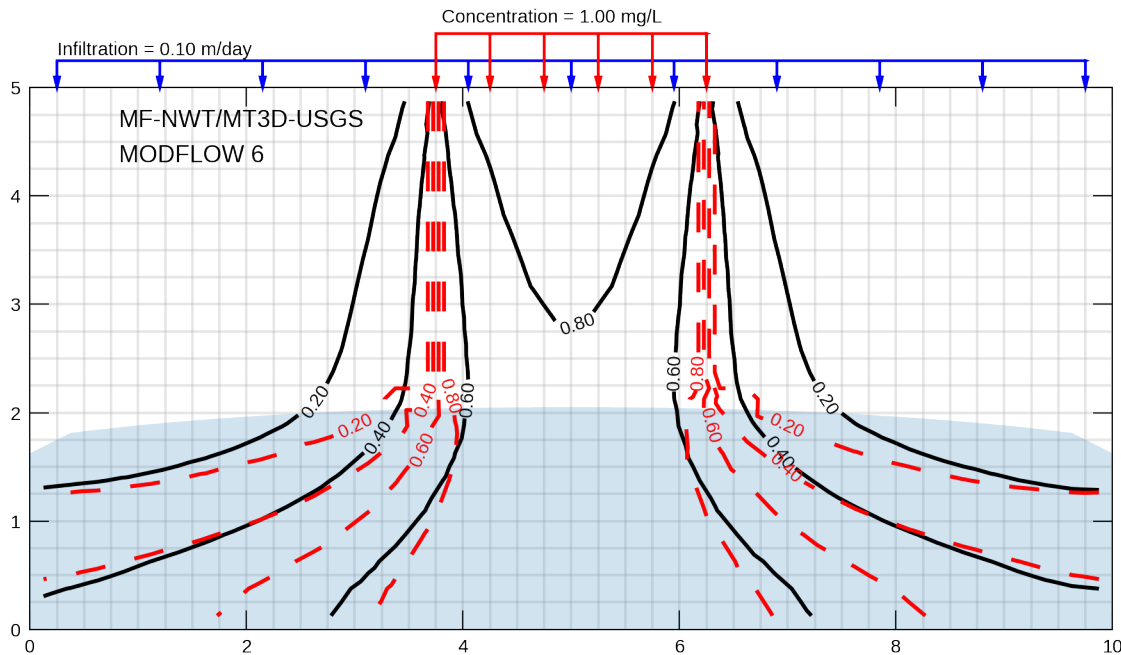


Figure 50–1: A two-dimensional problem first published in [Morway and others \(2013\)](#). MT3D-USGS results closely match a benchmark solution calculated by VS2DT ([Lappala and others, 1987](#)). The light blue shaded region shows the location of the saturated zone.

A second scenario in which longitudinal, transverse, and vertical dispersion are set equal to zero in the unsaturated zone of the MT3D-USGS solution was run. Because this setup more closely mimicks the MODFLOW 6 unsaturated zone solution, results between the respective models more closely match one another. We note, however, that because many transport problems originate at land surface, the final transport solution within the saturated zone may ultimately depend on accurately simulating unsaturated zone transport processes. That is, the extent and severity of the saturated zone plume may be inextricably tied to the spread and delay of migrating solute in the unsaturated zone, as demonstrated by the two different solutions within the saturated zone when dispersion is and is not accounted for in the unsaturated zone.

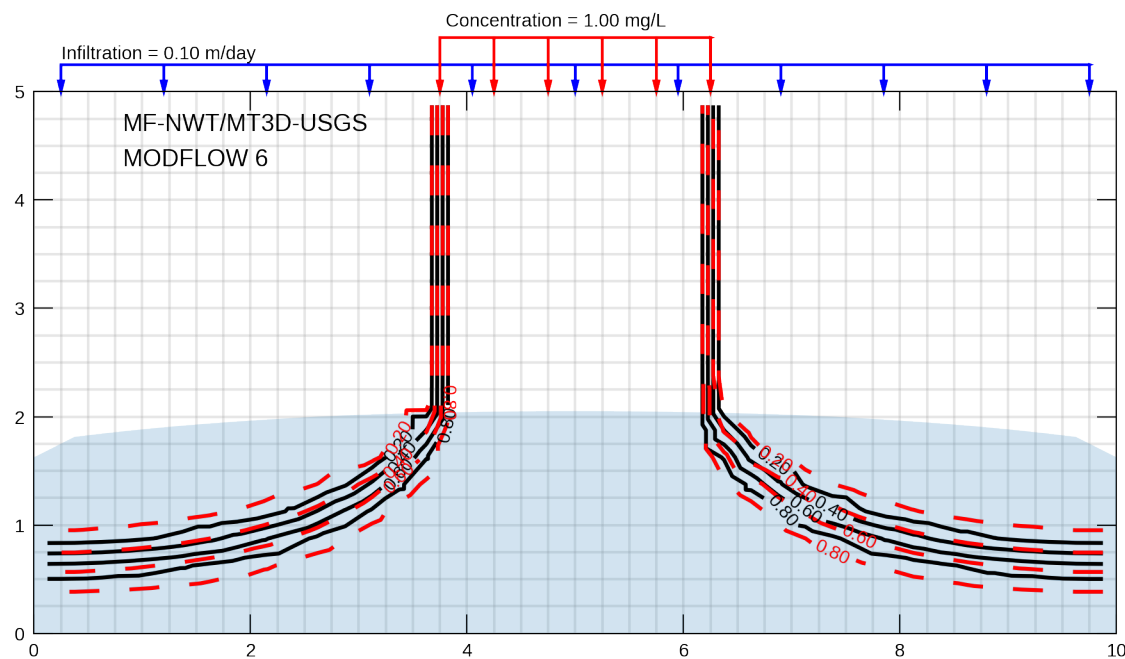


Figure 50–2: A two-dimensional transport problem with no dispersive fluxes in either MODFLOW 6 or MT3D-USGS within the unsaturated-zone. The light blue shaded region shows the location of the saturated zone.

## 51 Henry Problem

This problem simulates the classic Henry problem ([Henry, 1964](#)) for variable-density groundwater flow and solute transport. The MODFLOW 6 simulations presented here are based on the hydraulic-head formulation for variable-density flow as presented by [Langevin and others \(2020\)](#).

### 51.1 Example Description

Variations on the Henry problem ([Henry, 1964](#)) are commonly used as benchmark test problems for variable-density flow and transport codes. The model domain for the Henry problem is 2 m long by 1 m tall. In the original version of the problem, for which [Henry \(1964\)](#) presented a semianalytical solution, freshwater with a density of 1000  $kg/m^3$  flows into the domain through the left side at a rate of 5.7024  $m^3/d$ . [Simpson and Clement \(2004\)](#) reduced the rate of inflow to 2.851  $m^3/d$  in their numerical simulations, rendering the flow system less “advective dominant” and effecting “an increase in the relative importance of density-driven processes” ([Simpson and Clement, 2004](#)). This modified version of the problem, called the “low-inflow” version here, provides a better benchmark test of density-dependent flow behavior than Henry’s original version. Results from both versions of the problem are presented.

[Henry \(1964\)](#) and [Simpson and Clement \(2004\)](#) assign the same flow and transport boundary conditions at the right boundary. The boundary condition for flow is a hydrostatic condition based on seawater concentration, 35  $kg/m^3$ , which corresponds to a density of 1024.5  $kg/m^3$ . For transport, the concentration at the right boundary is fixed at seawater concentration. The simulations presented here use a variation in which the right boundary is assigned a mixed boundary condition: water that flows into the model from the right boundary enters at seawater concentration, and water that flows out of the model at the right boundary exits at the groundwater concentration computed for that boundary cell. Use of a mixed boundary condition in the Henry problem was introduced by [Segol and others \(1975\)](#), who imposed a Neumann-type condition for transport when water flows out of the model. The mixed boundary condition used here, in which outflow is at the prevailing groundwater concentration, is the condition used for the Henry problem by [Voss \(1984\)](#) and [Voss and Souza \(1987\)](#). This manner of representing the seawater boundary, which is often used in saltwater intrusion models, allows a freshwater outflow zone to form above the zone of recirculating saltwater.

The freshwater hydraulic conductivity is set to 864  $m/d$ , and the porosity to 0.35 (tab. 51–1). Mechanical dispersion is not represented; all mixing occurs solely by molecular diffusion with a diffusion coefficient of 0.57024  $m^2/d$ . The simulation begins with the model domain initially filled with seawater, although the problem can also be simulated with the domain initially filled with freshwater. If the hydraulic head is fixed for the seawater boundary and the mixed boundary condition is used for transport, then it may be necessary to start the simulation with some saltwater in the domain or there may be no seawater inflow. In the simulations presented here, the domain is divided into 40 layers and 80 columns of cells, and a simulation period of 0.5  $d$  is divided into 500 equally sized time steps of 0.001  $d$ .

Table 51–1: Model parameters for example ex-gwt-henry.

Parameter	Value
Number of periods	1
Number of time steps	500
Simulation time length ( $d$ )	0.5
Number of layers	40
Number of rows	1

Table 51–1: Model parameters for example ex-gwt-henry.

Parameter	Value
Number of columns	80
Length of system ( $m$ )	2.0
Column width ( $m$ )	0.025
Row width ( $m$ )	1.0
Layer thickness	0.025
Top of the model ( $m$ )	1.0
Hydraulic conductivity ( $md^{-1}$ )	864.0
Initial concentration (unitless)	35.0
porosity (unitless)	0.35
diffusion coefficient ( $m^2/d$ )	0.57024

## 51.2 Scenario Results

The original and low-inflow versions of the Henry problem (tab. 51–2) were simulated with a mixed boundary condition for concentration in cells along the right boundary. The mixed boundary condition is represented using the General-Head Boundary (GHB) Package, which allows the hydrostatic boundary condition to be effectively imposed at the right edge of the model domain by accounting for the conductance of aquifer material between the cell center and the right edge of the model domain. Conceptually, a seawater reservoir is attached to the edge of each model cell at the right boundary. Flow into the model domain enters at the concentration of seawater, and flow out of the model domain exists at the concentration computed in the corresponding boundary cell.

Figure 51–1 shows contours of concentration (relative seawater concentrations of 0.01, 0.1, 0.5, 0.9, and 0.99) at the end of the  $0.5\text{ }d$  simulation period for the classic Henry problem. Figure 51–2 shows results from the low-inflow version of the Henry problem. These same simulations were reported by [Langevin and others \(2020\)](#) and were shown to be in good agreement with results from SEAWAT simulations.

Table 51–2: Scenario parameters for example ex-gwt-henry.

Scenario	Scenario Name	Parameter	Value
1	ex-gwt-henry-a	inflow ( $m^3/d$ )	5.7024
2	ex-gwt-henry-b	inflow ( $m^3/d$ )	2.851

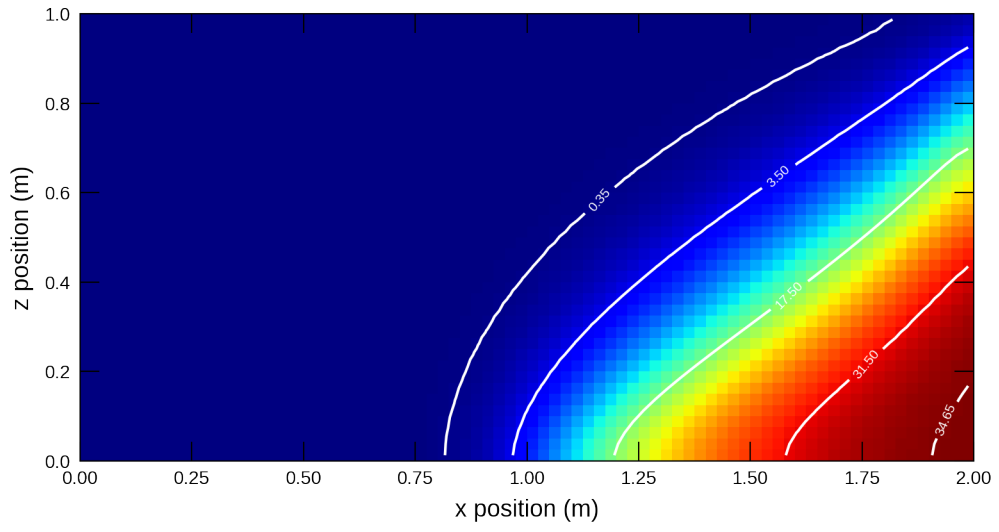


Figure 51–1: Simulation results for the classic Henry problem.

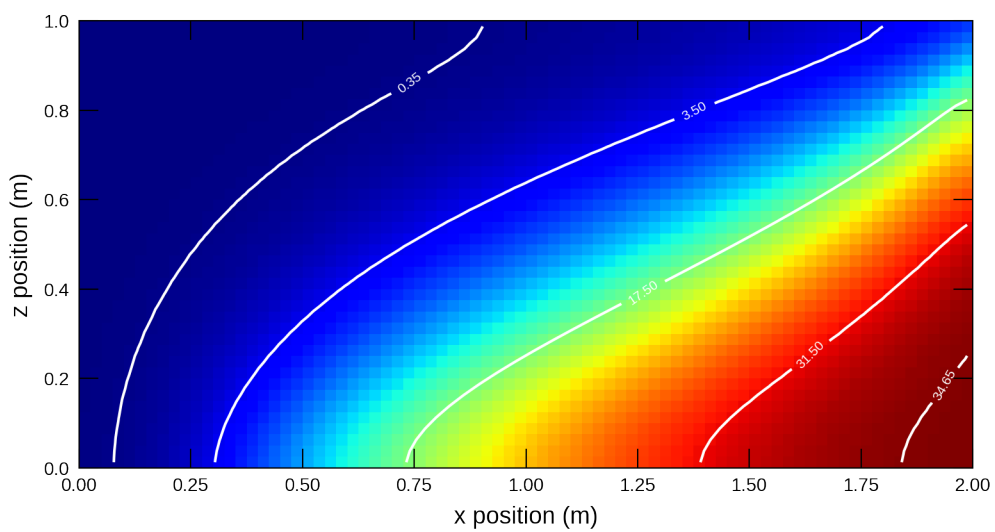


Figure 51–2: Simulation results for the low-inflow version of the Henry problem.

## 52 Salt Lake Problem

The salt lake problem was suggested by [Simmons and others \(1999\)](#) as a comprehensive benchmark test for variable-density groundwater flow models. The problem is based on dense salt fingers that descend from an evaporating salt lake. Although an analytical solution is not available for the salt lake problem, an equivalent Hele-Shaw analysis was performed in the laboratory to investigate the movement of dense salt fingers ([Wooding and others, 1997a,b](#)). In addition to the SUTRA simulation, this salt lake problem was simulated by [Langevin and others \(2003\)](#) using the MODFLOW-based SEAWAT-2000 program. The approach described by [Langevin and others \(2003\)](#) is followed here to reproduce the salt lake problem with MODFLOW 6.

### 52.1 Example description

Model parameters used for the MODFLOW 6 simulation of the salt lake problem are shown in table 52–1. The model grid and boundary conditions used for the MODFLOW 6 simulation are shown in figure 52–1. The model grid consists of 135 columns and 57 layers. To accurately capture the number and growth of salt fingers, the model grid has an increased level of resolution beneath the evaporative boundary. The evaporative boundary is represented in the model by using the Recharge (RCH) Package and specifying a negative recharge rate. [Simmons and others \(1999\)](#) describe the method for applying the SUTRA code to the salt lake problem. A random numerical perturbation was required to match the formation of the salt fingers observed in the Hele-Shaw experiment. Concentrations along the evaporative boundary were randomly assigned for each node and for each time step. A similar approach is used here for the MODFLOW 6 simulation, except that the random variations are not reassigned each time step. The inflow boundary is represented using constant-head cells with a constant inflow concentration. The MODFLOW 6 model was run for 24,000 seconds (400 minutes) using 60-second transport timesteps.

Table 52–1: Model parameters for example ex-gwt-saltlake.

Parameter	Value
Number of periods	1
Number of time steps	400
Simulation time length (s)	24000
Number of layers	57
Number of rows	1
Number of columns	135
Length of system (mm)	150.0
Column width (mm)	ranges from 0.75 to 1.5
Row width (mm)	1.5
Layer thickness	ranges from 0.75 to 1.5
Top of the model (mm)	75.0
Hydraulic conductivity ( $mms^{-1}$ )	3.05
Specific storage ( $mm^{-1}$ )	3.8e-10
Reference density	0.001065
Density and concentration slope	0.646
Initial and inflow concentration ( $gL^{-1}$ )	8.4e-5
Saturated concentration ( $gL^{-1}$ )	1.1e-4
Porosity (unitless)	1.0
Evaporation rate ( $mms^{-1}$ )	1.03e-3
Longitudinal dispersivity (mm)	9.0e-7
Transverse dispersivity (mm)	9.0e-7

Table 52–1: Model parameters for example ex-gwt-saltlake.

Parameter	Value
Diffusion coefficient ( $mms^{-1}$ )	9.0e-4

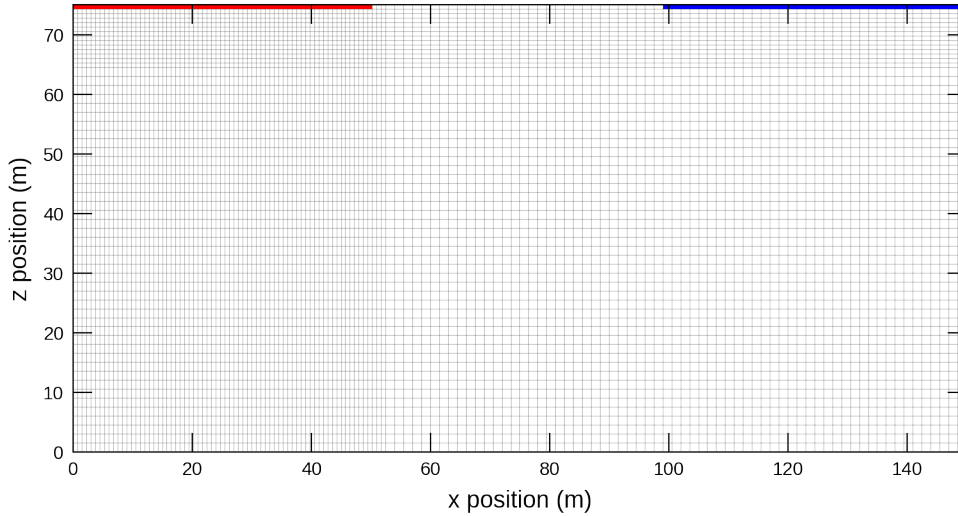


Figure 52–1: Model grid and boundary conditions used for the salt lake problem. Evaporation occurs from the cells highlighted in red. Inflow into the model grid occurs through the constant-head cells shown in blue.

## 52.2 Example Results

The salt lake problem represents a complex system of salt fingers that form, descend, and then coalesce due to the larger-scale flow system. Although the results from MODFLOW 6 are not identical with the results from the Hele-Shaw experiment, MODFLOW 6 seems capable of representing the growth rate and number of salt fingers (fig. 52–2). In the experiment and model, six or seven salt fingers are initially produced, of which only two persist. The rate of descent is similar for both the experiment and model.

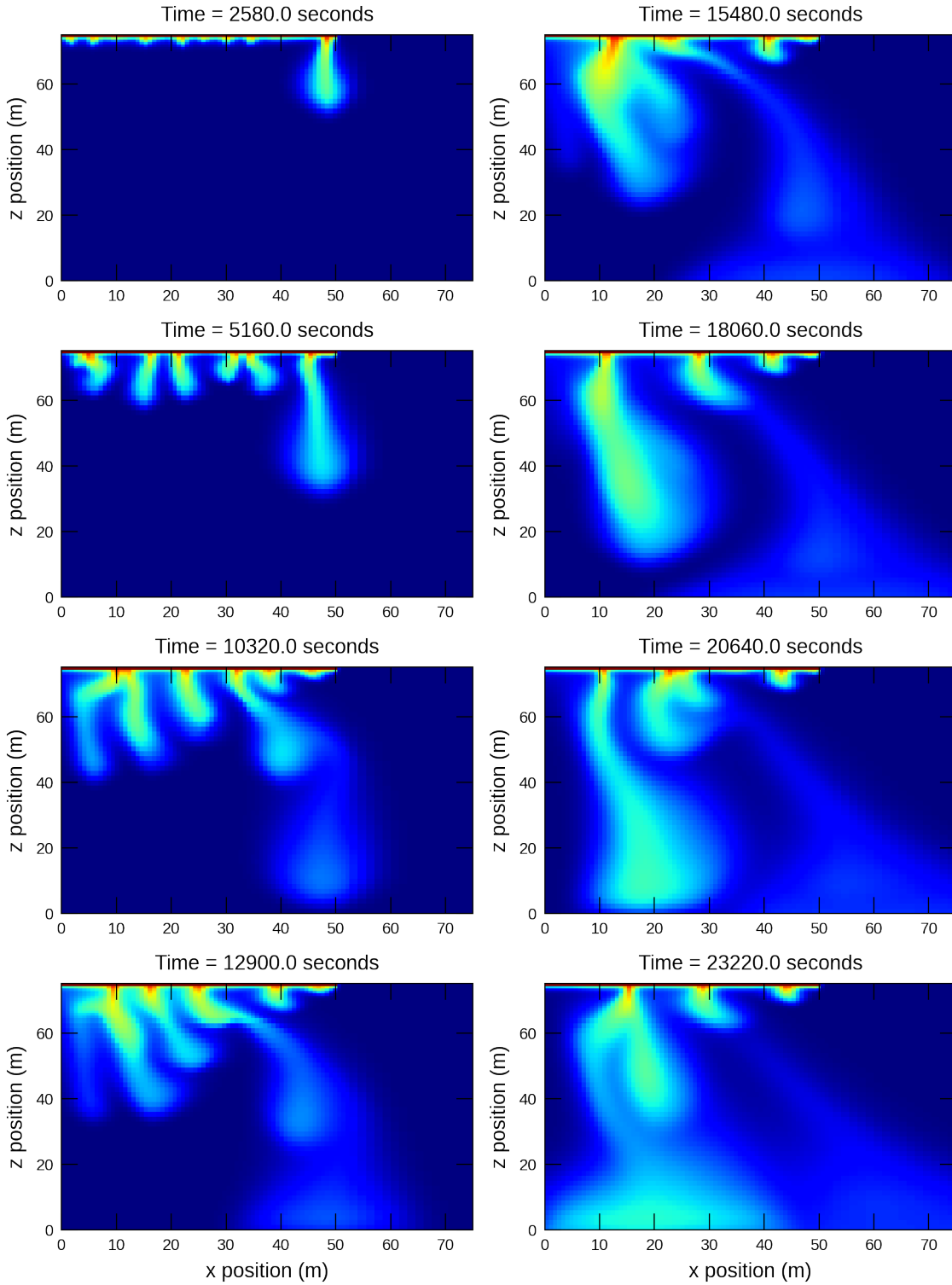


Figure 52–2: Color-shaded plots of concentration simulated by MODFLOW 6 for the [Simmons and others \(1999\)](#) problem involving density-driven groundwater flow and solute transport. Panels can be compared with the panels shown for the Hele-Shaw experiment ([Wooding and others, 1997b](#)) and for the SEAWAT-2000 numerical simulation ([Langevin and others, 2003](#)).

## 53 Rotating Interface Problem

The rotating interface problem was suggested by [Bakker and others \(2004\)](#) as a benchmark test for variable-density groundwater flow models. The problem consists of a box filled with three immiscible fluids that are separated by sharp interfaces. The fluid are initially in an unstable configuration that causes them to rotate. This rotating interface problem was simulated by [Langevin and others \(2003\)](#) using the MODFLOW-based SEAWAT-2000 program. [Bakker and others \(2004\)](#) also shows simulation results for the SWI Package for MODFLOW, MOCDEN3D, and for SEAWAT. There are two cases of this problem, one for symmetric rotational flow and one for asymmetric rotational flow. [Bakker and others \(2004\)](#) and [Langevin and others \(2003\)](#) show both the symmetric and asymmetric versions of the rotating interface problem; however, only the symmetric case is shown here.

### 53.1 Example description

The problem consists of a cross-sectional box filled with three fluids of different densities (fig. 53–1). The initial boundaries between the fluids are not horizontal, and thus, the fluids rotate. [Bakker and others \(2004\)](#) and [Langevin and others \(2003\)](#) compared simulated velocities at the onset of rotation with velocities obtained using an analytical solution. This same comparison with simulated velocities is also shown here for MODFLOW 6.

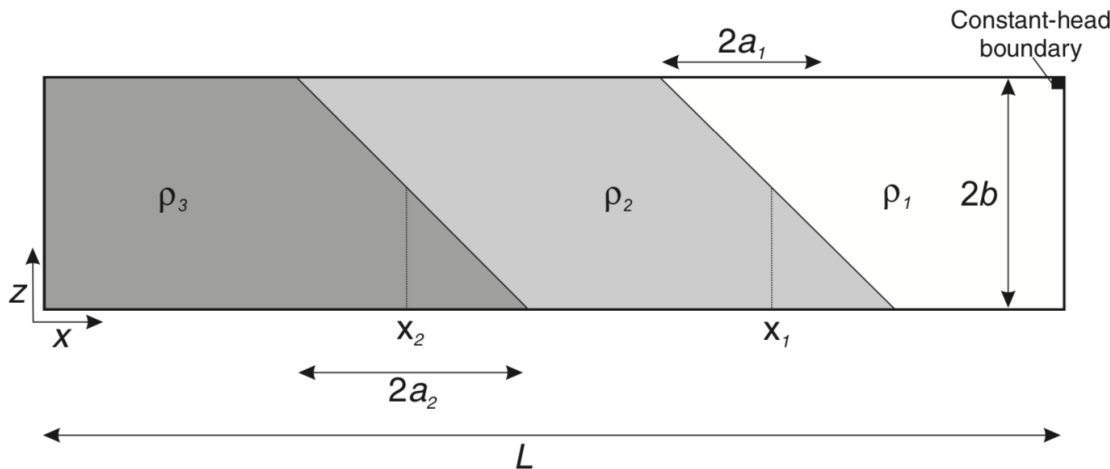


Figure 53–1: Configuration and variable definition for the rotating interface problem. From [Bakker and others \(2004\)](#) and [Langevin and others \(2003\)](#). Note that the constant-head boundary is not needed for the MODFLOW 6 simulation.

Model parameters used for the MODFLOW 6 simulation of the rotating interface problem are shown in table 53–1. The model grid and initial conditions used for the MODFLOW 6 simulation are shown in figure 53–2. The model grid consists of 300 columns and 80 layers. The interfaces between the three fluids are straight and slope down and to the right. The aquifer and fluids are assumed to be incompressible, and the effects of concentration on fluid viscosity are assumed to be negligible. The freshwater hydraulic conductivity is homogeneous and isotropic. Symmetric rotational flow results when the density for the middle fluid (zone 2) is set as the average of the two outer fluids (zone 1 and 3). Although a constant-head condition can be applied to help with convergence for this

problem, it was not required for this MODFLOW 6 simulation. The MODFLOW 6 model was run for 10,000 days divided into 1000 timesteps.

Table 53–1: Model parameters for example ex-gwt-rotate.

Parameter	Value
Number of periods	1
Number of time steps	1000
Simulation time length (d)	10000
Length of box (m)	300
Height of box (m)	40.0
Number of layers	80
Number of rows	1
Number of columns	300
Length of system (m)	150.0
Column width (m)	1.0
Row width (m)	1.0
Layer thickness	0.5
Top of the model (m)	height / 2
Hydraulic conductivity ( $md^{-1}$ )	2.0
Reference density	1000.0
Density and concentration slope	0.7
Density of zone 1 ( $kgm^3$ )	1000.0
Density of zone 2 ( $kgm^3$ )	1012.5
Density of zone 3 ( $kgm^3$ )	1025.0
Concentration of zone 1 ( $kgm^3$ )	0.0
Concentration of zone 2 ( $kgm^3$ )	17.5
Concentration of zone 3 ( $kgm^3$ )	35
Interface extent for zone 1 and 2	40.0
Interface extent for zone 2 and 3	40.0

## 53.2 Example Results

The rotating interface problem represents a complex variable-density flow system that results from an unstable initial density configuration. The analytical solution of [Bakker and others \(2004\)](#) is used here to calculate the horizontal interface velocity as a function of z for the left interface (fig. 53–3). Also shown on figure 53–3 is the horizontal interface velocity as simulated by MODFLOW 6.

During the simulation period, the fluid rotate toward a stable position with lighter water overlying denser water. Although the problem dictates that the fluids are immiscible, the MODFLOW 6 simulation shows some mixing caused by numerical dispersion.

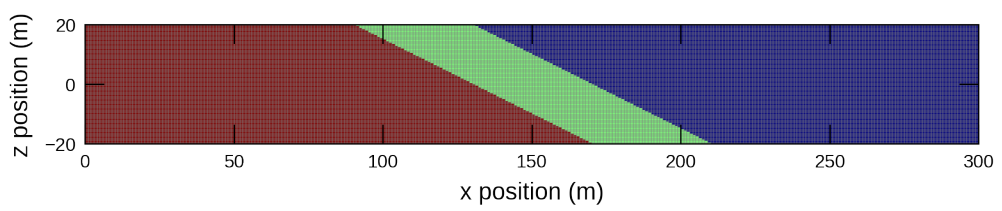


Figure 53–2: Model grid and initial conditions used for the rotating interface problem. Colors represent three different water types.

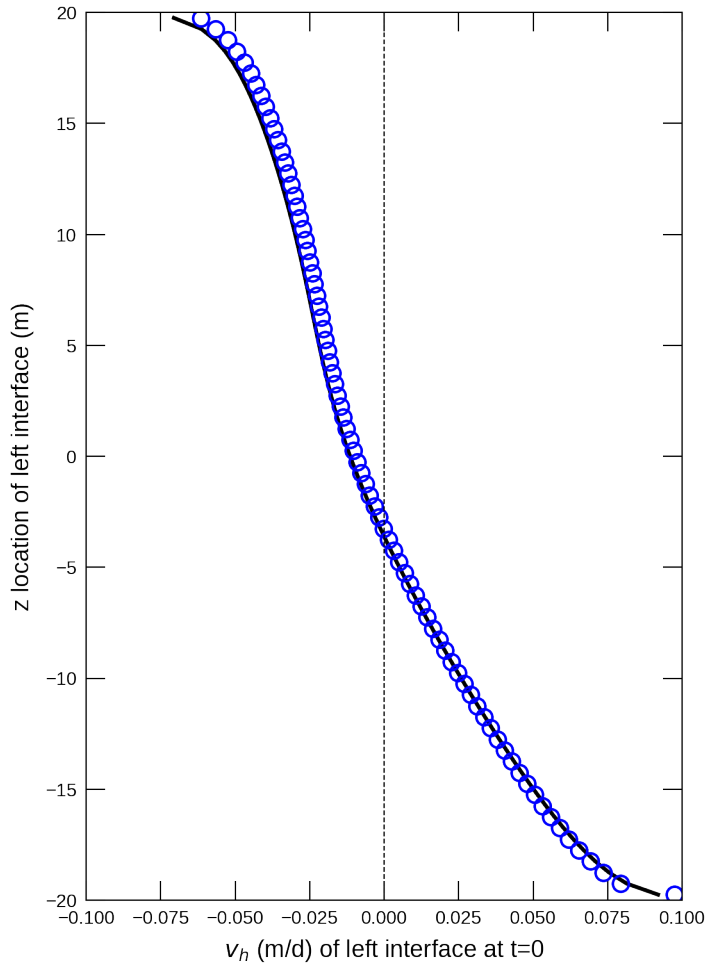


Figure 53–3: Initial horizontal velocity versus vertical position of the left interface, exact (solid), and MODFLOW 6 (blue circles).

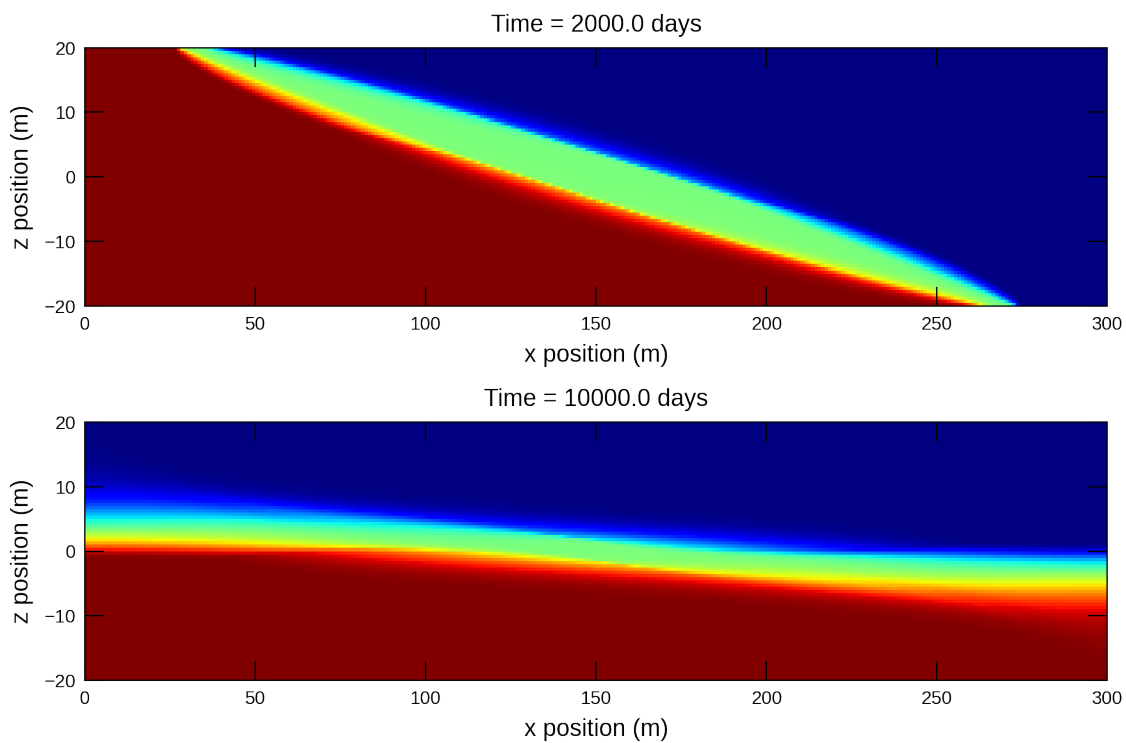


Figure 53–4: Color-shaded plots of concentration simulated by MODFLOW 6 for the [Bakker and others \(2004\)](#) problem involving rotating interfaces.

## 54 Hecht-Mendez 3D Borehole Heat Exchanger Problem

The models presented in [Hecht-Mendez and others \(2010\)](#) apply MT3DMS ([Zheng and Wang, 1999](#)) as a heat transport simulator. Both 2-dimensional and 3-dimensional demonstration problems are presented that explore the use of a “borehole heat exchanger” (BHE), a “closed” geothermal system that uses a heat pump for cycling water and anti-freeze fluids in pipes for mining heat from an aquifer ([Diao and others, 2004](#)). Figure 54–1 depicts the kind of system modeled in this example.

Among the examples presented in [Hecht-Mendez and others \(2010\)](#), this work recreates the 3D example that simulates heat exchange between a BHE and the aquifer it is placed in. Among the suite of examples included in the MODFLOW6-examples.git repo, this is the first one demonstrating the suitability of the GWT model within MODFLOW 6 for simulating saturated zone heat transport. To verify the applicability of MODFLOW 6 as a groundwater heat transport simulator, we compare the MODFLOW 6 solution to established analytical solutions. The analytical solutions are described in more detail below.

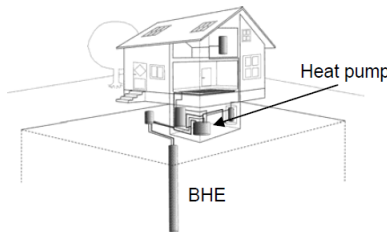


Figure 54–1: Example of a closed ground source heat pump extracting heat beneath a private residence, from [Hecht-Mendez \(2008\)](#).

### 54.1 Example description

Through appropriate substitution of heat-related transport terms into the groundwater solute transport equation, MODFLOW 6 (as is the case with MT3DMS and MT3D-USGS) may be used as a heat simulator for the saturated zone by observing that the heat transport equation,

$$\theta \rho_w C_w \frac{\partial T}{\partial t} + (1 - \theta) \rho_s C_s \frac{\partial T_s}{\partial t} = \operatorname{div} ((k_{T_m} + \theta \rho_w C_w \alpha_h v_a) \operatorname{grad} T) - \operatorname{div} (\theta \rho_w C_w v_a T) + q_h, \quad (54-1)$$

has a similar form as the groundwater solute transport equation,

$$\left[ 1 + \frac{\rho_b K_d}{\theta} \right] \theta \frac{\partial C}{\partial t} = \operatorname{div} [\theta (D_m + \alpha v_a) \operatorname{grad} C] - \operatorname{div} (v_a \theta C) + q_s C_s - \lambda \theta C, \quad (54-2)$$

Originally, [Hecht-Mendez and others \(2010\)](#) included three sub-scenarios for the 3D test model. The first sub-scenario used a Peclet number of 0, indicating no velocity and therefore explored a purely conductive environment. Owing to the fact that ([Hecht-Mendez and others, 2010](#)) did not publish results for this particular sub-scenario and because a 3D analytical solution for a purely conductive problem is not available, neither is this sub-scenario explored here. The two remaining sub-scenarios investigate the effect of groundwater velocity on the heat profile down-gradient of the BHE. To accomplish this goal, Peclet numbers of 1.0 and 10.0 are explored. A Peclet number of 1.0 indicates an approximate balance between convective (i.e., advective) and conductive heat transport.

Meanwhile, a Peclet number of 10.0 represents a convection-dominated transport environment. The parameters used in each of the two scenarios presented are listed in table 54–1.

Table 54–1: Scenario parameters for example ex-gwt-hecht-mendez.

Scenario	Scenario Name	Parameter	Value
1	ex-gwt-hecht-mendez-a	peclet ( <i>unitless</i> )	0.0
		gradient ( <i>m/m</i> )	0.0
		seepagevelocity ( <i>m/s</i> )	0.0
		constantheadright ( <i>m</i> )	14
2	ex-gwt-hecht-mendez-b	peclet ( <i>unitless</i> )	1.0
		gradient ( <i>m/m</i> )	0.00012
		seepagevelocity ( <i>m/s</i> )	3.7e-06
		constantheadright ( <i>m</i> )	13.964
3	ex-gwt-hecht-mendez-c	peclet ( <i>unitless</i> )	10.0
		gradient ( <i>m/m</i> )	0.0012
		seepagevelocity ( <i>m/s</i> )	3.7e-05
		constantheadright ( <i>m</i> )	13.64

The model grid consists of 83 row, 247 columns, and 13 layers. The flow model solves a steady, confined, uniform flow field moving from left to right, as shown in figure 54–2. No flow boundaries exist along the north, south, top, and bottom planes of the model domain. The velocity of the groundwater is varied in each of the two modeled scenarios (recall that scenario A is omitted) by varying the fixed head along the east (right) edge of the simulation domain. Cell lengths and widths vary across the model domain, beginning with  $0.5 \times 0.5 \text{ m}$  grid cells along the perimeter of the model domain, the grid cell resolution is refined to  $0.1 \times 0.1 \text{ m}$  in the vicinity of the BHE. All layers are set to an equal thickness of 1  $\text{m}$ . Additional flow related parameter values are listed in table 54–2.

Table 54–2: Model parameters for example ex-gwt-hecht-mendez.

Parameter	Value
Number of layers	13
Number of rows	83
Number of columns	247
Column width ( <i>m</i> )	varies
Row width ( <i>m</i> )	varies
Simulation width ( <i>m</i> )	200
Simulation length ( <i>m</i> )	300
Layer thickness ( <i>m</i> )	1.0
Top of the model ( <i>m</i> )	13.0
Saturated thickness ( <i>m</i> )	13.0
Horizontal hydraulic conductivity( <i>m/s</i> )	8.0e-3
Vertical hydraulic conductivity( <i>m/s</i> )	8.0e-3
Initial temperature of aquifer ( <i>K</i> )	285.15
Porosity	0.26
Longitudinal dispersivity ( <i>m</i> )	0.50
Ratio of horizontal transverse dispersivity to longitudinal dispersivity	0.1
Ratio of vertical transverse dispersivity to longitudinal dispersivity	0.1
Aquifer bulk density ( <i>kg/m<sup>3</sup></i> )	1961.0
Distribution coefficient ( <i>m<sup>3</sup>/kg</i> )	2.103e-4

Table 54–2: Model parameters for example ex-gwt-hecht-mendez.

Parameter	Value
Simulation time ( <i>seconds</i> ) (= 150 days)	12960000.0

Because the model is 3D, vertical heat transfer among the layers is considered. The BHE is vertically centered within the model grid, located in layers 6, 7, and 8 and is represented by a constant mass loading boundary condition. A negative mass (i.e., heat) loading rate of -60 W/m is constant throughout the simulation period and acts as a heat sink within the aquifer. Justification for the selected heat removal rate is given in [Hecht-Mendez and others \(2010\)](#). Initially, the entire model domain starts out with a constant temperature of 285.15 °K (12 °C). Additionally, groundwater enters the west boundary of the model at 285.15 °K and leaves at the calculated temperature of the groundwater along the east boundary. Heat exchange does not occur with the no-flow boundaries to facilitate comparison with analytical solutions.

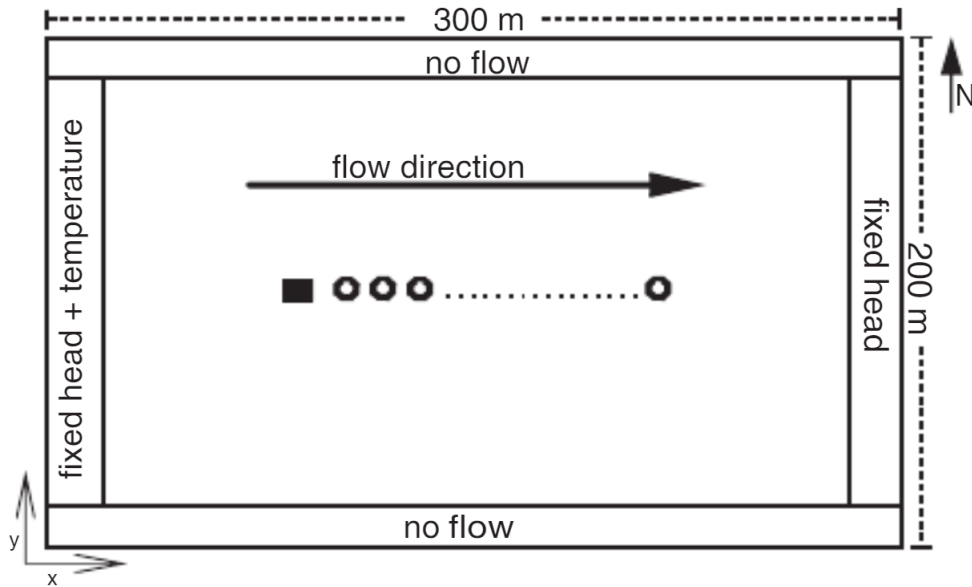


Figure 54–2: Model setup, from [Hecht-Mendez and others \(2010\)](#).

## 54.2 Analytical solutions

For each of the two scenarios simulated here, two points in time are compared to analytical solutions: 10 and 150 days from the start of the simulation representing transient and steady-state conditions. Although simulated results continue to change after 150 days, the magnitude of the change is relatively minor. Thus, 150 days was selected as “close enough” in order to help keep total simulation times to a minimum for obtaining the steady-state solution. Owing to numerical dispersion concerns, the total variation diminishing (TVD) schemes is activated in MODFLOW 6.

The analytical solution for a 3D planar source (or sink) is given in ([Domenico and Robbins, 1985](#)) as,

$$T(x, y, z, t) = \frac{T_o}{8} \cdot erfc \left[ \frac{Rx - v_a t}{2\sqrt{D_x R t}} \right] \cdot \left\{ erf \left[ \frac{(y + \frac{Y}{2})}{2\sqrt{D_y \frac{x}{v_a}}} \right] - erf \left[ \frac{(y - \frac{Y}{2})}{2\sqrt{D_y \frac{x}{v_a}}} \right] \right\} \cdot \left\{ erf \left[ \frac{(z + \frac{Z}{2})}{2\sqrt{D_z \frac{x}{v_a}}} \right] - erf \left[ \frac{(z - \frac{Z}{2})}{2\sqrt{D_z \frac{x}{v_a}}} \right] \right\}, \quad (54-3)$$

$Y$  and  $Z$  are the dimensions of the sink;  $D_x$ ,  $D_y$ , and  $D_z$  are the dispersion coefficients for dispersivities in the  $x$ ,  $y$ , and  $z$  directions, corresponding to  $\alpha_x$ ,  $\alpha_y$ , and  $\alpha_z$ ; and  $T_o$  is the starting temperature where the BHE is located and is given by,

$$T_o = \frac{F}{v_a \theta \rho_w C_w}, \quad (54-4)$$

where  $F$  is the energy extraction per area of the source ( $W/m^2$ ). Along the centerline of the plume, depicted in figure 54-3, the analytical solution under transient conditions reduces to the following,

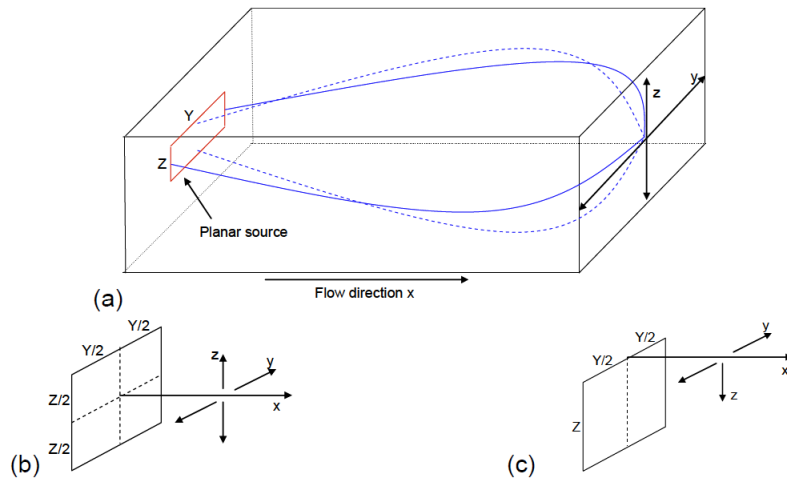


Figure 54-3: (A) Depiction of a heat plume spreading down gradient of a planar source (or sink) for which (Domenico and Robbins, 1985) gives an analytical solution for (B) two spreading directions in both  $y$  and  $z$  and finally (C) two spreading directions in  $y$  and one spreading direction in  $z$ , from Hecht-Mendez (2008).

$$T(x, t) = \frac{T_o}{2} \cdot erfc \left[ \frac{Rx - v_a t}{2\sqrt{D_x R t}} \right] \cdot erf \left[ \frac{Y}{4\sqrt{D_y \frac{x}{v_a}}} \right] \cdot erf \left[ \frac{Z}{4\sqrt{D_z \frac{x}{v_a}}} \right], \quad (54-5)$$

For steady-state conditions, the complementary error function ( $erfc$ ) term may be neglected while the  $\frac{T_o}{2}$  term reduces to  $T_o$ , leaving,

$$T(x) = T_o erf \left[ \frac{Y}{4\sqrt{D_y \frac{x}{v_a}}} \right] \cdot erf \left[ \frac{Z}{4\sqrt{D_z \frac{x}{v_a}}} \right], \quad (54-6)$$

Model results are compared to these analytical solutions.

### 54.3 Example results

Simulated temperature profiles downstream of the BHE are compared to steady-state and transient (10 days after the start of the simulation) analytical solutions in figures 54–4 (Peclet = 1.0) and 54–5 (Peclet = 10.0). In each scenario, simulated results compare well to the expected (i.e., analytical) temperature profiles, with some undersimulation of the temperature down gradient of the BHE shown in figure 54–4 (Peclet number equal to 1.0). Discrepancies between the simulated and analytical results are smaller in the scenario with a Pectlet number of 10.0. Moreover, under highly convective flow regimes, the transient solution is approximately equal to the steady state solution after 10 days, as shown in figure 54–5. These results confirm that MODFLOW 6 may be used as a heat transport simulator in the saturated zone.

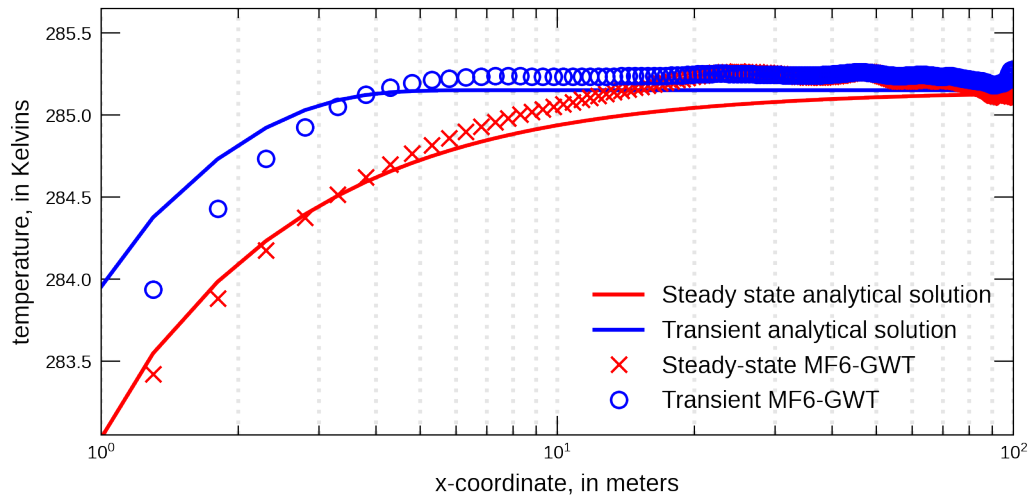


Figure 54–4: MODFLOW 6 simulated temperatures are compared to analytical solutions in a steady flow model with a Peclet number equal to 1.0. For this scenario, thermal transport is roughly split between convective and conductive processes. Temperature profiles are calculated along the centerline down gradient of a planar heat sink as shown in figure 54–3

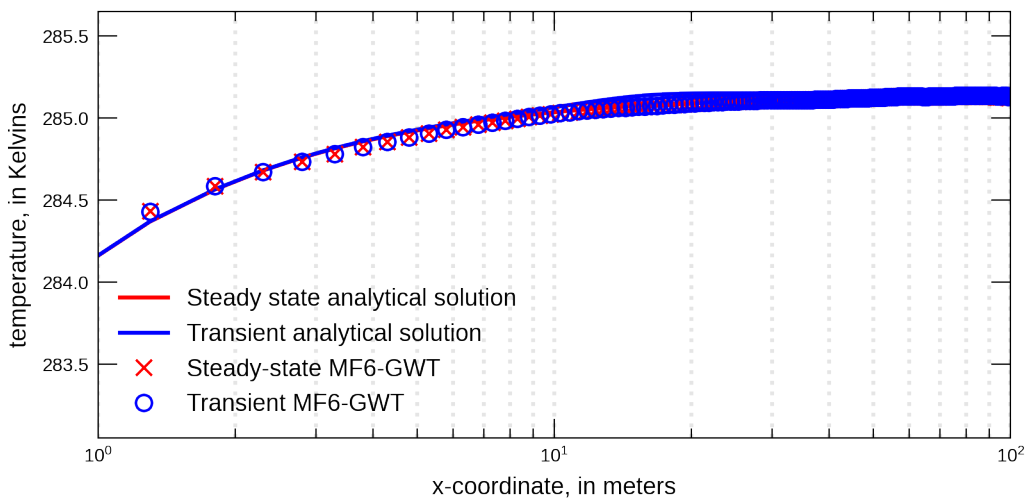


Figure 54–5: MODFLOW 6 simulated temperatures are compared to analytical solutions in a steady flow model with a Peclet number equal to 10.0. For this scenario, thermal transport is dominated by convective transport. Temperature profiles are calculated along the centerline down gradient of a planar heat sink as shown in figure 54–3

## 55 Stallman Problem

[Stallman \(1965\)](#) presents an analytical solution for transient heat flow in the subsurface in response to a sinusoidally varying temperature boundary imposed at land surface. The problem includes heat convection in response to downward groundwater flow. The problem also includes heat conduction through the fully saturated aquifer material. The analytical solution quantifies the temperature variation as a function of depth and time for this one-dimensional transient problem.

This section presents the results of a MODFLOW 6 simulation and the corresponding analytical solution presented by [Stallman \(1965\)](#). The MODFLOW 6 simulation includes a GWF Model and a GWT Model. Although the GWT Model was developed for solute transport, input parameters can be modified so that the GWT Model can approximate heat transport.

### 55.1 Example Description

The example problem presented here consists of a vertical profile from land surface (0 m) to a depth of 60 m. There are 120 model cells used to represent the profile. Groundwater flow is simulated using steady-state conditions with the top and bottom cells assigned as constant heads. The head in the top cell is given a value of 60 m and the head in the bottom cell is set to 59.701801 m. This results in a constant downward flow velocity that remains constant during the simulation.

The model simulates 10 sinusoidal periods over a total duration of 10 years (wave length = 1 year) with a total of 600 stress periods and 6 time steps per period (time step = 1 day).

For the GWT Model setup, an ambient temperature of 10 °C is given as the initial condition. The temperature variation at the surface boundary is 5 °C and varies with time according to  $T_{BC} = 10 + 5\sin(2\pi t/T)$ , where  $t$  is the current time and  $T$  is the wave length of one year. Solute analogs for the heat transport problem were calculated from thermal parameters. The diffusion coefficient is given as 1.02882E-06 ( $m^2/s$ ), and linear sorption is activated with porosity = 0.35, bulk density = 1709.5 ( $kg/m^3$ ) and the distribution coefficient = 0.000191663. Model parameters used for this example are shown in Table 55–1.

Table 55–1: Model parameters for example ex-gwt-stallman.

Parameter	Value
Number of periods	600
Number of time steps	6
Simulation time length (s)	525600
Number of layers	120
Number of rows	1
Number of columns	1
Length of system (m)	60.0
Column width (m)	1.0
Row width (m)	1.0
Layer thickness	ranges from 0.1 to 1
Top of the model (m)	60.0
Hydraulic conductivity ( $ms^{-1}$ )	1.0e-4
Porosity (unitless)	0.35
Longitudinal dispersivity (m)	0.0
Transverse dispersivity (m)	0.0
Diffusion coefficient ( $ms^{-1}$ )	1.02882e-06
Ambient temperature (°C)	10
Temperature variation (°C)	5
Bulk density ( $kg/m^3$ )	2630

Table 55–1: Model parameters for example ex-gwt-stallman.

Parameter	Value
Distribution coefficient (unitless)	0.000191663

## 55.2 Example Results

The simulated temperature profile from MODFLOW 6 shows good agreement with the temperature profile from the Stallman analytical solution for a simulation time of 9.02 yr (figure 55–1).

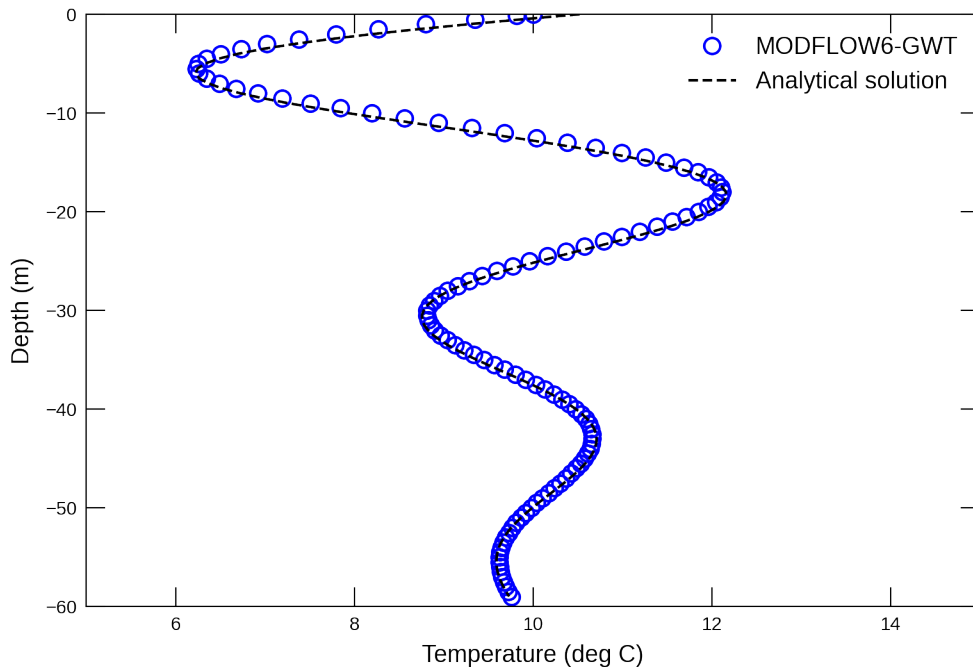


Figure 55–1: Comparison of the temperature profile simulated with MODFLOW 6 (blue circles) and calculated with the [Stallman \(1965\)](#) analytical solution (dashed line).

## 56 Synthetic Valley Problem

This example is based on a flow and transport problem described in [Hughes and others \(2023\)](#). The Synthetic Valley examples represents a developed alluvial valley surrounded by low permeability bedrock. The model includes the Blue Lake and Straight River surface water features (figure 56–1). The upper two layers represent an unconfined aquifer, the third layer represents a confining unit, and the lower three layers represent the lower aquifer unit. The confining unit only exists in the northern part of the model domain as shown in figure 56–1.

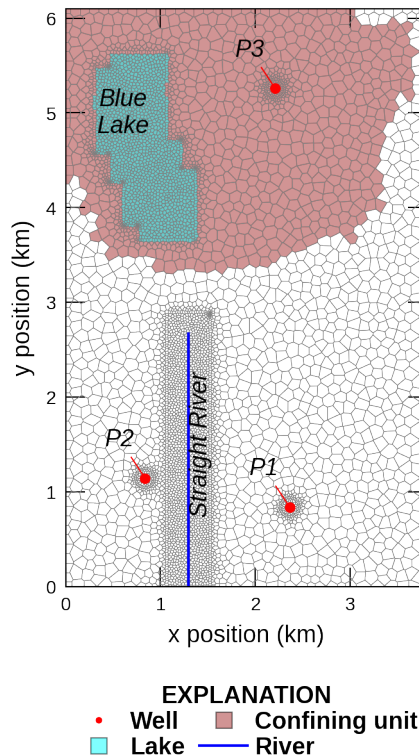


Figure 56–1: Map showing the Voronoi grid used to discretize the model domain and the location of Blue Lake, Straight River, and the areal extent of the confining unit separating the upper and lower aquifer units for the Synthetic Valley example in [Hughes and others \(2023\)](#).

### 56.1 Example description

The 6,096 m x 3,810 m model domain is discretized using a Voronoi grid, with 6,343 active cells per layer, and the discretization by vertices (DISV) package (figure 56–1). The model grid was refined

within Blue Lake, around Straight River, and around pumping wells P1, P2, and P3. The parameters used for this problem are listed in table 56–1.

Table 56–1: Model parameters for example ex-gwt-synthetic-valley.

Parameter	Value
Simulation length ( $d$ )	10957.5
Number of transport time steps	60
Number of layers	6
Rainfall ( $m/d$ )	0.0025
Potential evaporation ( $m/d$ )	0.0019
SFR package length unit conversion	1.0
SFR package time conversion	86400.0
Stream width ( $m$ )	3.048
Stream bed thickness ( $m$ )	0.3048
Stream Manning's roughness coefficient	0.030
Lake bed leakance ( $1/d$ )	0.0013
LAK package length unit conversion	1.0
LAK package time conversion	86400.0
Drain vertical hydraulic conductivity ( $m/d$ )	0.03048
Drain bed thickness ( $m$ )	0.3048
Drain linear scaling depth ( $m$ )	0.3048
Longitudinal dispersivity ( $m$ )	75.0
Transverse horizontal dispersivity ( $m$ )	7.5
Aquifer porosity (unitless)	0.2
Confining unit porosity (unitless)	0.4

In this example, both groundwater flow (Langevin and others, 2017a) and solute transport (Langevin and others, 2022) are simulated. To better represent solute transport, the lower aquifer has been discretized into three layers. Confining units have to be explicitly simulated in MODFLOW 6, therefore, a total of six layers are simulated. The bottom of layers 1, 2, 3, and 4 were set to constant values of -1.53, -15.24, -15.55 and -30.48 m, respectively. Model layer 3 represents the confining unit and is relatively thin (0.3 m). The IDOMAIN concept (Langevin and others, 2017a) was used to eliminate cells in model layer 3 (by setting IDOMAIN=-1) where the confining unit does not exist. In these areas, the thickness of layer 3 was set to zero and IDOMAIN was set to -1, which marks these cells in layer 3 as “vertical pass through cells” and results in cells in layer 2 being directly connected to cells in layer 4.

The bottom of the model (layer 6) is based on Hill and others (1998) and the bottom of layer 5 was specified to be half the distance between the bottom of layers 4 and 6. The top of the model was constructed from topographic contours developed for the model that was used as the starting point for Hill and others (1998); the top of the model is shown in Figure 56–2A. The top of the model and the bottom of layer 6 were resampled from the data used in Hill and others (1998).

The horizontal hydraulic conductivity was discretized into five zones with values of 45.72, 50.29, 60.96, 83.82, and 121.92 m/d; the lowest hydraulic conductivity zone was located south of Blue Lake and the highest hydraulic conductivity zone was located beneath Blue Lake. The vertical hydraulic conductivity in the upper and lower aquifer was specified to be one quarter of the horizontal hydraulic conductivity. The horizontal and vertical hydraulic conductivity in the confining unit was set equal to  $9.14 \times 10^{-4}$  m/d. The horizontal and vertical hydraulic conductivity were resampled from the data used in Hill and others (1998).

For the groundwater transport model, the porosity, longitudinal dispersivity, and transverse dispersivity were set to values specified in table 56–1. For the transport model, the Total Variation

Diminishing scheme available in the GWT model ([Langevin and others, 2022](#)) was used to simulate advection. Molecular diffusion was not represented.

Straight River is simulated using the streamflow routing (SFR) package, and Blue Lake is simulated using the LAK package (figure [56–1](#)). Straight River was discretized into 108 SFR reaches. The bed thickness and width of each SFR reach were set to values specified in table [56–1](#). The leakance for each SFR reach was calculated using the bed thickness, reach width, and reach length in each cell and based on a total Straight River conductance of  $50,971.72 \text{ m}^2/\text{d}$ . Specified rainfall and potential evaporation rates specified in table [56–1](#) were defined for each Straight River reach.

Blue Lake was simulated as a lake on top of the model grid and only had vertical connections to 1,406 cells in the underlying upper aquifer (model layer 1). A bed leakance of  $0.0013 \text{ l/d}$  was specified for each cell connected to Blue Lake. Specified rainfall and potential evaporation rates specified in table [56–1](#) were defined for Blue Lake.

Drain (DRN) cells were specified in each cell in model layer 1 that was not connected to Blue Lake to prevent water levels from exceeding the top of the model. The conductance of each DRN cell was based on the horizontal cell area and the drain bed thickness and vertical hydraulic conductivity specified in table [56–1](#). Linear scaling of the drainage conductance was applied to improve model convergence and ranged from  $0 \text{ m}^2/\text{d}$  when groundwater levels were greater than or equal to  $0.3048 \text{ m}$  below the top of the model to the specified conductance when groundwater water levels were greater than or equal to the top of the model.

Uniform recharge and potential evapotranspiration rates were specified using the recharge (RCH) and evapotranspiration (EVT) packages, respectively, and were equal to the rates specified in the SFR and LAK packages. The EVT surface was specified to be the top of the model and the EVT extinction depth was specified to be 1 m.

Pumping rates for wells P1, P2, and P3 were  $-7,600$ ,  $-7,600$ , and  $-1,900 \text{ m}^3/\text{d}$ , respectively. All groundwater pumping was extracted from model layer 6.

Transport was not simulated in the LAK and SFR packages. Instead, a specified concentration condition with a concentration of  $1.0 \text{ mg/L}$  was specified for Blue Lake. All other stress packages were assumed to have a concentration of  $0 \text{ mg/L}$ .

An initial head of 11 m was specified for every cell. An initial stage of 3.44 m was specified for Blue Lake. An initial concentration of  $0 \text{ mg/L}$  was specified for every cell in the transport model.

## 56.2 Example Results

The groundwater flow model used the Newton-Raphson Formulation with Newton under-relaxation to improve convergence. The groundwater flow and transport models used the Bi-conjugate Stabilized linear accelerator and simple solver settings.

The groundwater flow and transport models were run for a total of 30 years. The groundwater flow model used a single steady-state time step and groundwater flow results were used to run the transport model with a total of 60 time steps with a constant length of 182.625 days.

Simulated heads and vectors of specific discharge in model layer 1 are shown in figure [56–2B](#). Specific discharge is greatest on the east side of Blue Lake and in the vicinity of the three pumping wells and Straight River.

Simulated concentrations at the end of 30-years in all six model layers are shown in figure [56–3](#). Simulated concentrations are highest beneath Blue Lake in model layer 1 and do not vary much in model layers 1 and 2. Simulated concentrations in model layer 3 are limited to the extent of the confining unit because the remaining cells in the layer are defined to be “vertical pass through cells”. The lateral extent of the solute plume does not vary much south of Blue Lake because of the lack of confinement in these areas.

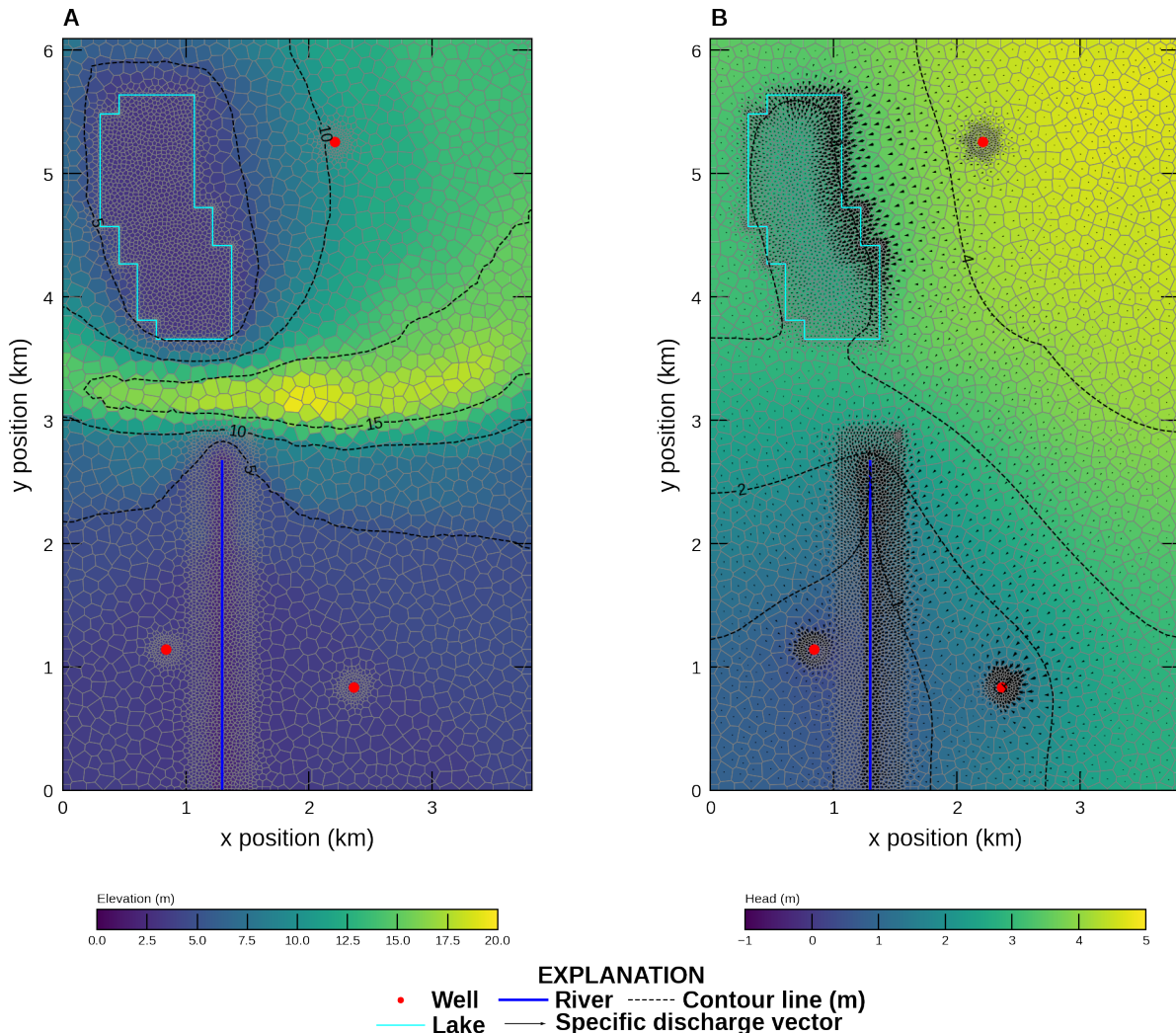


Figure 56-2: Color shaded plot of (A) topography and (B) simulated steady-state heads and specific discharge rates in model layer 1.

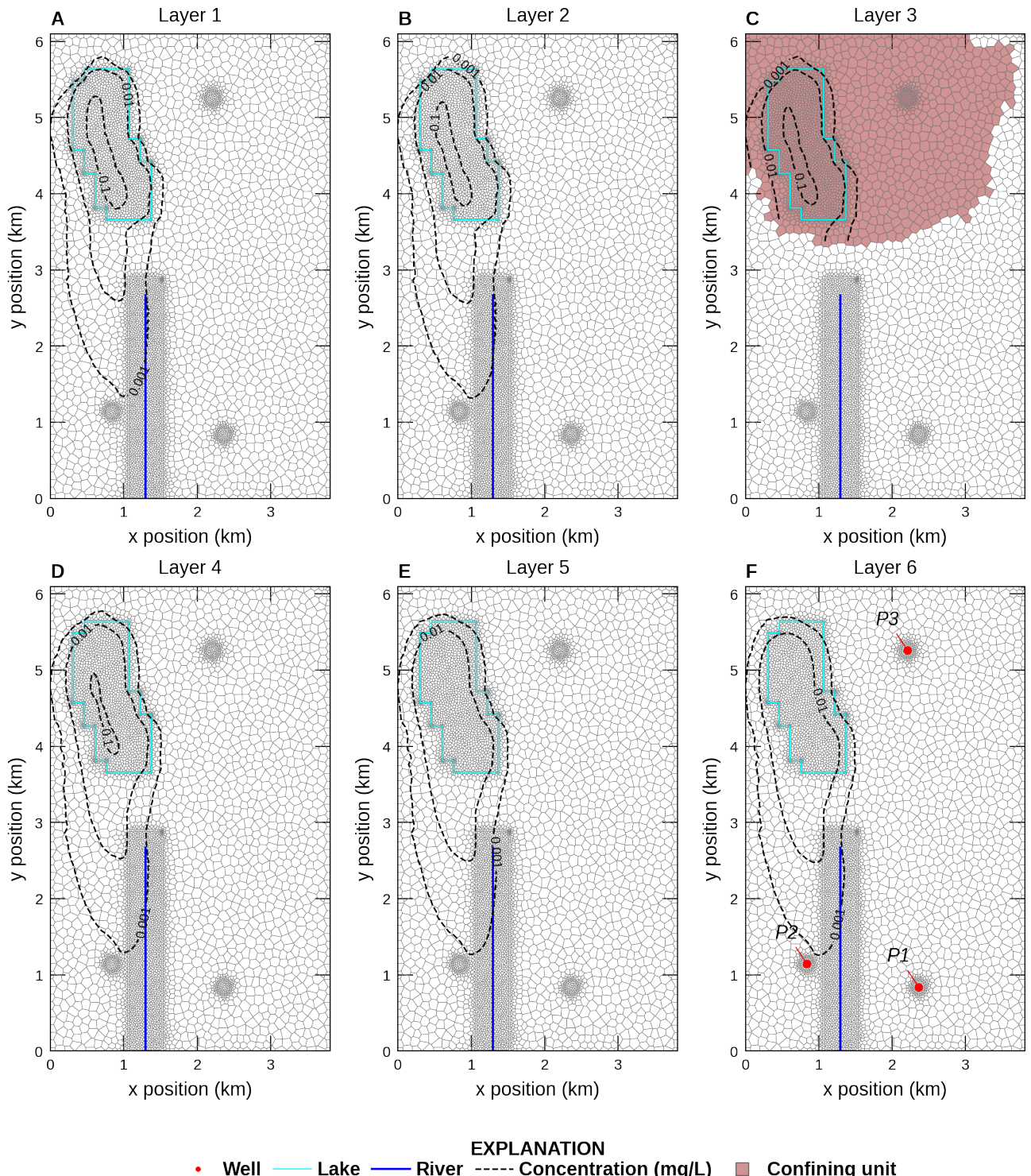


Figure 56–3: Contours of concentrations at the end of 30 years in model layer (A) 1, (B) 2, (C) 3, (D) 4, (E) 5, and (F) 6. The extent of the confining unit in model layer 3 is also shown on (C).

## 57 Radial Groundwater Flow Model

Radial groundwater models simulate and analyze the flow of groundwater in a radial coordinate system. The purpose of radial groundwater models is to understand the behavior of groundwater flow in response to groundwater extraction or to estimate aquifer properties. Radial groundwater models are axisymmetric with the constant aquifer properties defined in circular radial bands and vertical layers. The radial grid's innermost band is cylinder (single radius) and typically contains a groundwater well. Extending outward, the subsequent radial bands are ring shaped that are bound by an inner and outer radius (hollow cylinder). This example demonstrates the capability of the Unstructured Discretization (DISU) Package to represent a radial groundwater flow model.

This example replicates in MODFLOW 6 using FloPy the “Pumping Well” radial model described in [Bedekar and others \(2019\)](#). The original model used MODFLOW-USG to demonstrate that it is possible to use unstructured grid cells to simulate a banded, radial model. The MODFLOW 6 results are compared with the [Neuman \(1974\)](#) analytical solution for radial, unconfined flow with a partially penetrating well.

### 57.1 Example description

The example consists of a multi-layer, radial model representing an unconfined, homogeneous, and isotropic aquifer with a partially penetrating well. The radial grid represents the horizontal direction and is composed of 22 radial bands that vary in outer radius from 0.25 ft to 2000 ft (fig. 57–1A). Radial band 1 is a cylinder with a radius 0.25 ft and radial band 22 is a hollow cylinder with an inner and outer radius of 1500 ft and 2000 ft, respectively. The vertical direction consists of 25 uniform-layers that are 2 ft thick; with a total aquifer thickness of 50 ft. A partially penetrating well is located at radial band 1 (fig. 57–1B) and extracts water from the bottom 10 ft (layer 21 to 25) at a rate of 4000 ft<sup>3</sup>/day. The remaining model properties are summarized in table 57–1.

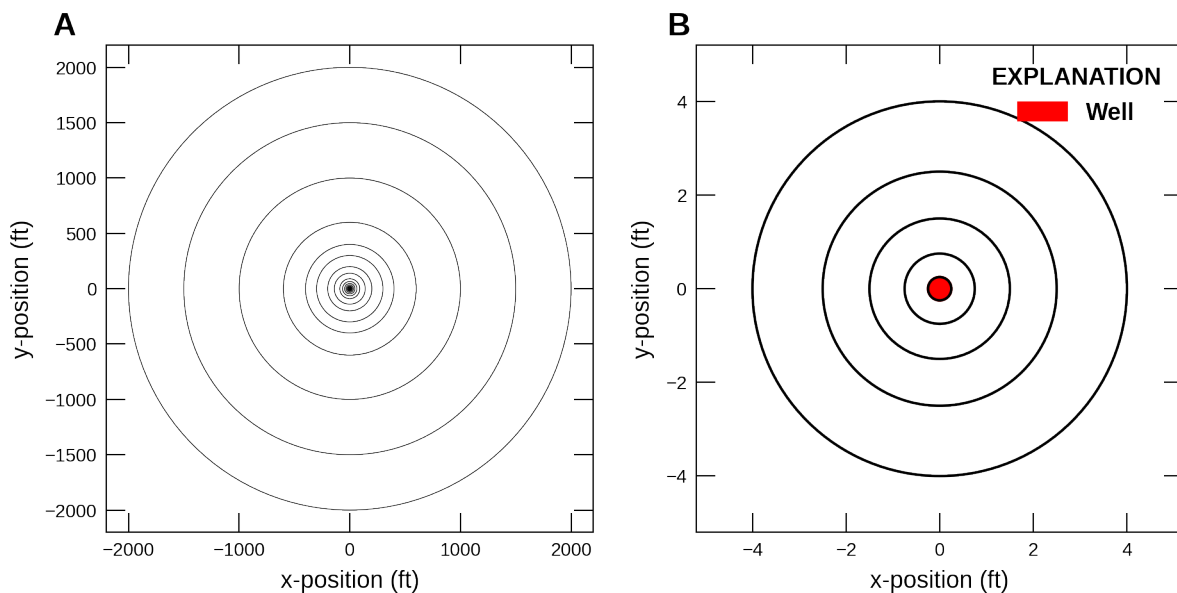


Figure 57–1: Plan view of the two-dimensional, radial model grid. *A*, plan view of entire model grid containing 22 radial bands, and *B*, plan view of the 5 innermost radial bands and the well location is marked in red.

The model simulation evaluates drawdown in response to pumping at an observation point. The simulation time frame is composed of 1 stress period of length 10 *days*, subdivided into 24 time steps with a multiplier of 1.24. The aquifer is initially saturated with an initial water level set to 50 *ft*, which is the reference level for drawdown. Observations are made at a radial distance of 40 *ft* (radial band 12) at the model's top (1 *ft* depth; layer 1), middle (25 *ft* depth; layer 13), and bottom (49 *ft* depth; layer 25) for every time step.

Table 57–1: Model parameters for example ex-gwf-radial.

Parameter	Value
Number of periods	1
Number of time steps	24
Simulation total time ( <i>day</i> )	10
Number of layers	25
Number of radial direction cells (radial bands)	22
Initial water table elevation ( <i>ft</i> )	50.0
Top of the radial model ( <i>ft</i> )	50.0
Base of the radial model ( <i>ft</i> )	0.0
Thickness of each radial layer ( <i>ft</i> )	2.0
Outer radius of each radial band ( <i>ft</i> )	0.25 to 2000
Horizontal hydraulic conductivity ( <i>ft/day</i> )	20.0
Vertical hydraulic conductivity ( <i>ft/day</i> )	20.0
Specific storage ( <i>1/day</i> )	1.0e-5
Specific yield (unitless)	0.1
Well screen elevation ( <i>ft</i> )	0.0 to 10
Well radial band location (unitless)	1
Well pumping rate ( <i>ft</i> <sup>3</sup> / <i>day</i> )	-4000.0
Observation distance from well ( <i>ft</i> )	40
“Top” observation elevation ( <i>ft</i> )	1
“Middle” observation depth ( <i>ft</i> )	25
“Bottom” observation depth ( <i>ft</i> )	49

## 57.2 Radial Setup with Unstructured Discretization (DISU)

To represent a radial grid, the DISU defines cell connectivity based on radial band circumference, circular areas, and the radial distance between bands. All radial bands have the same properties for each layer. That is, each layer's radial band has the same radius, circumference and area and only shifts the top and bottom elevation downward by 2 *ft*. A maximum of 4 connections is possible for any given node; the connections represent flow towards the inner band, to the outer band, upward flow, and downward flow.

Node numbers are assigned based on the radial band number (R), layer number (L), and the total number of radial bands (nradial) as described in equation 57–1.

$$\text{node} = \text{nradial} \cdot (L - 1) + R \quad (57-1)$$

To make the following more compact, radial band and layer numbers are presented as “(R, L)” pairs. The first node is (1, 1) and is a cylinder that is connected to the next radial band, (2, 1), and the cylinder beneath it, (1, 2). The nodal connections (JA) for node 1 is then nodes 2 and 23. The second node, (2, 1), is connected to the inner band at (1, 1), an outer band at (3, 1), and the downward band (2, 2). The JA connections for node 2 is then nodes 1, 3, and 24. Similarly node 24 is located at (2, 2) is connected to the inner band (1, 2), outer band (3, 2), upward band (2, 1), and downward band (2, 3). The JA connections for node 24 is then nodes 23, 25, 2, and 46, respectively.

The input requires specifying the plan view, cell surface area. This is calculated using equation 57–2.

$$\text{AREA}_j = \pi (r_j^2 - r_{j-1}^2) \quad (57-2)$$

where  $r$  is the outer radius for radial band  $j$  and  $r_0 = 0$ . The surface area for any radial band is the same for all layers.

The connection length (CL12) depends on if the cell connection is in the vertical or radial direction. Vertical connections are half the distance between the top and bottom elevation of the cell. Since all cells have a thickness of 2 ft, CL12 is 1 ft for all vertical connections. The radial direction has a CL12 for radial band 1 equal to its outer radius. For the rest of the radial bands CL12 is same for both the inner and outer directions and is half the distance between the inner and outer radius. That is,  $\text{CL12}_j = 0.5(r_j - r_{j-1})$ , where  $r$  is the outer radius for radial band  $j$  and  $r_0 = -r_1$ .

The input HWVA is the plan view area ( $\text{ft}^2$ ) for vertical connections and the width (ft) perpendicular to flow for horizontal connections. Since all layers have the same radii, the vertical  $\text{HWVA}_j$  is equal to  $\text{AREA}_j$ . The horizontal HWVA width is equal the radial band's circumference ( $2\pi r$ ) that the flow passes through. For flow towards the inner band,  $\text{HWVA}_{j, \text{inner}} = 2\pi r_{j-1}$ , and towards the outer band,  $\text{HWVA}_{j, \text{outer}} = 2\pi r_j$ .

To assist with the FloPy setup a script called `get_disu_radial_kwarg.py` is provided. This script provides the function `get_disu_radial_kwarg` that assembles the nodal connections and aforementioned properties (JA, AREA, CL12, HWVA). The function input expects the number of layers, number of radial bands, outer radius for each band, surface elevations, and layer thicknesses.

### 57.3 Example Results

Figures 57–2 and 57–3 present the simulated head and dimensionless drawdown results of the radial model with an initial head of 50 ft and 4000  $\text{ft}^3/\text{d}$  pumping for 10 days. In the figures the circles represent the MODFLOW 6 (MF6) solution at the end of the time step and the lines are the analytical solution from Equation 17 in Neuman (1974). The analytical solution uses dimensionless time and drawdown, so the results are presented in both head (MF6 native solution; fig. 57–2) and dimensionless drawdown (analytical native solution; fig. 57–3). Dimensionless time with respect to specific yield and dimensionless drawdown are defined as:

$$t_y = \frac{Tt}{S_y r^2} \quad (57-3)$$

$$s_d = \frac{4\pi T s}{Q} \quad (57-4)$$

where  $t_y$  is dimensionless time with respect to specific yield (-),  $T$  is the initial, radial direction transmissivity ( $\text{ft}^2/\text{d}$ ),  $t$  is the simulation time (d),  $S_y$  is the specific yield (-),  $r$  is the radial distance from the well to the observation point (ft),  $s_d$  is dimensionless drawdown (-),  $s$  is the drawdown from the initial water table elevation (ft), and  $Q$  is the pumping rate ( $\text{ft}^3/\text{d}$ ).

In figure 57–2, the MF6 head compare very well to the analytical solution. In figure 57–3, the MF6 dimensionless drawdown deviates from the analytical solution initially and then yields similar results. This deviation is more apparent in the first four circles (from the left) because of the small numbers presented on a log-log plot. These errors occur in the first 50 seconds of the 10-day simulation and are negligible in comparison to the rest of the simulation.

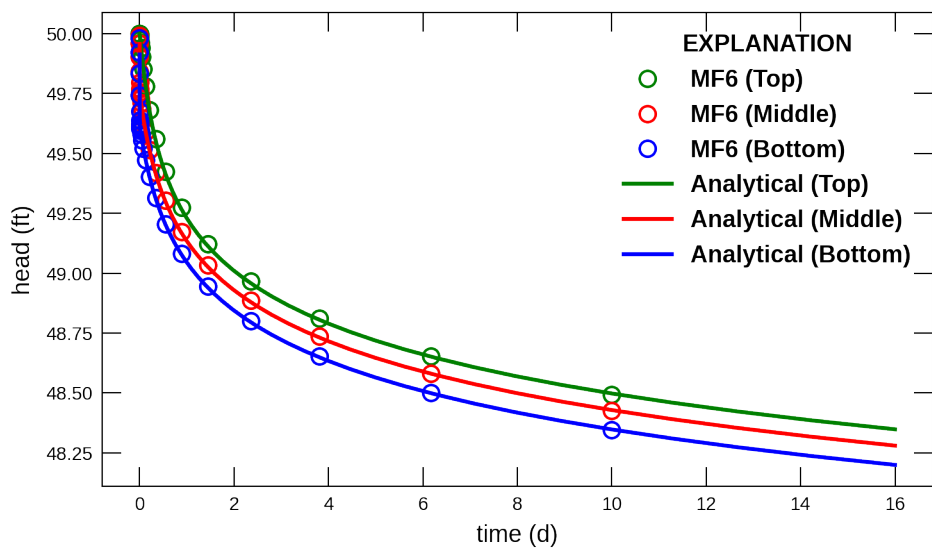


Figure 57–2: Radial model analytical solution (Neuman, 1974) and simulated groundwater (MF6) head 40 ft from the well (radial band 12) at the model's Top (1 ft depth; layer 1), Middle (25 ft depth; layer 13), and Bottom (49 ft depth; layer 25).

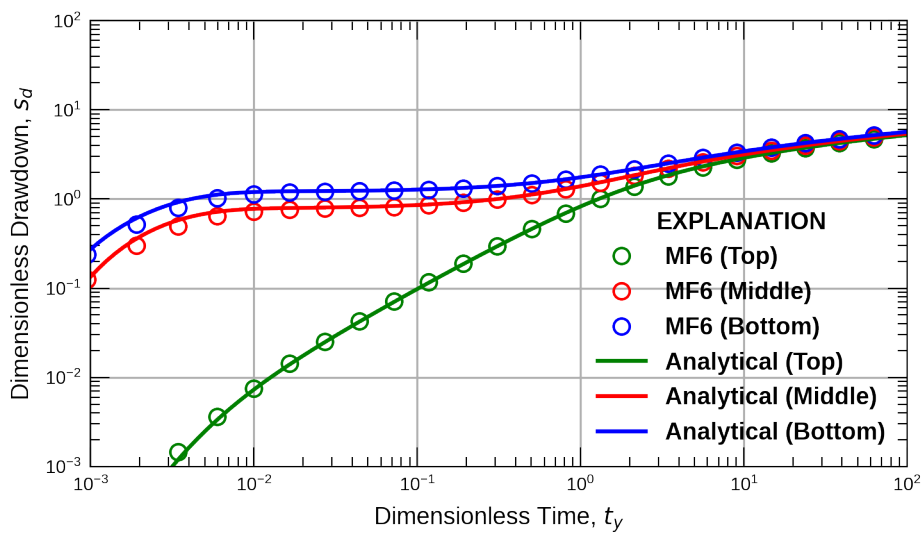


Figure 57–3: Radial model analytical dimensionless solution (Neuman, 1974) and simulated groundwater (MF6) dimensionless drawdown 40 ft from the well (radial band 12) at the model's Top (1 ft depth; layer 1), Middle (25 ft depth; layer 13), and Bottom (49 ft depth; layer 25).

## 58 Curvilinear Groundwater Flow Model

MODFLOW 6 vertex grids specify a set of vertices that define the edges of each model cell. Two (x, y) vertex pairs are connected in the horizontal plane by a straight line to represent edges of model cells. A set of vertices can represent a curvilinear grid ([Romero and Silver, 2006](#)) by a piecewise linear representation of the curved surfaces. Curvilinear grids can represent a radial model or replicate a curved flow domain with a major change in the dominant flow path. For example, a 90° curvilinear grid can change the dominant flow path from the x-direction to the y-direction along the same model “column”. This example demonstrates the capability of the Discretization by Vertices (DISV) Package to represent a curvilinear grid.

Using FloPy this example replicates the steady-state, curvilinear model described in [Romero and Silver \(2006\)](#) using the grid they show in Figure 3d. The original model used a modified MODFLOW-88 ([McDonald and Harbaugh, 1988](#)) code to demonstrate the ability of MODFLOW to simulate curvilinear models by distorting the model grid to use trapezoids. The results were validated against the analytical solution presented in equation 5.4 in [Crank \(1975\)](#).

### 58.1 Example Description

The example consists of a steady-state, 90° curvilinear model representing a single layer, confined, homogeneous, and isotropic aquifer (fig. 58–1). The positive x-axis represents the 0° angle and the positive y-axis is the 90° angle. The curvilinear model is discretized by radial bands and columns. The radial bands are a piecewise linear approximation of a curve and the columns are the discretization within a radial band.

The radial band numbering starts at 1 for the inner-most band and the column number starts at 1 for the column closest to the x-axis. For MODFLOW 6, the DISV package identifies cells by the CELL2D number (*icell2d*). For this example, *icell2d* starts at radial band 1, column 1 and increases sequentially in the column direction, then the radial direction (fig. 58–1).

All vertices between two radial bands have the same radial distance from the axis origin. The inner- and outer-most vertices have a radial distance of 4 ft and 20 ft, respectively. The radial distance between band vertices is 1 ft for a total of 16 curvilinear radial bands. The radial bands are discretized in 5° increments for a total of 18 columns per band. The single model layer is 10 ft thick with a transmissivity of 0.19 ft<sup>2</sup>/day. A constant head boundary condition is assigned to the inner- and outer-most radial bands at 10 ft and 3.334 ft, respectively. The remaining model properties are summarized in table 58–1.

Table 58–1: Model parameters for example ex-gwf-curvilinear-90.

Parameter	Value
Simulation Type	Steady-State
Number of periods	1
Number of time steps	1
Number of layers	1
Number of radial direction cells (radial bands)	16
Number of columns in radial band (ncol)	18
Degree angle of column 1 boundary	0
Degree angle of column ncol boundary	90
Degree angle width of each column	5
Model inner radius (ft)	4
Model outer radius (ft)	20
Model radial band width (ft)	1

Table 58–1: Model parameters for example ex-gwf-curvilinear-90.

Parameter	Value
Top of the model (ft)	10.0
Base of the model (ft)	0.0
Horizontal transmissivity ( $ft^2/day$ )	0.19
Horizontal hydraulic conductivity ( $ft/day$ )	0.019
Inner Constant Head Boundary (ft)	10
Outer Constant Head Boundary (ft)	3.334

## 58.2 Example Results

The curvilinear vertex model is solved using one, steady state, stress period and is compared to the analytical solution (eqn. 5.4 in [Crank \(1975\)](#)). Figure 58–2 presents the MODFLOW 6 simulated head and flow lines for all model cells. Figure 58–3 presents the head solution along column 9 from all radial bands ( $icell2d: 9, 27, 45, \dots, 261, 279$ ) and compares it to the analytical solution. The MODFLOW 6 head solution occurs at the cell center rather than the edge, so the radial distance of the inner most head solution is 4.5 ft instead of 4 ft. The MODFLOW 6 results are in agreement with the analytical solution with a relative error of 0.05% and root mean square error of 0.0037 ft.

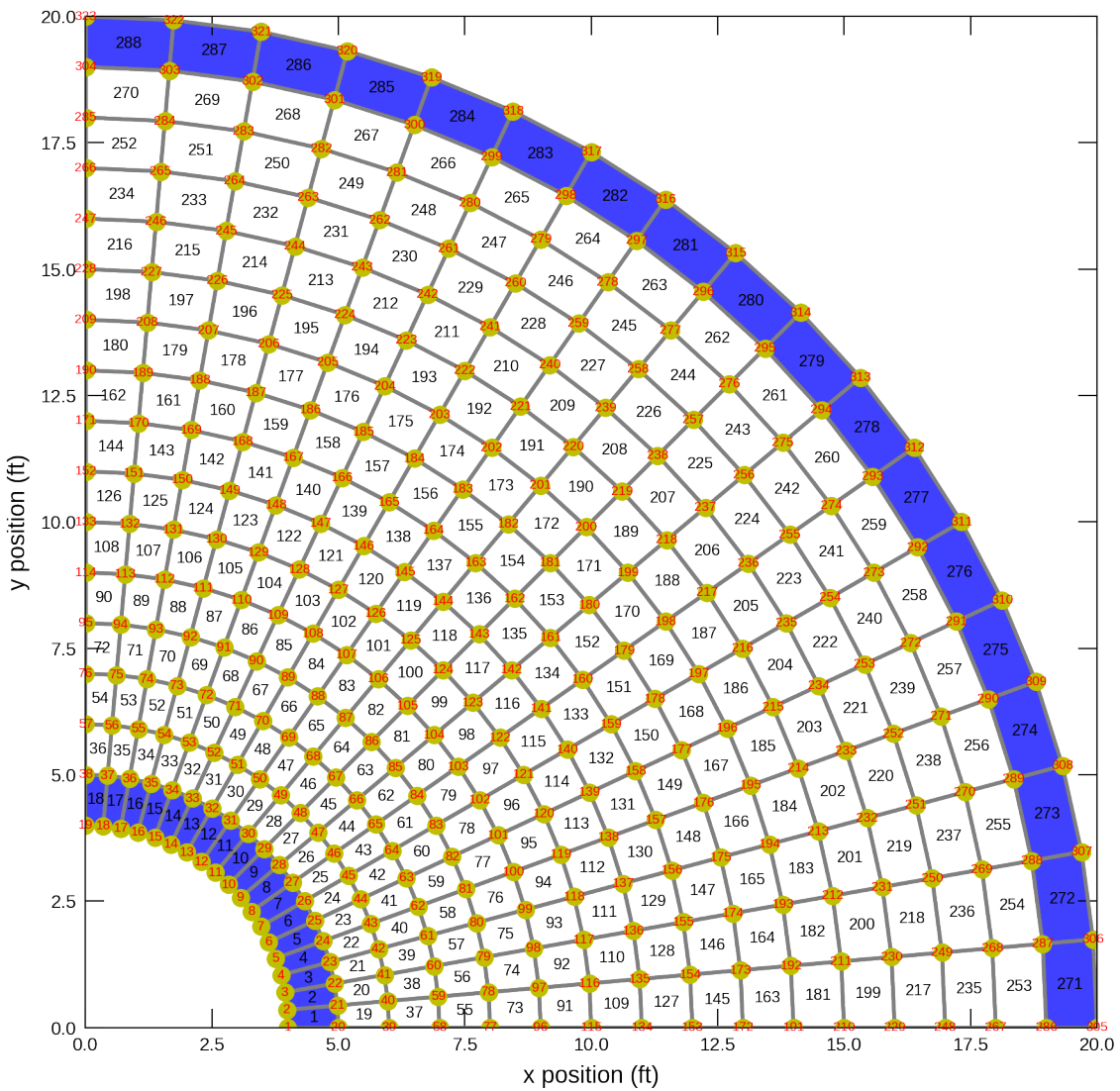


Figure 58–1: Model grid used for the  $90^\circ$  curvilinear vertex model. Constant-head cells are marked in blue. The inner constant head is 10 ft and the outer constant head is 3.33 ft. Cell numbers are shown inside each model cell. Vertices are also numbered and are shown in red.

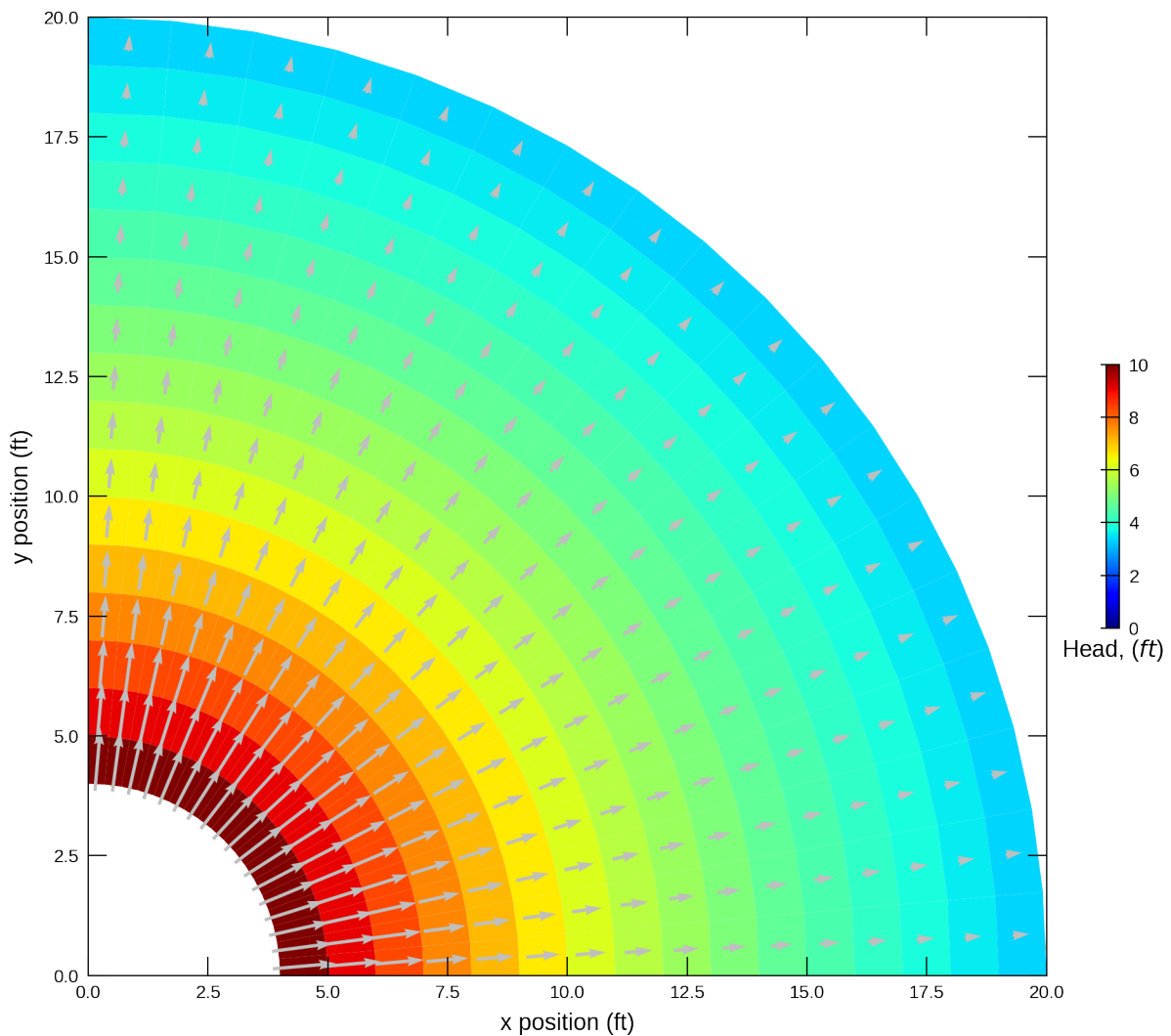


Figure 58–2: Steady state head solution and specific discharge vectors from the MODFLOW 6 curvilinear vertex model.

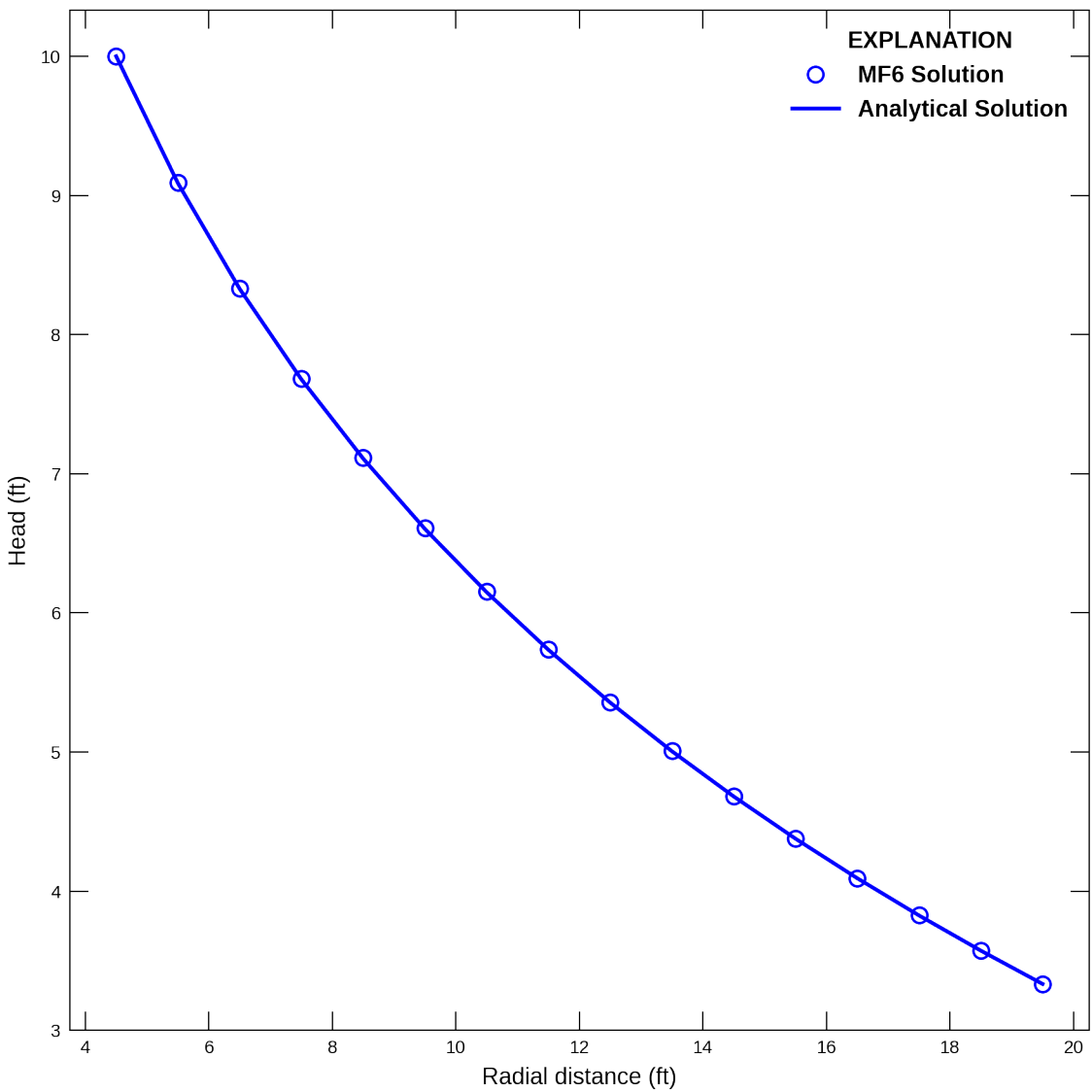


Figure 58–3: Steady state head solution from the MODFLOW 6 curvilinear vertex model (MF6) compared with the analytical solution (Crank, 1975). The MF6 head values are taken from each radial band along column 10. The radial distance of each MF6 solution is the distance from the vertex axis origin to the cell center.

## 59 Multipart Curvilinear Groundwater Flow Model

This example demonstrates how the MODFLOW 6 DISV Package can be used to simulate a multipart curvilinear model. This model extends the MODFLOW 6 “Curvilinear Groundwater Flow Model” example to reproduce the model grid presented in Figure 6 of [Romero and Silver \(2006\)](#). The hypothetical, curvilinear grid represents a meandering, curved flow path that traditional, structured grids cannot simulate. Figure 6 in [Romero and Silver \(2006\)](#) was introduced as an illustration of a curvilinear MODFLOW grid, but did develop it as a actual simulation model. This example illustrates that MODFLOW 6 can simulate this hypothetical grid.

### 59.1 Example Description

The hypothetical, curvilinear grid is composed of three distinct model regions that are combined to form the final grid. The first region (Left Grid; fig. 59–1A) is a curvilinear grid with 16 radial bands that start at  $180^\circ$  and end at  $270^\circ$  with a column discretization of  $5^\circ$  (18 columns). The Left Grid’s inner- and outer-most radius is  $4\text{ ft}$  and  $20\text{ ft}$ , respectively, and the radial direction vertices are  $1\text{ ft}$  apart. The second region (Center Grid; fig. 59–1B) is a  $1\text{ ft}$  rectangular, structured grid with 16 rows and 18 columns. The third region (Right Grid; fig. 59–1C) is an identical curvilinear grid as the first, but starts at  $90^\circ$  and end at  $0^\circ$ . The three regions are combined to derive the hypothetical, curvilinear grid presented in figure 59–2.

The hypothetical, curvilinear grid contains a single,  $10\text{ ft}$  thick, model layer with a transmissivity of  $0.19\text{ ft}^2/\text{day}$ . There are two constant head boundary conditions that are placed along the columns of the curvilinear regions (fig. 59–2). The first constant head boundary is  $10\text{ ft}$  and is along the first column of the Left Grid. The second constant head boundary is  $3.334\text{ ft}$  and is along the last column of the Right Grid. The remaining model properties are summarized in table 59–1.

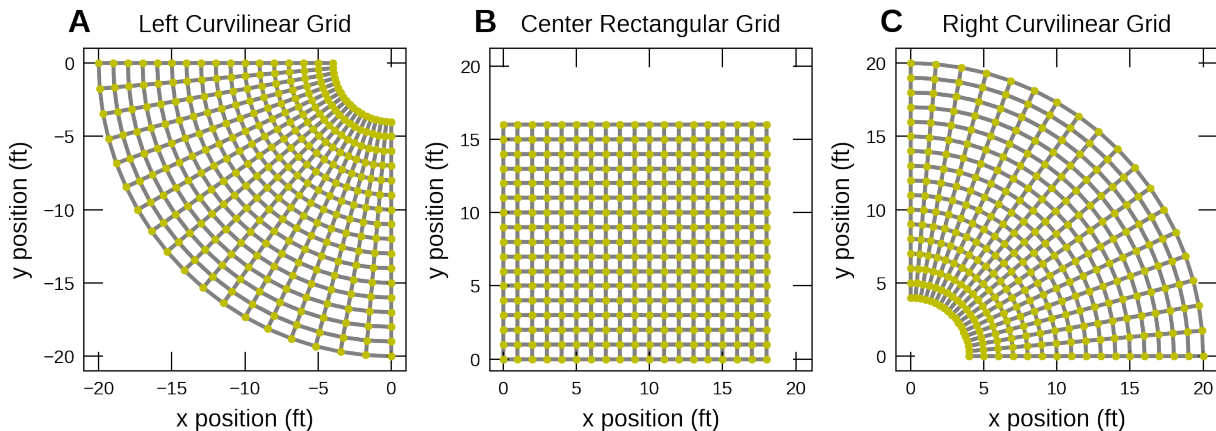


Figure 59–1: Three regions that combine to construct the hypothetical, curvilinear grid. A, Left curvilinear grid from  $180^\circ$  to  $270^\circ$ , B, Center 16 by 18 rectangular grid , and C, Right curvilinear grid from  $90^\circ$  to  $0^\circ$ . Grid vertices are marked in yellow. Note, the x, y coordinate positions are included for relative comparisons and not for the specific spatial location.

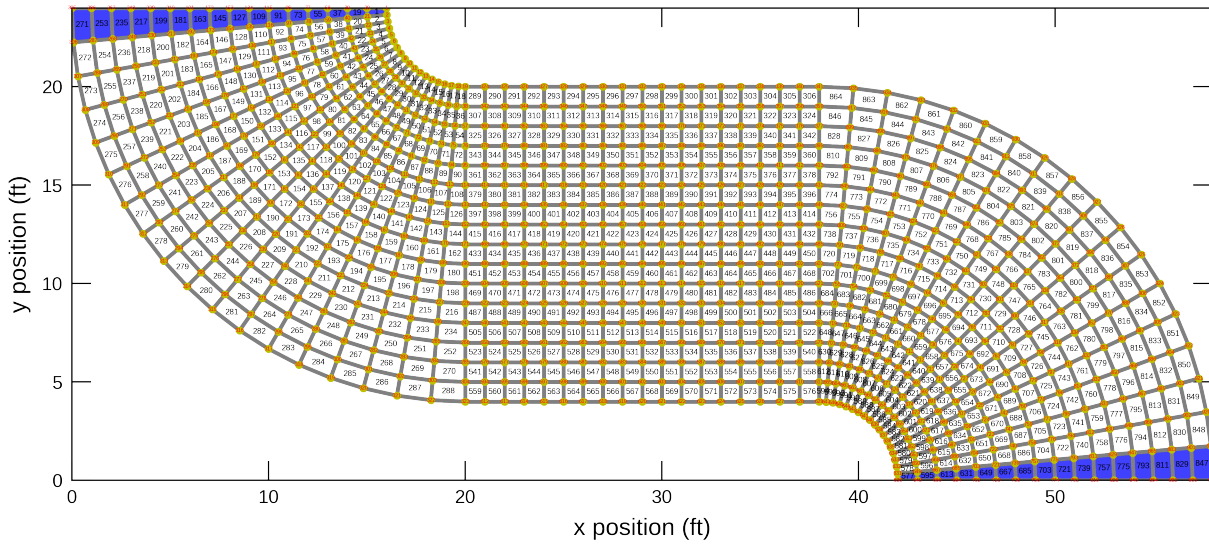


Figure 59–2: Plan view of the hypothetical, curvilinear grid with a meandering, curved flow path. Constant-head cells are marked in blue. The cell numbers  $1, 19, \dots, 253, 271$  constant head is 10 ft. The cell numbers  $577, 595, \dots, 829, 847$  constant head is 3.33 ft. Grid cell numbers are shown inside each model cell. Grid vertices are yellow with vertex numbers in red.

Table 59–1: Model parameters for example ex-gwf-curvilinear.

Parameter	Value
Simulation Type	Steady-State
Number of periods	1
Number of time steps	1
Number of layers	1
Number cells per layer	864
Top of the model (ft)	10.0
Base of the model (ft)	0.0
Horizontal transmissivity ( $ft^2/day$ )	0.19
Horizontal hydraulic conductivity ( $ft/day$ )	0.019
Left constant head boundary (ft)	10
Right constant head boundary (ft)	3.334
— Left Curvilinear Grid Properties —	
Degree angle of column 1 boundary	180
Degree angle of column ncol boundary	270
Degree angle width of each column	5
Number of radial direction cells (radial bands)	16
Number of columns in radial band (ncol)	18
Grid inner radius (ft)	4
Grid outer radius (ft)	20
Radial band width (ft)	1
— Middle Structured Grid Properties —	
Number of rows	16
Number of columns	18
Row width (ft)	1
Column width (ft)	1

Table 59–1: Model parameters for example ex-gwf-curvilinear.

Parameter	Value
<b>— Right Curvilinear Grid Properties —</b>	
Degree angle of column 1 boundary	0
Degree angle of column ncol boundary	90
Degree angle width of each column	5
Number of radial direction cells (radial bands)	16
Number of columns in radial band (ncol)	18
Grid inner radius (ft)	4
Grid outer radius (ft)	20
Grid radial band width (ft)	1

## 59.2 Example Results

The hypothetical, curvilinear grid (fig. 59–2.) is solved using one, steady state, stress period. Figure 59–3 presents the MODFLOW 6 simulated head and flow lines for all model cells.

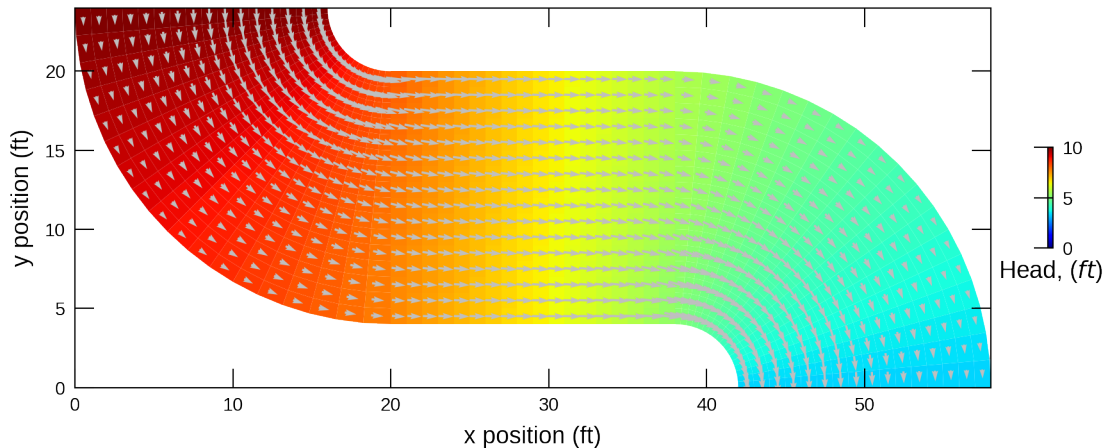


Figure 59–3: Steady state head solution and specific discharge vectors from the MODFLOW 6 curvilinear grid with a meandering, curved flow path.

## 60 Radial Heat Transport

A dedicated heat transport model referred to as the groundwater energy transport (GWE) model was released with version 6.5.0 of MODFLOW 6. Previously, to simulate groundwater heat transport in MODFLOW 6, a user could use the groundwater solute transport model, commonly referred to as simply groundwater transport (without specifying “solute” transport), to mimick heat transport by using its input parameters as surrogates for heat transport parameters ([Langevin and others, 2022](#); [Ma and Zheng, 2010](#); [Langevin and others, 2008](#)). Now, with GWE, users may specify native heat transport parameter values in the appropriate GWE package.

### 60.1 Example description

This example demonstrates use of the GWE model. This demonstration compares simulated results from a GWE model to an analytical solution that was published in [Al-Khoury and others \(2020\)](#). Both the groundwater flow (GWF) and GWE models employ a DISV grid type ([Langevin and others, 2017b](#)) with the numerical grid setup in a radial manner (fig. 60–1). The grid geometry facilitates outward propagation of heat from a borehole heat exchanger (BHE) ([Hecht-Mendez and others, 2010](#)) located in the center of the radially-symetric model grid (fig. 60–1). Groundwater flow moves from left to right. In this way, the model simulates heat flow in a convective and conductive heat transport environment moving past a cylindrical heat source.

Constant heads on the left and right sides of the model domain are specified such that the resulting left-to-right groundwater velocity is  $1 \times 10^{-5} \frac{m}{s}$  (fig. 60–3). The heat source located in the center of the numerical model is represented using the energy source loading (ESL) package with a known rate of energy input [referred to as a Dirichlet boundary condition in [Al-Khoury and others \(2020\)](#)]. The initial temperature throughout the model domain is  $0.0^{\circ}C$ . Energy is added to the grid cell in the middle of the model domain at a rate of  $100 \frac{W}{m}$ . Parameters used for the MODFLOW 6 simulation of the heat transport problem that uses a radially-symmetric grid are shown in table 60–1.

Table 60–1: Model parameters for example ex-gwe-radial.

Parameter	Value
Number of periods in flow model (–)	1
Number of layers (–)	1
Simulation radius (m)	20
Horizontal hydraulic conductivity (m/d)	1.0
Top of the model (m)	1.0
Bottom of the model (m)	0.0
Porosity (–)	0.2
Length of simulation (days)	2
Initial Temperature ( $^{\circ}C$ )	0.0
Advection solution scheme (–)	TVD
Thermal conductivity of water ( $\frac{W}{m \cdot ^{\circ}C}$ )	0.56
Thermal conductivity of aquifer material ( $\frac{W}{m \cdot ^{\circ}C}$ )	2.50
Density of water ( $kg/m^3$ )	1000.0
Heat capacity of water ( $\frac{J}{kg \cdot ^{\circ}C}$ )	4180.0
Density of dry solid aquifer material ( $kg/m^3$ )	2650.0
Heat capacity of dry solid aquifer material ( $\frac{J}{kg \cdot ^{\circ}C}$ )	900.0
Mechanical dispersion ( $m^2/day$ )	0.0
Transverse dispersivity ( $m^2/day$ )	0.0
Starting head (m)	1.0

Table 60–1: Model parameters for example ex-gwe-radial.

Parameter	Value
Groundwater seepage velocity 1 ( $m/s$ )	1.0e-5

## 60.2 Example Results

Results from the GWE model run are compared to a published analytical solution 48 hours after the start of the simulation ([Al-Khoury and others, 2020](#)). Isotemperature contours at 1, 2, 3, 4, 6, and 8  $^{\circ}C$  demonstrate that GWE results compare well with the analytical solution (fig. 60–4).

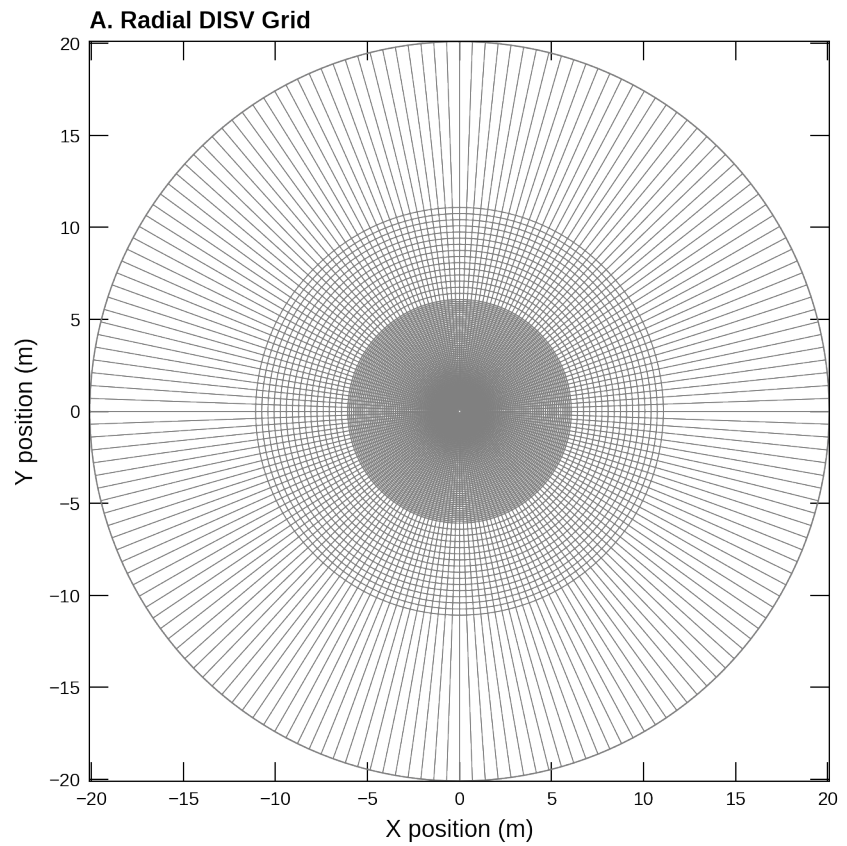


Figure 60–1: Configuration of the DISV model grid used in the radial transport problem. Model grid originally published in [Al-Khoury and others \(2020\)](#). Please refer to figure 60–2 for a zoomed-in view of the model grid in the vicinity of the BHE.

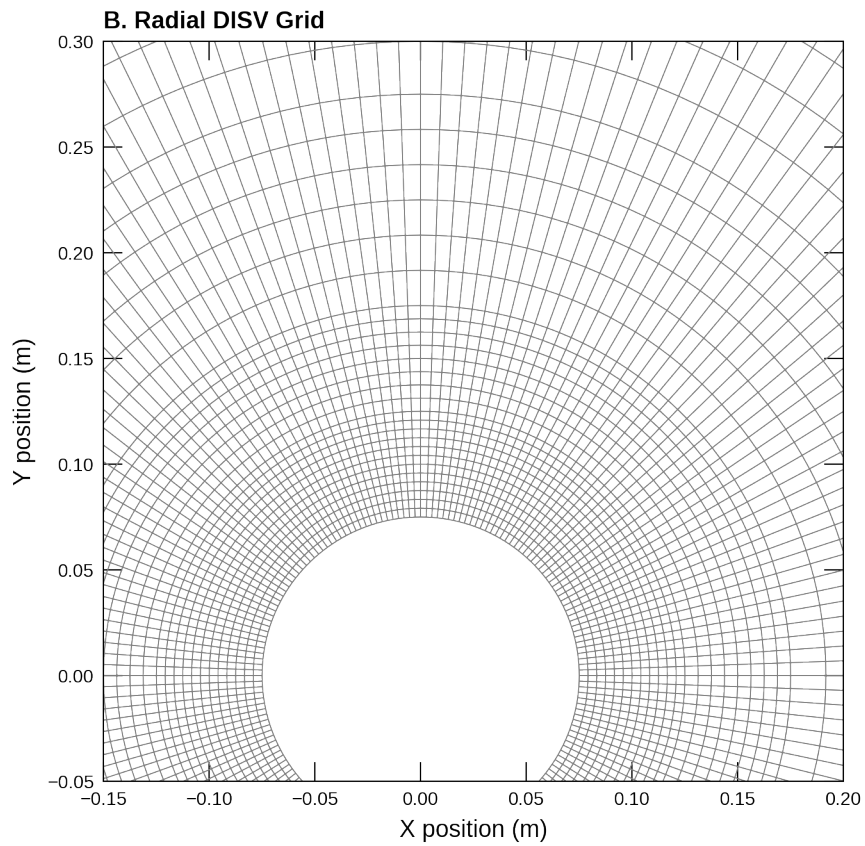


Figure 60–2: A zoomed-in view showing the refined discretization in close proximity to the BHE. Cell dimensions are sub-centimeter scale around the perimeter of the BHE. The radius of the BHE is 7.5 cm.

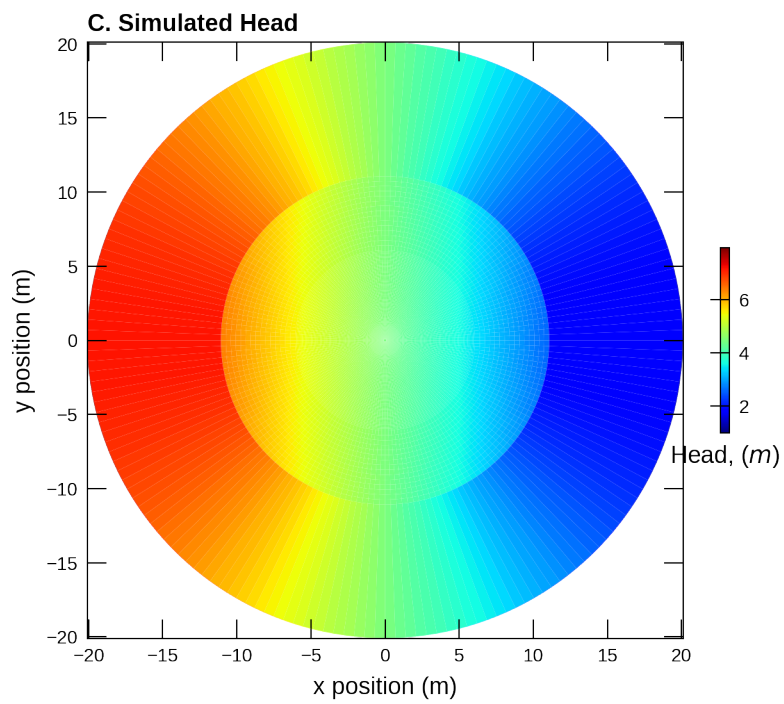


Figure 60–3: A head gradient is established in the outer-most ring of grid cells to drive groundwater flow from left to right. The combination of the groundwater head gradient with the hydraulic conductivity (table 60–1) results in a groundwater velocity of  $1 \times 10^{-5} \frac{m}{s}$ .

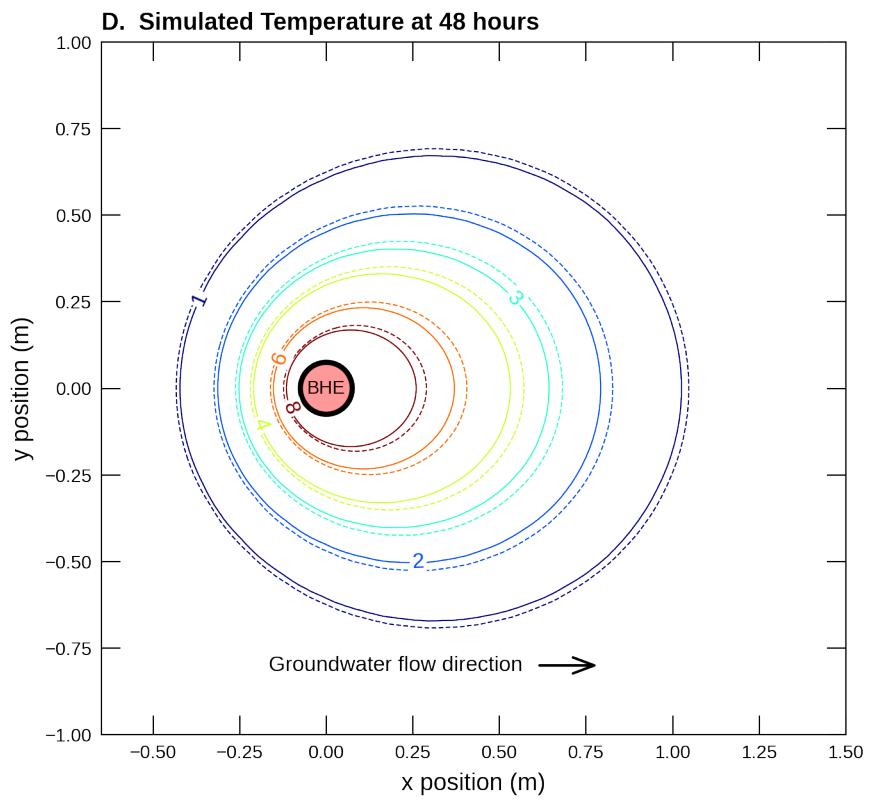


Figure 60–4: Simulation results for the GWE model run compared with an analytical solution.

# 61 Interacting Borehole Heat Exchangers in a Geothermal Setting

Shallow groundwater geothermal investigations often include more than one borehole heat exchanger (BHE) ([Al-Khoury and others, 2021](#)). In such applications, understanding the thermal interaction among multiple BHEs as well as on the flowing groundwater is made easier with a numerical groundwater flow and heat transport model. In this example, the accuracy of the groundwater energy transport (GWE) model is demonstrated for a convective-conductive porous domain with multiple thermally-interacting BHEs using an analytical solution first published in [Al-Khoury and others \(2021\)](#).

## 61.1 Example description

For this example nine BHEs are arranged in a  $3 \times 3$  configuration with a spacing of  $5\text{ m}$  from each other. The grid extent is  $90\text{ m} \times 60\text{ m}$ . Each BHE represents a cylindrical source of heat with energy being added at a rate of  $100\frac{\text{W}}{\text{m}}$  using the energy source loading (ESL) package. In order to better simulate the outward propagation of heat from each BHE, the discretization by vertices (DISV) grid type for both the groundwater flow (GWF) and GWE models was employed (fig 61–1). Grid refinement was added around each BHE (fig 61–2). Grid discretization is coarsened toward the perimeter of the model grid.

In order to test the MODFLOW 6 solution against the published analytical solution, the heat transport model simulates a porous media domain with a porosity of 0.20. Within the GWF model, two constant head (CHD) packages were setup on the left and right sides of the model, respectively, to drive groundwater flow from left to right with a velocity of  $1 \times 10^{-5}\frac{\text{m}}{\text{s}}$  (fig 61–3). The initial temperature throughout the model domain is  $0.0\text{ }^{\circ}\text{C}$ . Energy is added to the grid cell in the middle of the model domain at a rate of  $100\frac{\text{W}}{\text{m}}$ . Parameters used for the MODFLOW 6 simulation of the geothermal heat transport problem are shown in table 61–1.

Table 61–1: Model parameters for example ex-gwe-geotherm.

Parameter	Value
Number of periods in flow model (–)	1
Number of layers (–)	1
Simulation width (m)	60
Simulation length (m)	90
Horizontal hydraulic conductivity (m/d)	1.0
Top of the model (m)	1.0
Bottom of the model (m)	0.0
Porosity (–)	0.2
Length of simulation (days)	50
Initial Temperature ( $^{\circ}\text{C}$ )	0.0
Advection solution scheme (–)	TVD
Thermal conductivity of water ( $\frac{\text{W}}{\text{m}\cdot{}^{\circ}\text{C}}$ )	0.56
Thermal conductivity of aquifer material ( $\frac{\text{W}}{\text{m}\cdot{}^{\circ}\text{C}}$ )	2.50
Density of water ( $\text{kg}/\text{m}^3$ )	1000
Heat capacity of water ( $\frac{\text{J}}{\text{kg}\cdot{}^{\circ}\text{C}}$ )	4180.0
Density of dry solid aquifer material ( $\text{kg}/\text{m}^3$ )	2650.0
Heat capacity of dry solid aquifer material ( $\frac{\text{J}}{\text{kg}\cdot{}^{\circ}\text{C}}$ )	900.0
Latent heat of vaporization ( $\frac{\text{J}}{\text{kg}\cdot{}^{\circ}\text{C}}$ )	2500.0
No mechanical dispersion ( $\text{m}^2/\text{day}$ )	0.0
No transverse dispersivity ( $\text{m}^2/\text{day}$ )	0.0

Table 61–1: Model parameters for example ex-gwe-geotherm.

Parameter	Value
Starting head (m)	1.00

## 61.2 Example Results

Results from the geothermal model run are compared to a published analytical solution 50 days after the start of the simulation (Al-Khoury and others, 2021). Isotemperature contours at 1, 2, 3, 4, 6, and 8 °C provide a visual summary of the match between GWE and the analytical solution (fig. 61–4). Isotemperature contours match particularly well at the lower temperatures ( $\leq 2^{\circ}\text{C}$ ). At temperatures  $> 2^{\circ}\text{C}$ , the simulated temperatures have not advanced as far in the downgradient direction as the analytical solution would suggest.

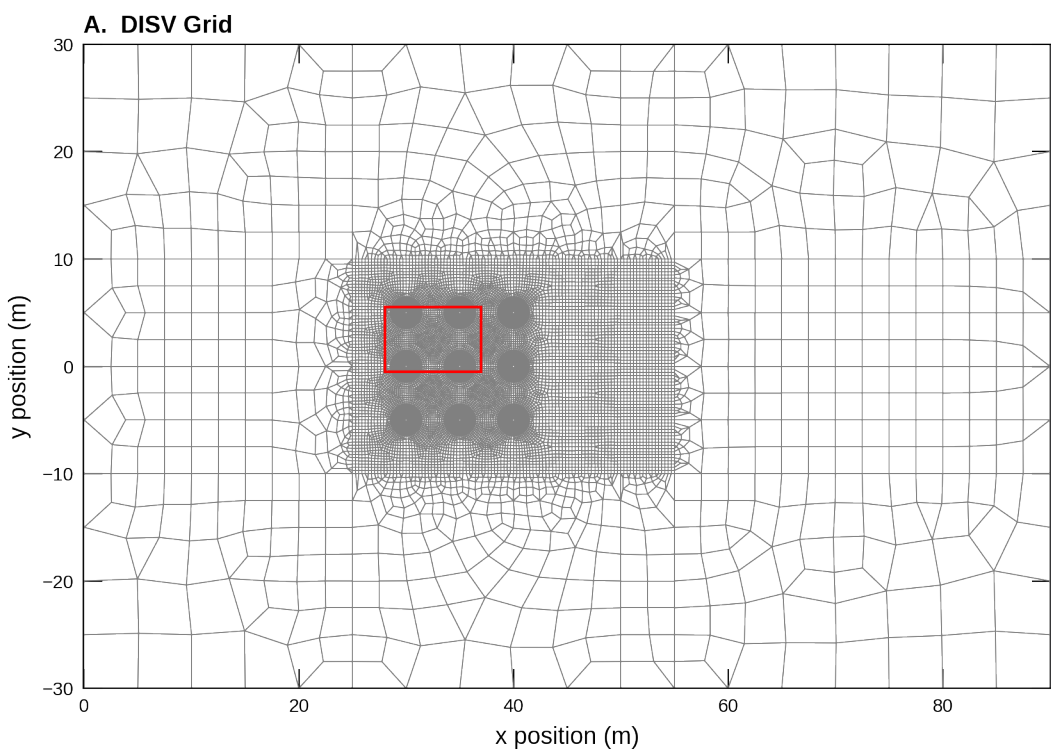


Figure 61–1: Configuration of the DISV model grid used to demonstrate the use of GWE in a geothermal transport problem. The original numerical model grid was published in [Al-Khoury and others \(2021\)](#). The red box shows the location of figure 61–2 which provides zoomed-in detail of the model grid in the vicinity of the BHEs.

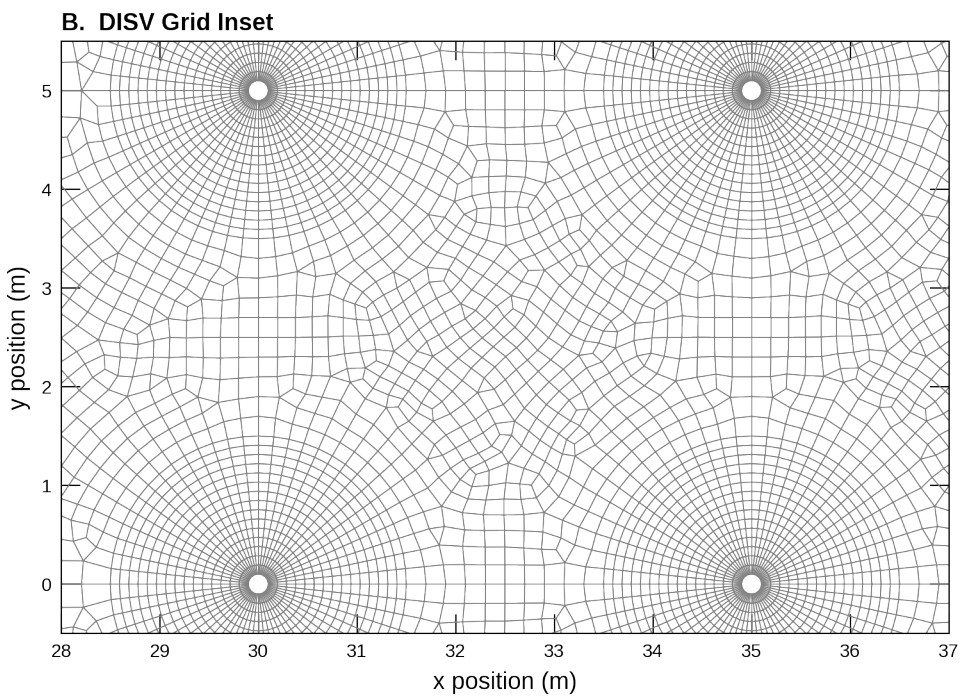


Figure 61–2: A zoomed-in view showing the refined discretization in close proximity to the BHEs. Cell dimensions are on the scale of centimeters around the perimeter of the BHEs. The diameter of each BHE is 10.0 cm.

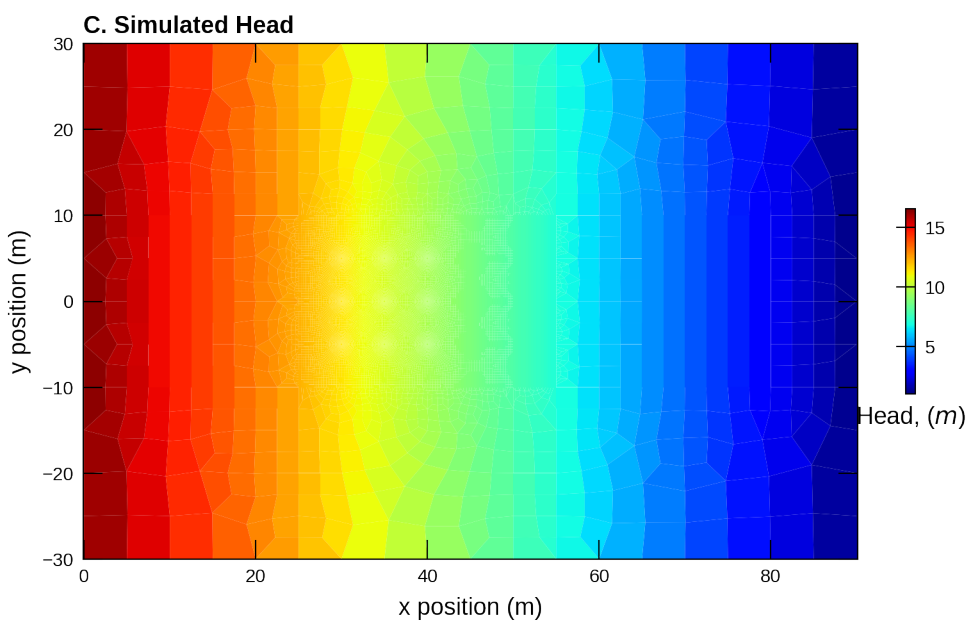


Figure 61–3: The established head gradient drives groundwater flow from left to right with a velocity of  $1 \times 10^{-5} \frac{m}{s}$ .

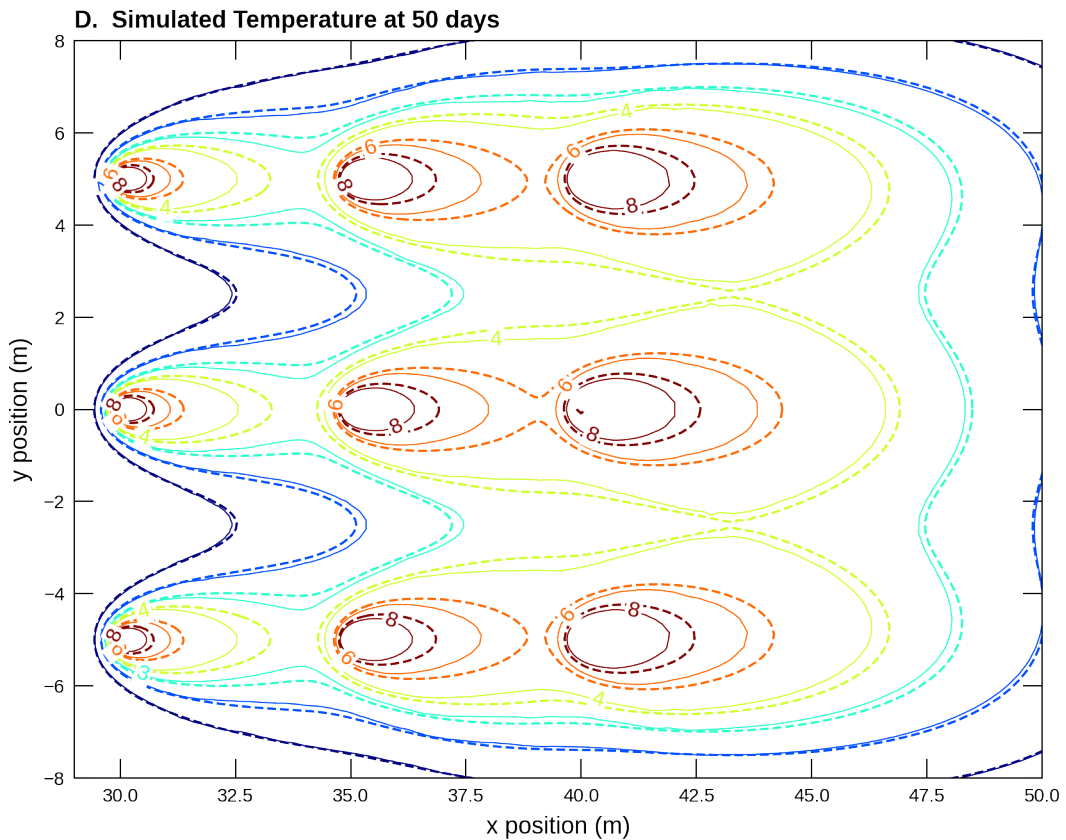


Figure 61–4: Simulated and analytical isolatitude contours for the geothermal example problem. The solid lines correspond to the GWE solution while the dashed line represents the analytical solution published by [Al-Khoury and others \(2021\)](#).

## 62 Infiltrating Heat Front

An analytical solution used in chemical engineering for modeling concentration in packed-bed reactors , commonly referred to as a “Danckwerts” (or “third-type”) boundary condition, is adapted here for confirming the accuracy of heat transport as solved by the UZE package in MODFLOW 6. The analytical solution has the following characteristics: (1) it solves for total energy flux (advection and conduction) along a 1-dimensional (1D) profile [i.e., there is no conduction (“thermal bleeding”) with the surrounding materials], (2) heat flux can only enter the active domain with the inflow (in this case, the infiltration) and it does not require the temperature at the boundary to be equal to the temperature of the infiltration, and (3) it solves for total heat flux (instead of temperature) throughout the 1D domain.

The Danckwerts analytical solution takes the following form:

$$q_{Tz} = q_{T_0} + \frac{1}{2} (q_{T_{infil}} - q_{T_0}) \left( \operatorname{erfc} \left\{ \frac{z - \nu t}{2\sqrt{Dt}} \right\} + \exp \left\{ \frac{\nu z}{D} \right\} \cdot \operatorname{erfc} \left\{ \frac{z + \nu t}{2\sqrt{Dt}} \right\} \right)$$

where  $q_{Tz}$  is the heat flux and depth  $z$ ,  $q_{T_0}$  is the infiltrating heat flux at  $t = 0$ ,  $q_{T_{infil}}$  is the amount of infiltrating heat flux at  $t > 0$ ,  $\operatorname{erfc}$  is the complementary error function,  $z$  is the distance from infiltrating heat flux boundary, which, in this example is the depth below land surface,  $t$  is time (in days),  $\nu$  represents the “thermal convection velocity” determined from,

$$\nu = q \cdot \frac{\rho_w C_{p_w}}{S_{w_z} \theta \rho_w C_{p_w} + (1 - \theta) \rho_s C_{p_w}}$$

with  $q$  equal to the volumetric infiltration rate,  $\rho_w$  is the density of water,  $C_{p_w}$  is the heat capacity of water,  $S_{w_z}$  is the saturation at depth  $z$ ,  $\theta$  is the water content,  $\rho_s$  is the density of a aquifer solids, and  $C_{p_w}$  is the heat capacity of the aquifer solids. Additionally,  $D$  represents the bulk thermal diffusivity,

$$D = \frac{k_{T_{bulk}}}{S_{w_z} \theta k_{T_w} + (1 - \theta) k_{T_s}}$$

and  $k_{T_{bulk}}$  is the bulk thermal conductivity represented by,

$$k_{T_{bulk}} = S_{w_z} \theta k_{T_w} + (1 - \theta) k_{T_s}$$

and  $k_{T_w}$  and  $k_{T_s}$  are the thermal conductivities of the water and aquifer material, respectively.

### 62.1 Example description

A 1D model grid of the unsaturated zone is used to simulate the downward migration of an infiltrating heat front (fig. 62–1). Steady flow conditions are simulated with the GWF model. The UZF package simulates flow through the unsaturated zone with a constant infiltration rate of  $0.01 \frac{m}{d}$ . An initial temperature of  $10^\circ C$  is specified for the entire model domain. After steady flow and transport conditions are established with a quasi-steady-state stress period, the temperature of the infiltration is increased to  $20^\circ C$  resulting in an energy source loading of  $9.68 \frac{J}{s}$  (calculated from  $q_{infil} \cdot T_{infil} \cdot \rho_w \cdot C_{p_w}$ ). Other pertinent parameter values are provided in table 62–1.

A constant head boundary is placed at the bottom of the model to remove water that recharges the water table in order to prevent the water table from rising into the unsaturated column (fig. 62–1).

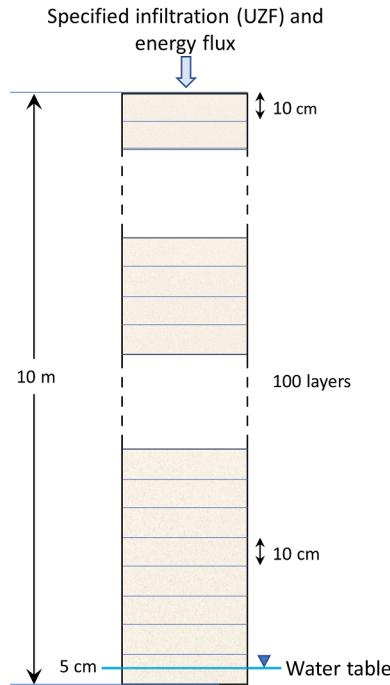


Figure 62–1: View of 1-dimensional model setup. Total thickness of the unsaturated zone is 10 m and is discretized with 100 cells that are each 10 cm thick.

Table 62–1: Model parameters for example ex-gwe-danckwarts.

Parameter	Value
Number of layers (-)	101
Number of rows (-)	1
Number of columns (-)	1
Number of simulated periods (-)	2
Cell width (m)	1.0
Cell length (m)	1.0
Cell thickness (m)	0.1
Initial head (m)	0.05
Top of the model grid (m)	10.00
Initial temperature ( $^{\circ}\text{C}$ )	10.0
Advection scheme (-)	Upstream
Longitudinal mechanical dispersion term (m)	0.0
Porosity (-)	0.2
Density of dry solid aquifer material ( $\frac{\text{kg}}{\text{m}^3}$ )	1500.0
Heat capacity of dry solid aquifer material ( $\frac{\text{J}}{\text{kg}\cdot{}^{\circ}\text{C}}$ )	760.0
Density of water ( $\frac{\text{kg}}{\text{m}^3}$ )	1000.0
Heat capacity of water ( $\frac{\text{J}}{\text{kg}\cdot{}^{\circ}\text{C}}$ )	4183.0
Thermal conductivity of water ( $\frac{\text{W}}{\text{m}\cdot{}^{\circ}\text{C}}$ )	0.5918
Thermal conductivity of solid aquifer material ( $\frac{\text{W}}{\text{m}\cdot{}^{\circ}\text{C}}$ )	0.27
Infiltration rate ( $\frac{\text{m}}{\text{d}}$ )	0.01
Contant head at the model outlet (m)	0.05
Residual water content of the unsaturated zone (-)	0.0001
Saturated water content of the unsaturated zone (-)	0.20

Table 62–1: Model parameters for example ex-gwe-danckwerts.

Parameter	Value
Initial water content of the unsaturated zone (–)	0.055
Brooks-Corey epsilon parameter (–)	4.0
Vertical hydraulic conductivity of the unsaturated zone ( $\frac{m}{d}$ )	1.0
Initial temperature in simulation domain ( $^{\circ}C$ )	10.0
Temperature of infiltrating water ( $^{\circ}C$ )	20.0

## 62.2 Example Results

The heat front that migrates downward through the unsaturated zone as a result of energy loading associated with the infiltration is shown in figure 62–2 at 10, 50, and 100 days. Figure 62–3 shows the same comparison broken out into 3 subplots, but further parses the downward heat migration into its advective (dark green) and conductive (light green) components. Where the temperature gradients are steepest, the conductive flux of energy plays a more prominent role in the downward migration of heat.

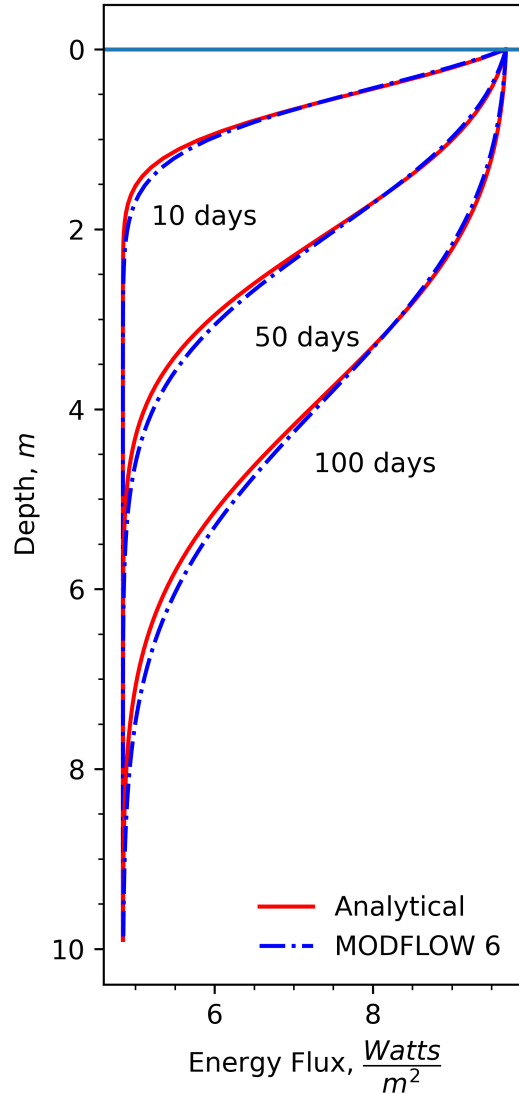


Figure 62–2: Comparison of simulated migration of infiltrating heat front to an analytical solution

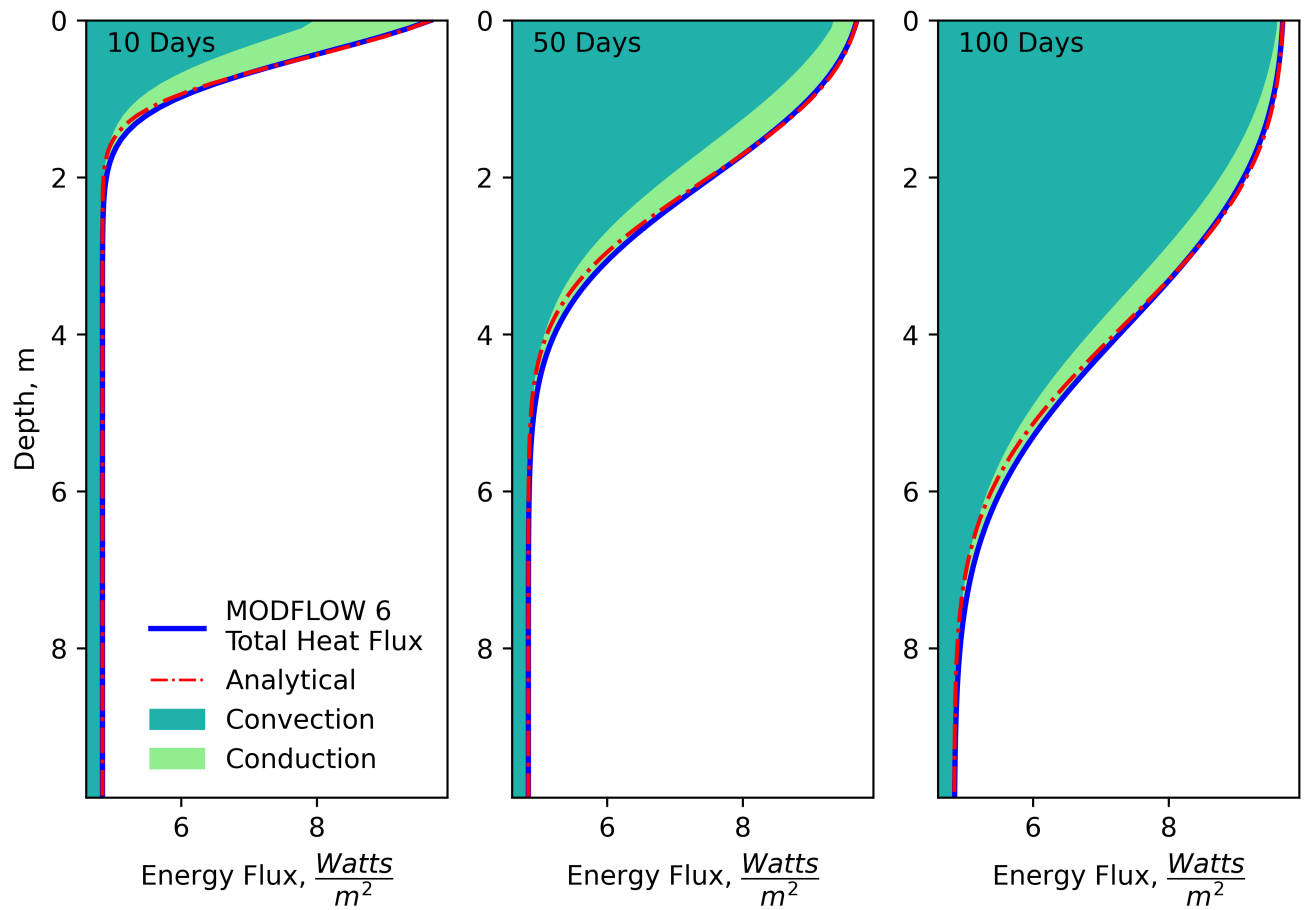


Figure 62–3: The same infiltrating heat fronts as shown in figure 62–2, but highlights the advective and conductive heat fluxes separately

## 63 Forward Particle Tracking, Structured Grid, Steady-State Flow

This example demonstrates a MODFLOW 6 particle tracking (PRT) model by reproducing example problem 1 from the MODPATH 7 ([Pollock, 2016](#)) example problems document ([Pollock, 2017](#)). An equivalent MODPATH 7 model is constructed for comparison, though only PRT results are shown.

### 63.1 Example description

The example first runs a groundwater flow (GWF) model simulating steady-state flow on a structured grid. The flow system includes an upper and lower aquifer separated by a confining layer with lower conductivity. The grid has 3 layers, 21 rows, and 20 columns, with square cells 500 feet to a side. The system includes two boundary conditions: a well in layer 3, row 11, column 10, and a river in layer 1, column 20 (fig 63–1). Model parameters for this example are summarized in table 63–1.

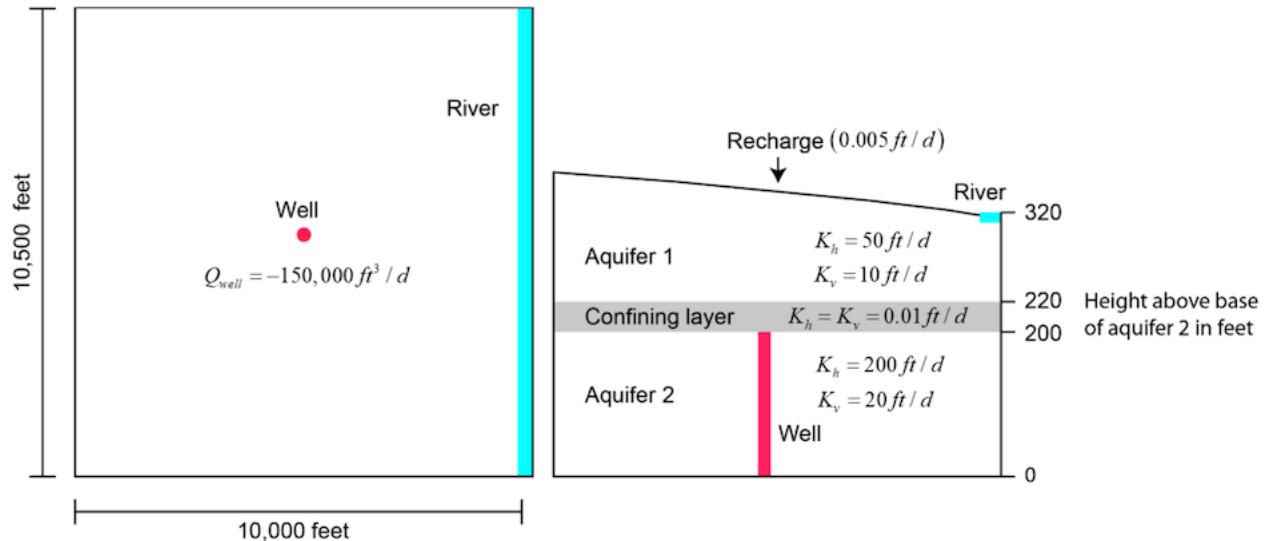


Figure 63–1: Conceptual model. Image reproduced from the MODPATH 7 examples document ([Pollock, 2017](#)).

Table 63–1: Model parameters for example ex-prt-mp7-p01.

Parameter	Value
Number of periods	1
Number of layers	3
Number of rows	21
Number of columns	20
Column width (ft)	500.0
Row width (ft)	500.0
Top of the model (ft)	400.0
Layer bottom elevations (ft)	220.0, 200.0, 0.0
Porosity (unitless)	0.1
Recharge rate (ft/d)	0.005
Horizontal hydraulic conductivity (ft/d)	50.0, 0.01, 200.0

Table 63–1: Model parameters for example ex-prt-mp7-p01.

Parameter	Value
Vertical hydraulic conductivity ( $ft/d$ )	10.0, 0.01, 20.0
Well pumping rate ( $ft^3/d$ )	-150000.0
River stage ( $ft$ )	320.0
River bottom ( $ft$ )	317.0
River conductance ( $ft^2/d$ )	1.0e5

## 63.2 Example Results

In this example a MODFLOW 6 particle tracking (PRT) model runs in the same simulation as a groundwater flow (GWF) model (fig 63–2), which provides it with intercell flows via a GWF-PRT model exchange.

In subproblem 1A, a line of 21 particles is placed at the water table in layer 1 for column 3, rows 1 through 21. In subproblem 1B, a denser release configuration is used which places a 3 x 3 array of particles on the top face of every cell in layer 1. Both simulations track particles forward to their discharge points.

Subproblem 1A path points on a 1000-day time interval are shown in fig 63–3.

To illustrate discharge points, pathlines are colored by discharge area (well or river) in fig 63–4. To show capture areas, starting locations of all particles are color-coded according to the zone value of the cells in which they terminate in fig 63–5. Travel time analysis is also a common use case for particle tracking. Particle release points are colored by total travel time to capture in fig 63–6.

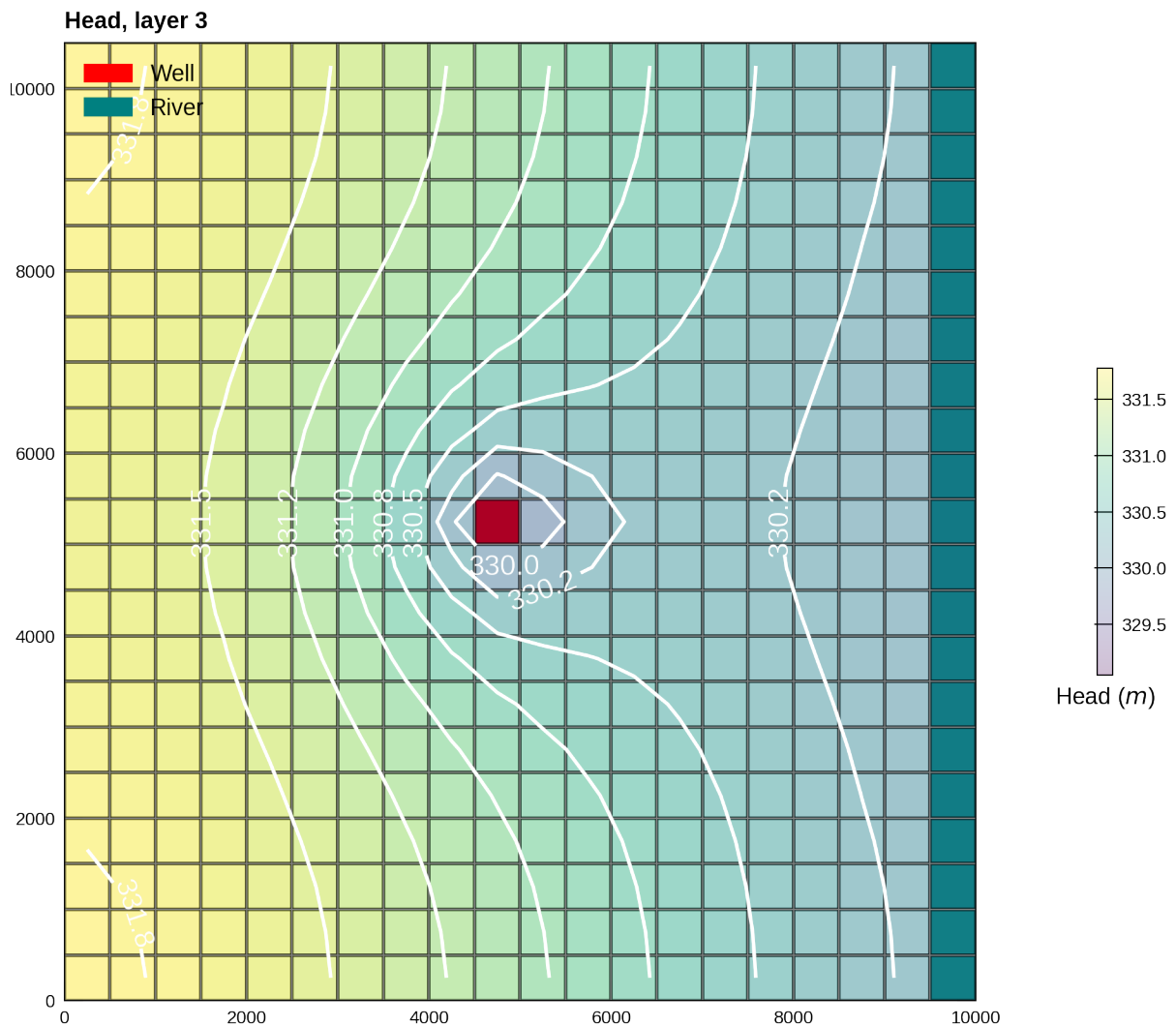


Figure 63–2: Heads simulated by the MODFLOW 6 groundwater flow (GWF) model.

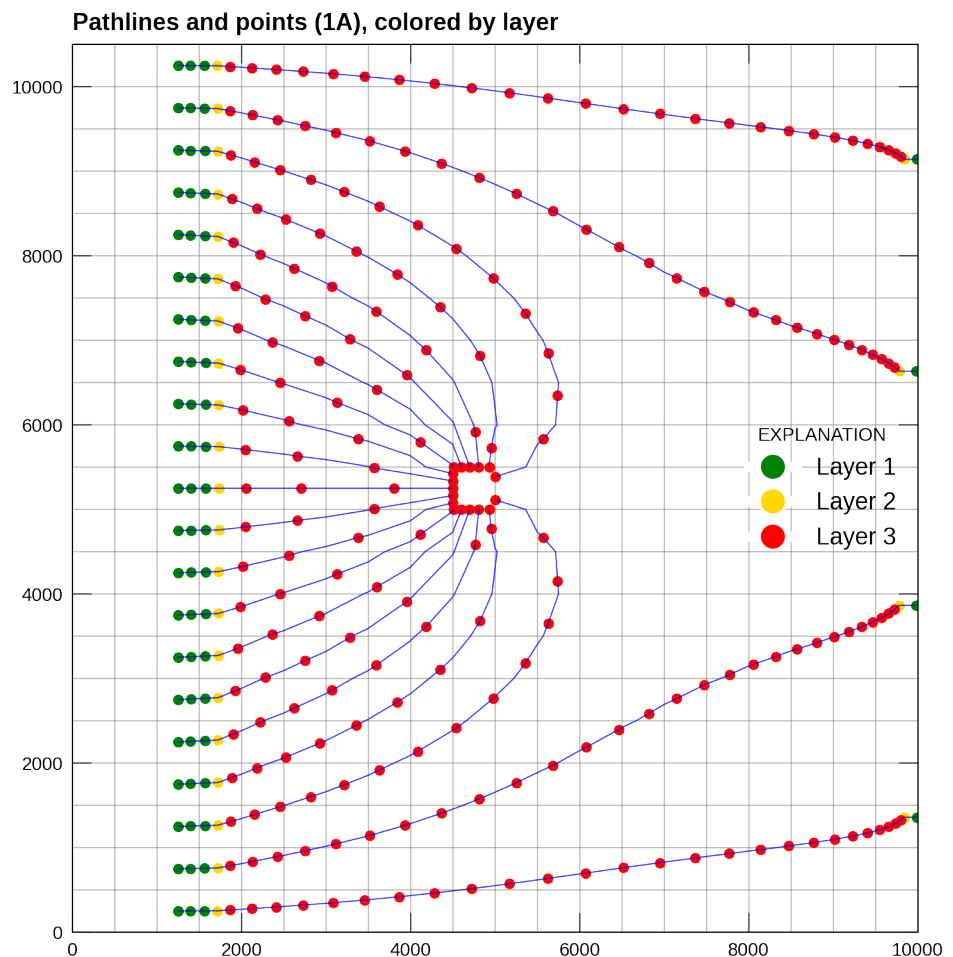


Figure 63–3: Particle pathlines and 1000-day points for subproblem 1A. Points are colored by layer.

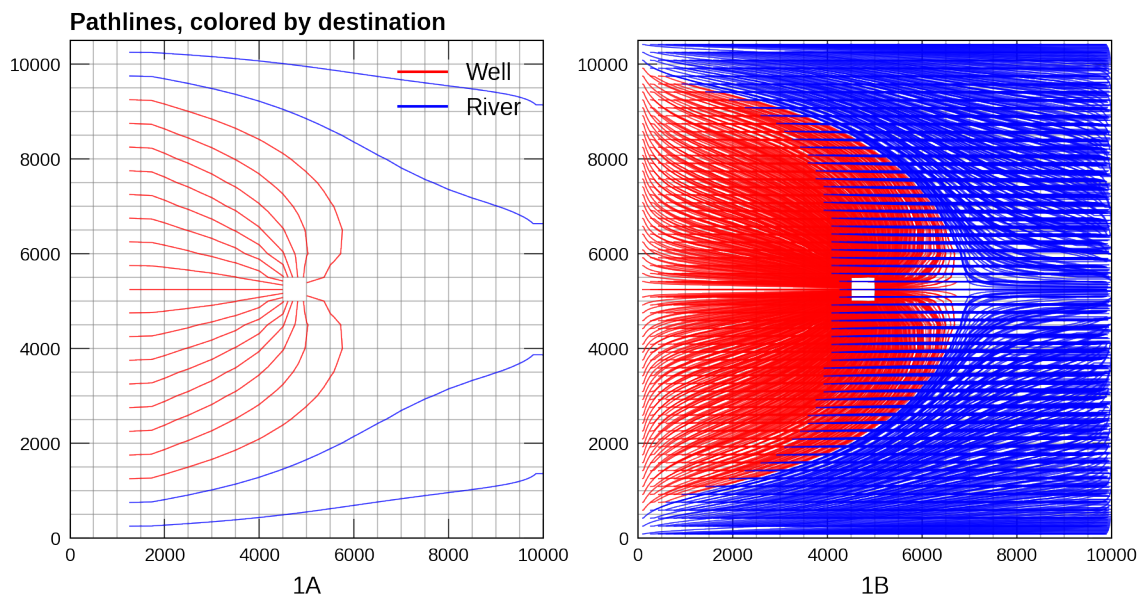


Figure 63–4: Particle pathlines, colored by destination: particles with red pathlines are captured by the well, particles with blue pathlines are captured by the river.

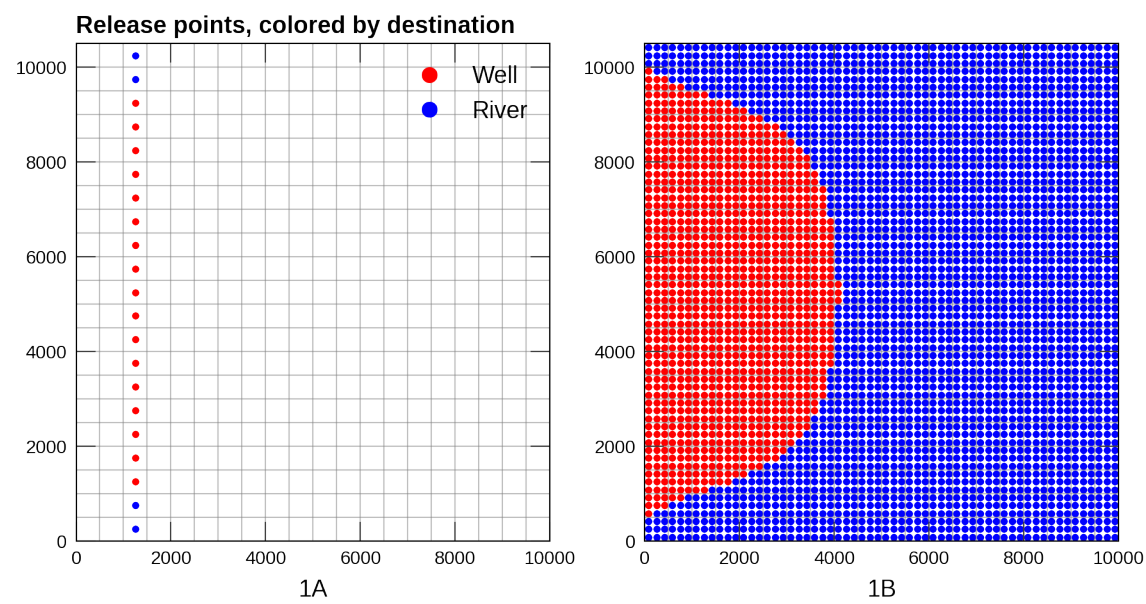


Figure 63–5: Particle release points, colored by destination.

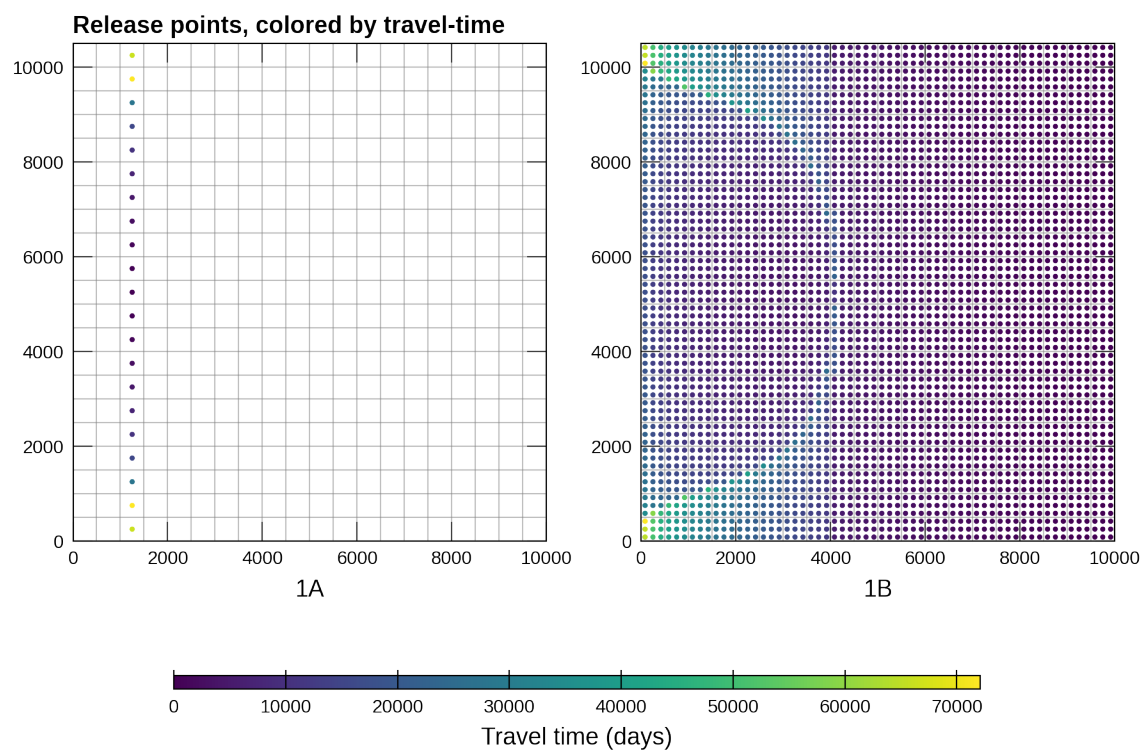


Figure 63–6: Particle release points, colored by travel time.

## 64 Forward Particle Tracking, Structured Grid, Transient Flow

This example demonstrates a MODFLOW 6 particle tracking (PRT) model by reproducing example problem 3 from the MODPATH 7 ([Pollock, 2016](#)) example problems document ([Pollock, 2017](#)). An equivalent MODPATH 7 model is constructed for comparison, though only PRT results are shown.

### 64.1 Example description

PRT/MP7 Example 3 modifies the flow system from PRT/MP7 Example 1 with three stress periods: first a steady-state period with a single time step, length 100,000 days, then a transient period with 10 time steps, each with length 36,500 days, and lastly a steady-state period with a single time step lasting 100,000 days.

Boundary conditions are also modified in this example. There is not one but two wells, one in the first layer and one in the third layer. There is also a drain in the first layer, extending from roughly the center of the grid to the river on the grid's right boundary. Both wells are inactive for the first stress period, then begin to pump as the 2nd stress period begins (after 100,000 days), and continue to pump at a constant rate for the rest of the simulation. Model parameters for this example are summarized in table 64-1.

Particles are released in batches from a 2x2-cell square (4 total cells) in the upper left quadrant of the grid. Ten batches are released in total: the first batch is released at 90,000 days, after which batches are released every 20 days until 200 days have elapsed.

Table 64-1: Model parameters for example ex-prt-mp7-p03.

Parameter	Value
Number of periods	3
Number of layers	3
Number of rows	21
Number of columns	20
Column width (ft)	500.0
Row width (ft)	500.0
Top of the model (ft)	350.0
Layer bottom elevations (ft)	220.0, 200.0, 0.0
Horizontal hydraulic conductivity (ft/d)	50.0, 0.01, 200.0
Vertical hydraulic conductivity (ft/d)	10.0, 0.01, 20.0
Recharge rate (ft/d)	0.005
River stage (ft)	320.0
River bottom (ft)	317.0
River conductance (ft <sup>2</sup> /d)	1.0e5
Soil porosity (unitless)	0.1

### 64.2 Example Results

In this example a MODFLOW 6 particle tracking (PRT) model runs in a separate simulation from the groundwater flow (GWF) model (fig 64-1). Intercell flows are read by the PRT model from the binary budget file written by the GWF model.

Path points on a 2000-day interval are visualized in plan view in fig 64-2 and in 3D in fig 64-3. Release and termination points are colored by destination in fig 64-4.

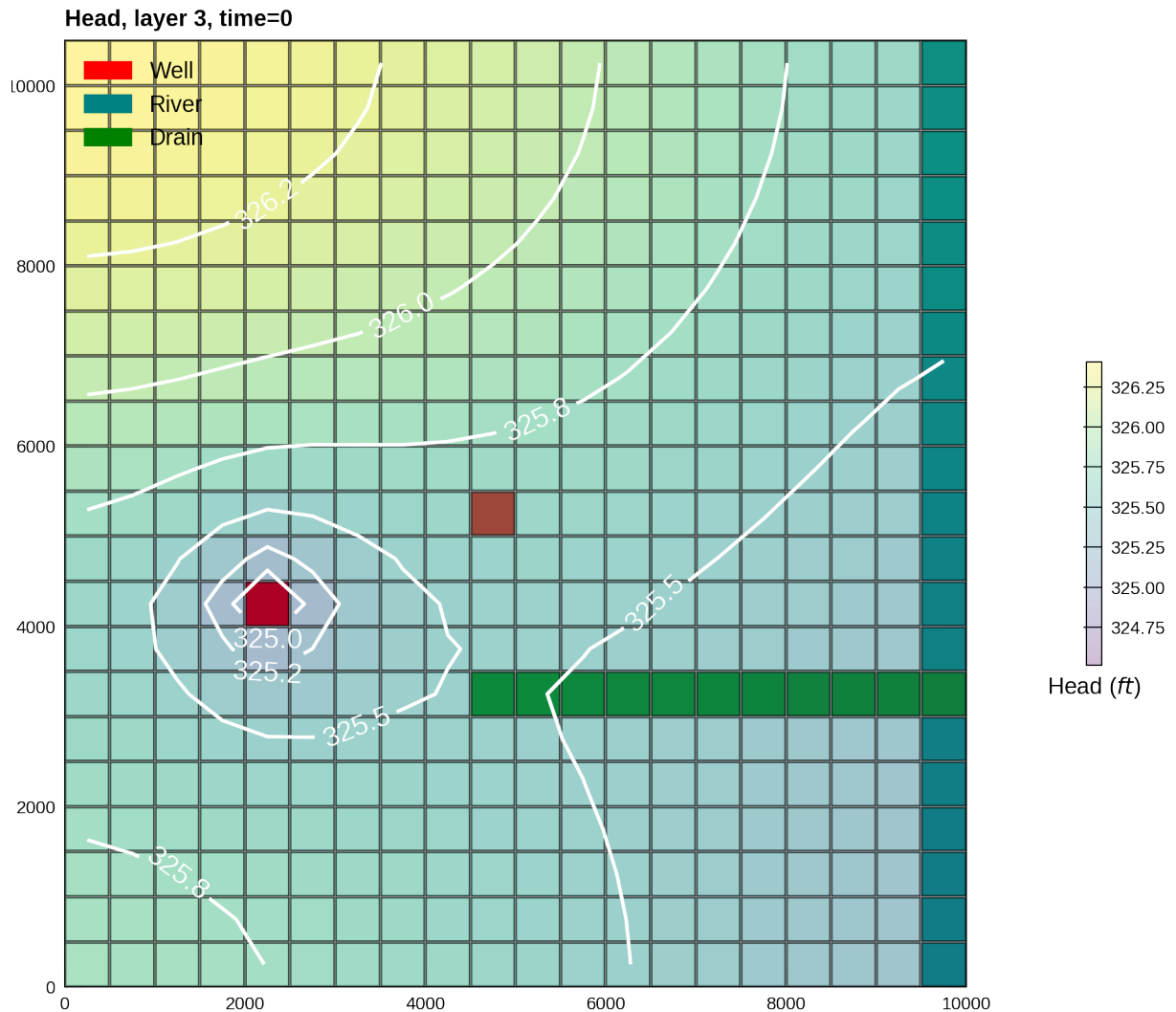


Figure 64–1: Head simulated by the MODFLOW 6 groundwater flow (GWF) model.

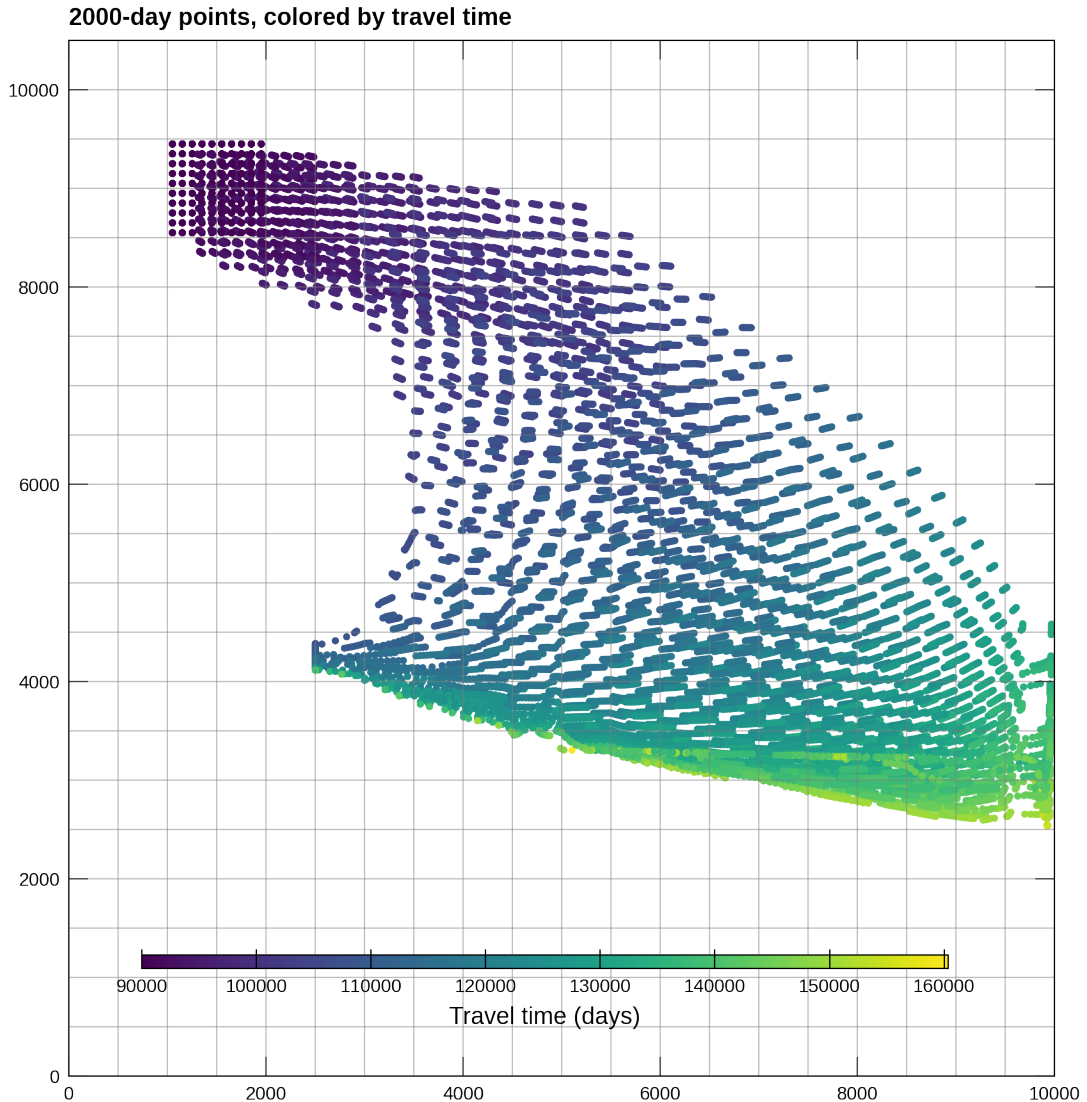


Figure 64–2: 2000-day particle path points. Points are colored by travel time.

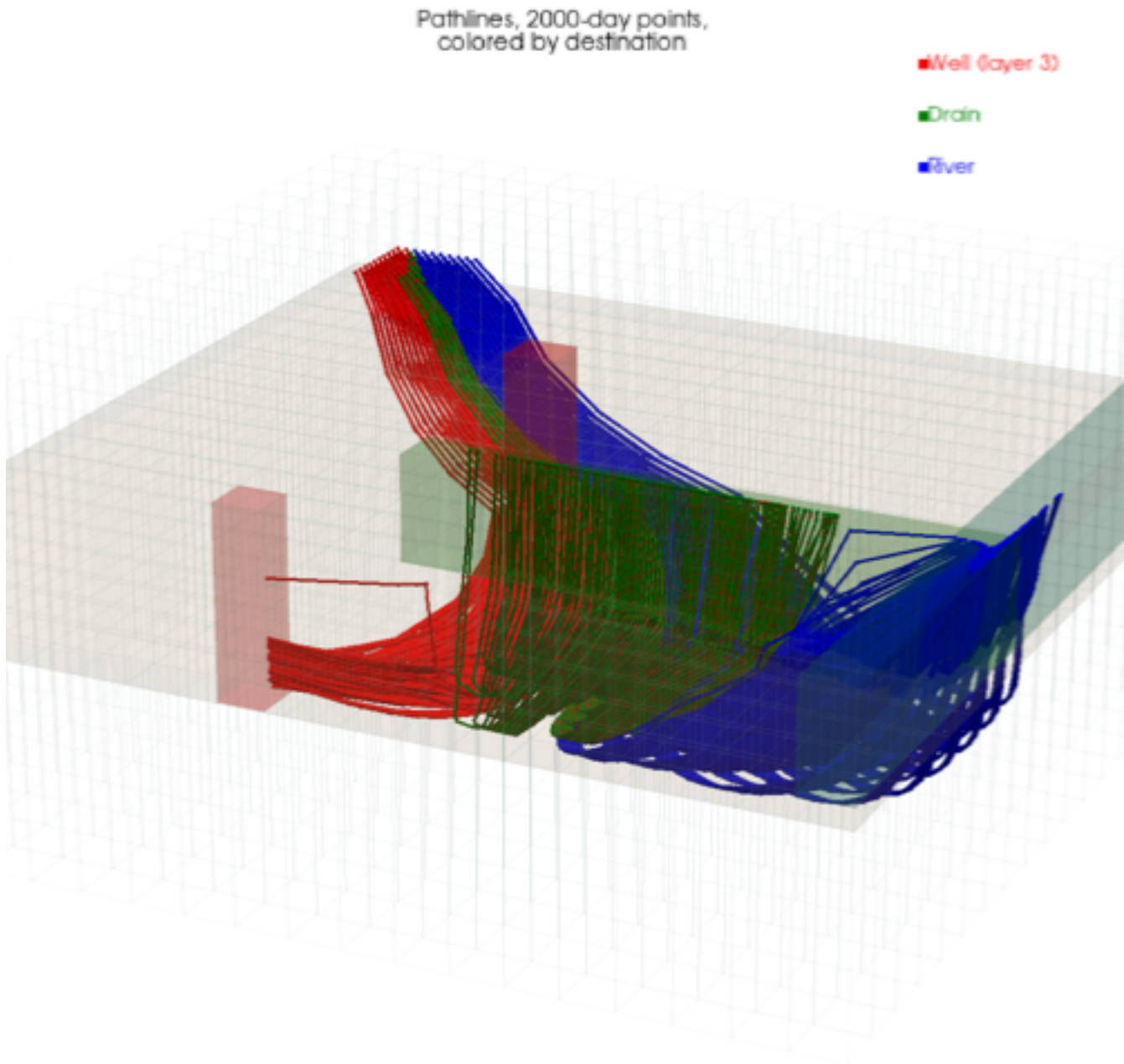


Figure 64–3: Three-dimensional perspective of pathlines and 2000-day points. Points are colored by destination.

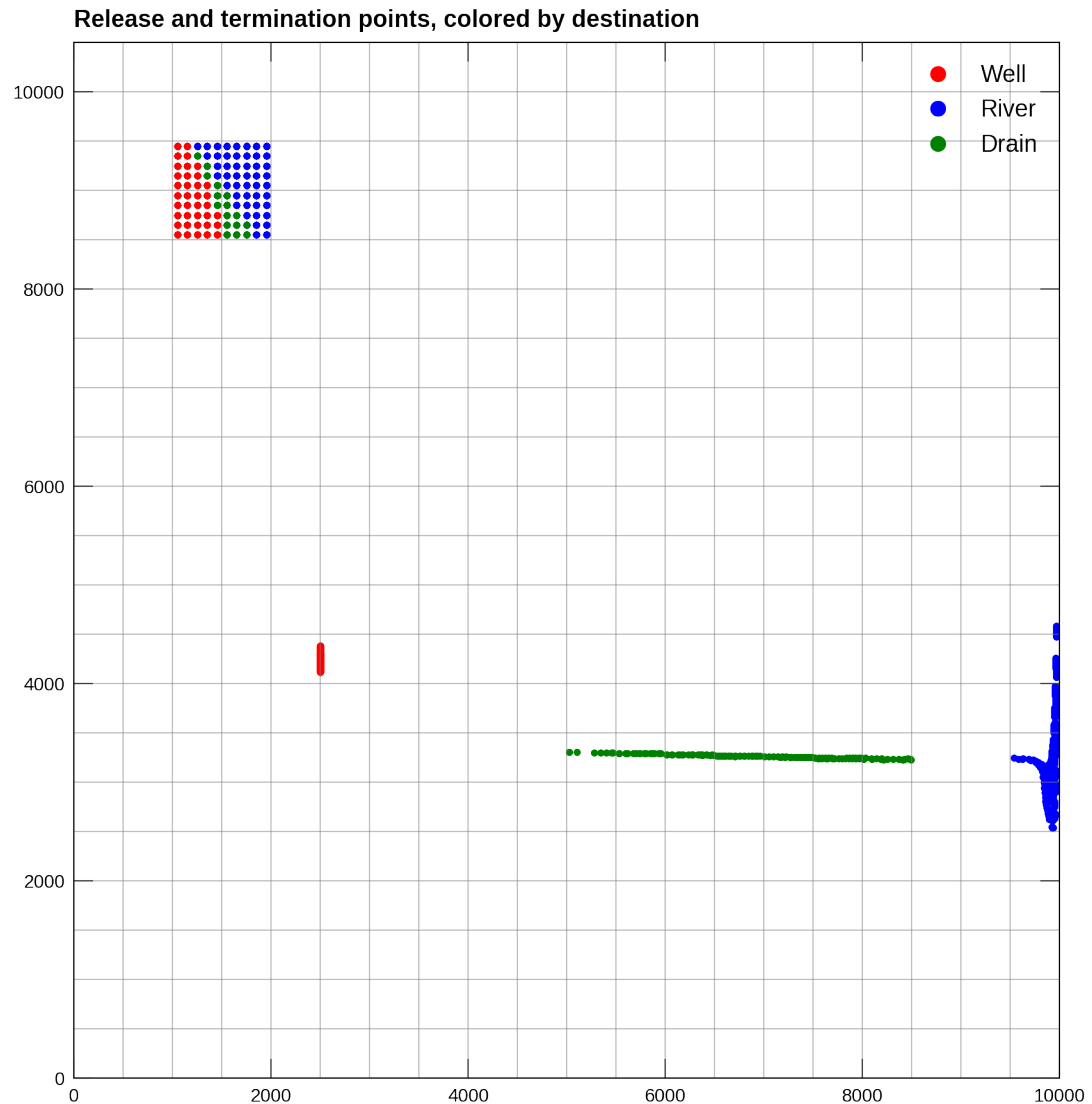


Figure 64–4: Particle release and termination points, colored by destination.

## 65 Thermal Profile along a Particle Path

This example demonstrates the simultaneous use of three different model types in MODFLOW 6: (1) groundwater flow (GWF), (2) groundwater energy transport (GWE), and (3) particle transport (PRT). Both GWF and GWE solve for steady flow and temperature conditions, respectively. PRT is used to route two particles through the steady flow and heat transport fields and once informed of the particle locations through time, each x-y location is mapped to a temperature that is then plotted.

### 65.1 Example description

A Voronoi model grid is simulated with the discretization by vertices package (DISV). The simulation domain is 2,000 m by 1,000 m and is used by all three model types mentioned above. In the flow model, arbitrarily configured specified head boundaries around the perimeter of the model are as follows: the left-hand boundary is set to 2.0 m, the bottom boundary cells are set to 1.8 m, and the right-hand boundary is set to 1.0 m. Two extraction wells are located in the model domain with the host cells shaded red (fig. 65–1). One is located near the lowerleft of the domain and the second extraction well is located just right of the center of the simulation domain. One injection well is located near the upper right portion of the active domain with the host cell also shaded red (fig. 65–1).

The GWE model uses a standard set of thermal parameters listed in table 65–1. A thermal gradient along the left-hand boundary and is setup such water entering the domain in the lower left corner starts at 0.0 °C with a linear gradient increasing to 100.0 °C in the upper-left corner of the simulation domain. Flow enters the bottom boundary at 80.0 °C. The injection well, or the furthest red shaded cell in figure 65–1, injects water at 80.0 °C.

PRT routes the two particles from their entry point on the left side of the model domain to where they exit along the right-hand boundary.

Table 65–1: Model parameters for example ex-gwe-prt.

Parameter	Value
Left model domain extent (m)	0.0
Right model domain extent (m)	2000.0
South model domain extent (m)	0.0
North model domain extent (m)	1000.0
Top of the model grid (m)	1.0
Bottom of the model grid (m)	0.0
Minimum angle of interior angle of a Voronoi grid cell (°)	30
Maximum area of a Voronoi grid cell (m <sup>2</sup> )	1000.0
Number of layers (–)	1
Porosity (–)	0.1
Starting temperature of model domain (°C)	10.0
Advection scheme (–)	TVD
Longitudinal mechanical dispersion term (m)	0.0
Transverse mechanical dispersion term (m)	0.0
Thermal conductivity of water ( $\frac{W}{m \cdot ^\circ C}$ )	0.56
Thermal conductivity of aquifer material ( $\frac{W}{m \cdot ^\circ C}$ )	2.5
Density of water (kg/m <sup>3</sup> )	1000
Heat capacity of water ( $\frac{J}{kg \cdot ^\circ C}$ )	4180.0
Density of dry solid aquifer material (kg/m <sup>3</sup> )	2650.0
Heat capacity of dry solid aquifer material ( $\frac{J}{kg \cdot ^\circ C}$ )	900.0

## 65.2 Example Results

Results from the GWE and PRT model runs are shown in figure 65–1. Blue dashed lines show each particles path through the simulation domain, with both particles moving from left to right through the domain. The total travel distance of each particle is different and as a result the total travel times also are different. Particle 2 (fig. 65–1) reaches a temporary stagnation point to the left of the injection well but eventually moves toward the lower boundary before being swept toward the right boundary where it eventually exits the simulation domain. The temperature experienced by each respective particle along its path is generally one of warming, both with respect to its x-position (fig. 65–1; middle plot) or time (fig. 65–1; bottom plot)

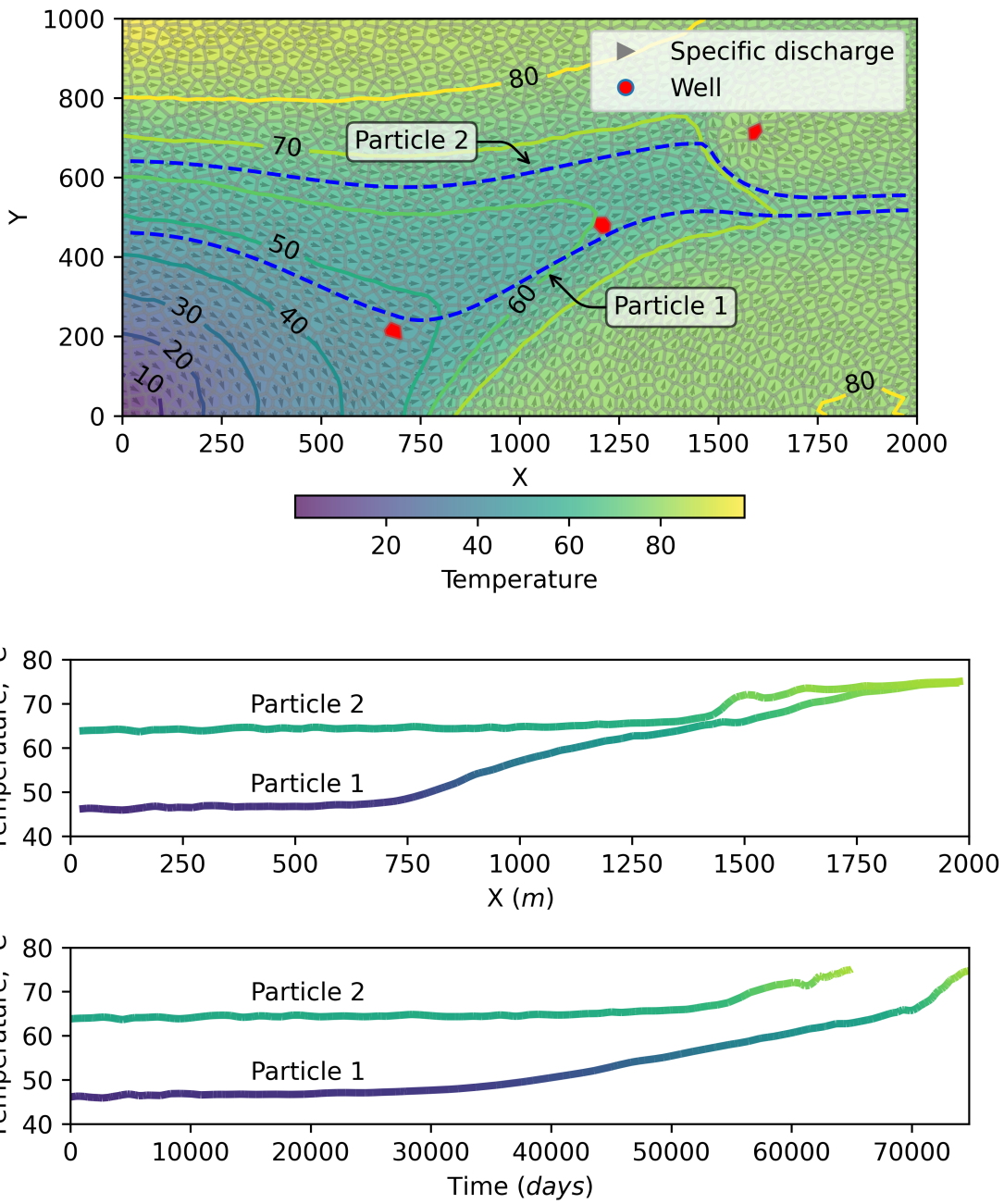


Figure 65–1: (Top) Model grid color-filled with the steady-state temperature field and specific discharge arrows. Dashed blue lines show the paths of particles 1 and 2 and they traverse the simulation domain. (Middle) The x-position of each particle is plotted against its temperature as it traverses the simulation domain. (Bottom) The travel time of each particle is plotted against its temperature as it traverses the simulation domain.

## References Cited

- Al-Khoury, R., BniLam, N., Arzanfudi, M.M., and Saeid, S., 2020, A spectral model for a moving cylindrical heat source in a conductive-convective domain: International Journal of Heat and Mass Transfer, v. 163, p. 120,517, accessed October 03, 2020, at <https://doi.org/10.1016/j.ijheatmasstransfer.2020.120517>.
- Al-Khoury, R., BniLam, N., Arzanfudi, M.M., and Saeid, S., 2021, Analytical model for arbitrarily configured neighboring shallow geothermal installations in the presence of groundwater flow: Geothermics, v. 93, p. 102,063, accessed February 23, 2021, at <https://doi.org/10.1016/j.geothermics.2021.102063>.
- Bakker, M., Oude Essink, G.H., and Langevin, C.D., 2004, The rotating movement of three immiscible fluids—a benchmark problem: Journal of Hydrology, v. 287, no. 1, p. 270 – 278, <https://doi.org/10.1016/j.jhydrol.2003.10.007>.
- Bakker, M., Post, V., Langevin, C.D., Hughes, J.D., White, J.T., Starn, J.J., and Fienen, M.N., 2016, Scripting MODFLOW model development using Python and FloPy: Groundwater, v. 54, no. 5, p. 733–739, accessed August 27, 2020, at <https://doi.org/10.1111/gwat.12413>.
- Bedekar, V., Morway, E.D., Langevin, C.D., and Tonkin, M.J., 2016, MT3D-USGS version 1: A U.S. Geological Survey release of MT3DMS updated with new and expanded transport capabilities for use with MODFLOW: U.S. Geological Survey Techniques and Methods, book 6, chap. A53, 69 p., <https://doi.org/10.3133/tm6a53>.
- Bedekar, V., Scantlebury, L., and Panday, S., 2019, Axisymmetric modeling using MODFLOW-USG: Groundwater, v. 57, no. 5, p. 772–777, <https://doi.org/10.1111/gwat.12861>.
- Brooks, R.H., and Corey, A.T., 1966, Properties of porous media affecting fluid flow: American Society of Civil Engineers, Journal of Irrigation and Drainage, v. 92, p. 61–90, <https://doi.org/10.1061/JRCEA4.0000425>.
- Burbey, T.J., 2001, Storage coefficient revisited—Is purely vertical strain a good assumption?: Groundwater, v. 39, no. 3, p. 458–464, accessed October 11, 2019, at <https://doi.org/10.1111/j.1745-6584.2001.tb02330.x>.
- Carslaw, H.S., and Jaeger, J.C., 1959, Conduction of heat in solids: Oxford: Clarendon Press, 1959, 2nd ed.
- Crank, J., 1975, The mathematics of diffusion. Second Edition, Oxford University Press.
- Diao, N., Li, Q., and Fang, Z., 2004, Heat transfer in ground heat exchangers with groundwater advection: International Journal of Thermal Sciences, v. 43, no. 12, p. 1203–1211, accessed February 19, 2021, at <https://doi.org/10.1016/j.ijthermalsci.2004.04.009>.
- Domenico, P.A., and Robbins, G.A., 1985, A new method of contaminant plume analysis: Groundwater, v. 23, no. 4, p. 476–485, accessed February 19, 2021, at <https://doi.org/10.1111/j.1745-6584.1985.tb01497.x>.
- El-Kadi, A.L., 1988, Applying the USGS mass-transport model (MOC) to remedial actions by recovery wells: Groundwater, v. 26, no. 3, p. 281–288, <https://doi.org/10.1111/j.1745-6584.1988.tb00391.x>.

- Freeze, R.A., and Cherry, J.A., 1979, Groundwater: Englewood Cliffs, N.J., Prentice-Hall, 604 p.
- Freyberg, D.L., 1988, An exercise in ground-water model calibration and prediction: *Groundwater*, v. 26, no. 3, p. 350–360, accessed June 23, 2021, at <https://doi.org/10.1111/j.1745-6584.1988.tb00399.x>.
- Gelhar, L.W., and Collins, M.A., 1971, General analysis of longitudinal dispersion in nonuniform flow: *Water Resources Research*, v. 7, no. 6, p. 1511–1521, accessed September 8, 2020, at <https://doi.org/10.1029/WR007i006p01511>.
- Harbaugh, A.W., 2005, MODFLOW-2005, the U.S. Geological Survey modular ground-water model—the Ground-Water Flow Process: U.S. Geological Survey Techniques and Methods, book 6, chap. A16, variously paged, accessed June 27, 2017, at <https://pubs.usgs.gov/tm/2005/tm6A16/>.
- Harbaugh, A.W., and McDonald, M.G., 1996, User's documentation for MODFLOW-96, an update to the U.S. Geological Survey modular finite-difference ground-water flow model: U.S. Geological Survey Techniques of Water-Resources Investigations, book 6, chap. A1, 586 p.
- Hecht-Mendez, J., 2008, Implementation and verification of the USGS solute transport code MT3DMS for groundwater heat transport modeling: Tübingen, University of Twente, Master's Thesis, 73 p., [https://www.hechtm.de/onewebmedia/Thesis\\_with\\_erratum.pdf](https://www.hechtm.de/onewebmedia/Thesis_with_erratum.pdf).
- Hecht-Mendez, J., Molina-Giraldo, N., Blum, P.D., and Bayer, P., 2010, Evaluating MT3DMS for heat transport simulation of closed geothermal systems: *Groundwater*, v. 48, no. 5, p. 741–756, accessed February 15, 2021, at <https://doi.org/10.1111/j.1745-6584.2010.00678.x>.
- Hemker, K., van den Berg, E., and Bakker, M., 2004, Ground water whirls: *Ground Water*, v. 42, no. 2, p. 234–242, accessed June 27, 2017, at <https://doi.org/10.1111/j.1745-6584.2004.tb02670.x>.
- Henry, H., 1964, Effects of dispersion on salt encroachment in coastal aquifers: *Sea Water in Coastal Aquifers*, U.S. Geol. Surv. Supply Pap., 1613-C, C71-C84.
- Hill, M.C., Cooley, R.L., and Pollock, D.W., 1998, A controlled experiment in ground water flow model calibration: *Groundwater*, v. 36, no. 3, p. 520–535, <https://doi.org/10.1111/j.1745-6584.1998.tb02824.x>.
- Hoffmann, J., Leake, S.A., Galloway, D.L., and Wilson, A.M., 2003, MODFLOW-2000 Ground-Water Model—User Guide to the Subsidence and Aquifer-System Compaction (SUB) Package: U.S. Geological Survey Open-File Report 03-233, 44 p., accessed June 27, 2017, at <https://pubs.usgs.gov/of/2003/ofr03-233/>.
- Hughes, J.D., Langevin, C.D., and Banta, E.R., 2017, Documentation for the MODFLOW 6 framework: U.S. Geological Survey Techniques and Methods, book 6, chap. A57, 36 p., accessed August 4, 2017, at <https://doi.org/10.3133/tm6A57>.
- Hughes, J.D., Langevin, C.D., Paulinski, S.R., Larsen, J.D., and Brakenhoff, D., 2023, FloPy workflows for creating structured and unstructured MODFLOW models: *Groundwater*, <https://doi.org/10.1111/gwat.13327>.
- Hunt, B., 1978, Dispersive sources in uniform ground-water flow: *Journal of the Hydraulics Division*, v. 104, no. ASCE 13467 Proceeding, accessed June 26, 2020, at <https://trid.trb.org/view/72451>.

- Hunt, R.J., Fienen, M.N., and White, J.T., 2020, Revisiting “an exercise in groundwater model calibration and prediction” after 30 years: Insights and new directions: *Groundwater*, v. 58, no. 2, p. 168–182, accessed June 23, 2021, at <https://doi.org/10.1111/gwat.12907>.
- Jacob, C., 1939, Fluctuations in artesian pressure produced by passing railroad-trains as shown in a well on Long Island, New York: *Eos, Transactions American Geophysical Union*, v. 20, no. 4, p. 666–674, <https://doi.org/10.1029/TR020i004p00666>.
- Keating, E., and Zyvoloski, G., 2009, A stable and efficient numerical algorithm for unconfined aquifer analysis: *Ground Water*, v. 47, no. 4, p. 569–579, accessed June 27, 2017, at <https://doi.org/10.1111/j.1745-6584.2009.00555.x>.
- Konikow, L.F., Goode, D.J., and Hornberger, G.Z., 1996, A three-dimensional method-of-characteristics solute-transport model (MOC3D): U.S. Geological Survey Water-Resources Investigations Report 96-4267, 87 p., accessed June 27, 2017, at <https://pubs.er.usgs.gov/publication/wri964267>.
- Laattoe, T., Post, V. E.A., and Werner, A.D., 2014, Spatial periodic boundary condition for MODFLOW: *Groundwater*, v. 52, no. 4, p. 606–612, accessed June 27, 2017, at <https://doi.org/10.1111/gwat.12086>.
- Langevin, C.D., Shoemaker, W.B., and Guo, W., 2003, MODFLOW-2000 the U.S. Geological Survey Modular Ground-Water Model—Documentation of the SEAWAT-2000 Version with the Variable-Density Flow Process (VDF) and the Integrated MT3DMS Transport Process (IMT): U.S. Geological Survey Open-File Report 03-426, 43 p., accessed July 25, 2019, at <https://pubs.er.usgs.gov/publication/ofr03426>.
- Langevin, C.D., Thorne Jr, D.T., Dausman, A.M., Sukop, M.C., and Guo, W., 2008, SEAWAT Version 4—A computer program for simulation of multi-species solute and heat transport: U.S. Geological Survey Techniques and Methods, book 6, chap. A22, 39 p., accessed June 27, 2017, at <https://pubs.er.usgs.gov/publication/tm6A22>.
- Langevin, C.D., Hughes, J.D., Provost, A.M., Banta, E.R., Niswonger, R.G., and Panday, S., 2017a, Documentation for the MODFLOW 6 Groundwater Flow (GWF) Model: U.S. Geological Survey Techniques and Methods, book 6, chap. A55, 197 p., accessed August 4, 2017, at <https://doi.org/10.3133/tm6A55>.
- Langevin, C.D., Hughes, J.D., Provost, A.M., Banta, E.R., Niswonger, R.G., and Panday, S., 2017b, MODFLOW 6, the U.S. Geological Survey Modular Hydrologic Model: U.S. Geological Survey Software Release, accessed August 4, 2017, at <https://doi.org/10.5066/F76Q1VQV>.
- Langevin, C.D., Panday, S., and Provost, A.M., 2020, Hydraulic-head formulation for density-dependent flow and transport: *Groundwater*, v. 58, no. 3, p. 349–362, <https://doi.org/10.1111/gwat.12967>.
- Langevin, C.D., Provost, A.M., Panday, S., and Hughes, J.D., 2022, Documentation for the MODFLOW 6 Groundwater Transport (GWT) Model: U.S. Geological Survey Techniques and Methods, book 6, chap. A61, 56 p., accessed July 28, 2022, at <https://doi.org/10.3133/tm6A55>.
- Lappala, E.G., Healy, R.W., Weeks, E.P., and others, 1987, Documentation of computer program VS2D to solve the equations of fluid flow in variably saturated porous media: U.S. Geological Survey Water-Resources Investigations Report 83-4099, 184 p., accessed June 27, 2017, at <https://pubs.er.usgs.gov/publication/wri834099>.

- Leake, S.A., and Galloway, D.L., 2007, MODFLOW Ground-water model—User guide to the Subsidence and Aquifer-System Compaction Package (SUB-WT) for Water-Table Aquifers: U.S. Geological Survey Techniques and Methods, book 6, chap. A23, 42 p., accessed June 27, 2017, at <https://pubs.er.usgs.gov/publication/tm6A23>.
- Leake, S.A., and Lilly, M.R., 1997, Documentation of computer program (FHB1) for assignment of transient specified-flow and specified-head boundaries in applications of the modular finite-difference ground-water flow model (MODFLOW): U.S. Geological Survey Open-File Report 97-571, 50 p., accessed June 27, 2017, at <https://pubs.er.usgs.gov/publication/ofr97571>.
- Leake, S.A., Reeves, H.W., and Dickinson, J.E., 2010, A new capture fraction method to map how pumpage affects surface water flow: Groundwater, v. 48, no. 5, p. 690–700, accessed June 23, 2021, at <https://doi.org/10.1111/j.1745-6584.2010.00701.x>.
- Ma, R., and Zheng, C., 2010, Effects of density and viscosity in modeling heat as a groundwater tracer: Groundwater, v. 48, no. 3, p. 380–389, accessed April 28, 2010, at <https://doi.org/10.1111/j.1745-6584.2009.00660.x>.
- McDonald, M.G., and Harbaugh, A.W., 1988, A modular three-dimensional finite-difference ground-water flow model: U.S. Geological Survey Techniques of Water-Resources Investigations, book 6, chap. A1, 586 p., accessed June 27, 2017, at <https://pubs.er.usgs.gov/publication/twri06A1>.
- McDonald, M.G., Harbaugh, A.W., Orr, B.R., and Ackerman, D.J., 1992, A method of converting no-flow cells to variable-head cells for the U.S. Geological Survey modular finite-difference ground-water flow model: U.S. Geological Survey Open-File Report 91-536, 99 p., accessed June 27, 2017, at <https://pubs.er.usgs.gov/publication/ofr91536>.
- Mehl, S.W., and Hill, M.C., 2013, MODFLOW-LGR Documentation of Ghost Node Local Grid Refinement (LGR2) for Multiple Areas and the Boundary Flow and Head (BFH2) Package: U.S. Geological Survey Techniques and Methods, book 6, chap. A44, 43 p., accessed August 27, 2020, at <https://doi.org/10.3133/tm6A44>.
- Merritt, M.L., and Konikow, L.F., 2000, Documentation of a computer program to simulate lake-aquifer interaction using the MODFLOW ground-water flow model and the MOC3D solute-transport model: U.S. Geological Survey Water-Resources Investigations Report 00-4167, 146 p., accessed June 27, 2017, at <https://pubs.er.usgs.gov/publication/wri004167>.
- Moench, A., and Ogata, A., 1981, A numerical inversion of the Laplace transform solution to radial dispersion in a porous medium: Water Resources Research, v. 17, no. 1, p. 250–252, accessed June 26, 2020, at <https://doi.org/10.1029/WR017i001p00250>.
- Morway, E.D., Niswonger, R.G., Langevin, C.D., Bailey, R.T., and Healy, R.W., 2013, Modeling variably saturated subsurface solute transport with MODFLOW-UZF and MT3DMS: Groundwater, v. 51, no. 2, p. 237–251, <https://doi.org/10.1111/j.1745-6584.2012.00971.x>.
- Neuman, S.P., 1974, Effect of partial penetration on flow in unconfined aquifers considering delayed gravity response: Water resources research, v. 10, no. 2, p. 303–312, <https://doi.org/10.1029/WR010i002p00303>.
- Neville, C.J., and Tonkin, M.J., 2004, Modeling multiaquifer wells with MODFLOW: Ground Water, v. 42, no. 6, p. 910–919, accessed June 27, 2017, at <https://doi.org/10.1111/j.1745-6584.2004.t01-9-x>.

Niswonger, R.G., and Pradic, D.E., 2005, Documentation of the Streamflow-Routing (SFR2) Package to include unsaturated flow beneath streams—A modification to SFR1: U.S. Geological Survey Techniques and Methods, book 6, chap. A13, 50 p., accessed June 27, 2017, at <https://pubs.er.usgs.gov/publication/tm6A13>.

Niswonger, R.G., Pradic, D.E., and Regan, R.S., 2006, Documentation of the Unsaturated-Zone Flow (UZF1) Package for modeling unsaturated flow between the land surface and the water table with MODFLOW-2005: U.S. Geological Survey Techniques and Methods, book 6, chap. A19, 62 p., accessed June 27, 2017, at <https://pubs.usgs.gov/tm/2006/tm6a19/>.

Niswonger, R.G., Panday, S., and Ibaraki, M., 2011, MODFLOW-NWT, A Newton formulation for MODFLOW-2005: U.S. Geological Survey Techniques and Methods, book 6, chap. A37, 44 p., accessed June 27, 2017, at <https://pubs.er.usgs.gov/publication/tm6A37>.

Panday, S., Langevin, C.D., Niswonger, R.G., Ibaraki, M., and Hughes, J.D., 2013, MODFLOW-USG version 1—An unstructured grid version of MODFLOW for simulating groundwater flow and tightly coupled processes using a control volume finite-difference formulation: U.S. Geological Survey Techniques and Methods, book 6, chap. A45, 66 p., accessed June 27, 2017, at <https://pubs.usgs.gov/tm/06/a45/>.

Pollock, D., 2017, Modpath version 7: Example problems.

Pollock, D.W., 2016, User guide for MODPATH Version 7—A particle-tracking model for MODFLOW: U.S. Geological Survey Open-File Report 2016-1086, 35 p., accessed June 27, 2017, at <https://doi.org/10.3133/ofr20161086>.

Provost, A.M., Langevin, C.D., and Hughes, J.D., 2017, Documentation for the “XT3D” Option in the Node Property Flow (NPF) Package of MODFLOW 6: U.S. Geological Survey Techniques and Methods, book 6, chap. A56, 46 p., accessed August 4, 2017, at <https://doi.org/10.3133/tm6A56>.

Pradic, D.E., Konikow, L.F., and Banta, E.R., 2004, A New Streamflow-Routing (SFR1) Package to simulate stream-aquifer interaction with MODFLOW-2000: U.S. Geological Survey Open File Report 2004-1042, 104 p., accessed June 27, 2017, at <https://pubs.er.usgs.gov/publication/ofr20041042>.

Reilly, T.E., Franke, O.L., and Bennett, G.D., 1989, Bias in groundwater samples caused by wellbore flow: Journal of Hydraulic Engineering, v. 115, no. 2, p. 270–276, [https://doi.org/10.1061/\(ASCE\)0733-9429\(1989\)115:2\(270\)](https://doi.org/10.1061/(ASCE)0733-9429(1989)115:2(270)).

Riley, F.S., 1969, Analysis of borehole extensometer data from Central California: International Association of Scientific Hydrology Publication 89, v. 2, p. 423–431.

Riley, F.S., 1998, Mechanics of aquifer systems—The scientific legacy of Joseph F. Poland, in Land subsidence case studies and current research: Proceedings of the Dr. Joseph F. Poland Symposium on Land Subsidence: Belmont, Calif., Star Publishing Co., Association of Engineering Geologists Special Publication, v. 8, p. 13–27.

Romero, D.M., and Silver, S.E., 2006, Grid cell distortion and modflow’s integrated finite-difference numerical solution: Groundwater, v. 44, no. 6, p. 797–802, <https://doi.org/10.1111/j.1745-6584.2005.00179.x>.

- Segol, G., Pinder, G.F., and Gray, W.G., 1975, A Galerkin-finite element technique for calculating the transient position of the saltwater front: Water Resources Research, v. 11, no. 2, p. 343–347, <https://doi.org/10.1029/WR011i002p00343>.
- Simmons, C.T., Narayan, K.A., and Wooding, R.A., 1999, On a test case for density-dependent groundwater flow and solute transport models: The Salt Lake Problem: Water Resources Research, v. 35, no. 12, p. 3607–3620, <https://doi.org/10.1029/1999WR900254>.
- Simpson, M.J., and Clement, T.P., 2004, Improving the worthiness of the Henry problem as a benchmark for density-dependent groundwater flow models: Water Resources Research, v. 40, no. W01504, p. 1152–1173, accessed July 1, 2019, at <https://doi.org/10.1029/2003WR002199>.
- Sneed, M., 2008, Aquifer-system compaction and land subsidence: data and simulations, the Holly site, Edwards Air Force Base, California: Sacramento, California State University, Master's Thesis, 40 p.
- Sneed, M., and Galloway, D.L., 2000, Aquifer-system compaction and land subsidence: measurements, analyses, and simulations: the Holly Site, Edwards Air Force base, Antelope Valley, California: U.S. Geological Survey Water-Resources Investigations Report 2000–4015, 65 p., accessed July 9, 2019, at <https://pubs.er.usgs.gov/publication/wri20004015>.
- Sokol, D., 1963, Position and fluctuations of water level in wells perforated in more than one aquifer: Journal of Geophysical Research, v. 68, no. 4, p. 1079–1080, <https://doi.org/10.1029/JZ068i004p01079>.
- Stallman, R., 1965, Steady one-dimensional fluid flow in a semi-infinite porous medium with sinusoidal surface temperature: Journal of geophysical Research, v. 70, no. 12, p. 2821–2827, <https://doi.org/10.1029/JZ070i012p02821>.
- Sudicky, E., 1989, The Laplace transform Galerkin technique—A time-continuous finite element theory and application to mass transport in groundwater: Water Resources Research, v. 25, no. 8, p. 1833–1846, accessed June 26, 2020, at <https://doi.org/10.1029/WR025i008p01833>.
- Van der Heijde, P. K.M., 1995, Model testing—A functionality analysis, performance evaluation, and applicability assessment protocol, CRC Press, Lewis Publishers, Boca Raton, FL.
- Van Genuchten, M.T., and Alves, W.J., 1982, Analytical solutions of the one-dimensional convective-dispersive solute transport equation: U.S. Department of Agriculture Technical Bulletin No. 1661, accessed June 25, 2020, at <https://naldc.nal.usda.gov/download/CAT82780278/PDF>.
- Vilhelmsen, T.N., Christensen, S., and Mehl, S.W., 2012, Evaluation of MODFLOW-LGR in connection with a synthetic regional-scale model: Groundwater, v. 50, no. 1, p. 118–132, accessed October 6, 2020, at <https://doi.org/10.1111/j.1745-6584.2011.00826.x>.
- Voss, C.I., 1984, SUTRA—a finite-element simulation model for saturated-unsaturated fluid-density-dependent ground-water flow with energy transport or chemically-reactive single-species solute transport: U.S. Geological Survey Water-Resources Investigations Report 84-4369, 409 p.
- Voss, C.I., and Souza, W.R., 1987, Variable density flow and solute transport simulation of regional aquifers containing a narrow freshwater-saltwater transition zone: Water Resources Research, v. 23, no. 10, p. 1851–1866, <https://doi.org/10.1029/WR023i010p01851>.

Welter, D.E., White, J.T., Hunt, R.J., and Doherty, J.E., 2015, Approaches in highly parameterized inversion–PEST++ Version 3, a Parameter ESTimation and uncertainty analysis software suite optimized for large environmental models: U.S. Geological Survey Techniques and Methods, book 7, section C12, 54 p. , accessed April 18, 2019, at <https://doi.org/10.3133/tm7C12>.

Wexler, E., 1992, Analytical solutions for one-, two-, and three-dimensional solute transport in ground-water systems with uniform flow: U.S. Geological Survey Techniques of Water-Resources Investigations, Book 3, Chapter B7, 190 p.

Wilson, J.L., and Miller, P.J., 1978, Two-dimensional plume in uniform ground-water flow: Journal of the Hydraulics Division, v. 104, no. 4, p. 503–514, accessed June 26, 2020, at <https://doi.org/10.1061/JYCEAJ.0004975>.

Wooding, R.A., Tyler, S.W., and White, I., 1997a, Convection in groundwater below an evaporating Salt Lake–1. Onset of instability: Water Resources Research, v. 33, no. 6, p. 1199–1217, <https://doi.org/10.1029/96WR03533>.

Wooding, R.A., Tyler, S.W., White, I., and Anderson, P.A., 1997b, Convection in groundwater below an evaporating Salt Lake–2. Evolution of fingers or plumes: Water Resources Research, v. 33, no. 6, p. 1219–1228, <https://doi.org/10.1029/96WR03534>.

Zaidel, J., 2013, Discontinuous steady-state analytical solutions of the Boussinesq equation and their numerical representation by MODFLOW: Groundwater, v. 51, no. 6, p. 952–959, <https://doi.org/10.1111/gwat.12019>.

Zheng, C., 1990, MT3D, A modular three-dimensional transport model for simulation of advection, dispersion and chemical reactions of contaminants in groundwater systems: Report to the U.S. Environmental Protection Agency, 170 p.

Zheng, C., 1993, Extension of the method of characteristics for simulation of solute transport in three dimensions: Groundwater, v. 31, no. 3, p. 456–465, accessed June 26, 2020, at <https://doi.org/10.1111/j.1745-6584.1993.tb01848.x>.

Zheng, C., 2010, MT3DMS v5.3—A modular three-dimensional multi-species transport model for simulation of advection, dispersion and chemical reactions of contaminants in groundwater systems; Supplemental user's guide: Technical Report, Department of Geological Sciences, The University of Alabama, 51 p.

Zheng, C., and Wang, P.P., 1999, MT3DMS—A modular three-dimensional multi-species transport model for simulation of advection, dispersion and chemical reactions of contaminants in groundwater systems; Documentation and user's guide: Contract report SERDP–99–1: Vicksburg, Miss., U.S. Army Engineer Research and Development Center, 169 p.